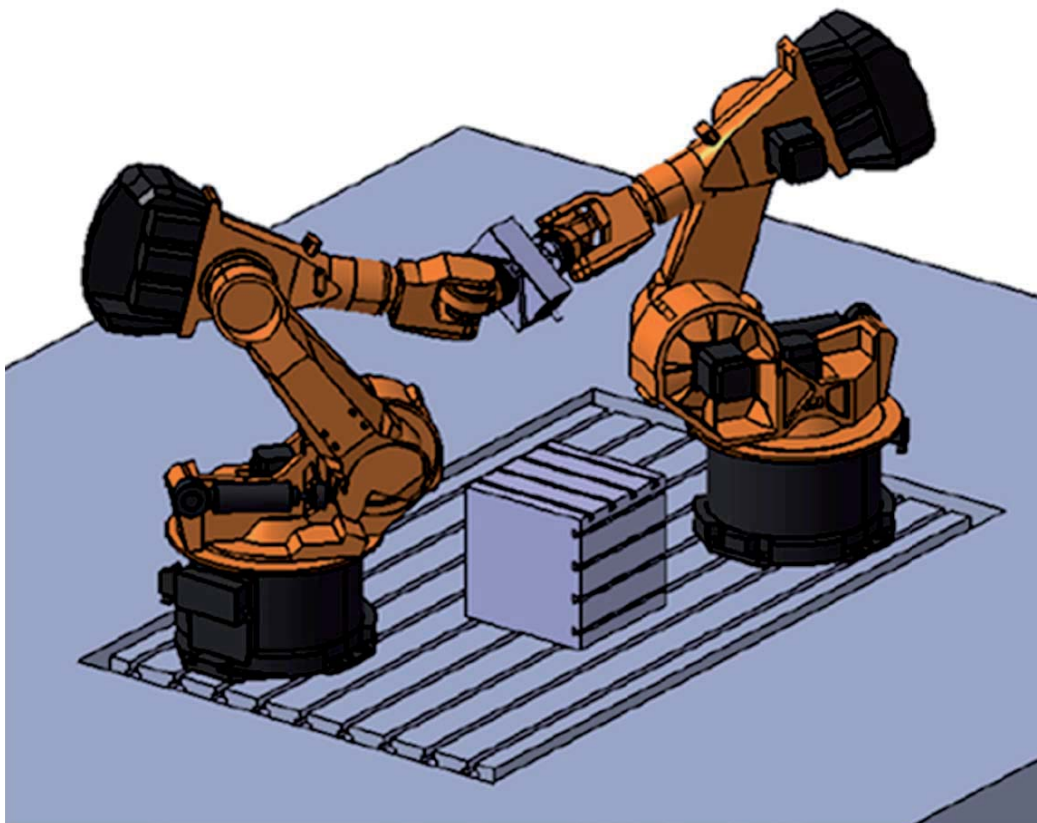


# Book of Abstracts

ECCOMAS Thematic Conference on  
**MULTIBODY DYNAMICS**  
Prague, June 19 - 22, 2017



CZECH TECHNICAL UNIVERSITY IN PRAGUE  
Faculty of Mechanical Engineering



# **Book of Abstracts of the 8<sup>th</sup> ECCOMAS Thematic Conference on MULTIBODY DYNAMICS 2017**

Prague, June 19 – 22, 2017  
Faculty of Mechanical Engineering  
Czech Technical University in Prague  
[www.multibody2017.cz](http://www.multibody2017.cz)

## **Editors:**

Michael Valášek, Zbyněk Šika, Tomáš Vampola, Michal Hajžman, Pavel Polach, Zdeněk Neusser, Petr Beneš, Jan Zavřel

## **Contact address:**

Czech Technical University in Prague  
Faculty of Mechanical Engineering  
Technická 4  
166 07 Prague  
Czech Republic  
Phone: +420 22435 5038

## **Design:**

Tomáš Prajs

## **Publisher:**

Nakladatelství ČVUT (CTN), Žitná 1903/4, 166 36 Praha 6 – Dejvice  
390 pages, 10 copies, 1. edition

ISBN 978-80-01-06171-8 (online)  
ISBN 978-80-01-06172-5 (printed)

## **Welcome to the Conference**

The ECCOMAS Thematic Conference on Multibody Dynamics is an international meeting held once every two years in a European country. The past conferences have been organized in Lisbon (2003), Madrid (2005), Milan (2007), Warsaw (2009), Brussels (2011), Zagreb (2013) and Barcelona (2015). The last predecessor of this conference that was held at Czech Technical University in Prague in 1994 was the Euromech Colloquium 320 on Multibody systems - Advanced Algorithms and Software Tools.

As the conference chair I cordially welcome you the Multibody Dynamics Conference held at Czech Technical University in Prague.

## **Conference Objectives**

Current conference on multibody dynamics takes place in Prague again after 23 years and will serve as a meeting point for the international researchers, scientists and experts from academia, research laboratories and industry working in the area of multibody dynamics.

Applications are related to many fields of contemporary engineering, from road and railway vehicles, aerospace, through robotic manipulators, machine tools, mechatronic systems, smart structures to biomechanical systems and nanotechnology. The theory and methods of multibody dynamics are also further developed.

## **Conference Focus**

However, as the conference chair I have raised a special attention on two topics in this conference that is visible in the choice of keynote lectures. One topic is the discussion on current problems and challenges in general multibody dynamics formalisms including the treatment of flexible multibody systems (Keynote lectures of Jorge Ambrósio and Peter Eberhard). The other topic is the advances in concepts, modelling and control of robots (Keynote lectures of Andreas Müller and Andreas Pott). I personally suppose these topics are very important and strongly developing with less attention than they deserve. The topic of robots is specially related to Prague where Karel Čapek wrote his theatre drama R.U.R. (Rossum's Universal Robots) and invented the word "robot".

*Michael Valášek, Conference Chair*

## Conference Topics

The Conference focuses on all aspects of multibody dynamics. Papers are especially solicited on the following topics:

**Formulations and Numerical Methods**  
**Efficient Methods and Real-Time Applications**  
**Parallelization methods**  
**Flexible Multibody Dynamics**  
**Contact Dynamics and Constraints**  
**Multiphysics and Coupled Problems**  
**Benchmark Problems**  
**Control and Optimization**  
**Software Development and Computer Technology**  
**Robotics**  
**Road Vehicle Dynamics**  
**Railroad Vehicle Dynamics**  
**Biomechanics**  
**Aerospace and Maritime Applications**  
**Machine Tools**

## Organizing Committee

Michael Valášek, Conference Chair (Czech Technical University in Prague)

Zbyněk Šika (Czech Technical University in Prague)

Pavel Polach (University of West Bohemia)

Michal Hajžman (University of West Bohemia)

Petr Beneš (Czech Technical University in Prague)

Jan Zavřel (Czech Technical University in Prague)

Zdeněk Neusser (Czech Technical University in Prague)

Tomáš Prajs (Czech Technical University in Prague)

Terézia Němcová, Secretary (Czech Technical University in Prague)

## Scientific Committee

Jorge Ambrósio (Instituto Superior Técnico, Portugal)  
Kurt Anderson (Rensselaer Polytechnic Institute, USA)  
Martin Arnold (Martin Luther Univ. Halle-Wittenberg, Germany)  
Joaquim A. Batlle (Univ. Politècnica de Catalunya, Spain)  
Olivier A. Bauchau (UM-SJTU Joint Institute, China)  
Wojciech Blajer (Univ. of Tech. and Hum. in Radom, Poland)  
Carlo L. Bottasso (Politecnico di Milano, Italy)  
Olivier Brùls (Univ. of Liège, Belgium)  
Alberto Cardona (Univ. Nacional del Litoral, Argentina)  
Javier Cuadrado (Univ. de La Coruna, Spain)  
Peter Eberhard (Univ. of Stuttgart, Germany)  
Paul Fiset (Univ. Catholique de Louvain, Belgium)  
Javier García de Jalón (Univ. Politècnica de Madrid, Spain)  
Juan Carlos García Orden (Univ. Politècnica de Madrid, Spain)  
Johannes Gerstmayr (Univ. of Innsbruck, Austria)  
Michal Hajžman (Univ. of West Bohemia, Czech Republic)  
Ben Jonker (Univ. of Twente, The Netherlands)  
Andrés Kecskeméthy (Univ. of Duisburg-Essen, Germany)  
Jozsef Kövecses (McGill Univ., Canada)  
Dirk Lefebber (Vrije Univ. Brussel, Belgium)  
Andreas Müller (Johannes Kepler University Linz, Austria)  
Dan Negrut (Univ. of Wisconsin-Madison, USA)  
Ettore Pennestrì (Univ. of Rome, Italy)  
Friedrich Pfeiffer (TU München, Germany)  
Dmitry Pogorelov (Bryansk State Technical Univ, Russia)  
Pavel Polach (Univ. of West Bohemia, Czech Republic)  
Werner Schiehlen (Univ. of Stuttgart, Germany)  
Arend Schwab (TU Delft, The Netherlands)  
Ahmed Shabana (Univ. of Illinois at Chicago, USA)  
Nobuyuki Shimizu (Iwaki Meisei Univ., Japan)  
Yoshihiro Suda (Univ. of Tokyo, Japan)  
Zbyněk Šika (Czech Tech. Univ. in Prague, Czech Republic)  
Yoshiaki Terumichi (Sophia Univ., Japan)  
Michael Valásek (Czech Tech. Univ. in Prague, Czech Republic)  
Tomáš Vampola (Czech Tech. Univ. in Prague, Czech Republic)  
Olivier Verlinden (Univ. Mons, Belgium)  
Wan-Suk Yoo (Pusan National Univ., Korea)  
Evtim Zahariev (Bulgarian Academy of Sciences, Bulgaria)

Special thanks belong to the members of Scientific Committee for their valuable support of selection and evaluation of papers presented at the conference.

*Michael Valasek, Conference Chair*



## **Section**

# **FORMULATIONS AND NUMERICAL METHODS**



# A Simple Energy-conserving Torsion-free Beam Element for Multibody Applications

Juan C. García Orden<sup>1</sup>

<sup>1</sup> Dep. de Mecánica de Medios Continuos y Teoría de Estructuras  
ETSI Caminos, Canales y Puertos  
Universidad Politécnica de Madrid  
Profesor Aranguren 3, 28040, Madrid, Spain  
juancarlos.garcia@upm.es  
ORCID 0000-0002-9063-6584

## Abstract

Slender flexible beams are very common in many applications in different fields related to multibody dynamics: robotics, aerospace mechanisms, computer graphics, etc. Typically, these components experience small strains but large displacements and rotations. What is more, often their torsional strains are very small or null, due to their slenderness or the specific type of kinematical pairs that connect them with other parts of the mechanism. The numerical simulation of the dynamical behavior of such systems demand the development of beam elements capable of representing these nonlinear effects, while providing accurate results when used with a time-marching scheme.

Many different approaches have been proposed in the literature for dealing with these types of problems. The main ones are segmentation or lumped methods [3, 4, 5], floating frame methods, and nonlinear finite element formulations. Naturally, each approach has different advantages and drawbacks for different applications, and can be used with different time integration schemes. Among these schemes, the so-called geometric integration methods have gained popularity in the last two decades. Specifically, energy-consistent (both energy-conserving or energy-decaying) methods present great appeal for the robust and physically-accurate integration of the dynamics of such systems.

Energy-consistent formulations for beams with the nonlinear finite element approach have been reported in the literature but, to the best of the author's knowledge, there are no such formulations available for the segmentation or lumped approach. We propose in this work the energy-conserving extension of the simple torsion-free beam element proposed in [2], which belongs to this category. In this model, the beam is a collection of articulated nonlinear trusses (large displacements and strains) with the proper tensile stiffness derived from a nonlinear potential, parametrized with the cartesian coordinates of the extremes. The bending stiffness is represented by another potential, such that a single element is composed by two segments (three nodes) that overlap with the neighbors. Since both tensile and bending forces are defined through discrete potentials, it is possible to develop a simple energy-conserving formulation, following [1]. With this formulation, total mechanical energy is exactly preserved in the discrete setting when no dissipative effects are present in the model. The main benefit of this approach is the enhancement of the stability of the numerical scheme. It is remarkable too that the formulation does not employ rotational degrees of freedom and can be applied to two and three-dimensional problems.

The basic formulation of this idea will be presented along with some validation tests that will assess the accuracy of the model, and some exploration on potential applications.

## Acknowledgments

Economy and Competitiveness Ministry of Spain supported this work under Project No. DPI2015-67667-C3-2-R. This support is gratefully acknowledged.

## References

- [1] J. C. García Orden and J. M. Goicolea. Conserving properties in constrained dynamics of flexible multibody systems. *Multibody System Dynamics*, 4:225–244, 2000.
- [2] Juan Carlos García Orden and Javier Cuenca Queipo. A simple shear and torsion-free beam model for multibody dynamics. *Journal of Computational and Nonlinear Dynamics*, 12(5):–, 03 2017.
- [3] Y. Wang and R.L. Huston. A lumped parameter method in the nonlinear analysis of flexible multibody systems. *Computers & Structures*, 50(3):421–432, 1994.
- [4] E. Wittbrodt, I. Adamiec-Wójcik, and S. Wojciech. *Dynamics of Flexible Multibody Systems. Rigid Finite Element Method*. Springer, 2006.
- [5] Y.X. Zhou and K.Y. Sze. A rotation-free beam element for beam and cable analyses. *Finite Elements in Analysis and Design*, 64:79–89, 2013.



# Adjoint sensitivity analysis of three-dimensional beam formulation

Alfonso Callejo<sup>1</sup>, Olivier A. Bauchau<sup>1</sup>

<sup>1</sup> Department of Aerospace Engineering  
University of Maryland  
3182 Glenn L. Martin Hall  
College Park, 20742 Maryland, U.S.A.  
{callejo, obauchau}@umd.edu

## Abstract

For decades, comprehensive rotorcraft analysis tools have been used to predict the aeroelastic response of helicopter rotors. These tools include coupled aerodynamics and flexible multibody dynamics modules to accurately predict the nonlinear dynamic behavior. They should also allow for optimization procedures to be used, in order to identify the most promising design configurations. On the aerodynamics side, design optimization involves thousands of design parameters, such as those defining the geometry of the airfoil; on the structural side, dozens of design parameters are involved, such as the wall thickness, the geometric configuration or the orientation of the composite laminates.

Many of the design optimization routines used in fluid mechanics and structural problems are gradient-based methods. The evaluation of the derivatives of the objective function with respect of the design parameters, often called design sensitivities, is the most costly step of the optimization process. As the number of design variables grows, the evaluation of design sensitivities becomes increasingly burdensome and the use of finite differences becomes prohibitive [1]. These requirements call for an efficient sensitivity analysis that covers all stages of the design process.

*SectionBuilder* is a finite element based code for the analysis of cross-sections of beams of arbitrary geometry made of anisotropic composite materials. It computes the beam's sectional stiffness matrix, the three-dimensional warping field, and the associated three-dimensional stress field at any point of the cross-sections when subjected to three-dimensional loading [2]. The formulation is based on a two-dimensional semi-discretization of the beam's cross-section. Because the computation does not require a three-dimensional mesh, it is computationally efficient. *SectionBuilder* serves as a preprocessor to a flexible multibody dynamics code that includes geometrically-exact beam elements, rigid bodies, and joints [3]. The multibody code is coupled with computational fluid dynamics tools to provide a comprehensive, multidisciplinary rotorcraft code [1, 4].

This paper presents the development of adjoint sensitivity analysis capabilities within *SectionBuilder*, as a first step towards the comprehensive evaluation of sensitivity derivatives for flexible multibody dynamics tools. Next, the governing equations, sensitivity analysis and conclusions are briefly presented.

**Governing equations** Most structural sensitivity analysis tools provide the derivatives of the outputs with respect to sectional properties such as the mass per unit span or the bending and torsional stiffnesses of beams. These codes, however, are unable to link these sectional properties to local design variables, such as sectional geometric configuration, material properties, or ply orientations of the composite lay-up. In contrast, *SectionBuilder* computes sectional properties based on the detailed description of the beam's sectional geometric configuration and material properties and, hence, it is well suited for the evaluation of the sensitivity derivatives of section properties with respect to the physical design parameters. Note that sectional properties are not independent design variables: indeed, changing a single physical characteristic such as a wall thickness alters all sectional properties.

Let  $N$  be the number of cross-section nodes and  $n = 3N$  the number of nodal coordinates. The main outputs of *SectionBuilder* are the beam's  $6 \times 6$  sectional compliance matrix,  $\underline{\underline{S}}^*$ , and the 6-dimensional stress vector,  $\underline{\underline{\tau}}^*$ , which require the computation of the  $n \times 6$  warping modes matrix  $\underline{\underline{W}}^*$ . The governing equations of the formulation can be summarized as

$$\underline{\underline{L}}_1(\underline{\underline{X}}_1) \equiv \underline{\underline{A}}\underline{\underline{X}}_1 - \underline{\underline{B}}_1 = \underline{\underline{0}}, \quad (1)$$

$$\underline{\underline{L}}_0(\underline{\underline{X}}^\dagger, \underline{\underline{X}}_1) \equiv \underline{\underline{A}}\underline{\underline{X}}^\dagger - \underline{\underline{B}}_0 + \underline{\underline{C}}\underline{\underline{X}}_1 = \underline{\underline{0}}, \quad (2)$$

$$\underline{\underline{Q}}(\underline{\underline{S}}^\dagger, \underline{\underline{W}}^\dagger) \equiv \underline{\underline{S}}^\dagger - \underline{\underline{S}}_r^* \left[ \underline{\underline{I}} - (\underline{\underline{M}}\underline{\underline{Z}}^*)^T \underline{\underline{W}}^\dagger \tilde{\underline{\underline{K}}}^{*T} - (\underline{\underline{C}}\underline{\underline{Z}}^*)^T \underline{\underline{W}}^\dagger \right] = \underline{\underline{0}}, \quad (3)$$

$$\underline{\underline{P}}(\underline{\underline{\alpha}}, \underline{\underline{S}}^\dagger, \underline{\underline{W}}^\dagger) \equiv \underline{\underline{\alpha}} + \left[ \underline{\underline{M}}(\underline{\underline{Z}}^* \underline{\underline{S}}^\dagger - \underline{\underline{W}}^\dagger \tilde{\underline{\underline{K}}}^{*T}) + \underline{\underline{C}}^T \underline{\underline{W}}^\dagger \right]^T \underline{\underline{W}}^\dagger = \underline{\underline{0}}, \quad (4)$$

$$\underline{\underline{Q}}(\underline{\underline{W}}^*, \underline{\underline{W}}^\dagger, \underline{\underline{\alpha}}) \equiv \underline{\underline{W}}^* - \underline{\underline{W}}^\dagger - \underline{\underline{Z}}^* \underline{\underline{\alpha}} = \underline{\underline{0}}, \quad (5)$$

$$\underline{\underline{R}}(\underline{\underline{S}}^*, \underline{\underline{S}}^\dagger, \underline{\underline{\alpha}}) \equiv \underline{\underline{S}}^* - \underline{\underline{S}}^\dagger + \tilde{\underline{\underline{K}}}^* \underline{\underline{\alpha}} + \underline{\underline{\alpha}} \tilde{\underline{\underline{K}}}^{*T} = \underline{\underline{0}}, \quad (6)$$

where  $\underline{\underline{X}}^\dagger = [\underline{\underline{W}}^{\dagger T}, \underline{\underline{S}}^{\dagger T}]^T$  and  $\underline{\underline{X}}_1 = [\underline{\underline{W}}_1^T, \underline{\underline{S}}_1^T]^T$ . Note that only state variables are highlighted as function dependencies. Please refer to Han and Bauchau [2] for further details. The linear systems in Eqs. (1) and (2) are six

times singular, hence Eqs. (1) and (2) provide particular solutions, denoted  $\underline{W}^\dagger$  and  $\underline{S}^\dagger$ , to the warping modes  $\underline{W}^*$  and the compliance matrix  $\underline{S}^*$ . Upon application of the correction term  $\underline{\alpha}$  (see Eqs. (3) and (4)) the final solution belonging to the null space,  $\underline{W}^*$ , as well as  $\underline{S}^*$ , are obtained (see Eqs. (5) and (6)). All other terms are calculated from the geometry and the material properties of the cross-section.

The three-dimensional stresses at any point of the cross-section can then be calculated as

$$\underline{\tau}_c^*(\underline{S}^*, \underline{W}^*) = \underline{\mathcal{D}}^* \left[ (\underline{A}\underline{N}) (\underline{Z}^* \underline{S}^* + \underline{W}^* \tilde{\mathcal{K}}^{*T}) + (\underline{B}\underline{N}) \underline{W}^* \right] \underline{\mathcal{F}}_c^*, \quad (7)$$

where  $\underline{\tau}_c^*$  is the 6-dimensional vector of Cauchy stresses,  $\underline{\mathcal{F}}_c^*$  is the 6-dimensional vector of sectional loads and  $\underline{\mathcal{D}}^*$  is the  $6 \times 6$  constitutive matrix. The effect of the design parameters on intermediate terms and state variables must be carefully assessed to correctly derive the sensitivity equations.

**Sensitivity equations** The three-dimensional stresses can be regarded as a set of objective functions whose sensitivities with respect to the design parameters are computed through the adjoint variable method. Consider a single component of the stress tensor,  $\tau_c^{j*}$ , and formulate the following Lagrangian:

$$\mathcal{L} = \tau_c^{j*} + \sum_{i=1}^6 \Lambda_{L_1}^{iT} L_1^i + \sum_{i=1}^6 \Lambda_{L_0}^{iT} L_0^i + \sum_{i=1}^6 \Lambda_O^{iT} O^i + \sum_{i=1}^6 \Lambda_P^{iT} P^i + \sum_{i=1}^6 \Lambda_Q^{iT} Q^i + \sum_{i=1}^6 \Lambda_R^{iT} R^i, \quad (8)$$

where 36 adjoint variable arrays ( $\Lambda_{L_0}^i$ ,  $\Lambda_{L_1}^i$ ,  $\Lambda_O^i$ ,  $\Lambda_P^i$ ,  $\Lambda_Q^i$ ,  $\Lambda_R^i$ ) that multiply each of the governing equations have been introduced. Because  $\mathcal{L} = \tau_c^{j*}$  as long as the governing equations are satisfied, Eq. (8) can be differentiated with respect to the design parameters to obtain the *design sensitivities*  $d\mathcal{L}/db = d\tau_c^{j*}/db$ . The fact that the multipliers are arbitrary can be used to cancel out all terms that contain *state sensitivities*, such as  $d\underline{W}^*/db$ ,  $d\underline{S}^*/db$ , etc. This then leads to an additional set of equations, namely the adjoint equations, that determine the value of the adjoint variables. Note that the adjoint equations are omitted here for the sake of brevity. The final expression for the global sensitivities in the case of, e.g., ply orientation parameters is

$$\frac{d\mathcal{L}}{db} = \frac{\partial \tau_c^{j*}}{\partial \underline{\mathcal{D}}^{j*}} \frac{d\underline{\mathcal{D}}^{j*}}{db} + \sum_{i=1}^6 \Lambda_{L_1}^{iT} \frac{\partial R^i}{\partial b} + \sum_{i=1}^6 \Lambda_O^{iT} \frac{\partial Q^i}{\partial b} + \sum_{i=1}^6 \Lambda_P^{iT} \left( \frac{\partial P^i}{\partial \underline{M}} \frac{d\underline{M}}{db} + \frac{\partial P^i}{\partial \underline{C}^T} \frac{d\underline{C}^T}{db} \right) \quad (9)$$

$$+ \sum_{i=1}^6 \Lambda_O^{iT} \left( \frac{\partial P^i}{\partial \underline{S}^T} \frac{d\underline{S}^T}{db} + \frac{\partial P^i}{\partial \underline{M}} \frac{d\underline{M}}{db} + \frac{\partial P^i}{\partial \underline{C}} \frac{d\underline{C}}{db} \right) + \sum_{i=1}^6 \Lambda_{L_0}^{iT} \left( \frac{\partial L_0^i}{\partial \underline{A}} \frac{d\underline{A}}{db} + \frac{\partial L_0^i}{\partial \underline{C}} \frac{d\underline{C}}{db} \right) + \sum_{i=1}^6 \Lambda_{L_1}^{iT} \left( \frac{\partial L_0^i}{\partial \underline{A}} \frac{d\underline{A}}{db} \right), \quad (10)$$

which can be directly computed once the adjoint variables are known and the remaining terms are analytically computed. These design sensitivities can then be efficiently used by a gradient-based design optimization routine to tune local design parameters. This strategy can be extended to different kinds of “objective functions” such as the compliance matrix  $\underline{S}^*$ . This would potentially be useful because  $\underline{S}^*$  is one of the inputs to the general-purpose flexible multibody dynamics formulation [3].

**Conclusion** This paper presents a detailed derivation of a state-of-the-art beam formulation adjoint, including all necessary terms, both theoretically and from a computational point of view. A number of numerical examples with specific design parameters such as material properties and ply orientations are presented. The resulting sensitivities are validated using finite differences (both real and imaginary). This work lays the groundwork for the sensitivity analysis of the associated flexible multibody dynamics formulation.

## References

- [1] L. Wang, B. Diskin, R. Biedron, E. Nielsen, and O. Bauchau, “Sensitivity analysis of multidisciplinary rotorcraft simulations,” in *55th AIAA Aerospace Sciences Meeting*, p. 1670, 2017.
- [2] S. Han and O. Bauchau, “Nonlinear three-dimensional beam theory for flexible multibody dynamics,” *Multibody System Dynamics*, vol. 34, pp. 211–242, July 2015.
- [3] O. Bauchau, C. Bottasso, and Y. Nikishkov, “Modeling rotorcraft dynamics with finite element multibody procedures,” *Mathematical and Computer Modeling*, vol. 33, no. 10-11, pp. 1113–1137, 2001.
- [4] K. Boopathy and G. Kennedy, “Adjoint-based derivative evaluation methods for flexible multibody systems with rotorcraft applications,” in *55th AIAA Aerospace Sciences Meeting*, p. 1671, 2017.

# Convergence Rate Improvement in The HHT Integration Method for Index-3 DAEs of Multibody Dynamics

Naresh Khude, Mike Collingridge, Jose Ortiz, Ashraf Hamed

MSC Software Corporation  
201 Depot Street, Ann Arbor, MI-48104, USA  
[naresh.khude, michael.collingridge, jose.ortiz, ashraf.hamed]@mscsoftware.com

## Abstract

This paper presents theoretical and implementation aspects related to a variant of the Hilber-Hughes-Taylor (HHT) integration method commonly used in index-3 DAEs of constrained mechanical systems. The HHT method was initially developed for the simulation of finite element models in structural dynamics. The HHT algorithm allows an efficient implementation with an optimal combination of accuracy at low-frequency and numerical damping at high-frequency. A variant of the HHT method was first proposed by Negrut et al. in [1] for the simulation of multibody dynamics system (MBS). In [1], the HHT algorithm was applied to the index-3 DAEs formulation of the constrained equations of motion and was implemented in a commercial MBS tool, Adams. In this paper, the drawbacks of the HHT algorithm in [1] are discussed and the improved HHT algorithm is proposed to eliminate these drawbacks.

In the context of a multibody dynamics, the constrained equations of motion and position kinematic constraint equations lead to the system of nonlinear equations. The time-discrete form of these equations at time  $t_{n+1}$  can be written as

$$\begin{aligned} (\mathbf{M}\ddot{\mathbf{q}})_{n+1} + (\Phi_{\mathbf{q}}^T \boldsymbol{\lambda})_{n+1} &= (\mathbf{Q})_{n+1} \\ \Phi(\mathbf{q}_{n+1}, \mathbf{t}_{n+1}) &= \mathbf{0} \end{aligned} \quad (1)$$

Vectors  $\mathbf{q}$  and  $\boldsymbol{\lambda}$  denote the generalized coordinates and the Lagrange multipliers, respectively,  $\mathbf{M}$  is the symmetric mass matrix, the vector of apparent forces  $\mathbf{Q}$  collects external forces, internal forces and complementary inertia forces, and  $\Phi_{\mathbf{q}}$  is the matrix of constraint gradients. Although commonly used BDF-based integrators in MBS use the constrained equation of motion given in equation (1), the HHT algorithm proposed in [1] modifies the constrained equation of motion as

$$\begin{aligned} (\mathbf{M}\mathbf{a})_{n+1} + (1 + \alpha)(\Phi_{\mathbf{q}}^T \boldsymbol{\lambda} - \mathbf{Q})_{n+1} - \alpha(\Phi_{\mathbf{q}}^T \boldsymbol{\lambda} - \mathbf{Q})_n &= \mathbf{0} \\ \Phi(\mathbf{q}_{n+1}, \mathbf{t}_{n+1}) &= \mathbf{0} \end{aligned} \quad (2)$$

where a parameter  $\alpha \in \left[-\frac{1}{3}, 0\right]$  controls the damping induced in the numerical solution. The HHT integration scheme draws on the Newmark formulas as

$$\begin{aligned} \mathbf{q}_{n+1} &= \mathbf{q}_n + h\dot{\mathbf{q}}_n + \frac{h^2}{2} [(1 - 2\beta)\mathbf{a}_n + 2\beta\mathbf{a}_{n+1}] \\ \dot{\mathbf{q}}_{n+1} &= \dot{\mathbf{q}}_n + h[(1 - \gamma)\mathbf{a}_n + \gamma\mathbf{a}_{n+1}]. \end{aligned} \quad (3)$$

where  $\gamma = \frac{1-2\alpha}{2}$ ,  $\beta = \frac{(1-\alpha)^2}{4}$  and  $h$  is an integrator step size. By design, the HHT algorithm uses a modified equation of motion to induce numerical damping. Note the notation used in Eq. (2) is meant to emphasize there is a distinction between  $\dot{\mathbf{q}}_{n+1}$  and  $\mathbf{a}_{n+1}$  (compare with Eq.(1)). Concretely,  $\mathbf{a}_{n+1}$  is an approximation of  $\ddot{\mathbf{q}}(t_n + (1 + \alpha)h)$ . In other words, the HHT algorithm solves the equations of motion at time  $\tilde{t}_{n+1} = (t_n + (1 + \alpha)h)$  to find the states of system at time  $t_{n+1}$ .

Although the generalized coordinates  $\mathbf{q}_{n+1}$  satisfy the kinematic constraint condition, the generalized accelerations  $\mathbf{a}_{n+1}$  do not satisfy Eq. (1) i.e. the original equation of motion. Moreover, the mass matrix is not constant in the case of generalized 3D motion of the rigid bodies and it depends on the generalized coordinates  $\mathbf{q}$ . Note that the mass matrix  $(\mathbf{M})_{n+1}$  is evaluated using the  $\mathbf{q}_{n+1}$ , i.e. the states of system at time  $t_{n+1}$ . Ideally the mass matrix should be evaluated using  $\mathbf{q}(t_n + (1 + \alpha)h)$  to be consistent with the equations of motion at time  $\tilde{t}_{n+1}$ . This inconsistency affects the accuracy of the solution and it is observed through the numerical experiments that though the HHT method is theoretically a second-order accurate method [2], the convergence order of this HHT algorithm is in fact one (see figure 1). It should be noted that this HHT algorithm shows the order-2 convergence only in the case of planar motions where the mass matrix is constant (e.g. see the numerical experiments in [3]) or in the case of  $\alpha = 0$ . Equation (1) is satisfied exactly with  $\alpha = 0$ ; however, in this case the

HHT method reduces to the trapezoidal method which is known in the literature to have stability problems when used with index-3 DAEs.

In order to increase the global convergence order and to obtain more accurate results for a given time step, an improved HHT algorithm based on the generalized-alpha method given in [4] is proposed here. The new HHT algorithm uses the following equation along with the constrained equation of motion given in Eq. (1) and the integration formulas given in Eq. (3),

$$\mathbf{a}_{n+1} = (1 + \alpha)\ddot{\mathbf{q}}_{n+1} - \alpha\ddot{\mathbf{q}}_n, \quad \mathbf{a}_0 = \ddot{\mathbf{q}}_0. \quad (4)$$

Here  $\mathbf{a}$  can be viewed as an auxiliary accelerations which depends on the physical acceleration  $\ddot{\mathbf{q}}$  through the recurrence relation as in Eq. (4). This algorithm satisfies the constrained equations of motion exactly and is consistent even in the case of non-constant mass matrix. The updated HHT algorithm has been implemented in Adams, and the global convergence analysis is done for a spatial slider crank model. Figure 1 shows that the updated HHT algorithm shows an order-2 convergence in agreement with the theoretical investigation in [3,4].

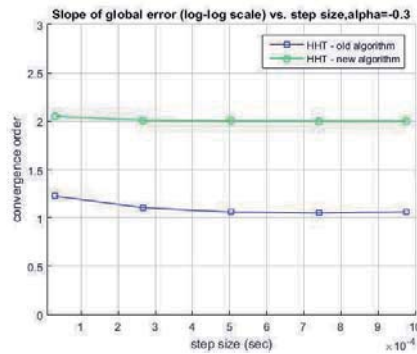


Figure 1. The convergence order of the HHT method

It has been observed that the updated HHT algorithm not only provides more accurate results (especially accelerations) but also improves the simulation speed significantly for many commercial multibody models as shown in figure 2. The details of implementation, the local error estimation, and the automatic control of integration step size will be given in the full length paper.

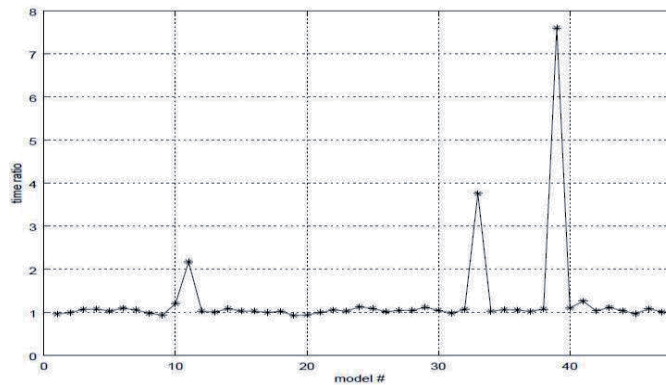


Figure 2. Simulation speed up (elapsed time ratio) with new HHT algorithm

## References

- [1] D. Negrut, R. Rampalli, G. Ottarsson, A. Sajdak. On an Implementation of the HHT Method in the Context of Index 3 Differential Algebraic Equations of Multibody Dynamics. *ASME Journal of Computational and Nonlinear Dynamics*, Vol. 2, No. 1, pp. 73-85, 2007.
- [2] L. O. Jay, D. Negrut. Extensions of the HHT-method to differential-algebraic equations in mechanics. *Electronic Transactions on Numerical Analysis*, Vol. 26, pp. 190-208, 2007
- [3] N. Khude, L. O. Jay, A. Schaffer, D. Negrut. A discussion of low order numerical integration formulas for rigid and flexible multibody dynamics. *Proceedings of the 6th ASME International Conference on Multibody Systems, Nonlinear Dynamics and Control*, Las Vegas, NV, 2007.
- [4] M. Arnold, O. Brüls. Convergence of the generalized-alpha scheme for constrained mechanical systems. *Multibody System Dynamics*, 2:185-202, 2007.

# Multibody Kinematics by Means of Dual Constraints

Ettore Pennestri<sup>1</sup>, Pier Paolo Valentini<sup>1</sup>

<sup>1</sup> Department of Enterprise Engineering  
University of Rome Tor Vergata  
via del Politecnico, 1 00133 Rome, Italy  
pennestri@mec.uniroma2.it      valentini@ing.uniroma2.it

## Abstract

The paper explores the possibility of expressing the constraints introduced by kinematic pairs by means of dual algebraic functions.

The dual vector

$$\hat{\mathbf{f}} = \vec{f} + \varepsilon \left( \vec{OP} \times \vec{f} \right) = \vec{f} + \varepsilon \vec{f}_O \quad (1)$$

represents a vector  $\vec{f}$  bound to a line containing point  $P$ . The components of  $\vec{f}$  and  $\vec{f}_O$  are the Plücker coordinates of such line vector.

## Dual vector products

Given the dual vectors  $\hat{\mathbf{a}} = \vec{a} + \varepsilon \vec{a}_O$  and  $\hat{\mathbf{b}} = \vec{b} + \varepsilon \vec{b}_O$  one can define the following products [1]:

- Vector product

$$\hat{\mathbf{a}} \times \hat{\mathbf{b}} = \hat{\mathbf{c}} = \vec{a} \times \vec{b} + \varepsilon \left( \vec{a} \times \vec{b}_O + \vec{a}_O \times \vec{b} \right) \quad (2)$$

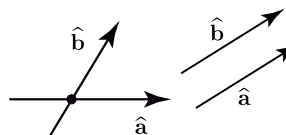
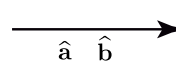
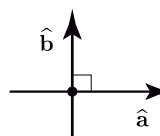
- Scalar product

$$\hat{\mathbf{a}} \cdot \hat{\mathbf{b}} = \vec{a} \cdot \vec{b} + \varepsilon \left( \vec{a} \cdot \vec{b}_O + \vec{a}_O \cdot \vec{b} \right) \quad (3)$$

- Inner product or Von Mises' scalar product

$$\hat{\mathbf{a}} \circ \hat{\mathbf{b}} = \vec{a} \cdot \vec{b}_O + \vec{a}_O \cdot \vec{b} = \mathcal{D} \left( \hat{\mathbf{a}} \cdot \hat{\mathbf{b}} \right) \quad (4)$$

Table 1: Basic constraints

Geometric condition	Algebraic condition	Vector representation
Intersection or parallelism	$\Psi_{di} \equiv \hat{\mathbf{a}} \circ \hat{\mathbf{b}} = 0$	
Alignment	$\Psi_{dv} \equiv \hat{\mathbf{a}} \times \hat{\mathbf{b}} = 0$	
Orthogonal intersection	$\Psi_{ds} \equiv \hat{\mathbf{a}} \cdot \hat{\mathbf{b}} = 0$	

As summarized in Table 1, these previously defined vector products are zero under certain geometric conditions between the line vector factors. The combination of such conditions can express the constraints introduced by the presence of kinematic pairs. In particular, Table 2 lists these combinations for the spherical, cylindrical, revolute and prismatic joints.

A dual algebraic equation is composed of two scalar equations, one for the real and the other for the dual part. As a consequence, it should be acknowledged that:

- the number of scalar constraint equations may exceed the degree of constraint of each joint;
- the system of kinematic constraints has a redundant number of equations and appropriate numerical tools are required for its solution;
- thank to its modularity, the approach herein proposed has the advantage of great algebraic compactness.

Table 2: Kinematic pairs and constraints between joint unit line vectors

Kinematic pair	Algebraic conditions	Vector representation
Spherical	$\begin{aligned}\widehat{\mathbf{x}}_{i_k} \circ \widehat{\mathbf{x}}_{j_k} &= 0 \\ \widehat{\mathbf{x}}_{i_k} \circ \widehat{\mathbf{y}}_{j_k} &= 0 \\ \widehat{\mathbf{x}}_{i_k} \circ \widehat{\mathbf{z}}_{j_k} &= 0 \\ \widehat{\mathbf{y}}_{i_k} \circ \widehat{\mathbf{x}}_{j_k} &= 0 \\ \widehat{\mathbf{y}}_{i_k} \circ \widehat{\mathbf{y}}_{j_k} &= 0 \\ \widehat{\mathbf{y}}_{i_k} \circ \widehat{\mathbf{z}}_{j_k} &= 0\end{aligned}$	
Cylindrical	$\widehat{\mathbf{z}}_{i_k} \times \widehat{\mathbf{z}}_{j_k} = 0$	
Revolute	$\begin{aligned}\widehat{\mathbf{z}}_{i_k} \times \widehat{\mathbf{z}}_{j_k} &= 0 \\ \widehat{\mathbf{x}}_{i_k} \circ \widehat{\mathbf{y}}_{j_k} &= 0 \\ \widehat{\mathbf{y}}_{i_k} \circ \widehat{\mathbf{z}}_{j_k} &= 0 \\ \widehat{\mathbf{z}}_{i_k} \circ \widehat{\mathbf{x}}_{j_k} &= 0\end{aligned}$	
Prismatic	$\begin{aligned}\widehat{\mathbf{z}}_{i_k} \times \widehat{\mathbf{z}}_{j_k} &= 0 \\ \widehat{\mathbf{x}}_{i_k} \cdot \widehat{\mathbf{x}}_{j_k} - 1 &= 0\end{aligned}$	

## References

- [1] L. Brand. *Vector Analysis*. Dover Publications Inc., 2006.

# Locally Nonlinear Strategies and Effective Preconditioners for Domain Decomposition Methods Applied to Large Flexible Multibody Systems

Eva-Maria Dewes<sup>1</sup>, Daniel J. Rixen<sup>2</sup>

<sup>1,2</sup> Institute of Applied Mechanics  
Technical University of Munich  
Boltzmannstr. 15, 85747 Garching, Germany  
{eva-maria.dewes, rixen}@tum.de

## Abstract

In structural mechanics, domain decomposition methods (DDM) have shown to be highly efficient in solving large finite element problems. Their good numerical and parallel scalability is promising also for time integration of large (flexible) multibody systems.

When applying domain decomposition methods to multibody systems, difficulties especially arise from nonlinear constraint equations which result in non-constant Jacobian matrices. This is an issue not yet tackled in domain decomposition approaches and it can result in exploding computational costs and poor convergence behaviour. Therefore, finding suitable preconditioners is crucial for the efficiency of the algorithm.

In this contribution the finite element tearing and interconnecting (FETI) method [1] is used and enhanced for application to multibody dynamics. In order to discuss different preconditioning techniques, we use a time integration scheme which is based on the generalized- $\alpha$  method [2] with an embedded FETI-method to solve the linear systems arising in every time step within the Newton iterations.

We consider mechanical systems with equations of motion represented by a system of differential-algebraic equations (DAE) in index- 3-formulation

$$\mathbf{M}(\mathbf{q})\ddot{\mathbf{q}} + \mathbf{f}(\mathbf{q}, \dot{\mathbf{q}}) + \mathbf{B}(\mathbf{q})^T \boldsymbol{\lambda} = 0 \quad (1)$$

$$\mathbf{g}(\mathbf{q}, t) = 0 \quad (2)$$

with dynamic equations (1) and kinematic constraints (2). The vector  $\mathbf{q}$  collects the generalized coordinates of the system and the vector of Lagrange multipliers  $\boldsymbol{\lambda}$  the constraint forces to enforce the nonlinear constraint equations (2).  $\mathbf{B}(\mathbf{q}) := \frac{\partial \mathbf{g}(\mathbf{q})}{\partial \mathbf{q}}$  denotes the non-constant Jacobian matrix and  $\mathbf{M}$  denotes the symmetric but not necessarily constant Mass matrix.

Discretization via generalized- $\alpha$  time integration scheme leads to the following system, where iteration indices  $n$  and  $k$  correspond to the time and Newton increments, respectively

$$\begin{bmatrix} \tilde{\mathbf{A}}_{n+1}^k & \mathbf{B}^T(\mathbf{q}_{n+1}^k) \\ \mathbf{B}(\mathbf{q}_{n+1}^k) & 0 \end{bmatrix} \begin{bmatrix} \Delta \mathbf{q}^k \\ \Delta \boldsymbol{\lambda}^k \end{bmatrix} = \begin{bmatrix} -\mathbf{r}_{\text{eq},n+1}^k \\ -\mathbf{r}_{\text{cons},n+1}^k \end{bmatrix}, \quad \tilde{\mathbf{A}}_{n+1}^k := \tilde{\boldsymbol{\beta}} \mathbf{M}_{n+1}^k + \tilde{\boldsymbol{\gamma}} \mathbf{C}_{n+1}^k + \mathbf{K}_{n+1}^k. \quad (3)$$

with scaled stepping matrix  $\tilde{\mathbf{A}}_{n+1}^k$ , tangent stiffness matrix  $\mathbf{K}_{n+1}^k$  and tangent damping matrix  $\mathbf{C}_{n+1}^k$ . For the choice of the parameters  $\tilde{\boldsymbol{\beta}}, \tilde{\boldsymbol{\gamma}}$  see [2]

In order to apply a DDM like FETI, we divide the global system (1), (2) into  $N_s$  substructures by partitioning the submatrices of system(3) as follows

$$\tilde{\mathbf{A}} := \text{diag}(\mathbf{A}^{(1)}, \dots, \mathbf{A}^{(N_s)}), \quad \mathbf{B} := (\mathbf{B}^{(1)} | \dots | \mathbf{B}^{(N_s)}) \quad (4)$$

$$\Delta \mathbf{q} := (\mathbf{q}^{(1)}, \dots, \mathbf{q}^{(N_s)})^T, \quad \mathbf{r}_{\text{eq}} := (\mathbf{r}_{\text{eq}}^{(1)}, \dots, \mathbf{r}_{\text{eq}}^{(N_s)})^T. \quad (5)$$

$$\mathbf{F}_I \Delta \boldsymbol{\lambda} = \mathbf{d} \quad \text{with} \quad \mathbf{F}_I := \tilde{\mathbf{B}} \tilde{\mathbf{A}}^{-1} \mathbf{B}^T, \quad \mathbf{d} := -\tilde{\mathbf{B}} \tilde{\mathbf{A}}^{-1} \mathbf{r}_{\text{eq}} + \mathbf{r}_{\text{cons}}. \quad (6)$$

The problem(6) is solved iteratively for the interface forces  $\Delta \boldsymbol{\lambda}$  via a preconditioned (projected) Conjugate Gradient (P(P)CG) algorithm. CG is applicable since we do not consider non-conservative forces in our model and this leads to symmetric positive definite (s.p.d.) tangent stiffness and damping matrices. This ensures a s.p.d. global iteration matrix  $\mathbf{F}_I$ , since the mass matrix is also s.p.d.. For unsymmetric problems one could use BiCGSTAB instead or transfer the results to another Krylov subspace method. In the dynamic case the global problem is non-singular due to the absence of floating subdomains and does not produce a so called natural coarse grid. However, finding good auxiliary coarse grids to ensure numerical scalability is important [3]. Furthermore, the iteration matrix  $\mathbf{F}_I$  is not constant and factorization of the local stepping matrices is time-consuming. In the case of multibody systems, when the system is partitioned bodywise, the  $\mathbf{B}$ -matrices are in general not constant due to nonlinear constraints. This makes computation of the preconditioner more costly. We thus investigate also different updating strategies to avoid full updates in every Newton step.

Define the preconditioner as proposed in [4]

$$\tilde{\mathbf{F}}_I^{-1} := \sum_{s=1}^{N_s} \tilde{\mathbf{B}}^{(s)} \tilde{\mathbf{S}}^{(s)} \tilde{\mathbf{B}}^{(s)T} \quad (7)$$

where  $\tilde{\mathbf{B}}^{(s)}$  are scaled assembly operators and  $\tilde{\mathbf{S}}^{(s)}$  local Schur complements or an approximation.

One possible choice for  $\tilde{\mathbf{B}}^{(s)}$  is [4]

$$\tilde{\mathbf{B}}^{(s)} := \underbrace{\left( \sum_{s=1}^{N_s} \mathbf{B}^{(s)} \mathbf{Q}^{(s)} \mathbf{B}^{(s)T} \right)^{-1}}_{(\mathbf{BQB}^T)^{-1}} \mathbf{B}^{(s)} \mathbf{Q}^{(s)} \quad (8)$$

where  $\mathbf{Q} = (Q_{ij})_{i,j}$  is a diagonal scaling matrix with  $Q_{ii} := \frac{1}{A_{ii}^{(s)}}$  for  $i = j$  and  $Q_{ij} = 0 \forall i \neq j$ , corresponding to the so called superlumped scaling in classical FETI. Here, the computation of  $\mathbf{BQB}^T$  can become costly for non-Boolean and non-constant  $\mathbf{B}$ -matrices. However, one can show that this is equivalent to choosing the Identity for  $\mathbf{Q}$  in the preconditioner and scaling the dynamic equations and the dynamic variables  $\Delta \mathbf{q}^k$  of the global uncondensed problem(3) via a diagonal scaling matrix  $\mathbf{W} = \left( (A_{ii}^{(s)})^{-\frac{1}{2}} \right)_{i,j:i=j}$ .

To illustrate the effect of applying different updating strategies for the FETI preconditioner a simple test model of a beam like structure is considered.

The model consists of three substructures, interconnected via nonlinear kinematic constraint equations of constant distance. Each substructure contains 24 point masses, which are connected via linear springs. The substructures are identical, except of the masses, which differ from substructure to substructure.

The following table shows selected solver statistics for different updating strategies for the lumped preconditioner with super-lumped scaling. Using no preconditioner leads to a high number of linear iterations, as expected. Updating the preconditioner in each Newton step with updated and constant  $\mathbf{B}_s$ -matrices, respectively, leads to the lowest number of iterations.

The trend already visible in this basic example needs to be further investigated using a more complex application.

Table 1: Solver statistics for different updating strategies of the preconditioner during Newton iterations

	full updated $\tilde{\mathbf{F}}_I^{-1}$	constant $\mathbf{B}_s$	constant $\mathbf{BQB}^T$	constant $\tilde{\mathbf{F}}_I^{-1}$	no Prec.
total no. of FETI iterations	16458	16400	18677	18133	33178
max. dim. of Krylov subspace	6	6	7	6	12
average dim. of Krylov subspace	5	5	6	6	11

## References

- [1] C. Farhat, F. Roux. A method of Finite Element Tearing and Interconnecting and its parallel solution algorithm. International Journal for Numerical Methods in Engineering, 32:1205-1227, 1991.
- [2] M. Arnold, O.Brüls. Convergence of the generalized- $\alpha$  scheme for constrained mechanical systems. Multi-body System Dynamics, 2:185–202, 2007.
- [3] C. Farhat, P. Chen, J. Mandel. A scalable Lagrange multiplier based domain decomposition method for time-dependent problems. International Journal for Numerical Methods in Engineering, 22:3831–3853, 1995.
- [4] D. Rixen. Extended preconditioners for the FETI method applied to constrained problems. International Journal for Numerical Methods in Engineering, 1:1–26, 2002.

## Interpolation schemes for geometrically exact beams: a motion approach

Valentin Sonneville<sup>1</sup>, Olivier Brüls<sup>2</sup> and Olivier A. Bauchau<sup>1</sup>

<sup>1</sup>Department of Aerospace Engineering  
University of Maryland  
College Park, MD, USA

<sup>2</sup>Department of Aerospace  
and Mechanical Engineering (LTAS)  
University of Liège  
Liège, Belgium

### Abstract

Many structural components of mechanical systems can be modeled accurately as flexible beams. When these components undergo finite motions, a non-linear approach is needed. The geometrically exact beam theory [1, 2] is often selected because it uses an exact kinematic description of the structure involving finite displacement and rotation fields, as expected for Cosserat solids. Because finite rotations are present, the configuration space is nonlinear and non-commutative.

The mechanical properties of the system are represented by a strain energy function that depends on sectional strain measures. Application of the fundamental principles of mechanics then yields the six nonlinear, ordinary differential equations of equilibrium. Typically, the finite element method is used to solve these nonlinear equations and because it is difficult to deal with nonlinear and non-commutative configuration spaces, numerous approaches to the problem have been proposed. The earliest researchers have used the classical interpolation tools of the finite element methods, see Simo and Vu-Quoc [3], Cardona and Geradin [4] or Ibrahimbegović [5]. While all these approaches use identical sectional strain measures to define the beam's strain energy, the numerical processes used to obtain the solution differ. Notable differences are found in the parametrization and interpolation of the rotation field.

Several issues with these early techniques have been documented in the literature. Crisfield and Jelenić [6, 7] were the first to point out that the strain measures used in the formulation should be objective, *i.e.*, should be invariant under the addition of a rigid-body motion to the configuration of the system. They showed that several commonly used discretization schemes for rotation fields do not satisfy these requirements: interpolated strain measures do not remain invariant under a superimposed rigid-body motion. Typically, the use of mesh and load step size refinements alleviate these problems. Another recurring issue of these schemes is the locking phenomenon. The requirement for the convergence of the finite element method is that the interpolated field be able to capture constant strain states accurately, see Zienkiewicz [8]. Unfortunately, when using the polynomial interpolation functions found in finite element textbooks for interpolating beam problems, it is not possible to represent constant or vanishing shear strain distributions, for instance, resulting in the well-known shear locking phenomenon. Typically, reduced integration, higher order-interpolation schemes, or both, are implemented to mitigate this problem.

The deficiencies of these schemes limit their performance and indicate that fundamental underlying concepts are not treated properly. In this work, a fresh look at beam problems is presented. The choice of an interpolation strategy is rooted in the kinematic description of the beam. In the classical approach, *e.g.* [3, 4, 9, 10, 11], the configuration space is considered as  $SO(3) \times \mathbb{R}^3$ : independent rotation,  $SO(3)$ , and displacement,  $\mathbb{R}^3$ , fields are used. In contrast, this work advocates the motion-based approach, in which the configuration space is selected as  $SE(3) = SO(3) \ltimes \mathbb{R}^3$ : the rotation and displacement fields are treated as a single, coupled entity, called a "frame field" or a "motion field." Although this motion framework is used widely in the robotic community, see, *e.g.*, Angeles [12] or Selig [13], it has been largely ignored by researchers modeling flexible structures. Such coupled approach for beams is found in the work of Borri and Bottasso [14] and Sonneville *et al.* [15]. Some researchers, *e.g.* Hodges [16] and Zupan and Saje [17] have advocated the use of the intrinsic formulation of the beam equations, which indirectly couples displacement and rotation. This approach is found to be consistent with the kinematic description of beams and handles the superposition of rigid-body modes easily, leading naturally to objective sectional strain measures.

In this work, two finite element interpolation strategies are presented and contrasted. The first interpolates the displacement and rotation fields separately, whereas the second interpolates both fields as a unit, in a manner consistent with the motion approach. The performance of the two approaches are evaluated in light of the fundamental requirements for the convergence of the finite element method: the ability to represent rigid-body motion and constant strain states. It is shown that the traditional uncoupled interpolation scheme for the position field approximates that based on the motion by neglecting the effect of the rotation field on the position field. Furthermore, it is shown that the coupling induced by the interpolation of motion yields superior convergence rates for the representation of constant strain states. This property is known to lead to finite elements that perform better, and, in particular, are less prone to the shear locking phenomenon.

## References

- [1] J.C. Simo. A finite strain beam formulation. The three-dimensional dynamic problem. Part I. *Computer Methods in Applied Mechanics and Engineering*, 49(1):55–70, 1985.
- [2] J.C. Simo and L. Vu-Quoc. On the dynamics in space of rods undergoing large motions - A geometrically exact approach. *Computer Methods in Applied Mechanics and Engineering*, 66(1):125–161, 1988.
- [3] J.C. Simo and L. Vu-Quoc. A three-dimensional finite strain rod model. Part II: Computational aspects. *Computer Methods in Applied Mechanics and Engineering*, 58(1):79–116, 1986.
- [4] A. Cardona and M. G eradin. A beam finite element non-linear theory with finite rotation. *International Journal for Numerical Methods in Engineering*, 26:2403–2438, 1988.
- [5] A. Ibrahimbegovi c. On the choice of finite rotation parameters. *Computer Methods in Applied Mechanics and Engineering*, 149:49–71, 1997.
- [6] M.A. Crisfield and G. Jeleni c. Objectivity of strain measures in the geometrically exact three-dimensional beam theory and its finite-element implementation. *Proceedings of the Royal Society, London: Mathematical, Physical and Engineering Sciences*, 455(1983):1125–1147, 1999.
- [7] G. Jeleni c and M.A. Crisfield. Geometrically exact 3D beam theory: Implementation of a strain-invariant finite element for static and dynamics. *Computer Methods in Applied Mechanics and Engineering*, 171:141–171, 1999.
- [8] O.C. Zienkiewicz, R.L. Taylor, and J.Z. Zhu. *The Finite Element Method: Its Basis and Fundamentals*. Elsevier, Butterworth Heinemann, Amsterdam, sixth edition, 2005.
- [9] A. Ibrahimbegovi c and R.L. Taylor. On the role of frame-invariance in structural mechanics models at finite rotations. *Computer Methods in Applied Mechanics and Engineering*, 191:5159–5176, 2002.
- [10] I. Romero and F. Armero. An objective finite element approximation of the kinematics of geometrically exact rods and its use in the formulation of an energy-momentum conserving scheme in dynamics. *International Journal for Numerical Methods in Engineering*, 54:1683–1716, 2002.
- [11] P. Betsch and P. Steinmann. Frame-indifferent beam element based upon the geometrically exact beam theory. *International Journal for Numerical Methods in Engineering*, 54:1775–1788, 2002.
- [12] J. Angeles. *Fundamentals of Robotic Mechanical Systems. Theory, Methods, and Algorithms*. Springer-Verlag, New York, 1997.
- [13] J.M. Selig. *Geometric Fundamentals of Robotics*. Monographs in computer science. Springer, New York, 2005.
- [14] M. Borri and C.L. Bottasso. An intrinsic beam model based on a helicoidal approximation. Part I: Formulation. *International Journal for Numerical Methods in Engineering*, 37:2267–2289, 1994.
- [15] V. Sonneville, A. Cardona, and O. Br uls. Geometrically exact beam finite element formulated on the special Euclidean group SE(3). *Computer Methods in Applied Mechanics and Engineering*, 268(1):451–474, 2014.
- [16] D.H. Hodges. A mixed variational formulation based on exact intrinsic equations for dynamics of moving beams. *International Journal of Solids and Structures*, 26(11):1253–1273, March 1990.
- [17] D. Zupan and M. Saje. Finite-element formulation of geometrically exact three-dimensional beam theories based on interpolation of strain measures. *Computer Methods in Applied Mechanics and Engineering*, 192:5209–5248, 2003.

# Computer Simulation of the Inverse Dynamics of Underactuated Mechanical Systems

Yinping Yang, Peter Betsch,

Institute of Mechanics  
 Karlsruhe Institute of Technology  
 Kaiserstraße 12, 76131 Karlsruhe, Germany  
 [yinping.yang, peter.betsch]@kit.edu

## Abstract

A new index reduction approach [1, 2] is developed for the inverse dynamics simulation of underactuated mechanical systems that have more degrees of freedom than control inputs. The formulation of this kind of inverse problems can be achieved by using servo constraints, in which the desired outputs (specified in time) are described in terms of state variables. In this case they are also called servo-constraint problems [3].

The servo-constraint problems of discrete underactuated mechanical systems are governed by differential-algebraic equations (DAEs) with high index (e.g. index 5). The servo constraints are contained in the algebraic equations of the DAEs. The numerical solution to the DAEs with high index is in general highly challenging and the flatness-based analytical solution is often not feasible for complicated underactuated multibody systems.

The newly proposed numerical method facilitates an index reduction from five to three and sometimes even to one. It makes possible the stable numerical integration of the resulting index-reduced DAEs. The new approach is also suitable to be applied to a very general and versatile formulation of cranes [2], which are classified as differentially flat systems [4]. Redundant coordinates or minimal coordinates can be applied to model the systems.

In this work we make use of redundant coordinates to formulate the mathematical model within the application of the new approach. The success and functional efficiency of the new method is demonstrated with a representative numerical example called cable suspension manipulator. A kinematically undetermined cable suspension manipulator is an underactuated mechanical system, which combines the capabilities of a crane and a robot to transport the payload from an initial position to an end position in the workspace precisely. The inverse dynamics simulation is achieved by using servo constraints. The governing equations are a set of differential-algebraic equations (DAEs) with index five.

A three-cable suspension manipulator CABLEV [5] is used to demonstrate the index reduction procedure for the trajectory tracking control problem. The model of cable suspension manipulator in Fig.1 is a differentially flat system, which has the property that all the state variables and control inputs can be algebraically expressed in terms of flat outputs and their time derivatives up to the fourth order. The solution to the trajectory tracking control problem leads to a feedforward control strategy.

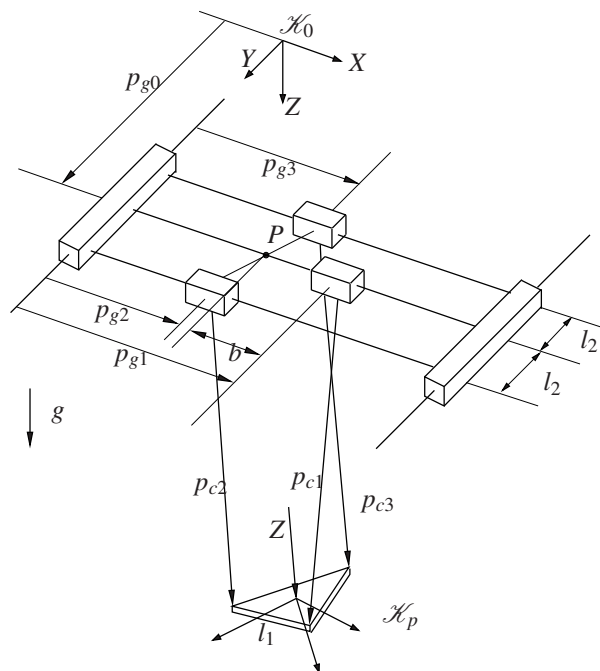


Figure 1: The three-cable suspension manipulator model (CABLEV)

## References

- [1] R. Altmann, P. Betsch and Y. Yang. Index Reduction by Minimal Extension for the Inverse Dynamics Simulation of Cranes. *Multibody System Dynamics*, 36(3):295-321, 2016.
- [2] P. Betsch, R. Altmann and Y. Yang. Numerical Integration of Underactuated Mechanical Systems Subjected to Mixed Holonomic and Servo Constraints. In J.M. Font-Llagunes, editor, *Multibody Dynamics: Computational Methods and Applications*, Series: Computational Methods in Applied Sciences, Vol. 42, 1-18, Springer Verlag, 2016.
- [3] V.I. Kirgetov. The motion of controlled mechanical systems with prescribed constraints (servoconstraints). *J. Appl. Maths. Mechs.*, 31(3):465-477, 1967.
- [4] M. Fliess, J. Lévine, P. Martin and P. Rouchon, "Flatness and defect of non-linear systems: Introductory theory and examples," *International Journal of Control*, vol. 61, no. 6, pp. 1327-1361, 1995.
- [5] T. Heyden and C. Woernle, "Dynamics and flatness-based control of a kinematically undetermined cable suspension manipulator," *Multibody System Dynamics*, vol. 16, no. 2, pp. 155-177, 2006.

# On the Proper Orthogonal Decomposition for the Reduced-Order Modelling of Geometrically Nonlinear Elastic Bodies

Olivier Brùls<sup>1</sup>, Vladimir Martinusi<sup>1</sup>, Valentin Sonneville<sup>2</sup>

<sup>1</sup> Department of Aerospace and Mechanical Engineering  
University of Liège  
Allée de la Découverte 9, 4000 Liège, Belgium  
[o.bruls,vladimir.martinusi]@ulg.ac.be

<sup>2</sup> Department of Aerospace Engineering  
University of Maryland  
College Park, MD 20742, USA  
vspsonn@umd.edu

## Abstract

This study addresses the development of model reduction methods for geometrically exact finite element models of elastic bodies. Following the formulations described in [1, 2, 3, 4], the nodal coordinates of the finite element mesh generally include finite translation and finite rotation variables. The rotation variables evolve on the special group of special orthogonal transformations  $SO(3)$ , which is a nonlinear space. Formally, the position and orientation of all the nodes of the mesh can then be collected in a matrix  $q \in G$ , where  $G$  is a matrix Lie group of dimension  $k$ . For a matrix Lie group, the composition operation is simply the matrix product. The construction of the matrix  $q$  from the set of nodal translation vectors and of nodal rotation matrices can be done in several different manners, which shall affect the nature of the composition operation [5].

In this mathematical setting, the equations of motion of the elastic body take the general form

$$\dot{q} = q\tilde{\mathbf{v}} \quad (1)$$

$$\mathbf{M}\dot{\mathbf{v}} = \mathbf{g}(q, \mathbf{v}, t) \quad (2)$$

where the first equation is a kinematic compatibility equation which defines the velocity vector  $\mathbf{v} \in \mathbb{R}^k$ , and the second equation represents the dynamic equilibrium with the mass matrix  $\mathbf{M}$  and the vector of internal, external and complementary inertia forces  $\mathbf{g}$ . This system of equations represents a differential equation on a Lie group, which can be solved using Lie group time integrators, see, e.g., [6].

In this work, model reduction methods based on the Proper Orthogonal Decomposition (POD), also known as the Karhunen-Loève decomposition or the Principal Component Analysis are investigated. These methods rely on some data about the dynamic system, which can be extracted either from simulation results of the full model or from experimental measurements. Here, the first option is considered. Then, these data should be organized in a so-called snapshot matrix, and a truncated orthogonal basis is constructed in order to capture the main variations that are present in the data. The algorithm can rely either on a singular value decomposition of the snapshot matrix or on eigenvalue analysis of the covariance matrix. The method is general and applicable to nonlinear dynamic systems evolving on a vector space. Also, it is optimal in the sense that it minimizes the average squared distance between the original signal and its reduced linear representation [7]. Then, a reduced-order model can be obtained by a projection of the dynamic system on the reduced basis.

The application of the POD method to dynamic systems evolving on a Lie group is, however, not straightforward. A first question is to construct the snapshot matrix in order to prepare the extraction of the truncated optimal basis. Each column of the snapshot matrix is a vector which should represent a configuration of the system coming from the simulation of the full model. Unfortunately, in our case, the configuration of the system is not represented by a vector but by a matrix  $q$  so that an additional step is needed to build the snapshot matrix. One possibility is to map the configuration  $q$  in the Lie algebra  $\mathfrak{g}$  of the group using the logarithm map  $\tilde{\mathbf{q}} = \log(q)$ . The Lie algebra has a linear structure so that any  $\tilde{\mathbf{q}} \in \mathfrak{g}$  can itself be represented by a vector  $\mathbf{q} = \text{vec}(\tilde{\mathbf{q}}) \in \mathbb{R}^k$ . If  $n$  snapshots  $q_1, \dots, q_n$  are available, the  $k \times n$  snapshot matrix  $\mathbf{S}$  is thus constructed as

$$\mathbf{S} = [\text{vec}(\log(q_1)), \dots, \text{vec}(\log(q_n))] \quad (3)$$

A second possibility is to define the snapshot matrix from  $n$  velocity vectors as

$$\mathbf{S}_{\text{vel}} = [\mathbf{v}_1, \dots, \mathbf{v}_n] \quad (4)$$

A third possibility is to combine the position and velocity snapshots in a single  $2k \times n$  snapshot matrix. An optimal and truncated basis can then be found using the standard POD procedure. The reduced basis shall be represented by a rectangular  $k \times l$  matrix  $\Psi$  with  $l < k$ .

A second question is related with the definition of the projection operator on the Lie group based on the matrix  $\Psi$ . For example, if the snapshots are constructed using Eq. (3), the projection can be based on the nonlinear formula

$$q = \exp(\widehat{\Psi\boldsymbol{\eta}}) \quad (5)$$

where  $\boldsymbol{\eta} \in \mathbb{R}^l$  is the vector of reduced coordinates. This formula is interpreted as a projection defined in the Lie algebra. As the exponential map is not injective, several values of  $\boldsymbol{\eta}$  can represent the same configuration  $q$ .

Therefore, the validity of this approach is restricted to regions of the configuration space and of the Lie algebra in which the exponential map is injective. A time derivation of the nonlinear formula (5) leads to a projection formula for the velocity, which turns out to be nonlinear in the general case. The equations of motion then take the form of a second-order differential equation in terms of the reduced coordinates  $\boldsymbol{\eta}$ .

In general, the reduced equations of motion resulting from this projection do not share the same Lie group structure as the initial equations of motion. However, it is possible to preserve the Lie group structure of the initial problem if some additional requirements are imposed on the choice of the subspace  $\boldsymbol{\Psi}$ . Indeed, if this subspace is actually a subalgebra of  $\mathfrak{g}$ , then the reduced-order model can be represented on a Lie subgroup, and thus inherits the Lie group structure of the initial problem, which appears as a substantial advantage. This additional requirement can be formulated as an involutivity condition for the columns of the matrix  $\boldsymbol{\Psi}$ .

A numerical study based on an highly elastic beam with large 3D motion is developed to illustrate the theoretical concepts. The influence of the choice of the initial Lie group structure, of the definition of the snapshot matrix and of the projection scheme are investigated numerically.

### Acknowledgments

This work was carried out within the EI-OPT project funded by the Walloon Region in Belgium (grant 7173), which is gratefully acknowledged.

### References

- [1] M. Géradin and A. Cardona. Flexible Multibody Dynamics: A Finite Element Approach. John Wiley & Sons, Chichester, 2001.
- [2] O.A. Bauchau. Flexible multibody dynamics. Springer, Dordrecht, 2011.
- [3] V. Sonneville, A. Cardona, and O. Brüls. Geometrically exact beam finite element formulated on the special Euclidean group SE(3). *Computer Methods in Applied Mechanics and Engineering*, 268:451–474, 2014.
- [4] V. Sonneville and O. Brüls. A formulation on the special Euclidean group for dynamic analysis of multibody systems. *ASME Journal of Computational and Nonlinear Dynamics*, 9:041002, 2014.
- [5] O. Brüls, M. Arnold, and A. Cardona. Two Lie group formulations for dynamic multibody systems with large rotations. In *Proceedings of the IDETC/MSNDC Conference, Washington D.C., U.S., August 2011*.
- [6] O. Brüls, A. Cardona, and M. Arnold. Lie group generalized- $\alpha$  time integration of constrained flexible multibody systems. *Mechanism and Machine Theory*, 48:121–137, 2012.
- [7] G. Kerschen, J.-C. Golinval, A.F. Vakakis, and L.A. Bergman. The method of proper orthogonal decomposition for dynamical characterization and order reduction of mechanical systems: An overview. *Nonlinear Dynamics*, 41(1-3):147–169, 2005.

# Velocity-Based Three-Dimensional Beam Using the Energy Preserving Approach

Eva Zupan, Dejan Zupan

University of Ljubljana  
Faculty of Civil and Geodetic Engineering  
Jamova 2, SI-1000, Ljubljana, Slovenia  
dejan.zupan@fgg.uni-lj.si

## Abstract

In numerical formulations of three-dimensional beams the choice of primary interpolated variables is highly important for the efficiency and accuracy of the method. Many numerical problems reported in literature are directly related to the properties of configuration space of the beam which incorporates three-dimensional rotations. From the perspective of total mechanical energy the spatial and temporal derivatives of configuration variables are more natural quantities. Additionally, when expressed with respect to the moving bases, the measures for the rate of change of rotations become additive. Despite these strong advantages they are rarely chosen to be the primary interpolated unknowns. This was the motivation for the strain-based beam formulation for static analysis [1] and the velocity-based beam formulation for dynamic analysis of three-dimensional beams [2]. The crucial idea exploited in our approaches is to employ velocities in fixed frame description and angular velocities in moving frame description as the primary unknowns. For such models standard additive interpolation is fully consistent with the configuration space. We further employ the algebra of quaternions as a suitable tool to express the governing equations and relate rotations with their derivatives. The initial investigations were performed without any additional measures taken to stabilize the calculations. Despite that, numerical investigations provided very promising results [2].

Unfortunately, a proper adaptation of time integration method to configuration space with three-dimensional rotations might still result in a loss of numerical stability even for conservative problems [3]. As the answer to this phenomenon several energy preserving and energy decaying algorithms were proposed, e.g., [3], [4], [5], [6], [7], [8], [9]. It is interesting to investigate the velocity-based beam elements in the framework of energy conserving algorithms. For this purpose we slightly modify the continuous balance equations of a Cosserat rod in quaternion notation:

$$\mathbf{n}' + \tilde{\mathbf{n}} - \frac{d}{dt}(\rho A \mathbf{v}) = \mathbf{0} \quad (1)$$

$$\mathbf{m}' + \mathbf{r}' \times \mathbf{n} + \tilde{\mathbf{m}} - \frac{d}{dt}(\hat{\mathbf{q}} \circ (\mathbf{J}_\rho \boldsymbol{\Omega}) \circ \hat{\mathbf{q}}^*) = \hat{\mathbf{0}}, \quad (2)$$

where  $\mathbf{v}$  and  $\boldsymbol{\Omega}$  are linear and angular velocity,  $\mathbf{r}$  is the position vector of the centroidal axis,  $\mathbf{n}$  and  $\mathbf{m}$  represent stress-resultant force and moment vectors of the cross-section with respect to the fixed basis;  $\rho$  is mass per unit of the initial volume;  $A$  is the area of the cross-section;  $\mathbf{J}_\rho$  is the centroidal mass-inertia matrix of the cross-section;  $\tilde{\mathbf{n}}$  and  $\tilde{\mathbf{m}}$  are vectors of applied distributed force and moment and  $\mathbf{q}$  is rotational quaternion.

The initial step in the time discretization follows directly from the mean value theorem:

$$\rho A \mathbf{v}^{[n+1]} - \rho A \mathbf{v}^{[n]} = h \left( \tilde{\mathbf{n}}' + \tilde{\mathbf{n}}^{[n+\alpha]} \right) \quad (3)$$

$$\mathbf{J}_\rho \boldsymbol{\Omega}^{[n+1]} - \mathbf{J}_\rho \boldsymbol{\Omega}^{[n]} = h \hat{\mathbf{q}}^{[n+\alpha]} \circ \left( \tilde{\mathbf{m}}' + \mathbf{r}^{[n+\alpha]} \times \tilde{\mathbf{n}} + \tilde{\mathbf{m}}^{[n+\alpha]} \right) \circ \hat{\mathbf{q}}^{*[n+\alpha]} - h \boldsymbol{\Omega}^{[n+\alpha]} \times \mathbf{J}_\rho \boldsymbol{\Omega}^{[n+\alpha]}, \quad (4)$$

where superscripts  $(\cdot)^{[n]}$  and  $(\cdot)^{[n+1]}$  are used to denote the values at two successive times  $t_n$  and  $(\cdot)^{[n]}$ , while  $h = t_{n+1} - t_n$  is the time step.  $(\cdot)^{[n+\alpha]}$  denotes the intermediate time, usually chosen to be  $\alpha = \frac{1}{2}$ . The newly introduced quantities  $\tilde{\mathbf{n}}$  and  $\tilde{\mathbf{m}}$  represent suitable approximations of stress resultants based on energy conservation constraint.

We will base the spatial discretization on incremental values of velocities and angular velocities  $\bar{\mathbf{v}}$  and  $\bar{\boldsymbol{\Omega}}$  representing the continuous update of the configuration. Using standard interpolation functions  $I_p(x)$  we have

$$\bar{\mathbf{v}}(x) = \sum_{p=1}^N I_p(x) \bar{\mathbf{v}}^p, \quad \bar{\boldsymbol{\Omega}}(x) = \sum_{p=1}^N I_p(x) \bar{\boldsymbol{\Omega}}^p. \quad (5)$$

Equations (3) and (4) are multiplied by the same test functions  $I_p(x)$  and integrated along the length of the

beam. After some terms are integrated by parts and the boundary conditions are considered, we have:

$$\int_0^L \left[ \rho A \mathbf{v}^{[n+1]} I_p - \rho A \mathbf{v}^{[n]} I_p + h \bar{\mathbf{n}} I_p' - h \tilde{\mathbf{n}}^{[n+\alpha]} I_p \right] dx - h \delta_p \mathbf{f} = \mathbf{0} \quad (6)$$

$$\int_0^L \left[ \mathbf{J}_p \boldsymbol{\Omega}^{[n+1]} I_p - \mathbf{J}_p \boldsymbol{\Omega}^{[n]} I_p + h \bar{\mathbf{M}} I_p' - h \mathbf{K}^{[n+\alpha]} \times \bar{\mathbf{M}} I_p - h \hat{\mathbf{q}}^{[n+\alpha]} \circ \left( \mathbf{r}'^{[n+\alpha]} \times \bar{\mathbf{n}} - \tilde{\mathbf{m}}^{[n+\alpha]} \right) \circ \hat{\mathbf{q}}^{*[n+\alpha]} I_p - h \boldsymbol{\Omega}^{[n+\alpha]} \times \mathbf{J}_p \boldsymbol{\Omega}^{[n+\alpha]} I_p \right] dx - h \delta_p \mathbf{H} = \mathbf{0} \quad (7)$$

where  $\bar{\mathbf{M}} = \hat{\mathbf{q}}^{*[n+\alpha]} \circ \bar{\mathbf{m}} \circ \hat{\mathbf{q}}^{[n+\alpha]}$  was introduced to describe the internal moment in local basis,  $\mathbf{K}^{[n+\alpha]}$  is the rotational strain, while  $\delta_p \mathbf{f}$  and  $\delta_p \mathbf{H}$  denote point forces and moments at the two boundaries.

After the kinematic compatibility equations for translational and rotational strain,  $\boldsymbol{\Gamma}$  and  $\mathbf{K}$ , are discretized in a similar manner, we have

$$\boldsymbol{\Gamma}^{[n+1]} - \boldsymbol{\Gamma}^{[n]} = h \left[ \hat{\mathbf{q}}^{*[n+\alpha]} \circ \mathbf{v}'^{[n+\alpha]} \circ \hat{\mathbf{q}}^{[n+\alpha]} + \left( \hat{\mathbf{q}}^{*[n+\alpha]} \circ \mathbf{r}'^{[n+\alpha]} \circ \hat{\mathbf{q}}^{[n+\alpha]} \right) \times \boldsymbol{\Omega}^{[n+\alpha]} \right] \quad (8)$$

$$\mathbf{K}^{[n+1]} - \mathbf{K}^{[n]} = h \left[ \boldsymbol{\Omega}'^{[n+\alpha]} - \boldsymbol{\Omega}^{[n+\alpha]} \times \mathbf{K}^{[n+\alpha]} \right], \quad (9)$$

which gives the update formulae for strains.

Considering the above results in the expression for the increment of the total mechanical energy between the two successive time steps leads to approximations for  $\bar{\mathbf{n}}$  and  $\bar{\mathbf{M}}$  that guarantee the algorithmic energy preservation under conservative load. We can conclude that the advantages of the velocity-based approach and the long-term stability based on energy conservation are successfully combined in the present approach.

## References

- [1] Dejan Zupan and Miran Saje. Finite-element formulation of geometrically exact three-dimensional beam theories based on interpolation of strain measures. *Computer Methods in Applied Mechanics and Engineering*, 192(49-50):5209–5248, 2003.
- [2] E. Zupan and D. Zupan. Velocity-based approach in non-linear dynamics of three-dimensional beams with enforced kinematic compatibility. *Computer Methods in Applied Mechanics and Engineering*, 310:406–428, 2016.
- [3] J. C. Simo, N. Tarnow, and M. Doblare. Nonlinear dynamics of 3-dimensional rods - exact energy and momentum conserving algorithms. *International Journal for Numerical Methods in Engineering*, 38(9):1431–1473, 1995.
- [4] O. A. Bauchau and N. J. Theron. Energy decaying scheme for non-linear beam models. *Computer Methods in Applied Mechanics and Engineering*, 134(1-2):37–56, 1996.
- [5] C. L. Bottasso and M. Borri. Energy preserving/decaying schemes for non-linear beam dynamics using the helicoidal approximation. *Computer Methods in Applied Mechanics and Engineering*, 143(3-4):393–415, 1997.
- [6] A. Ibrahimbegovic and S. Mamouri. Energy conserving/decaying implicit time-stepping scheme for nonlinear dynamics of three-dimensional beams undergoing finite rotations. *Computer Methods in Applied Mechanics and Engineering*, 191(37-38):4241–4258, 2002.
- [7] EV Lens, A Cardona, and M Geradin. Energy preserving time integration for constrained multibody systems. *Multibody System Dynamics*, 11(1):41–61, 2004.
- [8] I. Romero and F. Armero. An objective finite element approximation of the kinematics of geometrically exact rods and its use in the formulation of an energy-momentum conserving scheme in dynamics. *International Journal for Numerical Methods in Engineering*, 54(12):1683–1716, 2002.
- [9] Carlo Sansour, Tien Long Nguyen, and Mohammed Hjjaj. An energy-momentum method for in-plane geometrically exact Euler-Bernoulli beam dynamics. *International Journal for Numerical Methods in Engineering*, 102(2):99–134, 2015.

# Nullspace Method for the Analysis of Uniqueness of Reactions and Driving Forces in Redundantly Constrained Multibody Systems

Marcin Pełal, Janusz Frączek, Marek Wojtyra

Institute of Aeronautics and Applied Mechanics  
Warsaw University of Technology  
Nowowiejska 24, 00-665 Warsaw, Poland  
[mpekal, jfraczek, mwojtyra]@meil.pw.edu.pl

## Abstract

Redundantly constrained rigid multibody systems (MBS) are problematic in modelling. The difficulties occurring therein may be divided into two main groups: numerical problems and problems with the uniqueness of reactions. The first kind of problems may be reduced by using special algorithms devoted to such mechanisms and is not addressed in this paper. The second kind of problems is a direct consequence of the geometric structure of the considered overconstrained MBS [1, 2] and is observed regardless of the method adopted to handle the redundant constraints [3]. Similar issues are observed in overactuated systems, since overactuation may be treated as a special case of redundant constraints. For overconstrained mechanisms, reaction forces are indeterminate in general. However, some of the reactions (or reaction components) may be unique. Note that this phenomenon is very important in the simulation of MBS because it may cause ambiguous (arbitrary) results, e.g. when friction is present in joints with non-unique reactions [4]). Hence, for such analyzes, it should be known in advance which reactions are unique and which are not. In the case of complex MBS, it is not always easy to tell which reactions are unique. Thus, appropriate numerical methods for uniqueness tests seem to be necessary, especially for the use in large-scale multibody simulation packages. Note that the methods for dealing with the uniqueness problem are still under investigation and development.

In the papers studying joint reactions in overconstrained MBS, two different methods of redundancy analysis are exploited: one based on the constraint Jacobian matrix (described in, e.g. [1, 2, 4, 5]) and the other – quite novel – kinetostatics-based method (see, e.g. [6]). Moreover, redundant actuation is seldom investigated in the context of MBS modelling. This paper focuses on two issues. Firstly, a novel, nullspace-based approach to analysis of the constraint Jacobian matrix is proposed and analyzed. Secondly, it is shown that actuation redundancy, modelled in terms of redundant driving constraints, may affect uniqueness of reactions in joints without actuation.

The constraint Jacobian-based uniqueness analysis method was previously discussed, e.g. in [1, 2, 4, 5]. In paper [1] it was shown that some reactions in overconstrained rigid MBS (which have indeterminate reactions in general) may be unique; the conditions for reactions' uniqueness were introduced and proven. Three numerical methods, based on the concept of direct sum, were proposed to analyze the constraint Jacobian matrix, namely: rank comparison method, QR-based method and SVD-based method. In article [4] similar methods of constraint Jacobian analysis were employed to study the uniqueness of simulated motion in the presence of joint friction. It was shown that reactions non-uniqueness may affect the results of simulation of motion. The methods based on direct sum concept were subsequently utilized to investigate MBS with flexible bodies [5].

The nullspace method is an alternative to the direct sum-based methods. In paper [2] the nullspace method for reaction uniqueness analysis was used and the weighted minimum norm condition for the practical solution of non-unique reactions was formulated. Until now, the nullspace-based method allowed us to determine the uniqueness of the individual reaction components only. In the present paper we extend this approach to other, more general cases, e.g. to analysis of uniqueness of total joint reactions.

Let us discuss the nullspace method for Jacobian-based reaction uniqueness analysis. In order to perform the uniqueness test, the considered MBS must be described by coordinates for which Jacobian matrix includes information about all joints simultaneously, i.e. absolute or natural coordinates. For such system, a vector of generalized constraint reactions may be written in the following form

$$\mathbf{W} = \Phi_{\mathbf{q}}^T \boldsymbol{\lambda} = \mathbf{J}\boldsymbol{\lambda}, \quad (1)$$

where  $\Phi_{\mathbf{q}}$  is the Jacobian matrix of constraints (which transposition is denoted  $\mathbf{J}$ ) and  $\boldsymbol{\lambda}$  is the vector of Lagrange multipliers.

As mentioned before, in the case of redundant MBS, reactions are non-unique in general. However, some of them may be unique despite the global indeterminacy. One of the method allowing to check which reactions are determined is the nullspace method. In the previous papers, e.g. [2] or [7, p. 58], it was stated, that Lagrange multipliers lying in the nullspace of transposed Jacobian matrix  $\mathbf{J}$  are indeterminate, i.e. reaction components corresponding to these multipliers are non-unique. However, we are often interested in the total joint reaction (e.g. for proper dimensioning of the part). The information about the uniqueness of individual reaction components may be insufficient, because the total joint reaction may be unique, despite having non-unique components. This situation may be observed, e.g. in the case of a planar mechanism showed in Figure 1 (if we are interested in the

total reaction in doubled translational joint, rather than in separate reactions acting in each of the two co-linear translational joints). Hence, it is necessary to formulate appropriate criterion which takes this case into account.

In this paper it is proven that a reaction (regardless of whether it is a single reaction component, a set of components, a total joint reaction or a set of joint reactions) is unique if it is orthogonal to the nullspace of transposed Jacobian matrix  $\mathbf{J}$ . This theorem leads to the following orthogonality condition

$$\mathbf{J}_U \mathbf{N}_U = \mathbf{0}, \quad (2)$$

where  $\mathbf{J}_U$  is a submatrix of the transposed Jacobian matrix  $\mathbf{J}$ , created from these columns of  $\mathbf{J}$  that correspond to the reaction which uniqueness is studied;  $\mathbf{N}_U$  is a submatrix of the nullspace matrix  $\mathbf{N}$  (which contains the basis vectors of the nullspace of transposed Jacobian matrix  $\mathbf{J}$ ). Moreover,  $\mathbf{N}_U$  is build analogously to submatrix  $\mathbf{J}_U$ , but from the rows of matrix  $\mathbf{N}$  corresponding to the considered reaction.

In the next part of the paper the developed methods are extended to the case of redundantly actuated mechanisms. The study is based on expressing the actuation in terms of driving constraints. The derivatives of additional constraints are incorporated into the transposed Jacobian matrix  $\mathbf{J}$  (obviously, some additional Lagrange multipliers correspond to them). For such description, the uniqueness of driving forces may be analyzed just as the uniqueness of reactions. We show that the uniqueness of reactions should be studied together with the uniqueness of driving forces. It is vastly important to acknowledge the overactuation, since the redundancy of driving constraints may affect the uniqueness of joint reactions (in both actuated and not actuated joints).

To illustrate the issues discussed in this paper, a planar mechanism (presented in Figure 1) is investigated. This system has 1 degree of freedom and consists of 4 rigid bodies connected by 7 joints (5 translational and 2 revolute joints). Observe that the left-hand side translational joint is doubled. Various variants of joint actuation are considered, including redundant actuation. Note that overactuation increases the total number of redundant constraints. Hence, the system is characterized by at least 3 redundant constraints. The constraint Jacobian-based nullspace method is used to analyze the uniqueness of joint reactions and driving forces.

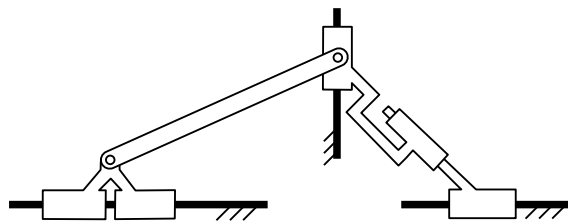


Figure 1: Planar mechanism

## Acknowledgments

This work has been supported by the National Science Centre of Poland under grant no. DEC-2012/07/B/ST8/03993.

## References

- [1] M. Wojtyra. Joint reactions in rigid body mechanisms with dependent constraints. *Mechanism and Machine Theory*, 44(12):2265–2278, 2009.
- [2] J. García de Jalón and M. D. Gutiérrez-López. Multibody dynamics with redundant constraints and singular mass matrix: existence, uniqueness, and determination of solutions for accelerations and constraint forces. *Multibody System Dynamics*, 30(3):311–341, 2013.
- [3] M. Wojtyra and J. Fraćzek. Comparison of Selected Methods of Handling Redundant Constraints in Multibody Systems Simulations. *Journal of Computational and Nonlinear Dynamics*, 8(2):021007 (1–9), 2013.
- [4] J. Fraćzek and M. Wojtyra. On the unique solvability of a direct dynamics problem for mechanisms with redundant constraints and Coulomb friction in joints. *Mechanism and Machine Theory*, 46(3):312–334, 2011.
- [5] M. Wojtyra and J. Fraćzek. Joint reactions in rigid or flexible body mechanisms with redundant constraints. *Bulletin of the Polish Academy of Sciences Technical Sciences*, 60(3):617–626, 2012.
- [6] M. Pękal, J. Fraćzek, and P. Tomulik. Solvability of reactions and inverse dynamics problem for complex kinematic chains. In *The 21st International Conference on Methods and Models in Automation and Robotics (MMAR 2016)*. Międzyzdroje, Poland, August 29–September 1 2016.
- [7] R. Featherstone and D. E. Orin. Dynamics. In B. Siciliano and O. Khatib, editors, *Springer Handbook of Robotics*. Springer-Verlag Berlin Heidelberg, 2008.

# Experimental Investigation and Numerical Modeling of Resultant-based Bending Plasticity in Cables

Vanessa Dörlich<sup>1,2</sup>, Peter Češarek<sup>3</sup>, Joachim Linn<sup>1</sup>, Stefan Diebels<sup>2</sup>

<sup>1</sup> Department Mathematical Methods in Dynamics and Durability  
 Fraunhofer Institute for Industrial Mathematics ITWM  
 Fraunhofer Platz 1, D-67663 Kaiserslautern, Germany  
 [vanessa.doerlich, joachim.linn]@itwm.fraunhofer.de

<sup>2</sup> Chair of Applied Mechanics  
 Saarland University  
 Campus A4 2, D-66123 Saarbrücken, Germany  
 s.diebels@mx.uni-saarland.de

<sup>3</sup> Faculty of Civil and Geodetic Engineering  
 University of Ljubljana  
 Jamova 2, SI-1115 Ljubljana, Slovenia  
 Peter.Cesarek@fgg.uni-lj.si

## Abstract

Flexible, slender structures like cables can be described by the Cosserat rod theory [1]. It yields models with geometrically exact kinematics, balance equations that govern the equilibrium of the sectional forces and moments and constitutive equations, which describe the relations between objective deformation measures and the sectional quantities. This contribution focuses on the constitutive modeling for cables displaying plastic deformation effects in bending from two different points of view: experiments and finite element modeling.

Cables typically consist of at least two layers and different kinds of materials, depending on the application. This complex multi-layer structure causes inelastic behavior, when the cable is under load. Friction, damage or delamination between the layers can occur. Furthermore, different material behavior has to be expected, because the constituents consist of a variety of materials, e.g. plastic metallic wires, hyper-elastic rubber jackets or visco-plastic insulators. The different structural and material effects can hardly be separated in experiments. Consequently, an approach in the framework of continuum mechanics is used in this work, where the inelastic effects are investigated on the macroscopic scale and modeled phenomenologically with suitable constitutive models formulated in the sectional quantities.

Three deformation modes and their combinations are relevant for flexible beam-like structures such as cables: tension, torsion and bending. It is state of the art to derive the corresponding elastic stiffnesses in uniaxial tensile tests, torsion tests and three-point bending. In [2, 3] it was already shown that plastic behavior can be observed, if these classic experiments are executed cyclically. Our first approach to model plasticity for cables based on sectional quantities covers bending, because this deformation case is the most relevant for applications of cables. In three-point bending tests, the specimen is supported symmetrically on both ends and loaded in the middle with a point load (Figure 1, left). The resulting kinematics yield a deformation state, where the bending moment and curvature are increasing linearly from the supports to the middle of the specimen. With this experimental setup, it is not possible to directly measure the constitutive law for the bending moment as a function of the curvature. Therefore, a new experimental device was designed which enables pure bending of cables, i.e. direct measurement of the bending moment as a function of bending curvature (Figure 1, right).

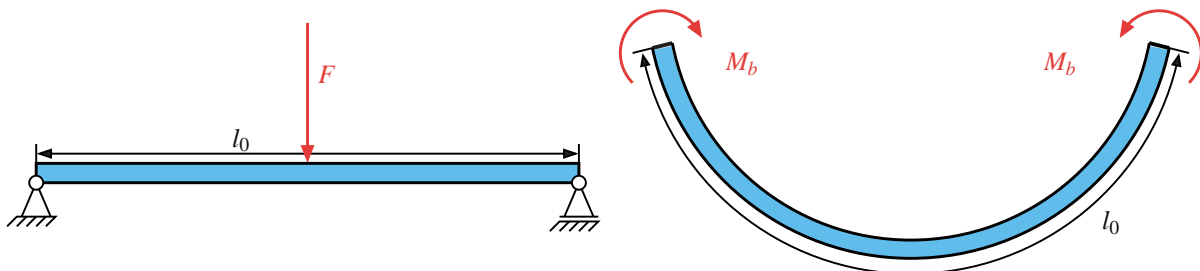


Figure 1: Schematic illustration of boundary conditions in three-point bending (left) and pure bending tests (right).

A two node geometrically exact beam element, which employs incremental displacements and rotations as primary variables, is derived for computational experiments. Following the concept presented in [4], the governing equations of the beam are developed from the generalized virtual work principle taking strains as independent variables. This leads to a mixed formulation with strains and internal forces as primary variables.

The main focus is on constitutive modeling, since plastic behavior with (strain) hardening can be observed in the force-displacement diagrams from three-point bending experiments. A rate-independent plasticity model with (isotropic) hardening [5] based on sectional quantities is formulated to include these effects of material nonlinearity.

The main ingredients of the model are: (i) the additive decomposition of the total strain into an elastic and a plastic part, (ii) a set of equations describing elastic (reversible) behavior, (iii) a yield curve in the bending moment plane and (iv) an associated flow rule and hardening law. For the associated flow rule, the direction of the plastic strain is assumed to be normal to the yield curve and its magnitude is given by the plastic multiplier, which is determined from the consistency condition that plastic flow remains on the yield surface. Loading and unloading are characterized by the Kuhn–Tucker complementarity conditions.

The plastic part of beam strains consists only of curvatures  $K_1^{pl}$  and  $K_2^{pl}$ , since the remaining deformation modes are assumed to stay elastic. Under this assumption, the yield function can be written as

$$f(M_1, M_2, \alpha) = (M_1^2 + M_2^2)^{\frac{1}{2}} - (M_0 + \alpha HI), \quad (1)$$

where  $M_0$  is the yield moment and  $HI$  the (constant) hardening bending stiffness. The internal hardening variable, i.e. accumulated plastic strain, is denoted by  $\alpha$ . For the resulting constitutive model, it is necessary to determine the elastic parameters (axial stiffness  $EA$ , torsional stiffness  $GJ$  and bending stiffnesses  $EI_1, EI_2$ ) and the plastic parameters (yield moment  $M_0$  and hardening bending stiffness  $HI$ ) of the cable.

In a first approach, three-point bending of a simple cable consisting of a core of metallic wires and a rubber jacket is modeled. While the elastic parameters can be estimated from the corresponding experiments, it is not possible to determine the plastic properties directly from three-point bending. Therefore, the plastic bending parameters are obtained from an optimization problem wherein the results of the beam model of the three-point bending test are fitted to the experimental data. The results of the least squares optimization, solved with algorithms for constrained optimization provided in Matlab, are presented in Figure 2.

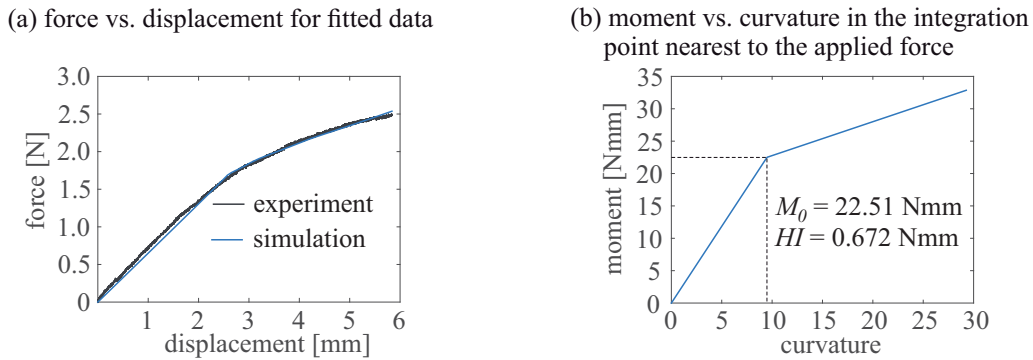


Figure 2: Three point bending: results of the optimization.

## References

- [1] J. C. Simo. A finite strain beam formulation: the three dimensional dynamic problem - Part I. *Computer Methods in Applied Mechanics and Engineering*, 49:55-70, 1985.
- [2] V. Dörlich, J. Linn, T. Scheffer, S. Diebels. Towards Viscoplastic Constitutive Models for Cosserat Rods. *Archive of Mechanical Engineering*, 63:215-230, 2016.
- [3] V. Dörlich, S. Diebels, J. Linn. Investigation of elastoplastic effects of cables under large spatial deformation. *Proceedings in Applied Mathematics and Mechanics*, 15:185-186, 2015.
- [4] P. Češarek, D. Zupan, J. Linn. Conceptual and numerical aspects of the mixed variational formulation of geometrically exact beam models. In J.M. Font-Llagunes, editor, *Proceedings of the ECCOMAS Thematic Conference on Multibody Dynamics 2015*, pages 66-76. Universitat Politècnica de Catalunya Barcelona, 2015.
- [5] J. C. Simo, T. J. R. Hughes. *Computational Inelasticity*. Springer, New York, 1998.

# Application of a DAE Approach to Nonlinear Sloshing Problems

Kensuke Hara

Department of Mechanical Engineering, School of Engineering,  
Tokyo Institute of Technology  
2-12-1 Ookayama, Meguro-ward, 152-8552, Tokyo, Japan  
hara@mech.titech.ac.jp

## Abstract

Liquid surface behavior in a partially filled liquid container (sloshing) is an important engineering problem for such applications as designs of liquid storage tanks, liquid cargo transportations, tuned liquid dampers (TLDs) and so on. The liquid in partially filled tanks tends to create a large liquid movement if the tank is subjected to the excitation with frequency components being close to the natural frequency of the sloshing. Therefore, many methods focusing on the nonlinearity have been developed. One of notable studies for the nonlinear sloshing has been developed by Faltinsen and his colleagues. In a series of their papers, multidimensional modal approaches have been presented for the nonlinear sloshing with irrotational inviscid flows in a tank having a rigid wall (e.g. [1]). On the other hand, numerical approaches have also been applied to this problem. There are typical methods with mesh discretization: the finite element method (FEM), the finite difference method (FDM) and the boundary element method (BEM). These numerical approaches are available for fully nonlinear problems. Moreover, incorporating the mesh discretization techniques into the numerical approaches has enabled us to analyze further applications. The methods based on the multibody dynamics (MBD) approach are effective in describing interaction between sloshing and structures. For example, in the case of TLD, which is used for suppressing the vibration of tall buildings, a lot of containers filled with liquid partially are installed in the building at the same time for improving its performance. Thus, it can be expected that MBD approaches are beneficial for describing the whole system. Moreover, liquid motion in the container is originally expressed as a constrained system since the free surface boundary conditions for a liquid domain lead to constraints. Once the system is formulated by the DAEs, methods based on the MBD are available. In addition, it could facilitate the extension of theory for the sloshing and structure interaction problem.

In this paper, we try to introduce a differential algebraic equation (DAE) approach to formulate the nonlinear sloshing problem. The present theory is based on the analytical dynamics framework such as Lagrangian mechanics and Hamiltonian mechanics. The resulting equations take the form of DAEs due to existence of algebraic equations given as a continuity equation and boundary conditions. Then, direct numerical integration technique known as the energy–momentum method[2, 3] is employed for calculating the derived DAEs. The proposed approach is validated by comparing with an existing model and an experiment in the time domain analysis.

We consider a two-dimensional nonlinear sloshing problem shown in Fig. 1. The quantities in the fluid domain are described by using the tank-attached Cartesian coordinate system ( $o-xy$ ). An assumption of inviscid irrotational flow is introduced for liquid. The tank has vertical side walls and a flat bottom, which can be regarded as rigid walls. The tank is subjected to external excitation in a horizontal direction.

According to the variational principle in continuum mechanics, the Lagrangian density of fluid is equivalent to pressure  $P(x, y, t)$ [4], that is,

$$L = \iiint_V P(x, y, t) dx dy dz, \quad (1)$$

where  $V$  is the volume of fluid. As a first step, this study considers the inviscid and irrotational flow. Therefore, the velocity potential  $\Phi = \Phi(x, y, t)$  can be introduced. It yields a following expression for the pressure  $P(x, y, t)$

$$P = -\rho \left\{ \frac{\partial \Phi}{\partial t} + \frac{1}{2} \nabla \Phi \cdot \nabla \Phi + \frac{1}{2} gy + x \ddot{x}(t) \right\}, \quad (2)$$

where  $\rho$  is the fluid density. The operator  $\nabla$  is defined by  $\nabla = (\partial/\partial x, \partial/\partial y)^T$ . Substituting Eq. (2) to Eq. (1), then applying integration by parts to Eq. (1), the Lagrangian of fluid is rewritten by

$$L = \rho \iint_S \Phi|_{y=\eta} \frac{\partial \eta}{\partial t} dx dy - T - U, \quad (3)$$

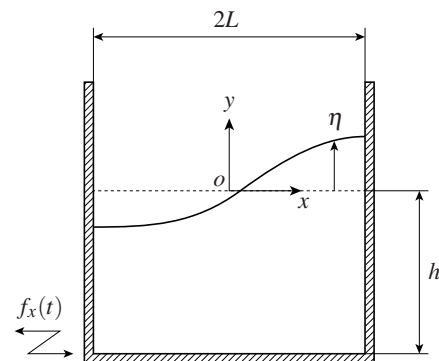


Figure 1: Analytical model for liquid in partially filled in a two-dimensional tank.

where functionals  $T$  and  $U$  denote kinetic and potential energies defined by

$$T = \rho \iiint_V \frac{1}{2} \nabla \Phi \cdot \nabla \Phi \, dx \, dy \, dz, \quad U = \rho \iiint_V (gy + x \dot{f}_x) \, dx \, dy \, dz.$$

One way to derive a set of equations of motion is to introduce the Euler-Lagrange equation (or Hamilton's principle). It gives a kinematic condition and an equilibrium of the pressure on the liquid surface as the boundary conditions, which govern time evolution for the velocity potential and the liquid surface elevation. In addition, a continuity equation (Laplace's equation) and boundary conditions on the bottom and the side walls can also be derived. Therefore, this approach leads to differential algebraic equations expressed as a well-known set of equations for the sloshing problem. Another way is to apply Hamiltonian formulation to Eq. (3). In this method, canonically conjugate momenta regarding the liquid surface displacement  $\eta$  and the velocity potential  $\Phi$  are introduced. Applying a functional derivative defined as  $\delta F[f(x)]/\delta f(\xi) = \lim_{\varepsilon \rightarrow 0} (1/\varepsilon) \{F[f(x) + \varepsilon \delta(x - \xi)] - F[f(x)]\}$  to Eq. (3), it gives

$$\pi^{(\eta)} = \frac{\delta L}{\delta \dot{\eta}} = \Phi|_{y=\eta}, \quad \pi^{(\Phi)} = \frac{\delta L}{\delta \dot{\Phi}} = 0, \quad (4)$$

where a dot ( $\dot{\phantom{x}}$ ) denotes a time-derivative  $d/dt$ . The resulting momentum in Eq. (4) imply that (i) the momentum  $\pi^{(\eta)}$  is given as a function of other (canonical) variables, and (ii) the momenta  $\pi^{(\Phi)}$  becomes 0. According to Dirac's method for constrained Hamiltonian system, these relations have to be considered as constraints (called "primary constraints"). Specifically, these constraints are expressed as

$$C_1 = \pi^{(\eta)} - \Phi|_{y=\eta} = 0, \quad C_2 = \pi^{(\Phi)} = 0. \quad (5)$$

Employing the Legendre transform for deriving the Hamiltonian, then modifying it by means of the method of Lagrange multipliers with the primary constraints (5), it gives an augmented Hamiltonian:

$$H = T + U + \lambda_1 C_1 + \lambda_2 C_2. \quad (6)$$

Let  $q$  and  $p$  be the canonical coordinates  $(\eta, \Phi)$  and momenta  $(\pi^{(\eta)}, \pi^{(\Phi)})$ , it gives a DAEs as follows:

$$\dot{q} = \frac{\delta H}{\delta p}, \quad \dot{p} = -\frac{\delta H}{\delta q}, \quad 0 = \frac{\delta H}{\delta \lambda_1} = C_1, \quad 0 = \frac{\delta H}{\delta \lambda_2} = C_2. \quad (7)$$

When dealing with the liquid surface displacement  $\eta$  and the velocity potential on the liquid surface  $\Phi|_{y=\eta}$  as the canonical coordinates, Equation (7) results in the kinematic condition and the equilibrium of the pressure on the liquid surface as well as the Euler-Lagrange equation. On the other hand, equation (7) also gives the continuity equation (Laplace's equation) and the boundary conditions on a bottom and side walls when dealing with the velocity potential in the fluid domain  $V$  and on the bottom and the side walls, respectively. In particular, the second equation of Eq. (7) leads to such boundary conditions as constraints in this case. Conventional asymptotic models (e.g. Faltinsen and Timokha[1]) and FEM models (e.g. Nakayama and Washizu[5], Wu and Taylor[6]) can be applied to the above Lagrangian and Hamiltonian formulations. Consequently, both formulations leads to the DAEs comprised of the equations of time evolution for the liquid surface displacement and the velocity potential and the boundary conditions. Then, direct numerical integration techniques are employed in order to solve the DAEs.

## References

- [1] O.M. Faltinsen and A.N. Timokha. An adaptive multimodal approach to nonlinear sloshing in a rectangular tank. *Journal of Fluid Mechanics*, 432:167–200, 2001.
- [2] O. Gonzalez. Mechanical systems subjected to holonomic constraints: Differential–algebraic formulations and conservative integration. *Physica D*, 132:165–174, 1999.
- [3] P. Betsch and P. Steinmann. Conservation properties of a time FE method–part III: Mechanical systems with holonomic constraints. *International Journal for Numerical Method in Engineering*, 53:2271–2304, 2002.
- [4] R. L. Seliger and G. B. Whitham. Variational principles in continuum mechanics. *Proceedings of the Royal Society of London, Series A, Mathematical and Physical Sciences*, 305:1–25, 1968.
- [5] T. Nakayama and K. Washizu. Nonlinear analysis of liquid motion in a container subjected to forced pitching oscillation. *International Journal for Numerical Method in Engineering*, 15:1207–1220, 1980.
- [6] G. X. Wu and R. E. Taylor. Finite element analysis of two-dimensional non-linear transient water waves. *Applied Ocean Research*, 16:363–372, 1994.

## Dynamic Analysis of Thin Cables with Time-Varying Unwinding Velocity Condition and Transient-Tension Equations

Jin-Seok Jang<sup>1</sup>, Ji-Heon Kang<sup>2</sup>, Kun-Woo Kim<sup>1</sup>, Jae-Wook Lee<sup>1</sup>, Hyung-Ryul Kim<sup>3</sup>, Seung-Hyun Jeong<sup>1</sup>, Wan-Suk Yoo<sup>2</sup>

<sup>1</sup>Construction Equipment R&D Group, Korea  
Institute of Industrial Technology, Daegu  
42994, Korea  
[jsjang, kwkim, jaewk, shjeong]@kitech.re.kr

<sup>2</sup>Faculty of Mechanical Engineering  
Pusan National University  
Geumjung-gu, Busan 609-735, Korea  
[kangji1226@naver,  
wsyoo@pusan.ac.kr]

<sup>3</sup>Agency for Defense Development  
Changwon, 51691, Korea

### Abstract

Steady-state unwinding systems had been studied during the past 50 years [1~4]. Unwinding dynamics during a transient state had also been studied [5~10] for military and electric fiber manufacturing applications. In this study, time-varying velocity conditions are considered for a transient unwinding dynamic system [11], including a time-varying velocity and transient tension equation.

Extended Hamilton's principles and the kinetic and potential energy are first used to derive the governing equations. The material derivative is then considered for the time-varying unwinding velocity. The transient tension equation is derived by utilizing the governing equations and inextensible conditions of the applied cable. Numerical methods, such as the finite difference method and Newmark integration algorithm, are suggested for a dynamic analysis of the unwinding behaviors for a time-varying unwinding velocity.

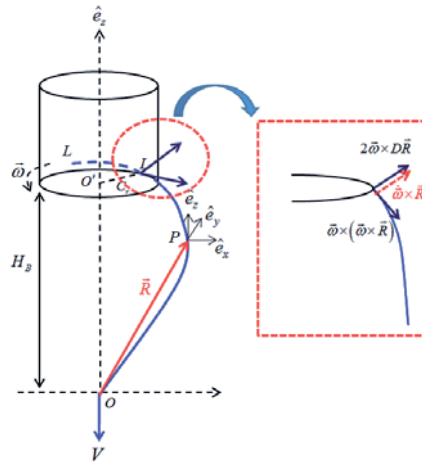


Figure 1. Acceleration vectors in unwinding dynamics

$$\rho A \left( \ddot{\vec{R}}_{tt} - 2V\ddot{\vec{R}}_{ts} + V^2\ddot{\vec{R}}_{ss} - V_t\ddot{\vec{R}}_s + 2\vec{\omega} \times (\dot{\vec{R}}_t - V\dot{\vec{R}}_s) + \vec{\omega} \times (\vec{\omega} \times \vec{R}) + \dot{\vec{\omega}}_t \times \vec{R} \right) = (T(s)\ddot{\vec{R}}_s)_s + \vec{F}_{air}(s,t) \quad (1)$$

$$\begin{aligned} T(s)R_s(0,t) &= 0 \quad \text{or} \quad R(0,t) = R_1(t) \quad \text{at eyelet} \\ T(s)R_s(s_1,t) &= 0 \quad \text{or} \quad R(s_1,t) = R_2(t) \quad \text{at lift-off point} \end{aligned} \quad (2)$$

The governing equations of motion and the boundary conditions at two points can be derived as Eq. (1) and Eq. (2), respectively. These equations of motion are derived by Lee [5].

$$\begin{aligned} T = \int T_s ds = T_o - \frac{1}{2} m x^2 \omega^2 - \frac{1}{2} m y^2 \omega^2 + m \dot{x}^2 + \{ m \ddot{x} - 2m\omega \dot{y} + m\omega V y_s - m\dot{\omega} y \} x \\ + m \dot{y}^2 + \{ m \ddot{y} + 2m\omega \dot{x} - m\omega V x_s - m\dot{\omega} x \} y + m \dot{z}^2 + \{ m \ddot{z} \} z - m V^2 - m \dot{V} \end{aligned} \quad (3)$$

Eq. (3) means transient-tension equation for time-varying unwinding equations of motion. Each terms are derived in inextensible condition. Using Eq. (3), the tension can be analyzed in the unwinding area which is difficult to measure as shown in figure 2.

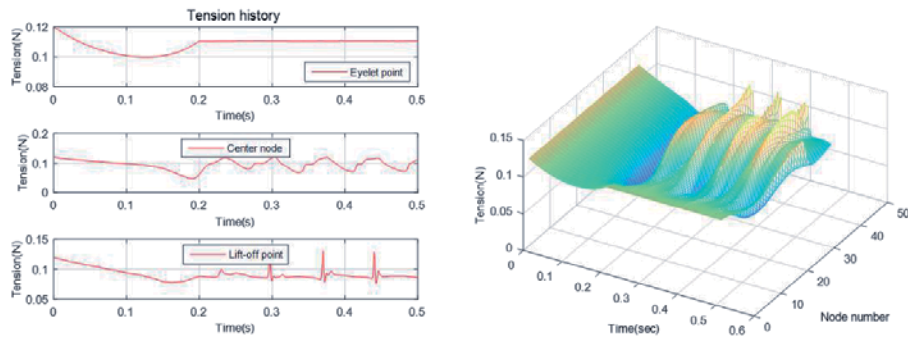


**Figure 2.** Tension profiles according to velocity change

The governing equations of motion and the boundary conditions at two points can be derived as Eq. (1) and Eq. (2), respectively. These equations of motion are derived by Lee[5].

In conclusion, transient-state unwinding dynamic equations were established, including time-varying unwinding velocity and transient-tension equations, which can be applied to the textile industry and military field.

## Acknowledgments

For *Acknowledgments* the heading should be treated as a section heading and should not be assigned a number.

## References

- [1] D. G. Padfield, A Note on the Fluctuations of Tension During Unwinding, *Journal of the Textile Institute Transactions*, vol. 47, pp. T301-T308, 1956.
- [2] D. G. Padfield, The motion and tension of an unwinding thread. I, in *Proceedings of the Royal Society of London A: Mathematical, Physical and Engineering Sciences*, 1958, pp. 382-407.
- [3] N. Isakov, Yarn tension in a balloon, *Technology of the Textile Industry USSR*, p. 92, 1961.
- [4] V. Kothari and G. Leaf, THE UNWINDING OF YARNS FROM PACKAGES PART I: THE THEORY OF YARN-UNWINDING, *Journal of the Textile Institute*, vol. 70, pp. 89-95, 1979.
- [5] J.-W. Lee, D.-M. An, and W.-S. Yoo, Derivation of equations of motion of an unwinding cable from a cylindrical spool package, *Journal of mechanical science and technology*, vol. 25, pp. 1287-1296, 2011.
- [6] J.-W. Lee, K.-W. Kim, H.-R. Kim, and W.-S. Yoo, Prediction of unwinding behaviors and problems of cables from inner-winding spool dispensers, *Nonlinear Dynamics*, vol. 67, pp. 1791-1809, 2012.
- [7] K. W. Kim, J. W. Lee, H. R. Kim, and W. S. Yoo, Experimental Verification of Unwinding Behavior of Fiber-Optic Cable and Prediction of High-Speed Unwinding, *Transactions of the Korean Society of Mechanical Engineers A*, 2014.
- [8] K.-W. Kim, J.-W. Lee, and W.-S. Yoo, Unwinding motion of cable by taking into consideration effect of bending on cable, *International Journal of Non-Linear Mechanics*, vol. 65, pp. 107-120, 2014.
- [9] K.-W. Kim, J.-W. Lee, and W.-S. Yoo, Verification of simulation for unwinding motion of cable in water by physical experiment, *Nonlinear Dynamics*, vol. 77, pp. 553-568, 2014.
- [10] K.-W. Kim, J.-W. Lee, H.-R. Kim, J.-S. Jang, and W.-S. Yoo, Necessity of transient-state unwinding equation of motion for analyzing unwinding motion of a thin cable, *Nonlinear Dynamics*, vol. 80, pp. 1565-1583, 2015.
- [11] J.-S. Jang, K.-W. Kim, J.-W. Lee, and W.-S. Yoo, Study on boundary conditions considering unwinding velocity in transient unwinding equations of motion, *Journal of Mechanical Science and Technology*, vol. 29, pp. 2587-2592, 2015.

# Condensed stiffness matrices for the model reduction of flexible multibody systems

Alessandro Cammarata<sup>1</sup>, Rosario Sinatra<sup>1</sup>

<sup>1</sup> Dipartimento di Ingegneria Civile e Architettura  
University of Catania  
Viale A.Doria 6, 95125, Catania, Italy  
acamma@dii.unict.it, rsinatra@dii.unict.it

## Abstract

Model reduction has been largely studied in structural and multibody dynamics as necessary to reduce the size of complex mechanical systems. Model reduction methods are varied. Some of these consider both the static modes at the boundaries of a domain and the restrained modes of the internal part when the boundary nodes are restrained. This method is used to obtain a *reduced impedance matrix* from a larger mechanical impedance matrix and to create a *superelement* [1], that is a subsystem able to interconnect to other superelements at the boundary nodes which takes into account its internal dynamics through a number of eigenmodes. The well-known Craig-Bampton representation is an impedance matrix reduction method in which the dynamics of the internal nodes is described by modal parameters, or intensities, of the internal modes [2]. Some reduction techniques do not consider the contribute of internal modes and are indicated as *static reduction methods*. The Guyan-Irons condensation method employs statically reduced stiffness matrices to reduce the stiffness of a mechanical system to the boundaries. The Guyan-Irons representation is based on the reduced stiffness matrix  $\mathbf{K}_{Or}$ , defined as:

$$\mathbf{K}_{Or} = \mathbf{K}_O - \mathbf{K}_{OI}\mathbf{K}_{II}^{-1}\mathbf{K}_{IO} \equiv \mathbf{\Xi}^T \mathbf{K} \mathbf{\Xi} \quad (1)$$

with the *static condensation matrix*  $\mathbf{\Xi}$  expressed as

$$\mathbf{\Xi} = \begin{bmatrix} \mathbf{1} \\ -\mathbf{K}_{II}^{-1}\mathbf{K}_{IO} \end{bmatrix} \quad (2)$$

in which the subscripts  $O$  and  $I$ , respectively, refer to the outer nodes of the boundary and to the inner nodes of the domain. In the physical domain a linear mechanical system is characterized by its mass  $\mathbf{M}$ , damping  $\mathbf{C}$  and stiffness  $\mathbf{K}$  matrices. Coupling different parts requires the use of *compatibility* and *equilibrium* conditions that, combined with the equation of motions, yield the general framework described by a system of three equations, [3]:

$$\begin{cases} \mathbf{M}\ddot{\mathbf{u}} + \mathbf{C}\dot{\mathbf{u}} + \mathbf{K}\mathbf{u} = \mathbf{f}_e + \mathbf{r} \\ \mathbf{B}\mathbf{u} = \mathbf{0} \\ \mathbf{L}^T \mathbf{r} = \mathbf{0} \end{cases} \quad (3)$$

in which  $\mathbf{u}$  is the array of generalized displacements,  $\mathbf{f}_e$  is the array of external forces and torques. Finally,  $\mathbf{B}$  expresses the compatibility conditions operating on the boundary nodes of two adjacent substructures and  $\mathbf{L}$  expresses the equilibrium conditions between the constraint forces  $\mathbf{r}$  at the boundaries. By introducing a set of independent nodes with displacements  $\mathbf{q}$ , such that

$$\mathbf{u} = \mathbf{L}\mathbf{q} \quad (4)$$

the system of equations (3) is reduced to the following form:

$$\mathbf{M}_r \ddot{\mathbf{q}} + \mathbf{C}_r \dot{\mathbf{q}} + \mathbf{K}_r \mathbf{q} = \mathbf{f}_{er} \quad (5)$$

in which  $\mathbf{M}_r = \mathbf{L}^T \mathbf{M} \mathbf{L}$ ,  $\mathbf{C}_r = \mathbf{L}^T \mathbf{C} \mathbf{L}$ ,  $\mathbf{K}_r = \mathbf{L}^T \mathbf{K} \mathbf{L}$  and  $\mathbf{f}_{er} = \mathbf{L} \mathbf{f}_e$  are the reduced matrices and array of generalized forces.

Here, the formulation adopted in [4] is used to create a general framework for the model reduction of flexible multibody systems in which two-node flexible beam elements are coupled by means of joints. The static reduction method is augmented with the compatibility conditions of the joints using a primal formulation without Lagrangian multipliers. In presence of joints the compatibility conditions must express the *Multi Point Conditions* (MPCs) linking the displacements of the two adjacent nodes composing the joint. In the proposed approach the compatibility conditions become:

$$\mathbf{u} = \mathbf{B}\mathbf{q} + \mathbf{H}\boldsymbol{\theta} \quad (6)$$

in which  $\mathbf{H}$  is a matrix or an array that includes the geometric features of the joint and  $\boldsymbol{\theta}$  is the array of joint displacements. It is noteworthy that eq.(6) expresses MPCs in which the joint contribute is not included inside  $\mathbf{B}$  but is explicit. This approach is useful to insert joint stiffness, joint preload forces/torques or to easily recover joint wrenches during the analysis. The compatibility conditions of (6) are coupled to the static equilibrium equations

to obtain a reduction technique analogous to the Guyan-Irons condensation method but augmented with MPCs. Then, the static equations are projected onto the joint-space through  $\mathbf{H}^T$  to solve for  $\theta$ , i.e.:

$$\mathbf{H}^T \mathbf{K}_{uu} \mathbf{u} + \mathbf{H}^T \mathbf{K}_{uq} \mathbf{q} + \mathbf{K}_\theta \theta + \mathbf{p} = \mathbf{0} \quad (7)$$

where  $\mathbf{K}_{uu}$  and  $\mathbf{K}_{uq}$  are the stiffness block matrices,  $\mathbf{K}_\theta$  is the joint stiffness matrix and  $\mathbf{p}$  is the array of joint preload. By introducing eq.(6) into (7),  $\theta$  can be obtained by the following equation:

$$\theta = -(\mathbf{K}_\theta + \mathbf{H}^T \mathbf{K}_{uu} \mathbf{H})^{-1} [\mathbf{H}^T (\mathbf{K}_{uu} \mathbf{B} + \mathbf{K}_{uq}) \mathbf{q} - \mathbf{p}] \quad (8)$$

By substituting the expression of  $\theta$  in eq.(6) an expression similar to eq.(4) can be derived:

$$\mathbf{u} = \mathbf{L} \mathbf{q} + \mathbf{l} \quad (9)$$

where  $\mathbf{l}$  depends only on the preload  $\mathbf{p}$ . The static condensation matrix  $\Xi$  becomes:

$$\Xi = \begin{bmatrix} \mathbf{1} \\ \mathbf{B} + \mathbf{H} \mathbf{L} \end{bmatrix} \quad (10)$$

and can be used to obtain the *statically reduced augmented stiffness matrix*  $\mathbf{K}_r = \Xi^T \mathbf{K} \Xi$  and the *statically reduced and consistent augmented mass matrix*  $\mathbf{M}_r = \Xi^T \mathbf{M} \Xi$  analogous to that reported in [1]:

$$\mathbf{M}_r = \mathbf{M}_{OO} - \mathbf{M}_{OI} \mathbf{K}_{II}^{-1} \mathbf{K}_{IO} - \mathbf{K}_{OI} \mathbf{K}_{II}^{-1} \mathbf{M}_{IO} + \mathbf{K}_{OI} \mathbf{K}_{II}^{-1} \mathbf{M}_{II} \mathbf{K}_{II}^{-1} \mathbf{K}_{IO} \quad (11)$$

Following a similar approach the method can be extended to impedance matrices, as demonstrated in [5]. Besides, the proposed static reduction is suitable to be used to include *constraint modes* of boundary points in the transformation matrix of the Craig-Bampton representation.

## References

- [1] M. Géradin, and A. Cardona. Flexible multibody dynamics: a finite element approach. Wiley, 2001.
- [2] M. C. Bampton, and JR, R. R. Craig. Coupling of substructures for dynamic analyses. Aiaa Journal, 6(7), pages 1313–1319, 1968.
- [3] R. R. Craig, and A. J. Kurdila. Fundamentals of structural dynamics. John Wiley & Sons, 2006.
- [4] A. Cammarata. Unified formulation for the stiffness analysis of spatial mechanisms. Mechanism and Machine Theory 105, pages 272-284, 2016.
- [5] A. Cammarata, I. Calì, A. Greco, M. Lacagnina, G. Fichera and D. D'Urso. Dynamic stiffness model of spherical parallel robots. Journal of Sound and Vibration, 384, pages 312-324, 2016.

# Recursive Solution Procedures for Flexible Multibody Systems: Comparing Condensation and Transfer Matrix Methods

Jurnan Schilder, Marcel Ellenbroek, André de Boer

Faculty of Engineering Technology  
University of Twente  
P.O. Box 217, 7500AE Enschede, The Netherlands  
j.p.schilder@utwente.nl

## Abstract

The dynamic behavior of flexible multibody systems that consist of a chain of bodies can be studied efficiently by recursive solution procedures. In these, it is common to express the kinematics using the relative coordinates formulation and the dynamics using the floating frame of reference formulation. A comprehensive overview of the developments in this field for open-loop and closed-loop rigid and flexible multibody systems is given in [1].

The purpose of this work is to provide additional insights to these recursive methods. Key concept in most recursive solution procedures is to recursively eliminate a body from the chain, upon which the mass matrix and interface forces of the remaining adjacent body must be updated appropriately. In this work, it is shown that by expressing the motion with respect to an inertial frame, the mass matrix update can directly be related to the effective mass of the eliminated body, giving it a clear physical interpretation. This method is compared with a recursive solution procedure based on transfer matrices. This transfer matrix method may have advantages in the case of closed-loop systems and systems that consist of a chain of identical bodies, which is often the case for solar panel arrays, robotic manipulators, offshore equipment, etcetera.

Consider the equation of motion of a single flexible body using the floating frame of reference formulation:

$$\begin{bmatrix} \mathbf{M}_r & \mathbf{\Gamma}^T \\ \mathbf{\Gamma} & \mathbf{M}_e \end{bmatrix} \begin{bmatrix} \dot{\mathbf{q}}_r \\ \dot{\mathbf{q}}_e \end{bmatrix} + \begin{bmatrix} \mathbf{0} & \mathbf{0} \\ \mathbf{0} & \mathbf{K}_e \end{bmatrix} \begin{bmatrix} \mathbf{0} \\ \mathbf{q}_e \end{bmatrix} = \begin{bmatrix} \mathbf{F}_r \\ \mathbf{F}_e \end{bmatrix}. \quad (1)$$

The rigid body coordinates  $\mathbf{q}_r$  describe the configuration of a floating frame with respect to an inertial frame. The elastic coordinates  $\mathbf{q}_e$  describe a linear elastic displacement field with respect to the floating frame, using a linear combination of deformation modes. The mass matrix consists of the rigid body mass matrix  $\mathbf{M}_r$ , the generalized mass matrix due to the elastic modes  $\mathbf{M}_e$  and the modal participation factors  $\mathbf{\Gamma}$  that couple rigid and elastic motions.  $\mathbf{K}_e$  is the generalized stiffness matrix due to the elastic modes.  $\mathbf{F}_r$  is the resultant generalized force acting on the body and  $\mathbf{F}_e$  is the generalized modal force. Here, quadratic velocity forces are contained in the right hand side generalized forces.

In [2], it is explained how this equation of motion can be used in a recursive order- $n$ -method that is applied for the simulation of flexible space structures. To explain the procedure, Figure 1 highlights the last two bodies,  $A$  and  $B$ , of an open-loop system. From the equation of motion of the last body  $B$ , the second line is solved for  $\dot{\mathbf{q}}_e$  and substituted in the first line. By doing so, it is possible to express the interface force between the two bodies in terms of the acceleration of the interface point and the generalized forces of body  $B$ . Next, this is substituted in the right hand side of the equation of motion of second to last body  $A$ . The term containing the acceleration of the interface point can be combined with the other inertia forces and forms the mass matrix update of this body. All other terms remain on the right hand side and form the update of the interface force. The procedure is repeated recursively, eliminating one body at a time, until one body remains. This equation of motion is solved and the result is back substituted in the equations of motion of the eliminated bodies subsequently. In case of a closed-loop system, a loop closure constraint is enforced using Lagrange multipliers.

If the elastic deformation is described by six appropriate modes, e.g. static Craig-Bampton modes, it can be shown that for a two-node body, it is always possible to find a coordinate transformation from  $\mathbf{q}_r$  and  $\mathbf{q}_e$  towards the global motion of the interface points, e.g.  $\mathbf{q}_i$  and  $\mathbf{q}_j$  for body  $A$ . With this, the equation of motion eq. (1) can be rewritten to the following form:

$$\begin{bmatrix} \mathbf{M}_{ii} & \mathbf{M}_{ij} \\ \mathbf{M}_{ji} & \mathbf{M}_{jj} \end{bmatrix} \begin{bmatrix} \dot{\mathbf{q}}_i \\ \dot{\mathbf{q}}_j \end{bmatrix} = \begin{bmatrix} \mathbf{F}_i \\ \mathbf{F}_j \end{bmatrix} + \begin{bmatrix} \mathbf{Q}_i \\ \mathbf{Q}_j \end{bmatrix}. \quad (2)$$

Note that these are nonlinear equations in terms of the (large) global motion of the interface coordinates.  $\mathbf{F}_i$  and  $\mathbf{F}_j$  are the interface forces of interface points  $i$  and  $j$ .  $\mathbf{Q}_i$  and  $\mathbf{Q}_j$  contains all other generalized forces acting on interface points  $i$  and  $j$ . This form is similar to the co-rotational frame formulation of a finite element, with the difference that in eq. (2) also quadratic velocity forces are included in  $\mathbf{Q}$ , which are normally neglected in a co-rotational formulation.

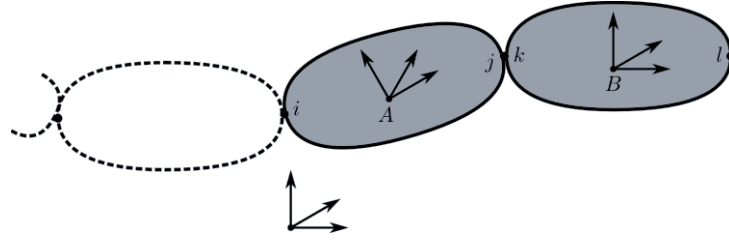


**Figure 1.** The last two bodies,  $A$  and  $B$ , of an open-loop flexible multibody system.

Using eq. (2) instead of eq. (1), a recursive solution procedure is set up similarly as explained above. The equation of motion of body  $B$  can be manipulated such that the interface force  $\mathbf{F}_k$  is expressed as:

$$\mathbf{F}_k = [\mathbf{M}_{kk} - \mathbf{M}_{kl}\mathbf{M}_{ll}^{-1}\mathbf{M}_{lk}]\ddot{\mathbf{q}}_k + \mathbf{M}_{kl}\mathbf{M}_{ll}^{-1}\mathbf{F}_l + \mathbf{Q}_k - \mathbf{M}_{kl}\mathbf{M}_{ll}^{-1}\mathbf{Q}_l. \quad (3)$$

The term in between square brackets can be recognized as the mass matrix condensed on interface point  $k$ , which consists of its relevant partition  $\mathbf{M}_{kk}$  and the added effective mass of the body  $-\mathbf{M}_{kl}\mathbf{M}_{ll}^{-1}\mathbf{M}_{lk}$ , similar to linear vibration problems [3]. Without loss of generality, it is assumed that the bodies are connected rigidly, such that the kinematic and dynamic coupling conditions are  $\ddot{\mathbf{q}}_j = \ddot{\mathbf{q}}_k$  and  $\mathbf{F}_j = -\mathbf{F}_k$ . With this, the equation of motion of body  $A$  can be expressed as:

$$\begin{bmatrix} \mathbf{M}_{ii} & \mathbf{M}_{ij} \\ \mathbf{M}_{ji} & \mathbf{M}_{jj} + \mathbf{M}_{kk} - \mathbf{M}_{kl}\mathbf{M}_{ll}^{-1}\mathbf{M}_{lk} \end{bmatrix} \begin{bmatrix} \ddot{\mathbf{q}}_i \\ \ddot{\mathbf{q}}_j \end{bmatrix} = \begin{bmatrix} \mathbf{F}_i \\ \mathbf{M}_{kl}\mathbf{M}_{ll}^{-1}\mathbf{F}_l \end{bmatrix} + \begin{bmatrix} \mathbf{Q}_i \\ \mathbf{Q}_j + \mathbf{Q}_k - \mathbf{M}_{kl}\mathbf{M}_{ll}^{-1}\mathbf{Q}_l \end{bmatrix}. \quad (4)$$

In this form, it is clear that the elimination of body  $B$  results in a mass matrix update of body  $A$ , but only in the partition directly related to interface point  $j$ . This can be physically interpreted as follows: In order to have equivalent motion of the system from which body  $B$  is eliminated, the appropriate condensed mass is added to interface point  $j$ . Simultaneously its interface force is updated to take into account the interface force  $\mathbf{F}_l$  and elastic and quadratic velocity forces of body  $B$ . By applying a coordinate transformation back to rigid and elastic coordinates on eq. (4), the same result is obtained as in [2]. With this, it can be understood that in this recursive solution procedure the mass matrix update can be related to a specific condensed mass matrix and a coordinate transformation.

With the equations of motion in the form of eq. (2), an alternative recursive formulation is possible in terms of transfer matrices. To this end, the acceleration and interface force of interface point  $j$  are expressed in terms of the acceleration and interface force of interface point  $i$  and generalized forces as:

$$\begin{bmatrix} \ddot{\mathbf{q}}_j \\ \mathbf{F}_j \end{bmatrix} = \begin{bmatrix} \mathbf{M}_{ij} & \mathbf{0} \\ \mathbf{M}_{jj} & -\mathbf{1} \end{bmatrix}^{-1} \begin{bmatrix} -\mathbf{M}_{ii} & \mathbf{1} \\ -\mathbf{M}_{ji} & \mathbf{0} \end{bmatrix} \begin{bmatrix} \ddot{\mathbf{q}}_i \\ \mathbf{F}_i \end{bmatrix} + \begin{bmatrix} \mathbf{M}_{ij} & \mathbf{0} \\ \mathbf{M}_{jj} & -\mathbf{1} \end{bmatrix}^{-1} \begin{bmatrix} \mathbf{Q}_i \\ \mathbf{Q}_j \end{bmatrix}. \quad (5)$$

The combination of acceleration and interface force of an interface point is referred to as the state vector of that interface point. In this formulation, the state vector of  $j$  is related to the state vector of  $i$  by a so-called transfer matrix and an additional vector due to elastic and quadratic velocity terms. With this, it is possible to eliminate all intermediate bodies from a multibody chain by successive multiplications of transfer matrices and to obtain a reduced equation of motion in terms of the first and last states only.

An advantage of this transfer matrix method is that these transfer matrices can be determined without any a priori knowledge of the boundary conditions of the entire structure, i.e. changing the boundary conditions on the first and last interface points does not influence the transfer matrices. As a consequence, no loop-closure constraints are required for closed-loop systems. Using the transfer matrix method becomes increasingly beneficial for systems that consists of a chain of identical bodies. In this case, the reduction of the full size equation of motion consists of multiplications of transfer matrices that are all the same, whereas when using techniques based on condensation and elimination of bodies, the mass matrix update still needs to be executed one body at a time. However, since this mass matrix update can be given the clear physical interpretation presented in this work, it is still an attractive alternative to the more mathematical transfer matrix method.

## References

- [1] T.M. Wasfy, A.K. Noor. Computational strategies for flexible multibody systems. *Applied Mechanics Reviews*, 56 (6), pages 553-613, 2003.
- [2] M.H.M. Ellenbroek. On the fast simulation of flexible space structures. PhD Thesis, University of Twente, Enschede, The Netherlands, 1994.
- [3] M. Géradin, D.J. Rixen. *Mechanical Vibrations*. Third Edition. Wiley, Chichester, United Kindom, 2015.

# Indirect State and Force Estimator Based on Multibody Models

Emilio Sanjurjo, Miguel Á. Naya, Daniel Dopico, Antonio J. Rodríguez

Laboratorio de Ingeniería Mecánica  
 University of A Coruña  
 C/ Mendizábal s/n, 15403, Ferrol, Spain  
 [emilio.sanjurjo, minaya, ddopico, antonio.rodriquez.gonzalez]@udc.es

## Abstract

Multibody simulations have already been used for a long time to reduce development time and cost in many sectors of the industry [1]. Although the first applications of multibody simulations were aimed at predicting the dynamic behavior of machines and/or mechanisms, the efficiency of the multibody formulations developed during the last years, combined with the increasing computational power available, have allowed new applications for multibody simulations, such as human-in-the-loop and hardware-in-the-loop simulations, which require real-time execution [2, 3].

During the last decade, some research groups started to employ multibody dynamics techniques to devise state observers [4, 5, 6, 7]. The advantages of this strategy with respect to state observers designed in a more conventional way are the accuracy of the multibody models with respect to simplified closed-form models, and the general methodology provided by the multibody formulations to develop models of new systems and sensors. Moreover, multibody models usually provide more information, which is usually neglected when using a closed-form model.

The main drawbacks of using multibody simulations for state observers include their high computational cost, not allowing to employ unscented Kalman filters in problems of moderate size, and the lack of accuracy of the force models employed.

Some of these problems can be overcome by using simple kinematic models, but at the cost of adding acceleration sensors to provide the input to the kinematic model [8, 9]. If the extra sensors are not available, then a dynamical model has to be used. However, if the force models are not accurate enough, the prediction of the model

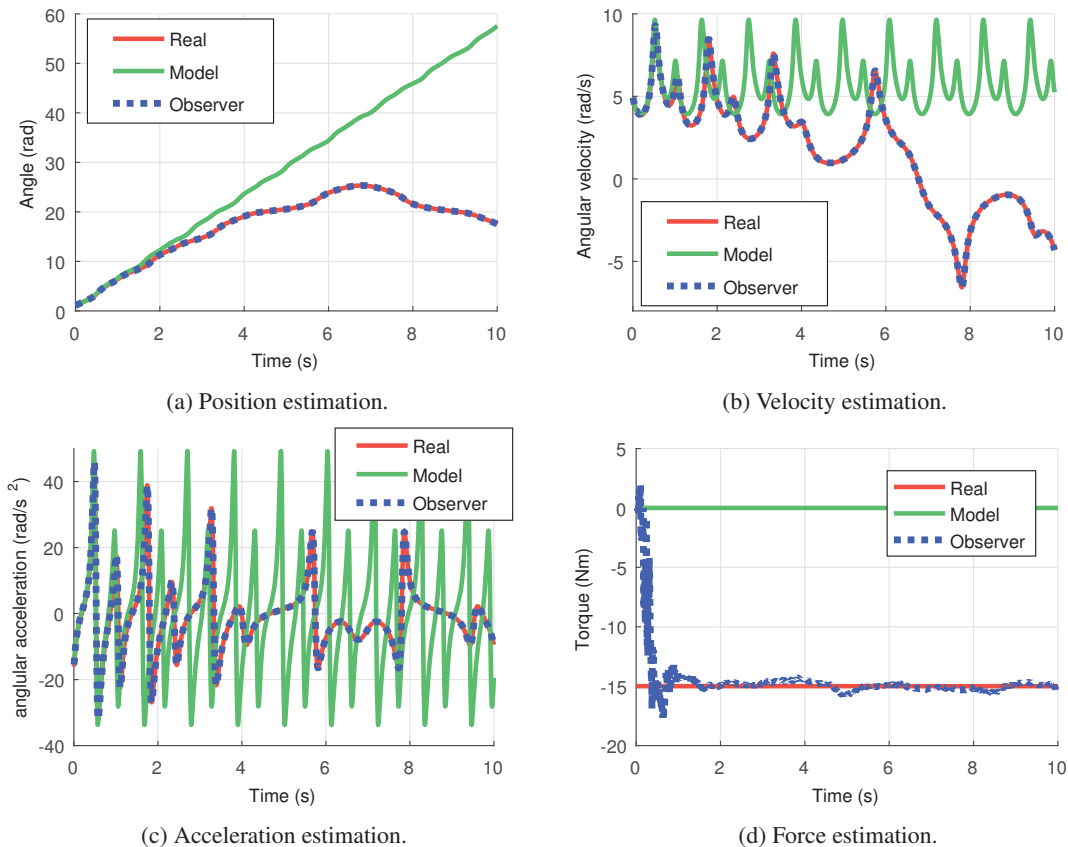


Figure 1: Estimation results from the test with the four-bar linkage. Plots (a) to (c) show the crank angle, angular velocity, and angular acceleration, while plot (d) shows the estimation of the torque applied to the crank.

will be biased. Although accurate results can be obtained with this approach if the values of the plant noise are properly adjusted [10], correcting the plant by estimating the actual force applied to the system should provide a more accurate solution. In some problems the force estimation can be the main aim, independently of the kinematic magnitudes.

In this work, an indirect Kalman filter estimating position, velocity and acceleration errors of a multibody simulation is proposed. The name *indirect* comes from the fact that the method does not estimate the magnitudes of interest, but the errors that the multibody model makes in tracking the real system. The acceleration errors are employed to calculate the force errors which would avoid the drift of the model, and these forces are applied to the model. Moreover, the kinematic magnitudes previously estimated are also corrected. This approach allows to obtain accurate state estimations, while estimating also the unknown forces.

In order to evaluate the behavior of this approach, two multibody models are employed. The first one is considered as the real mechanism. Its motion is measured with one or more sensors, which are corrupted by noise to simulate real sensors. The second multibody model acts as a model of the first one. They are similar, but there are some differences as if they were modeling errors, such as those produced due to unknown forces or parameters, or due to simplified force models. Finally, a state observer is built using the second multibody model and correcting it with information provided by the noisy measurements taken from the first model (the “real mechanism”).

This methodology has been applied in this work to a four-bar and a five-bar linkages. The mechanisms considered as real have constant torques applied to their cranks, while their corresponding models do not have any applied torque, thus simulating a situation in which the actual forces are unknown.

The results obtained from a test with the four-bar linkage can be seen in Figure 1. In this test, the real mechanism has a -15 Nm torque applied to its crank, while this torque is unknown to the model and the state observer. The only sensor considered for this test was an encoder measuring the crank angle. The results show how the errors in the multibody model make it diverge from the behavior of the real mechanism, while the state observer properly tracks both the kinematic magnitudes and the torque applied at the crank.

### Acknowledgments

This work has been partially financed by the Spanish Ministry of Economy and Competitiveness and EU-ERDF funds under the projects ‘Observadores de estados y entradas basados en modelos multicuerpo detallados aplicados al control de vehículos’ (TRA2014-59435-P). The research of Antonio J. Rodríguez was founded by fellowship BES-C-2015-0014 of Spanish Government.

### References

- [1] P. Eberhard, W. Schiehlen. Computational Dynamics of Multibody Systems: History, Formalisms, and Applications. *Journal of Computational and Nonlinear Dynamics*, 1:3–12, 2006.
- [2] R. Pastorino, F. Cosco, F. Naets, W. Desmet, J. Cuadrado. Hard real-time multibody simulations using ARM-based embedded systems. *Multibody System Dynamics*, 37:127–143, 2016.
- [3] J. García de Jalón, E. Bayo. *Kinematic and Dynamic Simulation of Multibody Systems: The Real Time Challenge*. Springer-Verlag, 1994.
- [4] J. Cuadrado, D. Dopico, A. Barreiro, E. Delgado. Real-time state observers based on multibody models and the extended Kalman filter. *Journal of Mechanical Science and Technology*, 23:894–900, 2009.
- [5] R. Pastorino, D. Richiedei, J. Cuadrado, A. Trevisani. State estimation using multibody models and non-linear Kalman filter. *International Journal of Non-Linear Mechanics*, 53:83–90, 2013.
- [6] F. Naets, R. Pastorino, J. Cuadrado, W. Desmet. Online state and input force estimation for multibody models employing extended kalman filtering. *Multibody System Dynamics*, 32:317–336, 2014.
- [7] J. L. Torres-Moreno, J. L. Blanco-Claraco, A. Giménez-Fernández, E. Sanjurjo, M. Á. Naya. Online Kinematic and Dynamic-State Estimation for Constrained Multibody Systems Based on IMUs. *Sensors*, 16:333, 2016.
- [8] I. Palomba, D. Richiedei, A. Trevisani. Kinematic state estimation for rigid-link multibody systems by means of nonlinear constraint equations. *Multibody System Dynamics*, 40:1–22, 2017.
- [9] I. Palomba, D. Richiedei, A. Trevisani. Two-stage approach to state and force estimation in rigid-link multibody systems. *Multibody System Dynamics*, 39:115–134, 2017.
- [10] E. Sanjurjo, M. Á. Naya, J. L. Blanco-Claraco, J. L. Torres-Moreno, A. Giménez-Fernández. Accuracy and efficiency comparison of various nonlinear Kalman filters applied to multibody models. *Nonlinear Dynamics*, 88:1935–1951, 2017.

# A Method for Calculating and Continuing Static Solutions for Flexible Multibody Systems

J. P. Meijaard

Faculty of Engineering Technology  
University of Twente  
Drienerlolaan 5, NL-7522 NB Enschede, The Netherlands  
J.P.Meijaard@utwente.nl

## Abstract

In the analysis of multibody dynamics problems, it is often useful to know the equilibrium configurations and the way in which these configurations change if a loading parameter changes. These solutions can often be considered initial quasistatic approximations of the true motion of a system if the loads change relatively slowly with respect to the eigenfrequencies of the system. Corrections can then be made with the aid of linearized dynamic equations. So here, a method for finding and continuing static equilibrium solutions of a flexible multibody system and obtaining the linearized equations in these equilibria is presented.

The flexible multibody systems are modelled by finite elements, as described earlier [1]. For each element with nodal coordinates  $\mathbf{x}^e$ , a number of generalized strains  $\boldsymbol{\varepsilon}^e$  are defined as functions of the nodal coordinates,

$$\boldsymbol{\varepsilon}^e = \mathcal{D}^e(\mathbf{x}^e). \quad (1)$$

These generalized strains are invariant under rigid-body displacements of the element and describe the state of deformation of the element, so constraining them to be zero enforces rigidity of the element. Generalized stresses  $\boldsymbol{\sigma}^e$  are defined as energetically dual to the generalized strains, so the inner product of them with a virtual variation of the generalized strain represent the negative virtual work of the internal forces in the element,  $\delta W_1^e = -\boldsymbol{\sigma}^T \delta \boldsymbol{\varepsilon}^e$ . If these strains are not prescribed, either as constant values or as prescribed functions of time, the associated generalized stresses are given by constitutive relations, which are assumed to be linear, so they can be specified by a stiffness matrix  $\mathbf{S}^e$  and a damping matrix  $\mathbf{S}_d^e$  as

$$\boldsymbol{\sigma}^e = \mathbf{S}^e \boldsymbol{\varepsilon}^e + \mathbf{S}_d^e \dot{\boldsymbol{\varepsilon}}^e. \quad (2)$$

A dot over a variable denotes a derivative with respect to time. The dynamic properties are described by a mass matrix and velocity-dependent convective terms, so the inertia force of the element is given by

$$-\mathbf{M}^e \ddot{\mathbf{x}}^e - \mathbf{h}^e(\dot{\mathbf{x}}^e, \mathbf{x}^e). \quad (3)$$

A system can be modelled by a number of elements of several kinds, which are linked by sharing nodal coordinates. Some coordinates and generalized strains can have prescribed values and applied forces can act on the system. The equations for the complete system can be obtained by the familiar finite-element assembly process.

Static solutions are found by equating the accelerations and velocities to zero and solving the resulting ordinary equations. The variables used in the present method are the nodal coordinates and the generalized strains that are not prescribed and all generalized stresses, for which the equations are simultaneously solved without further reductions.

Continuation methods to determine branches of equilibrium solutions have been used for some time. These methods consist of an explicit predictor, which estimates a new solution some distance away from a current solution, and an iterative corrector, which determines a more accurate solution on the branch of equilibria. One of the first to apply these methods was Haselgrove [2]; many fundamental ideas for continuation are contained in this article. Early applications to structural mechanics were made by Riks [3, 4] and Wempner [5], where an auxiliary equation that defined a hyperplane perpendicular to the tangent vector of a known solution was used to define a step size. Another auxiliary condition was used by Crisfield [6], whereas Fried [7] proposed a search direction orthogonal to the present level curve.

An application of continuation methods to the problem of finding equilibrium solutions for flexible multibody systems was reported by Cardona and Huespe [8]. Their method resembles somewhat the proposed model here, in that Lagrangian multipliers are included in the set of equations that has to be solved, but their formulation does not include generalized strains. The larger system of equations used in the present formulation is easier to evaluate, whereas the sparse structure of the matrix hardly influences the calculation time. In addition, the formulation appears to have better convergence properties. Also the linearized equations of motion in equilibria are formulated in a set of minimal coordinates, which are useful for obtaining stiffness values and natural frequencies. These can also be used with advantage for designing control systems.

The method is applied to large-deflection problems of a planar beam and a curved spatial beam, the buckling of a stylized parallel leaf-spring mechanism due to a misalignment and the deflection of a fluid-conveying pipe,

initially bent to a semicircle, due to the fluid flow. In the last two examples, stable as well as unstable branches could be traced.

### **Acknowledgments**

This research was supported by the Dutch Charity for Technical Sciences, STW, through the grant No 14152.

### **References**

- [1] J. B. Jonker. A finite element dynamic analysis of spatial mechanisms with flexible links. *Computer Methods in Applied Mechanics and Engineering*, 76:17–40, 1989.
- [2] C. B. Haselgrove. The solution of non-linear equations and of differential equations with two-point boundary conditions. *The Computer Journal*, 4:255–259, 1961.
- [3] E. Riks. On the numerical solution of snapping problems in the theory of elastic stability. Dissertation, Stanford University, Stanford, 1970.
- [4] E. Riks. The application of Newton's method to the problem of elastic stability. *ASME Journal of Applied Mechanics*, 39:1060–1065, 1972.
- [5] G. A. Wempner. Discrete approximations related to nonlinear theories of solids. *International Journal of Solids and Structures*, 7:1581–1599, 1971.
- [6] M. A. Crisfield. A fast incremental/iterative solution procedure that handles "snap-through". *Computers and Structures*, 13:55–62, 1981.
- [7] I. Fried. Orthogonal trajectory accession to the nonlinear equilibrium curve. *Computer Methods in Applied Mechanics and Engineering*, 47:283–297, 1984.
- [8] A. Cardona, A. Huespe. Continuation methods for tracing the equilibrium path in flexible mechanism analysis. *Engineering Computations*, 15:190–220, 1998.

# Stability Bounds For Step Size Ratios In Variable Time Step Implementations Of Newmark Integrators

Victoria Wieloch, Martin Arnold

06099 Halle (Saale), Germany  
Martin Luther University Halle-Wittenberg  
Institute of Mathematics  
[victoria.wieloch, martin.arnold]@mathematik.uni-halle.de

## Abstract

In structural dynamics, Newmark integrators are developed as methods with high-frequency dissipation and small low-frequency damping. The generalized- $\alpha$  method according to Chung and Hulbert [4] is such an integrator with second order accuracy. The algorithmic parameters are defined in terms of the desired amount of high-frequency dissipation. Brüls and Cardona [3] extended the method to constrained systems on matrix Lie groups  $G$ , that allow to describe large rotations without singularities. In this presentation, the Lie groups  $\mathbb{R}^3 \times SO(3)$  and  $SE(3)$  are considered.

The differential-algebraic equations of motion are either solved in the index-3 formulation (1) or in the stabilized index-2 formulation (2), see [1]:

<u>Index-3 formulation</u>	<u>Stabilized index-2 formulation</u>
$\dot{q} = DL_q(e) \cdot \tilde{\mathbf{v}}$ (1a)	$\dot{q} = DL_q(e) \cdot \tilde{\Delta \mathbf{q}}$ (2a)
$\mathbf{M}(q) \dot{\mathbf{v}} = -\mathbf{g}(q, \mathbf{v}, t) - \mathbf{B}^T(q) \boldsymbol{\lambda}$ (1b)	$\Delta \mathbf{q} = \mathbf{v} - \mathbf{B}^T(q) \boldsymbol{\eta}$ (2b)
$\mathbf{0} = \boldsymbol{\Phi}(q)$ (1c)	$\mathbf{M}(q) \dot{\mathbf{v}} = -\mathbf{g}(q, \mathbf{v}, t) - \mathbf{B}^T(q) \boldsymbol{\lambda}$ (2c)
	$\mathbf{0} = \boldsymbol{\Phi}(q)$ (2d)
	$\mathbf{0} = \mathbf{B}(q) \mathbf{v}$ , (2e)

with position coordinate  $q$ , velocity coordinate  $\mathbf{v}$ , holonomic constraints (1c) and (2d), constraint gradients  $\mathbf{B}(q)$ , mass matrix  $\mathbf{M}(q)$ , force vector  $\mathbf{g}(q, \mathbf{v}, t)$ , Lagrange multipliers  $\boldsymbol{\lambda}$  and an auxiliary vector  $\boldsymbol{\eta}$ . The tilde operator  $(\tilde{\bullet}) : \mathbb{R}^k \rightarrow \mathfrak{g}$  with the Lie algebra  $\mathfrak{g}$  and the directional derivative of the left translation  $DL_q(e) : \mathfrak{g} \rightarrow T_q G$ ,  $\tilde{\mathbf{v}} \mapsto DL_q(e) \cdot \tilde{\mathbf{v}}$  in  $e$  along  $\tilde{\mathbf{v}}$  are used to summarize the kinematic relations in their compact form (1a) and (2a), respectively. The numerical solution of the index-3 formulation does in general not preserve the hidden constraints at velocity level (2e), which is why an index reduction is useful [1].

For the generalized- $\alpha$  method with constant step sizes, the optimal parameters for accuracy and stability depend on the spectral radius at infinity  $\rho_\infty$ , see [4]. For fixed time step sizes  $h$ , the position and velocity coordinates in the index-3 formulation (1) are updated in time step  $t_n \rightarrow t_{n+1} = t_n + h$  according to

$$q_{n+1} = q_n \circ \exp(h \tilde{\Delta \mathbf{q}}_n) \quad (3a)$$

$$\Delta \mathbf{q}_n = \mathbf{v}_n + (0.5 - \beta) h \mathbf{a}_n + \beta h \mathbf{a}_{n+1} \quad (3b)$$

$$\mathbf{v}_{n+1} = \mathbf{v}_n + (1 - \gamma) h \mathbf{a}_n + \gamma h \mathbf{a}_{n+1} \quad (3c)$$

with the Lie group operation  $\circ : G \times G \rightarrow G$ , the exponential map  $\exp : \mathfrak{g} \rightarrow G$  and acceleration like vectors  $\mathbf{a}_n \approx \dot{\mathbf{v}}(t_n + \Delta_\alpha h)$  that satisfy

$$(1 - \alpha_m) \mathbf{a}_{n+1} + \alpha_m \mathbf{a}_n = (1 - \alpha_f) \dot{\mathbf{v}}_{n+1} + \alpha_f \dot{\mathbf{v}}_n. \quad (3d)$$

For the stabilized index-2 formulation (2), vector  $\mathbf{v}_n$  in (3b) must be replaced by  $\mathbf{v}_n - \mathbf{B}^T(q_n) \boldsymbol{\eta}_n$ , see [1]. The generalized- $\alpha$  method is characterized by its algorithmic parameters  $\alpha_m$ ,  $\alpha_f$ ,  $\beta$  and  $\gamma$  with  $\Delta_\alpha = \alpha_m - \alpha_f$  and considers the equilibrium conditions (1b,c) or (2c,d,e) with  $(q, \mathbf{v}, \dot{\mathbf{v}}, \boldsymbol{\lambda}) \rightarrow (q_{n+1}, \mathbf{v}_{n+1}, \dot{\mathbf{v}}_{n+1}, \boldsymbol{\lambda}_{n+1})$  at  $t = t_{n+1}$ , see [1,3,4].

In general, it is more efficient controlling the step size to improve the result accuracy and to keep the cost low at the same time. In a variable step size implementation of (3), step size  $h$  has to be replaced by  $h_n := t_{n+1} - t_n$  and the time shift of approximation  $\mathbf{a}_n \approx \dot{\mathbf{v}}(t_n + \Delta_\alpha h_{n-1})$  depends now on the *variable* time step size  $h_{n-1} = h_n / \sigma_n$  with the step size ratio  $\sigma_n := h_n / h_{n-1}$ . Therefore, the update formulae (3) have to be modified to guarantee (as before) local truncation errors of size  $\mathcal{O}(h_n^3)$  for second order convergence.

For variable time step sizes, the order conditions may be satisfied by variable algorithmic parameters  $\beta = \beta(\sigma_n)$ ,  $\gamma = \gamma(\sigma_n)$ , see [2], or by substituting  $\mathbf{a}_n \approx \dot{\mathbf{v}}(t_n + \Delta_\alpha h_{n-1})$  in (3) by  $\bar{\mathbf{a}}_n := \mathbf{a}_n + \Delta_\alpha (h_n - h_{n-1}) \dot{\mathbf{a}}_n \approx \dot{\mathbf{v}}(t_n + \Delta_\alpha h_n)$  with an approximation  $\dot{\mathbf{a}}_n$  of  $\dot{\mathbf{v}}(t_n)$ , see [5]. In the present paper, we follow the latter approach and furthermore substitute in the application to the index-3 formulation (1) the velocity coordinates  $\mathbf{v}_n \approx \mathbf{v}(t_n)$  by

$$\bar{\mathbf{v}}_n := \mathbf{v}_n + \mathbf{M}_n^{-1} \mathbf{B}_n (\mathbf{B}_n \mathbf{M}_n^{-1} \mathbf{B}_n^T)^{-1} \mathbf{B}_n (1 - 1/\sigma_n^2) ((1/6 - \beta - \Delta_\alpha/2) h_n^2 \dot{\mathbf{a}}_n + 1/12 \cdot h_n^2 \mathbf{R}_n) \quad (4)$$

to avoid order reduction in the Lagrange multipliers  $\boldsymbol{\lambda}$ , see [1]. In (4) the notations  $\mathbf{M}_n := \mathbf{M}(q_n)$ ,  $\mathbf{B}_n := \mathbf{B}(q_n)$  and  $\widetilde{\mathbf{R}}_n = [\tilde{\mathbf{v}}_n, \dot{\tilde{\mathbf{v}}}_n]$  with the matrix commutator  $[\mathbf{A}, \mathbf{B}] = \mathbf{AB} - \mathbf{BA}$  are used.

For a moderate number of random step size changes with step size ratios  $\sigma_n \in (0.5, 2)$  and spectral radius  $\rho_\infty = 0.8$ , second order convergence may be observed numerically. In Figure 1, the maximal absolute error of a position coordinate is shown in double logarithmic scale for two different Lie group formulations for the benchmark Heavy top [3]. The situation changes drastically if the step size is changed frequently. Rapidly growing numerical solutions and numerical instability are observed systematically, see Figure 2.

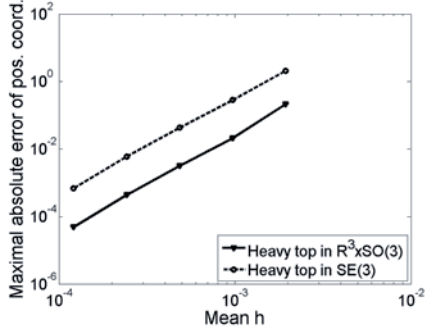


Figure 1: Global error for a small number of step size changes (position coordinates)

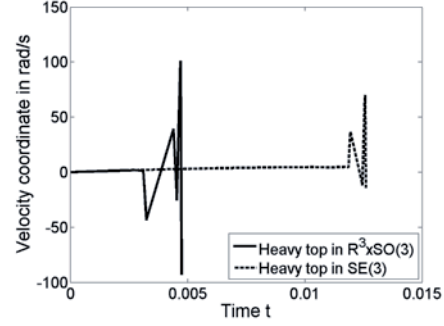


Figure 2: Time history of velocity coordinates for frequent step size changes,  $h_{\text{mean}} = 5 \cdot 10^{-4}$

To study these stability problems analytically, it is observed that the crucial point of the convergence analysis for fixed step sizes ( $\sigma_n \equiv 1$ ) is a contractivity condition for a matrix  $\mathbf{T} = \mathbf{T}(\rho_\infty) \in \mathbb{R}^{3 \times 3}$  with spectral radius  $\rho[\mathbf{T}(\rho_\infty)] = \rho_\infty < 1$ . By a continuity argument, we construct lower and upper bounds  $\underline{\sigma} = \underline{\sigma}(\rho_\infty)$  and  $\bar{\sigma} = \bar{\sigma}(\rho_\infty)$  such that this contractivity condition is satisfied also for variable step size implementations with step size ratios  $\underline{\sigma} \leq \sigma_n \leq \bar{\sigma}$  for all  $n \geq 0$ . Figures 3(a) and 3(b) show such bounds of  $\sigma_n$  for which the stability can always be guaranteed.

In the adaptation of the generalized- $\alpha$  method to variable step sizes an approximation  $\dot{\mathbf{a}}_n \approx \dot{\mathbf{v}}(t_n)$  occurred, which can be obtained by several difference quotients. The two applied approaches are

$$\text{Approach 1: } \dot{\mathbf{a}}_n = \frac{\mathbf{a}_n - \dot{\mathbf{v}}_n}{\Delta_\alpha h_{n-1}} \quad (5a) \quad \text{Approach 2: } \dot{\mathbf{a}}_n = \frac{\mathbf{a}_{n+1} - \mathbf{a}_n}{(\sigma_n + (\sigma_n - 1)\Delta_\alpha)h_{n-1}}. \quad (5b)$$

The bounds for the step size ratios for guaranteed stability become smaller with a bigger spectral radius  $\rho_\infty$ . In general the bounds are very small in the index-3 formulation. The stabilized index-2 formulation is much more robust. These observations are reproduced qualitatively by comprehensive numerical test results.

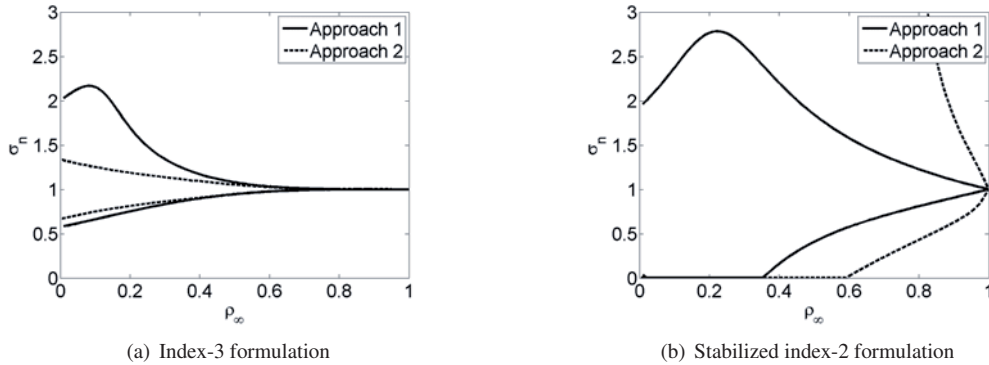


Figure 3: Lower and upper stability bounds of the step size ratios for variable step size changes

## References

- [1] M. Arnold, O. Brüls, A. Cardona. Error analysis of generalized- $\alpha$  Lie group time integration methods for constrained mechanical systems. *Numerische Mathematik*, 129:149-179, 2015.
- [2] O. Brüls, M. Arnold. The generalized- $\alpha$  scheme as a linear multistep integrator: towards a general mechatronic simulator. *Journal of Computational and Nonlinear Dynamics*, 3:041007, 2008.
- [3] O. Brüls, A. Cardona. On the use of Lie group time integrators in multibody dynamics. *Journal of Computational and Nonlinear Dynamics*, 5:031002, 2010.
- [4] J. Chung, G. M. Hulbert. A time integration algorithm for structural dynamics with improved numerical dissipation: The generalized- $\alpha$  method. *Journal of Applied Mechanics, Transactions of the ASME*, 60:371-375, 1993.
- [5] L. O. Jay, D. Negrut. Extensions of the HHT- $\alpha$  method to differential-algebraic equations in mechanics. *Electronic Transactions on Numerical Analysis*, 26:190-208, 2007.

# Towards Higher Order Multi-Symplectic Lie-Group Variational Integrators for Geometrically Exact Beam Dynamics – Avoidance of Shear Locking

Thomas Leitz<sup>1</sup>, Sigrid Leyendecker<sup>2</sup>

<sup>1</sup> Chair of Applied Dynamics  
University of Erlangen-Nuremberg  
Immerwahrstraße 1, 91058 Erlangen, Germany  
[Thomas.Leitz, Sigrid.Leyendecker]@fau.de

## Abstract

In geometrically exact beams dynamics [6], a model of slender structures is used, where the beam is represented by the position of points on the centerline and the orientation of the cross section at each point. In three-dimensional space, a point – comprised of the position and the orientation of the cross section – has six degrees of freedom, similar to a rigid body.

The derivation of higher order Lie-group variational integrators requires the interpolation of two or more points on the beam [1, 2, 4, 5]. Doing this, special care has to be taken in order to avoid shear locking. Since shear locking is independent of the velocity, we restrict ourselves in the following to an elastostatic analysis of the beam without loss of generality.

Shear locking is a phenomenon, that arises in the formulation of the deformation energy density, which is given as

$$U(\Omega, w) = U_1(w) + U_2(\Omega) = \frac{1}{2}(w - e_3)^T C_1 (w - e_3) + \frac{1}{2}\Omega^T C_2 \Omega$$

where  $w - e_3$  and  $\Omega$  are the linear and angular strains, given in the material frame, and  $C_1$  and  $C_2$  are symmetric positive definite matrices representing the linear and angular stiffnesses of the beam. Thereby  $C_1 = \text{diag}(GA, GA, EA)$  and  $C_2 = \text{diag}(EI_1, EI_2, G(I_1 + I_2))$  where  $A$  is the cross section area,  $I_1$  and  $I_2$  are the principal area moments of inertia and  $E$  and  $G$  are Young's modulus and the shear modulus respectively.  $U_1(w)$  is composed of tensile and shear energy and  $U_2(\Omega)$  is composed of bending and torsional energy. For the parametrization of a point on the beam, we use  $x \in \mathbb{R}^3$  for the position and a unit quaternion  $p \in \mathbb{H}^1 = \{p \mid p \in \mathbb{H}, \|p\| = 1\}$  for the orientation of the cross section. The arc-length parameter  $s \in [0, \ell]$  denotes the point in the undeformed configuration and the deformation map is  $\varphi : s \mapsto (p, x)$ . The linear strain then becomes  $w - e_3 = \bar{p}x'p - e_3$ , where  $\bar{p}$  is the conjugate quaternion and  $x' = \frac{dx}{ds}$  is treated as a pure quaternion, i.e. the real part  $\Re(x') = 0$  vanishes. The angular strain is given as  $\Omega = 2\bar{p}p'$ .

The beam is discretized into  $K$  elements and therefore  $K + 1$  nodes. The interpolation between the nodes is done by two different methods A and B, which are compared with respect to shear locking. In the following, the interpolation weights  $W_k$  depend on the parameter  $s$ .

## Interpolation method A

The interpolation between the nodes is done separately for the positions and the orientations. The positions are interpolated by a weighted sum, where the weights can e.g. be Lagrange polynomials. The orientations are interpolated by the normalized weighted sum of the unit quaternions, a.k.a. quaternion linear interpolation (QLERP) [3]. With

$$x(s) = \sum_{k=0}^K W_k(s)x_k \quad p(s) = \frac{P}{\|P\|} \quad \text{with} \quad P = \sum_{k=0}^K W_k(s)p_k$$

the angular strain and  $w$  are

$$\Omega = \frac{2}{\|P\|^2} \sum_{k=0}^{K-1} \sum_{l=k+1}^K (W_k W_l' - W_l W_k') \Im(\bar{p}_k p_l) \quad w = \frac{1}{\|P\|^2} \sum_{k=0}^K \sum_{l=0}^K \sum_{m=0}^K W_k W_l' W_m \Im(\bar{p}_k x_l p_m)$$

## Interpolation method B

The interpolation between the nodes is done using unit dual quaternions  $\tilde{p} = p + \frac{\varepsilon}{2}xp$  where  $\tilde{p} \in \tilde{\mathbb{H}}^1 = \{\tilde{p} \mid \tilde{p} = p_r + \varepsilon p_\varepsilon, \varepsilon^2 = 0, \|\tilde{p}\| = 1\}$  and  $x$  is treated as a pure quaternion. The interpolation is done by the normalized weighted sum of the unit dual quaternions, a.k.a. dual quaternion linear blending (DLB) [3]. Therefore the positions and the orientations are interpolated at the same time. With

$$\tilde{p}(s) = \frac{\tilde{P}}{\|\tilde{P}\|} \quad \text{with} \quad \tilde{P} = \sum_{k=0}^K W_k(s)\tilde{p}_k = P_r + \varepsilon P_\varepsilon$$

the angular strain and  $w$  are

$$\Omega = \frac{2}{\|P_r\|^2} \sum_{k=0}^{K-1} \sum_{l=k+1}^K (W_k W_l' - W_l W_k') \mathfrak{S}(\bar{p}_k p_l) \quad w = \frac{1}{\|P_r\|^2} \sum_{k=0}^{K-1} \sum_{l=k+1}^K (W_k W_l' - W_l W_k') \mathfrak{S}[\bar{p}_k (x_l - x_k) p_l] - \frac{P_r \cdot P_\varepsilon}{\|P_r\|^2} \Omega$$

### Pure bending

Consider a beam – or some part of a beam – of length  $\Delta s$  with the following deformed configuration

$$x(s) = \frac{\Delta s}{\varphi_0} \begin{bmatrix} 1 - \cos \alpha(s) \\ 0 \\ \sin \alpha(s) \end{bmatrix} \quad w = \bar{p} x' p = \begin{bmatrix} 0 \\ 0 \\ 1 \end{bmatrix}$$

$$p(s) = \begin{bmatrix} \cos \frac{\alpha(s)}{2} \\ 0 \\ \sin \frac{\alpha(s)}{2} \end{bmatrix} \quad \Omega = 2 \bar{p} p' = \begin{bmatrix} 0 \\ \frac{\varphi_0}{\Delta s} \\ 0 \end{bmatrix}$$

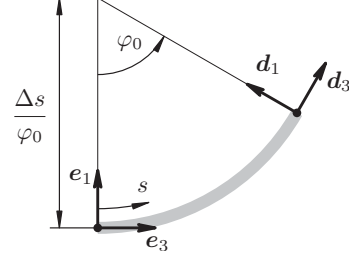


Figure 1: Pure bending

where  $\alpha(s) = \frac{\varphi_0}{\Delta s} s$ , i.e. the beam is bent into a circle without any elongation as depicted in Figure 1. Insertion into the deformation energy yields  $U_1 = 0$  and  $U_2 = \frac{1}{2} E I_2 \left(\frac{\varphi_0}{\Delta s}\right)^2$ , i.e. it is only composed of bending energy.

To compare the two interpolation methods, we insert the positions and orientations as  $x_k$  and  $p_k$  at  $\alpha_k$  into the equations for the strains and since  $P_r = P$ , the angular strain is the same for both methods

$$\Omega_A = \Omega_B = \frac{2}{\|P\|^2} \sum_{k=0}^{K-1} \sum_{l=k+1}^K (W_k W_l' - W_l W_k') \begin{bmatrix} 0 \\ -\sin \frac{\alpha_k - \alpha_l}{2} \\ 0 \end{bmatrix}$$

and represents bending around the  $e_3$ -axis as expected. The difference lies in the linear strain, where

$$w_A = \frac{2}{\|P\|^2} \frac{\Delta s}{\varphi_0} \sum_{k=0}^K \sum_{l=0}^K \sum_{m=0}^K W_k W_l' W_m \begin{bmatrix} -\sin \frac{\alpha_l}{2} \sin \frac{\alpha_k - \alpha_l + \alpha_m}{2} \\ 0 \\ \sin \frac{\alpha_l}{2} \cos \frac{\alpha_k - \alpha_l + \alpha_m}{2} \end{bmatrix}$$

$$w_B = \frac{1}{\|P_r\|^2} \frac{\Delta s}{\varphi_0} \sum_{k=1}^{K-1} \sum_{l=k+1}^K (W_k W_l' - W_l W_k') \begin{bmatrix} 0 \\ 0 \\ 2 \sin \frac{\alpha_l - \alpha_k}{2} \end{bmatrix}$$

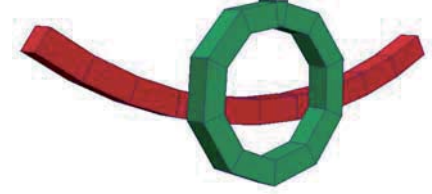


Figure 2: Results of dynamic simulation of method A (red) and method B (green)

The fact, that in  $w_A$  the  $e_1$  component is not equal to zero, is the reason why method A leads to shear locking and method B does not. This result is verified by a dynamics simulation, where a moment  $M_0$  is applied to the beam, which should deform it into a circle. The result is shown in Figure 2 and shows that method A leads to a beam with an unrealistic stiffness. Thus method B is superior and facilitates the derivation of higher order multi-symplectic Lie-group variational integrators for geometrically exact beam dynamics without shear locking.

### References

- [1] François Demoures, François Gay-Balmaz, Marin Kobilarov, and Tudor S. Ratiu. Multisymplectic Lie group variational integrator for a geometrically exact beam in  $R^3$ . *Communications in Nonlinear Science and Numerical Simulation*, 19(10):3492–3512, October 2014.
- [2] James Hall and Melvin Leok. Lie Group Spectral Variational Integrators. *Foundations of Computational Mathematics*, pages 1–59, November 2015.
- [3] Ladislav Kavan, Steven Collins, Jiří Žára, and Carol O’Sullivan. Geometric Skinning with Approximate Dual Quaternion Blending. *ACM Trans. Graph.*, 27(4):105:1–105:23, November 2008.
- [4] T. Leitz, S. Ober-Blöbaum, and S. Leyendecker. Variational integrators for dynamical systems with rotational degrees of freedom. In *11th World Congress on Computational Mechanics (WCCM XI)*, pages 3148–3159, Barcelona, Spain, 2014.
- [5] J.E. Marsden and M. West. Discrete Mechanics and Variational Integrators. *Acta Numerica*, 10:357–514, 2001.
- [6] J Simo. A finite strain beam formulation. The three-dimensional dynamic problem. Part I. *Computer Methods in Applied Mechanics and Engineering*, 49(1):55–70, May 1985.

## **Section**

# **EFFICIENT METHODS AND REAL-TIME APPLICATIONS**



## Real-Time Estimation based on Multibody Dynamics for Automotive Embedded Heterogeneous Computing

Antonio J. Rodriguez<sup>1</sup>, Roland Pastorino<sup>2,3</sup>, Miguel Á. Naya<sup>1</sup>, Emilio Sanjurjo<sup>1</sup>, Wim Desmet<sup>3,4</sup>

<sup>1</sup>Laboratorio de Ingeniería Mecánica  
University of A Coruña  
Mendizábal s/n, 15403 Ferrol, Spain  
antonio.rodriguez.gonzalez@udc.es  
minaya@udc.es  
emilio.sanjurjo@udc.es

<sup>2</sup>Siemens Industry Software NV  
Interleuvenlaan 68, 3001 Leuven,  
Belgium  
roland.pastorino@siemens.com

<sup>3</sup>KU Leuven, Division PMA  
Celestijnenlaan 300B, 3001  
Leuven, Belgium  
roland.pastorino@kuleuven.be  
wim.desmet@kuleuven.be

<sup>4</sup>Member of  
Flanders  
Make

### Abstract

For the last decades, the automotive industry has been improving the ride & handling and the safety of vehicles. Electronic Control Units (ECUs) have extensively contributed to these improvements [1]. Most of these ECUs need information from multiple sensors placed in the vehicle for getting all the information required to execute their control actions. However, in some cases, this information is not available or implies the use of expensive sensors. As an alternative, a state observer based on a model of the vehicle (or part of it) and a reduced number of sensors can be used to create virtual sensors [2, 3, 4] for the missing information required by the ECU. A difficulty linked to this solution is the execution of the state observer and the model of the vehicle in *real-time* on the ECU. Several studies have developed models of some parts of the vehicle or a simplified model of it with state observers for control applications [5-6]. In [2] the multibody model of a complete vehicle with a state observer is executed with good accuracy, but the computational complexity of the simulation was too high to be able to simulate it in *real-time*. Finally, in [7], an indirect state observer is presented and the simulation of a multibody model and its state observer reached *real-time* in an *on-board* CPU. This strategy is promising but the computing hardware used in this research does not correspond to the computational power available in ECUs of commercial vehicles. These Electronic Control Units often have low computational capabilities. However, new heterogeneous processors, embedding *ARM* cores and Field Programmable Gate Array (FPGA), are being used to develop the next generation ECUs. FPGAs are devices than can be fully reprogrammed to fit any application with high performance. ECUs in the automotive industry are mainly used in the execution of control algorithms. The implementation requirements of all the control systems that a vehicle includes, would need a high number of ECUs, which increase the complexity of the network system. For reducing the number of ECUs, powerful heterogeneous processors are chosen to execute these algorithms [8]. Nevertheless, at the date of writing, no approach exists for the use of heterogeneous FPGAs with multibody models.

The aim of this work is to satisfy the requirement of *real-time* implementing an *errorEKF* state observer [7] with a complete multibody model of a vehicle in an embedded heterogeneous processor. For this purpose, the multibody model of a car has been designed for embedded applications using tools previously developed by the authors [9]. The target hardware chosen for this work is the Zynq 7000 AP SoC of *Xilinx*. This System-On-Chip includes an *ARM* processor *Cortex-A9*, with two cores and an FPGA. In order to program the FPGA co-processor, the source code for the numerical computations has to be in the *VHDL* language. The source code has first been written in C/C++ and the translated into *VHDL* using the *Vivado* tool from *Xilinx*.

Different ways can be followed to test the computational efficiency of the implementation of the system (multibody model and observer) in the FPGA. First, the resources consumed in the FPGA must be taken into account: the more parallel the code is, the smaller execution time will be reachable, and the more area of the FPGA will be used. This requires, in case of complex models, to use a bigger FPGA at the expense of additional costs. Another option that is explored in this work is the use of different multibody formulations, which could result in a more efficient implementation. It is necessary to study different options regarding the computing time and consumed resources: execution of the entire multibody model in the FPGA and the state observer in the core of the *ARM* processor, implementation of some parts of the multibody model in the FPGA or execution of some matrix operations in the FPGA.

Preliminary results have been obtained in the simulation of a simple multibody model of a *quarter-car* following these different strategies. The *quarter-car* model was defined in natural coordinates [10], using the penalty formulation and with the trapezoidal-rule as integrator combined with the Newton-Raphson method. A 10 s maneuver has been executed with a time step of 4 ms at the heterogeneous processor.

Regarding to the different possibilities of combining the *ARM* processor with the FPGA, the first option explored was to execute the full model in the FPGA, and it was seen that the available resources of the FPGA were not enough, leading to the partitioning of the model. Two alternative options were compared: implementation of matrix multiplications in the FPGA co-processor or the matrix inversion on FPGA co-

processor. The results are shown in table 1.

**Table 1.** Time of execution of the quarter-car model

<b>Configuration</b>	All model in <i>ARM</i> processor	Matrix Multiplication in FPGA	Matrix Inversion in FPGA
<b>Clock Cycles</b>	1,55E+08	6,28E+08	1,44E+07
<b>Time (s)</b>	0.23	0.94	0.02

As can be seen, simulating the model with the matrix multiplications in the FPGA, leads to an excessive execution time. This could be due to the simplicity of the model, which results in small matrices and, therefore, the multiplication in the FPGA is not a significant computing time improvement, so the communication time makes the multiplication slower. However, the performance of the matrix inversion in the FPGA is substantially better than in the ARM processor, hence the communication times are far less relevant. It can be concluded that when complex models are used, the implementation of both matrix operations should lead to a more efficient and faster simulation.

### Acknowledgments

The support of the Spanish Ministry of Economy and Competitiveness (MINECO) under project TRA 2014-59435-P, cofinanced by the European Union through the EFRD program, is greatly acknowledged.

### References

- [1] E. Sanjurjo, R. Pastorino, P. Gallo, M.A. Naya. Implementation Issues of an on Board Real-Time Multibody Model. *Proceedings of the 3rd Joint Int. Conference on Multibody System Dynamics (IMSD) and 7th Asian Conference on Multibody Dynamics (ACMD 2014)*, 249-250. Busan, Korea, 2014.
- [2] J. Cuadrado, D. Dopico, J. A. Perez, R. Pastorino. Automotive observers based on multibody models and the extended Kalman filter. *Multibody System Dynamics*, Vol. 27, No. 1, pp. 3–19, 2012.
- [3] E. Sanjurjo, J.L. Blanco, J.L. Torres, M.A. Naya. Testing the efficiency and accuracy of multibody-based state observers. *ECCOMAS Thematic Conference on Multibody Dynamics*, Barcelona, Spain, 2015.
- [4] Pastorino, R., Richiedei, D., Cuadrado, J., Trevisani, A. (2013). State Estimation Using Multibody Models and Nonlinear Kalman Filters. *International Journal of non-Linear Mechanics*, 53, 83-90.
- [5] T. Wenzel, K. Burnham, M. Blundell and R. Williams. Dual extended Kalman filter for vehicle state and parameter estimation, *Vehicle System Dynamics*, 44, 153-171, 2006.
- [6] V. Sankaranarayanan et al. Observer Based Semi-Active Suspension Control Applied to a Light Commercial Vehicle. *2007 IEEE/ASME International Conference on Advanced Intelligent Mechatronics*. September 4-7, 2007, Zurich, Switzerland.
- [7] E. Sanjurjo, E. Sinigaglia, M.A. Naya. Multibody-based State Observer for Navigation Applications. *Proceedings of the 4th Joint Int. Conference on Multibody System Dynamics (IMSD 2016)*, a179. Montreal, Canada, 2016-05.
- [8] J. Becker, M. Hubner, G. Hettich, R. Constapel, J. Eisenmann, J. Luka. Dynamic and partial FPGA Exploitation. *Proceedings of the IEEE*, Volume: 95, Issue: 2, Feb. 2007.
- [9] R. Pastorino, F. Cosco, F. Naets, W. Desmet, J. Cuadrado. Hard real-time multibody simulations using ARM-based embedded systems. *Multibody System Dynamics* (2016) 37:127.
- [10] J. García de Jalón, E. Bayo. *Kinematic and Dynamic Simulation of Multibody Systems: The Real Time Challenge*, Springer-Verlag, 1994.

# Index-3 Divide And Conquer Algorithm For Efficient Multibody Dynamics Simulations

Paweł Malczyk<sup>1</sup>, Janusz Frączek<sup>1</sup>, Francisco González<sup>2</sup>, Javier Cuadrado<sup>2</sup>

<sup>1</sup> Institute of Aeronautics and Applied Mechanics  
Faculty of Power and Aeronautical Engineering  
Warsaw University of Technology  
Nowowiejska 24, 00-665 Warsaw, Poland  
[pmalczyk,jfraczek]@meil.pw.edu.pl

<sup>2</sup> Laboratorio de Ingeniería Mecánica  
Escuela Politecnica Superior  
University of La Coruña  
Mendizábal s/n, 15403 Ferrol, Spain  
[f.gonzalez,javicuad]@cdf.udc.es

## Abstract

There has been a growing attention to efficient simulations of multibody systems. This trend is apparently seen in many areas of computer aided engineering and design both in academia as well as in industry. The need for efficient or real-time simulations is readily observed in, e.g.: industrial or space robotics, in automotive industry or in a variety of simulators for mining, construction or crane operations including cables and ropes simulations. Additionally, there are interdisciplinary applications in molecular dynamics in which one can exploit the benefits associated with such simulations. Also hardware-in-the-loop or human-in-the-loop applications require specialized formulations to decrease the turnaround time associated with evaluation of multibody system responses. The real-time multibody simulator is typically connected with virtual reality environments and motion platforms to provide real sensations. Such complex simulation scenarios require better and faster formulations. Parallel computing is one of the approaches to achieve this objective. With the advances in parallel computer architectures equipped with cheap multi-core processors and graphical processor units, researchers pay more attention to the development of parallel algorithms for efficient multibody dynamics simulations.

Recently, the divide and conquer based schemes have attracted significant attention to the development of efficient parallel algorithms for complex multibody dynamics simulations. Various divide and conquer algorithms (DCA) based on Featherstone's original idea [1] are elaborated with a myriad of extensions to include constraint enforcement, rigid-flexible multibody dynamics, non-holonomic constraints, discontinuities in the system definition [2] or exploitation of Hamilton's canonical equations [3], [4]. This paper presents a novel DCA based algorithm for efficient multibody dynamics simulations of complex systems with the prospect for real-time applications. A redundant set of absolute coordinates is used for the system state description, similarly as in [5]. Initially, the algorithm is formulated by using a classical index-3 Lagrangian approach [6]. The resulting set of equations is written at discrete time instants. The trapezoidal rule is exploited as a numerical integrator. The divide and conquer scheme is used for the solution of nonlinear differential-algebraic equations. Figure 1 presents the flowchart of the algorithm. The most computationally intensive parts the formulation are marked as orange boxes. These procedures may be parallelized by using the approach proposed in the paper. The constraint equations for the velocities and accelerations may suffer from violation errors during the simulation. To overcome this difficulty, mass-orthogonal projections at the velocity and acceleration level are used in order to calculate the adjusted state of the system. Again, the projections are performed in a divide and conquer manner.

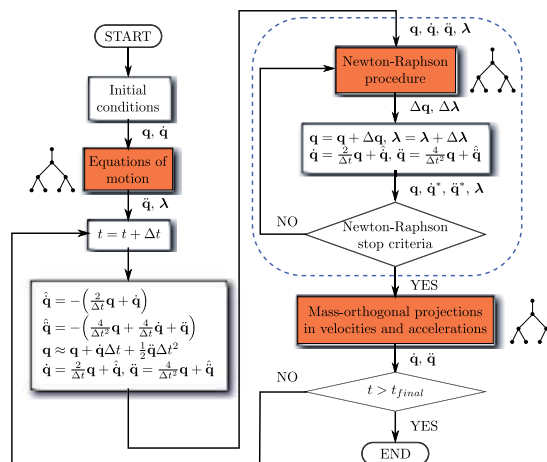


Figure 1: Flowchart of the algorithm. The orange boxes indicate parallelizable parts of the formulation.

Sample multibody system test cases are reported in the paper to indicate overall characteristics of the formulation measured in terms of constraint violation errors and total energy conservation. Figure 2 presents a planar

four-bar mechanism. The system is modeled as a spatial one. If absolute coordinates together with Euler parameters are used, there are 21 generalized coordinates for the three bodies. Since the mechanism possesses one degree of freedom, there must be three redundant constraints. Such over-constrained systems represent a challenge for numerical algorithms. In this situation one has to permanently deal with rank-deficient constraint Jacobian matrices. The existence of redundant constraints might have consequences in non-uniqueness of constraint reactions. Figure 3 presents the performance of the algorithm for the simulation that lasts 300 seconds. The method gives bounded response in terms of constraint violation errors as well as in terms of the total energy conservation. The constraint errors are kept under control. The total energy of the system indicates a small oscillatory behavior with the tendency to marginal energy dissipation. It can be noticed that the proposed formulation handles well the system with redundant constraints, which may repeatedly pass through the neighborhood of singular configuration.

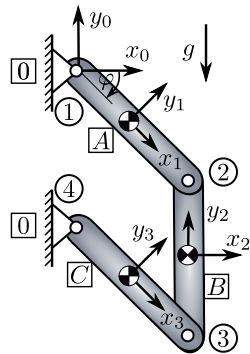


Figure 2: Sample test case. Planar four-bar mechanisms. Joints 1 – 4 are revolute joints.

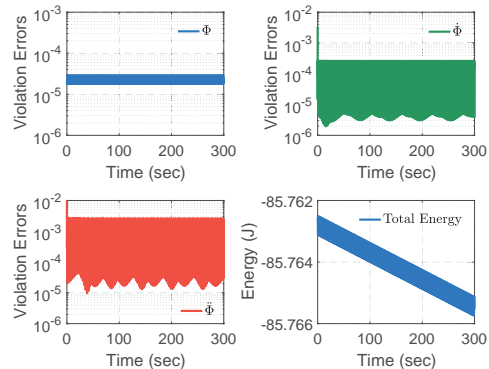


Figure 3: Constraint violation errors and total energy for the four-bar mechanism.

In summary, we propose a unified divide and conquer based formulation for efficient simulation of complex multi-rigid-body systems. The framework is employed on top of the index-3 formulation with mass-orthogonal projections. The trapezoidal rule is embedded into the solution process without the deterioration of the binary-tree structure of the algorithm. The efficiency gains might be obtained for the simulation of large multibody systems, especially those expected in real-time applications. The performance of the simulations might be further diminished by careful implementations on various embedded platforms as well as parallel computers involving multicore processor units or/and graphical processor units.

### Acknowledgments

This work has been supported by the National Science Center under grant no. DEC-2012/07/B/ST8/03993. The third author would like to acknowledge the support of the Spanish Ministry of Economy through its post-doctoral research program Juan de la Cierva, contract No. JCI-2012-12376.

### References

- [1] R. Featherstone. A Divide-and-Conquer Articulated-Body Algorithm for Parallel  $O(\log(n))$  Calculation of Rigid-Body Dynamics. Part 1: Basic Algorithm. *The International Journal of Robotics Research*, 18:867-875, 1999.
- [2] J. Laffin, K. Anderson, I. Khan, M. Poursina. Advances in the application of the divide-and-conquer algorithm to multibody system dynamics. *Journal of Computational and Nonlinear Dynamics*, 9, 2014.
- [3] K. Chadaj, P. Malczyk, J. Frączek. A Parallel Recursive Hamiltonian Algorithm for Forward Dynamics of Serial Kinematic Chains, *IEEE Transactions on Robotics*, 33(3), 2017.
- [4] K. Chadaj, P. Malczyk, J. Frączek. A parallel Hamiltonian formulation for forward dynamics of closed-loop multibody systems. *Multibody System Dynamics*, 39:51-77, 2017.
- [5] P. Malczyk, J. Frączek. A divide and conquer algorithm for constrained multibody system dynamics based on augmented Lagrangian method with projections-based error correction, *Nonlinear Dynamics*, 70:871-889, 2012.
- [6] D. Dopico, F. González, J. Cuadrado, J. Kövecses. Determination of Holonomic and Nonholonomic Constraint Reactions in an Index-3 Augmented Lagrangian Formulation With Velocity and Acceleration Projections. *Journal of Computational and Nonlinear Dynamics*, 9, 2014.

# In-Extensible ANCF Cable Element for Real-Time Simulations

Grzegorz Orzechowski, Aki M. Mikkola

Department of Mechanical Engineering  
Lappeenranta University of Technology  
Skinnarilankatu 34, 53850 Lappeenranta, Finland  
gorzeedu@gmail.com, aki.mikkola@lut.fi

## Abstract

Efficient dynamic analysis of the cable elements is of high demand in many practical applications. Cranes, reeving systems and offshore constructions are examples. Moreover, the rising requirements on human-in-the-loop software that requires real-time computations put even more constraints on computational efficiency of employed formulations. Therefore, it is in high demand to have a cable element formulation that captures the most important dynamical phenomena while offering real-time simulation capability.

The common approach in cable modeling is an approximation based on rigid bodies or physical particles interconnected with string-damper elements. This method has many advantages such as simplicity and reasonable efficiency. However, modern crane and reeving systems may consist of hundreds of meters of cables that require thousands of rigid bodies to obtain a reasonable cable response [1]. Therefore, other techniques are often used, including employment of cable finite elements or semi-analytical approach [2]. One possible solution is the use of absolute nodal coordinate formulation (ANCF). As pointed out in literature, however, ANCF is computationally expensive making it difficult to be used in cable applications. The main objective of this work is to present computational considerations which aims to make ANCF cable elements suitable for real-time.

The ANCF cable used in this work is originally introduced in [3]. The cable element under investigation is a simple two-node element with twelve degrees of freedom. Each node  $i$  has six coordinates  $\mathbf{e}_i^T = [ \mathbf{r}^T \quad \mathbf{r}_{,x}^T ]$  where  $\mathbf{r}$  is a position vector of node  $i$ , and comma indicates the partial derivative with respect to spatial coordinates. As usually for ANCF elements, the mass matrix is constant. More details about kinematic description of the element, including shape functions etc., can be found in work [3]. The virtual work of the elastic forces can be proposed as

$$\delta W = \delta W^a + \delta W^b = \int_0^l EA \varepsilon_x \delta \varepsilon_x dx + \int_0^l EI \kappa \delta \kappa \quad (1)$$

where  $\delta W^a$  and  $\delta W^b$  are components of the virtual work of internal forces produced, respectively, due to axial deformations and bending,  $E$  is Young modulus,  $A$  and  $I$  are cross section area and second moment of cable area, while  $\varepsilon_x = 0.5 (\mathbf{r}_{,x}^T \mathbf{r}_{,x} - 1)$  is axial strain and  $\kappa = |\mathbf{r}_{,x} \times \mathbf{r}_{,xx}| / |\mathbf{r}_{,x}|^3$  is element center-line curvature. Using Eq. (1) the expression for body vector of elastic forces can be easily established.

To make cable element suitable for real-time simulation, it can be assumed to be in-extensible. This assumption will remove the high frequencies that are associated with axial deformation modes. To model in-extensible cable the nonlinear constraint equations are proposed to restrict axial strain to remain zero at element center-line. Thus, one can write an axial strain constraint as

$$C = \mathbf{r}_{,x}^T \mathbf{r}_{,x} - 1 \quad (2)$$

Constraint Eq. (2) should be applied at several points along the element to ensure in-extensibility of the element. In general, five points should be constrained as cable element is described with polynomial of order four. It is worth to note that as all slope vectors in straight and undeformed configuration lies on the common line, more than three constraint equations for single element produces a singular constraint Jacobian matrix. Therefore, Eq. (2) is applied at three points along the element, which is sufficient especially when small deformations are assumed. Constraint equations may be imposed with Lagrange multiplier technique. When axial constraint is applied the axial part of the internal forces is omitted as it should be always equal to zero.

After the verification of cable formulation by employing static and dynamical tests, the simulation for simplified crane is performed. Long, slender structure is connected at one end to moving base and the mass is attached to the second, free end. The cable model is 40 m long with circular cross-section of 5 mm radius. The material properties of steel are assumed, i.e. Young modulus of 200 GPa and density equal to 7810 kg/m<sup>3</sup>. The structure is modeled with four ANCF cable elements and the end mass is considered by introduction of proper entries in body mass matrix (for details consult [4]). The modeled mass is a steel cube with equal sides with total mass of 100 kg, so all its second moment of inertia about main axes are equal to 0.9130 kg·m<sup>2</sup>. The gravity is acting in negative  $x$  direction. The displacement of the base along  $x$  axis  $u_x$  and velocity along  $y$  axis  $v_y$  is defined with a function that reaches maximum value of, respectively, 0.1 m and 0.1 m/s for time  $t \in [2, 3]$  s, while the transients from 0 to maximum for time from 0 to 2 s, and from maximum to 0 for time from 3 to 5 s are modeled smoothly with quarter cycle sine waves. Base movement in  $z$  direction is also constrained.

The simulation is carried out for 10 s motion using Matlab computational package with default solver error tolerances. Four different model variants are considered, all described in Table 1. Two constraint stabilization

Table 1: Model settings and simulation times. Time is taken as an average from seven consecutive simulations.

Name	Matlab Solver	Formulation	Axial Constraints	Time [s]
Model I	ode15s	SI1	no	204.4
Model II	ode15s	SI1	yes	28.9
Model III	ode45	Baumgarte	no	358.6
Model IV	ode45	Baumgarte	yes	3.1

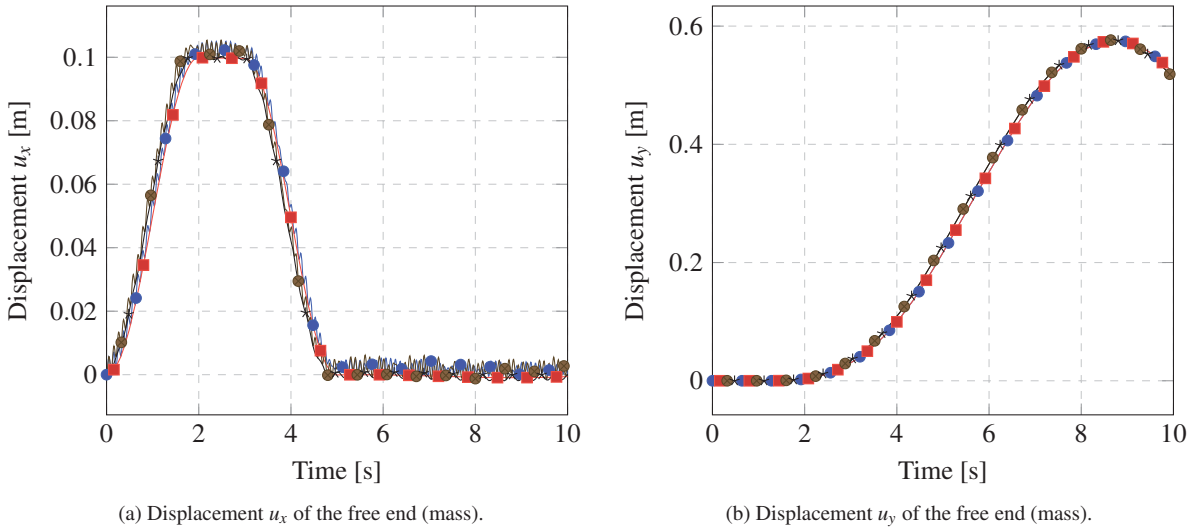


Figure 1: Results for four crane models: model I (—●—), model II (—■—), model III (—●—), model IV (—\*—).

techniques are considered: stabilized index 1 (SI1), and Baumgarte stabilization with parameters  $\alpha = \beta = 20$ . As it can be noticed, the simulation speedup for models with axial constraint included is from 7, in case of SI1 formulation, to almost 116, when Baumgarte stabilization is employed. It also means that the Matlab simulation of simple crane model (version IV) can be run in real time, despite the large overhead introduced by Matlab package.

Figure 1 shows a displacement of the mass attached to the cable free end. It can be seen that displacements of the mass are similar for all models, especially in the direction of y axis. In Figure 1a one can notice the oscillations for models without axial constraints, but they are expected as the simulation does not start at static equilibrium. In addition, for a Baumgarte solution a slight shift of the displacement with respect to SI1 solution can be noticed, while for model IV and displacement  $u_x$  some oscillations are noticeable for simulation time greater than 5 s. These effects are due to inexact fulfillment of the constraints in case of the Baumgarte stabilization.

Presented results indicate that the cable model with constrained axial mode can provide a reasonable solution when small deformations are considered. In addition, the computational speed-up due to axial mode suppression suggest that the ANCF cable element can be employed in real-time analysis of the crane model, especially when Baumgarte stabilization is employed. Presented research is a preliminary study that requires further examination and improvements, mainly to account for a variable length of elements.

## References

- [1] I. García-Fernández, M. Pla-Castells, and R. J. Martínez-Durá. Elevation cable modeling for interactive simulation of cranes. In M. Gross and D. L. James, editors, *Proceedings of the 2008 ACM SIGGRAPH/Eurographics Symposium on Computer Animation*, pages 173–181, Aire-la-Ville, Switzerland, 2008.
- [2] U. Lugrís, J. L. Escalona, D. Dopico, and J. Cuadrado. Efficient and accurate simulation of the rope–sheave interaction in weight-lifting machines. *Proceedings of the Institution of Mechanical Engineers, Part K: Journal of Multi-body Dynamics*, 225(4):331–343, 2011.
- [3] J. Gerstmayr and A. A. Shabana. Analysis of thin beams and cables using the absolute nodal co-ordinate formulation. *Nonlinear Dynamics*, 45(1):109–130, 2006.
- [4] A. A. Shabana. ANCF reference node for multibody system analysis. *Proceedings of the Institution of Mechanical Engineers, Part K: Journal of Multi-body Dynamics*, 229(1):109–112, 2015.

## Study on Model Order Reduction of Flexible Multibody Systems

Kai Luo<sup>1</sup>, Cheng Liu<sup>2</sup>, Qiang Tian<sup>3</sup>, Haiyan Hu<sup>4</sup>

School of Aerospace Engineering  
Beijing Institute of Technology  
5 South Zhongguancun Street, Haidian District, 100081 Beijing, China  
<sup>1,4</sup>[luokai1212, haiyan\_hu]@bit.edu.cn  
<sup>2,3</sup>[liucheng\_bit, tianqiang\_hust]@aliyun.com

### Abstract

The absolute nodal coordinate formulation (ANCF) [1-3] is used for modeling flexible multibody systems (FMBS) with geometrical nonlinearity of both overall motion and large deformation. However, significant computational cost is required when handling systems with a great number of degrees of freedom. In order to improve efficiency, reduced-order models (ROMs) are constructed based on the proper orthogonal decomposition (POD) [4] and Galerkin projection methods for multiple simulations of FMBS. The reduced stiffness matrices and generalized force vectors of ROMs are computed within each finite element via the OpenMP-based parallel technique. Besides, a simple approach for the selection of reduced constraint equations is proposed to deal with the singularity of the coefficient matrices of ROMs. After that, the method for adapting ROMs of pre-computed sampling points to new sets of physical or modeling parameters are presented. The interpolation of reduced-order basis vectors is performed on manifolds to obtain a parametric ROM [5]. Finally, numerical examples are given to validate the effectiveness and efficiency of the proposed model order reduction scheme for FMBS.

The FMBS in this study are modeled by using the finite elements of ANCF [1-3], of which the generalized coordinates contain the global position coordinates and the position gradient coordinates. Consequently, the derived dynamic equations of the system have a constant mass matrix and show no centrifugal and Coriolis forces explicitly. Therefore, the key issue of the present study is to solve efficiently the system dynamics equations, which are Differential Algebraic Equations (DAEs). The DAEs can be further transformed as a set of linear equations as following with the generalized- $\alpha$  method and Newton-Raphson iteration:

$$\begin{bmatrix} \mathbf{K}' & \Phi_q^T \\ \Phi_q & \mathbf{0} \end{bmatrix} \begin{bmatrix} \Delta \mathbf{q} \\ \Delta \lambda \end{bmatrix} = - \begin{bmatrix} \Gamma \\ \Phi \end{bmatrix} \quad (1)$$

where  $\mathbf{K}' = \hat{\beta} \mathbf{M} + (\Phi_q^T \lambda)_q + \mathbf{K}^{int}(\mathbf{q}) - \mathbf{K}^{ext}(\mathbf{q}, \dot{\mathbf{q}}) - \hat{\gamma} \mathbf{F}^{ext}(\mathbf{q}, \dot{\mathbf{q}})_q$ ,  $\Gamma = \mathbf{M} \ddot{\mathbf{q}} + \Phi_q^T \lambda + \mathbf{F}^{int}(\mathbf{q}) - \mathbf{F}^{ext}(\mathbf{q}, \dot{\mathbf{q}})$ .

The POD scheme [4] is performed to compute the reduced-order bases (ROBs) by extracting the solution snapshots (the time series of generalized coordinate increments) from the full-order model of high-fidelity. Then the truncated ROBs are carefully chosen according to the dominant oriented energy of the snapshot data. Afterwards, the ROM is obtained based on the Petrov-Galerkin projection of the full-order model onto the subspace of the ROBs, such that Eq. (1) is rewritten as:

$$\begin{bmatrix} \tilde{\mathbf{U}}^T \mathbf{K}' \tilde{\mathbf{U}} & (\Phi_q \tilde{\mathbf{U}})^T \\ \Phi_q \tilde{\mathbf{U}} & \mathbf{0} \end{bmatrix} \begin{bmatrix} \xi \\ \Delta \lambda \end{bmatrix} = - \begin{bmatrix} \tilde{\mathbf{U}}^T \Gamma \\ \Phi \end{bmatrix} \quad (2)$$

With the pre-computed sets of ROBs, a new set of ROBs with respect to arbitrary parameters in the neighborhood of the sampling ones can be obtained via interpolation. However, direct interpolation of the ROBs cannot guarantee the orthogonality of the constructed ones, which may lead to the breakdown of simulation. Since the ROBs belong to the Grassmann manifold, a manifold interpolation approach [5] can be applied. First, the sampling ROBs are mapped onto a tangent space to the manifold so as to release the orthogonality constraint. Subsequently, the mapped data is interpolated in this space using a preferable univariate or multivariate approximation method. Finally, the interpolated result is mapped back to the original manifold to derive the desired ROBs, and the ROBs is further applied to construction of a new ROM for online simulation.

The case study presents the effectiveness of the proposed method by simulating the dynamics of a flexible double-pendulum system with changes of parameters, including Young's modulus and gravitational acceleration. Figure 1 shows the initial configuration of the double pendulum composed of two beams with square cross-sections.

There involve two uncertain parameters, namely, Young's modulus of the two beams  $E \in [1.0e9 \text{ Pa}, 1.0e10 \text{ Pa}]$  and the gravitational acceleration  $g \in [g_{\text{earth}}/6, g_{\text{earth}}]$  where  $g_{\text{earth}}=9.81 \text{ m/s}^2$ . Other related geometry sizes and the connected relationship between ground and Beam1 and between the two beams are also shown in Fig. 1. The material density and Poisson's ratio are set to be  $1610 \text{ kg/m}^3$  and 0, respectively. Figure 2 a and b show the time histories of  $Y$ -displacement of the tip point C for different models corresponding to the desired parameters  $E$  and  $g$ , respectively. It can be indicated that the dynamics responses computed by the interpolated ROM are in good consistency with those of the full-order model and the directly computed ROM based on POD.

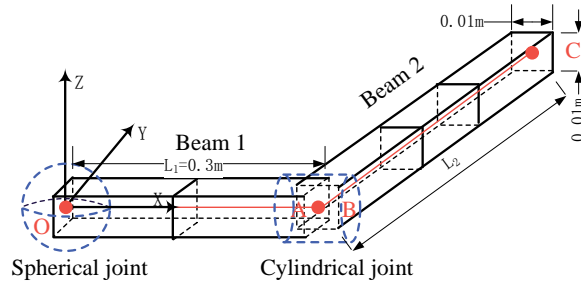


**Figure 1.** Initial configuration of a double pendulum

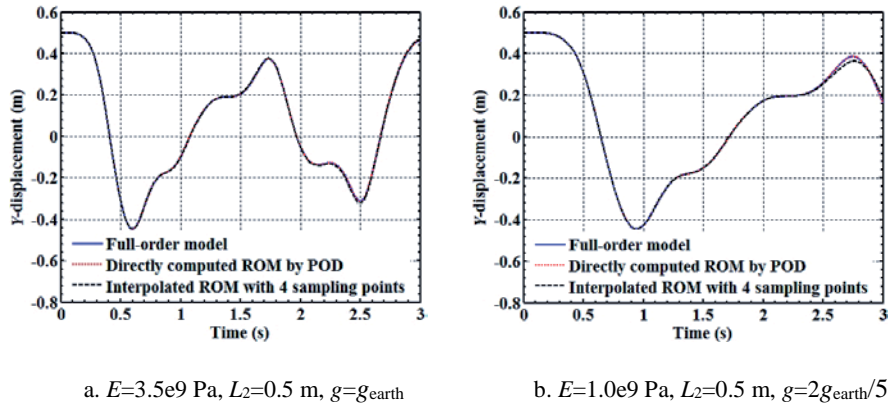


**Figure 2.** Curves of  $Y$ -displacement of tip C with respect to different uncertain parameters

## Acknowledgments

This research was supported by National Natural Science Foundations of China under Grants 11290151, 11221202 and 11302025.

## References

- [1] A. A. Shabana. An absolute nodal coordinates formulation for the large rotation and deformation analysis of flexible bodies. Technical Report, No. MBS96-1-UIC, University of Illinois at Chicago, 1996
- [2] C. Liu, Q. Tian, H. Y. Hu: Dynamics of a Large Scale Rigid-Flexible Multibody System with Composite Laminated Plates. *Multibody System Dynamics*, 26: 283–305, 2011.
- [3] K. Luo, C. Liu, Q. Tian, H. Y. Hu. Nonlinear static and dynamic analysis of hyper-elastic thin shells via the absolute nodal coordinate formulation. *Nonlinear Dynamics*, 85(2): 949-971, 2016.
- [4] G. Kerschen, J. C. Golinval, A. F. Vakakis, L. A. Bergman. The Method of Proper Orthogonal Decomposition for Dynamical Characterization and Order Reduction of Mechanical Systems: An Overview. *Nonlinear Dynamics*, 41(1-3): 147–169, 2005.
- [5] D. Amsallem, C. Farhat. An interpolation method for adapting reduced-order models and application to aeroelasticity. *AIAA Journal*, 46(7): 1803–1813, 2008.

# Constraint reordering for iterative multi-body simulation with contact

Sheldon Andrews<sup>1,2</sup>, Kenny Erleben<sup>3</sup>, Paul G. Kry<sup>1</sup>, Marek Teichmann<sup>2</sup>

<sup>1</sup> McGill University  
Montreal, Canada  
sheldon.andrews@mail.mcgill.ca  
kry@cs.mcgill.ca

<sup>2</sup> CM Labs Simulations, Inc.  
Montreal, Canada  
marek@cm-labs.com

<sup>3</sup> University of Copenhagen  
Copenhagen, DK  
kenny@di.ku.dk

## Abstract

Multi-body simulations with contact are non-smooth systems and wrought with discontinuities which arise due to non-interpenetration and frictional constraints. Linear systems are used for applications where real-time performance is a concern, such as interactive training or video games, which gives rise to a linear complementarity problem (LCP). A common mathematical formulation [5] of the LCP for the velocity-level equations of motion is

$$\underbrace{\mathbf{J}\mathbf{M}^{-1}\mathbf{J}^T}_{\mathbf{A}} \underbrace{\Delta t \boldsymbol{\lambda}}_{\mathbf{z}} + \underbrace{\mathbf{J}(\mathbf{v} + \Delta t \mathbf{M}^{-1} \mathbf{f}_{\text{ext}})}_{\mathbf{b}} = \mathbf{w} \quad (1)$$

$$\mathbf{z}_{\text{lo}} \leq \mathbf{z} \leq \mathbf{z}_{\text{hi}}, \quad \mathbf{w} \perp \mathbf{z},$$

where  $\mathbf{J} \in \mathbb{R}^{m \times n}$  is the Jacobian matrix encoding the non-penetration and friction constraints,  $\mathbf{M} \in \mathbb{R}^{n \times n}$  is the generalized mass matrix,  $\mathbf{v}$  and  $\mathbf{f}_{\text{ext}} \in \mathbb{R}^n$  are the generalized velocities and external forces of simulation bodies, respectively,  $\boldsymbol{\lambda} \in \mathbb{R}^m$  are Lagrange multipliers representing the non-interpenetration normal forces and tangential frictional forces of each contact. The box constraints defined by  $\mathbf{z}_{\text{lo}}$  and  $\mathbf{z}_{\text{hi}}$  contain the lower and upper bound, respectively, of the normal and frictional impulses.

The unilateral and discontinuous nature of the system in Eq.(1) is problematic for many numerical solvers. Previous work has solved the LCP using simplex based pivoting methods, such as Lemke's or the block pivoting approach by Judice and Pires [6]. These methods are able to provide exact solutions to the LCP, but are computationally infeasible for more than several hundred contact constraints. Iterative methods are more prolific for simulations involving a large number of contacts since an approximate solution can be found after only small number of iterations. Where performance is a concern, the algorithm can terminate early once specified error tolerance has been reached, or computational time budget has been exceeded.

Gauss-Seidel and Jacobi based solvers are among the most popular iterative methods for solving LCPs. Notably, the projected Gauss-Seidel (PGS) method [1, 2, 5], which has even been extended to handle non-linear complementarity problems [7]. These solvers are used extensively in computer graphics applications due to their speed, stability, and convergence properties. Briefly, the PGS algorithm works by splitting the lead matrix as  $\mathbf{A} = \mathbf{L} + \mathbf{D} + \mathbf{U}$ , where  $\mathbf{D}$ ,  $\mathbf{L}$ , and  $\mathbf{U}$  are the diagonal, strictly lower triangle, and strictly upper triangle parts of  $\mathbf{A}$ , respectively. The algorithm loops over each variable  $i \in m$  and updates its value at iteration  $k + 1$ , such that

$$\mathbf{z}_i^{k+1} \leftarrow \frac{\mathbf{b}_i - \sum_{j=1}^{i-1} \mathbf{L}_{i,j} \mathbf{z}_j^{k+1} - \sum_{j=i+1}^m \mathbf{U}_{i,j} \mathbf{z}_j^k}{\mathbf{D}_{i,i}}, \quad (2)$$

which is followed by a projection step  $\mathbf{z}_i^{k+1} = \min(\max(\mathbf{z}_{\text{lo}}, \mathbf{z}_i^{k+1}), \mathbf{z}_{\text{hi}})$ . It's obvious by inspection of Eq.(2) that the solution at each fixed-point iteration is dependent on the constraint order. This affects the number of iterations required to find a solution to the LCP, which is important if early termination is required. Furthermore, Stam [4] notes that for iterative solvers, the order in which constraints are solved has an effect on the resulting physical behavior. Likewise, Erleben [5] observes that correct stacking and shock propagation behavior cannot be simulated using standard PGS or Jacobi solvers and proposes a modified algorithm that sequentially solves blocks of contact constraints spatial ordering (e.g., in a bottom up order for stacking).

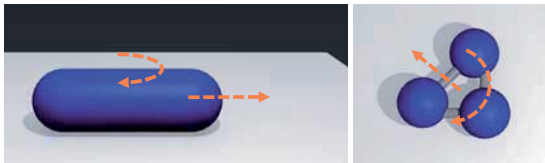


Figure 1: The examples used in our experiments. A capsule (left) and three sphere body (right) slide across a planar surface with an instantaneous angular velocity 1 rad/s and linear velocity of 10 m/s with directions shown as dashed orange arrows. The capsule and three sphere body are simulated using two and three frictional contact constraints, respectively, and coefficient of friction  $\mu = 1.0$ . Each body has a mass of 10 kg.

Our own experiments verify that the constraint order affects rate of convergence. We highlight this by simulating the examples shown in Fig. 1 using the complementarity formulation of [5]. Since the simulations involve only two or three frictional contacts, all possible permutations of constraint equation ordering can easily be evaluated (i.e. there are 720 and 362880 permutations, respectively, for the capsule and three sphere body example). The default constraint ordering is such that if  $j = (i \bmod 3)$  is zero, it corresponds to the non-interpenetration constraint of the  $j$ th contact, and rows  $i + 1$  and  $i + 2$  are the associated friction equations.

The convergence plots for the default, best, and worst orderings are show in Fig. 2. The best ordering converges in less than 20 iterations for both examples. However, for the worst ordering, the error remains high even

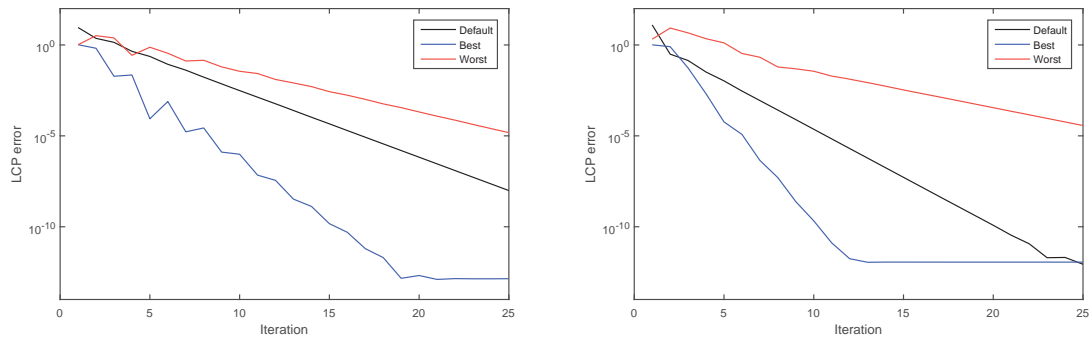


Figure 2: The convergence plots for the sliding capsule example (left) and three sphere body (right). The error at each iteration using the default order of the constraint equations (black) is compared versus the optimal order (blue) and worst case order (red).

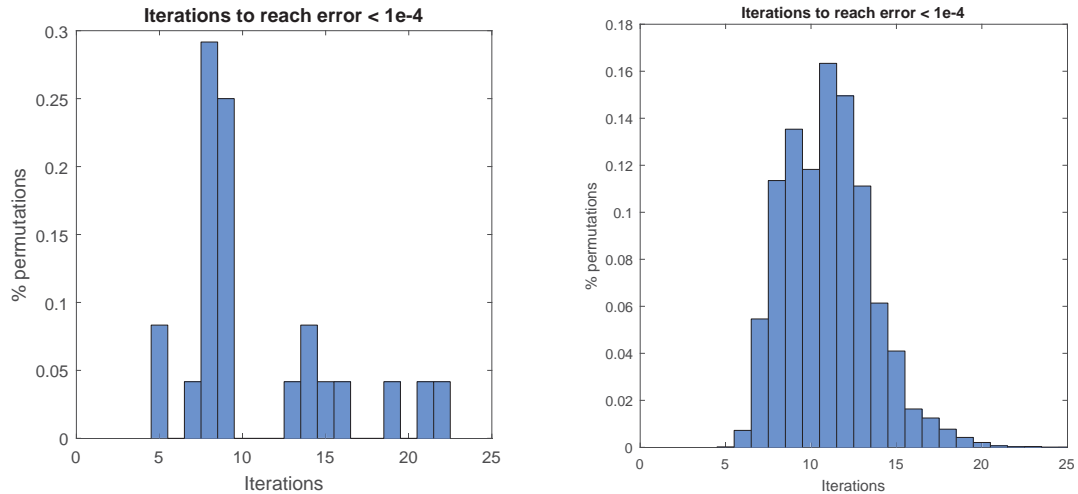


Figure 3: Histograms showing the number of iterations required to reach an error  $< 10^{-4}$  for the sliding capsule (left) and three sphere body (right).

after 25 iterations. Furthermore, as indicated by Fig. 3, there is a large variation in the number of iterations required to reach a reasonable error threshold.

Motivated by these results, our work investigates strategies to accelerate the convergence of iterative solvers for multibody simulation by reordering of the constraint equations. We present an analysis of the following strategies:

- Solving constraint equations in a randomized order;
- Re-ordering constraint equations by heuristics based on the complementarity error and the effective mass;
- Grouping constraint equations and solving for several variables at once by a blockwise PGS.

We investigate the viability of each strategy for a number of rigid body simulation scenarios involving frictional contact and develop heuristics that allow automatic re-ordering, and grouping, of constraint equations to improve solver performance.

## References

- [1] Mangasarian, O.L. (1977). Solution of symmetric linear complementarity problems by iterative methods. *Journal of Optimization Theory and Applications*, 22(4), p. 465.
- [2] Ko, M., and Zowe, J. (1994). An iterative two-step algorithm for linear complementarity problems. *Numerische Mathematik*, 68(1), p. 95.
- [3] Fratarcangeli, M., Tibaldo, V., and Pellacini, F. (2016). Vivace: a practical Gauss-Seidel method for stable soft body dynamics. *ACM Transactions on Graphics (TOG)*, 35(6), p. 214.
- [4] Stam, J. (2009). Nucleus: Towards a unified dynamics solver for computer graphics. In *11th IEEE International Conference on Computer-Aided Design and Computer Graphics*, (p. 1–11).
- [5] Erleben, K. (2007). Velocity-based shock propagation for multibody dynamics animation. *ACM Transactions on Graphics (TOG)*, 26(2), p. 12.
- [6] Júdice, J. J., and Pires, F. M. (1994). A block principal pivoting algorithm for large-scale strictly monotone linear complementarity problems. *Computers and Operations Research*, 21(5), p. 587-596.
- [7] Tasora, A., and Anitescu, M. (2009). A fast NCP solver for large rigid-body problems with contacts, friction, and joints. In *Multibody Dynamics*, pp. 45–55.

## Dynamic Relaxation Method to Determine Equilibrium Configuration of Dynamic Models

Samuel Jung<sup>1</sup>, Tae-Yun Kim<sup>2</sup>, Seul-Gi Yoon<sup>3</sup>, Wan-Suk Yoo<sup>4</sup>

<sup>1</sup>Research Institute of Mechanical Technology  
Pusan National University  
Busan, 609-735, Republic of Korea  
jung401@hanmail.net

<sup>2</sup>School of Mechanical Engineering  
Pusan National University  
Busan, 609-735, Republic of Korea  
tykid76@gmail.com

<sup>3</sup>School of Mechanical Engineering  
Pusan National University  
Busan, 609-735, Republic of Korea  
sgyoon0312@gmail.com

<sup>4</sup>School of Mechanical Engineering  
Pusan National University  
Busan, 609-735, Republic of Korea  
wsyoo@pusan.ac.kr

### Abstract

Most of dynamic models start their simulation from static equilibrium on the ground because of gravity force. When the dynamics system is in static equilibrium, the arrangement of inertia parts is called equilibrium configuration. The equilibrium configuration is so important information that can be used for various purposes for system analysis.

For examples, the form-finding method aims to find the equilibrium configuration of tensegrity structures.[1] In this method, equilibrium configuration is used as a result of simulation in various structures such as airbag design, large building design. And the equilibrium configuration is the most suitable initial condition for the dynamics analysis. In general, the initial conditions for dynamic analysis are set by design drawings or, in simple cases by intuition. The initial conditions selected in these way cause natural responses by gravity. Since this response is independent of the input of interest, unnecessary simulations are performed until static equilibrium is achieved. However, using the equilibrium configuration as an initial condition of the dynamics system, such unnecessary simulation process can be skipped. Thus, finding an equilibrium configuration is an important process in CAE and there are various ways to achieve it.

The most typical methods for finding an equilibrium configuration are dynamic relaxation[2] with kinetic damping.[3] This method produces a damping effect by forcing the velocity to zero when the velocity response reaches the peak as shown in Figure 1.

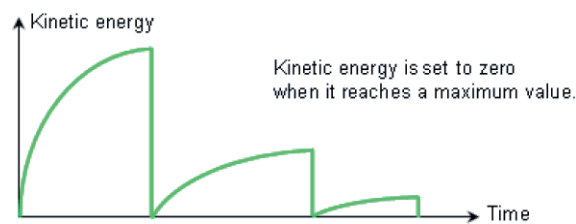


Figure 1. Typical result of kinetic relaxation[4]

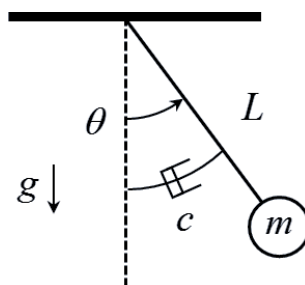
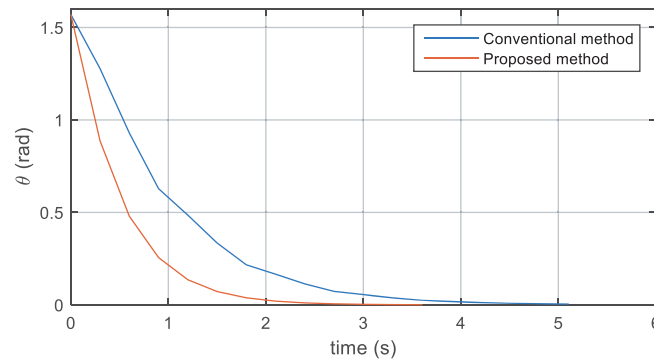


Figure 2. Simple pendulum model

This method ensures a fast convergence rate but the kinetic energy of the system must be measurable.

In this study, the characteristics and advantages and disadvantages of existing methods are analyzed through the verification simulation by using the simple model of Figure 2. We will discuss how to overcome the drawbacks and present various simulation results as shown in Figure 3.



**Figure 3.** Decay comparison for damping conditions

## Acknowledgments

This research was supported by a grant for the project managed by the Agency for Defense Development, "Technology development for rescue robots capable of lifting over 120 kgf", funded by Civil-Military Technology Cooperation Program.

## References

- [1] J. R. Garcia. Numerical study of dynamic relaxation methods and contribution to the modelling of inflatable lifejackets. Université de Bretagne Sud, 2011.
- [2] A. S. Day. An introduction to dynamic relaxation. *Eng.*, 219:218–221, 1965.
- [3] P. A. Cundall. Explicit Finite Difference Methods in Geomechanics. *Numer. Methods Geomech. Blacksbg. VA*, 1976.
- [4] Altair®. RADIOSS User's Guide : Example 16 - Dummy Positioning, 2011.

# Simplification of multibody direct dynamics models by parameter elimination

Javier Ros, Aitor Plaza, Xabier Iriarte

Mechanical, Energy and Materials Engineering Department  
Public University of Navarre  
Arrosadia Campus, 31006 Pamplona-Iruñea  
Navarre, Spain  
[jros, aitor.plaza, xabier.iriarte]@unavarra.es

## Abstract

As the number of applications which require real-time performance increases model order reduction and other simplification techniques have become an important topic in Multibody Dynamics. Most frequently, models are computationally expensive and reaching real-time constraints requires some sort of simplification.

The Lagrange equations of a multibody system can be written as:

$$\mathbf{d}(\mathbf{z}, \dot{\mathbf{z}}, \boldsymbol{\varphi}) = \mathbf{M}_{\mathbf{z}\mathbf{z}}(\mathbf{z}, \boldsymbol{\varphi})\ddot{\mathbf{z}} - \boldsymbol{\delta}_{\mathbf{z}}(\mathbf{z}, \dot{\mathbf{z}}, \boldsymbol{\varphi}) = \boldsymbol{\tau}_{\mathbf{z}} \quad (1)$$

where  $\mathbf{z}$ ,  $\dot{\mathbf{z}}$  and  $\ddot{\mathbf{z}}$  are respectively the sets of independent coordinates, velocities and accelerations,  $\boldsymbol{\varphi}$  is the model dynamic parameters vector,  $\mathbf{M}_{\mathbf{z}\mathbf{z}}$  represents the mass matrix,  $\boldsymbol{\tau}_{\mathbf{z}}$  is the vector of external generalized forces and  $\boldsymbol{\delta}_{\mathbf{z}}$  are the Coriolis, centrifugal and constitutive generalized forces. Equation (1) is not only linear with respect to the independent accelerations, but under some conditions, it can be expressed linearly with respect to the dynamic parameters. Therefore, in their Inverse Dynamics (ID) form, the model equations can be written as:

$$\mathbf{d}(\mathbf{z}, \dot{\mathbf{z}}, \boldsymbol{\varphi}) = \mathbf{K}_{\mathbf{z}\boldsymbol{\varphi}}(\mathbf{z}, \dot{\mathbf{z}}, \ddot{\mathbf{z}})\boldsymbol{\varphi} = \boldsymbol{\tau}_{\mathbf{z}} \quad (2)$$

where  $\mathbf{K}_{\mathbf{z}\boldsymbol{\varphi}}$  is the single instant Observation Matrix.

As exemplified in Equation (2), the ID model can always be written in linear form with respect to the inertial parameters. Friction and other phenomena can frequently be expressed as linear-in-the-parameter generalized forces. Linear-in-the-parameters models should be used if it is desired to preserve the linearity of the ID model with respect to  $\boldsymbol{\varphi}$ .

The goal of the *simplification by parameter elimination* presented here is to reduce the model computational complexity by removing some parameters of  $\boldsymbol{\varphi}$  (and the corresponding columns of  $\mathbf{K}_{\mathbf{z}\boldsymbol{\varphi}}$ ) so that:

$$\mathbf{K}_{\mathbf{z}\boldsymbol{\varphi}_R}(\mathbf{z}, \dot{\mathbf{z}}, \ddot{\mathbf{z}})\boldsymbol{\varphi}_R \approx \mathbf{K}_{\mathbf{z}\boldsymbol{\varphi}}(\mathbf{z}, \dot{\mathbf{z}}, \ddot{\mathbf{z}})\boldsymbol{\varphi} = \boldsymbol{\tau}_{\mathbf{z}} \quad (3)$$

where  $\mathbf{K}_{\mathbf{z}\boldsymbol{\varphi}_R}$  is the reduced single instant Observation Matrix and  $\boldsymbol{\varphi}_R$  is the reduced model parameter vector. As the number of columns of  $\mathbf{K}_{\mathbf{z}\boldsymbol{\varphi}_R}$  is smaller  $\boldsymbol{\tau}_{\mathbf{z}}$  can be computed more efficiently<sup>1</sup>.

For parameter estimation purposes the ID model for a set of  $n$  instants is used, leading to the following set of equations:

$$\mathbf{W}(\mathcal{E})\boldsymbol{\varphi} = \begin{bmatrix} \mathbf{K}_{\mathbf{z}\boldsymbol{\varphi}}(\mathbf{z}^1, \dot{\mathbf{z}}^1, \ddot{\mathbf{z}}^1) \\ \dots \\ \mathbf{K}_{\mathbf{z}\boldsymbol{\varphi}}(\mathbf{z}^n, \dot{\mathbf{z}}^n, \ddot{\mathbf{z}}^n) \end{bmatrix} \boldsymbol{\varphi} = \begin{Bmatrix} \boldsymbol{\tau}_{\mathbf{z}}^1 \\ \dots \\ \boldsymbol{\tau}_{\mathbf{z}}^n \end{Bmatrix} = \boldsymbol{\chi}(\mathcal{E}), \quad (4)$$

where  $\mathbf{W}(\mathcal{E})$  is the so called *Observation Matrix* for the data set  $\mathcal{E} = \{(\mathbf{z}^i, \dot{\mathbf{z}}^i, \ddot{\mathbf{z}}^i, \boldsymbol{\tau}_{\mathbf{z}}^i) \mid i = 1, \dots, n_{\mathcal{E}}\}$ . The previous equation can be seen as a linear regression problem, this in turn suggests to use model selection techniques found on regression bibliography [2, 3] to reduce the number of parameters, and therefore regressors, required to fit the data. This is the inspiration in this work.

Even for a “well exciting” data set  $\mathcal{E}$ , the matrix  $\mathbf{W}$  tends to be rank deficient meaning that linear dependencies between its columns exist. In this context one can reorder the columns of  $\mathbf{W}$  so that  $\mathbf{W}_{\boldsymbol{\varphi}_R}$  are the independent columns and  $\mathbf{W}_{\boldsymbol{\varphi}_E}$  are the dependent ones. Being  $\boldsymbol{\varphi}_R$  and  $\boldsymbol{\varphi}_E$  the parameters that multiply the columns of  $\mathbf{W}_{\boldsymbol{\varphi}_R}$  and  $\mathbf{W}_{\boldsymbol{\varphi}_E}$  respectively, the reduced model can be rewritten as:

$$\boldsymbol{\chi} = [\mathbf{W}_{\boldsymbol{\varphi}_R}, \mathbf{W}_{\boldsymbol{\varphi}_E}] \begin{Bmatrix} \boldsymbol{\varphi}_R \\ \boldsymbol{\varphi}_E \end{Bmatrix} = [\mathbf{W}_{\boldsymbol{\varphi}_R}, \mathbf{W}_{\boldsymbol{\varphi}_R}\boldsymbol{\beta}_R] \begin{Bmatrix} \boldsymbol{\varphi}_R \\ \boldsymbol{\varphi}_E \end{Bmatrix} = \mathbf{W}_{\boldsymbol{\varphi}_R}(\boldsymbol{\varphi}_R + \boldsymbol{\beta}_R\boldsymbol{\varphi}_E) = \mathbf{W}_{\boldsymbol{\varphi}_R}\boldsymbol{\varphi}'_R, \quad (5)$$

where the new parameters set of the model,

$$\boldsymbol{\varphi}'_R = \boldsymbol{\varphi}_R + \boldsymbol{\beta}_R\boldsymbol{\varphi}_E, \quad (6)$$

<sup>1</sup>consider this a convenient form to explain the procedure, for computational reasons the Jacobian  $\mathbf{K}_{\mathbf{z}\boldsymbol{\varphi}_R}$  does not need to be assembled in general, the parameters are directly removed from the symbolic functions involved in the problem setup Eq. 1 (i.e.  $\mathbf{d}(\mathbf{z}, \dot{\mathbf{z}}, \boldsymbol{\varphi}_R) \approx \mathbf{d}(\mathbf{z}, \dot{\mathbf{z}}, \boldsymbol{\varphi})$ )

is the so called *Base Parameter* set [1].

For this parametrization both Direct Dynamics (DD) and ID models can be simplified -without error- to:

$$\mathbf{M}_{zz}(\mathbf{z}, \boldsymbol{\varphi}'_R) \ddot{\mathbf{z}} - \boldsymbol{\delta}_z(\mathbf{z}, \dot{\mathbf{z}}, \boldsymbol{\varphi}'_R) = \boldsymbol{\tau}_z \quad (7a)$$

$$\mathbf{d}(\mathbf{z}, \dot{\mathbf{z}}, \boldsymbol{\varphi}'_R) = \mathbf{K}_{z\boldsymbol{\varphi}_R}(\mathbf{z}, \dot{\mathbf{z}}, \ddot{\mathbf{z}}) \boldsymbol{\varphi}'_R = \boldsymbol{\tau}_z. \quad (7b)$$

It is possible to define an approximate model using an even smaller number of parameters, smaller than the rank of the original  $\mathbf{W}$ . In this case the matrix  $\mathbf{W}_{\boldsymbol{\varphi}_E}$  is approximated by a linear combination of the columns of  $\mathbf{W}_{\boldsymbol{\varphi}_R}$ :

$$\mathbf{W}_{\boldsymbol{\varphi}_E} \approx \mathbf{W}_{\boldsymbol{\varphi}_R} \mathbf{W}_{\boldsymbol{\varphi}_R}^+ \mathbf{W}_{\boldsymbol{\varphi}_E} = \mathbf{W}_{\boldsymbol{\varphi}_R} \boldsymbol{\beta}_R \quad (8)$$

Based on the preceding equation,  $\mathbf{W}\boldsymbol{\varphi}$  can be approximated as:

$$\boldsymbol{\chi} = [\mathbf{W}_{\boldsymbol{\varphi}_R}, \mathbf{W}_{\boldsymbol{\varphi}_E}] \begin{Bmatrix} \boldsymbol{\varphi}_R \\ \boldsymbol{\varphi}_E \end{Bmatrix} \approx [\mathbf{W}_{\boldsymbol{\varphi}_R}, \mathbf{W}_{\boldsymbol{\varphi}_R} \boldsymbol{\beta}_R] \begin{Bmatrix} \boldsymbol{\varphi}_R \\ \boldsymbol{\varphi}_E \end{Bmatrix} = \mathbf{W}_{\boldsymbol{\varphi}_R} (\boldsymbol{\varphi}_R + \boldsymbol{\beta}_R \boldsymbol{\varphi}_E) = \mathbf{W}_{\boldsymbol{\varphi}_R} \boldsymbol{\varphi}'_R, \quad (9)$$

Using the smaller parameter set  $\boldsymbol{\varphi}'_R$  in Eqs. (7), approximate parameter-reduced DD and ID models can be derived. In this context the parameter-reduced model selection problem can be formulated as follows:

“Given a dynamic model with a known parameter set determine a minimal set of parameters of the model that approximate the characteristic model data with the desired accuracy.”

Two important issues remain to be solved in this problem: *a)* how to select the specific parameters that will be part of the reduced model and *b)* how to define an error criterion to choose one combination of parameters over another.

In order to solve the first issue, due to the enormous complexity of the problem, three candidate-model selection heuristics are proposed in this work: QR decomposition, Backward Elimination and Forward Selection [2, 3]. These heuristics do not assure the determination of the optimum reduced-parameter set, for a given number of parameters ( $< \text{rank}(\mathbf{W})$ ), but provide a *good* compromise between precision and computation time.

For the second issue the norm of an error vector is used as the objective function to be minimized. If one is focused on obtaining a parameter-reduced ID model, the norm of the difference between the actual external forces and their model based estimation can be used. On the other hand, if the focus is on simplifying the DD model, the norm of the difference between the accelerations calculated with the full and the parameter-reduced model seems appropriate. We propose to use these errors normalized as follows:

$$\varepsilon_{\boldsymbol{\tau}_z}(\boldsymbol{\varphi}_R, \mathcal{E}) = \frac{\|\text{col}({}^i\boldsymbol{\tau}_z - {}^i\boldsymbol{\tau}_{zR}(\mathcal{E}))\|}{\|\text{col}({}^i\boldsymbol{\tau}_z)\|} \quad (10a)$$

$$\varepsilon_{\ddot{\mathbf{z}}}(\boldsymbol{\varphi}_R, \mathcal{E}) = \frac{\|\text{col}({}^i\ddot{\mathbf{z}} - {}^i\ddot{\mathbf{z}}_R(\mathcal{E}))\|}{\|\text{col}({}^i\ddot{\mathbf{z}})\|} \quad (10b)$$

where the operator  $\text{col}(S)$  arranges the elements of  $S$  into a column and  ${}^i\boldsymbol{\tau}_{zR}$  and  ${}^i\ddot{\mathbf{z}}_R$  are the forces and independent accelerations for the  $i$ -th data sample in  $\mathcal{E}$ , calculated based on the reduced model parameters.

In a previous work [4] the force-based criterion has been used for the determination of ID parameter-reduced models. In this work the above defined acceleration-based error criterion will be used to measure the parameter-reduced model quality.

The reduction algorithm is applied to a 6-DOF serial and a 6-DOF parallel manipulator. The results show that very significant computational savings can be achieved with a very small approximation error. To be fair, these savings are demonstrated over the very efficient symbolical implementation of order 3 recursive formulations, and measured in terms of the number of operations.

## References

- [1] GAUTIER, M. Numerical calculation of the base inertial parameters of robots. *Journal of Robotic Systems* 8, 4 (1991), 485–506.
- [2] MILLER, A. J. *Subset selection in regression*. Chapman and Hall, 1990.
- [3] MYERS, R. *Classical and modern regression with applications*. PWS-KENT Publishing Company, 1990.
- [4] X. IRIARTE, J. ROS, V. MATA, A. PLAZA. *Multibody model reduction by parameter elimination*. ECCOMAS, Multibody Dynamics 2015. Barcelona, 2015.

# Comparative Analysis about High DOF Model and Low DOF Model of Rescue Robot

Tae-Yun Kim<sup>1</sup>, Samuel Jung<sup>2</sup>, Wan-Suk Yoo<sup>3</sup>

<sup>1</sup>School of Mechanical Engineering  
Pusan National University  
Geumjung-gu, Busan 609-735, Korea  
tykid76@gmail.com

<sup>2</sup>School of Mechanical Engineering  
Pusan National University  
Geumjung-gu, Busan 609-735, Korea  
jung40L@hanmail.net

<sup>3</sup>School of Mechanical Engineering  
Pusan National University  
Geumjung-gu, Busan 609-735, Korea  
wsyoo@pusan.ac.kr

## Abstract

Rescue robots had been developed in accordance with the tendency of unmanned combat systems for combat minimizing human loss. A rescue robot rescues injured soldiers in inaccessible areas, such as buildings that have been destroyed by bombing or places where toxic chemicals have leaked. Rescue robot is operated in the field or on the rough road. That is, since a rescue robot runs on the rough road, the risk of overturning and the impact on an injured person can be exerted. In addition, the rescue robot is operated by remote control using only limited vision information, so it is difficult to respond quickly to dangerous situations. This can't guarantee the stability of the rescue robot and patients.

Therefore, in order to pursue the stability of such the robot, an algorithm capable of supporting an operator's speed control is needed. It is possible to apply the limited speed determination technique through the real-time simulated driving. This algorithm is a technique for calculating the predicted response by running the road surface data obtained from the sensor in advance and estimating the safe speed that does not exceed the patient's limit response from the predicted response. In order to perform such an algorithm, a dynamic model capable of real-time analysis is needed. A rescue robot can be modeled as a multi-body system using several bodies, joints, and springs as shown in Figure 1.

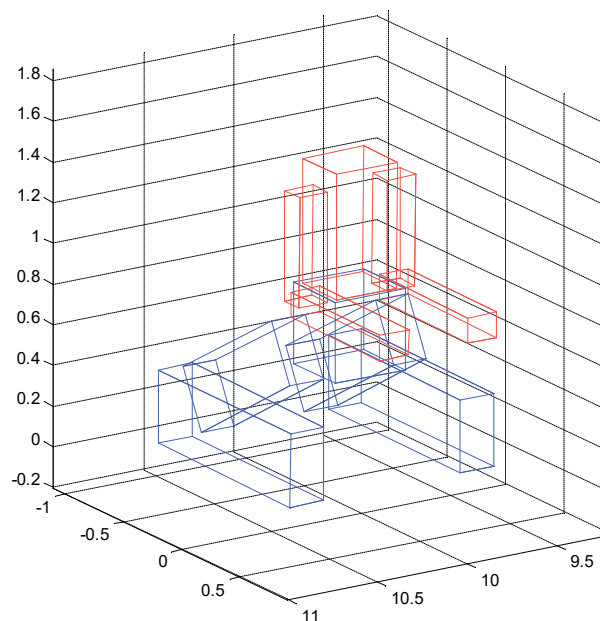


Figure 1. Multibody system of Rescue robot

The body, arms, legs and each joint position are made of revolute joints and can maintain the attitude of the robot through force control or rotary spring force at the joint position. The actual robot is controlled by the motor in the joint. However, reflecting the motor control to the dynamic analysis to reflect the characteristics of the actual robot has an adverse effect on the real-time analysis. It is also difficult to select specific rotary spring characteristics of each joint position due to motor control. It is impossible to model a reliable dynamic model with all degrees of freedom (DOF) maintained. Therefore, it is necessary to simplify model using only the position and inertia information of each body. Therefore, it is necessary to simplify the model to low DOF model using only the position and inertia information of each body.

In this paper, we verify the validity of the low DOF model by comparing the frequency and time domain responses for the high DOF model and low DOF models.

### **Acknowledgments**

This research was supported by a grant for the project managed by Agency for Defense Development, "Technology development for rescue robots capable of lifting over 120 kgf", funded by Civil-Military Technology Cooperation Program.

### **References**

- [1] Y. S. Jung. Development of Velocity Decision Algorithm for Autonomous Driving of Unmanned Ground Vehicle in Roughness Terrain, *M. S. thesis*, Pusan National University, Busan, 2011.
- [2] S. S. Kim, M. J. Vanderploeg. A State Space Formulation for Multibody Dynamic Systems Subject to Control, *Technical Report*, No. 84-20, 1984.
- [3] M. K. McCullough, E. J. Haug. Terra-dynamics of High Mobility Track Vehicles, *Technical Report*, Iowa, 1985.

# Performance Aspects of Real-Time Capable Flexible Multibody Simulations

Alexander Schmitt<sup>1</sup>, Robert Seifried<sup>1</sup>

<sup>1</sup> Institute of Mechanics and Ocean Engineering  
Hamburg University of Technology  
Eissendorfer Strasse 42, 21073 Hamburg, Germany  
[a.schmitt, robert.seifried]@tuhh.de

## Introduction

Real-time capable simulation models are becoming increasingly more important in development of lightweight structures and machines, e.g. for modern road vehicle development. The scope of application includes driver-in-the-loop simulation environments, test benches for electronic control units and control algorithms. However, current real-time capable simulation technologies usually neglect elastic deformations occurring in lightweight components.

To investigate the real-time capabilities of various modeling and integration options for flexible multibody systems, a real-time capable vehicle model including a flexible car body has been set up [1]. The flexible car body is thereby based on a high-detail finite element model and reduced to a low number of elastic coordinates using model order reduction technologies. This model features several challenges: The flexible car body is modeled as a free body with attached suspension parts which provide the connection to the environment. A vehicle suspension is considered as numerically stiff, since the ratio between suspension stiffness and suspension mass is high. In addition, due to the suspension kinematics each suspension yields to kinematic loops and hence additional algebraic equations have to be considered in the multibody system formulation, resulting in differential algebraic equations (DAE).

This work focuses on the performance enhancements feasible within the real-time simulation of such stiff flexible multibody systems. Since higher accuracy can be achieved when using a larger number of elastic degrees of freedom, faster and more efficient integration procedures are necessary. The investigated aspects include the use of various solvers, stabilization methods and efficient kinematics calculations.

## Modeling of a Real-Time Capable Flexible Multibody Simulation

Real-time capable simulation requires the calculation time of the equations of motion (EOM) to be known in advance. Fixed-step Runge-Kutta solvers can be used to solve the EOM in real-time if the system is formulated in minimal coordinates. However, kinematic loops require either additional iterative processes or calculation of the algebraic equations on acceleration level. In this research the flexible multibody simulation has been formulated in redundant cartesian coordinates instead of minimal coordinates. The cartesian position and velocity coordinates  $\mathbf{z}_I$  and  $\mathbf{z}_{II}$  respectively are defined for each body and the EOM are written as

$$\begin{aligned}\dot{\mathbf{z}}_I &= \mathbf{K}(\mathbf{z}_I) \mathbf{z}_{II} \\ \mathbf{M}(\mathbf{z}_I) \dot{\mathbf{z}}_{II} &= \mathbf{f}_a(\mathbf{z}_I, \mathbf{z}_{II}) - \mathbf{G}(\mathbf{z}_I)^T \boldsymbol{\lambda} \\ \mathbf{g}(\mathbf{z}_I) &= \mathbf{0}\end{aligned}\quad (1)$$

with the kinematic matrix  $\mathbf{K}$ , mass matrix  $\mathbf{M}$ , vector of applied forces  $\mathbf{f}_a$  and the constraint equations  $\mathbf{g}$ . The constraint equations are included in the EOM with their Jacobian  $\mathbf{G} = \frac{\partial \mathbf{g}}{\partial \mathbf{z}_I} \mathbf{K}$  and the Lagrange multipliers  $\boldsymbol{\lambda}$ .

For the case of an flexible multibody system and using the floating frame of reference method [2],  $\mathbf{z}_I$  and  $\mathbf{z}_{II}$  contain the rigid body coordinates of the floating frame as well as the elastic coordinates. This method is applicable to a vehicle dynamics simulation since the elastic deformations of a car body remain small compared to the overall motion of the vehicle itself.

The system of differential-algebraic equations is of index 3. By differentiation of the algebraic equations  $\mathbf{g}$  an index-2 formulation can be obtained. Solving a DAE-system usually requires iterative processes, whose calculation time is unknown in advance. However, non-iterative processes like the linear-implicit Euler-method [3] exist for solving index-2 DAE, which have been proven to be applicable for real-time capable flexible multibody simulations [1].

## Performance Aspects

For an efficient evaluation of the possible performance improvements, all major calculation steps during the integration cycle have to be evaluated. An overview of the performance-critical calculations analyzed in this work are shown in Figure 1. They include the evaluation of the kinematics and force calculation as well as the integration process itself.

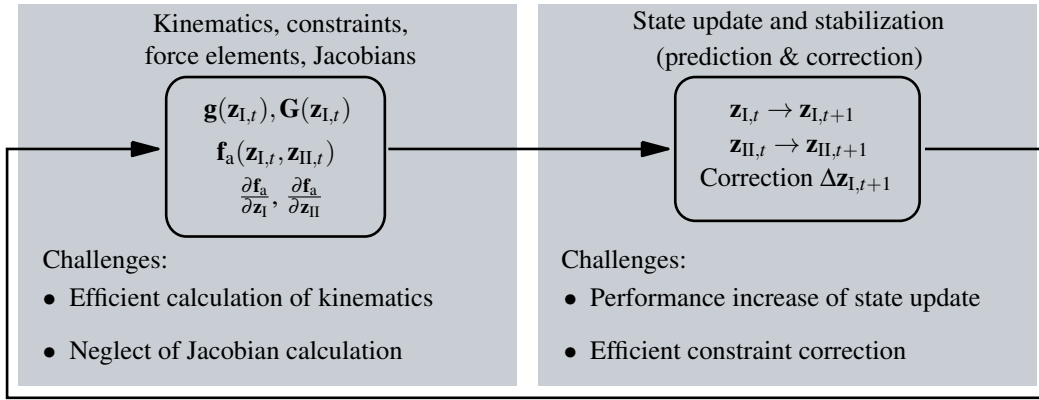


Figure 1: Performance options within the integration cycle

Linear-implicit Runge-Kutta methods require the calculation of the Jacobian matrices of all applied forces, which can be calculated either numerically or analytically. Calculation of Jacobians is very time consuming and calculating the exact Jacobian is often not necessary. Hence significant performance increase can be achieved by reducing the number of Jacobian evaluations or by neglecting certain parts of the Jacobians. Negligible components are usually changing slowly in time, for example it can be shown that this is true for some components of inertial forces or elastic forces. Other parts may be kept constant during time integration and hence can be calculated in advance, e.g. the Jacobians of some components of tire and suspension forces.

The kinematics of the points on an flexible body depend in general upon all elastic degrees of freedom, which yields a high computational effort for evaluating constraint equations and computing forces acting on a body. However, the kinematics may be calculated with less effort by using lower-order approximations of the elastic deformations.

Besides the linear-implicit Euler method, multi-stage methods of the group of W-solvers have been shown to be suitable for real-time vehicle dynamics simulation and show higher accuracy [4]. Methods with higher accuracy can be used at a larger integration step size, hence the additional calculation effort may be compensated and yield a performance increase.

Since the constraint equations of eq. (1) are only considered on velocity level by using the index-2 formulation, the position constraints  $\mathbf{g}$  have to be corrected after the integration process. Stabilization methods like the Baumgarte stabilization or GGL-formulation are suitable for this purpose. In [1] a mass-based projection method has been used to correct the constraints. Since in these simulations elastic deformations remain small compared to rigid body movement, the influence of stabilizing elastic coordinates on the simulation result are evaluated.

## The Vehicle Model

The vehicle simulation is set up in MATLAB/Simulink, which provides code generation tools for real-time targets and hence can be used to compare the performance of the suggested methods. It is equipped with the empirical MF-tire model and road model OpenCRG to provide a low-cost real-time capable connection of the vehicle model to the environment. The flexible car body itself is adopted from a frontal crash simulation model of a 2nd generation Ford Taurus and reduced with the Craig-Bampton method. The suspension is realized as McPherson suspensions at all four wheels, identical to the real car, consisting of two kinematic loops at each wheel. Overall, the vehicle model consists of nine bodies including the car body with 72 elastic coordinates.

## References

- [1] Schmitt, A.; Seifried, R.: Comparison of various models and integration method for real-time simulation of complex vehicle models with structural flexibility. In Proceedings of ISMA2016 International Conference on Noise and Vibration Engineering. 2016.
- [2] Schwertassek, R.: Dynamik flexibler Mehrkörpersysteme. Braunschweig [u.a.]: Vieweg, 1999.
- [3] Hairer, E.; Wanner, G.: Solving Ordinary Differential Equations II: Stiff and differential-algebraic problems. Berlin u.a.: Springer, 2., rev. ed., corrected 2. printing Edn., 2002.
- [4] Arnold, M.; Burgermeister, B.; Eichberger, A.: Linearly implicit time integration methods in real-time applications: DAEs and stiff ODEs. Multibody System Dynamics, Bd. 17, Nr. 2-3, S. 99–117, 2007.

## **Section**

# **PARALLELIZATION METHODS**



# Elimination Method for Parallelization of Flexible Multibody System Dynamics

Michael Valasek, Ladislav Mraz

Faculty of Mechanical Engineering  
Czech Technical University in Prague  
Technicka 4, 16607 Praha 6, Czech Republic  
Michael.Valasek@fs.cvut.cz

## Abstract

The most effective methods for the parallel multibody dynamics solution are the ones with the logarithmic complexity usually based on the Divide and Conquer (DAC) algorithm [1, 2, 3]. The paper describes the extension of the procedure [6] towards the parallelized dynamic solution of flexible multibody system. The method is based on the modified state space and the efficient set of natural coordinates [4] and modal coordinates for the description of the deformation in the system. The the equation of motion for single body  $i$  is derived as

$$\mathbf{M}_i \ddot{\mathbf{s}}_i + \mathbf{K}_i \mathbf{s}_i = \mathbf{Q}_i \quad (1)$$

where  $\mathbf{M}_i$  is the mass matrix,  $\mathbf{K}_i$  is the stiffness matrix and  $\mathbf{Q}_i$  is the vector of generalized forces. Using the procedure described in [5] exploiting the Schur complement the resulting system of equations of motion (EOM) is obtained

$$\mathbf{M} \dot{\mathbf{s}} + \mathbf{J}^T \boldsymbol{\mu} = \mathbf{p}^* \quad (2)$$

$$\mathbf{J} \dot{\mathbf{s}} = -\alpha \mathbf{f}(\mathbf{s}) \quad (3)$$

where  $\mathbf{M}$  is the diagonal mass matrix,  $\mathbf{J}$  is the Jacobi matrix corresponding to the constraints  $\mathbf{f}$ ,  $\alpha$  is the coefficient of the Baumgarte stabilization,  $\mathbf{s}$  is the vector of natural coordinates describing the absolute system position,  $\mathbf{p}^*$  is the modified momentum of the system and  $\boldsymbol{\mu}$  is the vector of the new Lagrange multipliers. Expressing  $\dot{\mathbf{s}}$  from (2) and substituting into (3) the resulting system for unknown  $\boldsymbol{\mu}$  is obtained

$$\mathbf{J} \mathbf{M}^{-1} \mathbf{J}^T \boldsymbol{\mu} = \alpha \mathbf{f}(\mathbf{s}) + \mathbf{J} \mathbf{M}^{-1} \mathbf{p}^* \quad (4)$$

which can be simply written as follows

$$\mathbf{A} \boldsymbol{\mu} = \mathbf{b} \quad (5)$$

The system of equations (5) is sparse, symmetric, positive definite with band structure for the case of a simple kinematic chain (Fig. 1 a). The system (4) has a structure of blocks (Fig. 1 b) corresponding to particular bodies with equivalent (small) sizes.

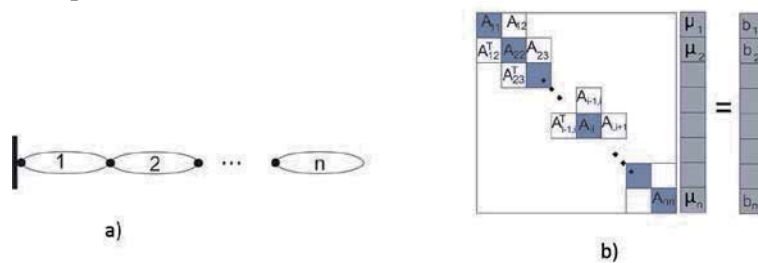


Figure 1 a): The simple kinematic chain b) The resulting matrix-structure

Thus the whole system of the equations can be understood as a set of the interconnected subsystems representing by the blocks for unknown vectors  $\boldsymbol{\mu}_i$ . Based on the comparison of the application of elimination process and Cholesky decomposition the combination of both approaches has been proposed [5]. The result is the efficient combination of elimination process and Cholmod procedure (Fig.2). This combination has been investigated for the small blocks (9x9). In the case, that the 9x9 division is used and there are not enough processors for the matrix transformations, the process is following. The number

of subsystems  $n_s$  for elimination is the same as the number of bodies  $n$ . The number of processors  $n_p$  is smaller than  $n$ . Therefore it is possible to evaluate only  $n_p$  elimination in parallel on one elimination level and the rest has to be carried out after that.

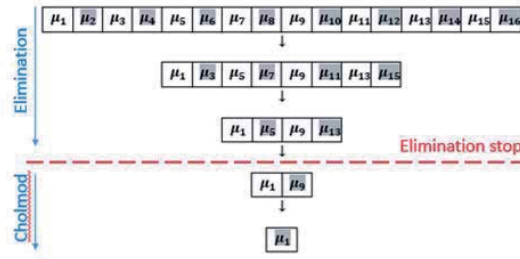


Figure 2: Efficient combination of the elimination with the Cholesky decomposition

It is obvious, that the system of equations (5) can be split into the sub-blocks which number corresponds to the number of processors ( $n_s = n_p$ ). However, it is always better from the complexity point of view to split the system in that way, that the number of sub-blocks corresponds to the number of particular bodies in the kinematical system ( $n_s = n$ ). Thus the optimal elimination process is obtained, see Fig. 3. The complexity of the solution is depicted for both the cases with different factors  $K = \frac{n}{n_p}$  representing the relation between number of bodies in the multibody system and the number of processors.

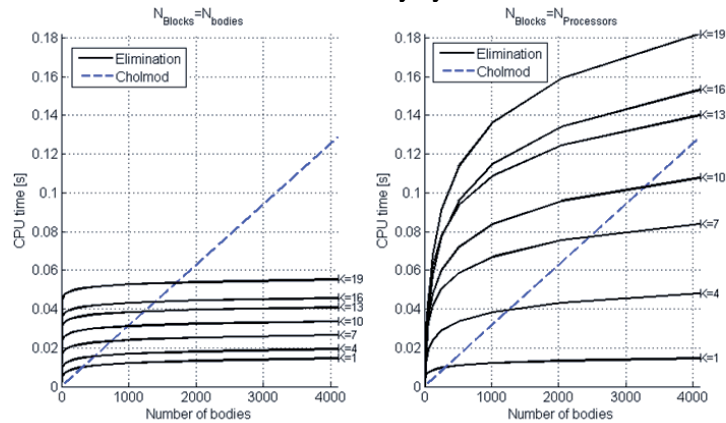


Figure 3: Comparison of the optimal and non-optimal system division

The resulting computational complexity is very promising. The elimination procedure is applied only to the computation of reaction forces (5) and the local equations of motion (1) are solved completely independently on parallel processors without any constraints between the processors.

## References

- [1] R. Featherstone. A Divide-and-Conquer Articulated-Body Algorithm for Parallel  $O(\log(n))$  Calculation of Rigid-Body Dynamics. Part 1: Basic Algorithm. *Int. J. Robotics Research*, vol. 18, no. 9, pp. 867–875, 1999.
- [2] R. Featherstone. A Divide-and-Conquer Articulated-Body Algorithm for Parallel  $O(\log(n))$  Calculation of Rigid-Body Dynamics. Part 2: Trees, Loops and Accuracy. *Int. J. Robotics Research*, vol. 18, no. 9, pp. 876–892, 1999.
- [3] M. Poursina, K. S. Anderson. An extended divide-and-conquer algorithm for a generalized class of multibody constraints. *Multibody Syst Dyn*, vol. 29, no. 3, pp. 235–254, 2013.
- [4] M. Valasek, Z. Sika, O. Vaculin. Multibody formalism for real-time application using natural coordinates and modified state space. *Multibody System Dynamics*. 17(2–3), 209–227 (2007)
- [5] M. Valasek, L. Mraz, Parallelization of Multibody System Dynamics by Additional Dynamics, *ECCOMAS Multibody Dynamics 2013*, 1-4 July, 2013, University of Zagreb, Croatia
- [6] Mraz, L., Valasek, M, The Logarithmic Complexity Procedure for Parallel Multibody Dynamics Solution, *ECCOMAS Multibody Dynamics 2015*, June 29- July 2, 2015, University of Barcelona, Spain

# A co-simulation framework for high-fidelity simulation of vehicle-terrain interaction

Radu Serban<sup>1</sup>, Antonio Recuero<sup>2</sup>, Nicholas Olsen<sup>1</sup>, Dan Negrut<sup>1</sup>

<sup>1</sup> Department of Mechanical Engineering  
University of Wisconsin-Madison  
Madison, WI 53706, USA  
[serban,nicholas.olsen,negrut]@wisc.edu

<sup>2</sup>The Goodyear Tire & Rubber Co  
200 Innovation Way, Akron, OH 44316, USA  
antonio\_recuero@goodyear.com

## Abstract

Assessing the mobility of off-road vehicles is a complex task that most often falls back on semi-empirical approaches to quantify the tire-terrain interaction. Herein, we present an open-source ground vehicle mobility analysis simulation framework called Chrono [1], which uses physics-based models of the vehicle, tires, and terrain to factor in both tire flexibility and terrain deformation. The tires are modeled using a nonlinear finite element approach that involves layers of orthotropic shell elements. The soil is represented as a large collection of rigid elements that mutually interact through contact, friction, and cohesive forces. The vehicle, which is a high-fidelity, template-based model that incorporates suspension, steering, driveline, and powertrain models, is driven through driver inputs to the appropriate subsystems.

A deformable-terrain vehicle mobility analysis in Chrono leads to a multi-physics, multi-scale problem in several millions degrees of freedom. To solve this and similar problems arising in multibody dynamics, finite element analysis, and granular dynamics, Chrono leverages parallel computing at several levels: (i) x86-AVX acceleration; (ii) multi-core, shared memory OpenMP; (iii) GPU-based parallel computing using CUDA; and, (iv) distributed parallel computing via MPI. Specifically, the nonlinear FEA component, which is computationally taxing when evaluating the tire internal force and Jacobian, is accelerated with OpenMP directives. Granular dynamics, including both the collision detection phase and the numerical solution of the discretized equations of motion, can be performed in parallel either on the GPU, or in a multi-core shared-memory OpenMP fashion, or else in a distributed MPI framework.

Chrono is designed in a modular fashion around a modeling and computational core which provides full support for modeling, simulation, and visualization of multibody systems. The optional modules (i) provide domain-specific support, e.g., (Chrono::FEA for finite element analysis, Chrono::FSI for computational fluid dynamics and fluid-solid interaction), (ii) allow rapid modeling and prototyping of specialized systems (Chrono::Vehicle for template-based modeling of wheeled and tracked vehicles, and Chrono::Granular for setting up large granular dynamics problems), or (iii) implement specialized parallel solution techniques (Chrono::Parallel for CPU shared memory or GPU computing and Chrono::Distributed for MPI distributed granular simulations).

To address the inherent multi-scale nature of the off-road mobility problem, Chrono has an additional co-simulation layer which decouples the vehicle, tire, and terrain subsystems. This approach allows further acceleration of the simulation by (i) allowing each subsystem to advance its state using a suitable integration time step; (ii) using different integration schemes (e.g., an implicit, adaptive HHT scheme for FEA tires and a semi-implicit Euler scheme for the granular terrain), as called for by the particular dynamics problem; and (iii) leveraging different and independent parallelization techniques, as dictated by the structure of each subsystem. Owing to its modular design, the co-simulation framework facilitates the swapping between a shared memory, OpenMP-based simulation of the granular terrain (using the Chrono::Parallel module), and an MPI-based distributed terrain simulation (provided by the Chrono::Distributed module).

The co-simulation framework itself, schematically illustrated in Fig. 1, is distributed and leverages MPI to perform the exchange of synchronization data in an explicit, force-displacement, co-simulation setup [2]. Chrono provides two co-simulation choices. The first one, tailored for a tire-test rig, is a two-way co-simulation scheme in which two MPI nodes control the simultaneous and independent simulation of the rig and tire on the one hand, and the granular terrain, on the other hand. The two nodes communicate through MPI messages the required synchronization data; i.e., positions and velocities of the tire FEA mesh in one direction, and tire contact forces at mesh vertices in the opposite direction. The rig mechanism, which is composed of a sequence of rigid bodies, joints, and actuators, enables one to control the toe angle, tire angular velocity, and rig linear velocity. The nonlinear finite element tire is modeled with shell finite elements using an Absolute Nodal Coordinate Formulation (ANCF) approach. A four-node, bilinear, and continuum mechanics-based shell element used was developed and validated for tire dynamics applications [3].

The second co-simulation setup supports full-vehicle mobility simulations. As illustrated in Fig. 1, it implements a three-way communication mechanism. The MPI node controlling the vehicle subsystem provides wheel states and receives cumulative tire forces at the wheel center to/from all tire nodes. The tire MPI nodes communicate with the terrain node to exchange FEA tire mesh vertex states, in one direction; and tire-terrain normal and

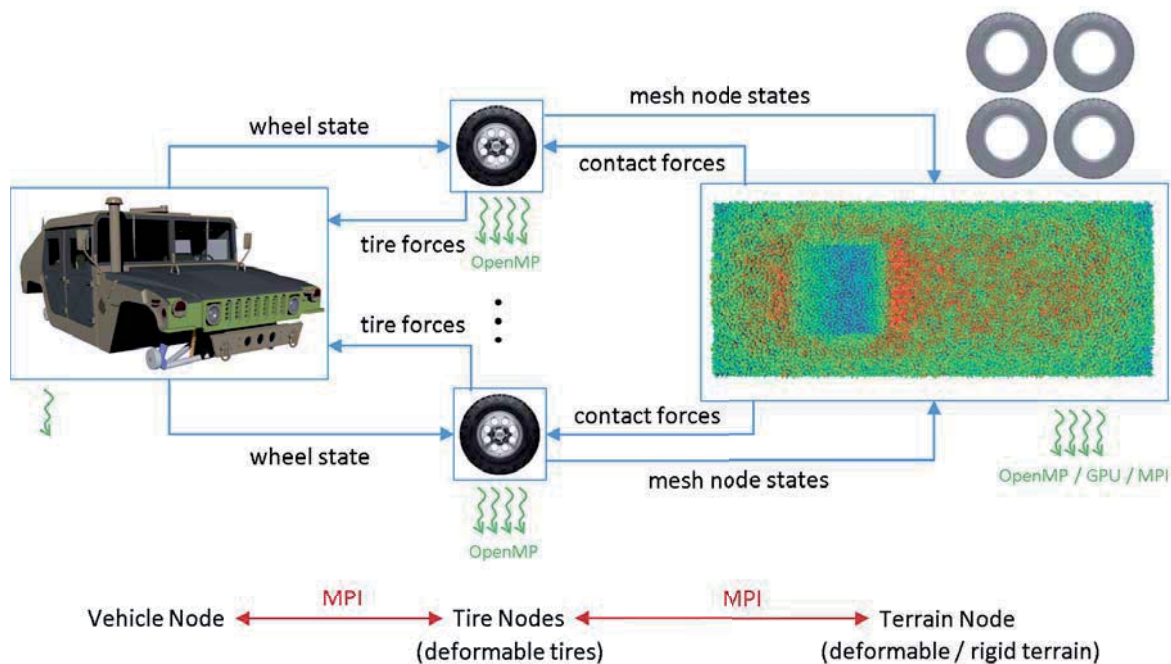


Figure 1: 3-way co-simulation scheme for the simulation of a HMMWV, ANCF tires, and granular terrain. Three types of MPI nodes exist: tire (4), terrain (1), and vehicle (1). The four ANCF tire nodes play a central role in the co-simulation scheme; at each communication time step, each tire node sends geometry information to the terrain node and receives the action of terrain on the tire in the form of nodal forces. Simultaneously, the tire receives the position of the rim body and sends an equivalent force and moment to a vehicle hub.

tangential contact forces, in the opposite direction. The simulation of the granular terrain and the tire-terrain interaction can be conducted either on one multi-core shared-memory node using up to 40 OpenMP threads, or else can be dispatched to a distributed memory HPC cluster, organized in a separate MPI communicator.

This co-simulation framework allows the expensive components of the solution process – the dynamics of the deformable tires and of the deformable terrain – to take place simultaneously. This has a significant impact on the overall simulation time. For instance, if the simulation of one deformable tire is slightly less time consuming than the computation of the terrain dynamics, all the four tires are going to be processed “in the shadow” of the terrain computation; i.e., the four tires add basically no additional wall-clock time to the total simulation time.

The physics-based co-simulation approach summarized here allows for the simulation of a variety of scenarios, e.g., deflated tires on hard terrain, overinflated tires on soft terrain, etc. The tire-test rig can be employed to compute key mobility measures parameters, such as drawbar pull, terrain resistance, and multi-pass effects, as well as assess the impact of various model parameters (e.g., tire inflation pressure, soil cohesion, coefficient of friction, etc.) on these mobility measures. The full-vehicle co-simulation framework enables the simulation of various maneuvers, such as straight line acceleration/deceleration, constant radius turn, or obstacle crossing.

### Acknowledgments

This research was supported in part by US Army Rapid Innovation Fund grant No. W911NF-13-R-0011.

### References

- [1] A. Tasora, R. Serban, H. Mazhar, A. Pazouki, D. Melanz, J. Fleischmann, M. Taylor, H. Sugiyama, and D. Negrut. Chrono: An open source multi-physics dynamics engine. In T. Kozubek, editor, *High Performance Computing in Science and Engineering – Lecture Notes in Computer Science*, pages 19–49. Springer, 2016.
- [2] A. Recuero, R. Serban, B. Peterson, H. Sugiyama, and D. Negrut. Wheeled Vehicle Mobility Studies in Chrono: Nonlinear Finite Element Tires Operating on Granular Terrain. Technical Report TR-2016-07: <http://sbel.wisc.edu/documents/TR-2016-07.pdf>, Simulation-Based Engineering Laboratory, University of Wisconsin-Madison, 2016.
- [3] Hiroki Yamashita, Paramsothy Jayakumar, and Hiroyuki Sugiyama. Development of shear deformable laminated shell element and its application to ancf tire model. In *Proceedings of the ASME 2015 International Design Engineering Technical Conferences & Computers and Information in Engineering Conference*. August 2-5, 2015, Boston, Massachusetts, USA, 2015.

## On-line Estimation of Wheel-Rail Contact Forces through Efficient Real-Time Models

José Escalona<sup>1</sup>, Emanuele Galardi<sup>2</sup>, Lorenzo Marini<sup>2</sup>, Enrico Meli<sup>2</sup>, Andrea Rindi<sup>2</sup>, Benedetta Romani<sup>2</sup>

<sup>1</sup>Department of Mechanical Engineering and Manufacturing  
University of Seville  
Camino de los Descubrimientos, 41092  
Seville, Spain  
escalona@us.es

<sup>2</sup>Department of Industrial Engineering  
University of Florence  
Via di S. Marta 3, 50139 Florence, Italy  
[emanuele.galardi, lorenzo.marini,  
enrico.meli, andrea.rindi,  
benedetta.romani]@unifi.it

### Abstract

The purpose of the proposed work is to develop a real-time model in order to estimate the wheel-rail contact forces in railway vehicles. This innovative model is characterized by both a 3D multibody model of bodies and suspension elements, which permits to describe the train dynamics, and a novel wheel-rail contact model, which estimates the wheel-rail contact points and the contact forces and torques, implementing the interaction between train and track.

The proposed model, developed for the contact forces estimation, will be implemented on the on-board subsystems of the vehicle, as, for example, Antiskid and Wheel Slide Protection systems [1], [2], [3], [4]. For this reason, the authors focused on obtaining the best trade-off between accuracy of results and computational efficiency. In addition, this work introduces an innovative technique to build up a hybrid Simulink-SimMechanics® [5] model (shown in Figure 1) whose computation load is distributed among different concurrent threads, exploiting parallel computing capabilities of modern multicore workstations and to achieve the best compromise between accuracy and efficiency.

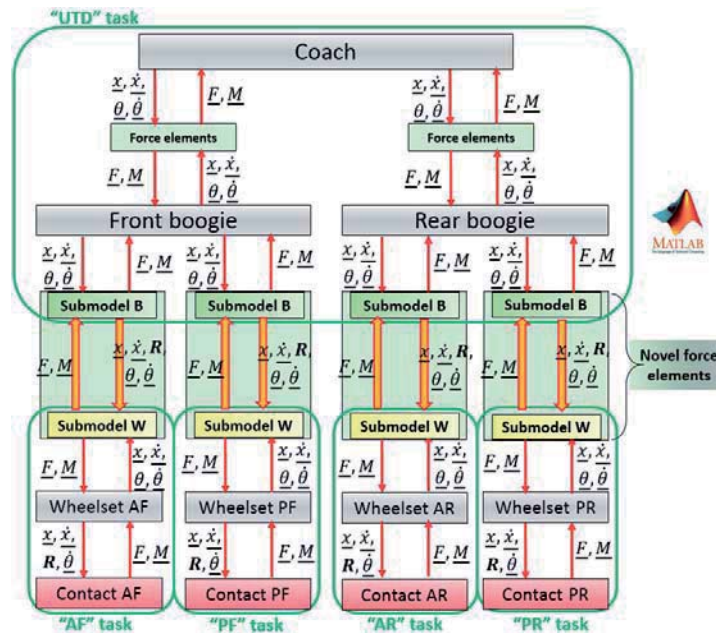


Figure 1. Multitasking implementation of the model and exchanged variables.

The multitasking model, developed by the authors, has been compiled and uploaded on an electronic multicore platform produced by Speedgoat® (the *Performance real-time target machine*) [6], suitable for real-time activities. The multitasking model was validated using the experimental data obtained on a scaled prototype, in order to obtain reduced development time and costs.

Therefore, the prototype was instrumented as shown in Figure 2. In particular, three Inertial Measurement Units acquired the 3D accelerations and angular velocities and they are positioned on the carbody, on the front bogie and on the anterior wheelset; two lasers, located the first one on the left side of the front bogie and the second one on the right side of the carbody, measured the vertical deflection between the vehicle bodies.

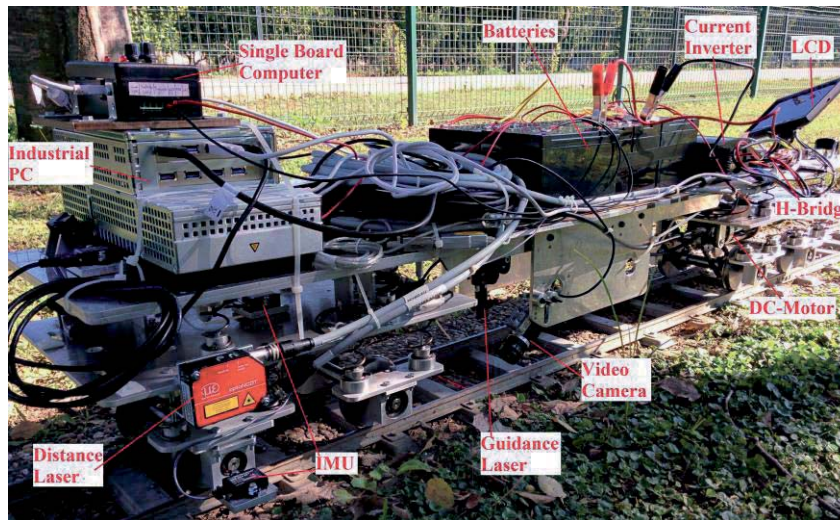


Figure 2. Sensors and actuators of the scaled vehicle prototype.

Finally, the comparison shows the good performances of the authors' model. In later research phases, the purpose will be the implementation of the innovative proposed architecture on the scaled vehicle and subsequently on a real train. The research activity was developed cooperating with University of Seville (Spain): the model was created and validated using the technical and experimental data provided by University of Seville. The prototype of the scaled train was tested on a scaled track, built in Seville.

## Acknowledgments

Thanks to the "Asociacion Sevillana de Amigos del Ferrocarril", for letting the authors to use the scaled track, which they had built in Parque de Alamillo.

## References

- [1] C.G. Kang, H.Y. Kim, M.S. Kim, B.C. Goo, Real-time simulations of a railroad brake system using a dSPACE board, *ICROS-SICE International Joint Conference 2009*, 4073-4078, 18-21 August 2009.
- [2] R. Conti, E. Meli, L. Pugi, M. Malvezzi, F. Bartolini, B. Allotta, A. Rindi, P. Toni, A numerical model of a HIL scaled roller rig for simulation of wheel-rail degraded adhesion condition, *Vehicle System Dynamics*, 50:5, 775-804, 2012.
- [3] C.-H. Jiang, W. You, L.-S. Wang, M. Chu, N. Zhai, Real-time monitoring of axle fracture of railway vehicles by translation invariant wavelet, *Proceedings of the Fourth International Conference on Machine Learning and Cybernetics*, 2409-2413, 18-21 August 2005.
- [4] N.G. Nenov, E.N. Dimitrov, G.S. Mihov, T.G. Ruzhekov, Sensor for Measuring Load on Wheels of Running Railway Vehicle, *28th Spring Seminar on Electronics Technology*, 24-28, 2005.
- [5] Matlab and Simscape® library informations available at the following site: <http://it.mathworks.com/products/simscape/>
- [6] Speedgoat® informations available at the following site: <https://www.speedgoat.ch/Products/Real-timetargetmachines-Performance/Default.aspx>, accessed the last time in 15/09/2015

## **Section**

# **FLEXIBLE MULTIBODY DYNAMICS**



# Implementation of shear deformable thin-walled beam element for flexible multibody dynamics

Ben Jonker

Faculty of Engineering Technology  
University of Twente  
Enschede, The Netherlands  
j.b.jonker@utwente.nl

## Abstract

Open section thin-walled members of flexible multibody systems are analyzed in the simplest approximation, as thin-walled beams with a cross-section that exhibits out-of-plane warping due to torsion. The beams undergo arbitrary large rigid body motions but small strains, requiring a non-linear beam formulation.

In this paper a geometrically non-linear beam finite element model is developed that captures non-uniform torsion and flexural-torsional coupling of shear deformable thin-walled beams with an open unsymmetrical cross-section. The beam model is based on the generalized strain beam formulation proposed by Besseling [1]. In this formulation, a set of independent discrete deformation modes is defined as generalized strains which are invariant under arbitrary rigid body motions of the element. For a 3D beam element, six independent deformation modes can be defined, see Fig. 1. The first deformation mode,  $\varepsilon_1$  describes the axial elongation, the second

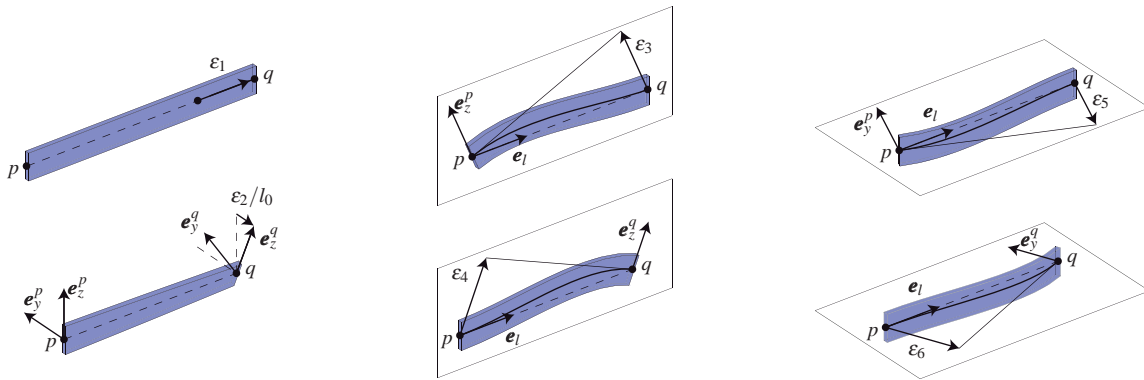


Figure 1: Visualization of deformation modes  $\varepsilon_1 - \varepsilon_6$ .

mode,  $\varepsilon_2$  describes the torsional deformation and the remaining modes,  $\varepsilon_3 - \varepsilon_6$  represent bending deformations. The discrete deformations are expressed as analytical functions of the nodal coordinates referred to a fixed global coordinate system. The deformation functions include the specification of rigid body motions as displacements and rotations for which the discrete deformations are zero. Flexible elements are modelled by allowing non-zero deformations. If the deformations remain sufficiently small, then in the elastic range they are linearly related to dual discrete stress-resultants in a single co-rotational frame which continuously translates and rotates with the element. In this way, discrete interpolation of finite rotations is avoided, leading to an intrinsic objective description. Since the elastic deformations can be assumed to be small with respect to the co-rotational frame, they can be modelled using existing linear beam models at various levels of sophistication ranging from elementary small-deflection beam theory to relatively advanced formulations for shear deformable thin-walled beams [9, 8]. The effect of warping shear may have significant influence on the vibration and stability behaviour of open thin-walled beams with low shear rigidity [3]. For complex-shaped flexible members a two-node superelement with deformable interface surfaces can be used [2]. Component mode substructuring methods are then employed to determine the dynamical properties of the super element using standard linear FEM software. The inclusion of deformable interface modes allows to capture out-of-plane warping deformation. Geometric non-linearities arising from change in configuration involving finite deflections and pre- and post-buckling are accounted for by additional second-order terms in the expressions for the discrete deformations, such that existing linear relationships between discrete stress resultants and discrete deformations are retained. This formulation combines the advantages of the co-rotational formulation with the consistency of the inertial frame approach, viz derivation of the inertia forces in terms of absolute nodal velocities and accelerations. A detailed description of the generalized strain beam formulation for flexible multibody dynamics is found in Jonker and Meijaard [7].

In formulating a shear-deformable finite element model, a local displacement field for unsymmetrical thin-walled cross-sections is introduced. In this formulation axial displacement and flexural rotations are defined at the centroid and lateral displacements and torsional rotation at the shear centre of the cross-section. The kinematics



Figure 2: Visualization of deformation modes  $\varepsilon_7/l_0$  and  $\varepsilon_8/l_0$ .

of the cross-sectional deformations is based on Timoshenko's bending theory and Reissner's torsion theory [11], where a single warping function and corresponding warping parameter are used [5]. Coupling effects between shear deformations due to the shear forces and the non-uniform torsion in two orthogonal principle planes are included using the procedure outlined in Kollar and Springer [9] and Kim et al.[8]. The stiffness matrix is derived by interpolating both flexure displacements and torsional rotations by means of locking-free Hermitian polynomials [10], using parameters indicating the influence of shear deformations. Additional degrees of freedom  $\varphi_{x,x}^p$  and  $\varphi_{x,x}^q$  at the end nodes  $p$  and  $q$  are defined, which represent the first derivative of the angle of twist to a coordinate  $x$  along the beam axis. Next two discrete deformations are defined by the relations  $\varepsilon_7/l_0 = \varphi_{x,x}^p$  and  $\varepsilon_8/l_0 = \varphi_{x,x}^q$ , where  $l_0$  is the reference length of the beam, see Fig. 2. Coupling among bending and torsion deformations due to non-coinciding centroid and shear centre is accomplished by transforming the element stiffness matrix from a parallel coordinate system passing through the shear centre to the system of principle axes passing through the centroid. A Taylor series expansion is used to expand the non-linear curvature and strain-displacement equations into a polynomial form of second-order. Integrating these equations over the length of the beam using the second moment-area theorem [4], yields the additional quadratic terms in the expressions for the discrete deformations describing the geometrically non-linear couplings such as extension-torsion, bending-torsion and bending-extension.

The inertia properties of the beam are described using both consistent and lumped mass formulations. The latter is used to model rotary and warping inertia of the beam cross-section. The derivation of the consistent mass matrix is based on a discretization of the beam's centroid axis in the global inertial coordinate system. The element has been implemented in an enhanced version of the computer program named SPACAR [6].

The efficiency and accuracy of the proposed beam finite element are tested for a thin-walled beam with C-shaped cross-section attached to a rigid hub rotating at constant angular velocity and subjected to an eccentric tip loading. The system exhibits flexural/torsional buckling behaviour. An incremental-iterative method based on the Newton-Raphson method combined with constant arc length of the incremental displacement vector is employed for the solution of the quasi-static equilibrium equations. A comparison of the obtained results with those computed by the commercial code ABAQUS using shell elements is presented.

## References

- [1] J.F. Besseling. Non-linear theory for elastic beams and rods and its finite element representation. *Computer Methods in Applied Mechanics and Engineering*, 31:205–22, 1982.
- [2] S.E. Boer, R.G.K.M. Aarts, J.P. Meijaard, D.M. Brouwer, and J.B. Jonker. A nonlinear two-node superelement with deformable-interface surfaces for use in flexible multibody systems. *Multibody System Dynamics*, 34:53–79, 2015.
- [3] V.A. Cortinez, and M.T. Piovan. Vibration and buckling of composite thin-walled beams with shear deformability. *Journal of Sound and Vibration*, 258:701–723, 2002.
- [4] J.M. Gere and S.P. Timoshenko. *Mechanics of Materials*. PWS, Boston, MA, 1997.
- [5] G.A. Gunnlaugsson, and P.T. Pedersen. A finite element formulation for beams with thin walled cross-sections. *Computers and Structures*, 15:691–699, 1982.
- [6] J.B. Jonker and J.P. Meijaard. SPACAR—computer program for dynamic analysis of flexible spatial mechanisms and manipulators. In W. Schiehlen (editor), *Multibody Systems Handbook*, pages 123–143. Springer-Verlag, Berlin, 1990.
- [7] J.B. Jonker and J.P. Meijaard. A geometrically non-linear formulation of a three-dimensional beam element for solving large deflection multibody system problems. *Int. J. of Non-Linear Mechanics*, 53:63–74, 2013.
- [8] N.I. Kim and M.Y. Kim. Exact dynamic/static stiffness matrices of non-symmetric thin-walled beams considering coupled shear deformation effects. *Thin-Walled Structures*, 43:701–734, 2005.
- [9] L.P. Kollar and G.S. Springer. *Mechanics of composite structures*. Cambridge University Press, 2003.
- [10] F. Minghini, N. Tullini and F. Laudiero. Locking-free finite elements for shear deformable orthotropic thin-walled beams. *Int. J. for Numerical Methods in Engineering*, 72:808–834, 2007.
- [11] E. Reissner. On non-uniform torsion of cylindrical rods. *Journal of Mathematical Physics*, 31:214–221, 1952.

## Kinetic aspects of discrete Cosserat rods

Joachim Linn<sup>1</sup>, Tomas Hermansson<sup>2</sup>, Fredrik Andersson<sup>2</sup>, Fabio Schneider<sup>1</sup>

<sup>1</sup> Fraunhofer ITWM

Fraunhofer-Platz 1, 67663 Kaiserslautern, Germany  
[joachim.linn, fabio.schneider]@itwm.fraunhofer.de

<sup>2</sup> Fraunhofer-Chalmers Centre FCC

Chalmers Science Park, SE-412 88, Gothenburg, Sweden  
[tomas.hermansson, fredrik.andersson]@fcc.chalmers.se

### Abstract

The theory of *Cosserat rods* [1] provides a self consistent framework for modeling large spatial deformations of slender flexible structures at small local strains. The main deformation modes of a Cosserat rod are *bending* and *twisting*, accompanied by very small, but in general non-zero amounts of longitudinal *stretching* (or compression), and *transverse shearing*, related to tiny out-of-plane cross section deformations.

Discrete Cosserat rod models may be derived in terms of a finite difference approximation that preserves essential geometric properties of the continuum theory [2, 3]. In a recent contribution [4], we discussed the *discrete kinematics* of Cosserat rods, based on the difference geometry of framed space curves defined on a staggered grid (see Fig. 1). The present work complements these considerations, with a focus on *kinetic* aspects.

As sketched on the left of Fig. 1, the kinematic skeleton of a Cosserat rod configuration mathematically corresponds to *framed curve* (or *Cosserat curve*), parametrized by the arc length  $s$  of its centerline  $\mathbf{r}(s)$ , augmented by a moving quaternion frame field  $\hat{\mathbf{q}}(s) \in S^3$ . The material curvature and tangent vector fields  $\mathbf{K} = 2\hat{\mathbf{q}}^* \circ \partial_s \hat{\mathbf{q}}$  and  $\mathbf{\Gamma} = \hat{\mathbf{q}}^* \circ \partial_s \mathbf{r} \circ \hat{\mathbf{q}}$  are the *differential invariants* that determine the geometry of a Cosserat curve uniquely, up to a global rigid body motion. In the case of *dynamic* motions, the *velocity*  $\mathbf{v} = \partial_t \mathbf{r}$  of points on the centerline and the *angular velocity*  $\boldsymbol{\omega} = 2\partial_t \hat{\mathbf{q}} \circ \hat{\mathbf{q}}^*$  of the local cross section rotations w.r.t. the global inertial frame, or equivalently its material counterpart given by  $\boldsymbol{\Omega} = \hat{\mathbf{q}}^* \circ \boldsymbol{\omega} \circ \hat{\mathbf{q}} = 2\partial_t \hat{\mathbf{q}}^* \circ \hat{\mathbf{q}}$ , are additional kinematical variables that characterize the space-time configuration of a Cosserat rod, subject to the *compatibility* condition  $\partial_s \boldsymbol{\Omega} - \partial_t \mathbf{K} \equiv \mathbf{K} \times \boldsymbol{\Omega}$ .

Local *strains* occurring in Cosserat rod configurations that are deformed w.r.t. a given reference state can be described in terms of the difference functions  $\Delta \mathbf{K}(s,t) \equiv \mathbf{K}(s,t) - \mathbf{K}_0(s)$  and  $\Delta \mathbf{\Gamma}(s,t) \equiv \mathbf{\Gamma}(s,t) - \mathbf{\Gamma}_0$  measuring the deviations of the invariants from their reference values  $\mathbf{K}_0(s)$  and  $\mathbf{\Gamma}_0 = (0, 0, 1)$ .

The basic *kinetic* quantities of a Cosserat rod are the force  $\mathbf{f}(s,t)$ , also denoted as *stress resultant*, and the moment  $\mathbf{m}(s,t)$ , also denoted as *stress couple*. Both vector fields are spatial quantities obtained by the integration of traction forces of the over the local cross section area, and respectively the integrated couples resulting from these traction forces w.r.t. the cross section center. The kinetic sectional quantities are both functions of the curve parameter  $s$ , usually chosen as the arc length of the centerline in its reference configuration, and the time  $t$ . Their dynamic equilibrium is governed by the balance equations

$$\partial_s \mathbf{f} + \boldsymbol{\beta} = \partial_t [\rho_L \mathbf{v}] \quad , \quad \partial_s \mathbf{m} + \partial_s \mathbf{r} \times \mathbf{f} + \boldsymbol{\mu} = \partial_t [\rho_L \mathbf{J} \cdot \boldsymbol{\omega}] \quad . \quad (1)$$

The inertial terms on the r.h.s. are the time derivatives of the translational momentum density  $\rho_L \mathbf{v}$  of infinitesimal mass segments with density  $\rho_L$  on the centerline of the rod, and the angular momentum density  $\rho_L \mathbf{J} \cdot \boldsymbol{\omega}$  of the corresponding cross sections, proportional to their rotational inertia tensor  $\rho_L \mathbf{J}$  w.r.t. the global inertial frame.

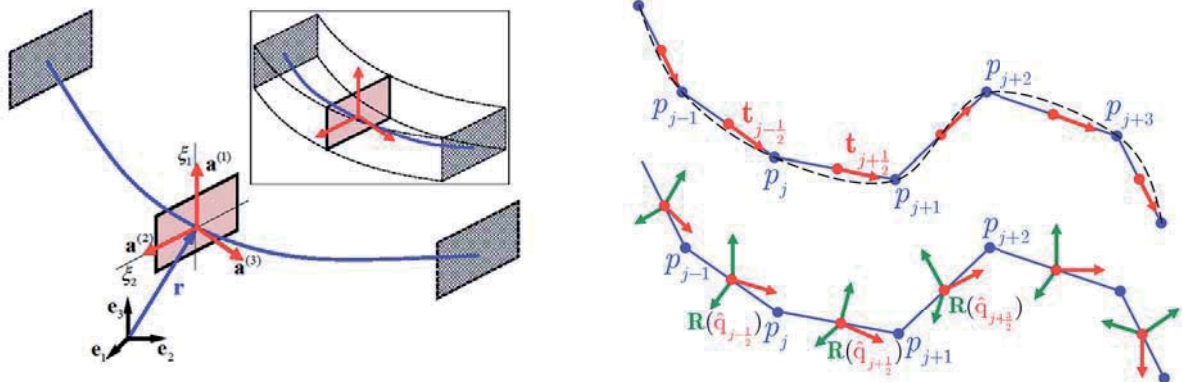


Figure 1: *Left*: Centerline curve  $\mathbf{r}(s)$  and attached moving frame  $\mathbf{R}(s) = \mathbf{a}^{(k)}(s) \otimes \mathbf{e}_k$  of a *Cosserat curve*, describing the geometry of the configurations of a prismatic rod in Euclidian space. The volumetric geometry is generated by sliding the cross section spanned by the frame directors  $\{\mathbf{a}^{(1)}, \mathbf{a}^{(2)}\}$  along the centerline. The position vectors of the material points in the rod volume are parametrized by:  $\mathbf{x} = \mathbf{r}(s) + \xi_\alpha \mathbf{a}^{(\alpha)}(s)$ . *Right*: Polygonal arc approximating a smooth regular geometric curve  $\mathcal{C}$ : The vertices  $p_j \in \mathcal{C}$  define edges  $[p_{j-1}, p_j]$  of length  $\ell_{j-1/2} > 0$ , with edge centered unit length tangent vectors  $\mathbf{t}_{j-1/2}$ . A *discrete Cosserat curve* consists of a polygonal arc with edge centered quaternions  $\hat{\mathbf{q}}_{j-1/2} \in S^3$ , representing the frames  $\mathbf{R}_{j-1/2} = \mathfrak{E}(\hat{\mathbf{q}}_{j-1/2})$  via the *Euler map*  $\mathfrak{E}: S^3 \rightarrow \text{SO}(3)$ .

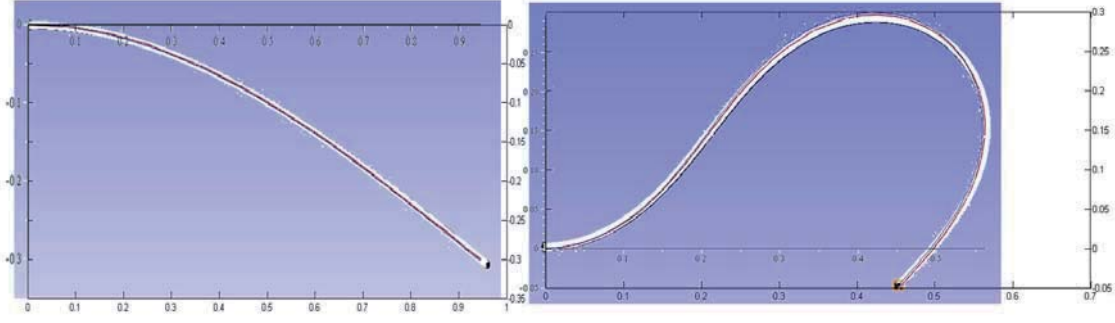


Figure 2: Overlay of screenshots from *IPS Cable Simulation* vs. *Matlab* plots of the centerline curves exported from *IPS* and the analytical solutions of the corresponding *inextensible Elastica* problem. The *IPS* solution is computed by minimization of the stored energy of the rod subject to given b.c., while the *Elastica* curves result from the analytical solutions of the corresponding b.v.p. for the centerline tangent angle computed in *Maple*.

Consistent with the staggered discretization approach for Cosserat rods [3], *semidiscrete balance equations* may be formally derived from the continuous ones by integrating the balance equations (1) over parameter intervals between adjacent edge centers  $s_{j\pm 1/2}$  around a vertex  $\mathbf{r}_j = \mathbf{r}(s_j)$ , and over intervals between adjacent vertices. With an approximation of various integral terms by midpoint quadrature one obtains the semidiscrete system of equations

$$\mathbf{f}_{j+1/2} - \mathbf{f}_{j-1/2} + \bar{h}_j \boldsymbol{\beta}_j = \bar{h}_j \rho_L \partial_t \mathbf{v}_j, \quad (2)$$

$$\mathbf{m}_{j+1} - \mathbf{m}_j + (\mathbf{r}_{j+1} - \mathbf{r}_j) \times \mathbf{f}_{j+1/2} + h_{j+1/2} \boldsymbol{\mu}_{j+1/2} = h_{j+1/2} \rho_L \partial_t [\mathbf{J}_{j+1/2} \cdot \boldsymbol{\omega}_{j+1/2}], \quad (3)$$

where  $\boldsymbol{\beta}_j$  and  $\boldsymbol{\mu}_{j+1/2}$  denote the integral averages of the external force and moment vector fields over the respective intervals of length  $\bar{h}_j := \frac{1}{2}(s_{j+1/2} - s_{j-1/2})$  and  $h_{j+1/2} := s_{j+1} - s_j$ .

While this semidiscrete system provides a consistent *finite difference discretization* of the continuous balance equations (1) displaying obvious formal similarities, it is less obvious that a semidiscrete system of this form results as an equivalent of the *Euler–Lagrange equations* of our discrete quaternionic Cosserat rod model, if a hyperelastic constitutive behaviour of the rod material is assumed. In this case the semidiscrete force and moment vectors  $\mathbf{f}_{j+1/2}(t)$  and  $\mathbf{m}_j(t)$  defined at the edge centers and the vertices of the staggered grid are given as gradients of a *stored energy potential function*  $\mathcal{V}(\{\boldsymbol{\Gamma}_{j-1/2}\}_{j=1,\dots,N}, \{\mathbf{K}_j\}_{j=0,\dots,N})$  w.r.t. the discrete material shear-extensional strain vectors given by  $\boldsymbol{\Gamma}_{j+1/2} := \hat{\mathbf{q}}_{j+1/2}^* \circ (\mathbf{r}_{j+1} - \mathbf{r}_j) / h_{j+1/2} \circ \hat{\mathbf{q}}_{j+1/2}$ , and material curvature vectors  $\mathbf{K}_j := 2 \log(\hat{\mathbf{q}}_{j-1/2}^* \circ \hat{\mathbf{q}}_{j+1/2}) / \bar{h}_j$  extracted from the difference rotations connecting adjacent frames  $\hat{\mathbf{q}}_{j\pm 1/2}$ , rotated to the global inertial frame according to:

$$\mathbf{f}_{j+1/2} = \hat{\mathbf{q}}_{j+1/2} \circ \frac{\partial \mathcal{V}}{\partial \boldsymbol{\Gamma}_{j+1/2}} \circ \hat{\mathbf{q}}_{j+1/2}^*, \quad \mathbf{m}_j = \hat{\mathbf{q}}_{j\pm 1/2} \circ \frac{\partial \mathcal{V}}{\partial \mathbf{K}_j} \circ \hat{\mathbf{q}}_{j\pm 1/2}^*.$$

While a derivation of the semidiscrete balance equations (2) of the sectional forces is straightforward, it is less obvious that the semidiscrete balance equations of the sectional momenta as given in [3] in quaternionic form are equivalent to equations of the form (3). Also, the relation of the latter to the *pair* of balance equations for the momenta as derived in [2] needs to be explained. In our contribution, we investigate these issues and thereby elucidate the seemingly differing kinetic aspects of discrete Cosserat rod models otherwise based on identical kinematic concepts.

We also present applications of our Lagrangian approach to (semi)discrete Cosserat rod models in computing equilibrium configurations of elastic cables by minimizing their potential energy w.r.t. external boundary conditions. Apart from a discussion of some interesting academic test examples (like e.g. the one shown in Fig. 2), we point out applications in cable assembly process simulation in automotive industry.

## References

- [1] S.S. Antman. *Nonlinear Problems of Elasticity*, Springer, 2005.
- [2] P. Jung, S. Leyendecker, J. Linn, M. Ortiz: A discrete mechanics approach to the Cosserat rod theory - Part 1: static equilibria, *Int. J. Numer. Methods Eng.*, 85:31–60, 2011.
- [3] H. Lang, J. Linn, M. Arnold: Multibody dynamics simulation of geometrically exact Cosserat Rods, *Multibody System Dynamics*, 25:285–312, 2011.
- [4] J. Linn: Discrete kinematics of Cosserat rods based on the difference geometry of framed curves, Proc. of *The 4<sup>th</sup> Joint International Conference on Multibody System Dynamics*, Montréal, 2016.

# Some Considerations on the Setup of Pseudo-Rigid Body Models for Single-Leaf Flexure Hinges in Compliant Mechanisms

Pier Paolo Valentini, Ettore Pennestri

Department of Enterprise Engineering  
University of Rome "Tor Vergata"  
Via del Politecnico, 1 – 00133 Rome, Italy  
valentini@ing.uniroma2.it; pennestri@mec.uniroma2.it;

## Abstract

Compliant mechanisms are widely used in different fields, such as robotics, micromechanics, aerospace and biomechanics. In order to address the design of such devices, engineers often localize the deformation zones in the so called "flexure hinges", as to mimic the presence of standard kinematic pairs. The kinematics and the dynamics of compliant mechanisms is often studied using the pseudo-rigid body approach [1]. For the definition of the pseudo-rigid body of leaf-type hinge, many authors suggest to include a revolute joint (pseudo-revolute joint) placed at a convenient location of the flexible beam and a torsion spring acting on the connected bodies [2-3]. In this way, only a first order approximation of the relative motion between the connected parts is achieved and the distributed elasticity of the flexible element is reduced to a lumped component.

In general, flexure hinges undergo large deformations and an intrinsic elasto-kinematic behavior is observed (*i.e.* the kinematics is affected by the loads). For the standard pseudo-revolute joint models currently available in literature, the matching between the actual relative motion of the bodies connected by the flexure hinge and the one reproduced by the model is limited within a few degrees rotation. This limitation requires a more careful study on the kinematic properties of the most used hinges especially for large deformation. A recent study [4] introduced the use of kinematic invariants for studying the kinematics of the flexure hinge in order to achieve a second order approximation of relative motion. The relative motion features between two rigid bodies are embedded in the kinematic invariants, independently from the actual structural embodiment of the mechanism [5]. The kinematic invariants relevant for this type of investigation are the fixed and moving polodes and the inflection circle. The first two invariants are the loci of the center of instantaneous rotation in the fixed and moving reference frames, respectively. The inflection circle is the locus of the points whose acceleration is parallel to velocity. Its diameter is related to centrodes radii of curvature.

The aim of the study is to investigate the second order kinematics of three types of common hinges (the circular profile flexure hinge, the elliptical profile flexure hinge, the leaf flexure hinge). The outcome is a pseudo-rigid mechanism with a second order approximation of the relative motion of the connected bodies in both small and large deformation. The inflection circle diameter is computed by postprocessing the results of full flexible multibody planar models (see Figure 1). The models include two rigid bodies and a variable flexible part meshed with plate elements. One of the rigid body is considered fixed and an enforced rotation of 90° is applied to the other one by means of a driving constraint. The connection between rigid and flexible parts is ensured with a force distributing rigid element (rigid spider).



**Figure 1.** Examples of the flexible multibody models of the flexure hinges (leaf hinge, on the left; elliptical profile hinge, in the middle; circular profile hinge, on the right).

Kinematic invariants are then computed according to the procedure discussed in [4]. The analysis of results show that the diameter of the inflection circle  $\delta$  is almost constant for the entire range of motion (Figure 2, on the

left). Since the diameter of the inflection circle and the radii of curvature of the two polodes ( $r_{c_f}$  and  $r_{c_m}$ ) are related by the following equation [6]

$$\frac{1}{\delta} = \frac{1}{r_{c_m}} - \frac{1}{r_{c_f}}, \quad (1)$$

the two connected rigid bodies evidenced an epicycloidal relative motion. This result suggests to reproduce the relative motion as the, without slipping, of two circles (see Figure 2, on the right). For sake of symmetry, the two circles should have the same radius that can be computed as the double of the inflection circle diameter:

$$r_{c_f} = r_{c_m} = 2\delta \quad (2)$$

The new pseudo-rigid mechanisms can include two circumferences (attached one on each body) and a rolling without slipping constraint, a trade-off between simplicity and accuracy in reproducing almost the same motion invariants of the actual flexible assembly.

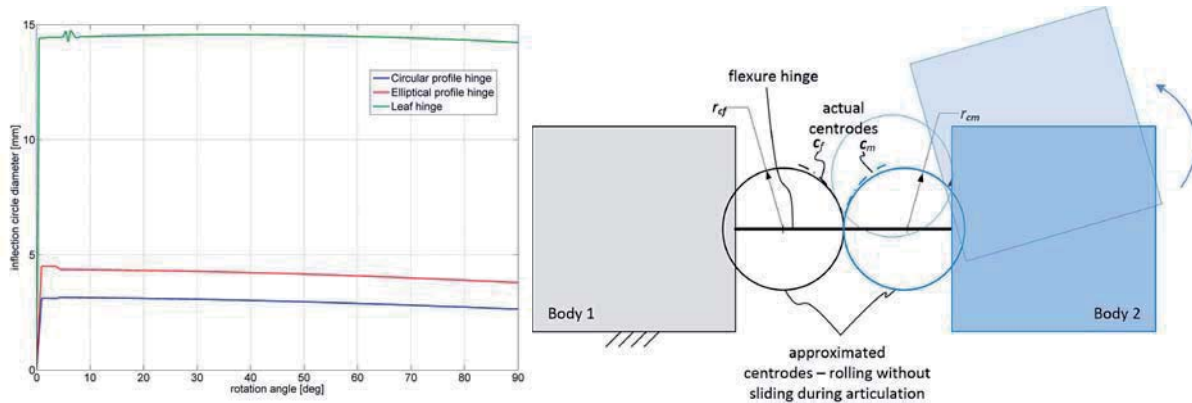


**Figure 2.** Inflection circle diameter as a function of rotation angle (on the left) and the precise pseudo-rigid model (on the right)

The accuracy of the proposed solution is assessed through the setup of three fully rigid multibody models (one for each hinge) including the pseudo-rigid arrangement and by comparing the results with those from the flexible models and from the traditional pseudo-hinge approach. The comparison confirms that the proposed pseudo-rigid body model can reproduce, for a large range of deformation, the relative motion with a feasible accuracy.

The results of the investigation encourage a more deep investigation of the kinematic properties of different types of flexure hinges and a parametric or preferred analytic study relating the dimension of the rolling circles to the dimensions of the actual flexible element in order to establish reliable design guidelines.

## References

- [1] Y.-Q. Yu, L.L. Howell, C. Lusk, Y. Yue, M.G. He. Dynamic Modeling of Compliant Mechanisms Based on the Pseudo-Rigid-Body Model, *ASME Journal of Mechanical Design*, 127:760-765, 2005.
- [2] L.L. Howell. *Compliant Mechanisms*, John Wiley and Sons, Inc., USA, 2001
- [3] P. Mandali, Q. Sun, Y. Kanamiya. A Pseudo-rigid model for the inverse dynamics of an Euler beam, *Applied Mathematical Modelling*, 35:3854–3865, 2011.
- [4] P.P. Valentini, E. Pennestrì. Elasto-kinematic comparison of flexure hinges undergoing large displacement, *Mechanism and Machine Theory*, 110:60-70, 2017.
- [5] B. Roth, A.T. Yang. Application of Instantaneous Invariants to the Analysis and Synthesis of Mechanisms. *ASME Journal of Engineering for Industry*, 99:97-103, 1997.
- [6] E. Pennestrì, N.P. Belfiore. On the Numerical Computation of Generalized Burmester Points, *Meccanica*, 30(2):147-153, 1995.

# The Use of Modal Derivatives in Determining Stroke-Dependent Frequencies of Large Stroke Flexure Hinges

Mieke van den Belt, Jurnan Schilder

Faculty of Engineering Technology  
University of Twente  
P.O. Box 217, 7500AE Enschede, The Netherlands  
[m.vandenbelt, j.p.schilder]@utwente.nl

## Abstract

Flexure hinges are frequently used in precision engineering for their deterministic behaviour, due to the absence of friction, hysteresis and backlash [1]. For their common applications, flexure hinges are compliant in driving directions, while constraining motion in other directions. This requires a high support stiffness throughout the entire range of motion. Figure 1 illustrates this concept for a single leaf spring. A commonly used measure for the performance of a flexure hinge is its first parasitic frequency, i.e. the lowest natural frequency in the support direction. Because the support stiffness typically decreases rapidly with the deflection, flexure hinges tend to have a reduced performance in their deflected state [1].

Recent development is aimed at the design of large stroke mechanisms for which this performance reduction is minimized. Shape and topology optimization is used to design sophisticated mechanisms, for which large stroke flexure hinges are included in geometrically nonlinear multibody analyses. As these forms of optimization require many design evaluations, model order reduction (MOR) is used to reduce computational costs. In [2], Wu and Tiso present a MOR technique suitable for multibody systems in the floating frame of reference (FFR) formulation using modal derivatives (MDs).

In the FFR formulation, the configuration of a flexible body is written as a combination of its global rigid body motion and a local elastic displacement field. When applying MOR, this local displacement field is expressed as a linear combination of a small number of mode shapes, e.g. Craig-Bampton modes. Geometric nonlinear effects in the displacement field are taken into account by the MDs, which are static corrections on the mode shapes.

In this work, this MD-based technique is extended to determine stroke-dependent natural frequencies. To this end, the frequency derivatives (FDs) are introduced as the derivatives of the natural frequencies with respect to the modal coordinates. The derivation of the FDs is presented. Using the FDs, the natural frequencies for any given configuration can be determined. For demonstration purposes, this method is used to determine the parasitic frequency as a function of the deflection in driving direction for the single leaf spring shown in Figure 1, using 3D beam elements.

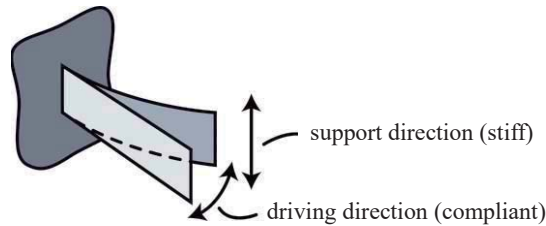


Figure 1. Single leaf spring flexure.

In order to derive MDs, the full nonlinear Green-Lagrange strain expression is taken into account, resulting in the configuration dependent stiffness matrix. The eigenvalue problem for free vibrations around the undeformed equilibrium configuration is given as:

$$(\mathbf{K} - \omega_i^2 \mathbf{M}) \boldsymbol{\phi}_i = \mathbf{0}, \quad (1)$$

where  $\mathbf{K}$  and  $\mathbf{M}$  are the stiffness and mass matrix respectively and  $\boldsymbol{\phi}_i$  is the natural mode shape corresponding to natural frequency  $\omega_i$ . Differentiation of the eigenvalue problem with respect to the modal coordinates  $\eta_j$  yields:

$$\left( \frac{\partial \mathbf{K}}{\partial \eta_j} - \frac{\partial \omega_i^2}{\partial \eta_j} \mathbf{M} \right) \boldsymbol{\phi}_i + (\mathbf{K} - \omega_i^2 \mathbf{M}) \boldsymbol{\theta}_{ij} = \mathbf{0}, \quad (2)$$

where  $\boldsymbol{\theta}_{ij}$  are the MDs, defined as the derivate of  $\boldsymbol{\phi}_i$  with respect to  $\eta_j$ .

The inertia terms in (2) can be neglected [3], therefore the expression for the modal derivatives yields:

$$\boldsymbol{\theta}_{ij} = -\mathbf{K}^{-1} \frac{\partial \mathbf{K}}{\partial \eta_j} \boldsymbol{\phi}_i. \quad (3)$$

With this, the local elastic displacement field can be written as a combination of mode shapes and modal derivatives. Since the MDs are now known, it is possible to determine the system's mode shapes for its deflected state. By pre-multiplying (2) with  $\boldsymbol{\phi}_i^T$ , it can be solved for the FDs as follows:

$$\boldsymbol{\gamma}_{ij} = \frac{\boldsymbol{\phi}_i^T \frac{\partial \mathbf{K}}{\partial \eta_j} \boldsymbol{\phi}_i + \boldsymbol{\phi}_i^T (\mathbf{K} - \omega_i^2 \mathbf{M}) \boldsymbol{\theta}_{ij}}{\boldsymbol{\phi}_i^T \mathbf{M} \boldsymbol{\phi}_i}, \quad (4)$$

where  $\boldsymbol{\gamma}_{ij}$  are the FDs, defined as the derivative of  $\omega_i^2$  with respect to  $\eta_j$ . The natural frequencies can now be written as a combination of the natural frequencies in undeformed equilibrium configuration and frequency derivatives:

$$\omega_i^2 = (\omega_i)_0^2 + \boldsymbol{\gamma}_{ij} \eta_j. \quad (5)$$

To demonstrate this method, the 3D example of the leaf spring in Figure 1 is analyzed. For numerical computations, the flexure is given length 0.1 m, height 0.04 m and width 0.0005 m. The material is given Young's modulus 210 GPa, shear modulus 79 GPa and density 7800 kg/m<sup>3</sup>. The first natural frequency of the system corresponds to a bending mode shape in the driving direction. When the system is deflected in this first mode, the natural frequency in the support direction is determined using the method as explained above. This is done until the angle of the end node reaches 45°.

Figure 2 shows the decrease of this parasitic frequency. It can be seen that already for relatively small deflections, the reduction in performance is indeed significant. A validation with software package SPACAR yields similar results. SPACAR uses a flexible multibody approach with nonlinear beam elements, which can also include large deformations. A detailed description of the formulation is found in [4]. In order to produce these results, SPACAR needs to solve a linearized eigenvalue problem for each incremental step in the deflection. The method presented here does not require this, which makes it attractive to apply on computationally expensive processes such as shape and topology optimizations.

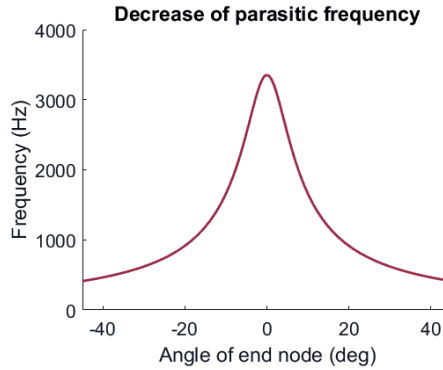


**Figure 2.** Decrease of parasitic frequency of a single leaf spring for increasing deflection in the first mode shape.

## References

- [1] K. Gunnink, R.G.K.M. Aarts and D.M. Brouwer. Performance optimization of large stroke flexure hinges for high stiffness and eigenfrequency. *Proceedings of the 28th Annual Meeting of the American Society for Precision Engineering*. Saint Paul, Minnesota, USA, 2013.
- [2] L. Wu and P. Tiso. Nonlinear model order reduction for flexible multibody dynamics: a modal derivatives approach. *Multibody System Dynamics*, 36: 405-425, 2015.
- [3] P.M.A. Slaats, J. de Jongh and A.A.H.J. Sauren. Model reduction tools for nonlinear structural dynamics. *Computers & Structures*, 54: 1155-1171, 1995.
- [4] J.B. Jonker and J.P. Meijaard. A geometrically non-linear formulation of a three-dimensional beam element for solving large deflection multibody system problems. *Int. J. Non-Linear Mech*, 53: 63-74, 2013.

## FLEGX: Multibody Approach in Flexible Structure Design and Control

**Mariapaola D'Imperio\***, **Daniele Ludovico#**, **Cristiano Pizzamiglio#**,  
**Lando Mentrasti\***, **Darwin G. Caldwell\*** and **Ferdinando Cannella\***

\* Istituto Italiano di Tecnologia  
Via Morego 30-16163, Genova, Italy  
{mariapaola.dimperio, darwin.caldwell, ferdinando.cannella}@iit.it.

# Politecnico di Torino, DIMEAS  
Corso Duca degli Abruzzi, 24 - 10129 Torino, Italy  
{cristiano.pizzamiglio, daniele.ludovico}@polito.it.

\* Università Politecnica delle Marche, DICEA  
Via delle Breccie Bianche, 60131, Ancona, Italy  
mentrasti@univpm.it

### ABSTRACT

Traditionally the Robotic Multibody Systems (*RMBS*) were considered composed by rigid bodies interconnected by rigid joints, thanks to the less difficult approach in studying their motion and performances. The limits of this method were faced with the increase of the robotic structures design complexity and with the growing demand of having safer and more efficient robots. In all the cases when the structural deformations determine the external forces acting on the system, the structural flexibility cannot be neglected. At the same time the design of a robot eligible for the Human Robotic Interaction requires a non-stiff and non-bulky robotic structure.

The computational effort for analysing a *RMBS* with flexible components is much heavier than the ones required for its rigid counterpart. This aspect caused a sharp slowdown of their research area development because the computers performances were not able to challenge with such effort. As shown from the state of the art, from the seventies to the early twenty-first century, the robotic research was more focused on design and control of rigid robots with some exception represented by the robots having flexible connections.

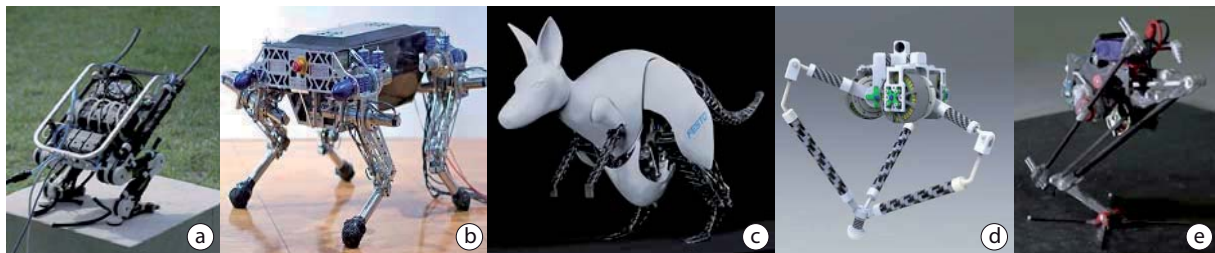


Figure 1: Flexible Jumping Robots: a) Mowgli; b) StralETH; c) Kangaroo; d) GOAT; e) SALTO; f) FLEGX

Later on, thanks to the advent of high-performance computers, the development of flexible robotic structures arose. In 2007 an artificial musculoskeletal system consisting of six pneumatic muscle actuators including bi-articular muscle and two legs with hip, knee and ankle joints was developed. It is called Mowgli (Fig. 1.a), it can jump as high as 0.5 m, more than 50% of its body height and can land softly. In 2012 StarLETH (Fig. 1.b) was born, it is fully actuated with high compliant series elastic actuation, making the system torque controllable and at the same time well suited for highly dynamic manoeuvres. The robot is able to jump up to 0.76 m, which corresponds to 150% of the leg length. In 2014 the German-based engineering company Festo developed a bionic kangaroo (Fig. 1.c) which, like its natural model, can recover the energy of a jumping phase, store it and efficiently use it for the next jump. In 2016 the Gearless Omni-directional Acceleration vectoring Topology (Fig. 1.d) was conceived, it is an electromechanically actuated robot with legs capable of dexterous walking, running, explosive omni-directional jumping and actively compliant landing. The robot can deliver 20 J in jumping experiments, achieving a height of 82 cm. In the same year of the previous, a one-legged hopper with the highest robotic vertical jumping agility ever recorded was designed. Its name is SALTO (Fig. 1.e) that stands for "SALTatorial Locomotion on Terrain Obstacles" and the motion of the mechanical jumping leg was modeled after *galagos*, a small jumping primates native to Africa. SALTO is 26 cm tall when fully extended and it can jump 400% of its tallness during its first leap and reach 500% with second one. [1].

A detailed analysis of the above mentioned robots shows that no one presents a flexible structure. The improvement we propose tends to add a contribution to the aforementioned panorama with the design of a 3 DoF underactuated mechanism with one flexible components. It is called FLEGX (FLEXible LEG) and it would be the first step in the design of a jumping humanoid robot with flexible limbs (Fig. 2.a). The two brushless DC motors

and their gearheads are directly mounted on a linear guide support plate and two tendons transfer the motion from the worm wheel to the knee joint. The virtual prototyping techniques played a key role in the identification of the optimal geometric and dynamic features of the system, such as the length and thickness of the flexible link or the inertial properties of the whole system, and in the choice of the most suitable mechanical and electromechanical components. An early system-level design validation of the FLEGX mechanical configuration was performed using the software MSC.Nastran<sup>®</sup> and MSC.Adams<sup>®</sup>-Matlab/Simulink<sup>®</sup> integrated environment.

The control architecture of the robotic structure here presented is based on a low level joint position control and an high level hybrid control. The low level control is based on the singular perturbation theory [2] applied to an hybrid system in order to obtain a order reduction model. Considering the Lagrangian-assumed modes dynamic model of the system:

$$\begin{bmatrix} m_{rr} & m_{rf} \\ m_{fr} & m_{ff} \end{bmatrix} \begin{bmatrix} \ddot{q} \\ \ddot{\delta} \end{bmatrix} + \begin{bmatrix} 0 & 0 \\ 0 & D_{ff} \end{bmatrix} \begin{bmatrix} \dot{q} \\ \dot{\delta} \end{bmatrix} + \begin{bmatrix} 0 & 0 \\ 0 & K_{ff} \end{bmatrix} \begin{bmatrix} q \\ \delta \end{bmatrix} + \begin{bmatrix} h_r(q, \dot{q}, \delta, \dot{\delta}) \\ h_f(q, \dot{q}, \delta, \dot{\delta}) \end{bmatrix} + \begin{bmatrix} G_r(q, \delta) \\ G_f(q, \delta) \end{bmatrix} = \begin{bmatrix} \tau \\ 0 \end{bmatrix} \quad (1)$$

where  $m$  is the inertia matrix,  $h$  represents the Coriolis vector,  $q$  is the rigid DoF,  $\delta$  is the flexible DoF while  $G$  is the vector containing the torque due to gravity. The subscript  $r$  is referred to joint variables while the subscript  $f$  is referred to deflection variables. Assuming that it is possible to chose as perturbation parameter  $\varepsilon^2 = k_m^{-1}$  which is the smallest value of the stiffness matrix ( $K_{ff}$ ). Thanks to a change of coordinates  $\phi = \frac{\delta}{\varepsilon^2}$  it is possible to decompose FLEGX dynamics into a slow and a fast subsystem, independent each other. The slow subsystem is obtained if  $\varepsilon$  tends to 0; while the fast subsystem can be estimated by applying a time scale  $T = t/\varepsilon$ . This decomposition allows to implement two independent control laws, one for the slow subsystem which allows to follow the joint trajectory using a simple PD controller as the robot was rigid, the other for the fast subsystem which allows to damp the oscillations of the flexible link.

The high level control is based on the theory of hybrid system [3]. The aim of this controller is to produce a stable orbit in the state space variable in order to obtain a controlled sequence of jumps.

As shown in Fig. (2.b) even if the high level control is not implemented, this mechanical structure is able to lift off and land taking advantage of the energy stored in the elastic link. In fact, the torques exerted/required to lift off and during the stance phase assume reasonable values compared to the one obtained for a complete rigid structure.

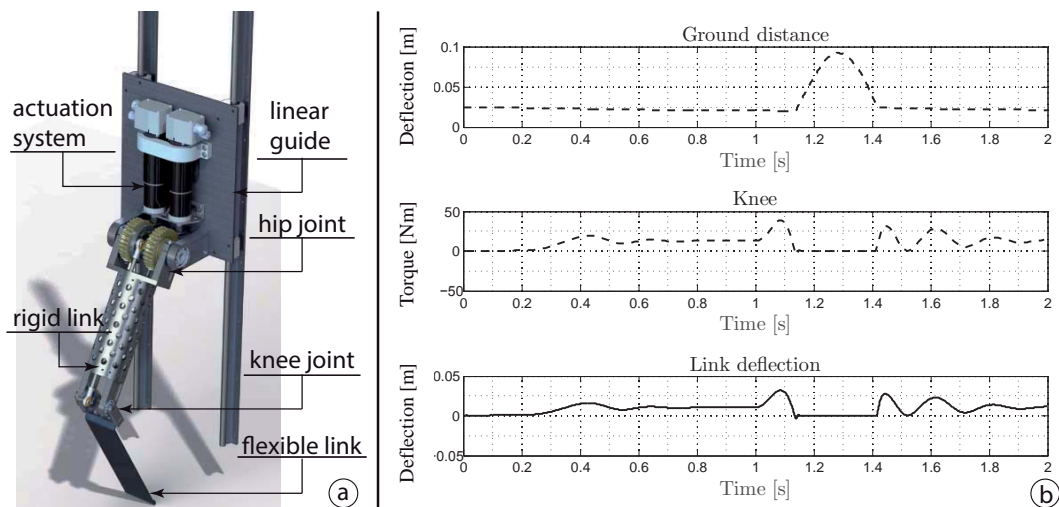


Figure 2: Adams-Matlab co-simulation of a single jump

Future works concern the accomplishment of an extended campaign of experimental test to collect data useful for the numerical model validation. The implementation of the squat jump will be also a further development of the numerical model in order to analyse more complex dynamic tasks.

## References

- [1] D. W. Haldane, M. Plecnik, J. Yim, and R. Fearing, “Robotic vertical jumping agility via series-elastic power modulation,” *Science Robotics*, vol. 1, no. 1, p. 2048, 2016.
- [2] A. D. Luca and B. Siciliano, “Trajectory control of a non-linear one-link flexible arm,” *International Journal of Control*, vol. 50, no. 5, pp. 1699–1715, 1989.
- [3] J. Kostamo, M. Focchi, E. Guglielmino, J. Kostamo, C. Semini, J. Buchli, M. Pietola, and D. Caldwell, “A magnetorheologically damped compliant foot for a legged robotic application,” *Journal of mechanical design*, p. 136, 2013.

# Approach for Modeling Flexible Bodies based on Experimental Data with Utilization in Elastic Multibody Simulation

Claudius Lein, Johannes Woller, Helge Hopf, Michael Beitelschmidt

Technische Universität Dresden, Faculty of Mechanical Engineering  
Institute of Solid Mechanics, Chair of Dynamics and Mechanism Design  
01062 Dresden, Germany  
[Claudius.Lein, Johannes.Woller, Michael.Beitelschmidt]@tu-dresden.de

## Abstract

The Elastic Multi-Body Simulation (EMBS) progressively constitutes the established method when dealing with elastic deformations of components in mechanical systems. This is motivated by the increasing complexity of technical assemblies and lightweight design. The Floating-Frame-of-Reference-Formulation (FFRF) is the state-of-the-art method, whereas the model of the elastic body is usually generated by the Finite-Element-Method (FEM) [1], see Figure 1. The validity of the FE-model is crucial for the simulation success. However, the FE-model consists of several uncertainties concerning geometry, mass distribution, local and directional stiffness as well as damping phenomena. For representing realistic components, a model-updating based on a tuning by measurement data would be mandatory. The updating procedure is highly expensive since a vast number of optimization parameter must be defined and evaluated [2]. Finally, a Model Order Reduction (MOR) condensates the elastic degrees of freedom, which embodies further approximation errors.

Due to the drawbacks of the conventional approach, a novel approach is suggested, where the data of the elastic body model is directly gained from the data of an Experimental Modal Analysis (EMA) without using any FE-model, see Figure 1. Using measured data to represent the global ansatz functions of the elastic body is also noted by other authors [1]. The novel approach makes the representation of very complex components available for EMBS considering any uncertainties of the real component. Since the FE-model becomes superfluous, a costly MOR is unnecessary. Besides, the expensive numerical eigenanalysis of the FE-model also vanishes.

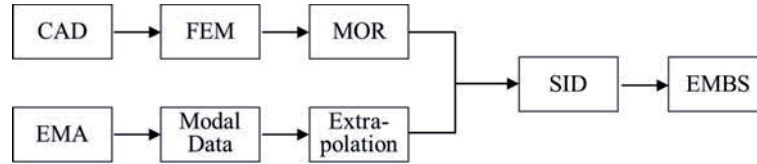


Figure 1: Generation of elastic body data by conventional approach (top) and novel approach (bottom)

All required data of the elastic body is obvious from the equation of motion 1 for a single body  $k$  [3]. With  $\mathbf{M}^k$  being the mass matrix,  $\mathbf{q}^k$  being the vector of generalized coordinates,  $\mathbf{h}_\omega^k$  being the vector of Coriolis and centrifugal forces,  $\mathbf{h}_e^k$  being the vector of inner elastic forces,  $\mathbf{h}_b^k$  being the vector of body forces and  $\mathbf{f}^k$  being the vector of external loads. Separating the generalized coordinates into translational (t), rotational (r) and elastic (e) coordinates, the terms of the required data are exposed, which are classified via the Standard Input Data (SID) definition [3]. The required data consists of eigenvalues  $\lambda$ , normal modes  $\Phi$ , modal mass  $\tilde{\mathbf{m}}$  and modal damping  $\tilde{\mathbf{d}}$ , which can be extracted from an EMA, see Table 1.

$$\mathbf{M}^k \ddot{\mathbf{q}}^k + \mathbf{h}_\omega^k + \mathbf{h}_e^k = \mathbf{h}_b^k + \mathbf{f}^k, \quad (1)$$

$$\begin{bmatrix} m\mathbf{E} & m\tilde{\mathbf{c}}^T & \mathbf{C}_t^T \\ m\tilde{\mathbf{c}} & \mathbf{J} & \mathbf{C}_r^T \\ \mathbf{C}_t & \mathbf{C}_r & \mathbf{M}_e \end{bmatrix}^k \begin{bmatrix} \ddot{\mathbf{q}}_t \\ \ddot{\mathbf{q}}_r \\ \ddot{\mathbf{q}}_e \end{bmatrix}^k + \begin{bmatrix} f(\mathbf{v}, \boldsymbol{\omega}, \dot{\mathbf{q}}, m, \mathbf{c}, \mathbf{C}_t) \\ f(\mathbf{v}, \boldsymbol{\omega}, \dot{\mathbf{q}}, m, \mathbf{c}, \mathbf{G}_r) \\ f(\mathbf{v}, \boldsymbol{\omega}, \dot{\mathbf{q}}, m, \mathbf{C}_t, \mathbf{G}_e, \mathbf{O}_e) \end{bmatrix}^k + \begin{bmatrix} \mathbf{0} \\ \mathbf{0} \\ \mathbf{D}_e \dot{\mathbf{q}}_e + \mathbf{C}_e \mathbf{q}_e \end{bmatrix}^k = \begin{bmatrix} mg\mathbf{E} \\ mg\tilde{\mathbf{c}} \\ g\mathbf{C}_t \end{bmatrix}^k + \begin{bmatrix} \mathbf{f}_t \\ \mathbf{f}_r \\ \mathbf{f}_e \end{bmatrix}^k.$$

Table 1: Required data (SID) for the representation of the elastic body

Symbol	Name	Required data for generation
$\mathbf{M}_e$	modal mass matrix	measured modal masses $\tilde{\mathbf{m}}^{\text{EMA}}$
$\mathbf{C}_e$	modal stiffness matrix	measured eigenvalues $\lambda^{\text{EMA}}$
$\mathbf{D}_e$	modal damping matrix	measured modal damping parameter $\tilde{\mathbf{d}}^{\text{EMA}}$
$m, \mathbf{c}, \mathbf{J}, \mathbf{C}_t, \mathbf{C}_r, \mathbf{G}_r, \mathbf{G}_e, \mathbf{O}_e$	rigid body parameter, elastic body parameter	artificial rigid body modes $\Phi^{\text{RB}}$ , measured elastic normal modes $\Phi^{\text{EMA}}$ , mass matrix of FE-model $\mathbf{M}^{\text{FE}}$ or via $\tilde{\mathbf{m}}^{\text{EMA}}$

The novel approach in Figure 1 yields five challenges that need to be dealt with. At first, a proper *measurement setup* that realizes a free-free support has to be established and a set of representative measurement points must be determined. Secondly, the *parameter identification* for the extraction of the modal information ( $\lambda^{EMA}$ ,  $\Phi^{EMA}$ ,  $\tilde{m}^{EMA}$ ,  $\tilde{d}^{EMA}$ ) is crucial as well as the realization (complex-to-real-conversion) of the complex eigenvectors. The representation of the *mass distribution* is the central issue, since the mass information ( $M^{FE}$ ) is usually not available from an EMA. Furthermore, the treatment of *rotational coordinates* is difficult for the reason that usually only translational coordinates can be detected using triaxial acceleration sensors. Finally, *interface nodes* are required for the EMBS-couplings (e.g. for bearings), which must be created artificially, if not being part of the FE-structure. Adequate solutions are presented in detail in the contribution.



Figure 2: Measurement setup

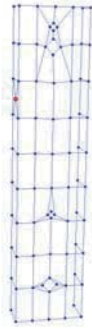
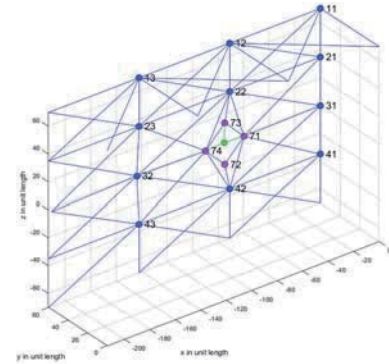


Figure 3: FE-model of U-section



# Parallel implementation of flexible multibody dynamics simulation based on the motion formalism

Valentin Sonneville, Olivier A. Bauchau

Department of Aerospace Engineering  
University of Maryland  
College Park, MD, USA

## Abstract

One of the most expensive operation in the numerical simulation of flexible multibody systems is the solution of the nonlinear equations of motion. Indeed, these equations may involve a large number of degrees of freedom due to the finite element discretization of the flexible components and to the Lagrange's multipliers used to enforce the kinematic constraints at the mechanical joints. Furthermore, the treatment of large amplitude motion, in particular large rotations, leads to strong kinematic non-linearities. The iterative solution of the nonlinear problems involves large, albeit sparse, iteration matrices. Therefore, streamlining the solution strategy would reduce computational costs significantly. The proposed strategy is based on three key aspects.

**Material frame formulation.** The equations of motion are expressed in a local material frame and all physical quantities are resolved in this frame. This reduces the nonlinearity of the governing equations that become invariant under rigid-body motions and furthermore, nonlinearities stem from local effects only. The use of the motion formalism [1, 2] allow change of frame operations to be performed naturally. Consider for instance the motion tensor, represented as the  $6 \times 6$  matrix  $\underline{\underline{\mathcal{C}}}$ ,

$$\underline{\underline{\mathcal{C}}} = \begin{bmatrix} \underline{\underline{R}} & \tilde{x}\underline{\underline{R}} \\ \underline{\underline{0}}_{3 \times 3} & \underline{\underline{R}} \end{bmatrix} ; \quad d(\underline{\underline{\mathcal{C}}}) = \underline{\underline{\mathcal{C}}}\tilde{d}\underline{\underline{\mathcal{U}}} = \underline{\underline{\mathcal{C}}}\begin{bmatrix} d\tilde{\psi} & d\tilde{u} \\ \underline{\underline{0}}_{3 \times 3} & d\tilde{\psi} \end{bmatrix}$$

where  $\underline{x} \in \mathbb{R}^3$  is a position or a displacement and  $\underline{\underline{R}} \in SO(3)$  is the rotation tensor representing an orientation. Matrix  $d\tilde{\psi}$  denotes the skew-symmetric matrix built on the three components of vector  $d\underline{\psi}$ . The local material frame derivative introduces  $d\underline{\underline{\mathcal{U}}} = [d\underline{u}^T \quad d\underline{\psi}^T]^T$ , a differential motion vector, where notation  $\tilde{\bullet}$  indicates the mapping of a  $6 \times 1$  vector into a  $6 \times 6$  matrix. Local frame velocities, strains, and variations can be introduced in a similar manner. A remarkable property of this local frame representation of derivatives is that it remains invariant under a rigid-body motion.

Typical mechanical components found in practical applications, such as rigid bodies, rigid-body connections, lower-pair joints, universal joints, flexible joints, and flexible beams, can be modeled using the motion formalism. Collecting the contributions from the different components of a system, the assembled, spatially discretized equations of motion at system level take the following form

$$\begin{aligned} \dot{\underline{\underline{\mathcal{C}}}}_k &= \underline{\underline{\mathcal{C}}}_k \tilde{\mathcal{V}}_k, \quad k = 1 \dots N, \\ \hat{\mathcal{F}}(\underline{\underline{\mathcal{C}}}_j^{-1} \underline{\underline{\mathcal{C}}}_k, \underline{\underline{\mathcal{V}}}, \dot{\underline{\underline{\mathcal{V}}}}) + \underline{\underline{B}}^T(\underline{\underline{\mathcal{C}}}_{rel}) \underline{\underline{\lambda}} &= \underline{\underline{0}}_{6N \times 1}, \\ \Phi(\underline{\underline{\mathcal{C}}}_{rel}, \underline{\underline{\mathcal{C}}}_j^{-1} \underline{\underline{\mathcal{C}}}_k) &= \underline{\underline{0}}_{6m \times 1}, \end{aligned}$$

where notation  $\dot{\bullet}$  indicates a time derivative,  $\underline{\underline{\mathcal{V}}}$  is the  $6N$ -dimensional velocity vector of the nodal velocities  $\underline{\underline{\mathcal{V}}}_k$ ,  $N$  is the number of motion nodes and  $\underline{\underline{\lambda}}$  is a  $6m$ -dimensional vector of Lagrange multipliers introduced to enforce the constraint equations  $\Phi$  arising from the  $m$  kinematic joints and whose gradient is denoted  $\underline{\underline{B}}$ . The relative motion variables at the joints is denoted  $\underline{\underline{\mathcal{C}}}_{rel}$ . Because the motion formalism is used, the equations of motion depend on the relative motions between the nodal motions only, not on their absolute position and orientation; this fundamental property of the formulation is expressed by the composition of motion,  $\underline{\underline{\mathcal{C}}}_j^{-1} \underline{\underline{\mathcal{C}}}_k$ , which remains invariant under a rigid-body motion.

The generalized- $\alpha$  scheme [3] is used to integrate these nonlinear differential-algebraic equations. The iteration process involves the iteration matrix given by

$$\underline{\underline{S}} = \begin{bmatrix} \beta \underline{\underline{M}} + \gamma \underline{\underline{G}} + \underline{\underline{K}} & \underline{\underline{B}}^T \\ \underline{\underline{B}} & \underline{\underline{0}}_{6m \times 6m} \end{bmatrix},$$

where  $\underline{\underline{M}}$ ,  $\underline{\underline{G}}$  and  $\underline{\underline{K}}$ , of size  $6N \times 6N$ , are the tangent mass, gyroscopic/centrifugal and stiffness matrices, respectively, stemming from the linearization of the equilibrium equations of the flexible components with respect to the accelerations, velocities, and incremental motions, respectively. Parameters  $\beta$  and  $\gamma$  pertain to the time integration scheme and are functions of the time step size and algorithmic damping. Because the local frame approach reduces the level of nonlinearity, the iteration matrices become nearly constant under the small strain assumption and nearly

steady velocity states. Clearly, efficient solution strategies should be explored that take advantage of these nearly constant iteration matrices. A general domain decomposition approach is proposed.

**Domain decomposition procedure.** A domain decomposition procedure has been developed to decrease the cost of the iterative solution. Each of the flexible components of the system is associated with a sub-domain. The mechanical joints connect the flexible components and become the physical interfaces between the sub-domains. Each flexible component is handled by a dedicated sub-domain.

Consider a flexible component  $i$  that is connected to the rest of the system at a set of interface nodes  $X$ . The contribution of the sub-domain to the iteration matrix can be partitioned as follows

$$\underline{\underline{S}}^i \underline{\underline{\mathcal{U}}}^i = \underline{\underline{r}}^i \Leftrightarrow \begin{bmatrix} \underline{\underline{S}}_{XX}^i & \underline{\underline{S}}_{XY}^i \\ \underline{\underline{S}}_{YX}^i & \underline{\underline{S}}_{YY}^i \end{bmatrix} \begin{bmatrix} \underline{\underline{\mathcal{U}}}_X^i \\ \underline{\underline{\mathcal{U}}}_Y^i \end{bmatrix} = \begin{bmatrix} \underline{\underline{r}}_X^i \\ \underline{\underline{r}}_Y^i \end{bmatrix},$$

where  $Y$  denotes the set of nodes which are not connected to the rest of the system. In practice, the set of nodes  $Y$  is much bigger than the set of interface nodes  $X$ . Because they do not interact directly with the rest of the system, the nodes in the set  $Y$  can be condensed, leading to a modified contribution of the remaining set  $X$  with respect to the rest of the system. This modified contribution is assembled with the rest of the system, handled by the main sub-domain. This approach corresponds to the well-known Schur complement reduction, which involves the following steps

$$\underline{\underline{\mathcal{U}}}_Y^i = (\underline{\underline{S}}_{YY}^i)^{-1} (\underline{\underline{r}}_Y - \underline{\underline{S}}_{YX}^i \underline{\underline{\mathcal{U}}}_X^i), \quad (1)$$

$$\underbrace{(\underline{\underline{S}}_{XX}^i - \underline{\underline{S}}_{XY}^i (\underline{\underline{S}}_{YY}^i)^{-1} \underline{\underline{S}}_{YX}^i)}_{\underline{\underline{S}}_{XX}^{i*}} \underline{\underline{\mathcal{U}}}_X^i = \underbrace{\underline{\underline{r}}_X - \underline{\underline{S}}_{XY}^i (\underline{\underline{S}}_{YY}^i)^{-1} \underline{\underline{r}}_Y}_{\underline{\underline{r}}_X^{i*}}. \quad (2)$$

During the assembly procedure of the entire system, each flexible component contributes a reduced stiffness matrix,  $\underline{\underline{S}}_{XX}^{i*}$ , and a reduced load vector,  $\underline{\underline{r}}_X^{i*}$ ; note that the condensed node set  $Y$  no longer appears. Consequently, the assembled iteration matrix of the main sub-domain is far smaller than the iteration matrix of the entire system. The assembled nonlinear system of equations of the main sub-domain is then solved to yield increments for the interface node set  $X$ ,  $\underline{\underline{\mathcal{U}}}_X^i$ . The corresponding increments at the condensed node set  $Y$ ,  $\underline{\underline{\mathcal{U}}}_Y^i$ , then follows from Eq. (1).

The domain decomposition strategy discussed above is based on the Schur complement reduction approach and hence, is quite general. When applied to flexible systems modeled with local frame motion formalism, it features particularly attractive numerical characteristics. If the iteration matrices are kept constant, the condensation process expressed by Eqs. (1) and (2) involves constant matrices only and hence, Schur complement matrix  $\underline{\underline{S}}_{XX}^{i*}$  remains itself constant. Consequently, Schur's reduction process, which involves the expensive factorization of matrix  $\underline{\underline{S}}_{YY}^i$ , is performed once only. On the other hand, the system of nonlinear equations for the global system is updated and factorized at each time step. This strategy may lead to a slight increase in the number of iterations at system level, but this global problem is far smaller than that involving all the flexible components.

The strategy outlined above can still accommodate changes in the iteration matrices for the flexible components. If required, the iteration matrix for the flexible component can be re-evaluated regularly and the associated Schur complement reduction repeated. Nevertheless, this re-evaluation takes place at sub-domain level. In many practical applications, the Schur complement reduction in each of the flexible sub-domains is performed once only at the beginning of the simulation.

**Parallel implementation.** The sub-domains created by the domain decomposition are independent and many operations can be performed in parallel on different processors. In particular, the evaluation of the equations of motion, their linearization, and the condensation process can be done in parallel.

The proposed solution strategy has been implemented in DYMORE 5 using the MPI environment. Its performance will be presented and assessed for academic examples as well as for practical flexible multibody system applications, such as a helicopter rotor.

## References

- [1] O.A. Bauchau. *Flexible Multibody Dynamics*. Springer, Dordrecht, Heidelberg, London, New-York, 2011.
- [2] V. Sonneville and O. Brüls. A formulation on the special Euclidean group for dynamic analysis of multibody systems. *Journal of Computational and Nonlinear Dynamics*, 9(4), 2014.
- [3] M. Arnold and O. Brüls. Convergence of the generalized- $\alpha$  scheme for constrained mechanical systems. *Multibody System Dynamics*, 18(2):185–202, 2007.

# A Discrete Hamilton-Pontryagin approach to the statics of Kirchhoff Rods

Alejandro Blumentals, Florence Bertails-Descoubes

Inria Grenoble  
Laboratoire Jean Kuntzmann  
{alejandro.blumentals,florence.bertails}@inria.fr

## Abstract

In this work we address the problem of computing stable static equilibria of Kirchhoff rods under different boundary conditions and possibly subject to contact constraints. Our approach relies on formulating the continuous problem as an Optimal Control Problem (OCP) and discretizing it using direct methods of numerical optimal control. Conceptually our approach is similar to the one developed in [3] in that we also leverage constructions from the discrete mechanics of rigid bodies ([1] in our case) in conceiving numerical schemes for the statics of rods.

A Kirchhoff rod is a thin elastic rod characterized by small strains (linear elasticity), large displacements and finite rotations (geometrical non linearities). It is assumed perfectly inextensible, and undergoes only pure bending and twisting deformations. The centerline of a Kirchhoff rod of length  $L$  is parametrized by a curve  $r$  mapping the arclength parameter  $s \in [0, L]$  to  $\mathbb{R}^3$ . The orientation of the cross sections is given by a material frame varying along the curve  $r$  and represented here as a rotation matrix  $R(s) \in SO(3)$ . As in [2] the configuration space of our geometrically exact rod is the special Euclidean group  $SE(3)$ . Accordingly the state of our OCP is  $(R, r) : [0, L] \rightarrow SE(3)$ . We collect the bending strains  $\kappa_1, \kappa_2$ , and the twisting strain  $\tau$  in a vector  $\kappa := (\kappa_1, \kappa_2, \tau)^T$  which will be interpreted as the control input in our OCP. The kinematics of the material frame read  $R' = R\hat{\kappa}$ , where  $\hat{\kappa}$  is the

skew symmetric matrix  $\hat{\kappa} = \begin{bmatrix} 0 & -\tau & \kappa_2 \\ \tau & 0 & -\kappa_1 \\ -\kappa_2 & \kappa_1 & 0 \end{bmatrix}$  and prime(') denotes derivation with respect to the arclength  $s$ .

The Euler-Bernoulli constraint reads  $r' = Re_3$ , where  $e_3 = (0, 0, 1)^T$ ; it encodes the incompressibility and no shear conditions, and couples the frame to the centerline (the frame is said to be adapted to the centerline). The  $SE(3)$  structure of the problem becomes apparent by rewriting the frame kinematics and Euler-Bernoulli constraint as the  $SE(3)$  reconstruction equation,

$$\frac{d}{ds} \begin{bmatrix} R(s) & r(s) \\ 0 & 1 \end{bmatrix} = \begin{bmatrix} R(s) & r(s) \\ 0 & 1 \end{bmatrix} \begin{bmatrix} \hat{\kappa} & e_3 \\ 0 & 0 \end{bmatrix}. \quad (1)$$

Finding the stable static equilibria of a Kirchhoff rod subject to boundary conditions and contact constraints can then be formulated as the OCP

$$\begin{aligned} \min_{R, r, \kappa} \quad & \int_0^L \mathcal{L}(R(s), r(s), \kappa(s)) ds \\ \text{s. t.} \quad & R' = R\hat{\kappa} \\ & r' = Re_3 \\ & g_I(R, r, \kappa) \leq 0 \\ & g_{bd}(R(0), r(0), R(L), r(L)) = 0, \end{aligned} \quad (2)$$

where the 'Lagrange cost' models in our example the sum of bending twisting and gravitational potential energies  $\mathcal{L} = \frac{1}{2}(EI_1 \kappa_1(s)^2 + EI_2 \kappa_2(s)^2 + \mu J \tau(s)^2) + U_g(r(s))$ , while  $g_I$  models inequality constraints and  $g_{bd}$  encodes the boundary conditions. Note that finding stable static equilibria of Cosserat rods could be formulated similarly, it would amount formally to doing a regularization of the Euler Bernoulli constraint: one would just have to add a shear and stretch degree of freedom  $v : [0, L] \rightarrow \mathbb{R}^3$ , an extra quadratic term  $\frac{1}{2}(v - e_3)^T C(v - e_3)$  in the elastic energy and to modify the kinematics as  $r' = Rv$ .

From the point of view of numerical optimal control there are two major categories of ways to find local solutions of the problem (2), namely *indirect methods* and *direct methods*. The indirect approach would be to first write the (infinite dimensional) first order optimality conditions of the OCP (2) and then to discretize it. In the absence of inequality constraints one would retrieve the Kirchhoff balance equations. However in the presence of inequality constraints the first order optimality conditions take on the form of a non smooth boundary value problem which is difficult to solve and one would not be guaranteed to find local minima but rather saddle points. In our opinion it is simpler to tackle the problem using direct methods, where one first discretizes the OCP (2), turning it into a finite dimensional Non Linear Program (NLP), and then optimizing it using standard NLP software like IPOPT [4].

From the point of view of direct methods of numerical optimal control the easiest technique to try is 'direct single shooting', where the controls (ie the strains  $\kappa$ ) are discretized into a suitable finite dimensional space and the states  $(R, r)$  are retrieved as functions of the strains by numerically solving the reconstruction equation in the OCP (2). In this case one then retrieves a 'strain based' finite element approach. Using piecewise constant strains and a Lie-Euler integrator on  $SE(3)$  for the kinematics, the formulation coincides precisely with the Super-Helix element for

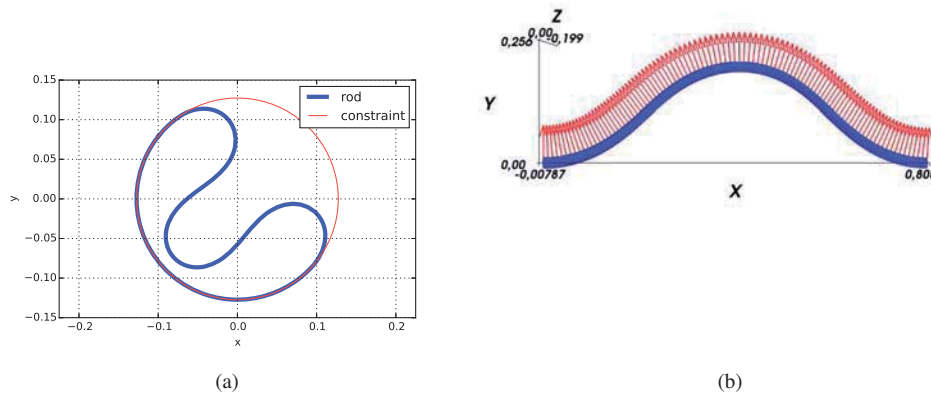


Figure 1: (a) Rod equilibrium under periodic boundary conditions and inequality constraints. (b) Rod equilibrium under fixed-fixed boundary conditions.

the statics of Kirchhoff rods [6]. More interestingly, the optimal control framework suggests a way to tackle higher order strains by simply using higher order Lie group integrators, for example general Runge Kutta Munthe-Kaas methods as employed in [1] in the similar context of Hamilton Pontryagin mechanics on Lie groups. The second branch of direct methods is 'direct multiple shooting' where both the strains  $\kappa$  and the states  $(R, r)$  are discretized, leading to a *mixed formulation*. The NLP in the mixed formulation is of higher dimensionality but with more sparsity and simpler non linearities. Using Lie group methods to discretize the kinematics allows us to avoid formulating supplementary orthogonality constraints for the frame  $R_i$  at each node  $s_i$ . In Figure (1b) we obtain a stable static equilibrium of a Kirchhoff rod subject to fixed-fixed boundary conditions, the director vectors are shown as red arrows. In Figure (1a) we obtain a stable static equilibrium configuration for a planar Kirchhoff rod with periodic boundary conditions and subject to the inequality constraint of remaining inside a circle, this curve can be found for example experimentally as the profile of a paper cylinder packed into a smaller cylinder of radius  $\rho_c$ . Using the mixed formulation allows to keep the inequality constraints  $\|r_i\|^2 \leq \rho_c^2$  convex albeit nonlinear. The simulation used 100 elements, total simulation time was 1.3s on a 2.6GHz Intel Core i7 processor parting from a random initial configuration using IPOPT. Our proposed method is quite robust to the choice of the initial configuration and could thus be used to initialize load displacements analyses. In conclusion the Optimal Control point of view provides a very useful theoretical and numerical framework to conceive, analyse and implement strain based and mixed finite element discretizations of rod statics under constraints.

### Acknowledgments

This work was supported in part by the ERC grant GEM (StG-2014-639139).

### References

- [1] N. Bou-Rabee and J.E. Marsden. Hamilton–Pontryagin integrators on Lie groups part I: Introduction and structure-preserving properties. *Foundations of Computational Mathematics*, 9:197-219, 2009.
- [2] V. Sonnevile, A. Cardona and O. Bruls. Geometrically exact beam finite element formulated on the special Euclidean group SE(3). *Computer Methods in Applied Mechanics and Engineering*, pages 451-474, 2014.
- [3] P. Jung, S. Leyendecker, J. Linn and M. Ortiz. A discrete mechanics approach to the Cosserat rod theory—Part 1: static equilibria. *International Journal for Numerical Methods in Engineering*, vol 85, pages 31-60, 2011.
- [4] L. Biegler and V. Zavala. Large-scale nonlinear programming using IPOPT: An integrating framework for enterprise-wide dynamic optimization. *Computers and Chemical Engineering*, vol 33, pages 575-582, 2009.
- [5] J. Andersson. A General-Purpose Framework for Dynamic Optimization. PhD Thesis KU Leuven, 2013.
- [6] F.Bertails, B.Audoly, M.P.Cani, B. Querleux, F. Leroy and J.L Leveque. Super-Helices for Predicting the Dynamics of Natural Hair. *ACM Transactions on Graphics (Proceedings of the SIGGRAPH conference)*, 2006.

# Dynamics of Spatial Flexible Multibody Systems with Interval Probabilities

Zhe Wang<sup>1</sup>, Qiang Tian<sup>2</sup>, Haiyan Hu<sup>3</sup>

<sup>1</sup> MOE Key Laboratory of Dynamics and Control of Flight Vehicle, School of Aerospace Engineering, Beijing Institute of Technology, Beijing 100081, China.  
cwangzhe@126.com

<sup>2</sup> MOE Key Laboratory of Dynamics and Control of Flight Vehicle, School of Aerospace Engineering, Beijing Institute of Technology, Beijing 100081, China.  
tianqiang\_hust@aliyun.com

<sup>3</sup> MOE Key Laboratory of Dynamics and Control of Flight Vehicle, School of Aerospace Engineering, Beijing Institute of Technology, Beijing 100081, China.  
haiyan\_hu@bit.edu.cn

## Abstract

A new computation methodology is proposed to study the dynamics of spatial flexible multibody systems with interval probabilities by taking into account interval mean values and interval variances. Within this consideration, the standard perturbation-based method is relaxed in order to incorporate interval probabilities in dynamics analysis of flexible multibody systems. The flexible multibody system is modeled in a unified Absolute Nodal Coordinate Formulation (ANCF) frame. Firstly, the second-order perturbation method is performed: the essential idea is to expand the items of dynamics equations about the mean of the uncertain input variables by means of the second-order Taylor series. Here, the first-order and the second-order sensitivity analysis of flexible multibody systems with interval parameters are performed. Based on the continuum mechanics, the computational efficient analytical formulations for the derivative items of the system sensitivity equations are deduced. Then, with the consideration of the interval parameters existing in the system, the Chebyshev collocation method (CCM) is utilized to generate the Chebyshev surrogate model for the dynamics and sensitivity equations. The interval bounds of the dynamics and sensitivity responses are determined by scanning the deduced Chebyshev surrogate model. Finally, the interval mean values and interval variances of the dynamics responses are obtained by using the interval arithmetic. Two numerical examples are studied to validate the proposed methodology. The first example is used to check the effectiveness of the proposed methodology. And the second one of a complex flexible robot with interval probabilities shows the effectiveness of the proposed computation methodology in the dynamics analysis of complicated spatial flexible multibody systems.

Most previous studies only studied the systems with random parameters with precise probabilistic information and interval parameters simultaneously. Few studies focused on imprecise probability. In fact, statements as “the mean is approximately equal to. . .” and “the variance lies in the range. . .” are common when handling real mechanical data. Qiu et al. [1] claimed the importance of “imprecise probability” in engineering applications. The dynamic equations in this section are carried out for uncorrelated interval probabilistic variables  $[\mathbf{b}] \sim \kappa([\boldsymbol{\mu}_b], [\boldsymbol{\Lambda}_b])$ , whose interval mean vector and variance matrix are, respectively.

$$\begin{cases} [\boldsymbol{\mu}_b] = [[\mu_{b_1}] \cdots [\mu_{b_n}]]^T \\ [\boldsymbol{\Lambda}_b] = \text{Diag}\{[\sigma_{b_1}^2] \cdots [\sigma_{b_n}^2]\} \end{cases} \quad (1)$$

According to the perturbation-based method, the interval mean generalized coordinates, interval mean Lagrange multipliers and the interval covariance matrix can be re-written, respectively, as follows

$$\begin{cases} [\boldsymbol{\mu}_q] = [\bar{\boldsymbol{\mu}}_q, \underline{\boldsymbol{\mu}}_q] = [\mathbf{q}^0] + \frac{1}{2} \sum_i^n \left[ \frac{\partial^2 \mathbf{q}^0}{\partial b_i^2} \right] [\sigma_{b_i}^2] \\ [\boldsymbol{\mu}_\lambda] = [\underline{\boldsymbol{\mu}}_\lambda, \bar{\boldsymbol{\mu}}_\lambda] = [\boldsymbol{\lambda}^0] + \frac{1}{2} \sum_i^n \left[ \frac{\partial^2 \boldsymbol{\lambda}^0}{\partial b_i^2} \right] [\sigma_{b_i}^2] \\ [\boldsymbol{\sigma}_{q_i}^2] = [\underline{\sigma}_{q_i}^2, \bar{\sigma}_{q_i}^2] = \sum_i^n \left[ \left( \frac{\partial q_i^0}{\partial b_i} \right)^2 \right] [\sigma_{b_i}^2] \\ [\boldsymbol{\rho}_{q_i, \lambda_i}] = [\underline{\boldsymbol{\rho}}_{q_i, \lambda_i}, \bar{\boldsymbol{\rho}}_{q_i, \lambda_i}] = \sum_i^n \left[ \frac{\partial q_i^0}{\partial b_i} \frac{\partial \lambda_i^0}{\partial b_i} \right] [\sigma_{b_i}^2] \\ [\boldsymbol{\sigma}_{\lambda_i}^2] = [\underline{\sigma}_{\lambda_i}^2, \bar{\sigma}_{\lambda_i}^2] = \sum_i^n \left[ \left( \frac{\partial \lambda_i^0}{\partial b_i} \right)^2 \right] [\sigma_{b_i}^2] \\ [\boldsymbol{\rho}_{\lambda_i, \lambda_i}] = [\bar{\boldsymbol{\rho}}_{\lambda_i, \lambda_i}, \underline{\boldsymbol{\rho}}_{\lambda_i, \lambda_i}] = \sum_i^n \left[ \frac{\partial \lambda_i^0}{\partial b_i} \frac{\partial \lambda_i^0}{\partial b_i} \right] [\sigma_{b_i}^2] \\ [\boldsymbol{\rho}_{q_i, \lambda_i}] = [\underline{\boldsymbol{\rho}}_{q_i, \lambda_i}, \bar{\boldsymbol{\rho}}_{q_i, \lambda_i}] = \sum_i^n \left[ \frac{\partial q_i^0}{\partial b_i} \frac{\partial \lambda_i^0}{\partial b_i} \right] [\sigma_{b_i}^2] \end{cases} \quad (2)$$

From above all, the interval displacement vector, interval Lagrange multiplier vector and their interval

derivatives should be obtained. It is obvious that the dynamic equations, first-order and second-order sensitivity equations are Interval Differential Algebraic Equations (IDAEs) if considering existing interval parameters. The Chebyshev sampling methods can obtain higher accuracy than most other sampling methods. They provide a non-intrusive computation methodology to study IDAEs system. In this study, the CCM sampling method proposed by Wang et al. [2] is used to study the dynamics of flexible multibody systems with interval probabilities. It worth noting the fact that the proposed methodology incorporates, both probabilistic method and interval method as special cases. Given interval mean parameters and zero variances, the proposed methodology can handle the dynamics of flexible multibody systems with interval parameters.

A spatial crank-slider mechanism is employed as shown in Fig. 1. Both the crank and connecting rod are flexible beams and modeled using 3-dimensional fully parameterized ANCF beam elements and their deterministic characteristic parameters can be found in Table 1 of the work by Pi et al. [3].

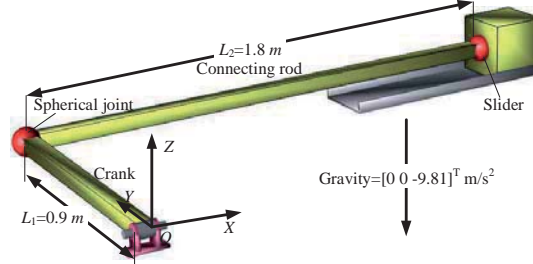


Figure 1. Schematic view of the spatial slider-crank mechanism

Figure 2a shows the X-displacement of the slider with interval parameters. It can be seen from Fig. 2a that the upper and lower bounds obtained by solving different scanned models are in good agreement with each other, and these bounds can wrap the results of the deterministic model very tightly. And it is very different from the results with deterministic parameters. It illustrates that the interval parameters influence the dynamic results. Figures 2b and 2c show the interval mean values and the interval variances of the X-displacement of the slider with interval probabilities. Actually, the numerical results shown in Fig. 2a can be regarded as the interval mean value of the X-displacement of the slider with zero variances. Comparing Figs.2a with 2b, it can be concluded that the ranges of the X-displacement of the slider intervals become wider when considering interval variances existing in the flexible multibody system. From Fig. 2b, it can be seen that the interval width of the interval mean value is dependent on the values of the interval variances. Other numerical examples will be presented on the conference.

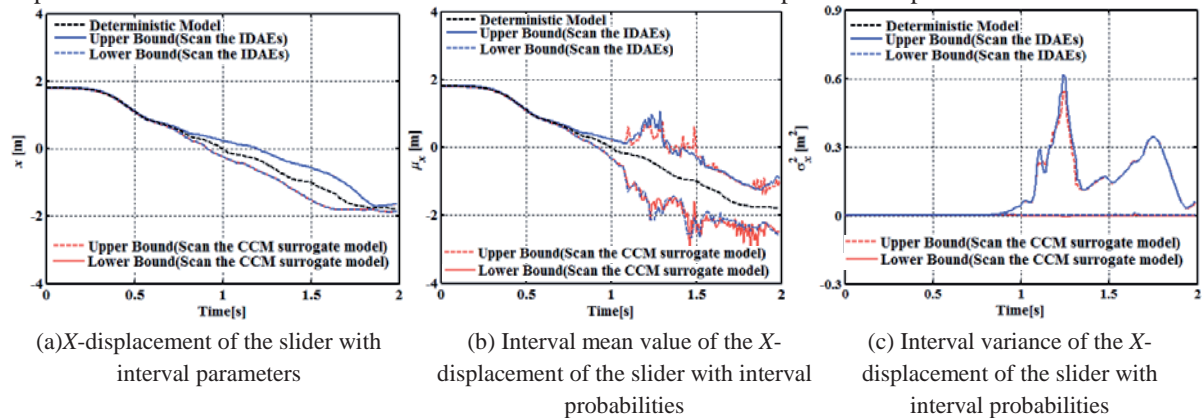


Figure 2. X-displacement of the slider

## Acknowledgments

This research was supported in part by National Natural Science Foundations of China under Grants 11290151 and 11472042.

## References

- [1] Z. Qiu, D. Yang, I. Elishakoff: Probabilistic interval reliability of structural systems, *International Journal of Solids and Structures*. 45: 2850–2860, 2008.
- [2] Z. Wang, Q. Tian, H.Y. Hu: Dynamics of spatial rigid–flexible multibody systems with uncertain interval parameters, *Nonlinear Dynamics*. 84:527-548, 2016.
- [3] T. Pi, Y. Zhang, L. Chen: First order sensitivity analysis of flexible multibody systems using absolute nodal coordinate formulation, *Multibody System Dynamics*, 27:153-171, 2012.

# Kinematic Calibration of a Six DOF Flexure-based Parallel Manipulator

J.H. Timmer Arends<sup>1</sup>, K.H.J. Voss<sup>2</sup>, W.B.J. Hakvoort<sup>1,2</sup>, R.G.K.M. Aarts<sup>1</sup>

<sup>1</sup>Faculty of Engineering Technology  
Structural Dynamics, Acoustics and Control  
University of Twente  
P.O. Box 217, 7500 AE Enschede, The Netherlands  
R.G.K.M.Aarts@utwente.nl

<sup>2</sup>DEMCON Advanced Mechatronics  
Institutenweg 25, 7521 PH Enschede, The Netherlands  
[Kevin.Voss,Wouter.Hakvoort]@demcon.nl

## Abstract

Flexure-based mechanisms enable high dynamic performance, repeatability and accuracy in high precision applications due to the absence of friction, hysteresis and backlash. However, the complicated non-linear behaviour of the deforming compliant joints has to be accounted for when deriving the far from trivial (inverse) kinematic relations between actuators and end-effector. In this paper we compare modelling approaches of varying complexity in terms of accuracy and computational load. Next a geometrical calibration is developed to realise the desired performance in an experimental set-up. The method is applied to a flexure-based parallel manipulator for a six degrees of freedom (DOF) mirror mount. The manipulator consists of a mirror mount to which six arms are attached, see Figure 1. The other end of each arm is translated by a linear direct drive motor that is fixed to a rigid frame. Each arm contains five joints that each release one DOF, see Figure 2. This means that each arm transfers one DOF to the mount. In  $x$ - and  $y$ -direction the translational and rotational strokes are respectively  $\pm 2.5$  mm and  $\pm 85$  mrad. The desired accuracy is  $50 \mu\text{m}$  (2%) for the translations and 1 mrad (2.2%) for the rotations.



Figure 1: Six DOF flexure-based parallel mechanism with the mirror mount in the origin of the coordinate system. The six linear motors are labelled 1–6.

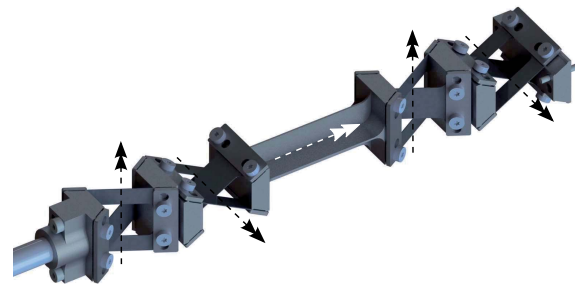


Figure 2: Single flexure arm in which the five arrows indicate the compliant motion of each joint: Black arrows for four Three Flexure Cross Hinges and a white arrow for a torsional compliant link.

The accuracy is mainly limited by the (inverse) kinematic model that is used to compute the motor positions from a desired end-effector pose. Effectively each arm can be described with five rotational joints or hinges connected by rigid links. A simple model is obtained when all hinges are assumed to be ideal. This is illustrated with the ideal hinge in Figure 3(a) where the pivot point remains fixed relative to the base link and all link lengths are constant. Using the Denavit-Hartenberg (D–H) notation [1] a kinematic model can be derived quite straightforwardly for each arm. However, the accuracy of this model is by far insufficient to meet the desired requirements.

Hence, the deformation of the flexures should be described more accurately. Four of the five flexures in each arm are Three Flexure Cross Hinges (TFCH) of which the deformed pose is illustrated in Figure 3(b). Their shape can be evaluated from a non-linear flexible multibody analysis. The SPACAR software [2] package has been used to build a flexure-based kinematic model that accounts accurately for these joint deformations. Spatial flexible beam elements are used to model all sheet flexures in the TFCH. The accuracy of this model is expected to be high, but it appears to be computationally too expensive as the elastic deformations of all flexures are evaluated from an equilibrium analysis.

Acceptable accuracy and numerical efficiency can be obtained by combining the results of the SPACAR analysis with a modified D–H model. This is accomplished by recognising that for both hinges shown in Figure 3 the position  $(y, z)$  of the arm is a function of the joint angle  $\theta$ . The result is a modified D–H model in which

the translation vector in the homogeneous transformation matrix depends on the joint angle. It was found that an approximation of the numerical data of the SPACAR analysis with a Taylor expansion with no more than three coefficients could offer close to nm accuracy for joint angles in the range of  $\pm 20^\circ$ . This modified D–H model can still be evaluated relatively fast. For the so-called nominal kinematic model the geometric parameters are retrieved from the CAD model of the mechanism.

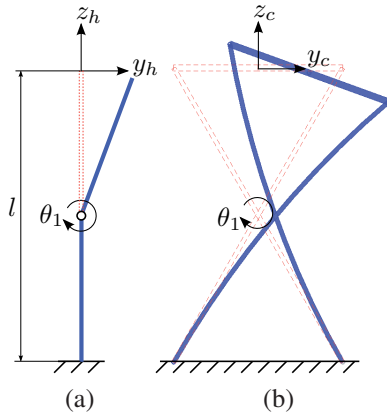


Figure 3: Deflected ideal hinge (a) and (b) Three Flexure Cross Hinge.

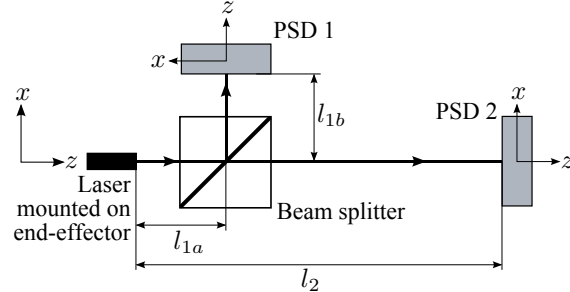


Figure 4: Measurement set-up with a beam splitter and two 2D lateral effect Position-Sensing Detectors (PSD) that jointly measure two positions ( $x, y$ ) and two rotations of the laser beam originating from the left.

The actual performance of this nominal kinematic model is evaluated with an experimental set-up, see Figure 4. The mirror mount on the end-effector is replaced by a laser and the position of the emitted laser beam is measured with two 2D lateral effect Position-Sensing Detector (PSD). Each PSD can measure 2D translations with a best resolution of  $0.75 \mu\text{m}$ . A beam splitter is used to be able to acquire data from two PSD that are placed at different distances from the laser source. In this way four of the six DOF of the end-effector can be measured, namely the positions  $x$  and  $y$ , and the rotations about the  $x$ - and  $y$ -axis, denoted  $a$  and  $b$ .

The measurements show a significant deviation of the end-effector pose compared to the nominal model. The mean errors in  $x$ ,  $y$ ,  $a$  and  $b$  are respectively 7.7%, 8.1%, 3.4% and 8.9%. The highest error of 20% was found in the translation  $y$ . Clearly, the desired accuracy is not achieved and the kinematic model parameters need to be estimated to improve the match between the kinematic model and the measurements. From a sensitivity analysis it appeared that offsets in the positions of the linear motors cause relatively large errors in the end-effector pose. These offsets could well be introduced by tolerances in assembly of the mechanism.

These parameter offsets are estimated with a calibration procedure. The model is linearised for small differences in these parameters to enable the use of linear regression techniques [3]. With a least squares estimate the parameters are updated. To avoid inaccuracies arising from overfit, the estimation is checked using singular value decomposition in combination with cross-validation. After applying the calibration method twice with updated regression matrices, the mean errors are reduced to respectively 1.3%, 1.7%, 3.0% and 0.8%. The highest error is now in rotation  $a$  and is 5%. Some non-repeatability was observed which is attributed to play in plain bearings used in the actuators.

It can be concluded that the modified D–H model after a kinematic calibration is able to remove the first order errors from the model. It is expected that further improvements can be realised by estimating more parameters and using sensors and motor encoders with better resolutions. Furthermore, the reproducibility is expected to improve by applying flexible guidances in the actuators as well.

### Acknowledgements

ATA, KV and WH acknowledge the support from the Horizon2020 program of the EU under project grant no. 637045 (“ADALAM”).

### References

- [1] B.W. Mooring, M.R. Driels, and Z.S. Roth. *Fundamentals of manipulator calibration*. Wiley-Interscience, 1991.
- [2] J.B. Jonker and J.P. Meijaard. Spacar - Computer program for dynamic analysis of flexible spatial mechanisms and manipulators. In W. Schiehlen, editor, *Multibody systems handbook*, pages 123–143. Springer-Verlag, Berlin, 1990.
- [3] A.Y. Elatta, L.P. Gen, F.L. Zhi, Y. Daoyuan, and L. Fei. An overview of robot calibration. *Information Technology Journal*, 3(1):74–78, 2004.

# Avoiding Unphysical Vibrations Caused by Statically Correct Reduction of Elastic Multibody Systems

Pascal Ziegler and Peter Eberhard

Institute of Engineering and Computational Mechanics  
University of Stuttgart  
Pfaffenwaldring 9, 70569 Stuttgart, Germany  
[pascal.ziegler, peter.eberhard]@itm.uni-stuttgart.de

## Abstract

Craig-Bampton, Rubin-MacNeal and other component mode synthesis (CMS) approaches for model order reduction of mechanical systems generally approximate the system behavior with two different sets of shape functions: normal modes and static modes. It is well known, that by reducing the system with only normal modes, i.e. eigenmodes, the global system dynamics is captured very well, yet the static approximation error is often unacceptably high and, therefore, static correction modes are added in order to address this problem. In case of a Craig-Bampton or Rubin-MacNeal approach these static modes are mechanically motivated unit displacements or unit loads, [1], hence they represent mechanically meaningful static deformation shapes. However, since these static correction modes are simply added to the reduction basis and both the mass and stiffness matrix of the system are reduced with the same reduction matrix, every static mode contributes one additional eigenfrequency to the reduced system. Contrary to the eigenfrequencies of normal modes, which are physically meaningful, a dynamical contribution of mode shapes that are by definition static deformation shapes, is unphysical. More recently developed reduction methods like Krylov-based schemes or balanced truncation, show the same behavior, [2]. A certain frequency range is approximated optimally, but usually at the cost of the same type of high frequency modes as introduced by static correction.

For mechanical systems, the frequency range of interest is often smaller than the frequency range of the excitation. This is particularly true for impact-like excitations. In these cases, classic CMS approaches cause severe problems. Even though the dynamical behavior of the system may very well be approximated for the frequency range of interest with acceptable error, the excitation excites those unphysical high frequency modes introduced by the static correction modes. This does not only result in increased integration times, but most importantly, in strong and totally unphysical high frequency oscillations. The common approach to remedy this problem is to either use implicit integration schemes with increased high frequency damping, like the generalized- $\alpha$  scheme, or, to explicitly damp the static modes. Nevertheless, the problems remain for both cases. With these approaches, static correction can only be obtained at the cost of artificial and mechanically invalid dynamics which cannot be avoided.

Instead of achieving static correction by using static correction modes with all mentioned disadvantages, we propose to obtain static correction by simply adding a constant term to the spectral sum. From a mechanical perspective, this can be interpreted as an infinitely fast dynamical approximation of the static behavior or as neglecting the inertia of the reduced system related to the static mode shapes. This approach avoids the unphysical dynamics in the reduced system by shifting them to a feedthrough term in the output equation. Since this reduction approach is not structure preserving, it can best be interpreted as an alternative modeling approach: The full system is approximated by any arbitrary reduction scheme of choice in any frequency range of interest, but at the same time the reduced system is guaranteed to only contain dynamics in this particular frequency range.

This approach has several advantages. First, compared to common CMS approaches, the number of degrees of freedom is further reduced by keeping the physical dynamics, yet at the same time avoiding unphysical and high frequency dynamics, and only those. Second, the reduction is still statically correct. Third, numerical efficiency increases considerably, since the highest eigenfrequency of the reduced system is further lowered and, fourth, neither artificial structural nor numerical damping is necessary. The potential and advantages of the approach will be demonstrated for numerical examples including contact problems.

## References

- [1] Craig, R.: Coupling of Substructures for Dynamic Analyses: An Overview AIAA Journal, Proceedings of the AIAA Dynamics Specialists Conference, Paper-ID 2000-1573, Atlanta, April 5, 2000.
- [2] Holzwarth, P.; Eberhard, P.: SVD-Based Improvements for Component Mode Synthesis in Elastic Multibody Systems European Journal of Mechanics - A/Solids, Vol. 49, pp. 408-418, 2014.



# Comparison of Local and Global Approaches for Parametric Model Order Reduction for Systems with Distributed Moving Loads

Benjamin Fröhlich, Peter Eberhard

Institute of Engineering and Computational Mechanics  
University of Stuttgart  
Pfaffenwaldring 9, 70569 Stuttgart, Germany  
[benjamin.froehlich, peter.eberhard]@itm.uni-stuttgart.de

## Abstract

The demand for energy-efficient machines with high processing speeds leads to the development of more and more lightweight machines. However, reducing the weight of a machine reduces the stiffness of a machine as well. Therefore, elastic deformations of the lightweight structures occur which have to be considered during the virtual product development. This can be done by incorporating flexible bodies in the equation of motion of classical rigid multibody systems, where such systems are called flexible multibody systems. Using the floating frame of reference formulation described in [1] the equation of motion reads

$$\begin{bmatrix} mE & m\tilde{c}^T(\mathbf{q}) & \mathbf{C}_t^T(\mathbf{q}) \\ m\tilde{c}(\mathbf{q}) & J(\mathbf{q}) & \mathbf{C}_r^T(\mathbf{q}) \\ \mathbf{C}_t(\mathbf{q}) & \mathbf{C}_r(\mathbf{q}) & \mathbf{M} \end{bmatrix} \cdot \begin{bmatrix} \mathbf{a}(t) \\ \boldsymbol{\alpha}(t) \\ \ddot{\mathbf{q}}(t) \end{bmatrix} = \begin{bmatrix} \mathbf{h}_t(t) \\ \mathbf{h}_r(t) \\ \mathbf{h}_e(t) \end{bmatrix} + \begin{bmatrix} \mathbf{0} \\ \mathbf{0} \\ -\mathbf{K} \cdot \mathbf{q}(t) - \mathbf{D} \cdot \dot{\mathbf{q}}(t) \end{bmatrix}. \quad (1)$$

Here,  $\mathbf{a}(t)$  and  $\boldsymbol{\alpha}(t)$  describe the rigid body motion. The matrices  $\mathbf{M}$ ,  $\mathbf{D}$  and  $\mathbf{K}$  are the mass, damping and stiffness matrix of the flexible structure, respectively. They are obtained by a spatial discretization of the elastic continuum with the Finite Element Method (FEM). The vector  $\mathbf{q}(t) \in N$  denotes the node displacement of the flexible structure.

Recently, there came up a demand for more and more accurate models describing the flexible bodies which leads to complex models of very high dimension. For example FEM-models for simple components such as piston rods can easily exceed hundreds of thousands degrees of freedom leading to long computation times. Therefore, model order reduction (MOR) is used to reduce the computational complexity of the underlying FEM-models. The flexible bodies are regarded as a linear time invariant multi-input-multi-output system

$$\mathbf{M} \cdot \ddot{\mathbf{q}}(t) + \mathbf{D} \cdot \dot{\mathbf{q}}(t) + \mathbf{K} \cdot \mathbf{q}(t) = \mathbf{B} \cdot \mathbf{u}(t). \quad (2)$$

The solution of the full order system is then approximated by  $\mathbf{q}(t) \approx \mathbf{V} \cdot \bar{\mathbf{q}}(t)$  in an  $n$ -dimensional subspace  $\mathcal{V}$  spanned by the columns of the projection matrix  $\mathbf{V} \in N \times n$ . By inserting the approximation and left multiplying with  $\mathbf{V}^T$  the reduced system reads

$$\bar{\mathbf{M}} \cdot \ddot{\bar{\mathbf{q}}}(t) + \bar{\mathbf{D}} \cdot \dot{\bar{\mathbf{q}}}(t) + \bar{\mathbf{K}} \cdot \bar{\mathbf{q}}(t) = \bar{\mathbf{B}} \cdot \mathbf{u}(t), \quad (3)$$

where the order of the reduced model  $n$  is much smaller than the order  $N$  of the original model. For linear time invariant systems this has been applied successfully with modern input-output based MOR-techniques such as Krylov subspace methods or reduction with Gramian matrices as described in [2]. However, in many engineering applications load positions are not constant but parameter dependent. These kinds of systems arise for example in simulation of gear trains, cranes or sliding components. Since the input and output matrices of such systems are not constant anymore, applying standard MOR techniques yields only very poor results. In the past years advances have been made in parameter preserving reduction of parameter dependent systems. A summary of methods suitable for parametric model order reduction in flexible multibody systems can be found in [3]. In [4] a distinction between local and global approaches is suggested. In local approaches the system matrices of several individual reduced systems are interpolated. In contrast, global approaches try to find one representative subspace capturing the entire parameter dependent dynamics of the system. In Figure 1 the reduction process for local and global approaches is shown.

As in in local approaches the size of the reduced parametric system does not depend on the number of parameter samples, small reduced models can be created. However, since the individual projection matrices are parameter dependent, all reduced system matrices are parameter dependent as well and have to be interpolated during time integration. This increases the computational effort since the mass matrix of the elastic body has to be inverted in every time step.

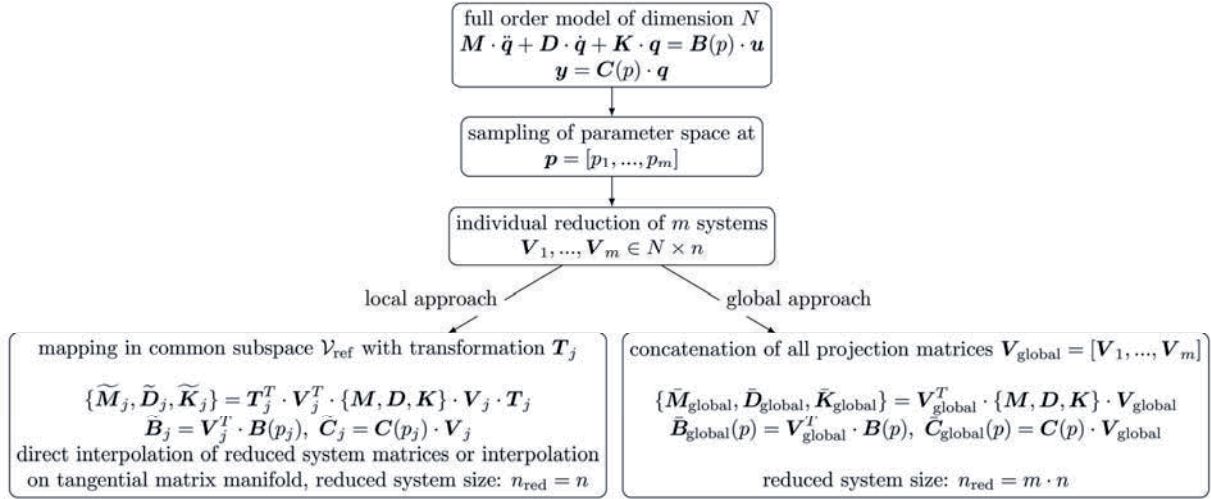


**Figure 1.** Reduction process for local and global approaches for parametric model order reduction.

To obtain parametric models with a comparable approximation quality by global approaches usually larger reduced models are necessary. An advantage is that only the reduced input and output matrix are parameter dependent. This enables a diagonalization of the mass and stiffness matrix which reduces the numerical effort during time integration.

In this contribution different approaches from [3] and [4] are applied and compared for systems with moving loads. A special interest lies on the simulation of systems with distributed loads acting on surfaces. Comparisons are made with respect to the approximation quality in time and frequency domain. Furthermore, the computational effort for generating the reduced order models and for the solution of initial value problems is compared. Suggestions for an automated and error-controlled reduction process for parametric systems with moving loads are made.

## Acknowledgments

The authors gratefully thank the German Research Foundation (DFG) for the support of this research work within the project EB 195/11-2.

## References

- [1] Schwertassek, R.; Wallrapp, O.: *Dynamik flexibler Mehrkörpersysteme* (in German). Vieweg, Braunschweig, 1999.
- [2] Fehr, J.: Automated and Error-Controlled Model Reduction in Elastic Multibody Systems. Dissertation, *Schriften aus dem Institut für Technische und Numerische Mechanik der Universität Stuttgart*, Vol. 21. Shaker Verlag, Aachen, 2011.
- [3] Baumann, M.: Parametrische Modellreduktion in elastischen Mehrkörpersystemen (in German). Dissertation, *Schriften aus dem Institut für Technische und Numerische Mechanik der Universität Stuttgart*, Vol. 43. Shaker Verlag, Aachen, 2016.
- [4] Benner, P.; Gugercin, S.; Willcox, K.: A Survey of Projection-Based Model Reduction Methods for Parametric Dynamical Systems. *SIAM Review*, Bd. 57, Nr. 4, S. 483-531, 2015.

## Estimating relative eigenvalue errors of dynamic model reduction for reliable flexible multibody simulation

Jin-Gyun Kim<sup>1</sup>, Hanmin Lee<sup>1</sup>, Juhwan Choi<sup>2</sup>, Jin Hwan Choi<sup>3</sup>

<sup>1</sup>Mechanical Systems Safety Research  
Division  
Korea Institute of Machinery and Materials  
Daejeon, 34103, Republic of Korea  
[jingyun, hmlee]@kimm.re.kr

<sup>2</sup>FunctionBay, Inc  
Pangyo Seven Venture Valley,  
Seongnam, Republic of Korea  
juhwan@functionbay.co.kr

<sup>3</sup>Department of Mechanical Engineering  
KyungHee University  
Giheung, Yongin, 17104, Republic of Korea  
jhchoi@khu.ac.kr

### Abstract

Coordinate reduction is essential for efficient modeling and simulation of flexible multibody dynamics (FMBD) [1]. Then, Guyan reduction and Craig-Bampton (CB) method are the most well-known dynamic model reduction techniques [2, 3]. To simplify model, Finite element (FE) based flexible body in general, the nodal coordinate of the original model is approximated by only using its dominant mathematical basis such as fixed interface normal and interface constraint modes. Therefore, the accuracy and efficiency of the FMBD simulation with the dynamic model reduction directly depend on number of the retained basis. The following question then arises: 'How many modes should be used?' The relative eigenvalue error is a common way to evaluate the accuracy of approximated models by dynamic model reduction techniques, and then we can manually determine the number of retained modes based on the relative eigenvalue error. However, it is quite expensive because it requires reference eigenvalues resulting by eigenvalue problem of original models.

To overcome this problem, robust estimation techniques of the relative eigenvalue error were recently developed by using the original eigenvalue formulation and its orthogonal condition [4-7] as follows:

$$\frac{\bar{\lambda}_i}{\lambda_i} - 1 \approx 2(\bar{\boldsymbol{\varphi}})_i^T \mathbf{T}_0^T \left[ \mathbf{M}_g - \frac{1}{\lambda_i} \mathbf{K}_g \right] \mathbf{T}_r (\bar{\boldsymbol{\varphi}})_i + (\bar{\boldsymbol{\varphi}})_i^T \mathbf{T}_r^T \left[ \mathbf{M}_g - \frac{1}{\lambda_i} \mathbf{K}_g \right] \mathbf{T}_r (\bar{\boldsymbol{\varphi}})_i. \quad (1)$$

The transformation matrices in Equation (1) are differently defined in the Guyan reduction and CB method. The proposed techniques can precisely estimate the relative eigenvalue errors without knowing the reference eigensolutions as shown in Figures (1) and (2). In this presentation, we introduce the key ideas and derivation procedures of the proposed error estimation methods including possible extensions in the FMBD simulation.

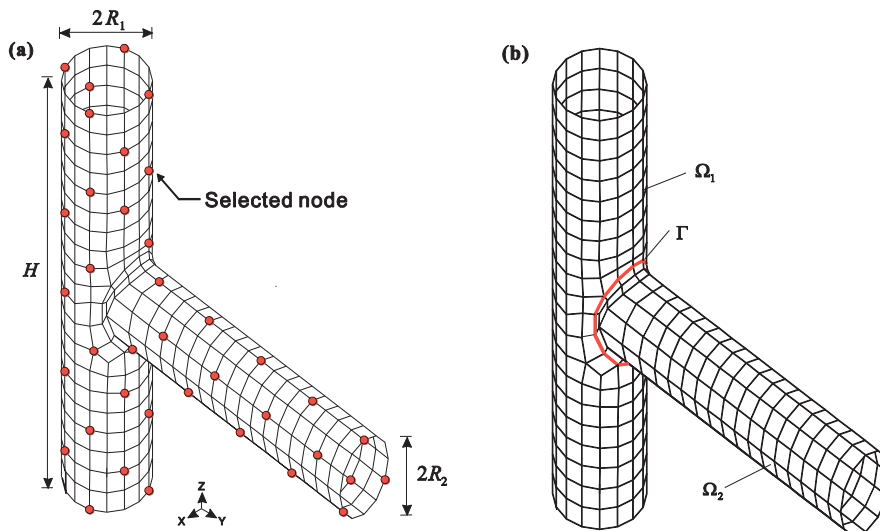


Figure 1. An shaft-shaft problem. (a) selected nodes in Guyan reduction, (b) partitioned type in CB method. [8]

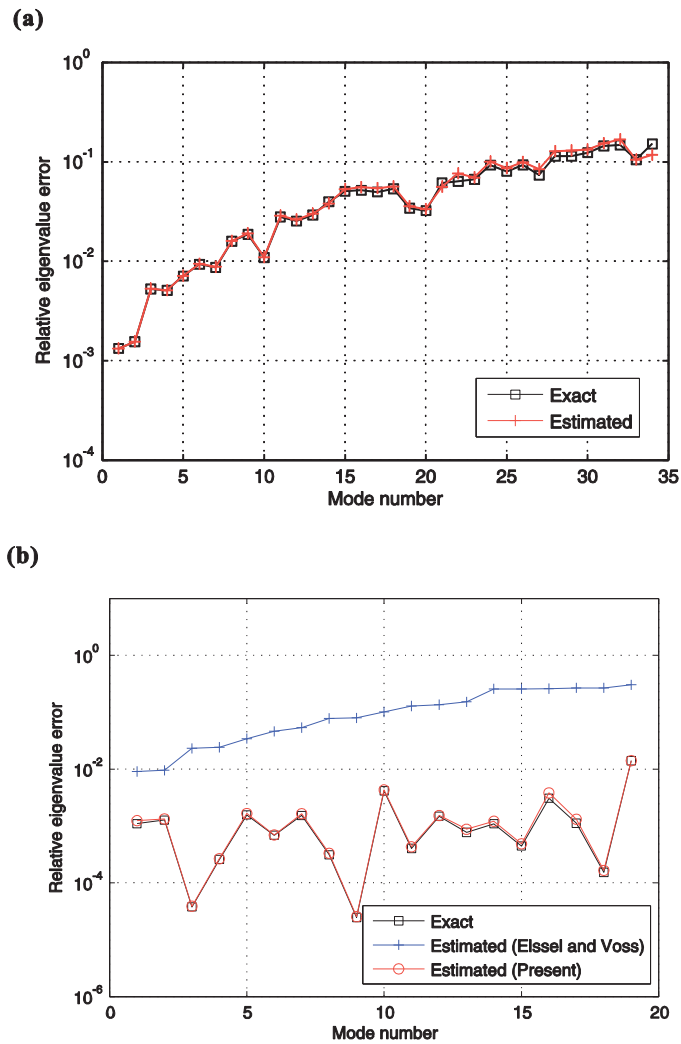


Figure 2. Exact and estimated relative eigenvalue errors. (a) Guyan reduction, (b) CB method [8].

## Acknowledgments

The first author has been supported by the Basic Science Research Program through the National Research Foundation of Korea (NRF) funded by the Ministry of Education, Science and Technology (NRF-2015R1C1A1A 01051499).

## References

- [1] Ahmed A. Shabana, *Dynamics of multibody systems*. Cambridge University Press. 3<sup>rd</sup> Edition, 2005.
- [2] R. Guyan, Reduction of stiffness and mass matrices. *AIAA Journal* 3(2) (1965) 380.
- [3] R.R. Craig, M.C.C. Bampton, Coupling of substructures for dynamic analysis. *AIAA Journal* 6(7) (1968) 1313-1319.
- [4] J.G. Kim, K.H. Lee, P.S. Lee, Estimating eigenvalue errors in the Craig–Bampton method. *Computers and Structures* 139 (2014) 54–64.
- [5] J.G. Kim, P.S. Lee, An accurate error estimator for Guyan reduction. *Computer Methods in Applied Mechanics and Engineering* 278 (2014) 1–19.
- [6] S.H. Boo, J.G. Kim, P.S. Lee, Simplified error estimator for the Craig–Bampton method and its application to error control. *Computers and Structures* 164 (2016) 53–62.
- [7] J.G. Kim, S.H. Boo, C.O. Lee, P.S. Lee, On the computational efficiency of the error estimator for Guyan reduction. *Computer Methods in Applied Mechanics and Engineering* 305 (2016) 759-776.
- [8] J.G. Kim, P.S. Lee, Reliability estimation of reduced-order models, *Proceedings of KSNVE conference 2014*, 698-699, Korea.

## Calibration of mechatronic flexible joint

Michael Valasek, Vaclav Bauma, Pavel Steinbauer

Faculty of Mechanical Engineering  
Czech Technical University in Prague  
Technicka 4, 16607 Praha 6, Czech Republic  
Michael.Valasek@fs.cvut.cz

### Abstract

The paper deals with the calibration of an example of multibody system with mechatronic flexible joint. Flexible joints are used in compliant mechanisms (e.g. robotic arm in Fig. 1). If they are actuated they are called mechatronic flexible joint. Precisely the flexible joint is a compliant body 1 fulfilling the function of movable connection of other bodies (e.g. Fig. 2). The mechatronic flexible joint is a flexible joint that is actuated and measured. If it is fulfilled the Saint-Venant principle then the mechatronic flexible joint can be described by finite number of parameters [1]. Therefore the existence of rigid flanges 10, 11 on both ends of flexible body 1 that creates the flexible joint is important (Fig. 2).

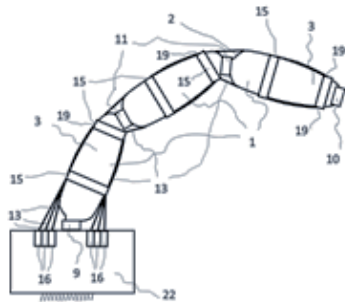


Figure 1. Robotic arm with mechatronic flexible joints.

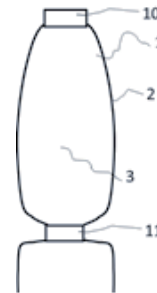


Figure 2. Mechatronic flexible joint.

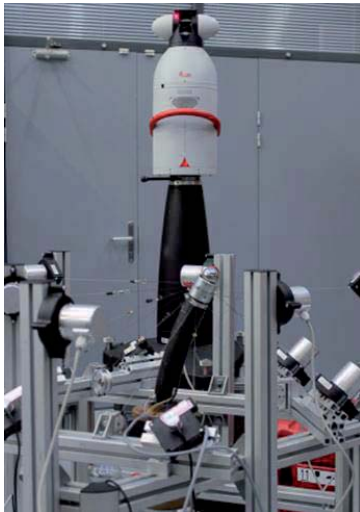


Figure 3. Experiment with calibration of mechatronic flexible joint based on inflated body.

A real example of mechatronic flexible body from the Fig. 1 is in Fig. 3. It consists of inflated body with constant air pressure in a body between two metallic flanges that are supposed to be rigid. The mechatronic flexible joint is fixed by one rigid flange to the frame and it is loaded by cables attached to the other rigid flange. Therefore the Saint-Venant principle is fulfilled and the mechatronic flexible joint can be described by finite number of parameters [1]. The position of this joint is measured by the distance sensors to fixed points at the frame (12 string distance sensors) and by the additional laser tracker for the reference.

The description naturally maps the applied forces (loading and actuating)  $F_L$  and  $u_F$  into the mechatronic flexible joint positions  $s$

$$s = MFJ(F_L, u_F) \quad (1)$$

It is described by LOLIMOT approach, that is an adaptive nonlinear description of input-output relation of a nonlinear system [2].

The calibration experiment is based on applying loading and actuating forces and the measurement of the mechatronic flexible joint position is carried out either by Laser tracker or by string distance measurements. The application of Laser tracker gives the mapping (1) from forces  $F_L$  and  $u_F$  to positions  $s$  of the mechatronic flexible joint and the application of string distance measurements  $d_k$  gives the possibility of self-calibration of the joint [1]. The self-calibration means that the redundant measurements of  $k$  string distance sensors enable to determine the positions of fixed points of the sensors at the frame, the offsets of distance sensors and finally the positions of the moving rigid flange of the mechatronic flexible joint. All these constant parameters are denoted as  $p$ . The function of distance sensors  $k$  can be generally described as

$$d_k = M(s, p) \quad (2)$$

If the number of sensors  $k$  and the number of measurements is large enough and the structural properties of the sensor scheme are suitable [1] then the self-calibration is possible and provides the results with reasonable accuracy. The paper describes the results of such experiment both computational and really experimental.

The practical importance of this self-calibration procedure for mechatronic flexible joint is the capability of on-line formulation of description (1) that cannot be derived just by geometric considerations. Despite of that a similar kinematic description of mechatronic flexible joint to the description of traditional kinematic joints is possible.

## Acknowledgements

This publication was supported by the project GA 101/13-39100S „ Mechatronic Flexible Joint“.

## References

- [1] Valasek, M., Bauma, V., Vampola, T.: Motion Description Of Mechatronic Flexible Joint, In: A.L. Araújo, C.A. Mota Soares, et al. (Editors): Proc. of 7th ECCOMAS Thematic Conference on Smart Structures and Materials (SMART 2015), IDMEC, Lisbon 2015, pp. 1-11
- [2] Štefan, M. - Šika, Z. - Valášek, M. - Bauma, V.: Neuro-Fuzzy Identification of Nonlinear Dynamic MIMO Systems, Engineering Mechanics. 2006, vol. 13, no. 3, p. 223-238.

# Modal Testing on Wind Turbines for Validation of a Flexible Multibody Model

János Zierath<sup>1</sup>, Roman Rachholz<sup>2</sup>, Sven-Erik Rosenow<sup>1</sup>, Reik Bockhahn<sup>1</sup>, Andreas Schulze<sup>2</sup>,  
Christoph Woernle<sup>2</sup>

<sup>1</sup> W2E Wind to Energy GmbH  
Strandstrasse 96, 18055 Rostock, Germany  
[jzierath, serosenow, rbockhahn]@wind-to-energy.de

<sup>2</sup> Chair of Technical Dynamics  
University of Rostock  
Justus-v.-Liebig-Weg 6, 18059 Rostock, Germany  
[roman.rachholz, andreas.schulze4, woernle]@uni-rostock.de

## Abstract

The life cycle of a wind turbine is mainly influenced by its dynamics. In order to avoid resonances in the variable speed range of a wind turbine, resonant frequencies of the entire turbine including substructure resonant frequencies as well as harmonic excitation must be known accurately. Whereas the harmonic excitation frequencies are multiples of the rotational speed and well known, resonant frequencies have to be calculated using a proper model or identified experimentally. A verification of calculated results by a measurement is the preferable approach. So the extensive knowledge and the deep understanding of the dynamics of a wind turbine allows the precise prediction of its behaviour. For the identification of the modal parameters the operational modal analysis (OMA) is chosen as it does not need any artificial excitation.

This contribution describes the identification of the modal parameters of the prototype W2E-93/2.0 wind turbine (Fig. 1), designed and manufactured by W2E Wind to Energy. The wind turbine prototype has been erected in 2011 in Tarnow, Mecklenburg-Western Pomerania, Germany (Fig. 1a). It has a hub height of 100 m, a rotor diameter of 93 m and a nominal rated power of 2.05 MW. A CAD sketch of the wind turbine labeling its main components is shown in Fig. 1b.

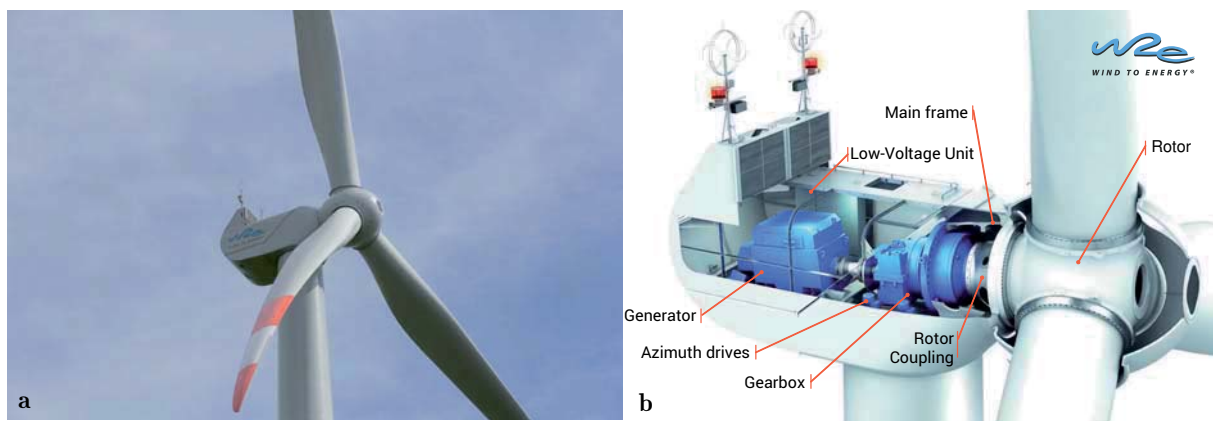


Figure 1: W2E-93/2.0 wind turbine **a** Wind turbine prototype, erected 2011 in Tarnow, Mecklenburg-Western Pomerania, Germany **b** CAD sketch of the nacelle of the 2.05 MW wind turbine

In a first step the OMA was conducted for the wind turbine with fixed rotor. During the measurement campaign the turbine and all mechanical devices such oil pumps and so on were stopped and the rotor blades were pitched out of the wind (feathered position). Several acceleration sensors were installed at different positions on the tower, the main frame, the gearbox, the generator, and the low-voltage unit. In order to achieve a high resolution of the measurements seven measurement cycles with different sensor positions keeping four reference sensors at the same positions were recorded. Altogether time data records for 61 measuring points were obtained. The vibration responses were recorded over a period of 90 minutes, sampled with a frequency of 512 Hz. For data acquisition a DYN-X system (Brüel & Kjær) with  $2 \times 24$ -bit AD converter (dynamic range 160 dB) in combination with seismic accelerometers (piezoelectric, sensitivity: 10 V/g, PCB) were applied.

Figure 2a shows exemplarily the first measurement cycle of the measurement campaign described above. The blue arrows represent the position and direction of the reference sensors which have been placed at the tower top position and at the rear end of the main frame. The green arrows represent the free placeable sensors, which have been applied on the tower during the first measurement cycle.

The software ARTEMIS Extractor was used for modal parameter identification. To extract resonant frequencies, corresponding to mode shapes and damping values, a frequency domain technique (Enhanced Frequency Domain Decomposition, EFDD) was applied for a preliminary analysis as well as a time domain technique (Stochastic Subspace Identification, SSI [1]) for a detailed analysis. Using the EFDD, a Singular Value Decomposition (SVD)

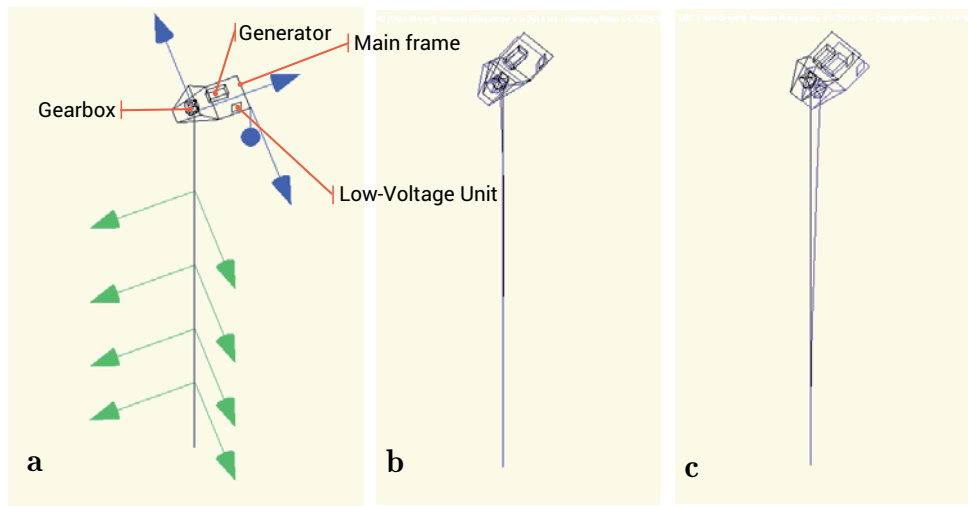


Figure 2: Measurement campaign **a** Measurement model with sensor setup for measurement series 1 (blue - reference sensors, green - free placeable sensors) **b** first measured tower mode in thrust direction **c** first measured tower mode in side-side direction

of the Power Spectral Density (PSD) was carried out in a first step. Since the singular values near the resonant frequency are proportional to the PSD of a SDOF system, it was used as a starting point for modal parameter estimation [2], [3]. To reduce random and leakage errors in PSD estimation, especially for damping identification of the first modes (starting from approx. 0.25 Hz), the long recording times (90 minutes) were necessary [4], [5]. Taking the advantage of the more sophisticated Stochastic Subspace Identification (SSI) [1], modal parameters were extracted in a detailed analysis. The SSI techniques rely on linear least squares estimation of the model using the raw measured time series. The Figs. 2b and 2c show the first tower modes in thrust and side-side direction obtained from the SSI extraction.

In a second step a measurement campaign has been carried out on a rotor blade on the ground during the replacement of the rotor main bearing of the wind turbine mentioned above. Here, the OMA has been applied to a rotor blade equipped with eight sensors. Furthermore a classical modal analysis measuring the artificial excitation and the response of the blade has been performed. The artificial excitation has been done by loading the structure by an specified weight and cutting off the line at which the weight is attached to the blade.

Finally the measured results are compared to a flexible multibody model that has been used for designing the wind turbine [6]. Some differences occurs due to uncertainties during the production of components, especially the blades, and some site-specific aspects of the foundation.

### Acknowledgement

The research presented here is part of the DynAWind project funded by the German Federal Ministry for Economic Affairs and Energy under the grant number FKZ 0325228C/D.

### References

- [1] Overschee P. V., Moor B. D. Subspace Identification for Linear Systems - Theory, Implementation, Applications, Kluwer, 1996.
- [2] Brincker R., Zhang L., Andersen P. Modal Identification for Ambient Responses Using Frequency Domain Decomposition, IMAC XVIII, 2000.
- [3] Brincker R., Ventura C., Andersen P. Damping Estimation by Frequency Domain Decomposition, IMAC XIX, 2001.
- [4] Uhlenbrock S., Rosenow S.-E., Schlottmann G. Application of Operational Modal Analysis to Marine Structures, IOMAC Workshop, 2006.
- [5] Tamura Y., Yoshida A., Zhang L., Ito T., Nakata S., Sato K. Examples of Modal Identification of Structures in Japan by FDD and MRD Techniques, 1<sup>st</sup> IOMAC, 2005
- [6] Zierath, J., Rachholz, R., Woernle, C. Field Test Validation of Flex5, MSC.Adams, alaska/Wind and SIM-PACK for Load Calculations on Wind Turbines. Wind Energy, 19(7):1201-122, 2016.

# A generalised Fourier method to solve the initial boundary value problem for free vibrating viscoelastic beam models

Holger Lang<sup>1</sup>, Sigrid Leyendecker<sup>1</sup>

<sup>1</sup> Chair of Applied Dynamics  
University of Erlangen-Nuremberg  
Immerwahrstrasse 1, 91058 Erlangen, Germany  
[holger.lang, sigrid.leyendecker]@fau.de

## Abstract

Fourier analysis is an extremely powerful and well-established tool for analysing oscillations of undamped linear mechanical structures, especially for beam structures [1, 2]. We extend this method to linear beam structures with viscoelastic damping mechanisms of Kelvin-Voigt kind, where the viscous stress contribution is proportional to the strain rate. In the following, we sketch the proposed generalised Fourier method.

The dynamic motion of a homogeneous and uniform axial beam with Kelvin-Voigt viscoelasticity can be described by its **normal displacement**  $u(x, t)$ , a real valued scalar function of the undeformed arclength parameter  $0 \leq x \leq 1$  and the time  $t \in \mathbb{R}$ . The equation of motion can be formulated as

$$\ddot{u} = u'' + 2\zeta \dot{u}', \quad \text{where } 0 \leq x \leq 1, \quad t \in \mathbb{R} \quad (1)$$

with the **viscosity**  $\zeta \geq 0$ . Here,  $' = \partial/\partial x$  and  $\dot{\phantom{x}} = \partial/\partial t$ . For a derivation of (1), which is formulated in non-dimensional form, see [4]. The internal **normal force** (or normal stress in the non-dimensional setting) is given by  $N = u' + 2\zeta \dot{u}'$ , where  $u'$  is the normal strain and  $\dot{u}'$  is its rate.

We impose the following initial resp. boundary conditions

$$u(x, 0) = u_0(x), \quad \dot{u}(x, 0) = \dot{u}_0(x) \quad \text{resp.} \quad u(0, t) \equiv 0, \quad u'(1, t) \equiv 0, \quad (2)$$

where  $0 \leq t$  and  $0 < x < 1$ . In (2), the initial positions  $u_0(x)$  and initial velocities  $\dot{u}_0(x)$  are prescribed functions of  $x$ . The boundary conditions in (2) belong to those of a cantilever. Note that  $u'(1, t) \equiv 0$  implies  $\dot{u}'(1, t) \equiv 0$ . Therefore, the normal force at the right free end vanishes identically, i.e.  $N(1, t) \equiv 0$ .

As demonstrated in [3], it is straightforward to see that real eigensolutions of (1), subjected to the boundary conditions (2), take the form

$$u_n(x, t) = f_n(t)U_n(x), \quad \text{where } U_n(x) = \sqrt{2} \sin(\omega_n x), \quad \omega_n = \left(n + \frac{1}{2}\right)\pi \quad (3)$$

and

$$f_n(t) = \exp(-\omega_n^2 \zeta t) \begin{cases} a_n \cos(\omega_n \sqrt{1 - \omega_n^2 \zeta^2} t) + b_n \sin(\omega_n \sqrt{1 - \omega_n^2 \zeta^2} t) & \text{if } \zeta < 1/\omega_n \\ a_n + b_n t & \text{if } \zeta = 1/\omega_n \\ a_n \exp(\omega_n \sqrt{\omega_n^2 \zeta^2 - 1} t) + b_n \exp(-\omega_n \sqrt{\omega_n^2 \zeta^2 - 1} t) & \text{if } \zeta > 1/\omega_n \end{cases} \quad (4)$$

for each  $n = 0, 1, 2, \dots$ . In (3), the number  $\omega_n$  denotes the  $n$ -th **undamped eigenfrequency**. Its corresponding **mode shape function** is  $U_n(x)$ , see [1]. The reciprocal  $1/\omega_n$  is the **critical viscosity** of the  $n$ -th eigenmode of the beam, the **total critical viscosity**  $\zeta^*$  is defined as the critical viscosity for the zeroth eigenmode, i.e.  $\zeta^* = 1/\omega_0 = 2/\pi$ , see [3, 4].

We assume, that the solution  $u(x, t)$  in (1) with (2) can be expanded into a **generalised Fourier series** of the form

$$u(x, t) = \sum_{n=0}^{\infty} f_n(t)U_n(x). \quad (5)$$

We let  $\langle v, w \rangle = \int_0^1 v(x)w(x) dx$  denote the  $L^2$  inner product, defined for square integrable functions  $v = v(x)$  and  $w = w(x)$  on the compact interval  $[0, 1]$ . Due to the orthonormality relationship  $\langle U_n, U_m \rangle = \delta_{nm}$  for  $n, m = 0, 1, 2, \dots$ , the well-known Fourier expansions  $u_0(x) = \sum_{n=0}^{\infty} \langle U_n, u_0 \rangle U_n(x)$  and  $\dot{u}_0(x) = \sum_{n=0}^{\infty} \langle U_n, \dot{u}_0 \rangle U_n(x)$  hold on  $[0, 1]$ , provided that the initial positions  $u_0(x)$  and initial velocities  $\dot{u}_0(x)$  are sufficiently regular.

Now, if (5) holds, it can be shown that the generalised Fourier coefficients  $a_n$  and  $b_n$  in (4) must take the following forms.

- If  $\zeta < 1/\omega_n$ ,

$$a_n = \langle U_n, u_0 \rangle, \quad b_n = \frac{1}{\omega_n} \left( \langle U_n, \dot{u}_0 \rangle + a_n \omega_n^2 \zeta \right) \sqrt{1 - \omega_n^2 \zeta^2}. \quad (6)$$

- If  $\zeta = 1/\omega_n$ ,

$$a_n = \langle U_n, u_0 \rangle, \quad b_n = \langle U_n, \dot{u}_0 \rangle + a_n \omega_n^2 \zeta. \quad (7)$$

- If  $\zeta > 1/\omega_n$ ,

$$a_n = \frac{1}{2\omega_n \sqrt{\omega_n^2 \zeta^2 - 1}} \left[ \omega_n \left( \sqrt{\omega_n^2 \zeta^2 - 1} + \omega_n \zeta \right) \langle U_n, u_0 \rangle + \langle U_n, \dot{u}_0 \rangle \right]$$

$$b_n = \frac{1}{2\omega_n \sqrt{\omega_n^2 \zeta^2 - 1}} \left[ \omega_n \left( \sqrt{\omega_n^2 \zeta^2 - 1} - \omega_n \zeta \right) \langle U_n, u_0 \rangle - \langle U_n, \dot{u}_0 \rangle \right]. \quad (8)$$

The proof can as well be carried out using the orthonormality of the eigenshapes  $U_n(x)$ . Note that in the non-dimensional setting – incidentally –  $\omega_n$  coincides with the  $n$ -th wave number of the beam [1, 4].

**Example** We consider the initial data

$$u_0(x) = x \quad \text{and} \quad \dot{u}_0(x) = 0, \quad \text{where} \quad 0 < x < 1. \quad (9)$$

Then, we have  $\langle U_n, u_0 \rangle = 4\sqrt{2}(-1)^n/\pi^2/(2n+1)^2$  and  $\langle U_n, \dot{u}_0 \rangle = 0$  for  $n = 0, 1, 2, \dots$ . These relations can be derived by induction, similarly as it is done in [2]. Figure 1 displays the Fourier resp. Finite Element solution for a sufficiently large number of elements. Both agree, which indicates the validity of the proposed method.

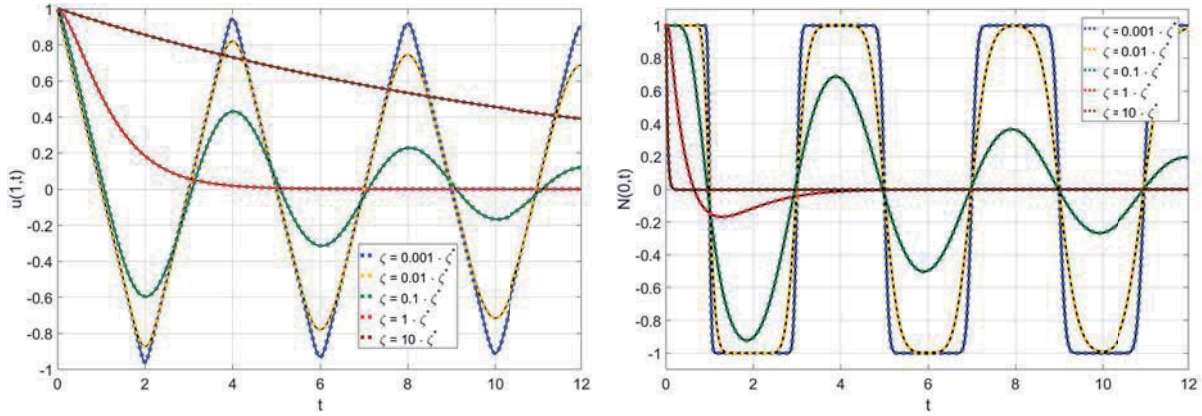


Figure 1: Solution of the IVBP (1), (2) with (9) for various viscosities  $\zeta$ . Left: Displacement  $u(1,t)$  at the right free end. Right: Normal force  $N(0,t)$  at the left clamped end. Colored: Fourier solution according to (5) together with (6), (7) and (8). Black: Finite Element solution according to [4, 5].

The extension of the proposed generalised Fourier method to viscoelastic torsional and Euler-Bernoulli bending beams of Kelvin-Voigt type, experimental convergence issues and the quantitative contribution of each eigen-solution  $u_n(x,t)$  to the series expansion (5) are part of the talk.

## References

- [1] R.R. Craig, A.J. Kurdila. Fundamentals of structural mechanics. John Wiley & Sons, 2006.
- [2] H. Heuser. Funktionalanalysis. Teubner, 1998.
- [3] H. Lang, S. Leyendecker, J. Linn. Numerical experiments for viscoelastic Cosserat rods with Kelvin-Voigt damping. In Proceedings ECCOMAS Thematic Conference on Multibody Dynamics, pp. 453–462, Zagreb, Croatia, 2013.
- [4] H. Lang, S. Leyendecker. Complex frequency response for linear beams with Kelvin-Voigt viscoelastic material. In Proceedings 4<sup>th</sup> Joint International Conference on Multibody System Dynamics, pp. 282–301, Montréal, Canada, 2016.
- [5] H.R. Schwarz. Finite element methods. Academic Press, 1988.

# Research on Form-finding and Deployment Dynamics for Modular Cable-Truss Antenna

Hanjiang Chang<sup>1</sup>, Kai Luo<sup>1</sup>, Qiang Tian<sup>1</sup>, Haiyan Hu<sup>1</sup>

<sup>1</sup> School of Aerospace Engineering  
Beijing Institute of Technology  
5 South Zhongguancun Street, Haidian District, 100081 Beijing, China  
hanjiangchang@163.com, luokai1212@bit.edu.cn,  
tianqiang\_hust@aliyun.com, haiyan\_hu@bit.edu.cn

## Abstract

Over the past years, the deployable space structure such as modular space deployable antenna with large aperture and high accuracy has a huge development potential to meet the increasing requirements of telecommunication industry. The antenna mesh reflector is a rigid-flexible coupling multibody system mainly composed of elastic supporting truss, flexible cable-net structure, metal mesh reflector and rigid joints. The form-finding of the antenna mesh reflector to design a reflective surface with accurate geometrical facet approximation is indispensable in the process of the reflector design. Besides, the deployment of the antenna mesh reflector is also a complicated process from the relative motions among its components to a rigid-flexible coupling system.

In order to obtain high precision reflector, the asymptotic iterative form-finding method is proposed based on the force density method<sup>[1]</sup> firstly. Figure 1 shows the reflector form-finding computation flowchart. The reflector geometric and material parameters are first specified. And then the desired cable tension force is specified, the initial cable force density coefficients of the reflector mesh can be evaluated. In the third part, the asymptotic iterative form-finding method is applied for the reflector form-finding. The desired reflector configuration is obtained when the criterion is satisfied; otherwise, the positions of the mesh boundary points will be updated according to the deformation of the reflector supporting truss. Figure 2 and 3 show the configuration of the reflector antenna before and after the form-finding process respectively. The positions of the points that connect the supporting truss also change after form-finding due to the truss deformation.

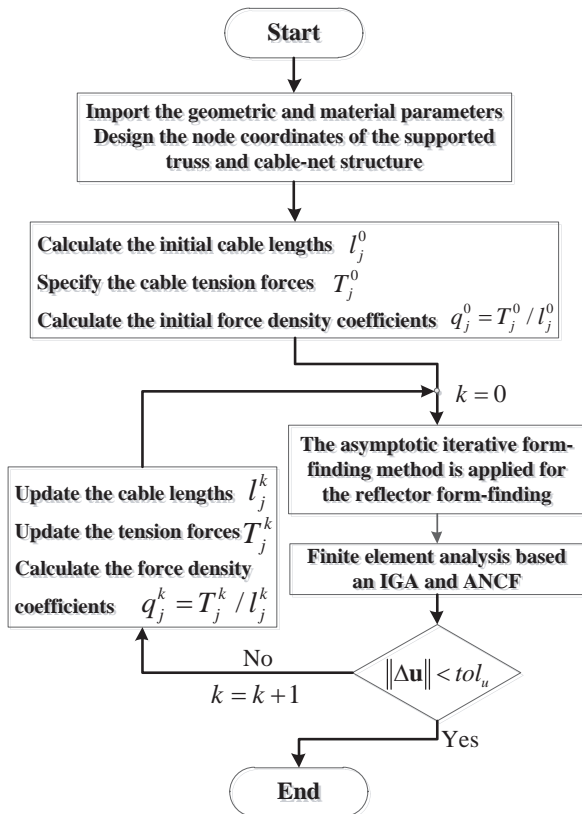


Figure 1. The reflector form-finding computation flowchart

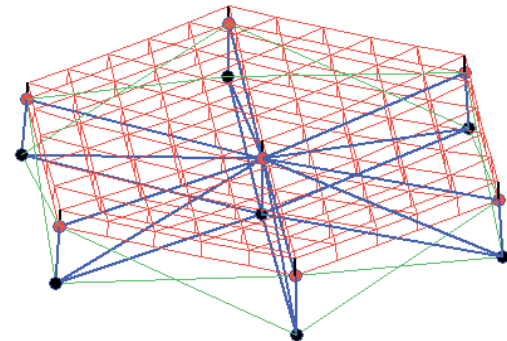


Figure 2. Configuration for the reflector before form-finding analysis

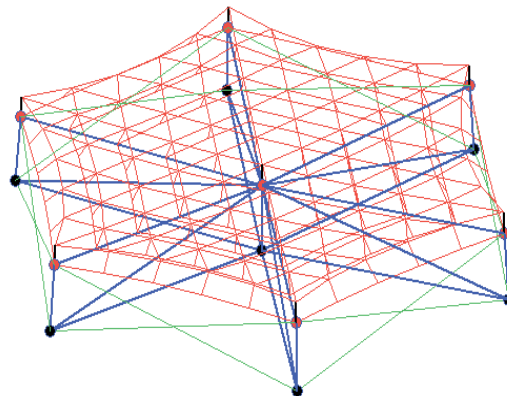
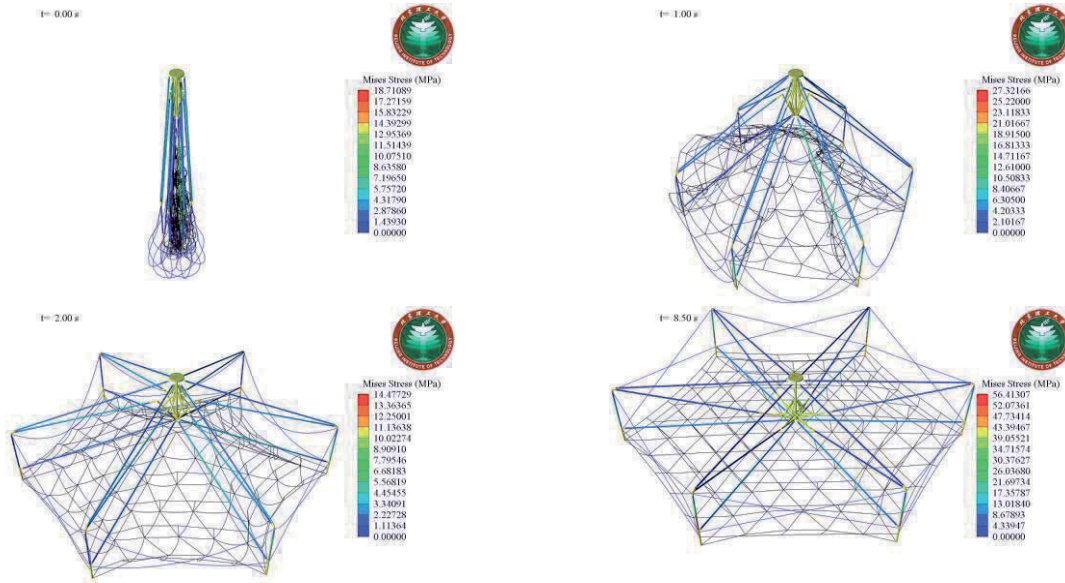


Figure 3. The Configuration for the reflector after form-finding analysis

In order to indicate the dynamic response of the space deployable antenna, the elastic flexible supporting truss is modeling with the fully parameterized beam elements in the frame of the absolute nodal coordinate formulation (ANCF)<sup>[2]</sup>, and the flexible cable-net structure is modeling with nonlinear NURBS cable elements<sup>[3]</sup>. Using the ANCF and IGA, the dynamic equations for the whole mesh reflector can be expressed as a set of differential algebraic equations with a constant mass matrix as following<sup>[4]</sup>:

$$\begin{cases} \mathbf{M}\ddot{\mathbf{q}} + \mathbf{F}(\mathbf{q}) + \mathbf{D}(\mathbf{q}, \dot{\mathbf{q}}) + \Phi_{\mathbf{q}}^T \lambda - \mathbf{Q}(\mathbf{q}, \dot{\mathbf{q}}, t) = \mathbf{0} \\ \Phi(\mathbf{q}, t) = \mathbf{0} \end{cases} \quad (1)$$

where  $\mathbf{M}$  is the constant mass matrix of the system,  $\mathbf{F}(\mathbf{q})$  is the elastic force vector which is a nonlinear function of nodal coordinates,  $\mathbf{D}$  is the damping force vector, in this study, the simple Rayleigh damping is used<sup>[5]</sup>.  $\Phi$  represents the vector that contains the system joint constraint equations,  $\Phi_{\mathbf{q}}$  is the derivative matrix of constraint equations with respect to the generalized coordinates  $\mathbf{q}$ ,  $\lambda$  is the Lagrange multiplier, and  $\mathbf{Q}$  is the external generalized forces.



**Figure 4.** Typical dynamic configurations of the deployment process

As shown in Figure 4, after form finding, the initial deployment configuration of the mesh reflector can be determined by shrinking the fully deployed mesh reflector to a quasi-static configuration. The deployment of the mesh reflector is achieved by applying the driving spring along the center bar. Finally, the typical four specific simulation moments of the mesh reflector dynamic configurations with von Mises stress contour are given in Figure 4. Other results will be shown on the conference report.

## Acknowledgments

This work was supported in part by National Natural Science Foundation of China under Grants Nos. 11290151 and 11302025. The work was also supported in part by Excellent Young Scholar Research Fund from Beijing Institute of Technology.

## References

- [1] K. Linkwitz. Formfinding by the "Direct Approach" and Pertinent Strategies for the Conceptual Design of Prestressed and Hanging Structures. *International Journal of Space Structures*, 14(2):73-87, 1999.
- [2] A. A. Shabana, R. Y. Yakoub. Three Dimensional Absolute Nodal Coordinate Formulation for Beam Elements: Theory. *Journal of Mechanical Design*, 123(4):614-621, 2001.
- [3] O. Weeger, U. Wever, B. Simeon. Isogeometric analysis of nonlinear Euler–Bernoulli beam vibrations. *Nonlinear Dynamics*, 72(4):813-835, 2013.
- [4] A. A. Shabana. *Computational dynamics*. John Wiley & Sons, 2010.
- [5] P. Li, C. Liu, Q. Tian, H. Hu, Y. Song. Dynamics of a Deployable Mesh Reflector of Satellite Antenna: Parallel Computation and Deployment Simulation. *Journal of Computational and Nonlinear Dynamics*, 11(6), 2016.

## Multibody dynamics of gear pairs: comparison among different models.

Marco Cirelli, Pier Paolo Valentini, Ettore Pennestri

Department of Enterprise Engineering  
University of Rome "Tor Vergata"  
Via del Politecnico 1, 00133, Italy  
marco.cirelli@uniroma2.it  
valentini@ing.uniroma2.it  
pennestri@mec.uniroma2.it

### Abstract

The paper reports about a comparison of different techniques for the dynamic simulation of spur gears. Dynamic analysis of gears represents an essential tool to identify and then to solve, motion irregularities, noise and vibration problems. Although the experimental approach is often adopted to understand the causes of noise, reliable analytical and numerical methods, with different complexity, are nowadays available. In the ideal case, gears are considered rigid with teeth meshing along the involute profiles. However, for the purpose of vibration phenomena simulation, gear flexibility, localized contact effects and speeds have all a significant influence on the dynamic behavior of gear mates and cannot be neglected.

For this kind of studies, different models based on multibody methodologies are available. The simplest model to simulate an approximate behavior of gears is the Rigid Multibody Gears (RMG). This model is generated considering gears as rigid bodies and the contact is simulated using a penetration law [1] between surfaces in contact. This kind of model has the great advantage to be light from the computational point of view, but doesn't provide accurate results in case of fast dynamics or variable loads. In fact, the flexibility of the components, one of the most important factor to evaluate noise or irregularities, is neglected. Furthermore, due to the displacement of gears, the RMG model does not replicate the effects connected to variation of the contact load direction during the engagement.

The setup of model with a realistic behavior requires to consider the gear deformation [2]. If we neglect shaft elasticity, the gear deformation can be associated mainly with three different causes [3,4]: the first one is the inflection of tooth due to bending and shear effects; the second one is the Hertzian type compression of the contact region [1]; the last one is the motion of the elastic foundation due to the thickness of the rim (Figure 1a). The Partial Flexible Multibody Gear (PFMG), based on the concept of flexible tooth, is a class of models that takes into account such effects. In these models, the tooth is considered as a rigid body connected to the main rigid body through a specific joint. In the translational tooth model (PFMGT), the joint used is a translational joint [5] located at the dedendum circle. In the rotational tooth model (PFMGR), the joint used, is a cylindrical or spherical joint [6] located on the midpoint of the segment that connects the extreme points of the tooth's arc (Figure 1b).

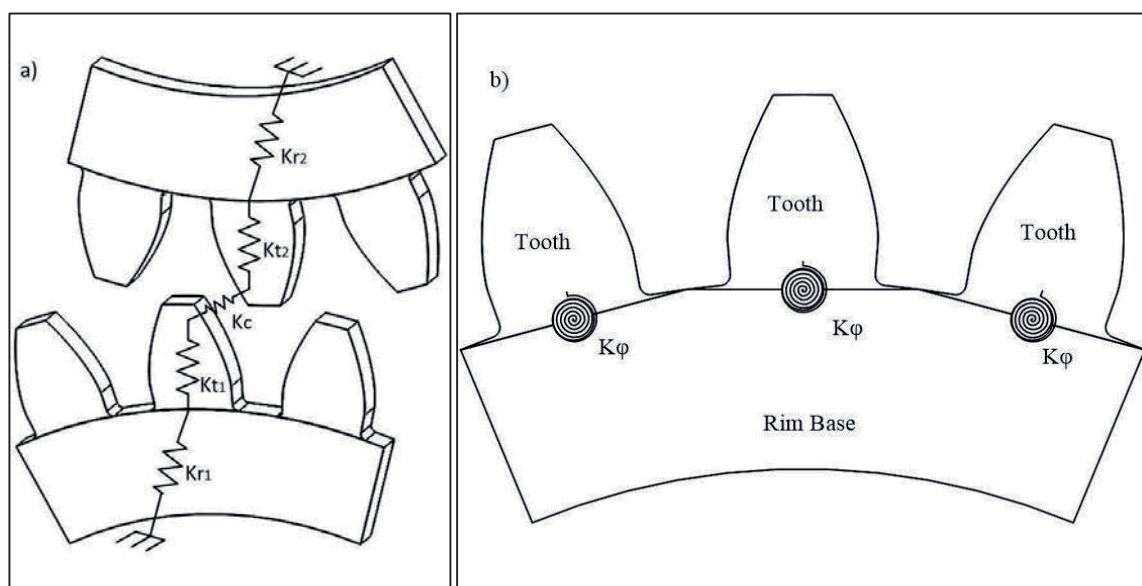


**Figure 1.** a) Construction of lumped method model of gear mates. b) Representation of flexible multibody model with rotational joints (PFMGR).

In this paper, a comparison among the three models (RMG, PFMGT and PFMGR) is discussed. A significant parameter to evaluate the dynamic behavior is the transmission error. It is defined as the deviation in position of the driven gear and the position it would occupy if the gear drive were perfectly conjugate. Using the subscript 1 and the subscript 2 to identify, respectively, the driving gear and the driven gear, the transmission error in an ordinary gear train can be expressed with the equation (1)

$$TE = \theta_2 - \frac{z_1}{z_2} \theta_1 \quad (1)$$

where  $\theta_i$  and  $z_i$  represent the angular position and the teeth number of  $i$ -th gear, respectively.

The transmission error, can be measured statically or dynamically. Static Transmission Error is evaluated when the loads are applied at very low speed (quasi-static situation), because it has the aim to give an evaluation of the effects due to the system's stiffness. Dynamic Transmission Error observed under dynamic conditions of mating is related to the noise.

The three models are also compared to a full flexible model of the gear pair in order to observe the differences in numerical results. Figure 2 shows the transmission error plots obtained with the full flexible model and the PFMGR model. This simulation was executed imposing a resisting torque of 2 Nm on the driven gear and an assigned ramp type rotational speed on the driving gear (starting from 0 rad/s at initial time and ending at 0.05s with 90 rad/s). The two spur gears are in steel, have a module  $m=2$  mm, same number of teeth (24) and pressure angle of 20 degrees.

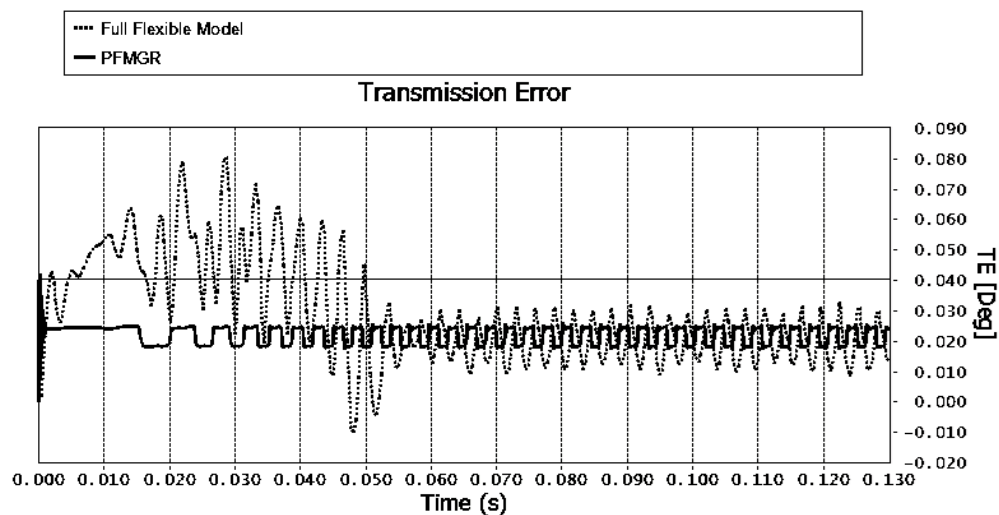


Figure 2. A comparison of transmission error in Full Flexible model and in PFMGR.

## References

- [1] Margarida Machado, Pedro Moreira, Paulo Flores, Hamid M. Lankarani. Compliant contact force models in multibody dynamics Evolution of the Hertz contact theory, *Mechanism and Machine Theory* 53 99–121, 2012.
- [2] Niels Leergaard Pedersen, Martin Felix Jørgensen. On gear tooth stiffness evaluation. *Computer and structures*, 135 109-117, 2015.
- [3] C. Weber. The Deformations of Loaded Gears and The Effect on Their Load-Carrying Capacity. Sponsored Research (Germany), British Dept. of Scientific and Industrial Research, Report No.3, 1949.
- [4] Zaigang Chen, Yimin Shao. Dynamic simulation of spur gear with tooth root crack propagating along tooth width and crack depth. *Engineering Failure Analysis*, Chongqing University, China, 2011.
- [5] Saeed Ebrahimi, Peter Eberhard. *Contact Modeling of Meshing Gear Wheels using Tangentially Movable Teeth*. Institute of Engineering and Computational Mechanics University of Stuttgart, Germany, 2006
- [6] Sunggyu Cho, Juhwan Choi, Jin Hwan Choi, Sungsoo Rhim. Numerical estimation of dynamic transmission error of gear by using quasi-flexible-body modeling method. *Journal of Mechanical Science and Technology* 29 2713-2719, 2015.

# Comparison of Model Order Reduction Techniques for Flexible Multibody Dynamics using an Equivalent Rigid-Link System Approach

Renato Vidoni<sup>1</sup>, Lorenzo Scalera<sup>2</sup>, Alessandro Gasparetto<sup>2</sup>, Marco Giovagnoni<sup>2</sup>

<sup>1</sup> Faculty of Science and Technology  
Free University of Bozen-Bolzano  
piazza Università 5, 39100, Bolzano, Italy  
renato.vidoni@unibz.it

<sup>2</sup> DPIA, Polytechnic Department  
of Engineering and Architecture  
University of Udine  
Via delle Scienze, 208, 33100, Udine, Italy  
scalera.lorenzo@spes.uniud.it  
alessandro.gasparetto@uniud.it  
giovagnoni@uniud.it

## Abstract

Nowadays, industrial robots and mechanisms are demanded to be lightweight, easily manoeuvrable and less energy-intensive. These features result in the design of manipulators in which structural flexibility has to be taken into account and, therefore, simulation and control become more difficult and challenging. For these reasons, the dynamic modeling of flexible multibody systems has become, in the last 20 years, a crucial research topic in both industry and academia and it is still an open area of investigation.

In multibody dynamics, the classical approach to take into account the flexibility of elastic mechanisms is based on the rigid-body dynamical model of the system and then the elastic deformations are introduced. The elastic deformations of the bodies are influenced by the rigid motion and vice versa. It results in a highly non-linear dynamic formulation described by a coupled set of partial differential equations. Two main methodologies can be found in literature for obtaining a set of ordinary differential equations: the nodal approach (i.e. the Finite Element Method, FEM) and the modal one [1]. However, since a high number of Degrees of Freedom is introduced by the discretization of the flexible bodies, proper reduction methods should be applied in order to allow an efficient simulation of the multibody system while keeping an accurate description of the predominant dynamic behaviour.

Different model reduction techniques have been studied and proposed by several authors, starting from the dynamic equilibrium equation such as:

$$M\ddot{x}(t) + C\dot{x}(t) + Kx(t) = F(t) \quad (1)$$

where  $M$ ,  $C$ ,  $K$  are the mass, dumping and stiffness matrices,  $x$  is the independent coordinates and  $F$  is the force vector acting on the system.

In particular, model reduction methods can be classified in physical coordinates techniques, generalized coordinates (i.e. modal coordinates) and hybrid methods, such as the Component Mode Synthesis (CMS). A review of model reduction techniques for structural dynamics, numerical mathematics and system and control is proposed in [2], whereas in [3] reduced order modeling strategies are applied in dynamics sub-structuring. An example of model reduction can be found in [4], in which a study on an elastic rod is proposed. Furthermore, in the field of multibody systems, an overview of the basic approaches to model elastic multibody systems with the help of Floating Frame of Reference formulation is given by [5]. A new ranking method (Interior Ranking Method, IMR) for the selection of interior normal modes in the Craig-Bampton technique [6] has been proposed in [7].

In this work, a theoretical and numerical comparison of different reduced order modeling strategies in flexible multibody dynamics is presented. In particular, an Equivalent Rigid-Link System (ERLS) formulation for modeling the dynamics of flexible multibody systems is applied [8] [9]. This approach, suitable in the case of large displacements and small elastic deformations, differently from other formulations, e.g. the Floating Frame of Reference (FFR), enables the kinematic equations of the ERLS to be decoupled from the compatibility equations of the displacement at the joints. It has been recently extended through a modal approach so as to obtain a more flexible solution based on a reduced-order system of equations. In particular, the dynamics of spatial flexible mechanisms is formulated with a Component Mode Synthesis technique (ERLS-CMS) and a Craig-Bampton approach has been adopted [10]. However, the Craig-Bampton reduction is not the only technique that is capable of reducing a high number degrees-of-freedom model. Indeed, it can be reduced either at substructure level, i.e. “component level reduction”, or at the whole model, i.e. “system level reduction”.

Different model reduction techniques such as Craig-Bampton, Interior Mode Ranking (IMR), Guyan, SEREP, Least Square Model Reduction (LSMR), Mode Displacement Method and Subspace Iteration Method are here implemented and the results compared. In order to assess the advantages and disadvantages of the different methodologies, these techniques can be applied to different benchmarks (Fig.1), e.g. L-shaped, slider-crank, double pendulum or four- and five- bar mechanisms.

FEM models for each link of the benchmark mechanisms are developed in Ansys<sup>®</sup> environment with different discretizations, whereas dynamics and post-processing are evaluated by means of Matlab<sup>™</sup>. The reduced model

accuracy is evaluated through the comparison of the computational time, the accuracy in the frequency domain and by means of vector correlation methods such as the Modal Assurance Criterion (MAC), the Cross-Orthogonality (CO) and the Normalized Cross-Orthogonality (NCO) [3] [7]. Moreover, the mechanisms behaviour is simulated under different input conditions, e.g. a step torque input and gravitational force, and nodal displacements, accelerations and frequency response compared. Results allow to obtain several different considerations about the effectiveness of different model reduction methods in different simulated cases.

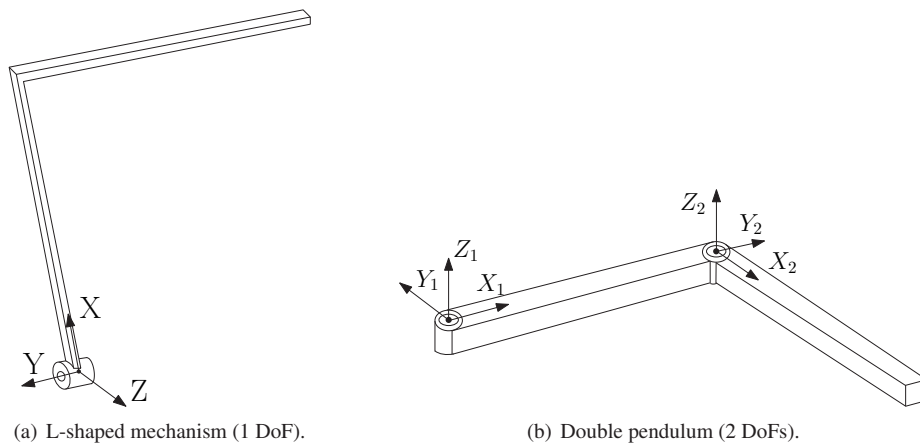


Figure 1: Examples of benchmark mechanisms.

## References

- [1] Shabana, A. A. Flexible multibody dynamics: review of past and recent developments. *Multibody system dynamics*, 1.2, 189-222, 1997.
- [2] Besselink, B., Tabak, U., Lutowska, A., Van De Wouw, N., Nijmeijer, H., Rixen, D. J., Hochstenbach, M. E., Schilders, W. H. A. A comparison of model reduction techniques from structural dynamics, numerical mathematics and systems and control. *Journal of Sound and Vibration*, 332(19), 4403-4422, 2013.
- [3] Roettgen, D., Seeger, B., Tai, W. C., Baek, S., Dossogne, T., Allen, M., Kuether, R., Brake, M. R. W., Mayes, R. A Comparison of Reduced Order Modeling Techniques Used in Dynamic Substructuring. In *Dynamics of Coupled Structures*, Volume 4, 511-528, Springer International Publishing, 2016.
- [4] Koutsovasilis, P., Beitelschmidt, M. Comparison of model reduction techniques for large mechanical systems. *Multibody System Dynamics*, 20(2), 111-128, 2008.
- [5] Nowakowski, C., Fehr, J., Fischer, M., Eberhard, P. Model order reduction in elastic multibody systems using the floating frame of reference formulation. *IFAC Proceedings Volumes*, 45(2), 40-48, 2012.
- [6] Bampton, M. C., Craig, R. R. Coupling of substructures for dynamic analyses. *Aiaa Journal*, 6(7), 1313-1319, 1968.
- [7] Palomba, I., Richiedei, D., Trevisani, A. Mode Selection for Reduced Order Modeling of Mechanical Systems Excited at Resonance. *International Journal of Mechanical Sciences*, 2016.
- [8] Vidoni, R., Gasparetto, A., Giovagnoni, M. Design and implementation of an ERLS-based 3-D dynamic formulation for flexible-link robots. *Robotics and Computer-Integrated Manufacturing*, 29(2), 273-282, 2013.
- [9] Vidoni, R., Gasparetto, A., Giovagnoni, M. A method for modeling three-dimensional flexible mechanisms based on an equivalent rigid-link system. *JVC/Journal of Vibration and Control*, 20(4), 483-500, 2014.
- [10] Vidoni, R., Gallina, P., Boscariol, P., Gasparetto, A., Giovagnoni, M. Modeling the vibration of spatial flexible mechanisms through an equivalent rigid-link system/component mode synthesis approach. *Journal of Vibration and Control*, 2015.

## Modelling and simulation of mechatronic flexible joint

Michael Valasek, Vaclav Bauma

Faculty of Mechanical Engineering  
Czech Technical University in Prague  
Technicka 4, 16607 Praha 6, Czech Republic  
[Michael.Valasek, Vaclav.Bauma]@fs.cvut.cz

### Abstract

The paper deals with the modeling and simulation of multibody systems where some of the joints are mechatronic flexible joints. Flexible joints are used in compliant mechanisms (e.g. robotic arm in Fig. 1). If they are actuated they are called mechatronic flexible joint. Precisely the flexible joint is a compliant body fulfilling the function of movable connection of other bodies(e.g. Fig. 2). The mechatronic flexible joint is a flexible joint that is actuated and measured. If it is fulfilled the Saint-Venant principle then the mechatronic flexible joint can be described by finite number of parameters [1]. Therefore the existence of rigid flanges 10, 11 on both ends of flexible body 1 that creates the flexible joint is important (Fig. 2).

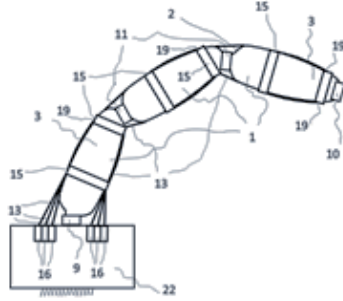


Figure 1. Robotic arm with mechatronic flexible joints.

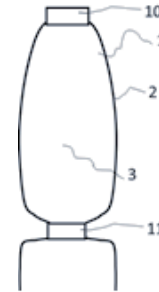


Figure 2. Mechatronic flexible joint.

The description naturally maps the applied forces (loading and actuating)  $F_L$  and  $u_F$  into the mechatronic flexible joint positions  $s$

$$s = MFJ(F_L, u_F) \quad (1)$$

The forces  $F_L$  includes the moments. It is described by LOLIMOT approach, that is an adaptive nonlinear description of input-output relation  $MFJ$  of a nonlinear system [2]. It is an adaptive nonlinear description of input-output relation of a nonlinear system [2]. The output  $\mathbf{y}$  is described as a function of input  $\mathbf{u}$  by summation of linear models with coefficients  $\mathbf{w}$  and weighting Gaussian functions  $\Phi$

$$\hat{y} = \sum_{i=1}^M \hat{y}_i \Phi_i(\mathbf{u}) = \sum_{i=1}^M (w_{i,0} + w_{i,1}u_1(k) + w_{i,2}u_1(k-1) + w_{i,n_1+1}u_1(k-n_1) + w_{i,n_1+2}u_2(k) + w_{i,n_1+3}u_2(k-1) + \dots + w_{i,n_1+n_2+2}u_2(k-n_2) + w_{i,n_1+\dots+n_{p-1}+p}u_p(k) + w_{i,n_1+\dots+n_{p-1}+p}u_p(k-n_p) + w_{i,n_1+\dots+n_{p-1}+p+1}y(k-1) + w_{i,n_1+\dots+n_{p-1}+p+n_y}y(k-n_y)) \Phi_i(\mathbf{u}) \quad (2)$$

The overall nonlinear function is replaced by local linear functions that are smoothed by Gaussian functions  $\Phi$  in weighted sum. Certainly, it must be taken into account that this description of mechatronic flexible joint is quasi-static as the identification experiments are carried out quasi-statically. Similar problem but with dynamic identification experiments are at damper description [3].

The description naturally maps the applied forces (loading and actuating) into the mechatronic flexible joint positions. This is however a difficulty for multibody modelling and simulation. The equations of motion are mapping the forces into the body accelerations, i.e. the opposite direction.

The simulation model is developed by the inverse of this mapping immediately or after the substitution of accelerations from the Newton-Euler law described in composite form [4]. Then the multibody simulation can be completed. The forces acting on the upper flange at Fig. 2 include the inertia forces in composite formulation

$$s = MFJ(F_L + I^P a^P - \beta^P, u_F) \quad (3)$$

where  $\mathbf{I}^P$  is composite inertia matrix,  $\mathbf{a}^P$  composite acceleration,  $\boldsymbol{\beta}^P$  composite dynamic forces. This equation is then inverted or solved for the composite acceleration that is then integrated. However, in order to do it is necessary to express the composite accelerations by the time derivatives of the relative physical coordinates of mutual positions of the subsequent flanges in the chain of flanges.

The other approach is based on the first inversion of the dependence (1)

$$F_L + I^P a^P - \beta^P = MFJ^{-1}(s, u_F) \quad (4)$$

This equation is simply resolved for the composite acceleration that is then integrated.

Both approaches lead to the description of composite acceleration of a body that is unified with the rigid flange of the mechatronic flexible joint. This enables to carry out the dynamic simulation of motion of mechatronic flexible joint similarly as the description of automotive dampers.

### **Acknowledgements**

This publication was supported by the project GA 101/13-39100S „Mechatronic Flexible Joint“.

### **References**

- [1] Valasek, M., Bauma, V., Vampola, T.: Motion Description Of Mechatronic Flexible Joint, In: A.L. Araújo, C.A. Mota Soares, et al. (Editors): Proc. of 7th ECCOMAS Thematic Conference on Smart Structures and Materials (SMART 2015), IDMEC, Lisbon 2015, pp. 1-11
- [2] Štefan, M. - Šika, Z. - Valášek, M. - Bauma, V.: Neuro-Fuzzy Identification of Nonlinear Dynamic MIMO Systems, Engineering Mechanics. 2006, vol. 13, no. 3, p. 223-238.
- [3] Šika, Z.; Valášek, M.; Bauma, V.; Bílkovský, A.: Efficient Nonlinear Models of Automotive Dampers, In: Proc. Of Multibody Dynamics 2009, Warszawa: Oficyna wydawnicza Politechniki Warszawskiej, 2009, pp. 1-9.
- [4] Stejskal, V., Valasek, M.: Kinematics and Dynamics of Machinery, Marcel Dekker, New York 1996.

## Two Approaches of the Rigid Finite Element Method to Modelling the Flexibility of Spatial Linkage Links

Krzysztof Augustynek, Andrzej Urbaś

Faculty of Mechanical Engineering and Computer Science  
University of Bielsko-Biala  
Willowa 2, 43-309 Bielsko-Biala, Poland  
[kaugustynek, aurbas]@ath.bielsko.pl

### Abstract

The paper presents dynamics analysis of spatial serial linkages. A mathematical model of a selected case of these linkages in the form of an RSUP linkage is considered. This model allows to take into account the links' flexibility and friction in the joints. The linkage is built of four links ( $n_i$ ) – Fig. 1. The first link of the linkage is loaded by both driving ( $\mathbf{t}_{dr}^{(1,1)}$ ) and resistance ( $\mathbf{t}_{res}^{(1,1)}$ ) torques.

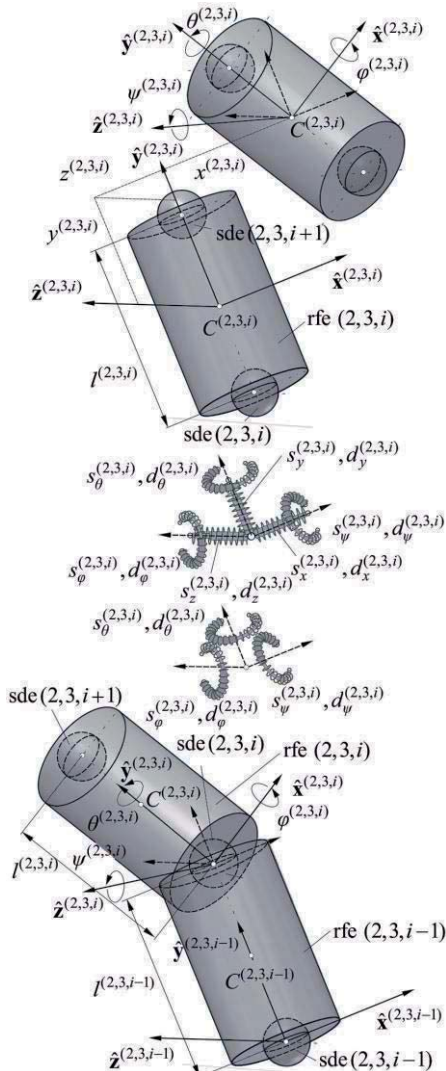


Figure 2. Discretisation of the link in:  
RFEM<sub>c</sub> (top) and RFEM<sub>m</sub> (bottom)

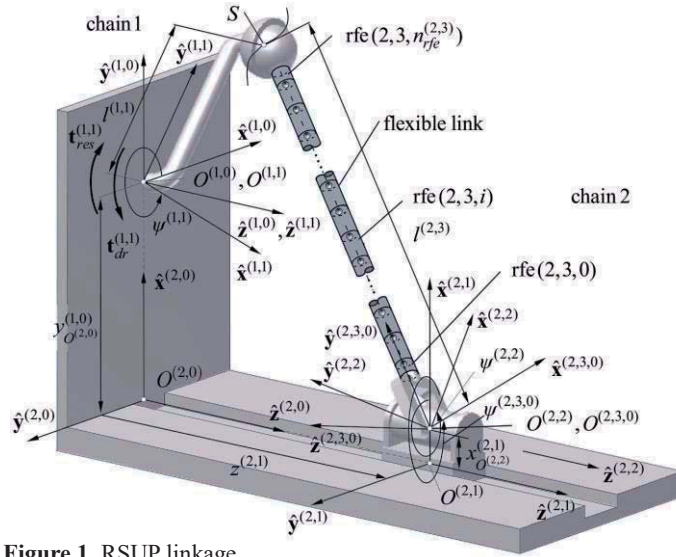


Figure 1. RSUP linkage

The second link (coupler) is considered as flexible. In order to model the flexibility of this link, the rigid finite element method [1,2] in the classical (RFEM<sub>c</sub>) and modified (RFEM<sub>m</sub>) formulations was taken into account – Fig. 2. In this method the flexible link is replaced by means of the system of  $n_{rfe}$  rigid elements interconnected by  $n_{sde}$  spring damping elements which describe the link's flexibility.

Friction is taken into account only in the prismatic joint. The LuGre model is proposed in order to determine the friction coefficient in this joint [3].

The cut-joint technique in an ideal spherical joint is used to eliminate the closed-loop kinematic chain from the system. As a result, the linkage is separated into two open-loop kinematic chains.

The formalism of joint coordinates and homogeneous transformation matrices [4] is used to describe the chains' geometry. The vector of generalised coordinates is defined in the following form

$$\mathbf{q} = \begin{bmatrix} \mathbf{q}^{(1,1)^T} & \mathbf{q}^{(2,3)^T} \end{bmatrix}^T = \begin{bmatrix} \tilde{\mathbf{q}}^{(1,1)^T} & \tilde{\mathbf{q}}^{(2,1)^T} & \tilde{\mathbf{q}}^{(2,2)^T} & \tilde{\mathbf{q}}^{(2,3)^T} \end{bmatrix}^T = \begin{bmatrix} \tilde{\mathbf{q}}^{(1,1)^T} & \tilde{\mathbf{q}}^{(2,1)^T} & \tilde{\mathbf{q}}^{(2,2)^T} & \tilde{\mathbf{q}}^{(2,3,0)^T} & \dots & \tilde{\mathbf{q}}^{(2,3,i)^T} & \dots & \tilde{\mathbf{q}}^{(2,3,n_{rfe}^{(2,3)})^T} \end{bmatrix}^T,$$

$$\text{where: } \tilde{\mathbf{q}}^{(1,1)} = [\psi^{(1,1)}], \quad \tilde{\mathbf{q}}^{(2,1)} = [z^{(2,1)}],$$

$$\tilde{\mathbf{q}}^{(2,2)} = [\psi^{(2,2)}], \quad \tilde{\mathbf{q}}^{(2,3,0)} = [\psi^{(2,3,0)}],$$

$$\tilde{\mathbf{q}}^{(2,3,i)} = \begin{cases} \begin{bmatrix} x^{(2,3,i)} & y^{(2,3,i)} & z^{(2,3,i)} & \psi^{(2,3,i)} & \theta^{(2,3,i)} & \varphi^{(2,3,i)} \end{bmatrix}^T & \text{– RFEM}_c \\ \begin{bmatrix} \psi^{(2,3,i)} & \theta^{(2,3,i)} & \varphi^{(2,3,i)} \end{bmatrix}^T & \text{– RFEM}_m \end{cases}$$

The  $RFEM_m$  takes into account only torsional and bending deformations, and motion  $rfe(2,3,i)$  is described in relation to the preceding element. In  $RFEM_c$ , each element has six degrees of freedom which allows to obtain also normal and shear forces that result from the deformation of the flexible link.

The equations of the chains' motion are derived by using the Lagrange equations and the algorithms presented in [2,5]. The Runge-Kutta method of the fourth order with a fixed step-size equal to  $10^{-5}$ s is used to integrate these equations.

Fig. 3 presents the slider displacements of the rigid and flexible link obtained when friction is omitted and when friction in the prismatic joint is taken into account. A significant influence of the friction phenomenon and the flexibility of the link on the motion of the slider can be observed. The stick phases are shorter and the motion of the linkage is smoother when flexibility of the coupler is considered. The difference between the courses obtained for both formulations of RFEM show that normal deformation of the link cannot be neglected when friction in the slider is considered.

The significant influence of the friction phenomenon on forces acting in the cut-joint is presented in Fig 4. When the flexibility of the coupler is taken into account the forces are significantly smaller because some part of the system's total energy is transformed into the link's spring deformation. This takes into account the normal and shear forces; therefore, forces in the cut-joint are slightly larger than those obtained from  $RFEM_m$ .

## References

- [1] J. Kruszewski, S. Sawiak, E. Wittbrodt. *The rigid finite element method in dynamics*, Science and Technical Publishers, Warsaw, 1999. (in Polish)
- [2] E. Wittbrodt, I. Adamiec-Wójcik, S. Wojciech. *Dynamics of flexible multibody systems. Rigid finite element method*, Springer, Berlin-Heidelberg, 2006.
- [3] C. Canudas de Wit, H. Ollson, K.J. Åström, P. Lischinsky. A new model for control of systems with friction, *IEEE Trans. Automat. Control*, 40:419-425, 1995.
- [4] J. J. Craig. *Introduction to robotics. Mechanics and control*, Addison-Wesley Publishing Company, Inc., 1989.
- [5] E. I. Jurevič. *Dynamics of robot control*, Nauka, Moscow, 1984. (in Russian)

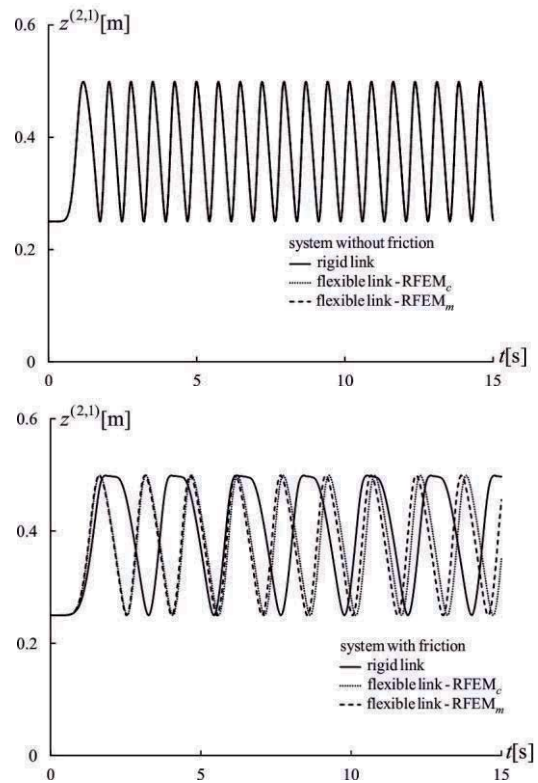


Figure 3. Slider's displacement

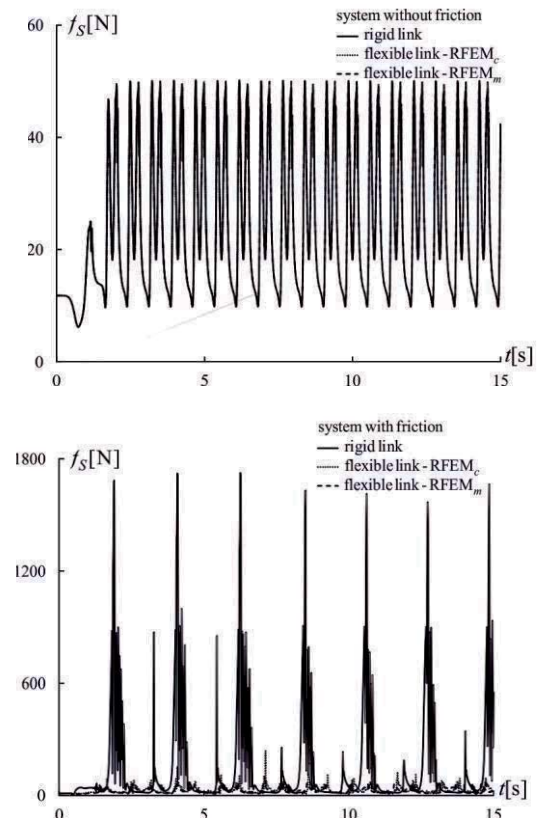


Figure 4. Courses of joint forces in spherical joint S

## Kinematic and Dynamic Behavior of Hyperelastic Plate with External Force via Absolute Nodal Coordinate Formulation

Haidong Yu<sup>1</sup>, Jingjing Luo<sup>1</sup>, Canming Yi<sup>1</sup>, Hao Wang<sup>2</sup>

<sup>1</sup>Key Laboratory of Digital Manufacture for Thin-walled Structure  
Shanghai Jiao Tong University  
Dongchuan Rd 800, 200240 Shanghai, P.R. China  
[hdyu, jingjing.luo, yicanming]@sjtu.edu.cn

<sup>2</sup>Key Laboratory of Mechanical System and Vibration  
Shanghai Jiao Tong University  
Dongchuan Rd 800, 200240 Shanghai, P.R. China  
wanghao@sjtu.edu.cn

### Abstract

Hyperelastic materials are widely used in soft robotics for their potential advantages of flexibility and efficiency in the complex work space. The large deformation during the motion will cause the variation of the stiffness matrix and lead to a change of kinematic behavior and accuracy of soft structures. The kinematic and dynamic behavior of the structures driven by external force is of great significance for the accurate control and performance of the soft machines. In this context, the dynamic models for two hyperelastic constitutive models is established based on the absolute nodal coordinate formulation. The kinematic and dynamic performances are investigated for thin plates with various geometrical parameters and mechanical behavior of materials.

In this study, the ANCF procedure is introduced to derive the dynamic model of the plate structure. The coordinate of the nodes in the plate structure can be described with high-order shape function and shown as

$$\mathbf{r} = \mathbf{S}\mathbf{e} = \begin{bmatrix} a_0 + a_1x + a_2y + a_3z + a_4xz + a_5yz + a_6xy + a_7x^2 + a_8y^2 + a_9x^3 + a_{10}y^3 + a_{11}x^2y + a_{12}y^2x + a_{13}xyz + a_{14}x^3y + a_{15}xy^3 \\ b_0 + b_1x + b_2y + b_3z + b_4xz + b_5yz + b_6xy + b_7x^2 + b_8y^2 + b_9x^3 + b_{10}y^3 + b_{11}x^2y + b_{12}y^2x + b_{13}xyz + b_{14}x^3y + b_{15}xy^3 \\ c_0 + c_1x + c_2y + c_3z + c_4xz + c_5yz + c_6xy + c_7x^2 + c_8y^2 + c_9x^3 + c_{10}y^3 + c_{11}x^2y + c_{12}y^2x + c_{13}xyz + c_{14}x^3y + c_{15}xy^3 \end{bmatrix} \quad (1)$$

where  $\mathbf{S}$  is the shape function matrix,  $\mathbf{e}$  is the absolute nodal coordinate vector.

For more efficient solutions in the case of large deformation, two hyper-elastic constitutive models, Neo-Hookean and Mooney-Rivlin material models, are applied for the plate structure. The generalized elastic force based on Neo-Hookean and Mooney-Rivlin material models, is presented as

$$\mathbf{Q}_{NHC} = \frac{\partial W_{NHC}}{\partial \mathbf{e}} = \frac{\mu}{2} \frac{\partial(\text{tr}(\mathbf{C}))}{\partial \mathbf{e}} + \left( \frac{\lambda \ln J - \mu}{J} \right) \frac{\partial J}{\partial \mathbf{e}} \quad (2)$$

$$\mathbf{Q}_{MRI} = \frac{\partial W_{MRI}}{\partial \mathbf{e}} = (C_1 + C_2 \text{tr}(\mathbf{C})) \frac{\partial(\text{tr}(\mathbf{C}))}{\partial \mathbf{e}} - \frac{C_2}{2} \frac{\partial(\text{tr}(\mathbf{C}^2))}{\partial \mathbf{e}} + k(J-1) \frac{\partial J}{\partial \mathbf{e}} \quad (3)$$

$$\mathbf{C} = \mathbf{J}^T \mathbf{J} \quad (4)$$

where  $\mathbf{J}$  is the Jacobian matrix,  $J$  is the determinant of the Jacobian matrix,  $\lambda$  and  $\mu$  are the Lamé's Constants.

With the help of the shape function matrix and the constitutive models, the dynamic model of plate based on Newton formulation is defined as

$$\mathbf{M}\ddot{\mathbf{e}} + \mathbf{Q} = \mathbf{Q}_a \quad (5)$$

where  $\mathbf{M}$  is the mass matrix of the structure,  $\mathbf{Q}$  is the generalized elastic force,  $\mathbf{Q}_a$  is the generalized force. The mass matrix and the generalized force can be given as

$$\mathbf{M} = \int_V \rho \mathbf{S}^T \mathbf{S} dV \quad (6)$$

$$\mathbf{Q}_a^T = \mathbf{F}^T \mathbf{S} \quad (7)$$

respectively, where  $\rho$  is the density of the material,  $\mathbf{F}$  is the force applied on the structure.

A flexible pendulum plane is employed to study the kinematic and dynamic behavior of plate structures and

is shown in Figure 1. Side AD is fixed with a revolute joint, while side BC is loaded by a force sinusoidal.

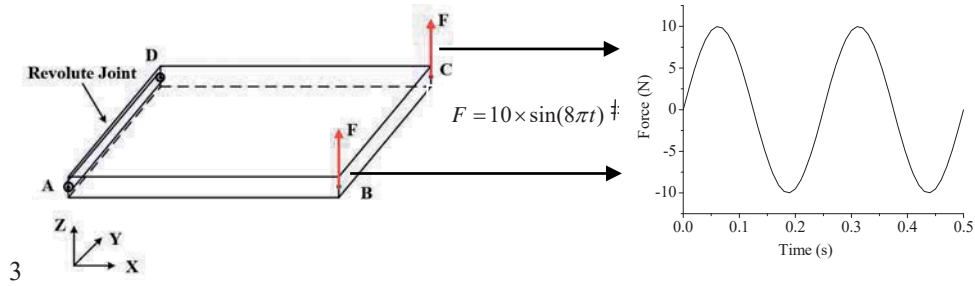


**Figure 1.** Flexible pendulum plane with the force sinusoidal

The deformations of plate at various times are shown in Figure 2. Here the time increment is 0.05s. The deformations of plates in different material models have certain similarity. At the first 0.05s, the displacement of plate using Hookean model is greater than that with hyper-elastic materials. It shows that the response driven by the external force of Hookean material is more efficient than the hyper-elastic materials.

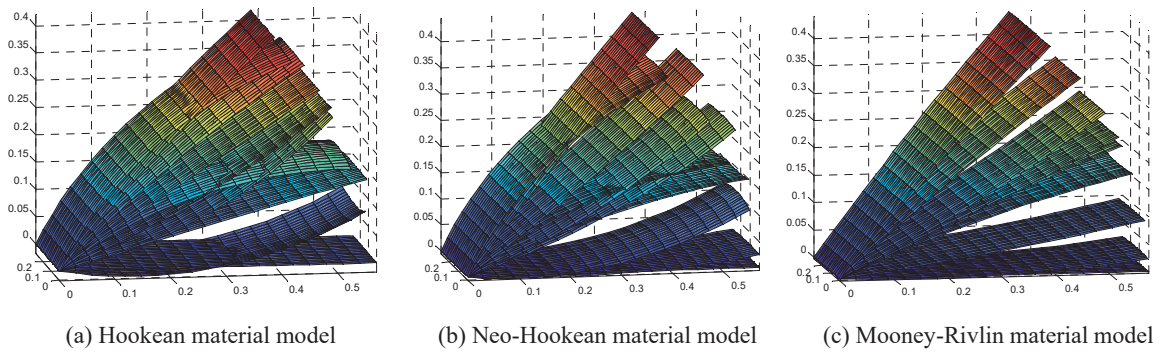


**Figure 2.** Deformed shape of the plate at different time step

Meanwhile, the kinematic and dynamic behavior of the plates with different geometrical parameters and Young's module are discussed and shown in Figure 3. The results may provide the guidance for the mechanical design of soft machines.

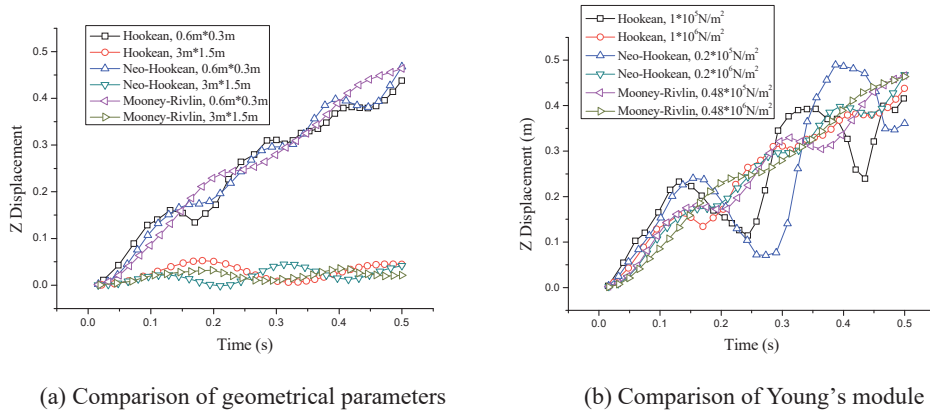


**Figure 3.** Displacement of node B with respect of time with various geometrical and material parameters

## Acknowledgments

The authors appreciate the financial support by the National Natural Science Foundation of China (51275292) and State Key Development Program of Basic Research of China (2014CB046600).

# On the Use of the Absolute Nodal Coordinate Formulation for the Dynamic Analysis of Rotating Shafts

Vesa-Ville Hurskainen<sup>1</sup>, Marko K. Matikainen<sup>1</sup>, Jia Wang<sup>2</sup>, Aki Mikkola<sup>1</sup>,

<sup>1</sup> School of Energy Systems

Lappeenranta University of Technology

Skinnarilankatu 34, 53851 Lappeenranta, Finland

vesa-ville.hurskainen@lut.fi

marko.matikainen@lut.fi

aki.mikkola@lut.fi

<sup>2</sup> School of Mechatronic Engineering

Harbin Institute of Technology

92 West Dazhi Street, 150001 Harbin, China

wangjia\_hit@163.com

## Abstract

When designing rotating machines, it is crucial to ensure that vibrations do not cause excessive wear on bearings, or additional noise at operating speeds or during running up. To predict vibrations and determine critical speeds of rotating machines, an often used approach is the Campbell diagram, constructed by solving the eigenvalue problem of the finite element model at each rotational speed and plotting the resulting natural frequencies. For this application, structural finite elements (such as Timoshenko beam elements) are often used due to their simplicity and low computational costs. It is, however, noteworthy that transient dynamic analyses are also sometimes needed in the design process to analyze rotor dynamics in case of acceleration, deceleration or component failure. Transient analysis can be carried out using nonlinear finite element methods [1], which is required e.g. when geometrically nonlinear effects should be taken into account. Considering this, it is advantageous to be able to use the same FE model in both modal and transient analyses.

The absolute nodal coordinate formulation (ANCF) is a finite element based approach in which the kinematics of beam and plate elements are described using an absolute (inertial frame) position and components of the deformation gradient [2]. By using the components of the deformation gradient instead of rotation angles, large reference rotations can be described without the singularity problems that may occur in the three-dimensional rotation description in a total Lagrangian formulation. The ANCF has been especially designed to predict the dynamic behavior of flexible bodies subjected to large deformations in multibody applications. As a geometrically exact formulation, it takes geometric nonlinearity into account [3], which is not the case in most commonly used structural beam based simulation approaches in the field of rotor dynamics. The aim of this research is to apply ANCF elements to the analysis of the critical speeds of a structure.

To compute a Campbell diagram using an ANCF element, the effect of rotor spin on the element's kinetic energy should be considered. In an element's cross-sectional reference frame, rotation at constant angular velocity  $\Omega$  around the rotor's longitudinal axis contributes to the velocity of an arbitrary point within the element as follows:

$$\mathbf{v}_{\Omega e}(x, y, z) = \Omega \mathbf{b}, \quad (1)$$

where  $\mathbf{b} = [0 \ -z \ y]^T$  and  $x, y, z$  are coordinates inside the cross-sectional frame,  $x$  denoting the lengthwise direction. Using the orthogonal rotation matrix  $\mathbf{A} = [\mathbf{e}_1 \ \mathbf{e}_2 \ \mathbf{e}_3]$ , which describes the element's cross-sectional coordinate frame, the total velocity of a point of the element in the inertial frame can be written as:

$$\mathbf{v}(x, y, z) = \dot{\mathbf{r}} + \mathbf{v}_{\Omega i} = \dot{\mathbf{r}} + \Omega \mathbf{A} \mathbf{b}, \quad (2)$$

and subsequently the total kinetic energy of the element (with  $dm = \rho dV$ ) as:

$$T = \frac{1}{2} \int_V |\mathbf{v}|^2 dm = \frac{1}{2} \int_V \mathbf{v}^T \mathbf{v} dm. \quad (3)$$

Substituting Eq. (2) into Eq. (3), the kinetic energy can be separated into three terms:

$$T_1 = \frac{1}{2} \int_V \dot{\mathbf{r}}^T \dot{\mathbf{r}} dm, \quad T_2 = \Omega \int_V \dot{\mathbf{r}}^T \mathbf{A} \mathbf{b} dm, \quad T_3 = \frac{1}{2} \Omega^2 \int_V \mathbf{b}^T \mathbf{b} dm. \quad (4)$$

When considering the contributions of these energy terms to the equations of motion, it is apparent that the first term involves translational inertia and results in the mass matrix. The second term involves the gyroscopic effect and results in the gyroscopic matrix. The third and final term has no relation to nodal coordinates, and thus no contribution to the equations of motion. Defining the base vectors of the cross-sectional frame exactly (e.g. as described by Nachbagauer et al. [4]) complicates the calculation of the gyroscopic matrix, due to the normed vectors' nonlinearity with respect to nodal coordinates. Calculation can be simplified by assuming small displacements, in which case  $\mathbf{A} \approx [\mathbf{r}_x \ \mathbf{r}_y \ \mathbf{r}_z]$ . Employing this approximation and definitions  $\mathbf{r} = \mathbf{S}_x \mathbf{q}$ ,  $\mathbf{r}_y = \mathbf{S}_y \mathbf{q}$  and  $\mathbf{r}_z = \mathbf{S}_z \mathbf{q}$ , the mass matrix and gyroscopic matrix can be written as follows:

$$\mathbf{M} = \int_V \mathbf{S}^T \mathbf{S} dm, \quad \mathbf{G} = 2 \int_V \mathbf{S}^T (y \mathbf{S}_z - z \mathbf{S}_y) dm. \quad (5)$$

The resulting system of equations of motion is of the form:

$$\mathbf{M}\ddot{\mathbf{q}} + \Omega\mathbf{G}\dot{\mathbf{q}} + \mathbf{K}\mathbf{q} = \mathbf{f}(t). \quad (6)$$

For comparison of results, a dynamic example was obtained from literature. The example case is a rotating shaft with a hollow cross-section and an unbalanced rigid disk attached at the midspan point. This example was originally presented by Bauchau et al. [1]. The numerically efficient quadratic ANCF beam element by Nachbagger et al. [4] was used in the computation. The stiffness matrix of the system was computed via finite differences from the elastic force vector, which in turn was computed from the Jacobian of the strain energy via Gaussian quadratures. A second order quadrature was used for the standard structural mechanics term and a third order quadrature for the cross-sectional term of the strain energy. A comparison of the Campbell results produced using the ANCF beam elements in MATLAB and BEAM188 elements in ANSYS is presented in Fig. 1 and Tab. 1.

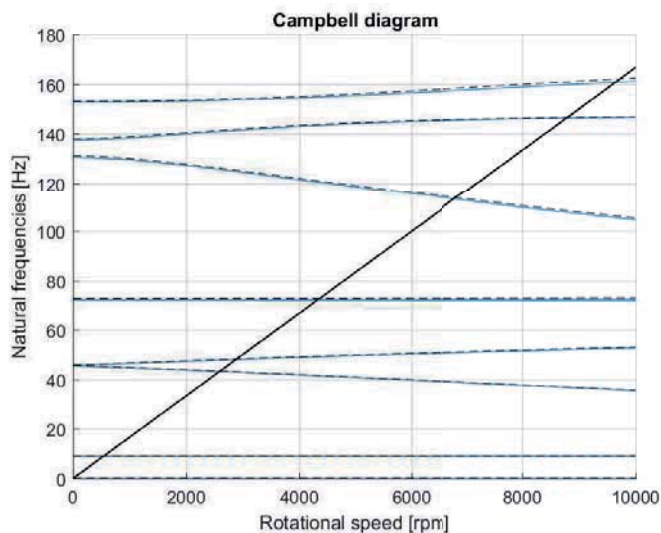


Figure 1: Campbell diagram comparison for the example structure. --- = 32 ANCF beam elements, — = 32 ANSYS BEAM188 elements. Diagonal line represents the  $1 \times$  spin frequency ( $\omega = \Omega$ )

Table 1: Critical speed [rpm] comparison for the lowest bending modes. BW = backward whirl, FW = forward whirl. Results are presented with an accuracy of 3 significant digits

Whirl	BEAM188	ANCF
BW	541	543
FW	556	558
BW	2590	2600
FW	2880	2900
BW	4320	4360
FW	4340	4380
BW	6790	6820
FW	8780	8790
FW	9650	9720

Fig. 1 and Tab. 1 show an acceptable level of agreement between the result sets. However, a small difference in natural frequencies is observed, even at zero spin speed. A probable cause for this difference is the definition of cross-sectional shear values in ANSYS.

### Acknowledgments

The authors would like to thank the Academy of Finland for supporting Marko K. Matikainen (Application No. 299033 for the funding of Academy Research Fellows).

### References

- [1] O. A. Bauchau, P. Betsch, A. Cardona, J. Gerstmayr, B. Jonker, P. Masarati, and V. Sonneville, "Validation of flexible multibody dynamics beam formulations using benchmark problems," *Multibody System Dynamics*, vol. 37, no. 1, pp. 29–48, 2016.
- [2] A. A. Shabana, "Definition of the slopes and the finite element absolute nodal coordinate formulation," *Multibody System Dynamics*, vol. 1, pp. 339–348, 1997.
- [3] J. Gerstmayr, M. K. Matikainen, and A. M. Mikkola, "A geometrically exact beam element based on the absolute nodal coordinate formulation," *Multibody System Dynamics*, vol. 20, no. 4, pp. 359–384, 2008.
- [4] K. Nachbagger, P. Gruber, and J. Gerstmayr, "A 3d shear deformable finite element based on the Absolute Nodal Coordinate Formulation," in *Multibody Dynamics* (J.-C. Samin and P. Fiset, eds.), vol. 28 of *Computational Methods in Applied Sciences*, pp. 77–96, Springer Netherlands, 2013.

## **Section**

# **CONTACT DYNAMICS AND CONSTRAINTS**



# Mathematical Tools for the Analysis of Smooth and Non-Smooth Systems with Redundant Constraints

Martin Arnold, Manuela Paschkowski

Institute of Mathematics  
Martin Luther University Halle-Wittenberg  
06099 Halle (Saale), Germany  
[martin.arnold,manuela.paschkowski]@mathematik.uni-halle.de

## Constrained systems with rank-deficient mass and constraint matrices

Following Glocker [1], mechanical systems with unilateral constraints and impacts can be described by a measure differential inclusion

$$d\mathbf{q} = \mathbf{v} dt, \quad (1a)$$

$$\mathbf{M}(\mathbf{q})d\mathbf{v} = \mathbf{f}(\mathbf{q}, \mathbf{v})dt + \mathbf{G}^\top(\mathbf{q})di, \quad (1b)$$

$$-di \in N_{C_N}(\boldsymbol{\xi})dt + N_{C_N}(\boldsymbol{\xi})dr \text{ with } \boldsymbol{\xi} := \mathbf{G}(\mathbf{q})(\mathbf{v}^+ + \varepsilon\mathbf{v}^-), \varepsilon \in [0, 1] \quad (1c)$$

with respect to the absolutely continuous position  $\mathbf{q} : [0, T] \rightarrow \mathbb{R}^k$  and the velocity  $\mathbf{v} : [0, T] \rightarrow \mathbb{R}^k$  of locally bounded variation with a Lebesgue decomposition for the differential measure  $d\mathbf{v} = \dot{\mathbf{v}}dt + (\mathbf{v}^+ - \mathbf{v}^-)dr$  referring to the Lebesgue measure  $dt$  and the jump measure  $dr := \sum_j \delta_{t_j}$  containing all Dirac measures  $\delta_{t_j}$  of the discontinuity points of  $\mathbf{v}$ . The set  $N_{C_N}(\boldsymbol{\xi}) := \{\mathbf{y} \in \mathbb{R}^k : \mathbf{y}^\top(\boldsymbol{\xi}^* - \boldsymbol{\xi}) \leq 0, (\boldsymbol{\xi}^* \geq \mathbf{0})\}$  defines the normal cone of the set of all non-negative real vectors being orthogonal to  $\boldsymbol{\xi}$ .

In (1), matrices  $\mathbf{M}(\mathbf{q})$  and  $\mathbf{G}(\mathbf{q})$  denote the mass and constraint matrix, respectively, and the force vector  $\mathbf{f}(\mathbf{q}, \mathbf{v})$  represents external and applied forces. The constraint matrix  $\mathbf{G}(\mathbf{q})$  summarizes gradients of active constraints  $\mathbf{g}(\mathbf{q}) \geq \mathbf{0}$ . For smooth systems with bilateral constraints  $\mathbf{g}(\mathbf{q}) = \mathbf{0}$ , it is given by  $\mathbf{G}(\mathbf{q}) := (\partial\mathbf{g}/\partial\mathbf{q})(\mathbf{q})$  and the equations of motion get the more compact form

$$\dot{\mathbf{q}} = \mathbf{v}, \quad (2a)$$

$$\mathbf{M}(\mathbf{q})\dot{\mathbf{v}} = \mathbf{f}(\mathbf{q}, \mathbf{v}) + \mathbf{G}^\top(\mathbf{q})\boldsymbol{\lambda}, \quad (2b)$$

$$\mathbf{0} = \mathbf{g}(\mathbf{q}) \quad (2c)$$

with Lagrange multipliers  $\boldsymbol{\lambda}$ . For physical reasons, the mass matrix  $\mathbf{M}(\mathbf{q})$  in (1) and (2) is symmetric, positive semi-definite. García de Jalón and Gutiérrez-López [2] point out that “in physical terms, ... any physically possible movement (i.e., which satisfies the constraint equations) cannot be associated with zero kinetic energy”.

This may be achieved by the condition

$$\ker \mathbf{M}(\mathbf{q}) \cap \ker \mathbf{G}(\mathbf{q}) = \{\mathbf{0}\} \quad (3)$$

which is equivalent to the condition that  $\mathbf{M}(\mathbf{q})$  is positive definite at  $\ker \mathbf{G}(\mathbf{q})$ . This setting is much more general than the full rank assumptions on  $\mathbf{M}$  and  $\mathbf{G}$  that are typical of the mathematical literature on DAE aspects of constrained systems (2), see, e.g., [3]. In particular, condition (3) covers the case of redundant constraints that result in rank-deficient constraint matrices and non-unique Lagrange multipliers [2, 4].

In the present paper, we discuss several mathematical tools for the analysis of systems (1) and (2) with redundant constraints and constraint matrices  $\mathbf{G}(\mathbf{q})$  satisfying (3).

## Lyapunov stability of measure differential inclusions

To analyse the Lyapunov stability of equilibria of the non-smooth system (1), we follow Leine and van de Wouw [5] and consider a more general problem class that is given by linear measure differential inclusions

$$\mathbf{B}(\mathbf{x})d\mathbf{x} \in \mathbf{F}(\mathbf{x}) \quad (4)$$

with a measure- and multi-valued right hand side and an admissible set  $A = \{\mathbf{x} : \mathbf{F}(\mathbf{x}) \neq \mathbf{0}\}$ . The challenge of stability analysis of such systems is their impulsive character and the resulting state discontinuities. According to Leine, van de Wouw [5], an equilibrium  $\mathbf{x}^*$  of (4) is said to be stable if there exists for every  $\varepsilon > 0$  a  $\delta > 0$  with

$$\|\mathbf{x}_0 - \mathbf{x}^*\| < \delta \Rightarrow \|\mathbf{x}(t) - \mathbf{x}^*\| < \varepsilon \text{ for almost all } t \geq t_0, \text{ all } \mathbf{x}_0 \in A$$

and all solutions  $\mathbf{x}(t)$  of (4) to initial values  $\mathbf{x}_0$ . Note, that the implication does not need to be true for the discontinuity points of function  $\mathbf{x}$ .

To generalize the direct method of Lyapunov to systems (4) with singular matrices  $\mathbf{B}(\mathbf{x})$ , we follow the considerations for smooth systems and present a theorem for the stability analysis of equilibrium points of (4). Applications to non-smooth systems with rank-deficient mass matrix  $\mathbf{M}(\mathbf{q})$  are discussed in more detail in [6].

**Theorem:** *An equilibrium  $\mathbf{x}^*$  of (4) is stable in the sense of Lyapunov if there exists a lower semicontinuous function  $V : \mathbb{R}^k \rightarrow \mathbb{R} \cup \{\infty\}$  and a neighborhood  $U := B(\mathbf{x}^*, h) \cap A$  for a  $h > 0$  with (i)  $V(\mathbf{x}) \geq 0$ , ( $\mathbf{x} \in U$ ),  $V(\mathbf{x}^*) = 0$ , (ii)  $dV(\mathbf{x}) \leq 0$ , ( $\mathbf{x} \in U$ ), (iii) the set  $\{\mathbf{x} \in U : V(\mathbf{x}) = 0\}$  contains no negative orbit of (4) except the trivial one.*

## Decomposition of rank-deficient systems by linear algebra methods

For the analysis of systems with redundant constraints, the separation of an equivalent regular system proves to be favourable [7]. We consider (constant) matrices  $\mathbf{M} \in \mathbb{R}^{k \times k}$  and  $\mathbf{G} \in \mathbb{R}^{m \times k}$  with  $\text{rank } \mathbf{M} = r \leq k$  and  $\text{rank } \mathbf{G} = s \leq m \leq k$  that satisfy condition (3). Using methods from numerical linear algebra, we get non-singular matrices  $\mathbf{U} \in \mathbb{R}^{k \times k}$  and  $\mathbf{Q} \in \mathbb{R}^{m \times m}$  such that

$$\left( \begin{array}{c|c} \mathbf{M} & \mathbf{G}^\top \\ \hline \mathbf{G} & \mathbf{0} \end{array} \right) = \left( \begin{array}{c|c} \mathbf{U} & \mathbf{0} \\ \hline \mathbf{0} & \mathbf{Q} \end{array} \right) \left( \begin{array}{c|c|c} \mathbf{0} & \mathbf{0} & \mathbf{0} & \mathbf{0} & \mathbf{I}_{k-r} \\ \hline \mathbf{0} & \bar{\mathbf{M}} & \bar{\mathbf{G}}^\top & \mathbf{0} & \mathbf{0} \\ \hline \mathbf{0} & \bar{\mathbf{G}} & \mathbf{0} & \mathbf{0} & \mathbf{0} \\ \hline \mathbf{0} & \mathbf{0} & \mathbf{0} & \mathbf{0} & \mathbf{0} \\ \hline \mathbf{I}_{k-r} & \mathbf{0} & \mathbf{0} & \mathbf{0} & \mathbf{0} \end{array} \right) \left( \begin{array}{c|c} \mathbf{U}^\top & \mathbf{0} \\ \hline \mathbf{0} & \mathbf{Q}^\top \end{array} \right) \quad (5)$$

with a non-singular matrix  $\bar{\mathbf{M}} \in \mathbb{R}^{r \times r}$  and a matrix  $\bar{\mathbf{G}} \in \mathbb{R}^{(s-(k-r)) \times r}$  that has full rank  $s - (k - r)$ , see [7, Lemma 2]. After decomposition, we have the  $5 \times 5$  block structure (5) with the second and third block row / block column corresponding to a regular subsystem satisfying the classical assumptions on constrained mechanical systems in DAE theory [3].

The zero blocks in the 4th block row of (5) represent redundant constraints. The corresponding zero blocks in the 4th block column refer to those components of the Lagrange multipliers  $\boldsymbol{\lambda}$  that remain undefined in the rank-deficient case. We discuss consistency conditions on the (bilateral or unilateral) constraints to distinguish redundant constraints from contradictory ones and get a local existence and uniqueness result for smooth systems with rank-deficient constraints matrices  $\mathbf{G}$ , see [7, Theorem 2].

The transformation (5) is based on QR-decompositions of rank-deficient matrices. In a practical implementation, it makes use of a small threshold  $\sigma_0 > 0$  to separate non-zeros being caused by round-off errors from structural non-zero elements. Special care is necessary to get transformation matrices  $\mathbf{U}$ ,  $\mathbf{Q}$  that vary smoothly for state dependent matrices  $\mathbf{M}(\mathbf{q})$  and  $\mathbf{G}(\mathbf{q})$ . Furthermore, the transformation (5) and its practical implementation may be generalized to systems with  $\mathbf{G}$  and  $\mathbf{G}^\top$  being evaluated at *different* arguments representing, e.g., different stage vectors of a half-explicit Runge-Kutta method for the index-2 formulation of smooth systems (2).

## Regularization of rank-deficient constraints

The non-uniqueness of Lagrange multipliers  $\boldsymbol{\lambda}$  is typical of systems with redundant constraints [2]. For systems with force vectors  $\mathbf{f}(\mathbf{q}, \mathbf{v})$  being independent of  $\boldsymbol{\lambda}$  this non-uniqueness does not affect the position and velocity coordinates. More sophisticated models are necessary for systems with friction forces depending on  $\boldsymbol{\lambda}$ . The qualitative consideration of elastic effects may help to regularize rank-deficient constraints without introducing (very) stiff contact forces. We recall a scalarization approach from multi-objective optimization that was used successfully to reduce a finite set of (redundant or even contradictory) constraints (2c) to a smooth scalar constraint equation [8] and discuss, how to extend this approach to non-smooth systems (1).

## References

- [1] C. Glocker. *Set-Valued Force Laws: Dynamics of Non-Smooth Systems*, volume 1 of *Lecture Notes in Applied and Computational Mechanics*. Springer-Verlag, Berlin Heidelberg, 2001.
- [2] J. García de Jalón and M.D. Gutiérrez-López. Multibody dynamics with redundant constraints and singular mass matrix: existence, uniqueness, and determination of solutions for accelerations and constraint forces. *Multibody System Dynamics*, 30:311–341, 2013.
- [3] E. Hairer and G. Wanner. *Solving Ordinary Differential Equations. II. Stiff and Differential-Algebraic Problems*. Springer-Verlag, Berlin Heidelberg New York, 2nd edition, 1996.
- [4] B. Brogliato and D. Goeleven. Singular mass matrix and redundant constraints in unilaterally constrained Lagrangian and Hamiltonian systems. *Multibody System Dynamics*, 35:39–61, 2015.
- [5] R. Leine and N. van de Wouw. *Stability and Convergence of Mechanical Systems with Unilateral Constraints*, volume 36 of *Lecture Notes in Applied and Computational Mechanics*. Springer, Berlin Heidelberg, 2008.
- [6] M. Paschkowski and M. Arnold. Lyapunov stability of measure differential inclusions - Applications in nonsmooth mechanics with singular mass matrices. Submitted to: 9th European Nonlinear Dynamics Conference (ENOC), 2017.
- [7] M. Arnold. DAE aspects of multibody system dynamics. To appear in A. Ilchmann and T. Reis, editors, *Surveys in Differential-Algebraic Equations IV*, Differential-Algebraic Equations Forum. Springer Berlin Heidelberg, 2017 (in print). - A preliminary version of this material is online available as Technical Report 01-2016 of the Institute of Mathematics, Martin Luther University Halle-Wittenberg, Germany.
- [8] M. Arnold and K. Frischmuth. Solving problems with unilateral constraints by DAE methods. *Mathematics and Computers in Simulation*, 47:47–67, 1998.

# Selection and Experimental Validation of Contact / Impact Models Suitable for Multibody Dynamics Simulations

Krystof P. Jankowski<sup>1</sup>, Salman Chaudhry<sup>2</sup>, Alex Czekanski<sup>3</sup>

<sup>1</sup>Magna Closures of America, Inc.  
750 Tower Drive, MC 2000  
Troy, Michigan 48098, USA  
Krystof.Jankowski@magna.com

<sup>2</sup>Department of Mechanical Engineering  
York University  
Toronto, ON M3J 1P3, Canada  
Salman01@yorku.ca

<sup>3</sup>Department of Mechanical Engineering  
York University  
Toronto, ON M3J 1P3, Canada  
Alex.Czekanski@lassonde.yorku.ca

## Abstract

Reliable numerical simulations of a multitude of multibody systems require proper modeling of contacts between elements of the considered system. In a general sense, modeling contacts between bodies involve both a continuous process occurring over a finite time and a short time events taking place when the bodies collide, i.e. during impacts. The reason for that is that generic multibody dynamics simulation codes should be able to account for the transition from the short time duration impacts toward a prolonged contact between bodies possibly occurring afterwards.

In the literature, there is a considerable amount of information on modeling contact phenomena, with only selected items cited here, such as, for example, published books [1, 2] and review papers [3, 4]. The most notable approach for contact modeling is based on Hertz theory [1, 2]. The pure elastic contact force model defines the force through a nonlinear power function  $F_N = K\delta^n$ , with  $K$  denoting the contact stiffness parameter and  $n$  the power exponent of the indentation  $\delta$  between contacting bodies. Both  $K$  and  $n$  depend on the material and geometric properties of the contacting bodies. The early Hertz model didn't account for energy dissipation during impact, and that is why subsequent approaches aimed at adding damping effects to the contact force definition. The simplest Kelvin and Voigt approach combines a linear spring ( $n=1$ ) and a linear damper with damping coefficient  $D$  to define the contact force as  $F_N = K\delta + D\dot{\delta}$ . As pointed out in the literature [3], although the Kelvin Voigt model can be used for some low speed impacts, it does not represent the nonlinear nature of the impact and also produces a discontinuous force at the onset of the impact when parts collide with a non-zero velocity. It also produces a 'sticky' contact force: non-zero attraction during part separation. A more elaborate approach, proposed by Hunt and Crossley [5], avoids the aforementioned inconsistencies. It uses Hertz theory in the elastic portion of the contact force expression, and a nonlinear damping term related to the coefficient of restitution  $c_r$  and the impact velocity  $\dot{\delta}^{(-)}$ :

$$F_N = K\delta^n [1 + 1.5(1 - c_r)\dot{\delta}/\dot{\delta}^{(-)}] \quad (1)$$

A modification of the Hunt and Crossley model proposed by Lankarani and Nikravesh [6] introduces a hysteresis damping factor obtained by relating the kinetic energy loss by the impacting bodies to the energy dissipated in the system due to internal damping. Their contact force model takes the form:  $F_N = K\delta^n [1 + 0.75(1 - c_r^2)\dot{\delta}/\dot{\delta}^{(-)}]$ . A number of similar approaches can be find in the literature, with varying definitions of the damping term in function of  $c_r$  and  $\dot{\delta}^{(-)}$ , each bringing certain improvements for particular impact conditions [3, 4]. It is known that they provide good predictions if coefficients of restitution are sufficiently high. All those approaches, however, are not suitable for generic multibody dynamics code implementation due to their dependence on the pre-impact velocity  $\dot{\delta}^{(-)}$  appearing in the denominator. Numerical problems may arise for small impact velocities, and the need to monitor and store pre-impact velocities may lead to cumbersome manipulations. Moreover, in multibody systems bodies are often in contact before separation and subsequent impact, after which they again may stay stationary. Not sure what values of  $\dot{\delta}^{(-)}$  should be used in the contact force equation in such cases.

A recently published contact force model [7] avoids some of the above mentioned limitations. It doesn't explicitly refer to the impact velocity, it doesn't produce 'sticky' contact forces, and it allows for non-zero indentation at the separation of the impacting bodies. The new model is defined by the following equations [7]:

$$\dot{a} = \max\left(-\frac{\gamma a}{1 + \gamma(\beta_1 + \beta_2 a)}, \gamma(\delta|\delta|^{\lambda-1} - a)\right) \quad (2a)$$

$$F_N = K \max\left(0, \delta|\delta|^{\lambda-1} + \gamma(\beta_1 + \beta_2 a)(\delta|\delta|^{\lambda-1} - a)\right) \quad (2b)$$

There are four constants used in the model:  $\lambda \geq 1$  determines the nonlinearity of the force-indentation relationship (similar to parameter  $n$  in Eq. (1)),  $\beta_1 \geq 0$  and  $\beta_2 \geq 0$  are damping parameters, and  $\gamma > 0$  is a tuning parameter. The variable  $a(t)$  is an internal state. The effects of model parameter changes have been investigated

[7]; it appears that  $\beta_1$  determines the residual indentation and the slope of the force profile in function of time at the beginning of impact,  $\beta_2$  influences the roundedness of the contact force – indentation curve, and  $\gamma$  influences the overall shape of that curve.

The main purpose of this paper is to investigate the applicability of the new contact force model (2) for selected materials and body shapes, and to establish a strategy to identify the parameters appearing in the contact force expression. The model described in Eq. (2) has been implemented in the multibody dynamics simulation code MSC ADAMS. The contact element computes the contact force through a user written subroutine, getting the local deformation between interacting bodies from ADAMS Solver. The implementation of the model (2) in the commercially available code is relatively easy because, as opposed to the Hunt-Crossley model (1), the impact velocity  $\delta^{(-)}$  does not appear in (2).

Typical experiments used to validate contact force models involve a ball falling onto a solid surface, with contact force measurements carried out directly through a piezoelectric element installed on top of the surface [8] or indirectly with an accelerometer mounted to the ball [9]. In the research described in this paper, together with the ball drop experiments, an alternative method is also used, based on a modified Kolsky bar apparatus [10] available at York University. The Kolsky bar test fixture, also called the split Hopkinson pressure bar, is composed of a striker bar, an incident bar and a transmission bar (Fig. 1). The specimen is sandwiched between the incident bar and the transmission bar. The impact of the striker on the end of the incident bar generates a longitudinal compressive wave in the incident bar propagating through the specimen to the transmission bar. The strain gauges mounted on the incident and the transmission bars monitor the wave propagation, allowing to compute the strain rate, strain and stress histories in the specimen, together with relative displacements and forces on both ends of the specimen. In order to increase the precision of measurements and to allow for dynamic characterization of softer materials, modifications to the original Kolsky bar were introduced [10], involving a pair of quartz crystal force transducers at the specimen ends of the incident and transmission bars (Fig. 1). A pulse shaping technique was also implemented, aimed at modifying the incident loading pulse in order to control the deformation strain rate and the inertia effects in the specimen. The results of experimental validation of the contact force model (2) using two aforementioned approaches will be presented in the full conference paper.

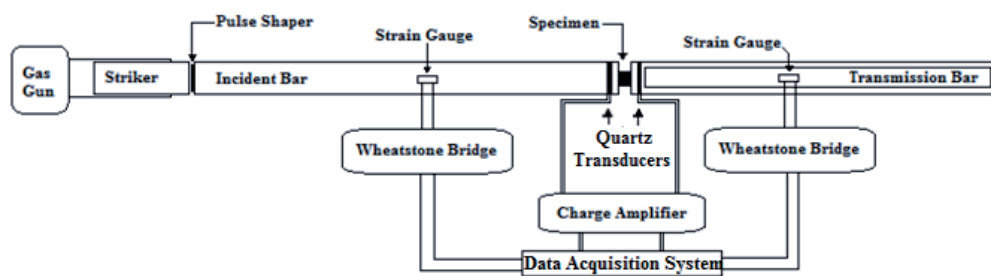


Figure 1. Schematic view of a modified Kolsky bar setup.

## References

- [1] W. Goldsmith. *Impact, the theory and physical behavior of colliding solids*. E. Arnold Ltd, London, 1960.
- [2] K.L. Johnson. *Contact Mechanics*. Cambridge University Press, Cambridge, 1999.
- [3] M. Machado, P. Moreira, P. Flores and H.M. Lankarani. Compliant contact force models in multibody dynamics: evolution of the Hertz contact theory. *Mechanism and Machine Theory*, 53:99-121, 2012.
- [4] J. Alves, P. Flores and N. Peixinho. Contact analysis for different viscoelastic contact force models. In Z. Terze, editor, *Proceedings of the ECCOMAS Thematic Conference on Multibody Dynamics*, pages 123-132. University of Zagreb, Zagreb, Croatia, 2013.
- [5] K.H. Hunt and F.R.E Crossley. Coefficient of restitution interpreted as damping in vibroimpact. *ASME Journal of Applied Mechanics*, 7:440-445, 1975.
- [6] H.M. Lankarani and P.E. Nikravesh. A contact force model with hysteresis damping for impact analysis of multibody systems. *ASME Journal of Mechanical Design*, 112:369-376, 1990.
- [7] X. Xiong, R. Kikuuwe and M. Yamamoto. A contact force model with nonlinear compliance and residual indentation. *ASME Journal of Applied Mechanics*, 81:021003-1-8, 2014.
- [8] R. Cross. The bounce of a ball. *American Journal of Physics*, 67:222-227, 1999.
- [9] Y. Zhang and I. Sharf. Validation of nonlinear viscoelastic contact force models for low speed impact. *ASME Journal of Applied Mechanics*, 76:051002-1-12, 2009.
- [10] W.W. Chen and B. Song. *Split Hopkinson (Kolsky) Bar: Design, Testing and Applications*. Springer, NY, 2011.

# Efficient Evaluation of Local and Global Deformations in Impact Simulations in Reduced Flexible Multibody Systems based on a Quasi-Static Contact Submodel

Stephan Tschigg and Robert Seifried

Institute of Mechanics and Ocean Engineering  
Hamburg University of Technology (TUHH)  
Eißenendorfer Straße 42, 21073 Hamburg, Germany  
[stephan.tschigg, robert.seifried]@tuhh.de

## Abstract

Due to increasing operation speed and lightweight construction, elastic deformations or component vibrations may occur in machines. These vibrations affect the system dynamics and cannot be neglected during the design of mechanical systems. For the efficient investigation of the global dynamic behavior of mechanical systems the approach of multibody systems (MBS) is widely used. In order to consider body flexibility, the approach of MBS can be extended by elastically deformable bodies, which leads to the method of flexible multibody systems (FMBS). The most widely used method for modeling FMBS is the floating frame of reference formulation. In this method, the motion of a body is separated into the nonlinear motion of the reference frame and the small linear elastic deformations with respect to the moving reference frame. If structural deformations remain small, which is the case in many dynamic systems, linear submodels can be used to describe the components' elastic deformation.

Impacts yield to complicated dynamical behavior in the involved bodies, like wave propagation, structural vibrations and change of rigid body motion. An accurate modeling of the high frequency vibration phenomena and the local deformation effects is possible using full finite element (FE) models. However, to capture all elastic effects, especially in the contact area, a very fine mesh is necessary. This results in high computation times and therefore the simulation of the overall motion of the system is usually not practical using FE models. For an efficient investigation of the contact behavior the FMBS approach can be combined with a contact model. In a simple approach a nonlinear force law including a energy loss factor, such as the coefficient of restitution, might be used [1]. However, which such an approach the local behavior cannot be reproduced accurately. Also the coefficient of restitution is defined for rigid bodies and cannot be transferred to flexible bodies in a straight forward way. Therefore, in this work a combination of reduced FMBS and nodal contact calculation [2] is used. The contact simulation consists of frictionless normal contact combined with the penalty method.

When investigating the system behavior during and after impacts, not only the correct rigid body motion but also the correct representation of local strains and stresses is of interest. Therefore an exact and efficient recovery of the local contact behavior as well as capturing the low frequency global motion with reduced flexible bodies is necessary. Using modally reduced models with a finite number of eigenmodes, a good approximation of the global elastic deformation in terms of wave propagation is possible [3]. However, to capture all local effects in the contact area, a very large number of high frequency eigenmodes is necessary. Due to the missing local deformations using a moderate number of low frequency eigenmodes, there is no convergence of the penalty factor like it occurs in the FE simulation. Therefore, it seems obvious to use additional static shape functions to approximate the local deformations. However, these static shape functions introduce high frequencies and thus the numerical stiffness increases. Hence, very small time steps during time integration are required, resulting in high computation times. Using reduced FMBS in contact simulations, the two challenging issues - accuracy and speed - are not yet satisfactorily solved together. Approaches like the static mode switching [2] require additional switching effort and result in numerical discontinuities. The use of high damping for example has a negative effect on the simulation of wave propagation.

In order to capture both the global motion in terms of wave propagation and the local deformation efficiently and accurately, alternative approaches are discussed in this work. The high frequency static shape functions are only necessary for capturing the local deformations in the contact area. They do not affect the wave propagation in the bodies and so they can be neglected in the dynamic simulation. The flexible part in the equations of motion of FMBS [4] can be divided in low (lf) and high (hf) frequency parts, such as

$$\begin{bmatrix} \mathbf{M}_{rr} & & \text{sym.} \\ \mathbf{M}_{er}^{lf} & \mathbf{M}_{ee}^{lf} & \\ \mathbf{M}_{er}^{hf} & \mathbf{0} & \mathbf{M}_{ee}^{hf} \end{bmatrix} \cdot \begin{bmatrix} \ddot{\mathbf{q}}_r \\ \ddot{\mathbf{q}}_e^{lf} \\ \ddot{\mathbf{q}}_e^{hf} \end{bmatrix} + \begin{bmatrix} \mathbf{0} & & \text{sym.} \\ \mathbf{0} & \mathbf{D}_{ee}^{lf} & \\ \mathbf{0} & \mathbf{0} & \mathbf{D}_{ee}^{hf} \end{bmatrix} \cdot \begin{bmatrix} \dot{\mathbf{q}}_r \\ \dot{\mathbf{q}}_e^{lf} \\ \dot{\mathbf{q}}_e^{hf} \end{bmatrix} + \begin{bmatrix} \mathbf{0} & & \text{sym.} \\ \mathbf{0} & \mathbf{K}_{ee}^{lf} & \\ \mathbf{0} & \mathbf{0} & \mathbf{K}_{ee}^{hf} \end{bmatrix} \cdot \begin{bmatrix} \mathbf{q}_r \\ \mathbf{q}_e^{lf} \\ \mathbf{q}_e^{hf} \end{bmatrix} = \begin{bmatrix} \mathbf{f}_{c,r} \\ \mathbf{f}_{c,e}^{lf} \\ \mathbf{f}_{c,e}^{hf} \end{bmatrix}. \quad (1)$$

The first approach for an efficient impact simulation presented in this work uses modal damping only on the high frequencies. Hence, in equation (1) the damping matrices of the low and high frequencies are defined as  $\mathbf{D}_{ee}^{lf} = \mathbf{0}$  and  $\mathbf{D}_{ee}^{hf} = 2\zeta\sqrt{\mathbf{K}_{ee}^{hf}}$  respectively, with the modal damping parameter  $\zeta$ . Using damping only on the high frequencies introduced by the static shape functions, there is no negative influence on the low frequency wave

propagation and the numerical difficulties can be eliminated. Moreover, a convergence of the penalty factor is possible, see [5]. But the modal damping parameter  $\zeta$  depends on the model and is unknown in the most cases. To avoid the determination of an optimal damping parameter, another approach is also presented in this work.

According to [6], the high frequency inertia coupling terms  $\mathbf{M}_{er}^{hf}$  can be neglected in the equations of motion (1) because they represent only local deformations. Considering the frequency range of interest, the high frequency parts will not be excited and a decoupling of the low and high frequency components is possible. Hence, the high frequency parts respond quasi-statically and its dynamics can be neglected in time integration. In this case, the last part of equation (1) is reduced to the pure static equation  $\mathbf{K}_{ee}^{hf} \cdot \mathbf{q}_e^{hf} = \mathbf{f}_{c,e}^{hf}$ . However, for the contact force calculation the influence of the local deformation field, represented by the static shape functions, has to be considered, see [6]. For this reason, the connection of the static and dynamic equations is made using the contact forces  $\mathbf{f}_{c,e}(\mathbf{q}_r, \mathbf{q}_e^{lf}, \mathbf{q}_e^{hf})$ . The unknown contact forces are highly dependent on the unknown local deformation field, which leads to a system of nonlinear equations. This system of nonlinear equations can be solved efficiently using a simplified Newton's method. With this quasi-static contact submodel, the influence of the high eigenfrequencies on the low frequency dynamic can be reduced. Consequently, an efficient time integration of the equations of motion is possible. For the calculation of the static shape functions the Craig-Bampton method should be used in this study. Due to the better approximation of the local deformation, a convergence of the penalty factor is expected and first preliminary results are presented. Also, besides local deformation, this work focuses on the efficient and precise stress recovery and simulation of the wave propagation. To evaluate this approach, the results will be compared with full FE simulations and experiments.

## References

- [1] H. M. Lankarani, P. Nikravesh. Continuous Contact Force Models for Impact Analysis in Multibody Systems. *Nonlinear Dynamics*, 5, 193-207, 1992.
- [2] T. Tamarozzi, P. Ziegler, P. Eberhard, W. Desmet. Static modes switching in gear contact simulation. *Mechanism and Machine Theory*, 63, 89-106, 2013.
- [3] W. Schiehlen, R. Seifried. Three Approaches for Elastodynamic Contact in Multibody Systems. *Multibody System Dynamics*, 12, 1-16, 2004.
- [4] A. A. Shabana. *Dynamics of Multibody Systems*. Cambridge University Press, New York, 2005.
- [5] S. Tschigg, R. Seifried. Impact Simulations Using a Quasi-Static Contact Submodel in Reduced Flexible Multibody Systems. *PAMM*, 16, 63-64, 2016.
- [6] K. Sherif, W. Witteveen, K. Mayrhofer. Quasi-static consideration of high-frequency modes for more efficient flexible multibody simulations. *Acta Mechanica*, 223, 1285-1305, 2012.

# On the Generalized Friction Cone for Multibody Systems

Albert Peiret<sup>1</sup>, József Kövecses<sup>1</sup>, Josep M. Font-Llagunes<sup>2</sup>

<sup>1</sup> Department of Mechanical Engineering,  
McGill University,  
Montréal, Canada  
alpeiret@cim.mcgill.ca — jozsef.kovecses@mcgill.ca

<sup>2</sup> Department of Mechanical Engineering,  
Universitat Politècnica de Catalunya,  
Barcelona, Spain  
josep.m.font@upc.edu

## Abstract

The use of the Coulomb friction model is considered to be representative for modelling contact. One of the most important element in this model is the *friction cone*. It arises from the fact that the static friction force has a threshold value, and therefore, all the possible contact force vectors of a sticking contact point must lie within the cone.

The *generalized friction cone* [1, 2] takes the dynamics of the system into account, and interprets the friction cone in the configuration space of the system. This representation is very useful to analyze different phenomena related to friction, such as the *Painlevé paradox* [2]. However, the fact that this cone is in the multi-dimensional configuration space makes it hard to visualize it. Here, the equation of the generalized friction cone projected to the contact velocity space is derived, so that it can be used to represent and visualize it in a 3-dimensional space.

Assuming isotropy in the tangent plane of the contact point, the limit of the friction force is defined as

$$\|\lambda_t\| = \sqrt{\lambda_t^T \lambda_t} \leq \mu \lambda_n \quad (1)$$

where  $\lambda_t$  is the friction force,  $\lambda_n$  is the normal force, and  $\mu$  is the friction coefficient, which is assumed to be equal for the static and kinetic friction. Equation (1) represents the *classic friction cone* ( $\kappa_\mu$ ), with the quadratic matrix form

$$\kappa_\mu(\lambda_c) = \lambda_c^T \mathbf{Q}_\mu \lambda_c = \begin{bmatrix} \lambda_t \\ \lambda_n \end{bmatrix}^T \begin{bmatrix} \mathbf{I}_{2 \times 2} & \mathbf{0} \\ \mathbf{0} & -\mu^2 \end{bmatrix} \begin{bmatrix} \lambda_t \\ \lambda_n \end{bmatrix} \leq 0 \quad (2)$$

where  $\lambda_n \geq 0$ , and  $\mathbf{I}_{2 \times 2}$  is the  $2 \times 2$  identity matrix.

For the analysis of the contact dynamics in a multibody system, it is useful to consider a *reduced representation* of the system in the space of the contact velocities

$$\mathbf{u}_c = \begin{bmatrix} \mathbf{u}_t \\ u_n \end{bmatrix} = \begin{bmatrix} \mathbf{A}_t \mathbf{v} \\ \mathbf{A}_n \mathbf{v} \end{bmatrix} = \mathbf{A} \mathbf{v} \quad (3)$$

where  $\mathbf{u}_t$  and  $u_n$  are the tangential and normal relative velocity components at the contact point of interest,  $\mathbf{A}$  is the contact Jacobian matrix, and  $\mathbf{v}$  contains the generalized velocities of the system with the mass matrix  $\mathbf{M}$ . The infinitesimal change of the contact velocities can be related to the contact forces by the effective mass matrix  $\mathbf{M}_c = (\mathbf{A} \mathbf{M}^{-1} \mathbf{A}^T)^{-1}$ , so that the differential of the contact force impulse  $d\Lambda_c = \lambda_c dt = \mathbf{M}_c d\mathbf{u}_c$ . Note that the incremental change  $\delta \mathbf{u}_c$  only accounts for the contact forces. Nevertheless, other forces might also contribute to the total incremental change of the contact velocities  $d\mathbf{u}_c = \delta \mathbf{u}_c + \delta \mathbf{u}_c^0$ , where  $\delta \mathbf{u}_c^0$  accounts for the change of  $\mathbf{u}_c$  due to the rest of forces acting on the system.

A quadratic expression for the contact velocity changes  $\delta \mathbf{u}_c$  can be derived from Eqn. (2) by using the aforementioned expression,

$$\kappa_g(\delta \mathbf{u}_c) = \delta \mathbf{u}_c^T \mathbf{Q} \delta \mathbf{u}_c = \delta \mathbf{u}_c^T (\mathbf{M}_c \mathbf{Q}_\mu \mathbf{M}_c) \delta \mathbf{u}_c = \begin{bmatrix} \delta u_t \\ \delta u_n \end{bmatrix}^T \begin{bmatrix} \mathbf{Q}_t & \mathbf{Q}_{tn} \\ \mathbf{Q}_{tn}^T & Q_n \end{bmatrix} \begin{bmatrix} \delta u_t \\ \delta u_n \end{bmatrix} \leq 0 \quad (4)$$

where  $\mathbf{Q}_t$  and  $Q_n$  are characteristic elements of the matrix  $\mathbf{Q}$  and will be defined below. This homogenous quadratic equation represents the projection of the generalized cone into the contact velocity space.

As in the classic cone  $\kappa_\mu$ , the friction coefficient affects the geometry of the generalized cone  $\kappa_g$ . For  $\mu = 0$  the cone degenerates into a line given by the parametrization  $\delta \mathbf{u}_c = \mathbf{A} \mathbf{M}^{-1} \mathbf{A}_n \lambda_n dt$ . This line represents the *space of constrained motion* associated with the contact constraint projected into the contact velocity space, also known as *natural contact direction* in [3]. It can be interpreted as the direction in which the contact velocity varies due to the normal contact force alone. In case of frictionless collisions, this direction is important because all non-impulsive forces are usually neglected and only the impulses of the normal force are taken into account. On the other hand, for  $\mu \rightarrow \infty$  the cone degenerates into a plane given by the parametrization  $\delta \mathbf{u}_c = \mathbf{A} \mathbf{M}^{-1} \mathbf{A}_t \lambda_t dt$ . This plane is not directly related to either the natural contact direction or the plane  $\delta u_n = 0$ , see Figure 1.

In general,  $\mathbf{Q}$  is a full-rank symmetric matrix that represents an elliptic cone  $\kappa_d$  without any particular shape. Nevertheless, its geometry in some cases can be of interest and help to better understand the dynamics of multibody systems with frictional contacts. For instance, it is clear from Eqn. (4) that the direction  $\delta \mathbf{u}_t = \mathbf{0}$  is located inside

the cone if and only if  $Q_n \leq 0$ . It can be shown that this occurs for values of the friction coefficient greater than a critical value [4],  $\mu \geq \mu_{\text{crit}} = \|\mathbf{M}_t \mathbf{h}\| = \sqrt{\mathbf{h}^T \mathbf{M}_t^2 \mathbf{h}}$ , where  $\mathbf{M}_t = (\mathbf{A}_t \mathbf{M}^{-1} \mathbf{A}_t^T)^{-1}$  and  $\mathbf{h} = \mathbf{A}_t \mathbf{M}^{-1} \mathbf{A}_n^T$  depend on the configuration of the system. The *critical friction coefficient*  $\mu_{\text{crit}}$  plays an important role in single-point collisions with friction, in which sliding cannot restart if  $\mu \geq \mu_{\text{crit}}$ . This fact is consistent with the dynamic cone, because  $\delta \mathbf{u}_t = \mathbf{0}$  is possible in such a case (i.e., it is inside the cone, see Figure 1), and therefore, the contact force alone can keep the contact point without sliding.

Another particular aspect of the generalized cone is its intersection with the plane  $\delta u_n = 0$ , which is a degenerate conic described by the quadratic equation  $\delta \mathbf{u}_t^T \mathbf{Q}_t \delta \mathbf{u}_t = 0$ . The intersection is different from a point (the vertex of the cone) if and only if  $\det \mathbf{Q}_t \leq 0$ , and it can be shown that this occurs if the friction coefficient is greater than a value,  $\mu \geq \mu_{\text{jam}} = \|\mathbf{M}_n \mathbf{h}\|^{-1} = (\mathbf{M}_n \sqrt{\mathbf{h}^T \mathbf{h}})^{-1}$ , where  $\mathbf{M}_n = (\mathbf{A}_n \mathbf{M}^{-1} \mathbf{A}_n^T)^{-1}$  also depends on the configuration of the system. In such a case, *dynamic jamming* (or *jamb*) [1, 2, 4] can happen if the contact point is sliding in a particular direction which gives  $\delta u_n \leq 0$ . This phenomenon gave rise to the *Painlevé paradox*, in which the dynamic equations of a rigid body with Coulomb friction in the contacts are shown to have no solution for certain kinematic states (i.e., configuration and velocity), or even several possible solutions [1, 2].

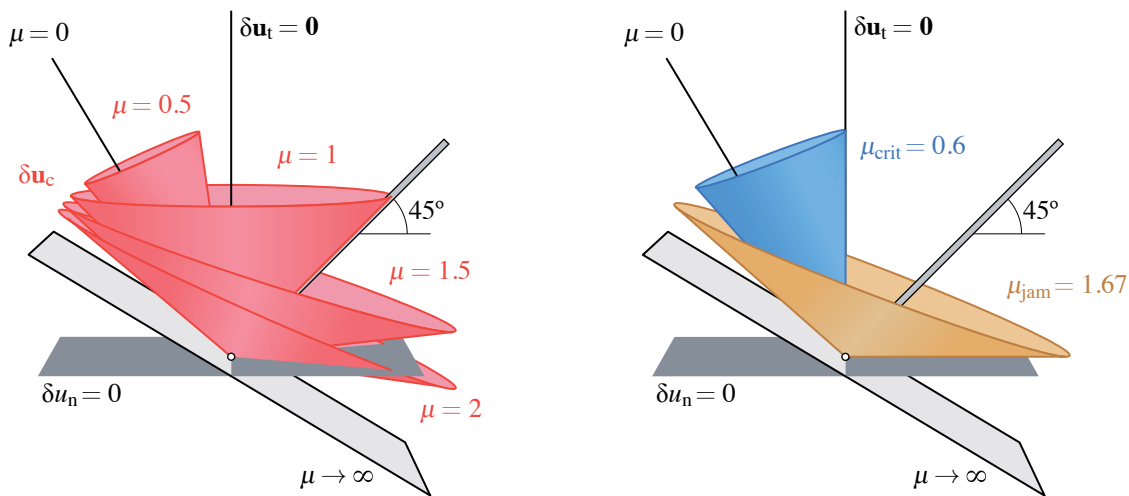


Figure 1: Projection of the generalized friction cone ( $\kappa_g$ ) to the contact velocity space of a rod at  $45^\circ$  with the ground for different friction coefficients.

As an example, let us consider a single rod in contact with the ground at  $45^\circ$ . Figure 1 shows the generalized cone for different friction coefficients, as well as the limit cases  $\mu = 0$  and  $\mu \rightarrow \infty$ . All the particular cases discussed above are also shown, and even though it is just one body in contact, this example is representative of a general case. Moreover, it is also shown the cone for the characteristic values  $\mu_{\text{crit}}$  and  $\mu_{\text{jam}}$ . For high friction coefficient ( $\mu > \mu_{\text{jam}}$ ), it can be seen how sliding to certain directions gives  $\delta u_n < 0$ , which presents the paradoxal situation where the dynamic equations have several solutions or none.

This new representation of the generalized friction cone gives a geometric tool that helps to understand the dynamics of multibody systems with frictional contacts. It is not only consistent with all the theories involving the Coulomb friction model [1, 2, 4], but it also captures the paradoxal behaviour of the model.

## References

- [1] J. J. Moreau. “Unilateral contact and dry friction in finite freedom dynamics.” *Nonsmooth Mechanics and Applications*. Springer Vienna, 1988. 1–82.
- [2] F. Génot, B. Brogliato. *New results on Painlevé paradoxes*. INRIA, 1998.
- [3] J. Kövecses, J. M. Font-Llagunes. “An eigenvalue problem for the analysis of variable topology mechanical systems.” *Journal of Computational and Nonlinear Dynamics*, 4(3), 031006, 2009.
- [4] J. A. Batlle, S. Cardona. “The Jamb (Self-Locking) Process in Three-Dimensional Collision.” *Journal of Applied Mechanics*, 65(2): 417–423, 1998.

## A discussion of two approaches for studying the dynamics of dry granular material

Michał Kwarta<sup>1</sup>, Arman Pazouki<sup>2</sup>, Radu Serban<sup>1</sup>, Dan Negrut<sup>1</sup>

<sup>1</sup> University of Wisconsin-Madison  
Department of Mechanical Engineering  
53706 Madison, Wisconsin, USA  
[kwarta, serban, negrut]@wisc.edu

<sup>2</sup> California State University, Los Angeles  
Mechanical Engineering Department  
90032 Los Angeles, California, USA  
apazouk@calstatela.edu

### Abstract

We summarized and numerically compared two different approaches for modeling and simulating the dynamics of dry granular matter. The first one, called DEM-P, from “discrete element method via penalty”, is commonly used in the soft matter physics and geomechanics communities. It can be traced back to [1, 2]. To compute the normal ( $F_n$ ) and tangential ( $F_t$ ) forces at the contact point it uses a viscoelastic model based on Hertzian contact theory, where  $F_n = \sqrt{\bar{R}\delta_n}(K_n\delta_n - C_n\bar{m}\mathbf{v}_n)$  and  $F_t = \sqrt{\bar{R}\delta_n}(-K_t\delta_t - C_t\bar{m}\mathbf{v}_t)$ . Here,  $\delta$  is the overlap of two interacting bodies;  $\bar{R}$  and  $\bar{m}$  represent the effective radius of curvature and mass, respectively; and  $\mathbf{v}$  is the relative velocity at the contact point [3].  $K_n$ ,  $K_t$ ,  $C_n$ , and  $C_t$  are the normal and tangential stiffness and damping coefficients.

The second approach, DEM-C (from “complementarity”), considers the bodies as rigid and enforces non-penetration via complementarity conditions. It is commonly used in robotics and computer graphics applications. It draws on a complementarity condition that imposes a non-penetration unilateral constraint, see Eq. (1a). That is, for a potential contact  $i$  in the active set,  $i \in \mathcal{A}(\mathbf{q}(t))$ , either the gap  $\Phi_i$  between two geometries is zero and consequently the normal contact force  $\hat{\gamma}_{i,n}$  is greater than zero, or vice-versa. The Coulomb friction model is posed via a maximum dissipation principle [4], which for contact  $i$  involves the friction force components  $(\hat{\gamma}_{i,w}, \hat{\gamma}_{i,u})$  and the relative velocity of the two bodies in contact, see Eq. (1b). The frictional contact force associated with contact  $i \in \mathcal{A}(\mathbf{q}(t))$  leads to a set of generalized forces, shown with an under-bracket in Eq. (1c), which are obtained using the projectors  $\mathbf{D}_{i,n}$ ,  $\mathbf{D}_{i,u}$ , and  $\mathbf{D}_{i,w}$  [5]. This leads in Eq. (1) to a so called differential variational inequality problem [4]

$$0 \leq \Phi_i(\mathbf{q}) \perp \hat{\gamma}_{i,n} \geq 0 \quad (1a)$$

$$(\hat{\gamma}_{i,u}, \hat{\gamma}_{i,w}) = \underset{\sqrt{\hat{\gamma}_{i,u}^2 + \hat{\gamma}_{i,w}^2} \leq \mu_i \hat{\gamma}_{i,n}}{\operatorname{argmin}} \mathbf{v}^T (\hat{\gamma}_{i,u} \mathbf{D}_{i,u} + \hat{\gamma}_{i,w} \mathbf{D}_{i,w}) \quad (1b)$$

$$\begin{aligned} \mathbf{M}(\mathbf{q})\dot{\mathbf{v}} = & \mathbf{f}(t, \mathbf{q}, \mathbf{v}) - \mathbf{g}_{\mathbf{q}}^T(\mathbf{q}, t)\hat{\lambda} \\ & + \underbrace{\sum_{i \in \mathcal{A}(\mathbf{q})} (\hat{\gamma}_{i,n} \mathbf{D}_{i,n} + \hat{\gamma}_{i,u} \mathbf{D}_{i,u} + \hat{\gamma}_{i,w} \mathbf{D}_{i,w})}_{i^{\text{th}} \text{ frictional contact force}}. \end{aligned} \quad (1c)$$

We reported numerical results for five granular dynamics experiments – shock wave propagation, direct shear (Fig. 1), static and dynamic cone penetration, triaxial loading, and hopper flow – for which we use, when feasible, both approaches. For the cone penetration test we compared numerical to experimental results of the cones’ displacement over time (Fig. 2a). The direct shear test was modified in a manner that would provide physical data to evaluate the ability of the software to track the particle motion (Fig. 2b). In the standard triaxial test the stress-strain curve obtained was compared to results published in literature [6] (Fig. 3).

The lesson learned from these and other similar granular dynamics simulations can be summarized in two observations. First, both the DEM-P and DEM-C methods are predictive; i.e., they estimate well the macroscale emergent behavior by capturing the dynamics of the material at the microscale. The remarkable aspect is that

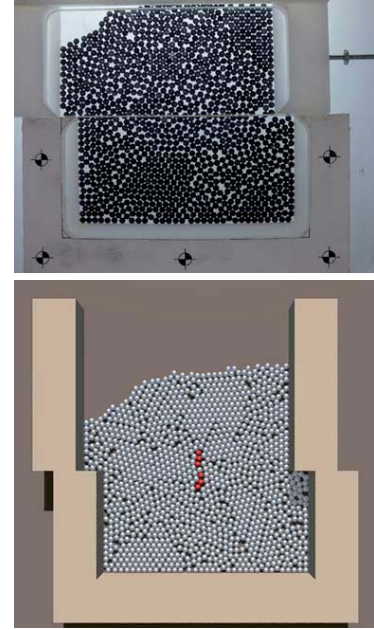
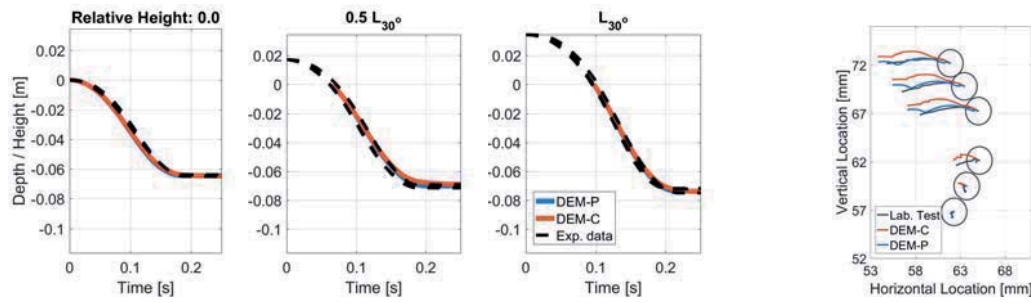


Figure 1: A comparison of the samples after the shear test seen in the laboratory test and numerical simulations. Six particles marked as red are the ones that had been monitored. Granular material packed loosely; incline angle 18°; shearing velocity 1.0 mm/min.



(a) Plots show the cones' displacement vs. time obtained from the simulations and experiments. Container with a 4-inches-wide diameter; cone  $30^\circ$  in apex angle; granular material packed loosely.

(b) Direct shear test - PIV results. Particles packed densely; the shear box inclined at  $30^\circ$ .

Figure 2: A comparison of the numerical to experimental results regarding (a) cone penetration test and (b) direct shear test with PIV.

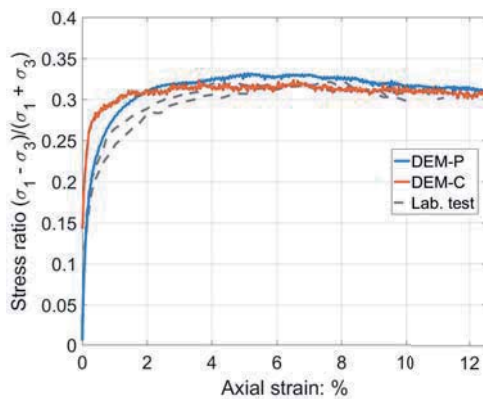


Figure 3: Standard triaxial test with polydisperse specimen.

DEM-P and DEM-C use vastly different (i) approaches to model the frictional contact problem; (ii) sets of model parameters required to capture the physics of interest; and, (iii) classes of numerical methods required to solve the differential equations that govern the dynamics of the granular material. Secondly, there are classes of problems for which one of the methods has the upper hand. While DEM-P can capture shock-wave propagation through granular media, DEM-C is proficient at handling arbitrary geometries and solving smaller problems (i.e., involving thousands of elements) with large integration step sizes very effectively. The results reported had been obtained using the open source software package Chrono.

## Acknowledgments

This research was supported in part by US Army Rapid Innovation Fund No. W911NF-13-R-0011, Topic No. 6a Maneuverability Prediction, and National Science Foundation grant GOALI-CMMI 1362583.

## References

- [1] Cundall, P., 1971. "A computer model for simulating progressive large-scale movements in block rock mechanics". In Proceedings of the International Symposium on Rock Mechanics. Nancy, France.
- [2] Cundall, P., and Strack, O., 1979. "A discrete element model for granular assemblies". *Geotechnique*, **29**, pp. 47–65.
- [3] Silbert, L. E., Ertas, D., Grest, G. S., Halsey, T. C., Levine, D., and Plimpton, S. J., 2001. "Granular flow down an inclined plane: Bagnold scaling and rheology". *Physical Review E*, **64**(5), p. 051302.
- [4] Stewart, D. E., 2000. "Rigid-body dynamics with friction and impact". *SIAM Review*, **42**(1), pp. 3–39.
- [5] Negrut, D., and Serban, R., 2016. Posing Multibody Dynamics with Friction and Contact as a Differential Algebraic Inclusion Problem. Tech. Rep. TR-2016-12: <http://sbel.wisc.edu/documents/TR-2016-12.pdf>, Simulation-Based Engineering Laboratory, University of Wisconsin-Madison.
- [6] Cui, L., O'Sullivan, C., and O'Neill, S., 2007. "An analysis of the triaxial apparatus using a mixed boundary three-dimensional discrete element model". *Geotechnique*, **57**, pp. 831–844.

# A spatial revolute joint model with clearance in mechanisms dynamics

Federico J. Cavalieri<sup>1</sup>, Alberto Cardona<sup>1</sup>, Olivier Brùls<sup>2</sup>, Javier Gálvez<sup>2</sup>

<sup>1</sup> Centro Internacional de Métodos Computacionales (CIMEC)  
Universidad Nacional del Litoral-CONICET  
Predio CONICET "Dr Alberto Cassano", Colectora Ruta 168 s/n, Paraje "El Pozo", 3000 Santa Fe, Argentina  
[fcavalieri, acardona]@cimec.unl.edu.ar

<sup>2</sup> Department of Aerospace and Mechanical Engineering (LTAS)  
University of Liège  
Chemin des Chevreuils 1 (B52), 4000 Liège, Belgium  
[o.bruls, jgalvez]@ulg.ac.be

## Abstract

Revolute joints are commonly represented with idealized models that restrict the components movement of the mechanism by a set of kinematic constraints. In a real mechanism, the unavoidable presence of misalignments, clearance between parts and assembly errors strongly affect the joints dynamic response and, consequently, of the whole system. These defects generate time variable loads with high frequency which propagate through the system increasing the possibility of breakage, fatigue and wear damage. Therefore, the mechanical system life is considerably reduced and operation costs are increased. In the last years, several numerical models of joints that include clearance, and where the contact/impact is modeled with a penalty method, have been proposed [1, 2, 4]. The penalty approach is relatively simple to implement. However, the main drawback associated with this method is the difficulty to choose the correct penalty parameters for the stiffness and damping of the contacting surfaces. Furthermore, it introduces high frequency dynamics into the system due to the presence of stiff springs that represent the contact surfaces, imposing the use of a very small time step in the integrator to correctly solve the impact. In this work, a new three-dimensional revolute joint is presented, which takes into account the components clearance and misalignment in the formulation. The equations of motion are integrated by using the nonsmooth generalized- $\alpha$  scheme proposed by Brùls *et al* [5]. Unlike the penalty approaches, the nonsmooth generalized- $\alpha$  integrator guarantees the exact satisfaction of bilateral and unilateral constraints both at position and velocity levels, avoiding the need of selecting any penalty parameter. It also avoids any unphysical penetration between the contacting bodies.

Joints clearance produces impacts in a small period of time, thus, the dynamic response of a system is conditioned to a correct selection of three main variables: i) the time step size; ii) the time integration scheme and iii) the numerical parameters of the integrators. The standard time integration algorithms such as the Newmark, Hilbert-Hughes-Taylor (HHT) or the smooth generalized- $\alpha$  methods, fail completely in the representation of rigid impacts represented by Lagrange multiplier techniques because the numerical response exhibits an important fictitious energy increase or decrease at the contact instant, completely affecting the computations. In contrast to these integrators, the nonsmooth generalized- $\alpha$  scheme makes an accurate description of impact and vibration phenomena of the system dynamics with a controllable numerical dissipation. Therefore, the nonsmooth generalized- $\alpha$  scheme leads to a qualitatively improved energy behaviour in the dynamic response.

The proposed joint model is composed by an internal cylinder, the *journal*, and an external cylinder, the *bearing* (Figure 1). Both bodies are assumed rigid and massless. Then, by ignoring the axial relative displacement between the journal and the bearing, four different movements which depend on the dynamic system configuration, are allowable: i) no contact between the components (free flight); ii) the journal and the bearing are in contact along a line; iii) the journal is in contact with the bearing at one point; iv) the journal is in contact with the bearing at two opposite points. Therefore, the dynamic behavior of the joint and the system is related with these four possible configurations, which depend on the the clearance and on the length of the journal. In the non contact condition, the joint does not introduce any forces to the system. On the contrary, in the contact condition, the changes of velocities and accelerations of the joints completely modify the dynamics of the system. To study the behavior of

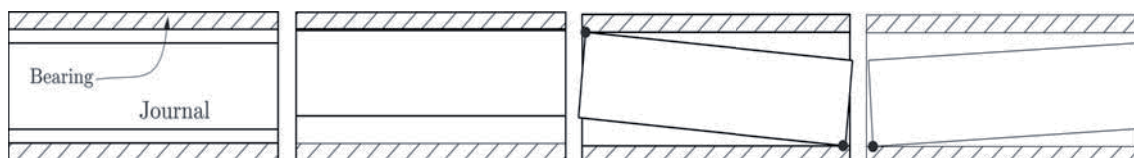


Figure 1: Four different contact modes between the journal and the bearing.

the proposed joint, a spatial three-dimensional mechanism is analyzed (Figure 2). The revolute joint with clearance is situated between the crank and the rigid frame. The dynamic behavior of the system is analyzed by plotting the displacement of the slider. The results are compared with another mechanism composed by ideal joints, i.e.

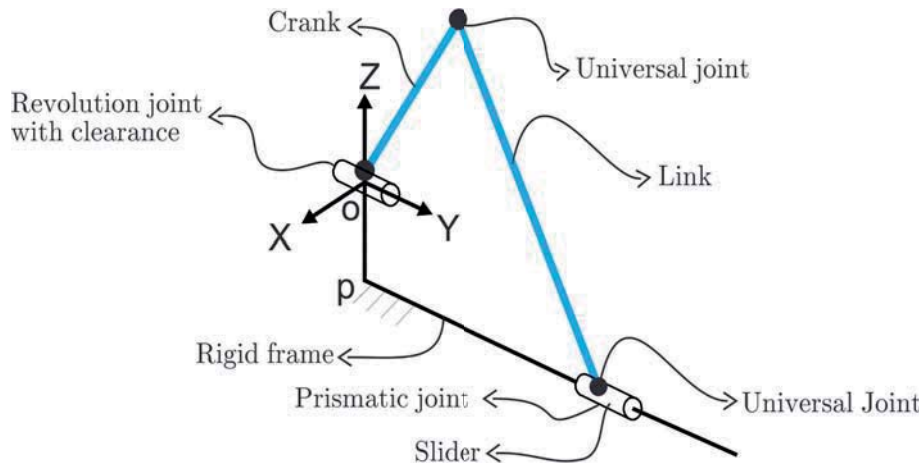


Figure 2: Configuration of the spatial mechanism.

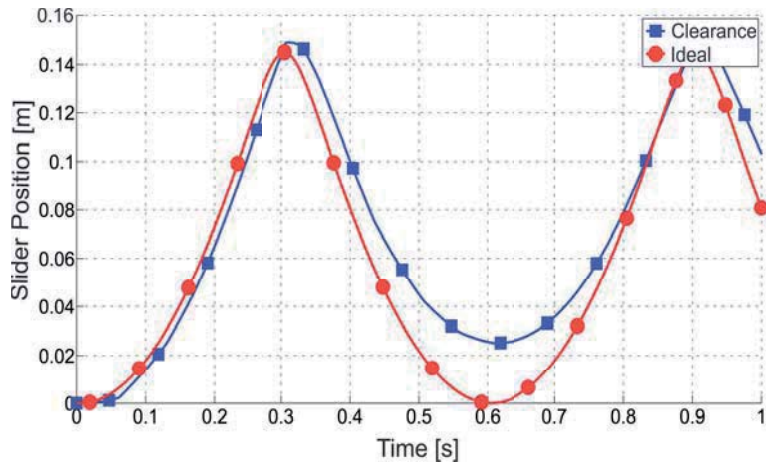


Figure 3: Slider position vs. time.

clearance is neglected. Figure 3 shows the time evolution of the position of the slider. The case with clearance is compared to the ideal case, showing that the dynamic system behavior is affected.

### Acknowledgments

This work has received financial support from Consejo Nacional de Investigaciones Científicas y Técnicas (CONICET) PIP-11220150100970CO, Agencia Nacional de Promoción Científica y Tecnológica (ANPCyT) PICT2015-1067, Universidad Tecnológica Nacional, Facultad Regional Santa Fe (UTN) PIDUTN3527.

### References

- [1] O. Bauchau and C. Ju. Modeling friction phenomena in flexible multibody dynamics. *Computer Methods in Applied Mechanics and Engineering*, 195(50-51):6909-6924, 2006.
- [2] P. Flores, J. Ambrósio and J.P. Claro. Dynamic analysis for planar multibody mechanical systems with lubricated joints. *Multibody System Dynamics*, 12(1):47-74, 2004.
- [3] P. Flores. A parametric study on the dynamic response of planar multibody systems with multiple clearance joints. *Nonlinear Dynamics*, 61(4):633-653, 2010.
- [4] P. Flores and J. Ambrósio. On the contact detection for contact-impact analysis in multibody systems. *Multibody System Dynamics*, 24(1):103-122, 2010.
- [5] O. Brüls, V. Acary and A. Cardona. Simultaneous enforcement of constraints at position and velocity levels in the nonsmooth generalized-alpha scheme. *Computer Methods in Applied Mechanics and Engineering*, 281:131-161, 2014.

# Geometrical Interpretation of LCP Pivoting in Contact Dynamics

Andreas Enzenhöfer<sup>1</sup>, Marek Teichmann<sup>2</sup>, József Kövecses<sup>1</sup>

<sup>1</sup> Department of Mechanical Engineering, Centre for Intelligent Machines  
McGill University  
817 Sherbrooke St. West, Room 270  
H3A 0C3, Montréal, Canada  
[andreas.enzenhofer@mail.mcgill.ca, jozsef.kovecses@mcgill.ca]

<sup>2</sup> CM Labs Simulations  
645 Wellington St., #301  
H3C 1T2, Montréal, Canada  
marek@cm-labs.com

## Abstract

Contact in multi-rigid-body systems can be modelled using *unilateral constraints*. The nonnegative *gap function*  $\phi \geq 0$  measures the distance between the closest points of two rigid bodies and prevents interpenetration of these bodies. Due to these inequalities, the dynamics formulation can be represented by a *linear complementarity problem* (LCP). The mathematical formulation of an LCP is given by

$$\begin{aligned} \mathbf{A}\mathbf{x} + \mathbf{b} &= \mathbf{w}, \\ \mathbf{0} &\leq \mathbf{w} \perp \mathbf{x} \geq \mathbf{0}, \end{aligned} \quad (1)$$

where the lead matrix  $\mathbf{A} \in \mathbb{R}^{n \times n}$  and the vector  $\mathbf{b} \in \mathbb{R}^n$  are known. It must hold that  $w_i x_i = 0$  with either  $x_i$  or  $w_i$  equal to zero for a solution to be admissible. The dynamics formulation of a multibody system without bilateral constraints using a finite difference approximation for the accelerations can be written as

$$\begin{aligned} \begin{bmatrix} \mathbf{M} & -\mathbf{J}_n^T \\ \mathbf{J}_n & \mathbf{0} \end{bmatrix} \begin{bmatrix} \mathbf{v}^+ \\ h\lambda_n^+ \end{bmatrix} + \begin{bmatrix} -\mathbf{M}\mathbf{v} - h\mathbf{f}_a \\ \mathbf{0} \end{bmatrix} &= \begin{bmatrix} \mathbf{0} \\ \dot{\phi}^+ \end{bmatrix}, \\ \mathbf{0} &\leq \dot{\phi}^+ \perp h\lambda_n^+ \geq \mathbf{0}, \end{aligned} \quad (2)$$

which represents a mixed LCP at the velocity level with mass matrix  $\mathbf{M}$ , unilateral constraint Jacobian  $\mathbf{J}_n$ , contact forces  $\lambda_n$ , generalized velocities  $\mathbf{v}$ , time step size  $h$ , applied forces  $\mathbf{f}_a$  and the time derivative of the gap function  $\dot{\phi}$ . The superscript  $+$  denotes the values at the next time step. This mixed LCP can be transformed into LCP-form (Eq. (1)) by substituting the unknown velocities  $\mathbf{v}^+$  [1]. This is equivalent to forming  $\mathbf{A} = \mathbf{J}_n \mathbf{M}^{-1} \mathbf{J}_n^T$  and  $\mathbf{b} = \mathbf{J}_n \mathbf{M}^{-1} (\mathbf{M}\mathbf{v} + h\mathbf{f}_a)$  in Eq. (1). Hence,  $\mathbf{x}$  and  $\mathbf{w}$  are the contact impulses and the gap velocities, respectively. According to complementarity, there are two possible configurations for each contact  $i$ : If two bodies in contact move away from each other ( $w_i > 0$ ), there must not be any additional impulse exchanged ( $x_i = 0$ ). Conversely, an impulse must be developed ( $x_i > 0$ ) in order to prevent two contacting bodies from moving toward each other ( $w_i = 0$ ).

This paper focuses on direct methods to solve LCPs, also known as *pivoting*, which systematically search for a solution to the LCP by interchanging components  $x_i$  or  $w_i$  between two different sets: *basic* and *nonbasic*. Basic components are nonnegative, nonbasic ones are zero. The objective of this paper is to geometrically interpret pivoting for LCPs in the context of contact dynamics. In Lemke's algorithm [2, 3], an artificial variable  $x_0$  is added to the nonbasic set if Eq. (1) is not satisfied by the initial guess. All  $2n + 1$  unknowns are regrouped to a single vector  $\mathbf{y} = [\mathbf{w}^T, \mathbf{x}^T, x_0]^T$ . This can be written as

$$\begin{aligned} \mathbf{A}\mathbf{x} + \mathbf{c}x_0 + \mathbf{b} &= \mathbf{w} \Leftrightarrow \mathbf{K}\mathbf{y} = \mathbf{b} \Leftrightarrow \mathbf{B}\bar{\mathbf{y}} = \mathbf{b}, \\ \mathbf{0} &\leq \mathbf{x} \perp \mathbf{w} \geq \mathbf{0}, x_0 \geq 0, \end{aligned} \quad (3)$$

where  $\mathbf{0} < \mathbf{c} \in \mathbb{R}^n$  and  $\mathbf{K} = [\mathbf{1}^{n \times n}, -\mathbf{A}, -\mathbf{c}] \in \mathbb{R}^{n \times (2n+1)}$ . The basis matrix  $\mathbf{B} \in \mathbb{R}^{n \times n}$  can be obtained by deleting all columns from  $\mathbf{K}$  that are multiplied by the  $n + 1$  nonbasic, hence zero, components in  $\mathbf{y}$ . Accordingly,  $\bar{\mathbf{y}}$  contains all basic components of  $\mathbf{y}$ . In order to get a solution to Eq. (3) after only one iteration,  $x_0$  is pivoted into the basic set and becomes nonzero. If  $x_0$  leaves the basic set, the LCP in Eq. (1) is fulfilled as well. Thus, Lemke's algorithm aims to remove  $x_0$  from the basic set, while complying with Eq. (3) at every pivoting step. For this purpose, single pivots are performed at each step, i.e. only one variable enters, another variable leaves the basic set. The *entering* variable  $y_s$  is chosen to be the complement of the variable which left the basic set in the previous iteration. This maintains an *almost-complementary* solution to Eq. (3) [3]. The *leaving* variable  $y_r$  is found by computing the componentwise minimum quotient

$$\alpha = \frac{\bar{y}_r}{v_r} = \min \left( \frac{\bar{y}_i}{v_i} : v_i > 0 \right), \quad (4)$$

where  $\bar{\mathbf{y}}$  is the current solution and  $\mathbf{v} = \mathbf{B}^{-1} \mathbf{k}_s$  is the column vector of  $\mathbf{K}$  corresponding to  $y_s$ , both expressed in the current basis  $\mathbf{B}$ . We can calculate the solution at the next pivoting step (indicated by  $*$ ) by  $\mathbf{y}^* = \mathbf{y} + \alpha \boldsymbol{\beta}$ . The components  $\boldsymbol{\beta} \in \mathbb{R}^{2n+1}$  are chosen as follows:  $\beta_i = v_i$  for all basic components  $i$  (including  $y_r$ ),  $\beta_s = 1$  for  $y_s$  and  $\beta_j = 0$  for all other components  $j$ . A detailed description of the above procedure can be found in [2].

We illustrate the geometrical interpretation of Lemke's algorithm with the 2D rigid rod at rest ( $\mathbf{v} = \mathbf{0}$ ) in Fig. 1. We apply an external moment,  $M_z = 6 \text{ Nm}$ , to the 4-kg, 1.5-m rod contacting the ground in two points at the ends under the effect of gravity ( $g = 9.81 \text{ m/s}^2$ ). The constraint Jacobian, mass matrix and applied forces are given by

$$\mathbf{J}_n = \begin{bmatrix} 0 & 1 & -\frac{l}{2} \\ 0 & 1 & \frac{l}{2} \end{bmatrix}, \mathbf{M} = \text{diag} \left( m, m, \frac{1}{12}ml^2 \right), \mathbf{f}_a = [ 0 \quad -mg \quad M_z ]^T. \quad (5)$$

The resulting MLCP (Eq. (2)) can be transformed into LCP form (Eq. (1)) with a time step size  $h = 0.1s$ :

$$\underbrace{\begin{bmatrix} \frac{4}{m} & -\frac{2}{m} \\ -\frac{2}{m} & \frac{4}{m} \end{bmatrix}}_{\mathbf{A}} \underbrace{\begin{bmatrix} h\lambda_1^+ \\ h\lambda_2^+ \end{bmatrix}}_{\mathbf{x}} + \underbrace{\begin{bmatrix} v_y - \frac{l}{2}\omega l - h(g + \frac{6}{ml}M_z) \\ v_y + \frac{l}{2}\omega l - h(g - \frac{6}{ml}M_z) \end{bmatrix}}_{\mathbf{b}} = \underbrace{\begin{bmatrix} 1 & -\frac{1}{2} \\ -\frac{1}{2} & 1 \end{bmatrix}}_{\mathbf{A}} \underbrace{\begin{bmatrix} h\lambda_1^+ \\ h\lambda_2^+ \end{bmatrix}}_{\mathbf{x}} + \underbrace{\begin{bmatrix} -1.581 \\ -0.381 \end{bmatrix}}_{\mathbf{b}} = \mathbf{w}. \quad (6)$$

Fig. 2 illustrates the column vectors  $\mathbf{k}_i$  of matrix  $\mathbf{K}$

$$\mathbf{K} = [\mathbf{1}^{n \times n}, -\mathbf{A}, -\mathbf{c}] = [\mathbf{k}_1, \mathbf{k}_2, \mathbf{k}_3, \mathbf{k}_4, \mathbf{k}_5] = \begin{bmatrix} 1 & 0 & -1 & \frac{1}{2} & -1 \\ 0 & 1 & \frac{1}{2} & -1 & -1 \end{bmatrix}.$$

We can express the right-hand side vector  $\mathbf{b}$  as a linear combination of two linearly independent basis vectors  $\mathbf{k}_j$ ,  $\mathbf{k}_l$ . If we allow nonnegative coefficients only, a nonnegative polygonal cone in 2D is defined by

$$C = \{ \lambda_j \mathbf{k}_j + \lambda_l \mathbf{k}_l : \lambda_j, \lambda_l \geq 0, j \neq l \}. \quad (7)$$

If no initial guess is given, Lemke's algorithm starts with the basis  $\mathbf{B} = [\mathbf{k}_1, \mathbf{k}_2]$ , i.e.  $y_1 (= w_1)$ ,  $y_2 (= w_2)$  are basic. We can see in Fig. 2 that  $\mathbf{b}$  is not in the nonnegative cone spanned by  $\mathbf{k}_1$ ,  $\mathbf{k}_2$ . Thus, one of the vectors  $\mathbf{k}_1$ ,  $\mathbf{k}_2$  needs to be removed from the basis and replaced by  $\mathbf{k}_3$ ,  $\mathbf{k}_4$  or  $\mathbf{k}_5$ . For the first pivot, we always choose the vector corresponding to the artificial variable  $y_5 (= x_0)$  as this ensures to form a nonnegative cone  $C$  with either  $\mathbf{k}_1$  or  $\mathbf{k}_2$  due to the strictly negative components of  $\mathbf{k}_5$ .

In this example, we replace  $\mathbf{k}_1$  by  $\mathbf{k}_5$  which leads to basis  $\mathbf{B}^* = [\mathbf{k}_2, \mathbf{k}_5]$  at the next pivoting step and delivers a nonnegative solution  $\bar{\mathbf{y}}$  (see Eq. (8)). This vector  $\bar{\mathbf{y}}$  is simply  $\mathbf{b}$  expressed in basis  $\mathbf{B}^*$  ( $\mathbf{B}^* \bar{\mathbf{y}} = \mathbf{b}$ ). To maintain complementarity, we choose the entering variable  $y_s$  to be  $y_3 (= x_1)$ , which is the complement of the formerly leaving variable  $y_1 (= w_1)$ . Its corresponding basis vector  $\mathbf{k}_3$  can be expressed in basis  $\mathbf{B}^*$  by solving the linear system  $\mathbf{B}^* \mathbf{v} = \mathbf{k}_3$  for  $\mathbf{v}$ :

$$\bar{\mathbf{y}} = \begin{bmatrix} y_2 \\ y_5 \end{bmatrix} = \begin{bmatrix} 1.2 \\ 1.581 \end{bmatrix}, \mathbf{v} = \begin{bmatrix} 1.5 \\ 1.0 \end{bmatrix}. \quad (8)$$

According to the minimum quotient rule in Eq. (4),  $\mathbf{k}_2$  will be replaced by  $\mathbf{k}_3$  as  $\frac{y_2}{v_1} < \frac{y_5}{v_2}$ . The minimum quotient contains information about the direction of  $\mathbf{b}$  and  $\mathbf{k}_3$  with respect to  $\mathbf{k}_2$ ,  $\mathbf{k}_5$  and to each other. It ensures to obtain another linear combination of  $\mathbf{b}$  in a nonnegative cone (Eq. (7)) after performing the pivot.

Lemke's method chooses the variable  $y_r$  leaving the basic set by computing the minimum quotient (Eq. (4)). We replace the basis vector  $\mathbf{k}_r$  by  $\mathbf{k}_s$  where the latter corresponds to the entering variable  $y_s$ . This choice ensures to always express the right-hand side  $\mathbf{b}$  in a nonnegative cone (Eq. (7)) which represents a solution to the generalized LCP in Eq. (3).

## References

- [1] K. Erleben, "Velocity-based shock propagation for multibody dynamics animation," *ACM Transactions on Graphics (TOG)*, vol. 26, no. 2, p. 12, 2007.
- [2] J. J. Júdice, "Algorithms for linear complementarity problems," in *Algorithms for continuous optimization*, pp. 435–474, Springer, 1994.
- [3] R. W. Cottle and G. B. Dantzig, "Complementary pivot theory of mathematical programming," *Linear algebra and its applications*, vol. 1, no. 1, pp. 103–125, 1968.

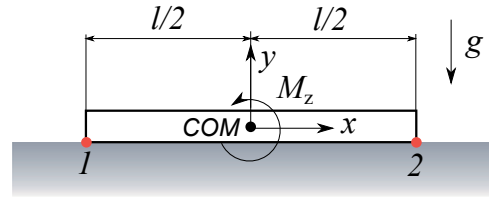


Figure 1: Rigid rod on the ground in 2D, 2 contact points at the ends

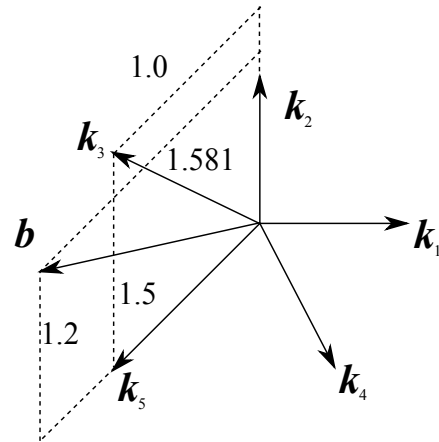


Figure 2: Geometrical interpretation: column vectors  $\mathbf{k}_i$  of  $\mathbf{K} = [\mathbf{1}^{n \times n}, -\mathbf{A}, -\mathbf{c}] = [\mathbf{k}_1, \mathbf{k}_2, \mathbf{k}_3, \mathbf{k}_4, \mathbf{k}_5]$  (Eq. (3))

# Geometric non-linear dynamics of shell system with large amount of contact based on the co-rotational formulation

Jiabei Shi, Zhuyong Liu, Jiazhen Hong

School of Naval Architecture, Ocean and Civil Engineering,  
Shanghai Jiao Tong University  
800 Dongchuan Road, 200240 Shanghai, P.R.China  
sjbnust@163.com, zhuyongliu@sjtu.edu.cn, jzhong@sjtu.edu.cn

## Abstract

In the multi-body system made of shell structures, the contact between shells usually happen at any time and any region of structures. For example, the solar cell system, Figure 1, at the initial/transportation mode, the solar cells are folded compactly. When the system extends to the final/working mode, because of the inertia and the geometric non-linear deformation, lots of the contact/impact between cells will come up and the contacted pairs may separate meanwhile. It is difficult and time-consuming to compute the geometric non-linear problem with frequent contact. The first reason is that the geometric non-linear dynamics shell problem itself is a complicated work[1] and the non-linear internal force and its complex linearization are both troublesome. The second, the contact problem make the time integration extremely slow for the collision detection runs for every time when solver access the iteration. That is why it is one of the most important factor to slow down the integration. From previous study, the node-surface contact mode may leads the penetration too deep, which will make the computation non-stable. Furthermore, if the continuous force[2] model is used in contact associated with thin shell or membrane, the integration step should be controlled carefully. Because the penetration is comparable with the shell thickness, which means that the contact pairs depend on the depth of the penetration, that's why the penetration depth needs to be limited.

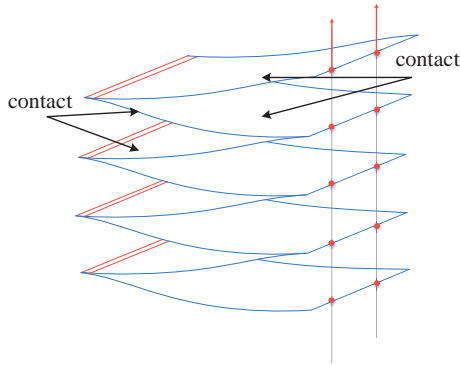


Figure 1: A part of solar cells

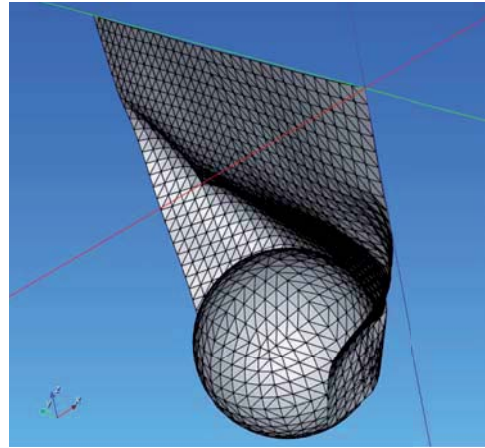


Figure 2: Numerical example of constrained cloth-ball contact

Considering the difficulty of computation of the non-linear shell contact, an enhanced model of dynamics of geometric non-linear shells with complete contact discretization is proposed. Based on the co-rotational formulation, a rotation-free form of geometric non-linear shell is developed, it is singularity free, efficient. By using of plane polar-based local frame, the deformation is accurate in the local frame, and the use of combined rotation-free element, the core element perform a better result.

$$\begin{aligned} \mathbf{f}^m + \mathbf{f}^i + \mathbf{f}^d + \mathbf{f}^c + \Phi_q^T \boldsymbol{\lambda} &= \mathbf{0} \\ \Phi &= \mathbf{0} \end{aligned} \quad (1)$$

where the items on the left-hand-side of the equation are inertial force vector, internal force vector, damping force vector, contact force vector and the force vector associated with constraint force. In handling the shell contact, a unified contact equation is derived to simplify the contact force and its linearization using continuous force model with augmented Lagrangian method.

$$\mathbf{f}_0^c = \varepsilon_g \mathbf{g}_k \quad (2)$$

$$\mathbf{f}_{k+1}^c = \mathbf{f}_k^c + \varepsilon_g \mathbf{g}_k \quad (3)$$

where the  $f_k^c$  denotes the iterative contact force, which is not sensitive to the penalty factor  $\epsilon_g$ . In the collision detection process, the low-order element is used, for the type of element in co-rotational formulation is always the low-order one, and which has a better computational efficient than high-order element. To extend the contact discretization type, the edge-edge contact mode is firstly introduced here. A complete contact primitives can be detected, which make the penetration smaller than ever. In time integration, generalized- $\alpha$  with constraint[3] is adopted, which provide numerical dissipation to stabilize the computation. The time step can be controlled by using the concept of continuous-collision-detection. First contact time can be predicted exactly and the next step is determined. Further- more the time step that associated with separation process controlled by error estimation. Using the above strategies and conventional parallel computation with bounding box hierarchy, we obtain a fine computational efficient. Several numerical examples show the effect of this contact model, and a complete practical application shows the efficient of the geometric non-linear model and the contact treatment method.

### **Acknowledgments**

This research was supported by the National Natural Science Foundation of China (No.11132007 , No.11202126), for which the authors are grateful.

### **References**

- [1] Felippa, C. A., Haugen, B. A Unified Formulation of Small-Strain Corotational Finite Elements: I. Theory. *Computer Methods in Applied Mechanics and Engineering*, Special Issue on Shells, 2005
- [2] Flores, P., Lankarani, H. M. *Contact Force Models for Multibody Dynamics*. Springer, Switzerland, 2016
- [3] Arnold, M., Brüls, O. Convergence of the generalized- $\alpha$  scheme for constrained mechanical systems. *Multi-body System Dynamics*, 18(2), 185–202,2007

# Comparison of Two Versions of the LuGre Model Under Conditions of Varying Normal Force

Marek Wojtyra

Warsaw University of Technology  
Institute of Aeronautics and Applied Mechanics  
Nowowiejska 24, 00-665 Warsaw, Poland  
mwojtyra@meil.pw.edu.pl

## Abstract

The LuGre model of friction is an effect of cooperation between Lund and Grenoble Universities [1]. This is a dynamic model, sometimes presented as an extension to the Dahl model. The important feature of dynamic models is that the same equations are used to describe both kinetic and static friction, and there is no need to switch between equation sets when the frictional pair transits from one mode to another. The LuGre model reproduces a range of friction-related phenomena: the Stribeck effect, presliding displacement, frictional lag, varying break-away force [1], [2]. The model is widely used in practice and has been thoroughly studied from the theoretical point of view. To use the model, six parameters must be matched to experimental data.

There are two variants of LuGre model. In the classical formulation [1], the normal force affects calculated friction indirectly (the normal force is used to calculate an auxiliary state variable, which is then utilized to determine friction). In the modified formulation [3], originally proposed to analyze tire-road contacts, the normal force directly affects friction (the auxiliary variable is used to calculate an instantaneous coefficient of friction). Differences between these variants manifest themselves mainly when the normal load is varying.

In this article two versions of the LuGre model are compared. Some important differences between the models are pointed out and their consequences are investigated. The applicability of the models to the systems working under conditions of variable normal load is discussed.

In its classical form, the LuGre model was proposed in [1]. To describe friction between two bodies, an additional state variable  $z$ , associated with micro-displacements, is introduced. The time evolution of this state variable is governed by the following equation:

$$\dot{z} = v - z \sigma_0 |v| / G(v), \quad (1)$$

where  $v$  is the relative velocity of the two surfaces in contact and  $\sigma_0$  is a constant coefficient. The velocity-dependent function  $G$  is defined as:

$$G(v) = F_C + (F_S - F_C) e^{-(v/\mathcal{G})^2}, \quad (2)$$

where  $F_C$  is the Coulomb friction force,  $F_S$  corresponds to the maximum of the stiction force, and parameter  $\mathcal{G}$  (sometimes, e.g. in [4], called the Stribeck velocity) determines how quickly  $G$  tends to  $F_C$ .

The friction force is calculated as:

$$F = \sigma_0 z + \sigma_1 \dot{z} + \sigma_2 v, \quad (3)$$

where constant  $\sigma_1$  represents micro-damping, whereas constant  $\sigma_2$  corresponds to macro-damping, namely viscous friction (note that more elaborated force-velocity relationship may be substituted for the  $\sigma_2 v$  term).

An alternative version of the LuGre model was proposed to model friction in tire-road contact [3] and later on was used to study a range of different mechanisms subjected to varying normal loads in frictional contacts between bodies (see, e.g., [5]).

In the modified version of the LuGre model the time derivative of the auxiliary state variable  $z$  is defined as:

$$\dot{z} = v - z \sigma_0^M |v| / G^M(v), \quad (4)$$

where  $\sigma_0^M$  is a constant coefficient.

The most important difference between the classic and the modified models consists in the definition of function  $G^M$ . This time coefficients of friction (in [3] referred to as normalized friction forces) rather than friction forces themselves are utilized:

$$G^M(v) = \mu_K + (\mu_S - \mu_K) e^{-|v/\mathcal{G}^\alpha|.} \quad (5)$$

In their calculations, the authors of [3] set  $\alpha = 1/2$ , however, in order to enable comparison with the classical version of the model, in this study  $\alpha = 2$  is used. Consequently, the argument of the exponential function in Eq. (5) equals  $-(v/\mathcal{G})^2$ , i.e., is the same as in Eq. (2).

In the modified LuGre model, friction is directly proportional to the magnitude of the normal force,  $N$ :

$$F = (\sigma_0^M z + \sigma_1^M \dot{z} + \sigma_2^M v)N = \mu \cdot N, \quad (6)$$

where  $\sigma_1^M$  and  $\sigma_2^M$  are constants which play roles analogous to constants  $\sigma_1$  and  $\sigma_2$  in the classical model. The friction to normal force ratio,  $\mu$ , may be understood as an instantaneous coefficient of friction.

In paper [1], a bristle analogy was proposed to visualize the idea behind equations describing the classical model (variable  $z$  may be interpreted as the average deflection of bristles at contacting surfaces; if the deflection is sufficiently large, the bristles will slip and the model will switch from stiction to sliding). In the present study it is pointed out that this analogy must be significantly amended to match the modified model. In the new interpretation the Amontons' paradox is involved to explain the fact that the stiffness of bristles, rather than their deflection, is proportional to the magnitude of normal force.

The potential equivalence of the two versions of the model was studied. It was shown that the models are equivalent only for one specific value of constant normal force. Both variants of the friction model were investigated with different constant normal forces. It was found that the changes of normal force levels resulted in changes of normalized break-away forces (i.e., in the friction to normal force ratio at which transition from stiction to sliding occurs). The classical model was found to be more sensitive to the changes of the level of the normal load than the modified model. Moreover, when the LuGre model, and especially its classical version, is tuned to match some constant normal force  $N_E$  (or, equivalently, to match kinetic and static friction levels,  $F_C$  and  $F_S$ , respectively) its applicability for normal forces  $N$  fairly different from  $N_E$  may be questionable. An experimental process intended to identify the parameters of the LuGre model should be organized in such a way as to take into account the variability of normal loads throughout the expected range.

Behavior of two versions of the friction model under conditions of time-varying normal force was investigated. It was found that the classical model (and only this one) may fail in two situations. Firstly, when the system under constant tangential load remains in the static mode, friction may remain constant even if the normal load significantly decreases (consequently, the friction to normal force ratio rises). Secondly, when the normal force  $N$  tends to zero, function  $G$  in the denominator of Eq. (1) tends to zero as well. As a result, large magnitudes of  $\dot{z}$  may be expected, and thus numerical problems are unavoidable.

The results of comparison show that the modified version of the LuGre model, while not being flawless, is much more suitable for simulation of frictional systems with varying normal forces. The usage of the classical version of the LuGre model should be avoided for systems with varying normal force, especially when the relative variations are large and the normal force can drop down to small, close to zero magnitudes. It was found that, in some situations involving varying normal force, the ratio of friction to normal force, predicted by the classical version of the model, may rise unbounded. Moreover, numerical problems appear when the normal force tends to zero. None of these problems are encountered when the modified model is used.

On the other hand, it was found that when the modified LuGre model is used to simulate the stiction mode, cyclical changes of the normal load may lead to drift of the mechanical system, even if the tangential load is constant and significantly less than the maximum stiction force. This property shall be recognized as a minor disadvantage of the modified model.

In the scientific literature the classical version of the LuGre model has been studied thoroughly from both theoretical and experimental perspectives. Number of papers dealing with the modified model is much less. As it can be demonstrated, properties of these two models are at some points very different. It should be concluded that the modified LuGre model deserves more attention.

## Acknowledgments

This research was supported by the National Science Centre (Poland) grant no. DEC-2012/07/B/ST8/03993.

## References

- [1] C. Canudas de Wit, H. Olsson, K. J. Astrom, P. Lischinsky. A New Model for Control of Systems with Friction. *IEEE Transactions on Automation and Control*, 40:419-425, 1995.
- [2] K. J. Astrom, C. Canudas de Wit. Revisiting the LuGre Friction Model. *IEEE Control Systems Magazine*, 28:101-114, 2008.
- [3] C. Canudas de Wit, P. Tsiotras, E. Velenis, M. Basset, G. Gissinger. Dynamic Friction Models for Road/Tire Longitudinal Interaction. *Vehicle Systems Dynamics*, 39:189-226, 2003.
- [4] N. B. Do, A. A. Ferri, O. A. Bauchau. Efficient Simulation of a Dynamic System with LuGre Friction. *Journal of Computational and Nonlinear Dynamics*, 2: 281-289, 2007.
- [5] M. Wojtyra. Modeling of static friction in closed-loop kinematic chains—Uniqueness and parametric sensitivity problems. *Multibody System Dynamics*, 39:337-361, 2017.

# Modeling Rigid Body Multi-point Contact-Impact Transition for Event-Based Simulation Schemes

Abhishek Chatterjee<sup>1</sup>, Alan Bowling<sup>2</sup>

<sup>1</sup> Department of Mechanical and Aerospace Engineering  
University of Texas at Arlington  
Box 19018, Arlington, TX, USA  
abhishek.chatterjee@mavs.uta.edu

<sup>2</sup> Department of Mechanical and Aerospace Engineering  
University of Texas at Arlington  
Box 19018, Arlington, TX, USA  
bowling@uta.edu

## Abstract

This work presents a modeling and simulation technique for handling rigid body contacts and impacts, particularly the transition from an impact to a contact problem. Impacts between rigid bodies are characterized by discontinuous changes in the system velocities due to infinitesimally large contact forces. In the proposed framework impacts are treated as discrete events during which the velocities of the system evolve in the impulse-domain. The impact model used in this work is developed based on Darboux-Keller shock dynamics [1]. Constraints consistent with the rigid body assumption are used to resolve indeterminacy associated with multi-point analysis [3]. An energetic coefficient of restitution based of Stronge's hypothesis establishes the termination criteria for the impact events [2]. The use of energetic coefficient of restitution ensures energy-consistency for the post-impact velocities found through this analysis.

An impact is considered to have a short duration, while contacts have a longer duration. During contact, the forces between the participating rigid bodies satisfy the: 1) non-penetrability condition and 2) frictional force constraints based on Coulomb Friction. The non-penetrability condition enforces normal velocity and acceleration constraints on the equations of motion. Whereas the Coulomb friction constrains the tangential forces at the contact points. These constraints placed on the equations of motion, lead to a reduction in the number of degrees of freedom of the system.

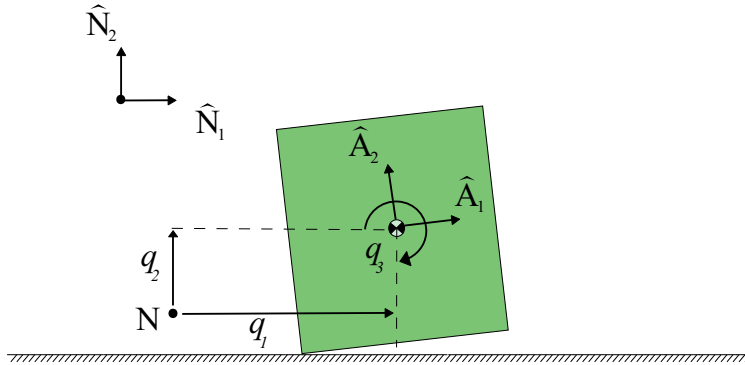


Figure 1: Rocking Block Schematic

The loss in degrees of freedom during contact varies depending upon the slip-state of the contact points. For example, consider the planar rigid block shown in Fig.(1). The planar block has three degrees of freedom (DOFs), described by a set generalized coordinates,

$$\mathbf{q} = [ q_1 \quad q_2 \quad q_3 ]^T \quad (1)$$

where  $q_1$  and  $q_2$  represents the position and  $q_3$  describes the orientation of the block. Then, the general form for the equations of motion is given by,

$$A\ddot{\mathbf{q}} + \mathbf{b}(\dot{\mathbf{q}}, \mathbf{q}) + \mathbf{g}(\mathbf{q}) = J^T \mathbf{F} \quad (2)$$

where  $A$  is the mass matrix, while  $\mathbf{b}$  and  $\mathbf{g}$  are vectors of Coriolis terms and gravity. The contact constraint forces  $\mathbf{F}$  are related to the generalized active forces through a Jacobian matrix,  $J$ . The planar block in the configuration shown in Fig.(1), contacts the ground at one of the vertex points. If this contact point sticks, both normal and tangential velocities of this contact point become zero, such that  $q_3$  becomes the only independent coordinate for the system, thereby dropping the number of DOFs to one. On the other hand, when the contact point slips, constraints are applied at the force-level. Furthermore, during dynamic simulation contact points can also switch

between contact and separation. This work uses a constraint embedding technique similar to [4, 5], to enforce all the different types constraints into the equations of motion. During slipping, the force constraints from the Coulomb friction law are embedded into the equations of motion by the virtue of velocity projection method [3].

An event-based simulation scheme is used in this work for detection and analysis of impacts. A criterion is proposed, based on normal velocities and acceleration of contact points, to accommodate the transition between impact and contact states. This approach yields an energetically consistent method for handling the impact, the transition from impact to contact, contact, separation, and the transition from contact to impact. Simulation results of a three-dimensional rocking block example using the proposed method are presented and are compared with experimental results from the literature.

## References

- [1] J. Keller, "Impact with friction," *Journal of Applied Mechanics, Transactions ASME*, vol. 53, pp. 1–4, Mar. 1986.
- [2] W. J. Stronge, *Impact mechanics*. Cambridge university press, 2004.
- [3] A. Rodriguez, A. Chatterjee, and A. Bowling, "Solution to three-dimensional indeterminate contact and impact with friction using rigid body constraints," in *ASME 2015 International Design Engineering Technical Conferences and Computers and Information in Engineering Conference*, pp. V006T10A037–V006T10A037, American Society of Mechanical Engineers, 2015.
- [4] R.A. Wehage, E.J. Haug, "Generalized coordinates partitioning for dimension reduction in analysis of constrained dynamic systems" *J. Mech. Design*, 104 (1982), pp. 247-255
- [5] R.B. Gillespie, V. Patoglu, I.I. Hussein, E.R. Westervelt, "On-line symbolic constraint embedding for simulation of hybrid dynamical systems," *Multibody Syst. Dyn.* 14(3–4), 387–417 (2005)

# Modelling of the Nuclear Fuel Assembly Components as a Flexible 1D Continua with Inner and Outer Impact Interactions

Štěpán Dyk<sup>1</sup>, Vladimír Zeman<sup>1</sup>

<sup>1</sup>NTIS, Faculty of Applied Sciences  
University of West Bohemia  
Univerzitní 8, 306 14 Plzeň, Czech Republic  
[sdyk, zemanv]@ntis.zcu.cz

## Abstract

A nuclear fuel assemblies (FAs) consist of a large number of the beam-type components. The assembly includes mainly fuel rods (FRs) which are its key part as that is where the nuclear fission occurs. Each FR, see Fig. 1a, consists of the fuel rod cladding (Zr thin-walled tube) filled with the uranium fuel pellets stack with the clearance between pellets and the cladding. Other important components of the FA are guide thimbles (GTs), see Fig. 1b, placed between the fuel rods and securing control rods (CRs) drop which slow down the nuclear reaction if necessary. All these components are linked together by several spacer grids (SGs) which fix them in the appropriate cross section shape (square or hexagonal, depending on the FA type). In case of TVSA-T fuel assemblies applied in VVER-1000 type reactors, the cross-section of the assembly is hexagonal and it includes 312 FRs, 18 GTs, one central tube (CT), vertices of cross-section hexagon are stiffened by six angle-pieces and there are 8 spacer grids placed regularly over the FA length. FRs are fixed into spacer grids with radial prestress. Between GTs and SG cells, there is a radial clearance. At the level of the highest SG, there is an added sleeve.

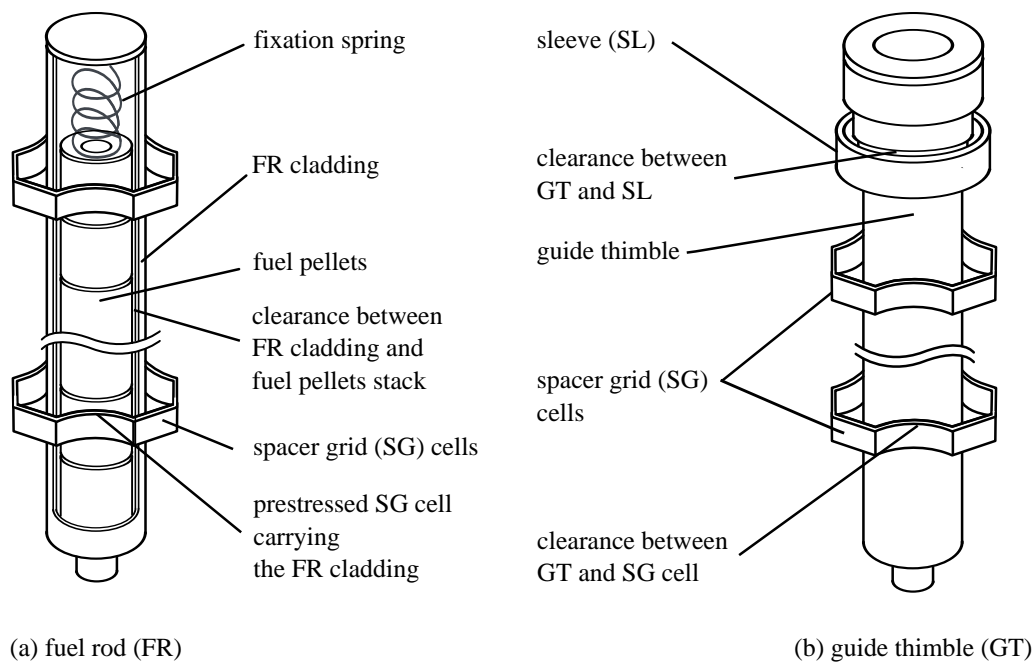


Figure 1: A fuel rod model (a) as a system consisting of two flexible 1D subsystems and spacer-grids, and guide thimble (b) as a system consisting of 1D flexible body, spacer grids and sleeve

For many reasons, it is important to estimate the motion of the FA components. The deformation of the GT is key factor for the smooth control rod drop that is critical during the operation of the reactor. Basically, there are two main causes of the GT deformation – static and dynamical. Static deformation, often called FA bow, is given by the axial loading on the GTs and irradiation and it is not taken into account in this paper. The dynamical deformation is given by the pressure pulsations of the coolant and fluid-flow forces. Due to clearances between the GTs and SG cells or sleeve, impact forces are possibly generated during the GT vibration [2]. The control rod drop can be modelled using multibody approaches [5, 1, 3] and it helps to estimate the time of the CR fall.

In case of FRs, it is important as well to know its vibration because the *grid-to-rod fretting wear* occurs in the contact points between FR cladding and SG cells. This phenomenon makes the cladding thinner in the contact point and the loss of the mass occurs during the reactor operation-cycle. In critical case, the thickness of the FR cladding can reach the limit value that can cause undesirable leak of fission products into the coolant. For the estimation of the fretting wear, it is necessary to know the FR vibration [8].

Considering all the nonlinearities and complex phenomena such as a fluid-structure interaction of FA components with the coolant or contacts, it is impossible to create a detail and complex model of the whole assembly or even the whole reactor. However, there is a possibility to create a model of a single chosen component (FR, GT or CT) and include approximately the influence of the whole FA using the data obtained from higher-scale models such as model of the reactor or simplified linearised model of the FA. The highest-scale model is the model of the reactor [6] that consists of a large number of rigid bodies (pressure vessel, core barrel, reactor core, etc.) and flexible bodies (e.g. each FA is idealized as a 1D lumped-mass continuum) coupled by linearised couplings. Considering pressure pulsations of coolant caused by the main circulation pumps, it is possible to investigate the spatial motion of supporting plates that are FAs fixed in. The motion of the supporting plates is used as kinematical excitation in the model of the chosen FA (middle-scale model) which consists of large number of linearized 1D continua (FRs, GTs, central tube, angle pieces, etc.) and coupled by linear couplings [7]. Using this model, a motion of SG cells is investigated which is used as a kinematical excitation in the detail nonlinear model of the single component (FR, GT or CT) including all the mechanical nonlinearities such as impact forces, prestress effect with possible loose of contact or friction forces in contact points. The single component motion is modelled using FEM for flexible 1D continua. In case of FR, there are two main subsystems (FR cladding and fuel pellets stack) that can possibly impact interact. At the level of all the eight spacer grids, there are three SG cells that are radially prestressed and the possible loose of contact of the FR cladding with any cell at the end of the reactor operational-cycle is respected. The kinematical excitation is present in the lower node as well where the FR is fixed into the lower piece of the FA. Contact forces include both normal and friction components. In case of the GT, the model consists of one flexible body (a tube), SG cells and the sleeve which are kinematically excited together with the lower and upper pieces of the FA. In the model of GT discussed in the presented paper, the CR drop is not considered although there is a methodology for considering it with rigid GT and flexible CT [1, 3] and it could be possibly extended in this way.

The developed methodology enables to create a mathematical model of the main components of the nuclear FA and to simulate its vibration caused by pressure pulsation of coolant. Model includes all the relevant mechanical nonlinearities such as impact and friction forces in the contact points and prestress effects with possible loose of contact. There is a wide class of problems to be solved using this simulation including simulations of fretting wear of the FR cladding in the contact points with the spacer grids and estimation of maximal lateral deformations of the GT which is important for the CR drop. These models shows one of the possible ways how to simulate such a complex systems using a multi-scale modelling. However, there is a disadvantage of not included backward influence of the models of higher scale by the results from the lower scale.

### Acknowledgments

This publication was supported by the project LO1506 of the Czech Ministry of Education, Youth and Sports.

### References

- [1] R. Bulín, M. Hajžman, P. Polach. Nonlinear dynamic analysis of a single control rod in nuclear reactors. L. Pešek, editor, *National Colloquium with International Participation Dynamics of Machines 2014*, 2014.
- [2] Š. Dyk, V. Zeman. Impact vibrations of guide thimbles in nuclear fuel assembly, *Archive of Applied Mechanics*, 87(2): 231–244, 2017.
- [3] M. Hajžman, P. Polach. Two Approaches to The Modelling of The Control Rods in Nuclear Reactors. *The Fourth Asian Conference on Multibody Dynamics ACMD2008*, Jeju, Republic of Korea, 2008.
- [4] H.-K. Kim, S.J. Kim, K.H. Yoon, H.-S. Kang, K.-N. Song. Fretting wear of laterally supported tube. *Wear*, 250(1-12): 535-534, 2001.
- [5] P. Polach and M. Hajžman. Approaches to the Creation of Multibody Models of the VVER 1000 Nuclear Reactor Control Assembly. In M. Papadrakakis, V. Papadopoulos, G. Stefanou, V. Plevris, editors, *VII European Congress on Computational Methods in Applied Sciences and Engineering*, 2016.
- [6] V. Zeman, Z. Hlaváč. Dynamic response of VVER 1000 type reactor excited by pressure pulsations. *Engineering MECHANICS* 15(6): 435–446, 2008.
- [7] V. Zeman, Z. Hlaváč. Dynamic response of nuclear fuel assembly excited by pressure pulsations. *Applied and Computational Mechanics* 6(2): 219-230.
- [8] V. Zeman, Š. Dyk, Z. Hlaváč. Mathematical Modelling of Nonlinear Vibration and Fretting Wear of the Nuclear Fuel Rod. *Archive of Applied Mechanics* 86(4): 207-212, 2016.

# Numerical Prediction and Experimental Validation of a Three-Dimensional Rod-Plate Impact

Jianyao Wang<sup>1</sup>, Zhuyong Liu<sup>1</sup>, Jiazhen Hong<sup>1</sup>

<sup>1</sup>Department of Engineering Mechanics  
Shanghai Jiao Tong University  
800 DongChuan R.D., 200240 Shanghai, P.R.China  
[wjy2011, zhuyongliu, jzhong]@sjtu.edu.cn

## Abstract

The impact problem of flexible multibody system is a non-smooth, high-transient and strong-nonlinear dynamic process with variable boundary. The numerical approaches which are being used widely in contact/impact analysis can be divided into two categories: computational contact mechanics based on finite element methods (FEM) [1] and approaches based on multibody system dynamics (MSD) [2]. FEM is well suited for particularly high accuracy requirements, yet causes very high computational effort; while approaches based on MSD acquire considerably less computational effort yet cannot provide accurate local deformation information.

To bridge the gap between accuracy and efficiency, a sub-region method (SRM) for the description of multibody system with impact is proposed, in which the contact body is divided into two parts called non-impact region and impact region. The non-impact region is modelled using the modal reduction approach to raise the solving efficiency. The impact region is modelled using FEM for high accuracy requirement. With this method, the solving efficiency of the whole system and the computation accuracy in the local impact region are both raised.

For the experimental investigation of impact problems, the main difficulty is that the impact duration is very short and the impact responses have extremely high frequencies, so they are very difficult to measure. Early experimental investigation mainly focused on transient strain response and the measurement instruments were strain gauges [3]. Accelerometers were also used in some impact experiments to measure points located not close to the impacts [4]. With the advancement of laser techniques, some impact experiments were conducted using Laser-Doppler-Vibrometers (LDVs), however, mainly for one-dimensional rod impact or two-dimensional planar impact problems [5].

To validate the presented simulation method, a three-dimensional rod-plate impact is designed and performed. Strain gauges and LDVs are employed to measure the high-frequency impact responses. A schematic diagram of the impact experiment is shown in Figure 1. A cylindrical steel rod with hemispherical tip is used to strike an aluminum plate. The two colliding bodies are suspended by thin lines. The strains are measured with strain gauges which are bonded to the contact surface of the plate in three directions 15mm away from the center point. Two LDVs are used to measure the displacement and velocity of the back point of the rod and the center point of the plate.

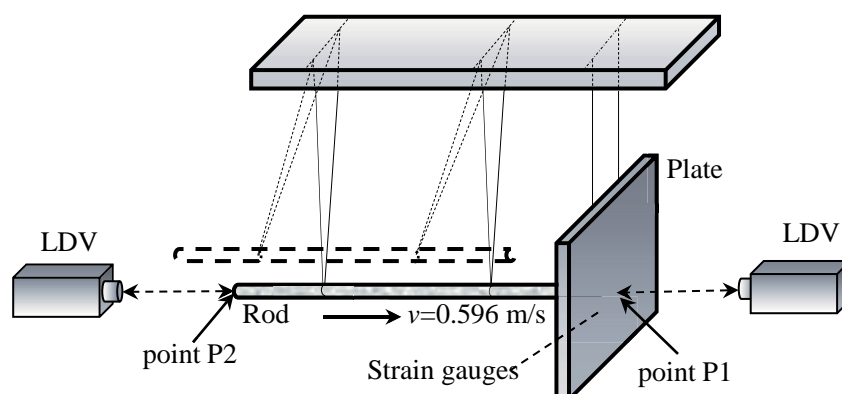


Figure 1. Schematic diagram of the impact experiment

Both FEM and SRM are used to simulate the experimental case. For SRM, a very important problem is how to partition the contact bodies to ensure the accuracy of simulation. That is to say, how many nodes should be used to describe the impact region and how many orders of modes should be applied to describe the non-impact region? The principle for how to partition the contact bodies is proposed. The numerical results agree well with the experimental measurements, as shown in Figure 2. It is shown that SRM is an effective formulation

considering both accuracy and efficiency.

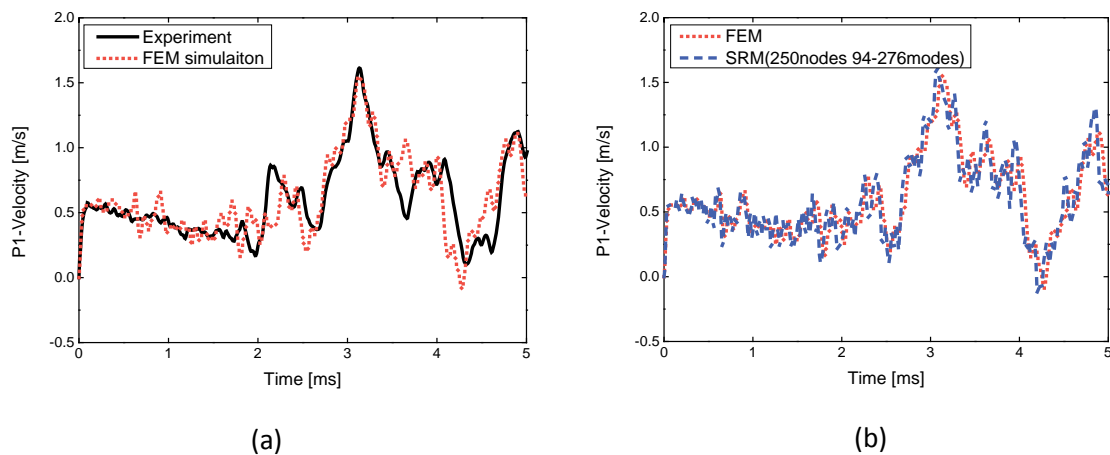


Figure 2. Comparisons of simulation and experimental results

## Acknowledgments

This research work is supported by the National Science Foundation of China (No.11132007, No.11202126), for which authors are grateful.

## References

- [1] T. A. Laursen. *Computational Contact and Impact Mechanics*. Springer, Berlin Heidelberg, 2003.
- [2] M. Machado, P. Moreira, P. Flores, H. M. Lankarani. Compliant contact force models in multibody dynamics: Evolution of the Hertz contact theory. *Mechanism and Machine Theory*, 53:99-121, 2012.
- [3] M. M. Al-Mousawi. On Experimental Studies of Longitudinal and Flexural Wave Propagations: An Annotated Bibliography. *Applied Mechanics Reviews*, 39: 853-865, 1986.
- [4] I. Khemili, L. Romdhane. Dynamic analysis of a flexible slider–crank mechanism with clearance. *European Journal of Mechanics-A/Solids*, 27:882-898, 2008.
- [5] R. Seifried, W. Schiehlen, P. Eberhard. The role of the coefficient of restitution on impact problems in multi-body dynamics. *Proceedings of the Institution of Mechanical Engineers, Part K: Journal of Multi-body Dynamics*, 224: 279-306, 2010.

# Experimental Investigation of Contact-impact In Multi-body System Using DIC Technique

Peng Chen<sup>1</sup>, Jinyang Liu<sup>2</sup>, Xiaowei Deng<sup>3</sup>

<sup>1</sup>Department of Engineering Mechanics  
Shanghai Jiao Tong University  
No. 800, Dongchuan Road, 200240  
Shanghai, China  
cpsjtu@sjtu.edu.cn

<sup>2</sup> Department of Engineering Mechanics  
Shanghai Jiao Tong University  
No. 800, Dongchuan Road, 200240  
Shanghai, China  
liujy@sjtu.edu.cn

<sup>3</sup>Department of Engineering Mechanics  
Shanghai Jiao Tong University  
No. 800, Dongchuan Road, 200240  
Shanghai, China  
dxw913@sjtu.edu.cn

## Abstract

In the investigation of contact-impact problems, the experimental validations are very important. Seifried et al [1] designed impact experiments between bodies with different geometrical shapes to validate their theoretical models. Hu compared the analytical and experimental results of an impact example between a steel sphere and an aluminum rod [2]. Their investigations proved that the wave propagation can be observed with Laser Doppler Vibrometers and the strain history of certain points can be measured by strain gauges precisely. With the innovation of technology, the resolution ratio and the shooting speed of digital cameras have been improved greatly. Within milliseconds, hundreds and even thousands of images with sufficient resolution ratio can be captured [3, 4]. DIC is a non-contact optical measure technique which acquires the images of an object and performs image analysis to obtain displacements and strains. Different from the strain gauges which can only measure the strains of the special points, DIC can measure the full-field distribution of strains.

In this investigation, a dynamic formulation based on the penalty method and component mode synthesis method is presented for solving the normal contact-impact problems in multibody system. The contact bodies are divided into contact zones and un-contact zones. The degrees of freedom of the un-contact zones can be reduced by modal reduction. In the process of finite element discretization, sufficient elements in the contact zones are needed to satisfy the accuracy demand. However, the excessive refinement may lead to the waste of elements and extremely small time step. Based on the sub-region mesh method, the allowed maximum element sizes within the contact area, the local contact region and the wave propagation region are presented for the contact-impact of flexible bodies according to the description of the contact surface, stress distribution of the local contact area and the propagation of the high-frequency elastic wave, respectively.

In order to verify the numerical results, experiment of contact-impact in multi-body system is carried out using DIC technique. The experimental setup is demonstrated in figures 1 and 2. A steel rod is put within an ejection device and a PVC plate is put on a supporting platform. In order to reduce the influence of boundary constraints, the plate is supported by three tip screws with same height. Upward the plate, a high speed camera of type Photron FASTCAM SA-X2-1000k-M2 is set up perpendicularly to the plate surface. Under the plate, three strain gauges are glued on the bottom surface of the plate, which are located 15mm, 30mm, and 45mm from the contact point. Besides, a Laser Doppler Vibrometer of type Polytec OFV-3000 is used to capture the velocity of the rod.

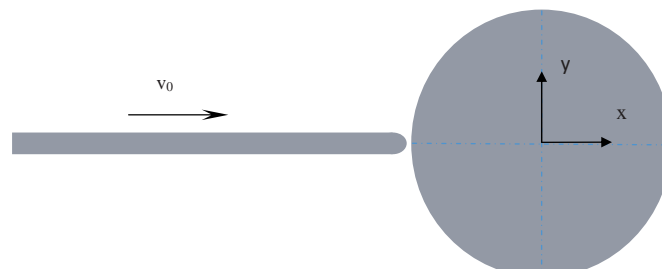


Figure 1. Geometry of the impact system

The rod is ejected by the ejection device and impacts the plate right in the middle. The initial impact velocity of the rod is measured by the Laser Doppler Vibrometer. Firstly, the strain gauge and the DIC technique are both used to validate the normal strain of the special points. The normal strain of a special point of the plate (15 mm from the impact point) is shown in figure 3. It can be seen that the normal strain in the impact direction obtained by simulation coincides with the experiment results. In addition, DIC technique is used to measure the full normal strain field of the plate, which was commonly used in the stationary experiments. Figure 4 shows the

strain field of the plate in the impact direction at 0.32ms after impact. It is indicated that the strain distribution obtained by simulation with sufficiently small meshes in the local contact region is approximately consistent with the result obtained by DIC measurement.



**Figure 2.** Experimental setup of the system

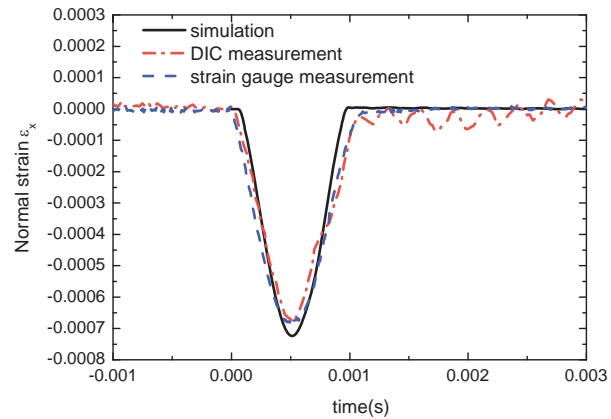


**Figure 3.** Normal strain in contact direction

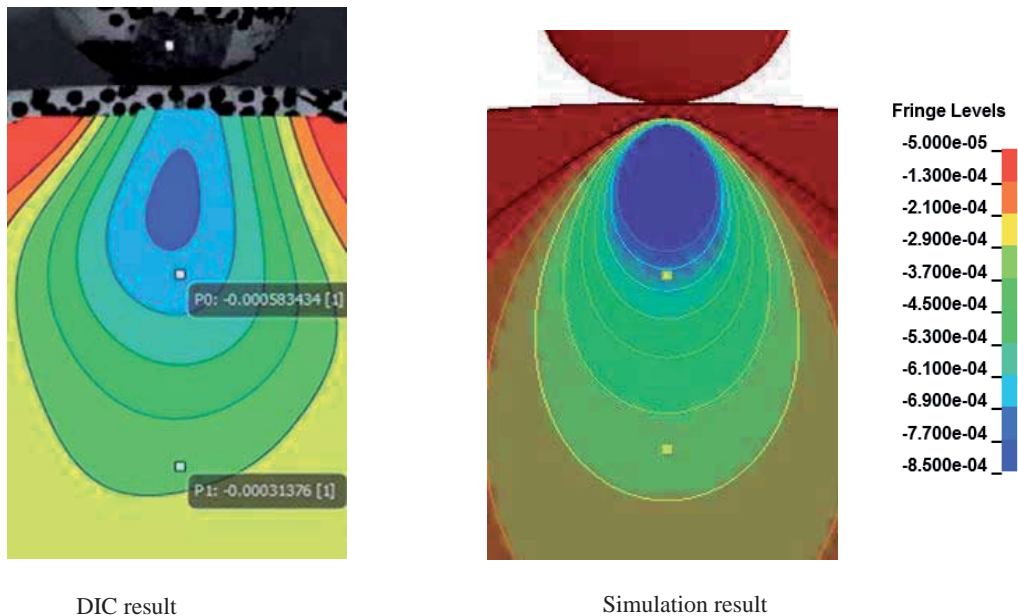


**Figure 4.** Strain field in the impact direction at 0.32ms after impact

## Acknowledgments

This research was supported by the National Natural Science Foundation of China (No. 11272203, No. 11132007) for which the authors are grateful.

## References

- [1] W. Schiehlen, R. Seifried. Three approaches for elastodynamic contact in multibody systems. *Multibody System Dynamics*, 12: 1-16, 2004.
- [2] B. Hu, W. Schiehlen, P. Eberhard. Comparison of analytical and experimental results for longitudinal impacts on elastic rods. *Journal of Vibration and Control*, 9(1-2): 157-174, 2003.
- [3] M. A. Sutton, J. H. Yan, V. Tiwari et al. The effect of out-of-plane motion on 2D and 3D digital image correlation measurements. *Optics and Lasers in Engineering*, 46(10): 746-757, 2008.
- [4] H. Wang, H. Xie, L. Wu et al. Study on the effect of DIC deformation sensor on mechanical property of substrate. *Measurement*, 49: 283-288, 2014.

## Contact and Constraints in Analytical Dynamics.

Souchet René, *rp.souchet@orange.fr*  
Buxerolles, France

### Abstract

Recently Udawadia et al. [1] have proposed to obtain dynamical equations using Lagrange method with generalised parameters as quaternions  $q$ . In 2014 a different point of view was applied by the actual author: since rigidity is not (a priori) included, the main aim is the necessary use of stress tensor in the Virtual Work Principle (VWP), then its elimination is required for rigid bodies. Here we propose to show the applicability of our method to friction leading to an inequality problem.

### Background.

We suppose that body forces  $f$  are not present. Then the VWP is written for a body  $B$

$$-\int_B \rho a \cdot v dx + \int_{\Gamma} \varphi \cdot v da - \int_B \sigma : grad v dx = 0$$

where  $\rho$  is the density,  $a$  the acceleration,  $\varphi$  the surface forces,  $\sigma$  the stress tensor, and  $v$  the virtual piecewise displacements. In the application of some rotational motion,  $x=R(q(t))X$ ,  $x$  being the actual position of the particle  $X$ , the virtual displacements are  $v=(R'_i R^j x)w_i$  where the  $w_i$ 's are arbitrary and  $R$  is a 3x3 matrix function of quaternions.  $R'_i$  is the partial derivative of  $R(q_1, \dots, q_n)$ .  $R$  is not necessarily a rotation, i.e. the constraint  $q^T q = I$  is not fulfilled as an a priori condition.

If we take account of the actual virtual displacements in the above formula, the first term is the virtual work (denoted  $L_i w_i$ ) of acceleration. Then we have

$$grad v = (R'_i R^j)w_i = S_i w_i + A_i w_i, \quad \sigma : grad v = (\sigma : S_i)w_i$$

where  $S_i$  and  $A_i$  are resp. the symmetrical and anti-symmetrical parts of the matrix  $R'_i R^j$ . But for a rigid body we must eliminate the stress tensor, requiring the relations  $S_i w_i = 0$  (sum on  $i$ ), a priori realised if  $R$  is a rotation. In addition, it is seen that surface forces  $\varphi$  occur by global quantities  $R(f)$  and  $M(f)$  only. So the following compatibility conditions result: whatever the  $w_i$ 's such that  $S_i w_i = 0$ , we have

$$[-L_i + M(f) a_i] w_i = 0 \quad (\text{sum on } i)$$

( $a_i$ : dual vector of matrix  $A_i$ ) under the only above hypotheses.

Finally we write the rigidity constraint  $q^T q = I$  when quaternions are used. In the following part we give an example of the actual method.

### Example: Contact with friction.

We consider an homogeneous rigid wheel (centre  $O$ , radius  $r$  and mass  $m$ ) rolling in a vertical plane  $O_0 x_0 y_0$  on an inclined line (or surface)  $O_0 X_0$  under the gravitational acceleration  $g$  downwards, the gravitational force being ( $f = -mg y_0$ ) applied on the centre  $O$  of the wheel. We use the referential  $Ref = O_0 X_0 Y_0 Z_0$  with the angle between  $O_0 x_0$  and  $O_0 X_0$  noted  $\alpha$ . Two-dimensional Euler parameters ( $p, q$ ) are introduced to specify the rotation of the wheel, so

$$R_{11} = R_{22} = 1 - 2q^2, \quad R_{12} = -R_{21} = -2pq, \quad R^{-1} = R^T / \Delta, \quad \Delta = 1 + 4q^2(p^2 + q^2) - 1$$

Now we define the virtual coefficients ( $w_x, w_y, w_p, w_q$ ) associate to the parameters ( $x, y, p, q$ ) and the condition  $w_i S_i = 0$ , i.e.  $p w_p + q w_q = 0$ . Under the above condition, the VWP is writing

$$-\int_B \rho a \cdot v dx - mgy_0 \cdot v(O) + Tv_1(A) + Nv_2(A) = 0$$

where  $(T, N, 0)$  are the components of the two-dimensional contact force on the wheel applied at the contact point A. Now we must use the contact law of friction, by example in the hypothesis of a bilateral contact ( $y=r$ ) at the point  $A=(x, y-r, 0)$  of the wheel, implying the geometric constraint  $y=r$ , together with the Coulomb law of friction equivalent to the inequality of Duvaut and Lions [3]

$$T[v_1(A) - u_1(A)] + k|N| \left| |v_1(A)| - |u_1(A)| \right| \geq 0$$

First the parameters are specified such that  $w_x = w_p = w_q = 0$ , satisfying  $w_i S_i = 0$ . It results  $v(x) = (0, w_y, 0)$  so that by taking account of the bilateral contact  $y=r$

$$mg \cos \alpha - N = 0 \text{ and } \dot{K} + mg \sin \alpha \dot{x} + k|N| |u_1(A)| = 0$$

$$\int_B \rho a \cdot v dx + mgy_0 v(O) - Nv_2(A) + k|N| |v_1(A)| \geq 0 \text{ where } N = mg \cos \alpha$$

that is available whatever the parameters  $(w_x, w_p, w_q)$ . After some straightforward calculus, the acceleration term is obtained under the form

$$\int_B \rho a \cdot v dx = m\ddot{x}w_x + a_{11}\ddot{p} + a_{22}\ddot{q} + 2a_{12}\dot{p}\dot{q} + 2b\dot{q}^2$$

$$a_{11} = 2mr^2(q^2 w_p + pqw_q), \quad a_{22} = 2mr^2(pq + p^2 + 4q^2)w_q, \quad a_{12} = 2mr^2(qw_p + pw_q), \quad b = 4mr^2qw_q$$

Taking account of this expression, the differential variational inequality follows

$$(m\ddot{x} + mg \sin \alpha)w_x + kmg \cos \alpha |w_x + r(\alpha_p w_p + \alpha_q w_q)| + 2mr^2(Aw_p + Bw_q) \geq 0$$

(where  $\alpha_p, \alpha_q$  and  $A, B$  are given functions) under the compatibility condition  $pw_p + qw_q = 0$ . That is the basic relation to solve the problem completed naturally by initial conditions on velocities (and positions) [4].

## Conclusion.

The present work has presented a natural link existing between Analytical Dynamics and Continuum Mechanics. The key of our scheme was the use of the Virtual Work Principal leading to Cauchy stresses. Then the elimination of Cauchy stresses introduces compatibility relations between virtual coefficients when rigidity conditions are not fulfilled. Finally the actual method is easily extended to multibody dynamics.

## References.

- [1] Schutte, A., Udewadia, F., (2011) "New Approach to the Modelling of Complex Multibody Dynamical Systems", J. Appl. Mech., Vol.78, 021018-1,11.
- [2] Souchet R., (2004) Leçons sur les Grandes Déformations, Cépadues Editions, Toulouse, France.
- [3] Duvaut G., Lions J.L., (1972) Les inéquations en Mécanique et en Physique, Dunod, Paris, (chapitre 3)
- [4] Souchet R., (2014) "Continuum Mechanics and Lagrange equations with generalized coordinates", *Int. J. Engng Sc.*, 76C, pp.27-33.

# A 3D Volumetric Foot-Ground Model for Forward Dynamics

Peter Brown, John McPhee

Systems Design Engineering  
 University of Waterloo  
 200 University Ave W, Waterloo, ON, Canada N2L 3G1  
 [pm2brown, mcphee]@uwaterloo.ca

## Abstract

In forward dynamics human models, particularly when modelling gait, the foot-ground contact plays an important role on the system dynamics and is challenging to model. The plantar surface is a large, compliant, and conforming surface, so an accurate and computationally efficient model is hard to find. Efficient and commonly used point contact models may not be accurate unless the surface is finely discretised [1], and more accurate finite element models are too computationally expensive for use in optimisations or real-time simulations.

Volumetric contact has been proposed as a computationally efficient modelling method for conforming surfaces [2]. Based on elastic foundation theory, volumetric contact treats the contact surfaces as a continuous collection of springs. Contact forces can be described as functions of the geometry of the two surfaces—particularly the volume of penetration of the two surfaces. Thus, analytical equations of the contact forces can be derived for simple geometry.

Volumetric contact has previously been used for foot-ground contact, but was limited to 2D motion and the contact surface was approximated as spheres [3]. To expand this work, equations describing the reaction forces of an ellipsoid contacting a plane were derived based on the volumetric contact model. The volumetric contact model analytically describes the normal contact force (with damping), centre of pressure location, and rolling resistance.

A foot model was made of three of these ellipsoid-plane contacts to represent a bare foot in contact with the ground (one at the heel, one at the ball of the foot, and one at the toe). The foot is modelled as two separate segments (the foot and the toe) joined by a revolute joint (representing the toe joint). This resulted in a foot model with 29 contact parameters (27 parameters to describe the geometry, a stiffness parameter, and a damping parameter).

The model was parametrised by optimising to match experimental gait reaction forces. The foot model was driven to match the experimentally measured motion, and optimal parameters were determined by minimising differences in normal reaction force, centre of pressure (COP) position, and pressure distribution across the surface. The optimiser was allowed to adjust the foot motion by small amounts (2mm translation or 0.05 rad rotation) to account for measurement errors in the experiment. The optimised model was able to reproduce the normal force and centre of pressure position with less than 4% RMS (root-mean-square) error, as shown in Figure 1. The simulated and experimental pressure profiles are shown in Figure 2.

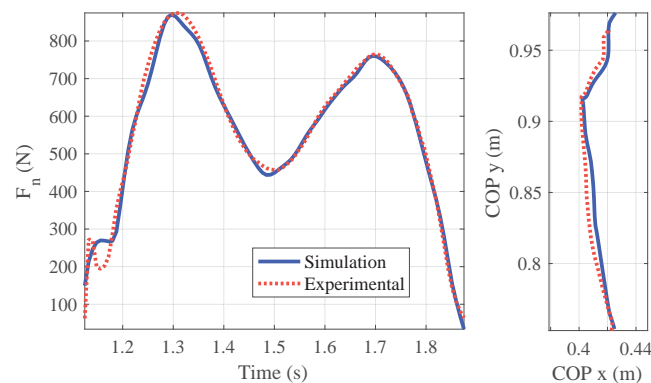


Figure 1: Simulated and experimental normal force (left) and centre of pressure location (right)

For verification, the foot model with the same parameters was used to recreate experimental gait at several cadences. The RMS errors for these additional experiments are shown in Table 1.

As would be expected, the calibration trial had the lowest RMS errors, followed by gait trials at the same cadence. The higher cadence trials had the largest RMS values, though none of the trials had very different RMS errors from the calibration trial. The largest difference is between the calibration trial and the high cadence trial COP error, which was doubled. The pressure had the largest errors by almost an order of magnitude. Part of this error is due to inaccuracies in representing the shape of the plantar surface with simplified shapes (see the pressure profiles in Figure 2), and errors in the pressure measurements (the pressure mat was noted to have a low response time).

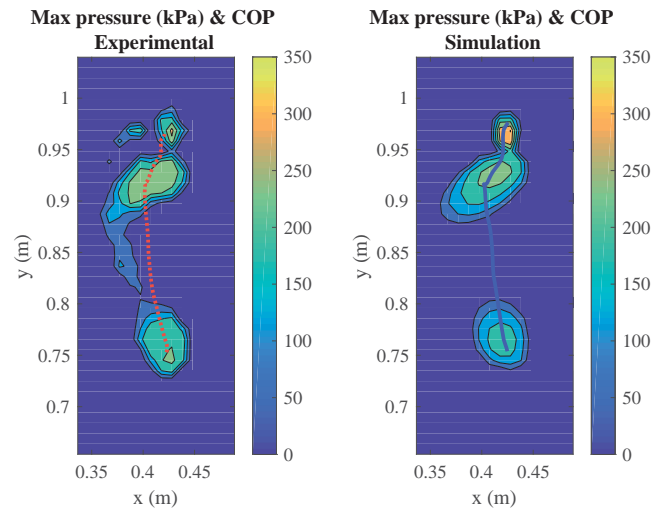


Figure 2: Simulated and experimental surface pressure (maximum pressure over contact shown)

Table 1: RMS error for foot-ground contact model

Cadence (strides/minute) (number of trials)	Normal force	COP	Pressure
Calibration: 92 (1)	3.4%	3.2%	33.9%
92 (3 <sup>a</sup> )	4.2%	4.2%	38.1%
112 (5)	4.9%	6.6%	44.1%
72 (4 <sup>a</sup> )	4.4%	5.0%	40.0%

<sup>a</sup> Some trials ignored due to unusual values or processing errors

The foot model ran over 100 times faster than real-time in an inverse simulation (although the simulation took longer when the pressure distribution was calculated for use in the optimisation). The parameter optimisation minimising error in normal force, COP position, and pressure took, on average, 164 seconds.

The developed foot-ground contact model was able to match experimental normal force and COP position within 5% for trials at the same or lower gait cadence. The COP position had higher levels of error for a higher gait cadence (6.6%). This is of similar accuracy to a recent model using a large number of point contacts [1] (the model presented here has better COP position accuracy, but poorer normal force accuracy). The volumetric contact model requires a smaller number of parameters than models with a large number of point contacts (since each contact point may use a different stiffness and damping). Ignoring the friction parameters, the model by Jackson et al. [1] had 77 parameters, compared with the 29 parameters of this model.

### Acknowledgments

This research was funded by NSERC and the Canada Research Chairs program.

Special thanks to Dr. Stacey Acker and David Kingston for the use of their lab space and assistance running the gait experiments.

### References

- [1] J. N. Jackson, C. J. Hass, and B. J. Fregly, "Development of a Subject-Specific Foot-Ground Contact Model for Walking," *ASME J. Biomech. Eng.*, vol. 138, no. 9, 091002:1–12, 2016.
- [2] Y. Gonthier, J. McPhee, C. Lange, and J.-C. Piedbœuf, "A Contact Modeling Method Based on Volumetric Properties," in *ASME IDETC*, 2005, pp. 477–486.
- [3] M. Sharif Shourijeh and J. McPhee, "Forward Dynamic Optimization of Human Gait Simulations: A Global Parameterization Approach," *ASME J. Comput. Nonlin. Dyn.*, vol. 9, no. 3, 031018:1–11, 2014.

## Gear Contact Model: Simulations and Measurement

Zdeněk Neusser<sup>1</sup>, Tomáš Vampola<sup>1</sup>, Michael Valášek<sup>1</sup>, Matěj Sulitka<sup>1</sup>

<sup>1</sup>Faculty of Mechanical Engineering  
Czech Technical University in Prague  
Technická 4, 166 07 Prague, Czech Republic  
[Zdenek.Neusser, Tomas.Vampola, Michael.Valasek, Matej.Sulitka]@fs.cvut.cz

### Abstract

Gearboxes are widely used in the engineering applications and mechanical engineers need to know their properties. Specific parameters are needed to be used for multibody modeling of gearboxes. Such parameters are mainly mass, moment of inertia, stiffness and damping. Properties of shafts and wheels could be obtained from the analytical formulas or from finite element models. Simulations verified by measurements in [1] and [2] prove this. The only part of gear mesh process, which is not covered in details, is teeth contact area, see Figure 1.



Figure 1. Teeth contact area.

Teeth contact area has its static stiffness, which varies with the gear rotation – the teeth are approaching into the contact, leaving the contact and teeth surfaces move during the contact between each other. This also causes energy dissipation, gear rattling, hammering and gear whine. Such effects must be covered in the gear mesh dynamics in combination with stiffness calculation. The analytical and FEM (Finite Element Method) based approaches are developed.

At first is presented analytical approach. Analytical formula [3] combines calculation of teeth contact stiffness (based on Hertz theory) with tooth flexibility (derived in [4]) and gear wheel deformations in the tooth root (see [5]). Combining the stiffness calculation of all teeth in the contact and used in dynamic simulation the gear mesh behavior is predicted, see [6]. Stiffness evaluation is decomposed into tooth flexibility (bending), gear wheel deformations (tilting) and teeth deformation due to the contact itself. The decomposition is shown in the Figure 2.

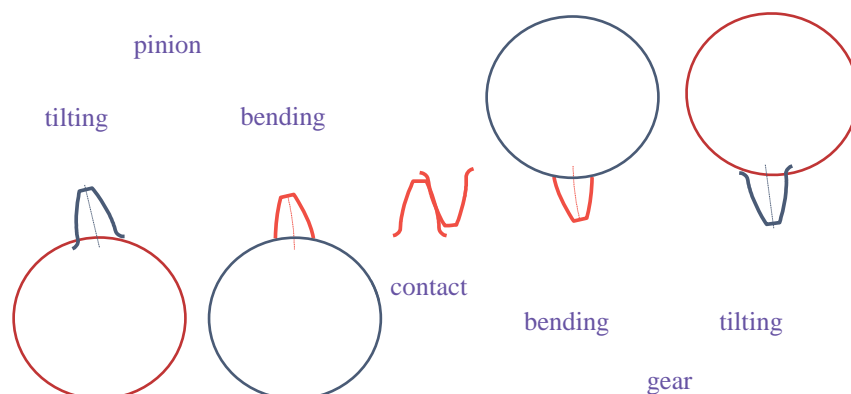
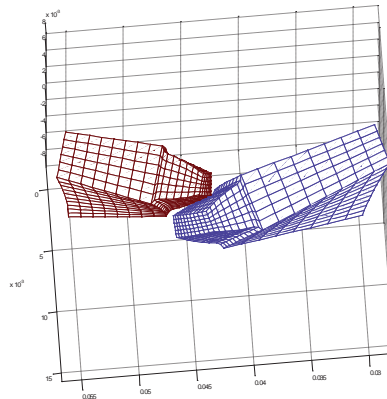


Figure 2. Teeth contact calculation using analytical model.

There is developed FEM (Finite Element Method) based approach for static stiffness evaluation. The gear with teeth is meshed with structural mesh and appropriate constraint is applied. Nodes placed on teeth contact flanks are found and using static reduction the stiffness matrix is obtained. The resulting flank deformation and corresponding contact force are used in the gearbox dynamic simulation. Two teeth in contact are shown in the Figure 3.



**Figure 3.** Teeth contact evaluation using FEM model.

Developed methods for gear meshing behavior needs to be validated by measurement. There is proposed method, how to measure gear contact area excluding gear wheel and shafts flexibility. The test bed is shown in the Figure 4. Gear contact area is measured by angular sensors measuring the gear wheel rotation under the root circle.

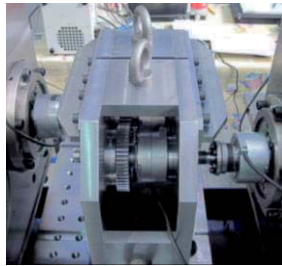


**Figure 4.** Test bed with gearbox and sensors.

Gearbox model is needed in many parts of mechanical engineering industry and effectivity together with quality demand leads to development of computationally efficient approach covering all gear meshing aspects. The experimental verification must be appropriately proposed and performed.

## Acknowledgments

This research has been realized using the support of The Ministry of Education, Youth and Sports program NPU I (LO), project # LO1311 Development of Vehicle Centre of Sustainable Mobility. This support is gratefully acknowledged.

## References

- [1] M. Sulitka, J. Veselý, Z. Neusser. Coupled model of the machine tool motion axis with a multi-stage tooth gear system. *MM Science Journal*, Prague, 2012.
- [2] M. Sulitka, J. Veselý, Z. Neusser. Analysis of dynamic properties of a multi-stage gear system using the flexible multi-body system modelling technique. *Proceedings of the 37th International MATADOR Conference*, Manchester, 2012.
- [3] D. Petersen. *Auswirkung der Lastverteilung auf die Zahnfußtragfähigkeit von hochüberdeckenden Strinradpaarungen*. Technische Universität Braunschweig, 1989.
- [4] C. Weber, K. Banaschek. Formänderung und Profilrücknahme bei Gerad- und Schrägverzahnten Rädern. *Schriftenreihe Antriebstechnik*, Braunschweig, Friedr. Vieweg & Sohn, 1953.
- [5] P. Sainsot, P. Velez, O. Duverger. Contribution of Gear Body to Tooth Deflections - A New Bidimensional Analytical Formula. *Journal of Mechanical Design*, 126:748-752, 2004.
- [6] Z. Neusser, M. Sopouch, T. Schaffner, H.-H. Pribsch. Multi-body Dynamics Based Gear Mesh Models for Prediction of Gear Dynamics and Transmission Error. *SAE Technical Paper 2010-01-0897*, 2010.

# Multibody Modelling of Friction Based Interaction Between Turbine Blades

Olivier Verlinden<sup>1</sup>, Michal Hajžman<sup>2</sup>, Hoai Nam Huynh<sup>1</sup>, Miroslav Byrtus<sup>2</sup>

<sup>1</sup> Department of Theoretical Mechanics, Dynamics and Vibration  
University of Mons  
31, Bd Dolez, B-7000 Mons, Belgium  
Olivier.Verlinden@umons.ac.be, Hoainam.Huynh@umons.ac.be

<sup>2</sup> Faculty of Applied Sciences  
University of West Bohemia  
Univerzitni 22, 306 14 Plzen, Czech Republic  
mhajzman@kme.zcu.cz, mbyrtus@rice.zcu.cz

## Abstract

Turbine blades are subjected to severe vibration environments. Especially, nozzle excitation frequencies can correspond to eigen frequencies during acceleration and deceleration phases so that it is necessary to introduce some form of damping. Friction based solutions [1] are nonlinear and offer the interesting property to operate only when the level of vibrations reaches some threshold. But they can be difficult to tune and the availability of a model proves helpful for the designer.

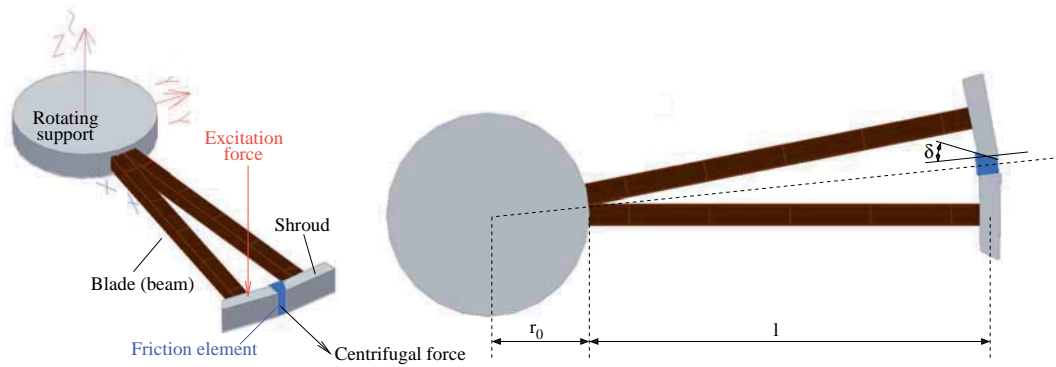


Figure 1: Model and geometry of the experimental system with 2 blades

The system which is analysed in this paper is the experimental prototype studied in [2], whose model is illustrated in Figure 1. It consists of 2 blades, which interact with each other through a so-called friction element (FE), in contact with the shrouds placed at the tip of the blades. During the experimental procedure, one of the blades is excited out-of-plane by an electromagnet and the displacements of the blade tips and friction element are measured. An in-house model of the device has been specifically developed under Matlab [3, 2].

In this paper, we present a multibody model directly inspired from the latter. To properly implement the nonlinear effects of friction, the equations of motion are solved in the time domain, as in [2]. The harmonic balance method was used in [3], friction being replaced by viscous damping so as to dissipate the same amount of energy. The blades are modelled as flexible bodies comprising 4 Euler-Bernoulli beam elements while the shrouds and the friction element are modelled as rigid bodies. All motions are defined with respect to a rotating basis so that the centrifugal and Coriolis effects are naturally taken into account in the equations of motion.

In [3, 2], the normal component of the contact force between the surfaces is introduced through translational and rotational stiffnesses and dampings between the surfaces. In the present model, the contact is introduced by defining, for each surface, 4 points of the friction element interacting with a plane attached to the shroud. At each point, the normal contact force  $F_n$  is calculated from the penetration  $\delta$  of the contact point in the plane according to the well-known Hunt and Crossley law

$$F_n = K\delta^{p_k} + C\delta^{p_d}\dot{\delta} \text{ if } \delta > 0 \text{ and } F_n = 0 \text{ otherwise.} \quad (1)$$

while the tangential force  $\vec{F}_t$  can be computed from the sliding velocity vector  $\vec{v}_s$  according to

- a regularized Coulomb friction model:  $\vec{F}_t = -\mu_d F_n \frac{\vec{v}_s}{v_s^*}$
- a regularized GKF (General Kinetic Friction) model

$$\vec{F}_t = -(\mu_d + (\mu_s - \mu_d) \exp(-(\|\vec{v}_s\|/V_{str})^\gamma)) F_n \frac{\vec{v}_s}{v_s^*} - f_d \vec{v}_s \quad (2)$$

with  $\mu_s$  and  $\mu_d$  the static and dynamic friction coefficients respectively,  $V_{str}$  the Stribeck velocity,  $\gamma$  an exponent to adjust,  $f_d$  the damping coefficient and  $v^* = \max(\|\vec{v}_s\|, V_{lim})$ ,  $V_{lim}$  being a threshold velocity to avoid numerical pitfalls for small sliding velocities.

The elastic parameters for the contact points are chosen so as to reproduce the hypotheses in [3]:  $p_K=2$  and  $K = \frac{A}{c^{1/p_K}}$  with  $A$  the contact area and  $c$  the compliance. Moreover, the spacing between contact points is chosen so as to get the same torsional stiffness as in [3].

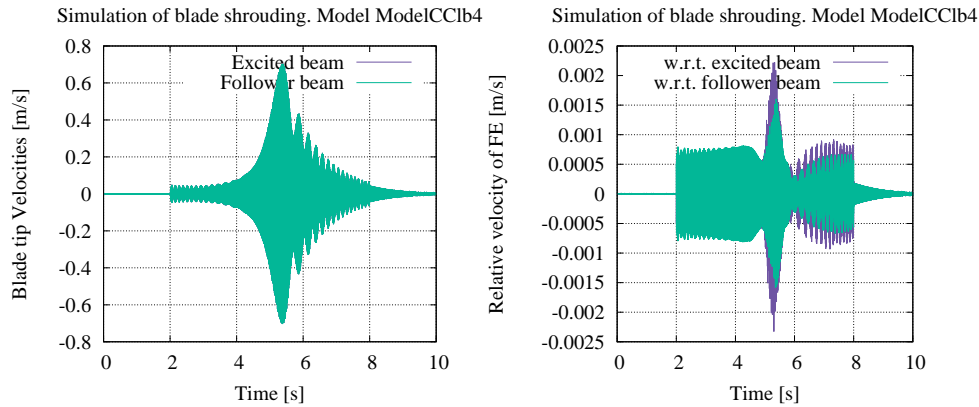


Figure 2: Swept sine response of blades (Coulomb friction and rotating FE)

Table 1: Comparison of some results in terms of the adopted model: max. velocity of follower tip, max. sliding velocity (B=contact with excited beam)

(Values in m/s)	<i>Coulomb model</i>	<i>GKF model</i>
FE free in rotation	$V_{tip,max}=0.704$ $V_{sA}=0.007$ $V_{sB}=0.008$	$V_{tip,max}=0.714$ $V_{sA}=0.002$ $V_{sB}=0.003$
FE locked in rotation	$V_{tip,max}=0.44$ $V_{sA}=0.15$ $V_{sB}=0.42$	$V_{tip,max}=0.60$ $V_{sA}=0.13$ $V_{sB}=0.37$

The purpose of the paper is to compare the models and to investigate the influence of some parameters. As an example, Figure 2 presents the response of the system when it is excited with a logarithmic swept sine from 125 to 145 Hz (between instants  $t=2$  and 8 s), so as to excite the first flexural mode of the beam at about 135 Hz, when the Coulomb model is used and the friction element is free to rotate. The left and right graphs show the time history of the out of plane motion of the blade tips (shroud) and the relative velocity of the friction element with respect to the blade tips. It appears that only microslips occur with this model whatever the friction model. On the contrary, macroslips appear with a simplified model where the rotation of the friction element is not taken into account. This is illustrated in Table 1, which compares some typical maximum velocities for different modelling options. This difference apparently issues from the increase of the normal contact forces during resonance when the rotation is taken into account.

## References

- [1] A. Rizvi, C. W. Smith, R. Rajasekaran and K. E. Evans. Dynamics of dry friction damping in gas turbines: literature survey. *Journal of Vibration and Control*, 22:296-305, 2016.
- [2] L. Pešek, M. Hajžman, L. Půst, V. Zeman, M. Byrtus, J. Brůha. Experimental and numerical investigation of friction element dissipative effects in blade shrouding. *Nonlinear Dynamics*, 79:1711-1726, 2015.
- [3] M. Byrtus, M. Hajžman, V. Zeman. Linearization of friction effects in vibration of two rotating blades. *Applied and Computational Mechanics*, 7:5-22, 2013.

# Dynamics of falling dominoes

Tengfei Shi, Caishan Liu

State Key Laboratory for Turbulence and Complex Systems  
College of Engineering  
Peking University  
Beijing, 100871, China  
liucs@pku.edu.cn

## Abstract

Putting an array of rectangular blocks equally spaced in a straight line on the ground, then toppling the first block to initiate a sequence of collisions, one easily observes a wave propagation. Modeling the dynamics of the domino game has attracted the attention of scientists for a long time. Most of the studies often introduced several simplifying assumptions to develop general theories quantifying the intrinsic velocity existing in the domino wave. Although some of the theoretical results were available in certain limiting cases [1, 2], there still lacks an effective model accurately capturing the details of the domino dynamics.

The domino wave concerns a group of neighboring blocks that interact with each other. These interactions are nonsmooth, and consist of many discrete events such as stick-slip behavior of friction, separation and impacts between blocks, as well as the detachment followed by impacts between the blocks and the ground. Obviously, the domino system is a typical multibody system that consists of complex multiple impacts with friction.

For such complex multibody systems, one may select a convenient way of directly quantifying the interactions between two bodies into some kind of constitutive equation with a relation between the contact force and the small deformation. However, simulations of using this method will encounter various difficulties in determining physical parameters and in numerically integrating the differential equations with small scales of time and size. Recently, a multiple impact model, referred to as LZB, was introduced in [4, 5]. The main idea of this method is that the interface behaviors due to impact are described by a force-energy relationship between the contact force and the elastic potential energy transferred from the kinetic energy of impacting bodies. Energy dissipation at each contact point is quantified by an energetic coefficient, and the coupling effects among simultaneous contact points are reflected by the ratios of potential energy at each contact point. Moreover, numerical integration is performed in the level of impulse to avoid the usage of small variables (impact time and local deformation). The LZB model does encapsulate the main dynamical effects of multiple impacts with Coulomb friction, and has been successfully validated by the detailed comparisons with experimental data for many mechanical systems. [6, 7, 8].

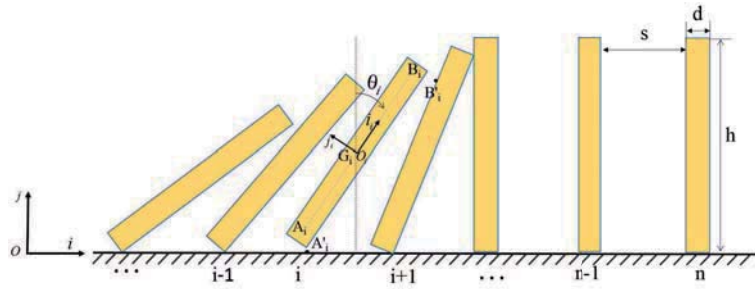


Figure 1: A falling dominoes system on the ground

The objective of this work is to demonstrate that the LZB model can be useful for the study of domino dynamics. This system not only concerns the problem of multiple impacts with friction, but also is related to an edge contact between the block and the ground, which should be carefully treated in modeling impacts. Figure 1 sketches a typical domino system, whose dynamics is generally governed by equations as follows:

$$\mathbf{M}\ddot{\mathbf{q}} = \mathbf{G} + \mathbf{W}(\mathbf{q})\mathbf{F}^n + \mathbf{N}(\mathbf{q})\mathbf{F}^t, \quad (1)$$

where  $\mathbf{M} = \text{diag}(1, 1, I, 1, 1, I, \dots, 1, 1, I) \in \mathbb{R}^{3\kappa \times 3\kappa}$  is generalized mass matrix,  $\mathbf{G} = [0, -1, 0, 0, -1, 0, \dots, 0, -1, 0]^T \in \mathbb{R}^{3\kappa \times 1}$  is generalized gravity,  $\mathbf{W}$  and  $\mathbf{N}$  are Jacobian matrixes of the normal and tangential constraint of the contact set, respectively.

Based on the general equations, together with LZB method handling the impact events, we can simulate the domino dynamics in detail. In order to check the numerical accuracy, we revisit the experiments performed by Stronge in [1]. Fig 2 shows the comparisons between the numerical and experimental results for the propagation

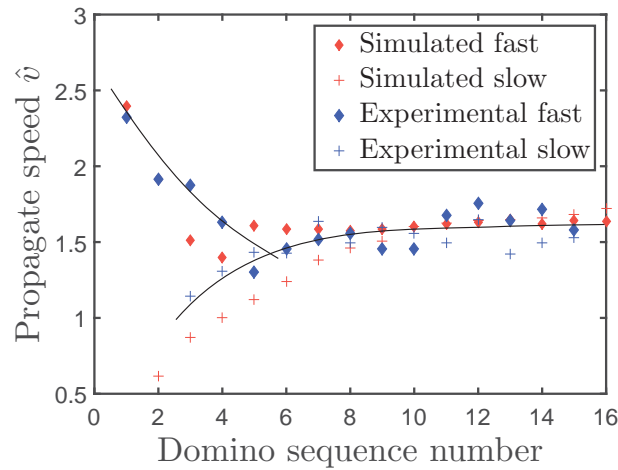


Figure 2: Comparison between numerical and experimental results.

speed, which is defined as  $\hat{v}_i = (s + d)/t_i$ , and  $t_i$  is the time interval between two neighboring events of the domino toppling. Good agreement is achieved between them.

Through comprehensive numerical investigations, we find that the domino wave propagates with an intrinsic constant speed. The origin of the phenomenon comes from the balance between the energy released from gravity and the dissipation by the impact and friction during the cooperative action of a group of falling neighbours. Actually, the value of the intrinsic speed is mainly influenced by the spaced distance and the coefficient of restitution, while it changes little with the coefficient of friction.

In summary, we propose a general model for simulating the domino effects exhibited in a regularly spaced domino array. Though the system has a simple topological configuration, it is indeed extremely complex due to the impact and friction among the interactions of the dominos and ground. We validate our numerical model by comparing with the experimental data reported in existing literature. How the physical parameters affect the intrinsic wave speed is also investigated. This work brings out some hints for deep understanding the fundamental properties of systems with strong nonlinearity: Impact and friction may be taken as internal mechanism for a complex system converging to an equilibrium state.

### Acknowledgments

This work was performed under the support of the National Natural Science Foundation of China (NSFC:11472011).

### References

- [1] Stronge, W.J.: The domino effect: a wave of destabilizing collisions in a periodic array. *Proc. R. Soc. A.* **409**,199-208 (1987)
- [2] Stronge WJ, Shu D.: The domino effect: successive destabilization by cooperative neighbours. *Proc. R. Soc. A.* **418**,155-163 (1988)
- [3] Pfeiffer F., Glocker C., Glocker C., *Multibody Dynamics with Unilateral Contacts*. Wiley, New York. Wiley, 1996.
- [4] Liu, C., Zhao, Z., Bernard, B., Frictionless multiple impacts in multibody systems: Part II. Numerical algorithm and simulation results. *Proc. R. Soc. A* **465**, 123 (2009)
- [5] Zhao, Z., Liu, C., Brogliato, B., Planar dynamics of a rigid body system with frictional impacts. II. Qualitative analysis and numerical simulations. *Proc. R. Soc. A* **465**, 2267-2292 (2009)
- [6] Zhao, Z., Liu, C., Brogliato, B., Energy dissipation and dispersion effects in a granular media. *Phys. Rev. E* **78**(3), 031307 (2008)
- [7] Liu C., Zhang H., Zhao Z., Brogliato B., Impact-contact dynamics in a disc-ball system. *Proc. R. Soc. A.***469**, 20120741 (2013).
- [8] Wang J., Liu C., Ma D.: Experimental study of transport of a dimer on a vertically oscillating plate. *Proc. R. Soc. A.* **470**, 20140439 (2014)

# Multibody Dynamics of a Flexible Legged Robot with Wheeled Feet

Giovanni Gerardo Muscolo, Darwin Caldwell, Ferdinando Cannella

Istituto Italiano di Tecnologia (IIT)  
Advanced Robotics Line  
Via Morego, 30, 16163, Genova, Italy  
[giovanni.muscolo, darwin.caldwell,  
ferdinando.cannella]@iit.it

## Abstract

Humanoid robots are complex multibody machines. Many dynamic balance systems of biped robots are proposed and tested in literature, but the problem of falling down during walking is unsolved. This problem is caused by the complexity of the control of a legged machine. Some major difficulties for the control system are the following [1]: 1) the robot kinematics and dynamics are non-linear and difficult to accurately model. Robot parameters such as center of mass, moment of inertia, etc. are not known exactly; 2) the dynamics of the robot depend on which legs make contact with the ground. In other word, the dynamics change whenever the robot makes a transition between a single support phase and a double support phase or a flight phase, and vice-versa. Moreover, exchange of leg support is accompanied by an impact disturbing the robot's motion; 3) a legged robot is submitted to intermittent holonomic and nonholonomic constraints; 4) the environment is unknown and dynamic. The surface might be elastic, sticky, soft or stiff; 5) vertical contact forces on the surface are unilateral, meaning that they can not pull the robot against the surface; 6) the goal of keeping dynamic balance is difficult to decompose into actuator commands; 7) many degree of freedom have to be controlled real-time. To summarize one can conclude that controlling a bipedal walking robot that is able to negotiate different terrains and walk/run at high speeds is still an unsolved problem. In order to simplify the control of biped locomotion, the most important research institutes and companies with background in legged robots proposed alternative solutions such as the use of wheels on behalf of the legs or used in combination with these. In 2007, the Jet propulsion Laboratory (JPL-NASA) developed the All-Terrain Hex-Limbed Extra-Terrestrial Explorer (ATHLETE) vehicle used for space applications [2]. Its concept is based on 6 DoF (Degrees-of-Freedom) limbs, each with a 1 DoF wheel attached. ATHLETE uses its wheels for efficient driving over stable, gently rolling terrain, but each limb can also be used as a general purpose leg. In 2010, EMIEW 2, a biped service robot with wheels, has been developed by Hitachi [3]. In 2015, a Korean biped robot with wheels won the last edition of the DARPA Robotics Challenge, thanks to the mounted wheels on the robot [4]. Boston Dynamics is known for its advanced legged robots including the world's fastest robot, Cheetah (with 29 mph), Big Dog, and the latest Atlas. Recently, in 2017, the Boston Dynamics published the novel robot with biped wheels [5]. The biped locomotion capabilities shown with this robot confirmed how wheels can solve many of the big problems in biped locomotion in order to have a more robust biped dynamic walking, running, and jumping. In the meanwhile, a small Company named Humanot patented and published a unique and completely innovative biped robot with wheeled feet including the novelty of flexible legs [6], called ROLLO (see Fig.1). The authors in [6] presented the robot and its applications but without including in the paper the multibody model of the robot. The objective of this paper is to show the completely new multibody dynamic model of a biped flexible robot with wheeled feet, a dynamic analysis and a comparison of this model with the real robot proposed in [6]. The following two points underline the novelty of this paper: 1) a novel physical and analytical model of a biped wheeled robot with flexible legs; 2) a biped locomotion composed by a combination of flexible links and wheeled feet. The validation of the model with the real robot allows to give to the scientific community a key reference to design future biped wheeled and flexible robots. ROLLO solves the points from 2 to 7 presented above and it cannot falls because its center of mass is approximately in contact with the ground. It can be moved in a plane with the two motors on the feet and a human-like motion can be reproduced moving the two feet in opposite and alternate way. ROLLO can be moved in a rectilinear or curvilinear way and they are both possible only thanks to the flexible structure of the robot. The critical points of the multibody analysis presented in this paper can be synthetized in: 1) Tire friction on each foot during rotation around Z axis and alternate and opposite forward motion of the two feet in Y direction (see Fig. 1); 2) Number and length of flexible and rigid modules in each leg in order to reproduce a human-like motion. The experimental tests performed in [6] underlined how the two critical points presented above have influences on the dynamic balance of the robot. In particular, ROLLO is able to turn left or turn right with different speeds thanks to a correct combination of: 1) speed and acceleration of each foot; 2) number and length of flexible and rigid modules in each leg; 3) dimensions of wheels; 4) friction between the wheels and the ground; 5) weight of feet. A typical helical spring, as shown in Figures 1c and 1d, is a spiral wire or rod with mean diameter of coil  $D=2R$ , wire diameter  $d$ , number of active coils  $i$ , helical degree  $\alpha$ , uniform pitch of the helix  $p= \pi*D*\tan \alpha$ , free length  $H=i*p$ , length of the wire or rod  $L= \pi*D*i$ . The unconventional use of the spring (as shown in Fig. 1) allows the unique motion of the ROLLO robot. Figure 2a shows some output signals (only z axis, see Fig. 1) of the

accelerometers mounted on the leg of the ROLLO robot during a motion with an intermediate velocity value (0.2 m/s); Figure 2b shows pitch and roll angles for the ankle and hip passive joints during a rotation of 360 degrees clockwise. The used formulation in the model will be presented on the paper (if accepted) because more space is necessary to explain all used variables. The paper will be structured as follows: section I will present a detailed introduction on biped wheeled and flexible robots; section II will show the proposed physical and analytical modeling of the biped wheeled and flexible robot; section III will show the simulation of the model; section IV will present results and discussions including a comparison between simulations and real tests. The paper will end with conclusion and future works.

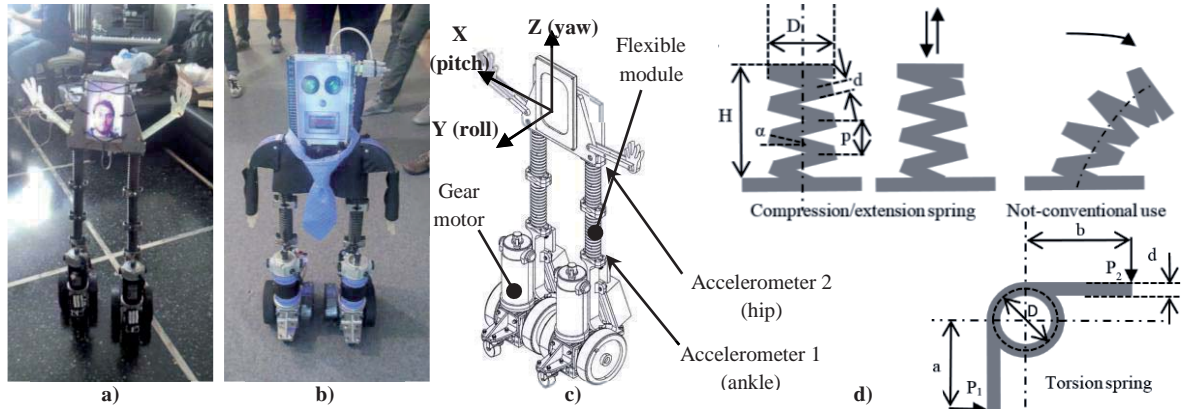


**Figure 1.** ROLLO biped avatar robot with wheeled feet and three (a) or two (b) flexible modules in each leg, its sketch (c), and behavior of the flexible module (d) (courtesy of Humanot company) [6].

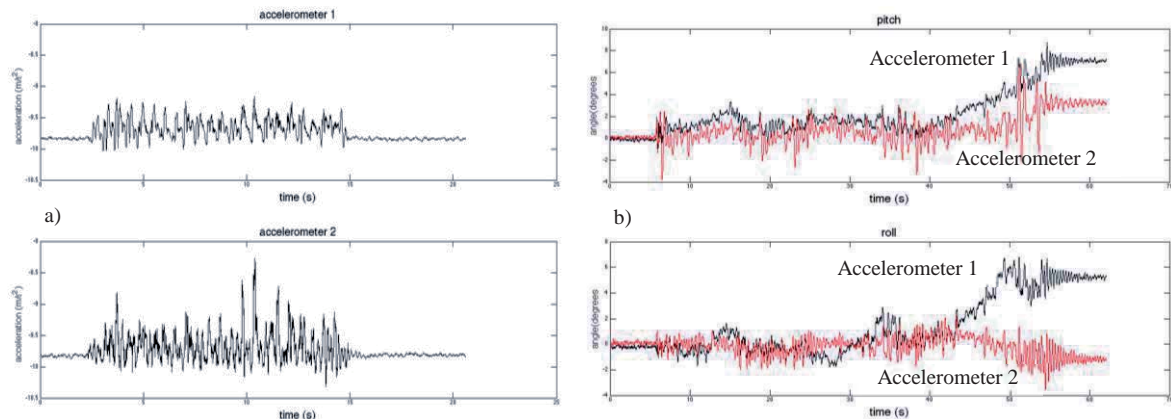


**Figure 2.** Three springs in each leg: a) Output signals (only z axis) of the accelerometers on the right leg of the ROLLO robot during a motion with an intermediate velocity value (0.2 m/s); b) Pitch and roll angles for the ankle and hip passive joints (red = hip, black = ankle) during a rotation of 360 degrees clockwise.

## Acknowledgments

The authors would like to thank to Humanot Team.

## References

- [1] Pratt, J., 2000. "Exploiting inherent robustness and natural dynamics in the control of bipedal walking robots". Ph.D. thesis, Massachusetts Institute of technology.
- [2] Wilcox B.H., et al., 2007. "ATHLETE: A Cargo Handling and Manipulation Robot for the Moon" *Journal of Field Robotics* 24(5), 421–434 (2007) © 2007 Wiley Periodicals, Inc.
- [3] Hitachi 2012. Hitachi Emiew two wheeled robot. Available: <http://www.hitachi.com/New/cnews/050315a.html>
- [4] Lim, J., et al. 2016, Robot System of DRC-HUBO+ and Control Strategy of Team KAIST in DARPA Robotics Challenge Finals. *J. Field Robotics*. doi:10.1002/rob.21673.
- [5] Boston Dynamics "nightmare inducing" wheeled robot "Handle". Published on 1st February 2017. <https://www.youtube.com/watch?v=giS41utjlbU>
- [6] Muscolo G. G. and Recchiuto C. T., 2017. "Flexible Structure and Wheeled Feet to Simplify Biped Locomotion of Humanoid Robots", *International Journal of Humanoid Robotics*. Volume 14, Issue 1, 26 p..

## **Section**

# **MULTIPHYSICS AND COUPLED PROBLEMS**



# Dynamic simulation of the inflation gas of a tire under operational conditions

Axel Gallrein, Manfred Bäcker, Francesco Calabrese

Fraunhofer-Institut für Techno-  
und Wirtschaftsmathematik ITWM  
Fraunhofer-Platz 1, 67663 Kaiserslautern, Germany  
[axel.gallrein, manfred.baecker, francesco.calabrese]@itwm.fraunhofer.de

## Abstract

In the virtual development process, the assessment and optimization of vehicle suspension and chassis performance are based on the forces that are transferred by the tire from road into the suspension. In this load transfer, the tire is one of the most critical components because the tire has a strong nonlinear behavior and is very difficult to model.

ITWM's tire model CDTire supports engineers in almost all analysis scenarios used in modern vehicle development processes from within modern multi body simulation (MBS) tools [3,4]. Special focus on tire belt dynamics and interaction with 3D road surfaces accurately captures the vibrations in both amplitude and frequency behavior.

The CDTire/3D is structural 3D shell based bead-to-bead model with sidewalls and belt that separately models all functional layers of a modern tire [2]. In this model, the inflation pressure is modeled as a uniform stress acting normal to the shell's faces. The pressure can vary depending on the application: prescribed by the MBS-tool to align to a constant pressure specified for a vehicle or scenario, but it can also be modified dynamically to simulate e.g. a sudden pressure loss in a tire. The authors have also show in previous publications that the pressure dependency is modeled physical correct.

For many applications, this description of the inflation pressure as a time dependent quantity is sufficient. However, there are tire applications where it is needed to describe the inflation gas using a dynamic gas equation (Euler or Navier-Stokes). One such example is when the tire model is used in NVH (Noise-Vibration-Harshness) applications [1] where the frequency range extends the 250 Hz range. For passenger car tires, a first mode of the inflation gas is at around 230. This mode couples with the tire structure and yields significant peaks in the spindle force spectrum, which have to be considered in the NVH assessment of a car.

In this paper, we are modeling the inflation gas of a tire by an isentropic compressible Euler equation and couple it to the tire dynamics in the nonlinear transient application range. After validation of the overall model by comparison with respective measurements, the authors are also describing how one can derive a linear model from the overall transient tire model, which can be used in linear FEM based NVH-tools.

Conservation of mass (1), conservation of momentum (2) and an isentropic relation (3) for an ideal gas yields the following equations, where the interaction with the tire and rim structure is realized via the local cross section area  $A$  and the local inflation pressure  $p$ .

$$\partial_t(\rho A) + \partial_s(\rho A v) = 0 \quad (1)$$

$$\partial_t(\rho A v) + \partial_s(\rho A v^2 + p A) = p \partial_s A \quad (2)$$

$$p = p(\rho) \quad (3)$$

It should be pointed out that the tire rotation will yield a split in the aforementioned cavity mode which increases with rotational velocity as is shown in the following comparison between measurements and simulation with and without cavity model.

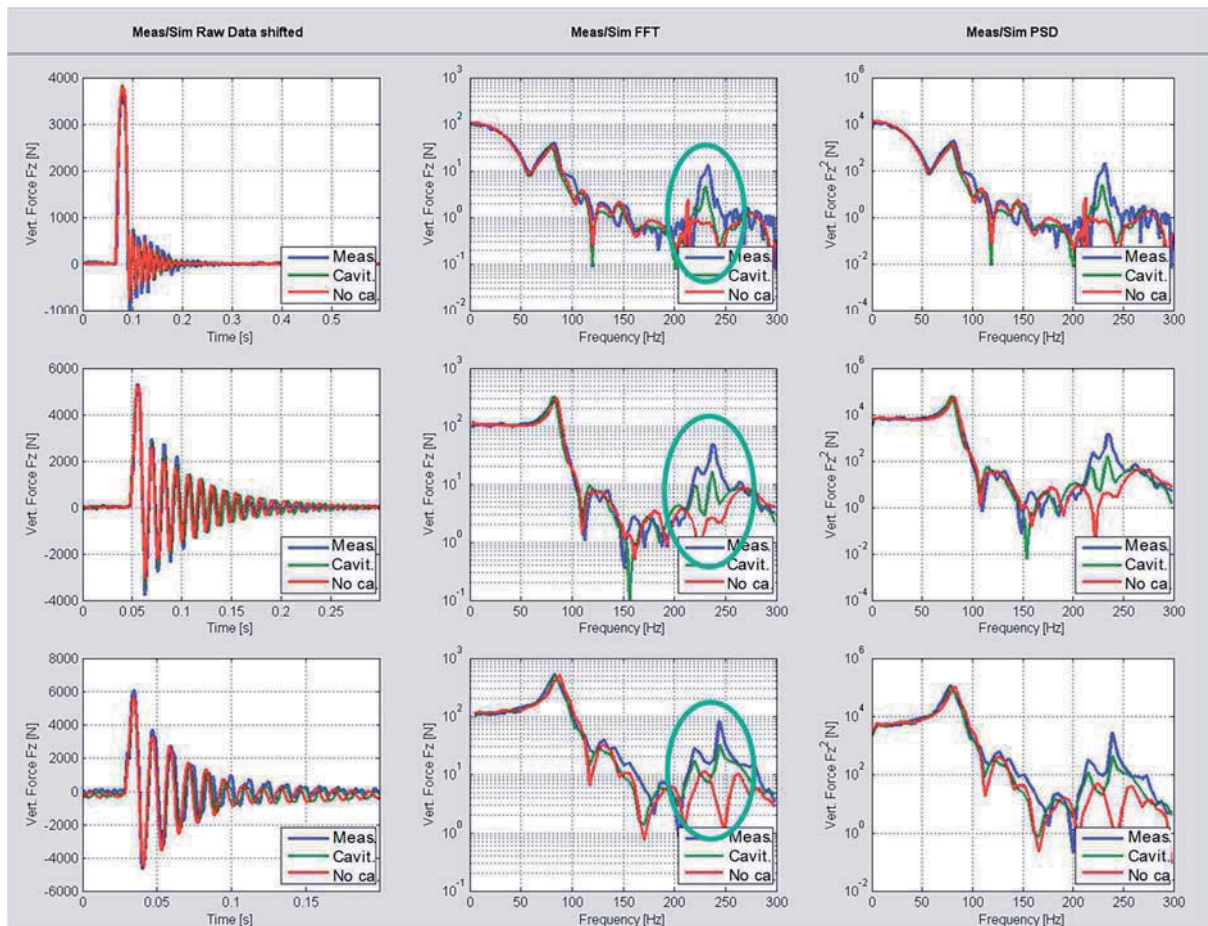


**Figure 1.** Comparison vertical force for cleat runs (30,60,90 km/h) of measurement (blue), tire with cavity model (green) and without cavity model (red) at low preload on drum test rig

## References

- [1] M. Baecker, A. Gallrein, M. Roller: Noise, vibration, harshness model of a rotating tyre, *Vehicle System Dynamics* Vol.54 – Issue 4, pp. 474-491, 2016, doi: 10.1080/00423114.2016.1158844, <http://dx.doi.org/10.1080/00423114.2016.1158844>
- [2] A. Gallrein, M. Bäcker, A. Gizatullin: Structural MBD tire models: Closing the gap to structural analysis – history and future of parameter identification, *SAE Technical Paper* 2013-01-0630, 2013, doi:10.4271/2013-01-0630
- [3] A. Gallrein, M. Bäcker: Structural MBD Tire Models: Evolving from Spindle Load to Deformation Measurements, in: *Proceedings of ECCOMAS Multibody Dynamics 2013*
- [4] M. Baecker, A. Gallrein, M. Hack, A. Toso: A Method to Combine a Tire Model with a Flexible Rim Model in a Hybrid MBS/FEM Simulation Setup, *SAE Int.* SP-2307, 2011-01-0186, 2011

# Coupling a DEM material model to multibody construction equipment

Michael Burger<sup>1</sup>, Klaus Dressler<sup>1</sup>, Torbjörn Ekevid<sup>2</sup>, Stefan Steidel<sup>1</sup>, Dietmar Weber<sup>1</sup>

<sup>1</sup> Mathematical Methods in Dynamics and Durability  
 Fraunhofer Institute for Industrial Mathematics ITWM  
 Fraunhofer-Platz 1, 67663 Kaiserslautern, Germany  
 {michael.burger, klaus.dressler, stefan.steidel, dietmar.weber}@itwm.fraunhofer.de

<sup>2</sup> Virtual Product Development  
 Volvo Construction Equipment AB  
 Carl Lihnell's väg, 360 42 Braås, Sweden  
 torbjorn.ekevid@volvo.com

## Abstract

Particle simulation with the Discrete Element Method (DEM) is well-established and widely used in soil dynamics related applications as, for instance, described in [1, 2, 3, 4] and references therein. The wide range of applications can be envisaged in automotive engineering (e.g. soil interaction with wheels/tracks, earth moving equipment, ...), material handling (e.g. conveyer belt load extraction, material spread in hopper, ...), manufacturing/processing (e.g. granulation/agglomeration of powders, crushing, grinding, ...), etc.

In recent years, the Fraunhofer ITWM has developed and implemented its own DEM code entitled “GRANular Physics Engine (GRAPE)” which is currently specialized for granular materials. Particles are represented by 3-dimensional spheres with 3 translational degrees of freedom interacting with each other and external tools via (repulsive) contact forces. On the implementation side, we focus on performant simulations following a strict parallelization algorithm so that we particularly achieve a real time factor well below 100 for 150000 particles and 40000 triangles in mesh. Physically our focus lies on the prediction of correct reaction forces, which implies the necessity of an appropriate model parameterization.

Another major target is GRAPE’s capability in closed-loop scenarios, i.e. the particle interaction with external tools in a general sense. Therefore we have implemented a generic interface to any multibody simulation tools that is aligned with the FMI 1.0 interface standard. In this context, we interpret an external tool as a rigid body with its geometry represented and imported into GRAPE by a triangular mesh. Regarding the implementation a major and time-consuming task consists of collision detection between particles and particles with mesh triangles. Hence, we pay special attention to this problem by splitting it into two phases with different time steps: a broad phase with complete collision detection utilizing octal trees yielding a relatively small list of potential contacts for each particle, and a narrow phase checking this potential contact list for actual contacts by calculating the actual distance. This approach shows good scaling with respect to the number of particles and triangles and the number of cores. The program can be driven in two basic modes: standalone and interactive for closed-loop scenarios. In the first mode, GRAPE processes the instructions given in an input file and provides the requested results in a file based system. In the second mode, GRAPE operates in a server mode waiting for external requests via TCP/IP. These requests are generally produced by an external application (e.g. an MBS program) through a GRAPE client (DLL) which exposes the FMI 1.0 standard and communicates with the GRAPE server.

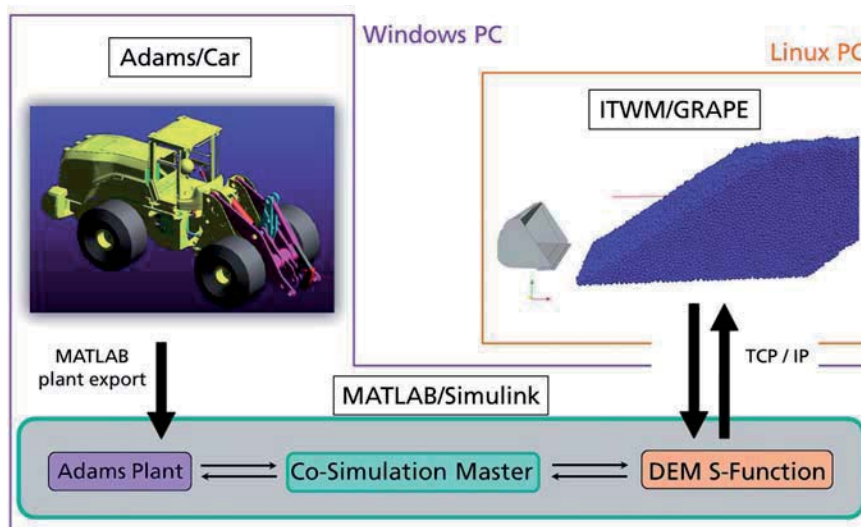


Figure 1: Realization of co-simulation setup between wheel loader (Adams/Car) and particles (ITWM/GRAPE).

We exemplify the technical realization of GRAPE's application in the wheel loader development context that has been evolved during a project collaboration between the Fraunhofer ITWM and Volvo CE. In particular, we implement a co-simulation scenario that couples Volvo CE's wheel loader model in Adams/Car 2013.1 with GRAPE for soil simulation, in order to realize a framework in which different loading maneuvers can be simulated and analyzed. An important issue for such analyses is to provide reaction forces during digging and loading that are sufficiently accurate to address questions of durability and energy efficiency. We conceptually establish a force-displacement coupling for the co-simulation setup where the bucket is modelled and simulated within GRAPE, the section forces are transmitted to the wheel loader which, in turn, provides the bucket kinematics for GRAPE. In practice, MATLAB/Simulink is chosen as the platform for setting up the co-simulation scenario. Particularly, we make use of the plant export to MATLAB provided by Adams/Car whereas GRAPE is integrated as an S-Function into the scheme and the co-simulation master is implemented in a MATLAB/Simulink subsystem. The communication, i.e. the exchange of the coupling quantities, especially on the DEM S-Function side, is realized via a TCP/IP network protocol such that it is possible to run GRAPE and MATLAB/Simulink together with Adams/Car on different host PC's, as illustrated in Figure 1.

A validation of the prescribed coupling environment by comparing simulation results with existing real measurements has partly been presented in [5]. In this work, we moreover address numerical studies with a focus on GRAPE internal parameters and co-simulation settings. Finally, we illustrate the transferability of the setup by analyzing the tire forces of a multibody hauler model when discharging granular material.

## References

- [1] M. Obermayr, K. Dreßler, C. Vrettos, P. Eberhard. A bonded-particle model for cemented sand. *Computers and Geotechnics*, 49:299-313, 2013.
- [2] M. Obermayr. Prediction of Load Data for Construction Equipment using the Discrete Element Method. PhD thesis, University of Stuttgart, 2013.
- [3] M. Obermayr, C. Vrettos, P. Eberhard, T. Däuwel. A discrete element model and its experimental validation for the prediction of draft forces in cohesive soil. *Journal of Terramechanics*, 53:93-104, 2014.
- [4] J. Kleinert, B. Simeon, M. Obermayr. An inexact interior point method for the large-scale simulation of granular material. *Computer Methods in Applied Mechanics and Engineering*, 278:567-598, 2014.
- [5] M. Balzer, M. Burger, T. Däuwel, T. Ekevid, S. Steidel, D. Weber. Coupling DEM Particles to MBS Wheel Loader via Co-Simulation. In K. Berns et. al., editors, *Proceedings of the 4<sup>th</sup> Commercial Vehicle Technology Symposium (CVT 2016)*, pages 479-488. University of Kaiserslautern, 2016.

# A unitary framework for handling Fluid-Solid Interaction (FSI) problems

Dan Negrut<sup>1</sup>, Hammad Mazhar<sup>1</sup>, Milad Rakhsha<sup>1</sup>, Arman Pazouki<sup>1</sup>

<sup>1</sup> Department of Mechanical Engineering, University of Wisconsin-Madison, Madison, WI, USA  
{negrut,mazhar,rakhsha,pazouki}@wisc.edu

The solution of fluid-solid interaction (FSI) problems is most often anchored by an established approach to solving the fluid dynamics component. The handling of the solid phase is subsequently folded into this fluid solution framework. The current contribution takes a different tack. It starts with a differential variational framework to handle the solid phase; i.e., the rigid multi-body dynamics problem in the presence of contact, friction, and bilateral kinematic constraints. The dynamics of the fluid phase, which is captured via smoothed particle hydrodynamics (SPH), is subsequently embedded into this framework in which *the incompressibility attribute of the flow is enforced via kinematic constraint equations that involve SPH particles*. The resulting FSI solution methodology, called CF-SPH, is scalable owing to reliance on a matrix-free iterative solver for the solution of a cone constrained quadratic optimization problem that yields the contact forces, friction forces, boundary condition Lagrange multipliers, fluid-solid coupling terms, and bilateral constraint Lagrange multipliers. The numerical experiments performed include a scaling analysis; three validation studies (incompressibility, dam break, and sloshing); and a vehicle fording.

**Handling of the solid “s” phase.** The time-evolution of a collection of  $n_b$  rigid bodies interacting through friction and contact is described using Cartesian coordinates. The array of generalized coordinates  $\mathbf{q} = [\mathbf{r}_1^T, \boldsymbol{\epsilon}_1^T, \dots, \mathbf{r}_{n_b}^T, \boldsymbol{\epsilon}_{n_b}^T]^T \in \mathbb{R}^{7n_b}$ , and its time derivative  $\dot{\mathbf{q}} = [\dot{\mathbf{r}}_1^T, \dot{\boldsymbol{\epsilon}}_1^T, \dots, \dot{\mathbf{r}}_{n_b}^T, \dot{\boldsymbol{\epsilon}}_{n_b}^T]^T \in \mathbb{R}^{7n_b}$ , are used to represent the state of the system, where for body  $j$ ,  $\mathbf{r}_j$  and  $\boldsymbol{\epsilon}_j$  are the absolute position of the center of mass and the body orientation Euler parameters, respectively. The time evolution of a system of bodies that can interact with each other through contact, friction, external forces, and bilateral constraints is the solution of [3]

$$\dot{\mathbf{q}} = \mathbf{L}^s(\mathbf{q})\mathbf{v} \quad (1a)$$

$$\mathbf{M}^s \dot{\mathbf{v}} = \mathbf{f}^s(t, \mathbf{q}, \mathbf{v}) + \mathbf{G}^s \boldsymbol{\lambda}^s + \underbrace{\sum_{i \in \mathcal{A}^s(\mathbf{q}, \delta)} (\hat{\gamma}_{i,n}^s \mathbf{D}_{i,n}^s + \hat{\gamma}_{i,u}^s \mathbf{D}_{i,u}^s + \hat{\gamma}_{i,w}^s \mathbf{D}_{i,w}^s)}_{i^{th} \text{ frictional contact force}} \quad (1b)$$

$$\mathbf{0} = \mathbf{g}^s(\mathbf{q}, t) \quad (1c)$$

$$i \in \mathcal{A}^s(\mathbf{q}(t)) : \begin{cases} 0 \leq C_i^s(\mathbf{q}) \perp \hat{\gamma}_{i,n}^s \geq 0 \\ (\hat{\gamma}_{i,u}^s, \hat{\gamma}_{i,w}^s) = \underset{\sqrt{\gamma_u^2 + \gamma_w^2} \leq \mu_i^s \hat{\gamma}_{i,n}^s}{\text{argmin}} \mathbf{v}^T \cdot (\gamma_u \mathbf{D}_{i,u}^s + \gamma_w \mathbf{D}_{i,w}^s) \end{cases} \quad (1d)$$

**Handling of the fluid “f” phase.** The time evolution of the fluid phase is the solution of a set of partial differential equations that capture the mass and momentum balance [5]

$$\dot{\rho} = -\rho \nabla \cdot \mathbf{v}^f \quad (2a)$$

$$\dot{\mathbf{v}}^f = -\frac{1}{\rho} \nabla p + \frac{\mu}{\rho} \nabla^2 \mathbf{v}^f + \hat{\mathbf{f}}^f, \quad (2b)$$

where  $\mu$  is the fluid viscosity,  $\rho$  the fluid density,  $\mathbf{v}^f$  and  $p$  are the flow velocity and pressure, respectively, and  $\hat{\mathbf{f}}^f$  is the fluid external body force. The approach embraced for the spatial discretization of the Navier-Stokes equations in Eq. (2b) draws on the Smoothed Particle Hydrodynamics (SPH) methodology [2], a meshless method that dovetails well with the Lagrangian modeling perspective adopted for the dynamics of the solid phase.

**Discretization of the coupled equations of motion.** In discretized form, the equations of motion for the coupled FSI problem are listed in Eq. (3). Therein,  $\mathbf{z} \equiv [\mathbf{v}^{f,T}, \mathbf{v}^{s,T}]^T$  are the system-level generalized velocities and the  $\mathbf{D}$  and  $\mathbf{G}$  operators are used to compute generalized forces using the unilateral  $\gamma$  and bilateral  $\lambda$  Lagrange multipliers, respectively. The discretization is based on a half-implicit symplectic Euler scheme, which updates the position of the SPH particles and rigid bodies as shown in Eqs. (3a) and (3b), as soon as the velocities are known. The momentum balance equations for the fluid and solid phases yield the conditions in Eqs. (3c) and (3d). The kinematic constraints on fluid density are imposed at velocity level, see Eq. (3e), just like the bilateral constraints associated with mechanical joints, see Eq. (3f). The last three sets of unilateral constraints are combined with maximum dissipation conditions to capture friction and contact in the boundary conditions, Eq. (3g); between the solid bodies, Eq. (3h); and, between the solid and fluid components, Eq. (3i). Upon further manipulations, these equations lead to a complementarity problem that is solved via a matrix free iterative algorithm [4]. In Fig. 1 we compare against results produced by the most established open-source SPH solver [1]. Figure 2 shows one frame of a simulation of a tracked vehicle, which weighs 15973.8 kg. The model has 154 bodies connected together through 761 bilateral kinematic constraints with collisions being modeled using a total of 544 different convex shapes. The fluid is modeled using 1426663 SPH particles each with a mass of  $3.96 \times 10^{-3}$  kg, a kernel radius of 0.032 m and a rest

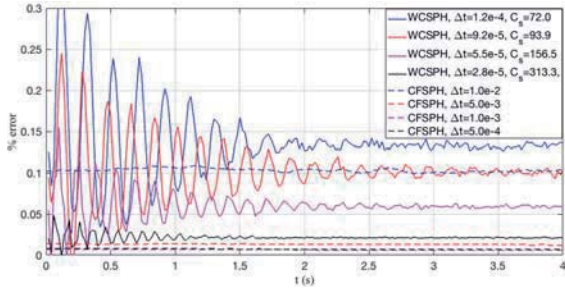


Figure 1: Error in density; CFSPH vs. WCSPH [1].

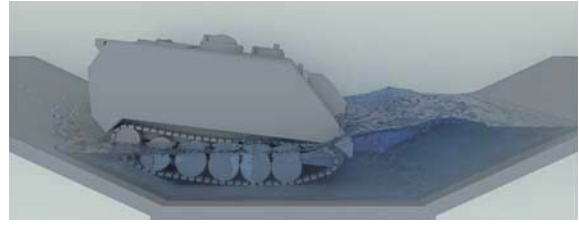


Figure 2: M113 performing fording operation. At each time step, an optimization problem in more than two million variables is solved.

density of  $1000 \text{ kg/m}^3$ . The fording simulation was 20 s long and for a step size  $\Delta t = 0.001 \text{ s}$  required 59 hours of run time when executed on a 40 core Intel(R) Xeon® CPU E5-2650 v3 @ 2.30GHz processor.

$$\mathbf{x}^{(l+1)} = \mathbf{x}^{(l)} + \Delta t \mathbf{v}^{f,(l+1)} \quad (3a)$$

$$\mathbf{q}^{(l+1)} = \mathbf{q}^{(l)} + \Delta t \mathbf{L}^s(\mathbf{q}^{(l)}) \mathbf{v}^{(l+1)} \quad (3b)$$

$$\mathbf{v}^{f,(l+1)} - \mathbf{v}^{f,(l)} = \Delta t \mathbf{f}^f(t^{(l)}, \mathbf{x}^{(l)}, \mathbf{v}^{f,(l)}) + \mathbf{G}^f \lambda^{f,(l+1)} + \mathbf{D}^{bc} \gamma^{bc,(l+1)} + \mathbf{D}^F \gamma^{FS,(l+1)} \quad (3c)$$

$$\mathbf{M}^s(\mathbf{v}^{(l+1)} - \mathbf{v}^{(l)}) = \Delta t \mathbf{f}^s(t^{(l)}, \mathbf{q}^{(l)}, \mathbf{v}^{(l)}) + \mathbf{G}^s \lambda^{s,(l+1)} + \mathbf{D}^s \gamma^{s,(l+1)} + \mathbf{D}^S \gamma^{FS,(l+1)} \quad (3d)$$

$$0 = \frac{1}{\Delta t} \mathbf{g}^f(\mathbf{x}^{(l)}) + \mathbf{G}^{f,T} \mathbf{v}^{f,(l+1)} \quad (3e)$$

$$0 = \frac{1}{\Delta t} \mathbf{g}^s(\mathbf{q}^{(l)}, t^{(l)}) + \mathbf{G}^{s,T} \mathbf{v}^{(l+1)} + \mathbf{g}_t^s(\mathbf{q}^{(l)}, t^{(l)}) \quad (3f)$$

$$k \in \mathcal{A}^{bc,(l)} : \begin{cases} 0 \leq \frac{C_k^{bc}(\mathbf{x}^{(l)})}{\Delta t} + \mathbf{D}_{k,n}^{bc,T} \mathbf{v}^{f,(l+1)} - \mu_k^{bc} \sqrt{\left(\mathbf{D}_{k,u}^{bc,T} \mathbf{v}^{f,(l+1)}\right)^2 + \left(\mathbf{D}_{k,w}^{bc,T} \mathbf{v}^{f,(l+1)}\right)^2} \pm \gamma_{k,n}^{bc,(l+1)} \geq 0 \\ \left(\gamma_{k,u}^{bc,(l+1)}, \gamma_{k,w}^{bc,(l+1)}\right) = \underset{\sqrt{\gamma_u^2 + \gamma_w^2} \leq \mu_k^{bc} \gamma_{k,n}^{bc,(l+1)}}{\text{argmin}} \mathbf{v}^{f,(l+1),T} \left(\gamma_u \mathbf{D}_{k,u}^{bc} + \gamma_w \mathbf{D}_{k,w}^{bc}\right) \end{cases} \quad (3g)$$

$$i \in \mathcal{A}^{s,(l)} : \begin{cases} 0 \leq \frac{C_i^s(\mathbf{q}^{(l)})}{\Delta t} + \mathbf{D}_{i,n}^{s,T} \mathbf{v}^{(l+1)} - \mu_i^s \sqrt{\left(\mathbf{D}_{i,u}^{s,T} \cdot \mathbf{v}^{(l+1)}\right)^2 + \left(\mathbf{D}_{i,w}^{s,T} \cdot \mathbf{v}^{(l+1)}\right)^2} \pm \gamma_{i,n}^{s,(l+1)} \geq 0 \\ \left(\gamma_{i,u}^{s,(l+1)}, \gamma_{i,w}^{s,(l+1)}\right) = \underset{\sqrt{\gamma_u^2 + \gamma_w^2} \leq \mu_i^s \gamma_{i,n}^{s,(l+1)}}{\text{argmin}} \mathbf{v}^T \cdot \left(\gamma_u \mathbf{D}_{i,u}^s + \gamma_w \mathbf{D}_{i,w}^s\right). \end{cases} \quad (3h)$$

$$j \in \mathcal{A}^{FS,(l)} : \begin{cases} 0 \leq \frac{C_j^{FS}(\mathbf{x}^{(l)}, \mathbf{q}^{(l)})}{\Delta t} + \mathbf{D}_{j,n}^{FS,T} \mathbf{z}^{(l+1)} - \mu_j^{FS} \sqrt{\left(\mathbf{D}_{j,u}^{FS,T} \mathbf{z}^{(l+1)}\right)^2 + \left(\mathbf{D}_{j,w}^{FS,T} \mathbf{z}^{(l+1)}\right)^2} \pm \gamma_{j,n}^{FS,(l+1)} \geq 0 \\ \left(\gamma_{j,u}^{FS,(l+1)}, \gamma_{j,w}^{FS,(l+1)}\right) = \underset{\sqrt{\gamma_u^2 + \gamma_w^2} \leq \mu_j^{FS} \gamma_{j,n}^{FS,(l+1)}}{\text{argmin}} \mathbf{z}^{(l+1),T} \left(\gamma_u \mathbf{D}_{j,u}^{FS} + \gamma_w \mathbf{D}_{j,w}^{FS}\right) \end{cases} \quad (3i)$$

**Acknowledgments.** Partial funding was provided by US Army TARDEC under RIF grant W56HZV-14-C-0254.

## References

- [1] Alejandro JC Crespo, José M Domínguez, Benedict D Rogers, Moncho Gómez-Gesteira, S Longshaw, R Canelas, R Vacondio, A Barreiro, and O García-Feal. Dualsphysics: Open-source parallel cfd solver based on smoothed particle hydrodynamics (sph). *Computer Physics Communications*, 187:204–216, 2015.
- [2] R. A. Gingold and J. J. Monaghan. Smoothed particle hydrodynamics-theory and application to non-spherical stars. *Monthly Notices of the Royal Astronomical Society*, 181(1):375–389, 1977.
- [3] E. J. Haug. *Computer-Aided Kinematics and Dynamics of Mechanical Systems Volume-I*. Prentice-Hall, Englewood Cliffs, New Jersey, 1989.
- [4] T. Heyn, M. Anitescu, A. Tasora, and D. Negrut. Using Krylov subspace and spectral methods for solving complementarity problems in many-body contact dynamics simulation. *International Journal for Numerical Methods in Engineering*, 95(7):541–561, 2013.
- [5] Lawrence E. Malvern. *Introduction to the Mechanics of a Continuous Medium*. Prentice Hall, 1969.

# An Efficient and Robust Standard Particle Interface for Multi-Flexible-Body Dynamics

Juhwan Choi<sup>1</sup>, Jin Hwan Choi<sup>2</sup>

<sup>1</sup>R&D Center, FunctionBay, Inc.  
Chief Product Officer

5F, Pangyo Seven Venture Valley 1 danji 2 dong, 15, Pangyo-ro 228  
beon-gil, Bundang-gu, Seongnam-si, Gyeonggi-do, Republic of Korea  
[juhwan@functionbay.co.kr](mailto:juhwan@functionbay.co.kr)

<sup>2</sup>Department of Mechanical Engineering  
KyungHee University

1, Seochun, Kihung, Yongin, Gyeonggi, 449-701, Republic of Korea  
[jhchoi@khu.ac.kr](mailto:jhchoi@khu.ac.kr)

## Abstract

The computer simulation of Multi-Body Dynamics (MBD) and Finite Element Analysis (FEA) is an important part of computational dynamics. In addition, the integrated simulation of MBD and FEA becomes more important in order to analyze the dynamic system more accurately and efficiently. We call that Multi-Flexible-Body Dynamics (MFBD). As the computational performance of computers and numerical methods has improved, it has become possible to simulate the dynamics of very complex systems that include flexible bodies in the integrated MFBD system. This integrated MFBD system is well defined and developed in the commercial software RecurDyn. By using RecurDyn/MFBD technologies, the model generation and analysis for various complex dynamic systems can be efficiently performed. On the other hand, the particle-based simulation approach has become more popular to analyze the fluid and granular materials as the computational performance has improved dramatically by using many CPUs (Central Processing Units) and GPUs (Graphical Processing Units). As the computational performance become more powerful, particle-based simulations are used for various applications to solve more complex and multi-physics problems. In addition, the particle-based approaches are very good for the coupling with the dynamic analysis compared to the original mesh grid approach because the dynamic analysis inherently involves the large displacement and rotations in the model. As a result, the boundary of the geometries of dynamics model should be handled efficiently. For this moving boundary problem, the particle-based approaches are much efficient than the original mesh grid approaches.

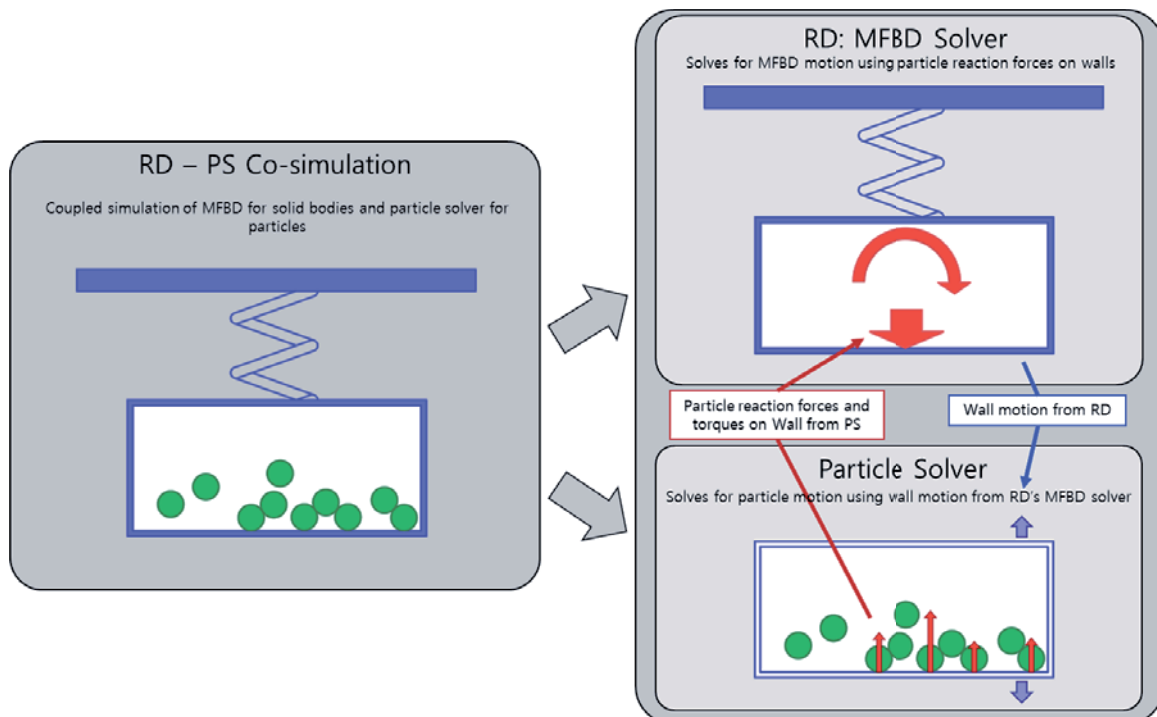


Figure 1. Co-simulation concept of MFBD and Particle Models

As a result, the needs for the efficient and robust coupling between multi-body dynamics and particle-based simulations has been increased more and more. In order to resolve this kind of important demands, we propose a new standard particle interface which can be used for any kind of particle-based solvers such as the solid or fluid particle solver. This standard particle interface will be developed in RecurDyn V9R1 and this interface can be used for coupling with various particle-based solvers.

Fig. 1 shows a co-simulation concept of MFBD and particle models. “RD” means “RecurDyn” and “PS” means “Particle Solver”. As shown in Fig. 1, the users can build a dynamic model in RD and a particle model can be defined in the PS. Because the dynamics simulation has to handle whole simulation, RD should be set as the master for co-simulation and the PS should be set as the slave. Additionally, Fig. 2 shows the co-simulation coupling strategy and time integration strategy which can be used in the standard particle interface.

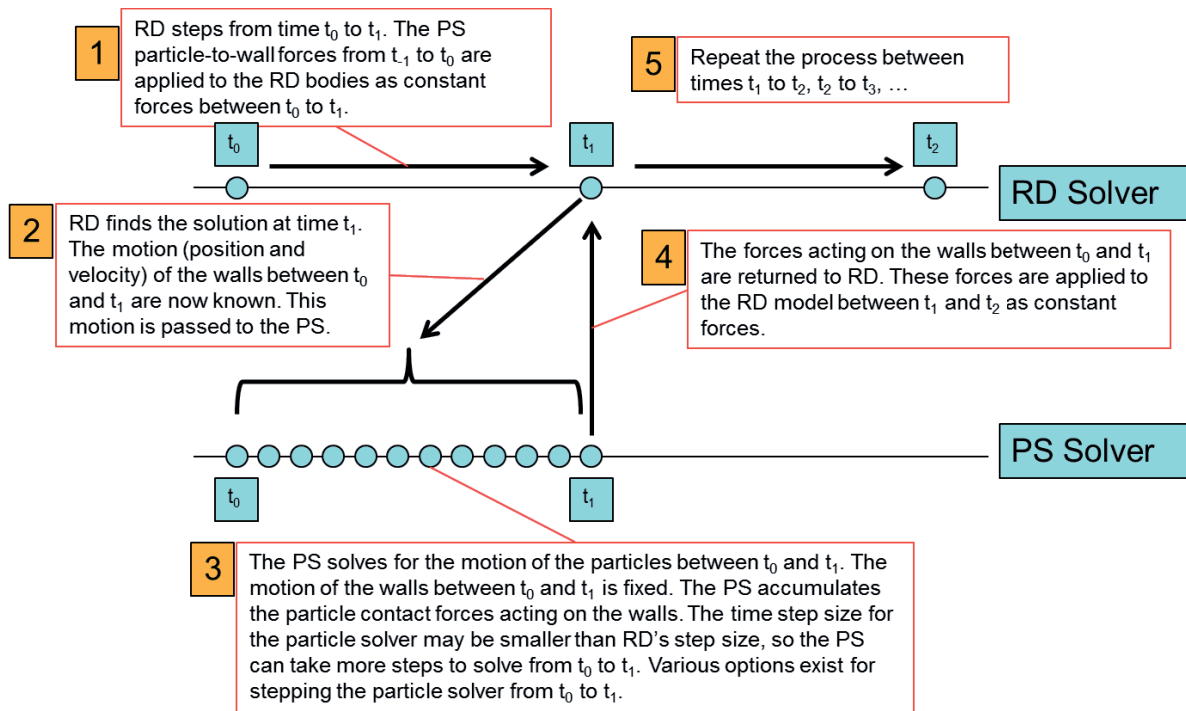


Figure 2. Co-simulation coupling strategy and time integration strategy

## Acknowledgments

This work is supported by the Industrial Strategic Technology Development Program (10051136, Development of an integrated analysis software coupled between particle-based fluid dynamics and multibody dynamics for predicting motion of floating offshore structures (MOTIE)).

## References

- [1] A.A. Shabana. *Dynamics of Multibody Systems*, Cambridge University Press, 2005.
- [2] RecurDyn™ Help Library, FunctionBay, Inc., 2017.
- [3] J. Choi. Study on the analysis of rigid and flexible body dynamics with contact, PhD Dissertation, Seoul National University, Seoul, 2009.
- [4] J. Choi, S. Rhim, and J.H. Choi. A general purpose contact algorithm using a compliance contact force model for rigid and flexible bodies of complex geometry, *International Journal of Non-Linear Mechanics*, 2013.

## Coupled Model for Simulating Turbocharger Rotors with Ball Bearings

Daixing Lu, Ioannis Chatzisavvas, Robert Schmoll and Bernhard Schweizer

Institute of Applied Dynamics  
Technical University of Darmstadt  
Otto-Berndt-Str. 2, 64287 Darmstadt, Germany  
[lu, chatzisavvas, schmoll, schweizer]@ad.tu-darmstadt.de

### Abstract

On the one hand, stringent emission regulations are challenging automobile manufacturers to design engines that meet the needs of these environment regulations. On the other hand, vehicles are desired that are enjoyable to drive. Turbochargers meet that challenge and deliver significant benefits to end users. A turbocharger is a system which uses the exhaust gas of the engine in order to compress the air, which is supplied to the engine. The main part of a turbocharger consists of a rotating shaft with two wheels, namely a turbine wheel and a compressor wheel, see Fig 1. The rotating shaft is supported by an appropriate bearing system. Usually, oil-film bearings are used in turbocharger applications [1]. Alternatively, ball bearings can be applied, which have the advantage that the friction losses are reduced. Since ball bearings exhibit only less damping/friction, squeeze-film dampers are used in order to introduce damping into the rotor system.

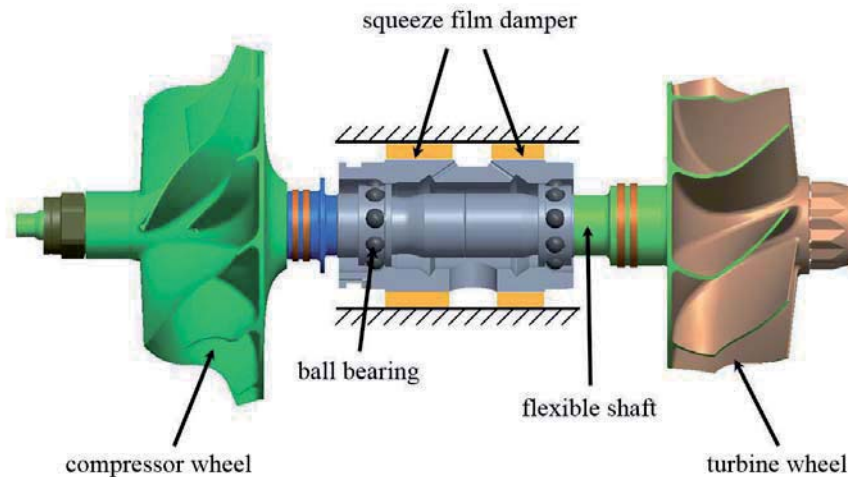


Figure 1. Turbocharger Rotor

Here, a detailed numerical model is presented for turbochargers supported by ball bearings; the model also includes an external squeeze-film damper. For the ball bearings, an analytical 2D-model approach based on Hertzian contact theory is used. The bearing forces acting in the squeeze-film damper, see Fig. 1, are calculated with the Reynolds equation for thin fluid films [2]. The Reynolds equation is a partial differential equation, which is solved numerically by a finite element approach. The rotor is modeled as a flexible multibody system. Hence, the discretized Reynolds equation – represented by a system of nonlinear algebraic equations – has to be solved in every time integration-step in parallel with the multibody system. To reduce the simulation time, a computationally efficient semi-implicit co-simulation approach is used here, see ref. [3].

### References

- [1] B. Schweizer, M. Sievert. Nonlinear oscillations of automotive turbocharger turbines. *Journal of Sound and Vibration*, 321, pp. 955–975, 2009.
- [2] Y. Hori. *Hydrodynamic Lubrication*. Springer, Tokyo, 2006.
- [3] M. Busch, B. Schweizer. Coupled simulation of multibody and finite element systems: an efficient and robust semi-implicit coupling approach. *Arch. Appl. Mech.*, 82, pp. 723–741, 2011.



# Multibody Formulation of a Load-out Problem of a Mega Block Using Modular Transporters in Shipbuilding Industry

Seung-Ho Ham<sup>1</sup>, Myung-II Roh<sup>2</sup>

<sup>1</sup>Department of Naval Architecture and Ocean Engineering,  
Seoul National University,  
1 Gwanak-ro, Gwanak-gu, 08826, Seoul,  
Republic of Korea  
hsh0930@snu.ac.kr

<sup>2</sup>Department of the Naval Architecture and Ocean Engineering, and Research Institute of Marine Systems Engineering, Seoul National University,  
1 Gwanak-ro, Gwanak-gu, 08826,  
Seoul, Republic of Korea  
miroh@snu.ac.kr

## Abstract

A ship or an offshore structure is built by erecting several blocks one by one. To enhance the efficiency, many shipbuilding companies have tried to erect a huge block at once. For example, a ring block which is almost one fifth of the entire ship is built in another facility for block production, and then is transported to the shipyard by being tied up on the barge. To lift this huge block of which weight is more than 2,000 tons, a floating crane has been used until now. However, it took much time to prepare the connection and disconnection of wire ropes. In addition, because the floating crane is greatly affected by weather condition, the operation may be delayed. In order to overcome these drawbacks, a new way of using modular transporters (MTPs) instead of the floating crane has been proposed. MTPs lift the block directly and move to the quay or the floating dock. It is shown in Figure 1.



Figure 1. Example of load-out using modular transporters.

However, several things should be checked before executing the operation for the safety. Different from the operation using the floating crane, MTPs are continuously crossing over from the barge to the quay (or the floating dock). Therefore, the load acting on both the barge and the quay is also continuously changed. Besides, the connection equipment like a link beam is designed enough to endure the load due to the relative motion when MTPs cross over.

Therefore, the needs for the dynamic simulation has increased. However, existing dynamics engines for the simulation are not suitable to be applied because it should be combined by two or more physical theories simultaneously. For example, wheels of MTPs are made by hydraulic cylinders. Pressurized fluid is supplied to each hydraulic cylinder to maintain the horizontal position of MTPs. Moreover, the wheels have contact with the deck of the barge. Another example is the connection equipment. It should be modeled by the flexible element to take into account the concentrated load. The connection equipment is connected by hinge joints. Therefore, rigid and flexible multibody formulation is necessary to solve the equations of motion of the bodies explained above.

For this, we adopted the discrete Euler-Lagrange (DEL) equation derived by Lacoursière [1]. The integration scheme mixes the well-known Störmer-Verlet method for dynamic equations with the linearly implicit Euler method for constraint equations. This makes the numerical integration be more stable. The final form of the DEL equation is shown in Eq. (1).

$$\begin{bmatrix} \mathbf{M}_{rigid} & -\mathbf{G}_k^T \\ \mathbf{G}_k & \Gamma \frac{4\epsilon}{h^2} \end{bmatrix} \begin{bmatrix} \mathbf{v}_{k+1} \\ \boldsymbol{\lambda}_{k+1} \end{bmatrix} = \begin{bmatrix} \mathbf{M}_{rigid} \mathbf{v}_k - h \frac{\partial V}{\partial \mathbf{q}_k} + h \mathbf{f}(\mathbf{q}_k, \mathbf{v}_k) \\ -\frac{4\Gamma}{h} \mathbf{g}_k + \Gamma \mathbf{G}_k \mathbf{v}_k \end{bmatrix}. \quad (1)$$

where, the subscript  $k$  means the  $k^{\text{th}}$  step of the simulation,  $\mathbf{M}_{rigid}$  is mass matrix of the rigid bodies,  $h$  is time step,  $\mathbf{v}$  is velocity,  $\mathbf{f}$  is external forces,  $\mathbf{g}_k$  and  $\mathbf{G}_k$  is constraint and constraint Jacobian, respectively. Meanwhile, for the flexible body, we used absolute nodal coordinate formulation (ANCF) which is well described in Bezeri and Shabana [2] and Shabana [3]. In ANCF, the nodal coordinates and slope are defined in the inertial frame.

$$\mathbf{r}(x) = \mathbf{S}\mathbf{q} = \begin{bmatrix} s_1\mathbf{I} & s_2\mathbf{I} & s_3\mathbf{I} & s_4\mathbf{I} \end{bmatrix} \begin{bmatrix} \mathbf{r}_0 \\ \mathbf{r}'_0 \\ \mathbf{r}_l \\ \mathbf{r}'_l \end{bmatrix}, (0 \leq x \leq l). \quad (1)$$

where,  $\mathbf{S}$  is cubic Hermite shapesfunction, and  $\mathbf{r}_0$  and  $\mathbf{r}_l$  are displacement node vectors at both ends. Based on this kinematic description of the beam element, we can derive the kinetic energy and strain energy. Finally, the equations of motion of the flexible multibody system can be derived from the Euler-Lagrange equation. The equations of motion for rigid and flexible multibody systems are shown in Eq. (2).

$$\begin{bmatrix} \mathbf{M}_{rigid} & \mathbf{0} & -\mathbf{G}_{k,(rigid-rigid)}^T & -\mathbf{G}_{k,(flex-rigid)}^T \\ \mathbf{0} & \mathbf{M}_{flex} & -\mathbf{G}_{k,(rigid-flex)}^T & -\mathbf{G}_{k,(flex-flex)}^T \\ \mathbf{G}_{k,(rigid-rigid)} & \mathbf{G}_{k,(rigid-flex)} & \Gamma_1 \frac{4\boldsymbol{\varepsilon}_1}{h^2} & \mathbf{0} \\ \mathbf{G}_{k,(flex-rigid)} & \mathbf{G}_{k,(flex-flex)} & \mathbf{0} & \Gamma_2 \frac{4\boldsymbol{\varepsilon}_2}{h^2} \end{bmatrix} \begin{bmatrix} \mathbf{v}_{k+1}^{(rigid)} \\ \mathbf{v}_{k+1}^{(flex)} \\ \bar{\boldsymbol{\lambda}}_{k+1}^1 \\ \bar{\boldsymbol{\lambda}}_{k+1}^2 \end{bmatrix} = \begin{bmatrix} \mathbf{M}_{rigid} \mathbf{v}_k^{(rigid)} - h \frac{\partial V}{\partial \mathbf{q}_k} + h \mathbf{f}(\mathbf{q}_k, \mathbf{v}_k) \\ \mathbf{M}_{flex} \mathbf{v}_k^{(flex)} - h \frac{\partial V}{\partial \mathbf{q}_k} + h \mathbf{f}(\mathbf{q}_k, \mathbf{v}_k) \\ -\frac{4\Gamma_1}{h} \mathbf{g}_k + \Gamma_1 \mathbf{G}_k \mathbf{v}_k \\ -\frac{4\Gamma_2}{h} \mathbf{g}_k + \Gamma_2 \mathbf{G}_k \mathbf{v}_k \end{bmatrix}. \quad (2)$$

The contacts between the wheel and the barge are constructed by non-interpenetration constraints which are signed distance functions between two collision bodies. Between bodies and wheels of MTPs, hydraulic cylinders are implemented to account for equalizing forces acting on each wheel. As a result, we applied the derived multibody formulation to a load-out problem of moving a mega block to a transportation barge by using MTPs. From this, we could check whether the safety margin of the connection equipment is suitable or not during the operation. Simulation results are depicted in Figure 2.

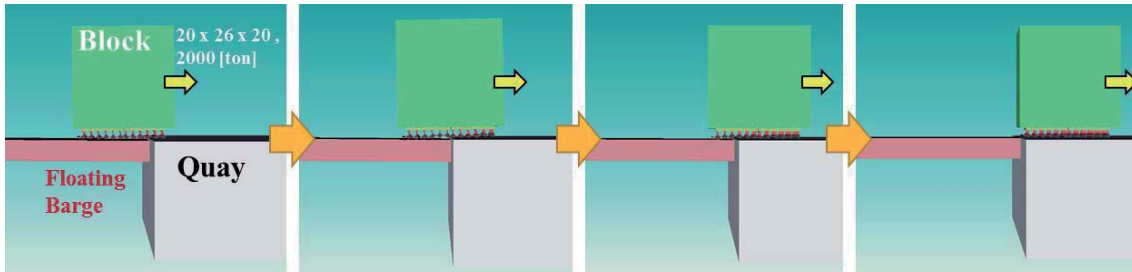


Figure 2. Simulation results of a load-out problem of a mega block using modular transporters.

## Acknowledgments

This work was partially supported by

- BK21 Plus, Education & Research Center for Offshore Plant Engineers (COPE) of Seoul National University, Republic of Korea,
- Program of University Specialized for Offshore Plant Engineering funded by the Ministry of Trade, Industry and Energy, Republic of Korea, and
- Research Institute of Marine Systems Engineering of Seoul National University, Republic of Korea.

## References

- C. Lacoursière, *Ghosts and machines: regularized variational methods for interactive simulations of multibodies with dry frictional contacts*. Ph. D. Thesis. Umea University, Sweden, 2007.
- M. Berzeri, A. A. Shabana, Development of Simple Models for the Elastic Forces in the Absolute Nodal Coordinate Formulation, *Journal of Sound and Vibration*, 235(4):239-565, 2000.
- A. A. Shabana, *Dynamics of multibody systems*, Cambridge University Press, New York, 2005.

# Damping effect on tall building low frequency vibration using two degree-of-freedom enhanced Coriolis effect damper

Mario Walker, Masaaki Okuma, Yuuki Hira

Faculty of Mechanical and Aerospace Engineering  
Tokyo Institute of Technology  
2-12-1Ookayama, Meguro-ku, 152-8550 Tokyo, Japan  
walker.m.aa@m.titech.ac.jp

## Abstract

This paper proposes and investigates a multi-body system that enhances Coriolis effect to be used to attenuate the low-frequency vibration of building structures in the event of large excitations.

Urbanisation and population increase has forced mankind to build upwards. Additionally, the evolution of building structures is towards lightness, increased flexibility and usually associated with low inherent damping [1]. These structures are more vulnerable and in the event of large excitations may experience large displacements which are hazardous to the structures, unpleasant for occupants and may pose serious serviceability issues [2]. Researchers have placed significant efforts in finding measures to reduce responses of structures.

The use of mass dampers to reduce the response of structures has been investigated by many researchers in the past years. Den Hartog [3] investigated a tuned mass damper (TMD) system showing that linear mass dampers can be quite effective for reducing the vibration amplitude of a periodically forced structure. Over the years many mass-damping system have been developed for the purpose of reducing the response of building structures. Up until 1999, it was reported that over 97 auxiliary damping systems were installed in buildings in Japan alone [2].

However, conventional damping systems require space in the horizontal direction. But as these structures become taller and thinner, the space for effective damping becomes less adequate.

The aim of this work is to investigate the idea of using the space in the longitudinal direction which is significantly greater. When tall structures vibrate they undergo some amount of rotational motion and any motion in the longitudinal direction will induce Coriolis effect. This, added with the mass inertia can be used to reduce the response of structures. However, Coriolis effect is greatly influenced by the angle of rotation and while the longitudinal motion will provide damping effect, for effective damping a significant angle of rotation is required. This concept was investigated in [4] and [5] for mass moving in radius direction of a gondola system inducing Coriolis effect to reduce its swing. They found that damping was only effective when the swing of the gondola was large and ineffective for small angles.

For the proposed model (See Figure 1), the structural system is simplified as a single degree-of-freedom (DOF) system which is coupled with a 2 DOF damping system. The primary system has motion in the horizontal direction with displacement  $x$ . The proposed damping system consists of a moving mass along a massless rod which is allowed rotational motion. The 2 DOF damping system is attached to the top of the primary system. It should be noted that the pivot of the damping system can be placed at the top or at the bottom. Depending on the pattern of motion of the damping system, it can either provide damping effect or amplification effect. An appropriate pattern of motion is chosen for damping effect based on assessment of the equations of motion.

The equations of motion of the entire system are derived using the extended Hamilton's principle. Three second order differential equations containing nonlinear terms are obtained. The response of the system is analysed numerically using Newmark's method. The damping effectiveness of the proposed system is examined. The transient response of the system is investigated under harmonic excitation until a desired displacement is achieved after which the excitation is removed and free response is allowed. The performance of the proposed system is evaluated by comparing the damping ratio found using the logarithmic decrement, and the reduction of response to harmonic excitation with those of the primary system coupled with a conventional TMD.

The results showed the concept to be relatively effective for low-frequency vibration of structures. Indications are that future works should be done on the concept in order to derive optimal parameters and appropriate control law to improve effectiveness. Additionally, investigations into how this concept would perform if higher modes of vibration are to be reduced would be interesting. This concept provides new possibilities for vibration control of tall flexible structures dominated by low mode frequency. This concept may be quite attractive in particular to structural systems where the longitudinal dimension is significantly greater than the horizontal dimension and inherent damping is extremely low.

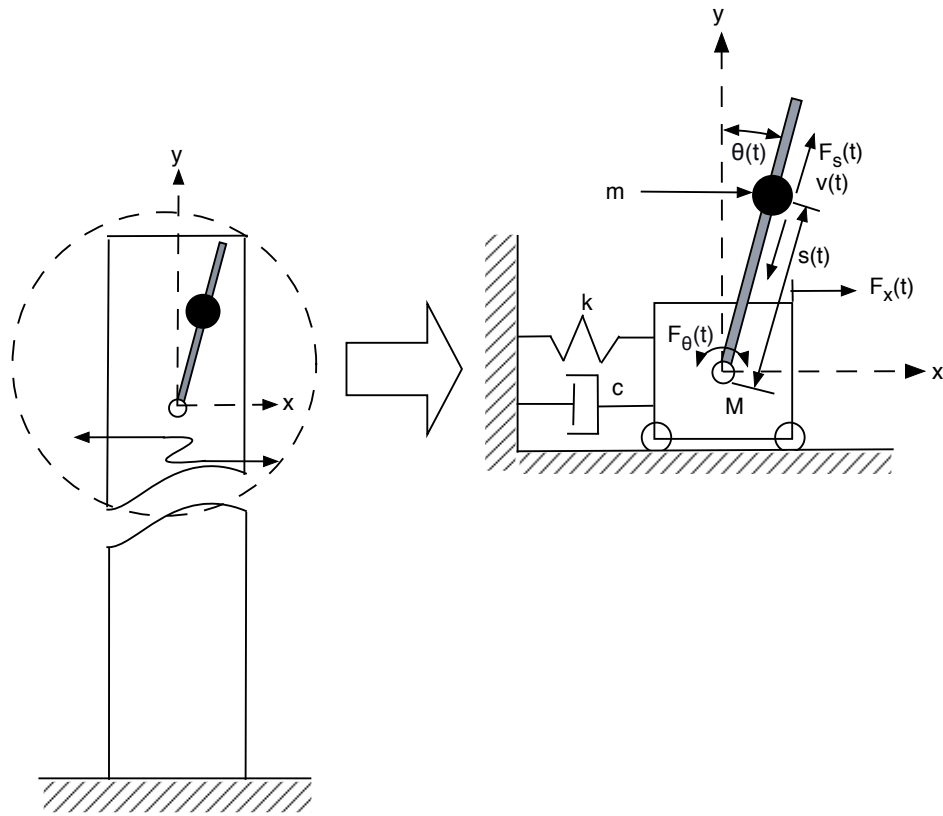


Figure 1: Simplified model of the building structure coupled with the proposed 2 DOF damping system

## References

- [1] M. M. Ali and K. S. Moon . Structural Developments in Tall Buildings: Current Trends and Future Prospects. *Architectural Science Review*, volume 50, number 3, pages 205-223. 2007.
- [2] A. Kareem, T. Kijewski, and Y. Tamura. Mitigation of motions of tall buildings with specific examples of recent applications. *Wind and structures*, volume 2, number 3, pages 201-251. 1999.
- [3] J. P. D. Hartog. *Mechanical Vibrations*. McGraw-Hill Book Company. New York. 1956.
- [4] H. Matsuhisa, R. Gu, Y. Wang, O. Nishihara and S. Sato. Vibration Control of a Ropeway Carrier by Passive Dynamic Vibration Absorbers. *The Japan Society of Mechanical Engineers International Journal*, volume 38, number 4, pages 657-662. 1995.
- [5] L. D. Viet, N. D. Anh and H. Matsuhisa. The Effective Damping Approach to Design a Dynamic Vibration Absorber Using Coriolis Force. *Journal of Sound and Vibration*, volume 330, number 9, pages 1904-1916. 2011.

# A Study on the Steering Jerk of a Wheel Loader Using MBD Simulation Including Hydraulic System

Heejong Lee<sup>1</sup>, Jimin Lee<sup>1</sup>, Minseok Kim<sup>1</sup>, Wansuk Yoo<sup>2</sup>

<sup>1</sup>Construction Equipment R&D Center  
Hyundai Heavy Industries Co., Ltd.  
Dong-gu, 44032, Ulsan, Korea  
[runnerlhj, jmlee0105,  
mskim77]@hhi.co.kr

<sup>2</sup>Faculty of Mechanical Engineering  
Pusan National University  
Geumjeong-gu, 46241, Busan, Korea  
wsyoo@pusan.ac.kr

## Abstract

A wheel loader is an off-road heavy vehicle which is widely used in construction sites. It generally consists of two frames which are connected by vertical hinge. Each frame has a fixed centre of gravity, but the resulting center of gravity of the equipment changes as a function for the yaw angle of the hinge. An articulated steering system of the wheel loader is a hydro-mechanical system that directly controls the yaw angle at the hinge. There are two cylinders on each side of the hinge, each of which connects the front and rear frame. Counter clockwise steering implies that the left cylinder is pulled in and the right cylinder is pulled out through hydraulic power steering system. In specific circumstances, an operator can feel that the wheel loader shakes laterally during steering even though the vehicle is not in operating. This jerk motion is unpleasant and sometimes even unsafe. To provide customers with a comfortable and safe operating environment, it is necessary to quantify and eliminate the jerk motion.

Many researchers have carried out static and dynamic analysis to improve and optimize the design of the steering system for the articulated vehicle. Dudzinski[1, 2] compared the basic advantages and disadvantages of steering systems for mobile earthmoving equipment. Oida[3, 4] derived an equation of motion for the turning in horizontal plane of a tractor with articulated steering. Cave[5] explained the jerk motion by the relation between acceleration of the operator seat and the derivation of pressure difference in the left and right steering cylinders. This paper presents the results of a study to improve the steering performance using MultiBody Dynamic simulation including hydraulic system. At first, I developed a detailed hydraulic power steering model (Figure 1) consisting of steering cylinders, power steering unit, pump, pressure relief valve and etc. using AMESim. The other mechanical parts of the wheel loader such as tires, axles, frames, steering cylinders, attachment and etc. were built by RecurDyn. The developed co-simulation model was verified through comparison of test results.

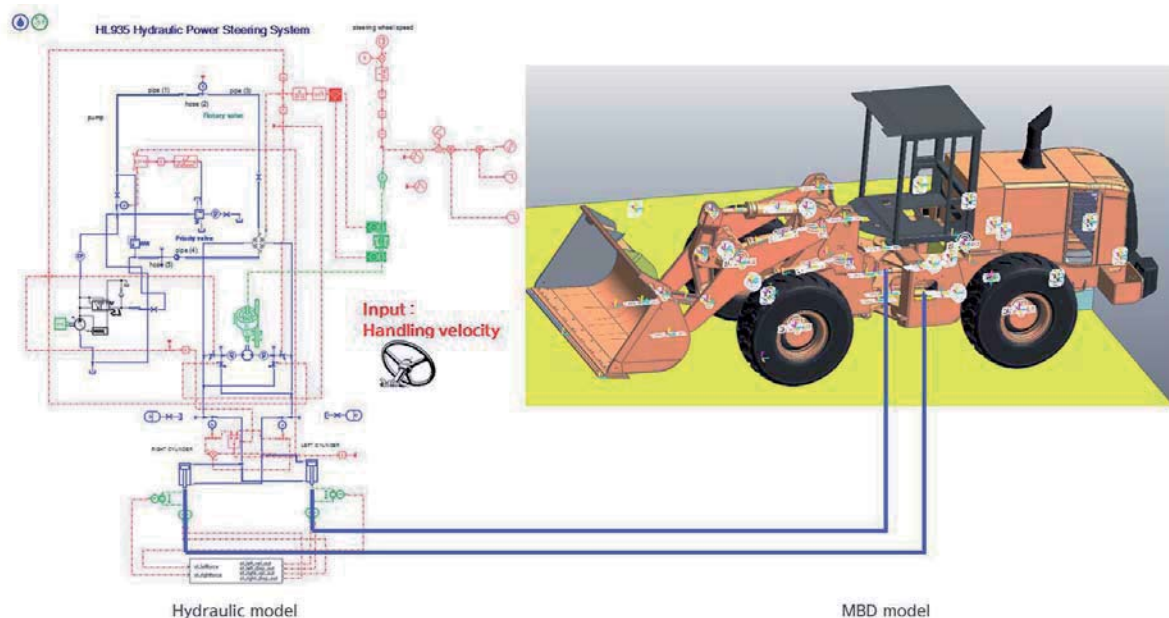


Figure 1. Co-simulation model consisting of MBD and hydraulic steering system

Using this simulation model, I identified the repeatable input condition which gives rise to jerk motion. Figure 2 shows the analysis results for three sine waves for operator's steering control. Each sine wave input means rotating the steering wheel from left to right starting and stopping at the same angle. As the frequency of the sine wave decreases, the cabin's lateral acceleration decreases remarkably. It was confirmed that 1 Hz sine wave condition is suitable for quantitatively analyzing the jerk motion and that the lateral oscillation of the cabin

is induced by the rate of change for flow in steering cylinder. With this input condition, I analyzed jerk motion sensitivity for various operating environment (posture, loading weight, tire pressure, road friction and etc.) and proposed an improved design to reduce the jerk motion. Figure 3 shows the analysis result of the improved design, where an accumulator was mounted on the hydraulic system. It is confirmed that the oscillation of lateral acceleration disappears and the maximum lateral acceleration is reduced by 73%.

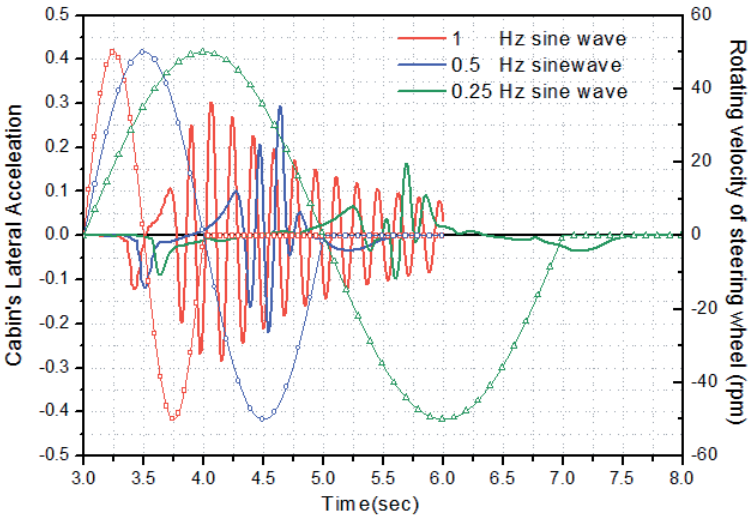


Figure 2. Co-simulation results for the sine wave input conditions

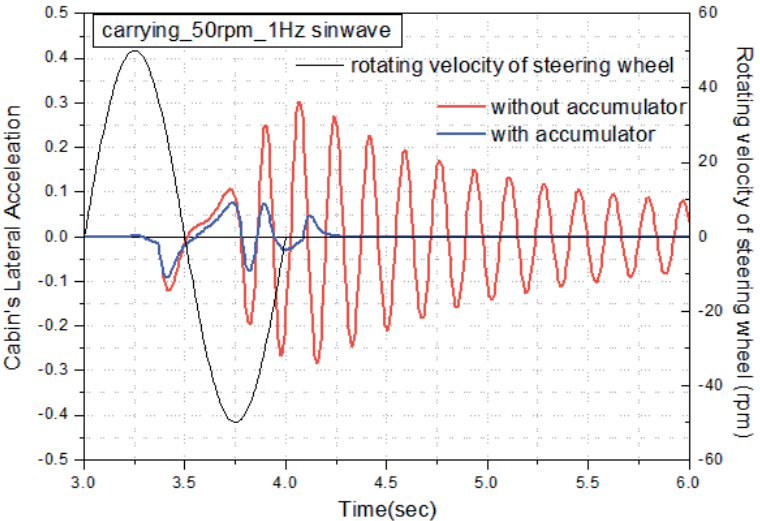


Figure 3. Co-simulation results for the improved design of hydraulic system

References

- [1] P. Dudzinski. Problems of turning process in articulated terrain vehicles. Journal of Teramechanics, 19:4:243-256, 1983.
- [2] P. Dudzinski. Design characteristics of steering systems for mobile wheeled earthmoving equipment. Journal of Teramechanics, 26:1:25-82, 1989.
- [3] A. Oida. Turning behavior of articulated frame steering tractor – part 1 motion of tractor without traction. Journal of Teramechanics, 20:3/4:153-165, 1983.
- [4] A. Oida. Turning behavior of articulated frame steering tractor – part 2 motion of tractors with drawball pull. Journal of Teramechanics, 24:1:57-73, 1987.
- [5] J. Cave. Hydraulic steering jerk on articulated vehicle. IFPE paper 3.3, 2013.

# Investigation of Numerical Stability and Local Error for Continuous Co-Simulation Methods

Martin Busch

Wiesenstraße 28, 91469, Hagenbüchach, Germany  
 busch@research-multibodydynamics.de

## Abstract

In the field of dynamic simulation, co-simulation methods are often used in order to simulate multidisciplinary systems or to improve the calculation efficiency, e.g., by applying a multirate or a parallelization technique. To accomplish the co-simulation, the overall system is decomposed into subsystems by defining appropriate input and output variables. In Fig.1, a common force/displacement coupling is shown for a simple example model where subsystem 1 obtains the coupling force as an input and subsystem 2 obtains the motion of the first body.

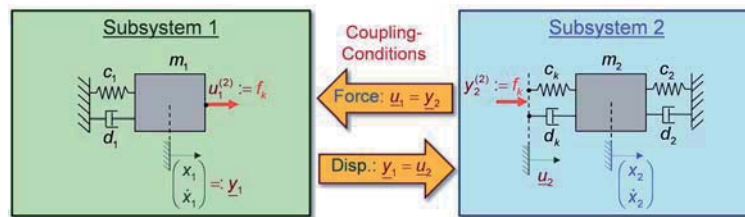


Figure 1: Modular modeling of 2-DOF oscillator with common force/displacement coupling.

During the time integration of the subsystems, the input vectors  $u_1$ ,  $u_2$  have to be updated, see Fig.2. For this purpose, the time is discretized into macro points  $T_N$  where the subsystems exchange their coupling data  $u_1 = y_2$ ,  $u_2 = y_1$ . Between the macro points, i.e., in the macro step  $T_N \rightarrow T_{N+1}$  with step size  $H$ , the unknown inputs are approximated by means of extrapolation (blue curve) or interpolation polynomials (green curve) which are calculated from the discrete output vectors  $y_1$ ,  $y_2$ .

As a drawback of classical co-simulation approaches, the extrapolation polynomials are discontinuous at the end of each macro step, see the blue curve in Fig.2. Consequently, the subsystem solvers may strongly reduce their integration step size which raises the number of right-hand side calls and makes the co-simulation inefficient. To overcome the discontinuity issue, a so-called *extrapolated interpolation (EXTRIPOL)* approach was introduced by Dr. J. Rauh (Daimler AG) in Ref. [3]. In each macro step, a classical polynomial extrapolation is carried out to obtain coupling data at  $T_N$  (blue circles). These extrapolated data are smoothed with an interpolation polynomial  $\tilde{u}_1(h)$  (red curve) which is continuous over the macro steps.

In the talk, the EXTRIPOL approach will be analyzed regarding numerical stability and local error. The results are compared to the corresponding results of the Lagrange polynomial approach, for the latter, see Ref.[1].

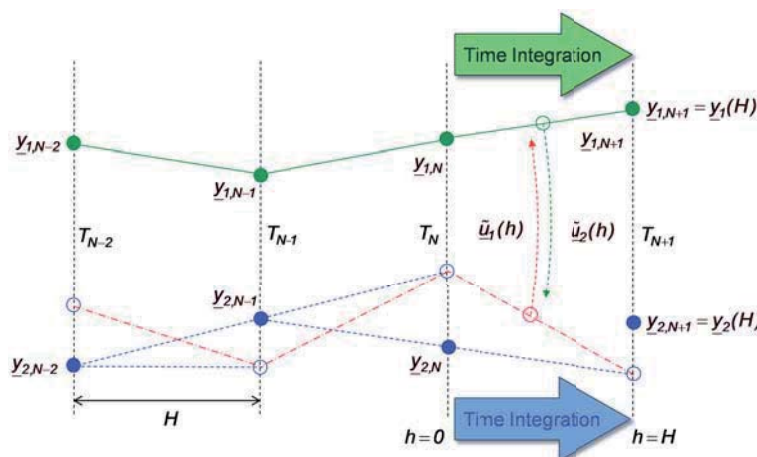


Figure 2: Sequential Gauss-Seidel scheme using a macro step  $T_N \rightarrow T_{N+1}$  with constant macro step size  $H$  and a Lagrange extrapolation (blue curve) or an EXTRIPOL method (red curve) for generating inputs for subsystem 1.

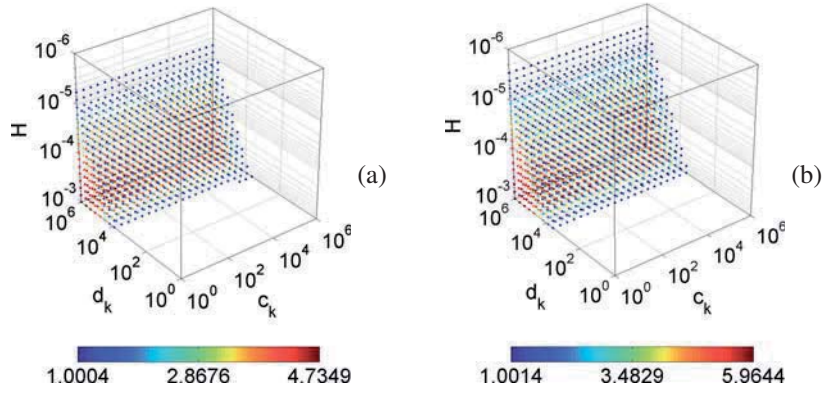


Figure 3: Instability regions for a force/displacement coupling approach in combination with the sequential Gauss-Seidel scheme. Plot (a) shows the EXTRIPOL method and plot (b) the classical cubic Lagrange approach.

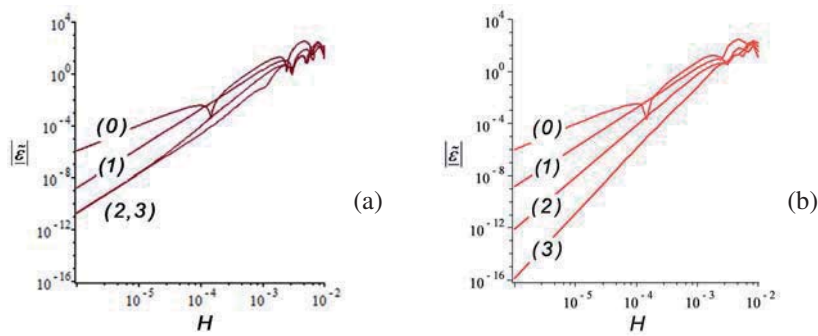


Figure 4: Local error over the macro-step size for increasing polynomial degrees ( $k = 0, 1, 2, 3$ ) of the EXTRIPOL method (a) and the Lagrange approach (b).

In Fig.3, the instability region of the EXTRIPOL method (a) and of the Lagrange approach (b) are plotted for varying macro step size  $H$ , varying coupling stiffness  $c_k$  and varying coupling damping coefficients  $d_k$  of the example model. A cubic polynomial degree is used for the Lagrange approach and for the underlying extrapolation polynomial in the EXTRIPOL method. As can be seen in the plot, both co-simulation approaches are zero-stable since the instability regions vanish for decreasing macro step size  $H$ . Increasing  $d_k$ , the instability of the system increases so that smaller macro step sizes have to be used to accomplish a stable co-simulation. Comparing the plots (a) and (b), the EXTRIPOL method is slightly more stable but basically the stability behavior is similar.

Analyzing the local error of the two methods, see Fig.4, the error reduces for decreasing macro step size  $H$ . Hence, both methods converge for sufficiently small  $H$  since they are consistent and zero-stable. However, the local error of the Lagrange approach decreases with higher order than the EXTRIPOL approach which makes the Lagrange approach the better method (at least, regarding the local error). The order drop is related with the fact that the EXTRIPOL method uses a linear interpolation polynomial for the smoothing technique which limits the error.

In the presentation, a  $C^1$ -continuous approximation method will be introduced which combines the advantages of the afore-mentioned methods, see Ref.[2]. This method is continuous and even differentiable, and it possesses similar stability and error properties than the Lagrange approach. Further, the method can be implemented in simulation programs as easy as the above methods and does not require additional information from the solvers.

## References

- [1] M. Busch. *Zur effizienten Kopplung von Simulationsprogrammen (On the efficient coupling of simulation codes)*. PhD thesis, University of Kassel, Kassel, 2012. ISBN-13: 978-3862192960.
- [2] M. Busch. Continuous approximation techniques for co-simulation methods: Analysis of numerical stability and local error. *ZAMM - Journal of Applied Mathematics and Mechanics - Zeitschrift für Angewandte Mathematik und Mechanik*, 96(9):1061–1081, 2016.
- [3] S. Dronka and J. Rauh. Co-simulation-interface for user-force-elements. In *Proceedings of SIMPACK user meeting*, Baden-Baden, 2006.

# Dynamic Analysis of a 3D Printer based on the Delta Mechanism

Eduardo Paiva Okabe<sup>1</sup>, Pierangelo Masarati<sup>2</sup>

<sup>1</sup> School of Applied Sciences  
University of Campinas - UNICAMP  
PO Box 1068, Limeira, Brazil  
eduardo.okabe@fca.unicamp.br

<sup>2</sup> Dipartimento di Scienze e Tecnologie Aerospaziali  
Politecnico di Milano  
Via La Masa 34, 20156, Milano, Italy  
pierangelo.masarati@polimi.it

## Abstract

This work presents the computational modeling and dynamic analysis of a three dimensional printer based on a delta mechanism using a multidisciplinary open source software. The flexible components of the printer (parallel arms) were modeled using the finite volume beam developed by Ghiringhelli et al. [6].

Three dimensional printers are revolutionizing the manufacturing and development of new products. These machines can make complex parts in a matter of few hours with a minimum waste of material. One of the most common techniques of 3d printing is the fused deposition method (FDM), which consists in building a part through the movement of a deposition head that adds melted plastic direct to the part.

The majority of the FDM printers uses a gantry (cartesian) mechanism to move the deposition head. However, another types of mechanism such as Delta and SCARA have been adopted in open source 3D printers because they are faster and simpler than cartesian mechanisms. One the most popular projects of delta printer is the Rostock printer [5], which was used as a reference for the computer model presented in this work.

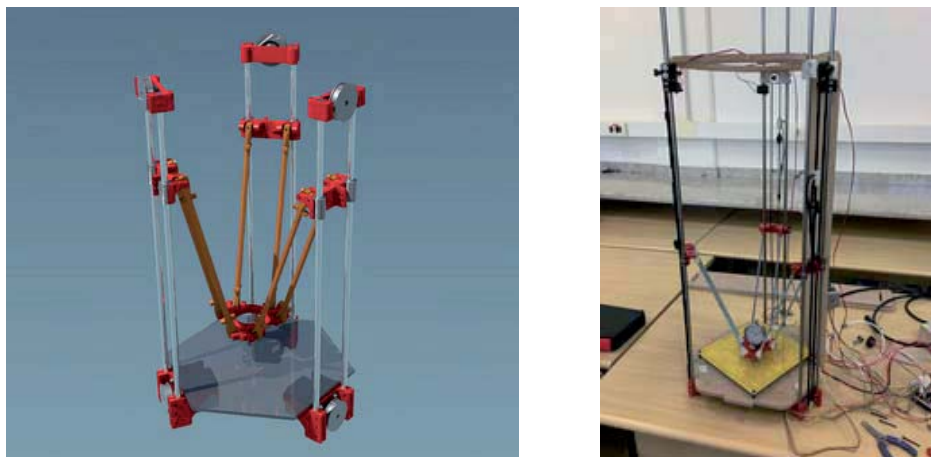


Figure 1: Rendered model of the delta printer based on the Rostock project (left) and the prototype printer during calibration (right).

The origin of delta robots is controversial [1]. The conceptual design was presented by Pollard in a patent of 1942 [2], and presented again by prof. Clavel in the 1980s [3]. The delta mechanism is based on a set of parallel arms (usually three) that are connected to a platform. In 3d printers, the deposition head is attached to this platform, and the delta mechanism can move it at a high speed ( $>3000\text{mm/s}$ ), which translates into a faster printing process. However, the trajectory calculation of the head requires an inverse kinematic (or dynamic) analysis, due to the fact that this motion is a nonlinear function of the motion of the actuators.

Fig.1 shows a rendered model of the printer and the prototype model that was built in the LAPS/Unicamp (Laboratory of Automation, Prototyping and Simulation). The prototype was depicted during the calibration phase, which explains the probe indicator on the platform instead of the extruder head.

Three dimensional printers are complex machines that integrate software and hardware with elements of several disciplines (electrical motors, elastic beams, bearings). One of the softwares that can combine all these elements in one system is the MBDyn [4]. This software can simulate multibody systems with several features, such as elastic and nonlinear components, control systems, hydraulic circuits and aerodynamic effects. MBDyn has also an inverse kinematic and dynamic analysis which is essential to study the delta mechanism, since it requires the translation of the desired trajectory of the deposition head into motor rotations.

The simulation of the delta printer in the MBDyn follows the workflow described in [7]. The first step is modeling the part that is going to be printed. Then a slicing software generates the g-code to make this part, that is translated into displacement, velocity and acceleration of the deposition head, which is the input of the inverse dynamic analysis. This analysis yields the displacement of each one of the carriages of the delta printer, and it is

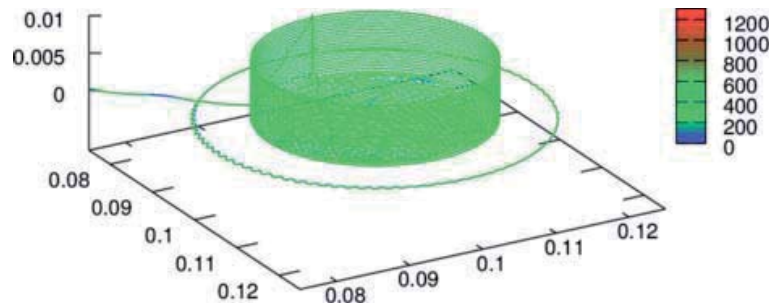


Figure 2: Simulated trajectory of the delta printer.

translated by another script into discrete steps that are used to feed the stepper driver model. The inverse dynamic simulation of the model considers rigid arms, but they are replaced by flexible arms in the final simulation.

It is important to consider the flexibility of the parallel arms, because they are the link between the platform that supports the extruder and carriages connected to the actuators. Therefore evaluate the dynamic effect of the flexibility of these components is essential to determine which material is going to be used in their construction.

Fig. 2 shows the simulated trajectory in space of the deposition head during the printing process. The color variation means the deviation [ $\mu m$ ] of the head in relation to the planned trajectory. In this case, the arms were modeled using the properties of the ABS plastic, which is the original material adopted in the Rostock project.

The maximum deviation is 1.2 mm, and is associated to the high speed displacements of the head, which occur when the head has to be positioned in a new printing area. The average deviation of the printer with ABS arms is  $296.45 \mu m$  and the standard deviation is  $55.6 \mu m$ . Usually the positioning error of this kind of printer is lower than 0.1 mm; however, the flexibility of the ABS arms caused an error of almost 0.3 mm.

## References

- [1] I. Bonev, The true origins of parallel robots. [www.parallemic.org/Reviews/Review007.html](http://www.parallemic.org/Reviews/Review007.html), May 2013.
- [2] W.L.V. Pollard, Position Controlling Apparatus. Patent US 2286571, 1942.
- [3] R. Clavel, Device for Displacing and Positioning an Element in Space. Patent WO/1987/003528, 1987.
- [4] P. Masarati, M. Morandini, P. Mantegazza, An efficient formulation for general-purpose multi-body/multiphysics analysis. *J. Comp. Nonlin. Dyn.* 9(4), October 2014, doi:10.1115/1.4025628.
- [5] J.C. Rocholl, Concept for a delta robot 3D printer. <https://github.com/jcrocholl/rostock>, 2012.
- [6] G.L. Ghiringhelli, P. Masarati, P. Mantegazza, A multibody implementation of finite volume beams. *AIAA Journal*, 38(1), pp. 131–138, 2000.
- [7] E.P. Okabe, P. Masarati, Dynamic modeling of a 3d printer based on a four arms scara mechanism. In *Proceedings of the ECCOMAS Thematic Conference on Multibody Dynamics*, 2015.

## Advance Modeling of Machine Tool Machining Process

Frédéric Cugnon<sup>1</sup>, Luke Berglind<sup>2</sup>, Denys Plakhotnik<sup>3</sup>, Erdem Ozturk<sup>2</sup>

<sup>1</sup>Samtech s.a.  
A Siemens company  
8 rue des chasseurs Ardennais, 4030 Liège,  
Belgium  
Frederic.cugnon@siemens.com

<sup>2</sup>AMRC  
University of Sheffield  
Wallis Way, Catcliffe  
Rotherham, S60 5TZ, UK  
l.berglind@sheffield.ac.uk  
e.ozturk@sheffield.ac.uk

<sup>3</sup>Moduleworks GmbH  
Henricistr. 50, 52072, Aachen, Germany  
denys@moduleworks.com

### Abstract

The Twin-Control European project [1] aims to develop a simulation system that integrates the different aspects that affect machine tool and machining performance, including lifecycle concepts, providing better estimation of machining performance than single featured simulation packages. This holistic simulation model will be linked to the real machines in order to update itself according to their real condition and to perform control actions that will lead to performance improvements.

The focus of this paper is on the dynamic modeling of the machine tool including its Computer Numeric Control (CNC), and its interaction with the machining process. To properly simulate modern high-speed machine tools, which show close interaction between the dynamic behavior of the mechanical structure, drives, and the CNC, it is crucial to build models that represent the flexibility of all components and their interactions [2][3]. To answer such requirements, we use 3D MBS and FEA methods for mechanical aspects, and 1D modeling for the CNC. Even if the concurrent use of these technologies is already used in some industrial sectors, it is quite new in the machine tool industry. This multi-model approach is usually inefficient because of limited integration between the different tools. This paper introduces an integrated methodology that combines MBS capabilities in a nonlinear FEA solver called SAMCEF Mecano [4][5]. It enables accurate modeling of the machine by considering FEA models of the components connected together by a set of flexible kinematical joints. Particular models are implemented to deal with drive-trains and motors dynamics.

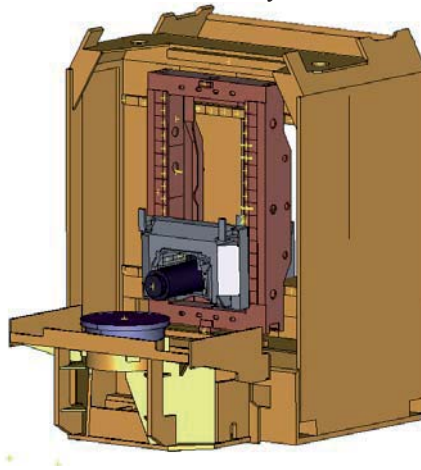


**Figure 1.** Multibody model of the test machine tool

To fully capture the dynamic behavior of the machine tool, force interactions between the cutting tool and the workpiece are also considered in this model. The general process for obtaining cutting forces is illustrated in Figure 2. First, the motions of the machine structure are coupled with workpiece CAD files to define how the tool is engaged in the workpiece at any point of the CNC program. Calculation of tool-workpiece engagement is based on a mixed discrete-continuous representation of the stock material, also known as the tri-dexel model [6]. Each discrete intersection point between the tri-dexel model representation and the cutting data (the sweep envelope surface of the moving tool geometry) is mapped, according to the tool feed direction, onto the milling tool surface. Due to discrete nature of the underlying model, a rasterization routing is used to provide a heuristic detecting continuous contact areas between the cutting tool and stock material. The resulting tool workpiece engagement data is then applied to a mechanistic cutting force model [6] to determine average cutting forces and spindle torque, or force and torque variations based on the rotation of the tool. The cutting forces obtained using this process is then applied to the machine structure model.

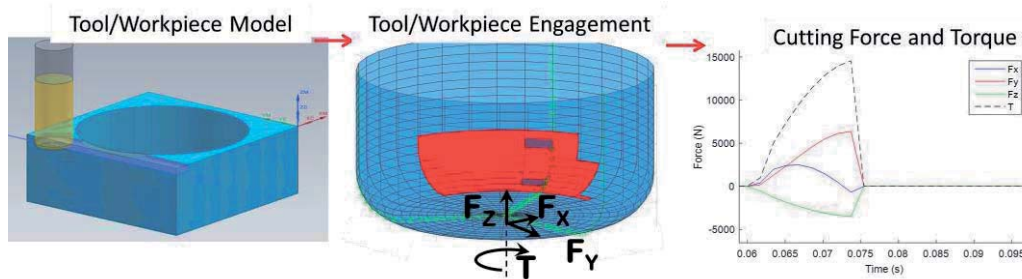


Figure 2. Process of obtaining cutting forces

A strong coupling between the mechatronic model of the machine tool and the machining simulation tool is implemented. Practically, a specialized cutting force element has been developed. It considers the dynamics of the tool tip combined with the tool-workpiece engagement determined from Module Works CAD/CAM for toolpath generation and simulation. The resulting relative dynamics of the tool with respect to the workpiece is used as input to generate cutting forces. Those are applied on the machine model at the spindle tip level, and generate some excitation of the model. To fulfill equilibrium at each step of the time integration process a Newton-Raphson iterative scheme is used, where cutting forces are updated and the associated iteration matrix is generated at each iteration.

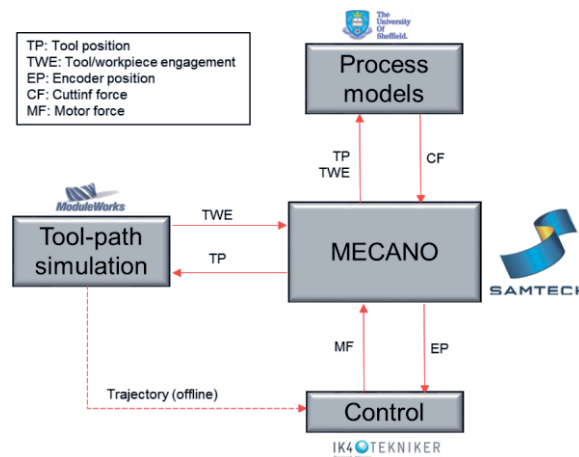


Figure 3. Coupling scheme

To illustrate this technology, a high-speed box-in-box 4 axes Urane25V3 machine from Comau is considered. A SIEMENS 840D CNC controls the motors of the different axis in order to follow the desired trajectories with minimum errors. In the built model, all frames are fully flexible, as the rails and skates that connect them. Those, as the linear motors, are represented by sets of flexible slider elements based on beam formulation. The control loops are modelled in MATLAB/Simulink, translated into a dynamic library that is associated to a specific control element used to manage the coupling between 1D models and the full flexible 3D model. The presented machine tool model will be validated considering simple machining sequences.

## Acknowledgments

The work presented in this paper is part of the research work still in progress in the project Twin-Control, funded under H2020 under grant agreement no. 680725, as part of the Factories of the Future initiative.

## References

- [1] Twin-Control website (<http://twincontrol.eu/>)
- [2] M. Ghassempouri, E. Vareilles and C. Fioroni. *Modelling and simulating the dynamic behavior of a high speed machine tool*, Samtech Users conference, 2003.
- [3] P. Morelle, D. Granville and M. Goffart. *SAMCEF for Machine Tools resulting from the EU MECOMAT project*, NAFEMS Seminar – Mechatronics in Structural Analysis, Wiesbaden, Germany, May 5-6, 2004
- [4] M. Géradin and A. Cardona A. (2001). *Flexible multi-body dynamics: a finite element approach*, John Wiley & Sons, 2001
- [5] Samtech. *SAMCEF V17.1 User manual*. 2016.
- [6] Moduleworks website (<http://www.moduleworks.com>)
- [7] Y. Altintas, Manufacturing Automation; Metal Cutting Mechanics, Machine Tool Vibrations, and CNC Design, 2nd Edition, Cambridge University Press, 2012.

## **Section**

# **BENCHMARK PROBLEMS**



# Comparison of Classical Multibody Simulation Methods with regard to the DAE Mathematica Solver

Rémi BARRERE<sup>1</sup>, Benjamin BOUDON<sup>2</sup>

<sup>1</sup>ENSMM  
University of Bourgogne Franche-Comté  
Besançon, France  
remi.barrere@ens2m.fr

<sup>2</sup>ISM (CNRS)  
Aix-Marseille Université,  
Institute Movement Science,  
Marseille, France  
benjamin.boudon@amu.univ.fr

## Abstract

Most complex mechanical systems are composed of kinematic closed loops or more generally are expressed with a dependent coordinate formulation. The dynamic equations for these systems without preliminary analysis of study of the geometry lead to differential algebraic equations (DAEs) which need special care to be solved.

The difficulties in solving numerical DAEs are summarized in [1, 2]. A recent and concise review of the methods for solving DAEs can also be found in [3]. One can find four main groups of methods: the direct resolution of the DAEs thanks to specific solvers [4], the reduction of the DAEs to ODEs using stabilization techniques such as the Baumgarte stabilization method to circumvent the drift of the constraints [5], the reduction of ODEs by solving the constraints to obtain a minimal coordinate formulation [6], and the conversion to ODEs by modifying the model (the penalty formulation or the singular perturbation method when only the fictitious potential energy and Rayleigh's damping function are considered [7]).

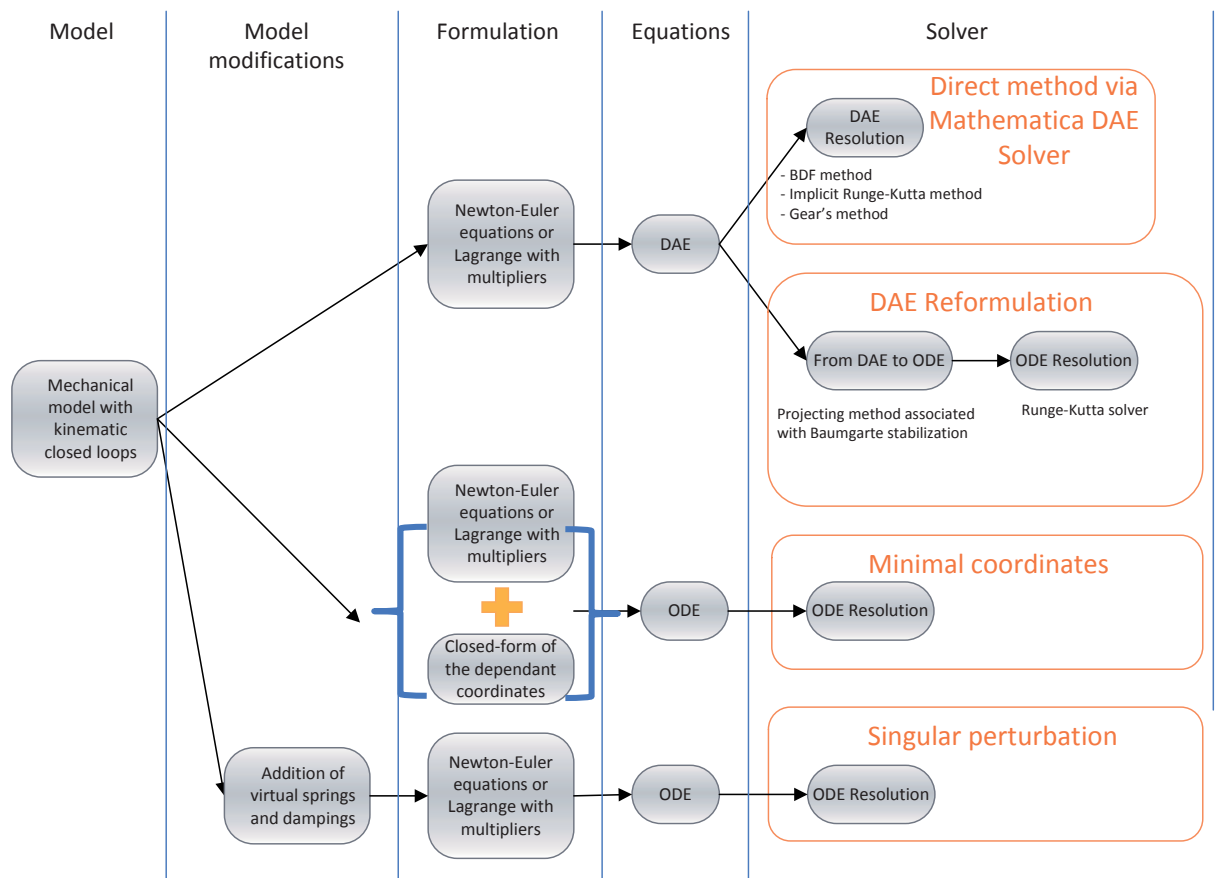


**Figure 1 - Simulation methods compared in this investigation**

In parallel, symbolic manipulations are used more and more in the multibody community either for modeling and simulation or in view of the pre-processing of embedded code. Moreover, it is worth noting that symbolic manipulation software such as Mathematica has also improved its numerical differential solvers. Besides, Mathematica coherently combines an editing front end, a computer algebra system, a symbolic programming language, numerical solvers, high quality visualization tools, various data processing modules, a C

code generator, parallel programming capabilities, plus cloud computing features in the latest versions [8, 9]. So, a trend emerges that consists of managing whole (multibody) projects within such a framework, including system modeling, equation generation, and symbolic, numerical or hybrid solving with the advantage of an integrated environment which remains the same.

In this context, the question arises: what level of confidence can we give to the DAE Mathematica solver? The main objective of this paper is to compare the Mathematica solver with classic simulation methods. Three methods have been considered: DAE to ODE reformulation, minimal coordinates and singular perturbations. These methods have been tested on simple case studies such as a slider crank.

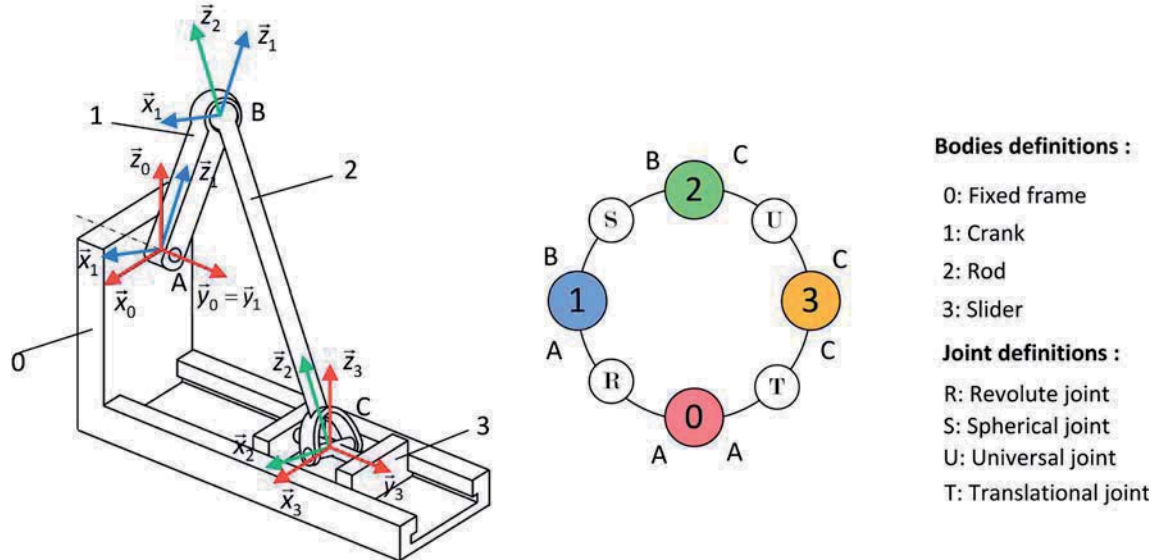


Figure 2 – Kinematic scheme and joints graph of the slider crank

## References

- [1] BAUCHAU O. A., LAULUSA A., Review of contemporary approaches for constraint enforcement in multibody systems, *Journal of Computational and Nonlinear Dynamics*, vol. 3, p. 011005, 2008.
- [2] LAULUSA A., BAUCHAU O. A., Review of classical approaches for constraint enforcement in multibody systems, *Journal of Computational and Nonlinear Dynamics*, vol. 3, p. 011004, 2008.
- [3] UCHIDA T. K., Real-time Dynamic Simulation of Constrained Multibody Systems using Symbolic Computation, PhD Thesis, University of Waterloo, Ontario, 2011.
- [4] BRENAN K. E., CAMPBELL S. L., PETZOLD L. R., *Numerical solution of initial-value problems in differential-algebraic equations* vol. 14: Siam, 1996.1611971225 1611971225
- [5] BAUMGARTE J., Stabilization of constraints and integrals of motion in dynamical systems, *Computer methods in applied mechanics and engineering*, vol. 1, pp. 1-16, 1972.
- [6] HILLER M., KECSKEMETHY A., Dynamics of multibody systems with minimal coordinates, in *Computer -Aided Analysis of Rigid and Flexible Mechanical Systems*, M. F. O. S. PEREIRAJ. A. C. AMBROSIO, Eds.: Kluwer Academic Publishers, pp. 61-100, 1994
- [7] WANG J., GOSSELIN C., CHENG L., Modeling and Simulation of Robotic Systems with Closed Kinematic Chains Using the Virtual Spring Approach, *Multibody System Dynamics*, vol. 7, pp. 145-170, 2001.
- [8] WOLFRAM S., *The Mathematica Book*: Wolfram Media, 2003
- [9] WOLFRAM S., *An Elementary Introduction to the Wolfram Language*: Wolfram Media, 2015

# Benchmark Problems for the Linearization of Multibody Dynamics

Francisco González<sup>1</sup>, Bruce Minaker<sup>2</sup>, Pierangelo Masarati<sup>3</sup>,  
Alberto Luaces<sup>1</sup>, David Vilela<sup>1</sup>, Javier Cuadrado<sup>1</sup>

<sup>1</sup>Laboratorio de Ingeniería Mecánica  
University of La Coruña  
Mendizábal s/n, 15403 Ferrol, Spain  
[f.gonzalez, aluaces,  
david.vilela]@udc.es, javicuad@cdf.udc.es

<sup>2</sup>Mechanical, Automotive, & Materials Engineering  
University of Windsor  
401 Sunset Avenue, Windsor, ON, Canada  
bminaker@uwindsor.ca

<sup>3</sup>Dipartimento di Scienze e Tecnologie Aerospaziali  
Politecnico di Milano  
via La Masa 1, 20156, Milano, Italy  
pierangelo.masarati@polimi.it

## Abstract

Multibody formulations express the dynamics of a mechanical system in terms of a set of  $n$  generalized coordinates  $\mathbf{q}$  and their derivatives. These may be independent; alternatively they can be related by  $m$  kinematic constraint equations  $\Phi(\mathbf{q}, t) = \mathbf{0}$ . In the latter case, the dynamics is expressed by a system of Differential Algebraic Equations (DAEs)

$$\mathbf{M}\ddot{\mathbf{q}} = \mathbf{f} + \mathbf{f}_c \quad (1a)$$

$$\Phi(\mathbf{q}, t) = \mathbf{0} \quad (1b)$$

where  $\mathbf{M}$  is the  $n \times n$  mass matrix,  $\mathbf{f}$  comprises the applied and velocity-dependent forces, and  $\mathbf{f}_c$  stands for the constraint reactions. If the coordinates  $\mathbf{q}$  are independent, then the dynamics is described by Eq. (1a) alone with  $\mathbf{f}_c = \mathbf{0}$ , which is a system of Ordinary Differential Equations (ODEs).

A wide variety of coordinate selections, formulations, and numerical methods to deal with the solution of such systems have been proposed during the last decades [1], which has prompted the multibody dynamics community to put forward a significant number of benchmark problems [2]. These benchmark problems serve two purposes. First, they allow researchers to validate newly proposed methods or software implementations. Second, they can be used as a means to compare the efficiency, ease of use, and accuracy of different algorithms and codes, providing useful information for the selection of the most appropriate ones for a given application.

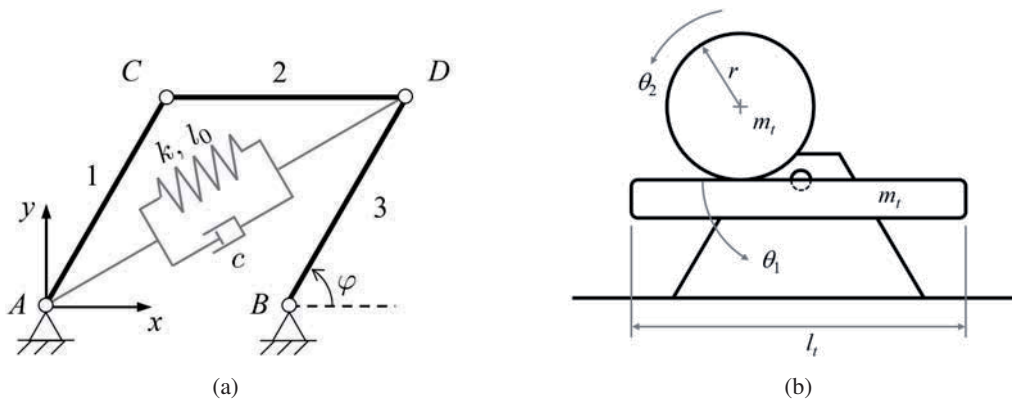


Figure 1: Two of the proposed benchmark problems: (a) Four-bar linkage with spring and damper elements; (b) A wheel rolling on a tipping table.

Regardless of the approach followed to obtain Eqs. (1), the resulting system is highly nonlinear in most cases. However, some applications such as modal analysis require a linearized expression of the dynamics. In others, like stability analysis, the availability of a linear model makes it simpler to gain insight into the system behaviour. The linearization of Eqs. (1) can be achieved in many different ways and several approaches have already been published in the multibody literature. The properties of each approach depend on the coordinate selection and the way in which kinematic constraints are treated [3]. Each method has different accuracy and efficiency properties and conveys information about the system dynamics in its own particular way.

In this work, we introduce a series of test problems to benchmark linearization methods for multibody dynamics. Some of these have already been added to the IFToMM library of Computational Benchmark Problems [2]. The examples can be categorized into two main groups:

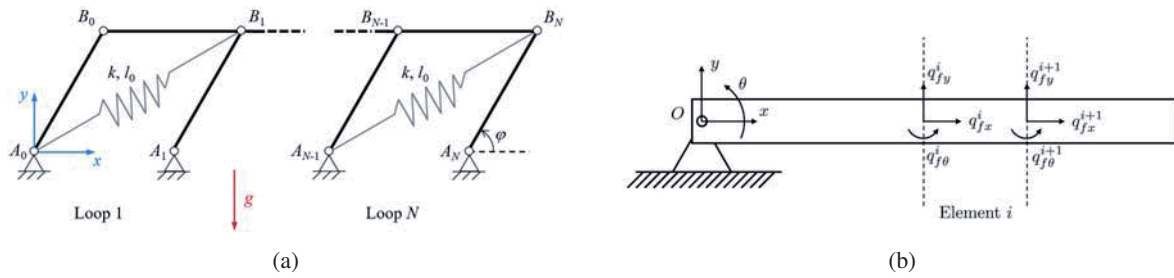


Figure 2: Benchmark problems with variable dimensions: (a)  $N$ -loop four-bar linkage; (b) A flexible pendulum modelled with finite elements.

- Simple problems with known analytical solutions (Fig. 1): a simple rigid pendulum, a four-bar linkage with spring and damper elements, a wheel rolling on a tipping table.
- Variable-size problems that can be used to assess the computational efficiency of the methods. Among these, two kinds of problems can be distinguished: heavily constrained systems with relatively few degrees of freedom, e.g., the  $N$ -loop version of the four-bar linkage in Fig. 2a, in which the number of kinematic constraints is similar to system size ( $m \approx n$ ); and systems with many more variables than constraints ( $m \ll n$ ), such as flexible beams and pendulums (Fig. 2b).

The proposed test problems have been used to validate and compare the performance of three multibody linearization methods based on velocity transformations, direct eigenanalysis, and a penalty formulation respectively [3]. Results showed that these methods were able to match the theoretical solutions of the first type of problems. The linearization of the proposed examples highlighted the differences between the three approaches in terms of computational efficiency and accuracy of the obtained eigenvalues.

### Acknowledgments

The first author acknowledges the support of the Spanish Ministry of Economy through its post-doctoral research program Juan de la Cierva, contract No. JCI-2012-12376.

### References

- [1] O. A. Bauchau. Flexible Multibody Dynamics, Springer, 2011.
- [2] IFToMM Technical Committee for Multibody Dynamics. Library of Computational Benchmark Problems. URL: <http://www.iftomm-multibody.org/benchmark>, 2014.
- [3] F. González, P. Masarati, J. Cuadrado, and M. A. Naya. Assessment of Linearization Approaches for Multibody Dynamics Formulations, accepted in Journal of Computational and Nonlinear Dynamics, d.o.i.: 10.1115/1.4035410, 2016.

## Computational modelling of the parallel cable mechanism with the added active structure

Radek Bulín<sup>1</sup>, Michal Hajžman<sup>1</sup>, Pavel Polach<sup>1</sup>, Zbyněk Šika<sup>2</sup>, Jan Zavřel<sup>2</sup>

<sup>1</sup> Faculty of Applied Sciences  
University of West Bohemia  
Univerzitní 22, 306 14 Pilsen, Czech Republic  
[rbulin, mhajzman, ppolach]@ntis.zcu.cz

<sup>2</sup> Faculty of Mechanical Engineering  
Czech Technical University in Prague  
Technická 4, 166 07 Prague, Czech Republic  
[zbynek.sika, jan.zavrel]@fs.cvut.cz

### Abstract

The main advantages of the cable-driven parallel kinematic mechanisms (PKM) are the achievement of a lower moving inertia, which leads to a higher mechanism speed, lower production costs, a large range of motion, the possibility of antibacklash property and easy reconfiguration. The typical disadvantages of the cable-driven PKM are the relatively narrow frequency bandwidth of their feedback motion control and the problems with the accurate positioning of the end-effector. The promising research direction for solution of problems is the concept of multi-level mechanisms with the hierarchical structure composed of a parallel cable-driven mechanism for large and slow motions and an active structure connected to the mechanism platform for the low and high frequency motions [1]. Parallel structures consisting of cables with negligible flexural stiffness have to deal with the problem of complex vibrations. This paper deals with the creation of the multibody model of a particular multilevel mechanism combining the cable-driven parallel mechanism and the added piezo structure.

The Quadrosphere mechanism was chosen as a reference cable manipulator mechanism equipped with the active structure. This mechanism consists of a platform connected with the active piezo structure to the spherical joint, which is mounted to the basis frame. The cardan angles of the spherical joint are accurately measured by sensors. In each corner of the platform a lightweight fiber is connected. Each fiber is led through a guiding pulley to the vertically placed linear drive. All of the fibers should operate only in tension and the general position of the platform is determined by the vertical positions of the drives. The active piezo structure consists of six piezo-actuators, which are designed to enhance accuracy of the platform positioning and also compensate the platform vibrations.

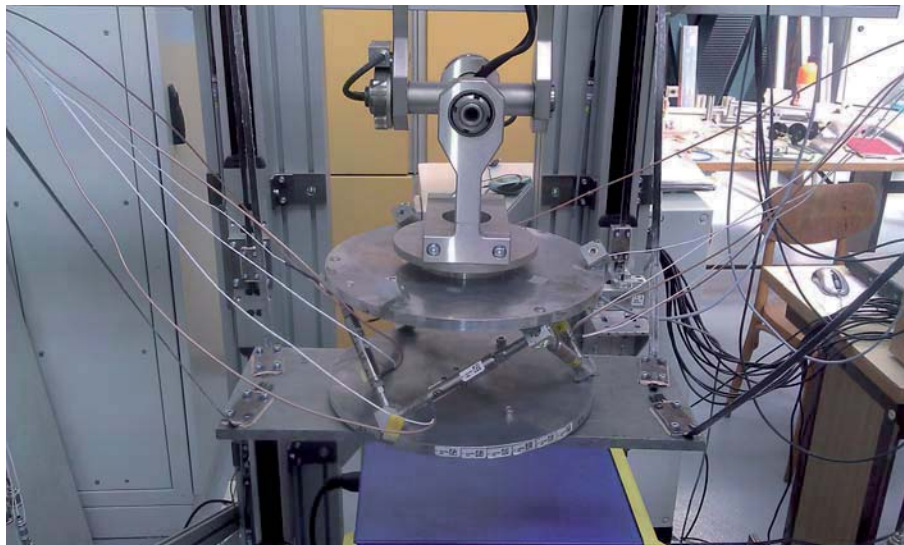


Figure 1: Quadrosphere mechanism with added piezostructure.

The multibody model of the Quadrosphere mechanism was created in the MSC.Adams code. It consists of 16 bodies, which are connected by various constraints. In Figure 2 left, the kinematic scheme of the mechanism is shown. The bodies are represented by rectangles and the connections are represented by circles. Letter R means rotational constraint and T means translational constraint. The dot-dash line represents the fibers, which goes from the drives through the pulleys to the platform corners. A simplified cable model of the MSC.Adams Machinery plugin was used for the modelling of fibre and thus the fibers are modelled using nonlinear forces, which are active only in tension. Due to the low weight of the fiber, the inertia and gravitational effect on the fiber was neglected.

The paper also deals with various modelling techniques of the proposed active structure. The basic model of the active structure contains six linear springs, each for each piezo-actuator. The stiffness of the spring is calculated to reflect the axial stiffness of the piezo-actuator defined by the manufacturer and the stiffness of the used flexible

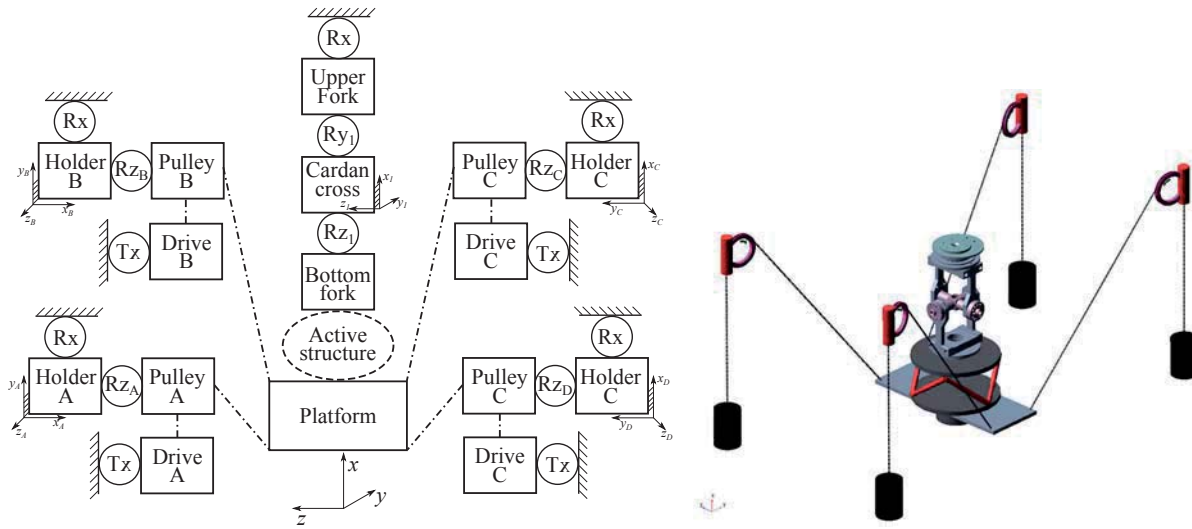


Figure 2: Kinematic scheme of the Quadrosphere mechanism and the visualisation in MSC.Adams.

connections. The ejection of the actuator is performed by the changing of the spring free length. A complex model representing the piezo-actuator was also employed. The complex model contains several bodies in order to reflect the bending stiffness of the flexible connections, too.

In order to investigate the dynamic properties of the whole model one of the piezo-actuators was excited using chirp signal, which goes up to 400 Hz in 5 seconds. The resultant single-sided amplitude spectra of two selected rotation angles of the spherical joint are shown in Figure 3.

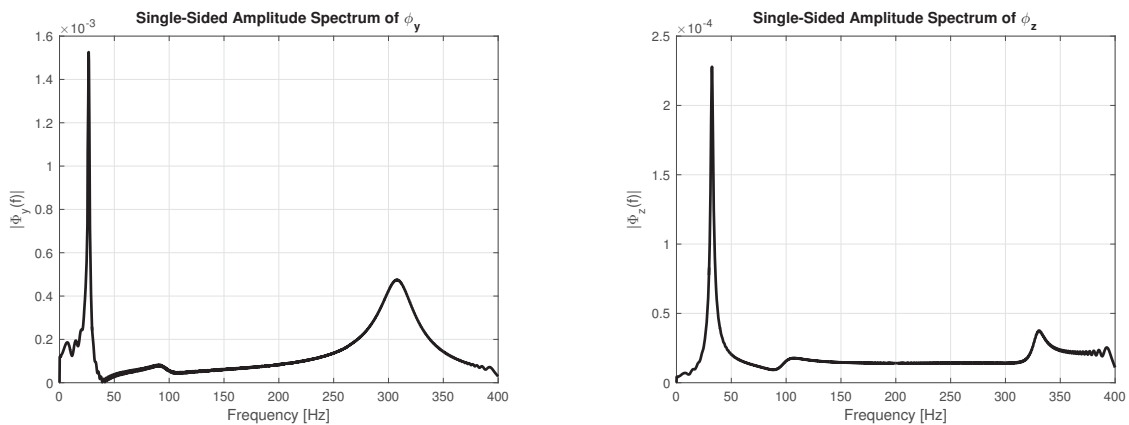


Figure 3: The amplitude spectra of two rotation angles using chirp excitation of selected piezo-actuator.

## Acknowledgments

The paper has originated in the framework of solving the project of the Czech Science Foundation No. 15-20134S entitled “Multi-level Light Mechanisms with Active Structures”.

## References

- [1] X. Duan, Y. Qiu, J. Du, Z. Zhao, Q. Duan. Real-time motion planning for the macro-micro parallel manipulator system. *Proceedings of IEEE International Conference on Robotics and Automation*, pages 4214-4219, Shanghai, 2011.
- [2] M. Hajžman, R. Bulín, Z. Šika, P. Svatoš. Usage of the particle swarm optimization in problems of mechanics. *Applied and Computational Mechanics*, 10:15-26, 2016.
- [3] P. Svatoš. *Optimization and motion control of cable-driven parallel mechanisms*. Ph.D. Thesis, Czech Technical University, Prague, 2016.

## **Section**

# **CONTROL AND OPTIMIZATION**



# Fully Coupled Topology Optimization of Flexible Multibody Systems with Constraints

Alexander Held<sup>1</sup>, Thomas Kohlsche<sup>2</sup>, Robert Seifried<sup>1</sup>

<sup>1</sup>Institute of Mechanics and Ocean Engineering  
Hamburg University of Technology  
Eißendorfer Straße 42, 21073 Hamburg, Germany  
{alexander.held,robert.seifried}@tuhh.de

<sup>2</sup>Institute of Modelling and Computation  
Hamburg University of Technology  
Denickestraße 17, 21073 Hamburg, Germany  
thomas.kohlsche@tuhh.de

## Abstract

In the last years considerable progress has been made in the topology optimization of flexible multibody systems. On the one hand, a variety of methods for the efficient and precise modeling and simulation of flexible multibody systems has been developed as, for instance, nonlinear finite element methods or the floating frame of reference approach, see [2]. On the other hand, weakly and fully coupled optimization procedures have been studied and presented in which the structure of the flexible components are best adapted to the dynamical loads. In this structural optimization stress and displacement constraints often have to be considered, which is, in particular for fully coupled methods, a difficult task. In this work, two different strategies are used to take constraints into account in the fully coupled optimization of flexible multibody systems. First, the pointwise constraints are transformed into functional constraints [1]. Second, the constraints are aggregated using the Kreisselmeier-Steinhausen function [4,5].

## Constrained Dynamic Optimization Problems

Fully coupled methods consider the whole dynamic behavior of the flexible multibody system within the simulation period. Provided that the geometry or the material properties of the flexible bodies are parameterized by the vector of design variables  $\mathbf{p} \in \mathbb{R}^h$  the equations of motion of the flexible multibody system reads

$$\begin{aligned} \dot{\mathbf{y}} &= \mathbf{v}(\mathbf{y}, \mathbf{z}, t) \\ \mathbf{M}(\mathbf{y}, t, \mathbf{p})\dot{\mathbf{z}} &= \mathbf{f}(\mathbf{y}, \mathbf{z}, t, \mathbf{p}) \end{aligned} \quad (1)$$

where  $\mathbf{M}$  is the mass matrix,  $\mathbf{f}$  the right-hand-side vector, and  $\mathbf{y} = \mathbf{y}(t, \mathbf{p})$  and  $\mathbf{z} = \mathbf{z}(t, \mathbf{p})$  are the generalized position and velocity coordinates. Given the initial conditions  $\mathbf{y}(t=0) = \mathbf{y}^0$  and  $\mathbf{z}(t=0) = \mathbf{z}^0$  the equations of motion (1) can be solved by a numerical integration. The performance of the current design  $\mathbf{p}$  can be determined by evaluating a scalar objective function  $\psi(\mathbf{p}) \in \mathbb{R}$  from the results of the time integration.

Mathematically the optimization problem of a fully coupled structural optimization problem can be formulated as

$$\begin{aligned} &\underset{\mathbf{p}}{\text{minimize}} && \psi(\mathbf{p}) \\ &\text{subject to} && \dot{\mathbf{y}} - \mathbf{v} = \mathbf{0}, \\ & && \mathbf{M}\dot{\mathbf{z}} - \mathbf{f} = \mathbf{0}, \\ & && h_j(\mathbf{y}, \mathbf{p}, t) \leq 0, \quad t^0 \leq t \leq t^1, \quad j = 1(1)m, \\ & && p_i^l \leq p_i \leq p_i^u, \quad i = 1(1)h. \end{aligned} \quad (2)$$

That is, the objective function  $\psi$  shall be minimized for a flexible multibody systems which is subjected to the equations of motion (1) and, in addition,  $m$  pointwise inequality constraints  $h_j$ , as well as lower and upper bounds of the design variables,  $p_i^l$  and  $p_i^u$ , respectively.

The solution of the optimization problem (2) is not trivial. In particular, the inequality constraints  $h_j$  are difficult to consider in the optimization process, since they have to be fulfilled at each time point between the initial time  $t^0$  and the final time  $t^1$ . One possibility is to discretize the problem and consider the constraints only at the grid points of the time integration of the dynamic system. However, depending on the dynamic system the number of grid points might become very large and, hence, this approach very costly. Alternatively, in [1] the pointwise inequality constraints  $h_j$  are transformed into an integral-type constraint  $\bar{h}_j$  as follows

$$\bar{h}_j = \int_{t^0}^{t^1} \langle h_j(\mathbf{y}, \mathbf{p}, t) \rangle dt = 0, \quad \text{where} \quad \langle h_j \rangle = \begin{cases} h_j, & h_j \geq 0 \\ 0, & h_j < 0 \end{cases}. \quad (3)$$

Thus, instead of considering the inequality constraint  $h_j$  at a large number of discrete time points, only a single equality constraints has to be evaluated and taken into account.

A third way is to aggregate the constraints into a single composite function as, for instance, the Kreisselmeier-Steinhauser (KS) function

$$\text{KS}(\mathbf{p}, \gamma) = h_{\max} + \frac{1}{\gamma} \ln \left( \frac{1}{m} \sum_j \sum_i \exp(\gamma(h_j(\mathbf{y}(t_i), \mathbf{p}, t_i) - h_{\max})) \right), \quad (4)$$

where pointwise constraints are evaluated at discrete time points, see [5] for details. In the KS function  $h_{\max}$  is the maximal value of all inequality constraints and  $\gamma$  is the aggregation parameter. It is worth noting that for the efficient sensitive analysis of Eq. (3) and (4) semi-analytical approaches, such as the adjoint variable method, can be used.

In this work, both the transformation (3) and the KS function (4) are used to consider displacement constraints in the fully coupled topology optimization of a flexible slider-crank mechanism [3]. The results of both approaches are compared with regard to the efficiency of the optimization procedure, including the sensitivity analysis, and the quality of the optimization results.

## References

- [1] E. J. Haug, J. S. Arora. Applied optimal design: mechanical and structural systems. John Wiley & Sons, 1979.
- [2] A. Shabana. *Dynamics of Multibody Systems*. Cambridge University Press, Cambridge, 2005.
- [3] A. Held, S. Knüfer, R. Seifried. Topology Optimization of Members of Dynamically Loaded Flexible Multi-body Systems using Integral Type Objective Functions and Exact Gradients. Proceedings of the 11th World Congress on Structural and Multidisciplinary Optimization, Sydney, Australia, 2015.
- [4] N. M. Poon, J. R. Martins. An adaptive approach to constraint aggregation using adjoint sensitivity analysis. *Structural and Multidisciplinary Optimization*, 34(1), 61-73.
- [5] K. F. Bloss, L. T. Biegler, W. E. Schiesser. Dynamic Process Optimization through Adjoint Formulations and Constraint Aggregation. *Industrial & engineering chemistry research*, 38(2), 421-432.

# Variational multirate integration in discrete mechanics and optimal control

T. Gail<sup>1</sup>, S. Ober-Blöbaum<sup>2</sup>, S. Leyendecker<sup>1</sup>

<sup>1</sup> Department of Mechanical Engineering  
University Erlangen-Nuremberg  
Immerwahrstrasse 1, 91058 Erlangen, Germany  
[tobias.gail, sigrid.leyendecker]@fau.de

<sup>2</sup> Department of Engineering Science  
University of Oxford  
Parks Road, OX1 3PJ Oxford, United Kingdom  
sina.ober-blobaum@eng.ox.ac.uk

## Abstract

We consider mechanical systems with dynamics on different time scales. They impose contradicting requirements on the numerical integration. For a stable integration of the fast dynamics, tiny time steps are needed. However, for the slow dynamics, larger time steps are accurate enough. In this work, this contradiction is addressed using multirate integration schemes. The mechanical system is split into slow and fast parts and simulated on a macro and a micro time grid, [1, 2], leading to computing time savings. Since computing time is also an issue when solving optimal control problems numerically, we introduce the variational multirate integration scheme, derived in [3], into discrete mechanics and optimal control (DMOC) [4].

Let a mechanical system be described by a Lagrangian  $L(q, \dot{q}) = T(q, \dot{q}) - U(q)$ , where  $T$  is the kinetic energy and  $U$  is the potential energy, with configuration  $q \in \mathbb{R}^{k_q}$  and velocity  $\dot{q} = \frac{dq}{dt} \in \mathbb{R}^{k_q}$ . We assume it to be possible, to split the configuration into slow variables  $q^s \in \mathbb{R}^{k_q^s}$  and fast variables  $q^f \in \mathbb{R}^{k_q^f}$  where  $q = (q^s, q^f)^T$  and  $k_q = k_q^s + k_q^f$ . Further, we assume that  $U$  can be split into a slow potential  $V$  and a fast potential  $W$  where  $U(q) = V(q) + W(q^f)$ . The action  $S$  is the time integral over the Lagrangian. In the Lagrange-d'Alembert principle, the virtual work of the external forces  $f(q, \dot{q}, u)$ , which depend on the control path  $u \in U \subset \mathbb{R}^{k_u}$ , is added to the first variation of the action [4]. To account for the slow and fast dynamics, the forces are split into slow forces  $f^s \in \mathbb{R}^{k_u^s}$  and fast forces  $f^f \in \mathbb{R}^{k_u^f}$  with  $f = (f^s, f^f)^T$ . Then, also the controls need to be split into slow controls  $u^s \in \mathbb{R}^{k_u^s}$  and fast controls  $u^f \in \mathbb{R}^{k_u^f}$  where  $u = (u^s, u^f)^T$  and  $k_u = k_u^s + k_u^f$ . The equations of motion for the slow and fast part, the multirate forced Euler-Lagrange equations, of the mechanical system can be derived with the Lagrange-d'Alembert principle. A continuous optimal control problem with the multirate forced Euler-Lagrange equations in the time interval  $[t_0, t_1]$  reads

$$\begin{aligned}
 \min_{q, u} J[q, u] &= \int_{t_0}^{t_1} C(q, \dot{q}, u) dt \\
 \text{subject to} \quad 0 &= \frac{\partial [T(q, \dot{q}) - V(q)]}{\partial q^s} - \frac{d}{dt} \left( \frac{\partial T(q, \dot{q})}{\partial \dot{q}^s} \right) + f^s(q, \dot{q}, u) \\
 0 &= \frac{\partial [T(q, \dot{q}) - (V(q) + W(q^f))]}{\partial q^f} - \frac{d}{dt} \left( \frac{\partial T(q, \dot{q})}{\partial \dot{q}^f} \right) + f^f(q, \dot{q}, u) \\
 0 &= a(q, \dot{q}, u) \\
 0 &\leq b(q, \dot{q}, u)
 \end{aligned} \tag{1}$$

with the objective functional  $J$  being the time integral over the cost function  $C$ , equality constraints  $a$  representing e.g. initial and final boundary conditions, and inequality and path constraints  $b$ .

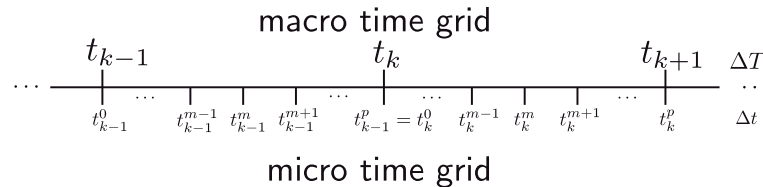


Figure 1: Synchronised macro and micro time grids

Following the first discretise then optimise approach in DMOC, we replace the optimal control problem in Equation (1) with its discrete counterpart. For the multirate integration, we introduce two synchronised time grids, a macro and a micro time grid, as illustrated in Figure 1, where there are  $p$  micro time steps per macro time step. The discrete slow variables and controls are approximated on the macro time grid and the discrete fast variables and controls on the micro time grid. Using the multirate forced variational integrator and discrete

equality constraints and inequality constraints the discretised optimal control problem can be stated as a non linear constrained optimisation problem.

Using the multirate forced variational integrator, the number of optimisation variables is reduced compared to the use of DMOC on the fine grid for the complete system. The number of optimisation variables is  $\frac{t_N}{\Delta t} \left( \frac{1}{p} (k_q^s + k_u^s) + (k_q^f + k_u^f) \right)$ , where  $t_N$  is the simulation end time. Then, there are  $1/p$  times less slow configuration and control variables using the multirate integrator ( $p > 1$ ) than for DMOC ( $p = 1$ ). We expect that we need less computing time in solving the optimal control problem. We show that this is the case numerically by means of an example systems. The spring pendulum is a pendulum where a small point mass is attached to a large mass with a passive spring. This underactuated pendulum is illustrated in Figure 2 and it shows the angle  $\phi$  which is actuated with the torque  $\tau$  and the length of the spring  $\psi$ , where there is no angular degree of freedom between the small and large mass.

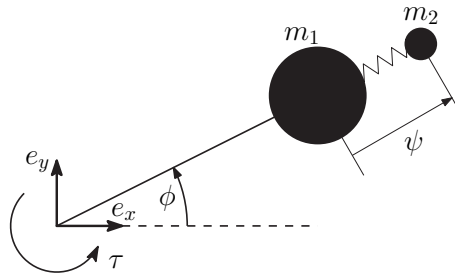


Figure 2: The spring pendulum with forcing and variables

In the computations, the example system performs an upswing from the lower equilibrium position to the upper equilibrium position and the spring goes from a stretched length to its gravitational slack length while the control effort is minimised. Figure 3 shows an example for such a rest to rest manoeuvre for the spring pendulum for  $p = 20$ . The plot on the left shows the angle of the pendulum  $\phi$  in blue and the length of the spring  $\psi$  in green on the macro time grid and  $\psi_{mic}$  in red on the micro time grid versus time. The plot on the right shows the  $x$ - and  $y$ -coordinates of the two point masses. The computing time for the shown rest to rest manoeuvre was reduced from 10.45s for single rate to 1.19s using the multirate integrator with  $p = 20$ .

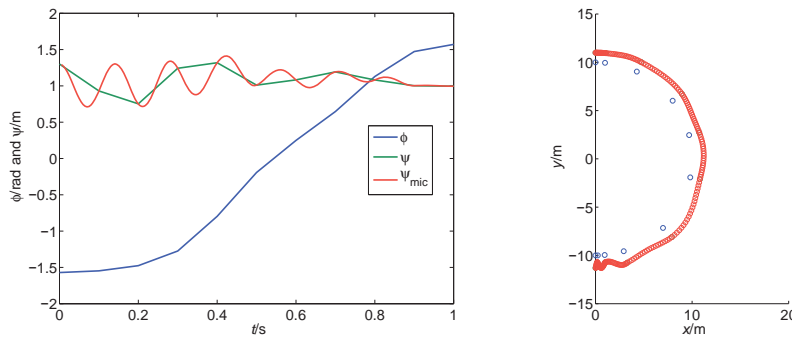


Figure 3: Example of a rest to rest manoeuvre for the spring pendulum with  $p = 20$

## References

- [1] M. Arnold. Multi-rate time integration for large scale multibody system models. In P. Eberhard, editor, IUTAM Symposium on Multiscale Problems in Multibody System Contacts, pages 1-10, Springer, 2007.
- [2] C.W. Gear, D.R. Wells. Multirate linear multistep methods. BIT, 24:484-502, 1984.
- [3] S. Leyendecker, S. Ober-Blöbaum. A variational approach to multirate integration for constrained systems. In J. Samin and P. Fiset editors, Multibody Dynamics, Computational Methods in Applied Sciences, pages 97-121, Springer, 2013.
- [4] S. Ober-Blöbaum, O. Junge, J.E. Marsden. Discrete Mechanics and Optimal Control: An Analysis. ESAIM: Control, Optimisation and Calculus of Variations, 17:322-352, 2011.

# Forward sensitivity analysis of the index-3 augmented Lagrangian formulation with projections

Daniel Dopico, Francisco González, Mariano Saura, Daniel García-Vallejo

Laboratorio de Ingeniería Mecánica  
Universidade da Coruña  
C/ Mendizábal s/n, 15403, Ferrol, Spain  
[ddopico,f.gonzalez]@udc.es

Dpto. de Ingeniería Mecánica.  
Universidad Politécnica de Cartagena  
Cartagena, Spain  
msaura.sanchez@upct.es

Dpto. de Ingeniería Mecánica y Fabricación  
Universidad de Sevilla  
Sevilla, Spain  
dgvallejo@us.es

## Abstract

Sensitivity analysis of the dynamics of multibody systems is essential for design optimization and optimal control. Dynamic sensitivities, when needed, are often calculated by means of finite differences but, depending on the number of parameters involved, this procedure can be very demanding in terms of time, and the accuracy obtained can be very poor in many cases.

In previous works, the sensitivity equations of index-3 DAE, index-1 DAE, Baumgarte and penalty formulations [1, 2, 3, 4, 5, 6] were derived, using either direct differentiation (forward sensitivity), adjoint variable (adjoint sensitivity) or both methods depending on the publication.

The index-3 augmented Lagrangian formulation with velocity and acceleration projections (the ALI3-P formulation) is an efficient and robust method to carry out the forward dynamics simulation of multibody systems modeled in dependent coordinates, which outperforms the behavior of the aforementioned formulations. It was extensively used for the real-time simulation of different systems with human and hardware in the loop, some of them including complex phenomena like flexibility [7], contact with friction [8, 9] or non-holonomic constraints [10].

In this paper, the forward sensitivity equations of the ALI3-P formulation presented in [10] are derived and applied to a test case.

Let us consider the equations of motion (EOM) depending on the vector of parameters  $\boldsymbol{\rho} \in \mathbb{R}^p$ . The objective function is defined in terms of the parameters, on the states  $\mathbf{q}, \dot{\mathbf{q}}, \ddot{\mathbf{q}} \in \mathbb{R}^n$ , and on the Lagrange multipliers  $\boldsymbol{\lambda} \in \mathbb{R}^m$ ,

$$\psi = w(\mathbf{q}_F, \dot{\mathbf{q}}_F, \ddot{\mathbf{q}}_F, \boldsymbol{\rho}_F, \boldsymbol{\lambda}_F) + \int_{t_0}^{t_F} g(\mathbf{q}, \dot{\mathbf{q}}, \ddot{\mathbf{q}}, \boldsymbol{\lambda}, \boldsymbol{\rho}) dt. \quad (1)$$

The problem is to obtain the sensitivity of such a cost function, expressed by the following gradient,

$$\nabla_{\boldsymbol{\rho}} \psi^T = (w_{\mathbf{q}} \mathbf{q}_{\boldsymbol{\rho}} + w_{\dot{\mathbf{q}}} \dot{\mathbf{q}}_{\boldsymbol{\rho}} + w_{\ddot{\mathbf{q}}} \ddot{\mathbf{q}}_{\boldsymbol{\rho}} + w_{\boldsymbol{\lambda}} \boldsymbol{\lambda}_{\boldsymbol{\rho}} + w_{\boldsymbol{\rho}})_{t_F} + \int_{t_0}^{t_F} (g_{\mathbf{q}} \mathbf{q}_{\boldsymbol{\rho}} + g_{\dot{\mathbf{q}}} \dot{\mathbf{q}}_{\boldsymbol{\rho}} + g_{\ddot{\mathbf{q}}} \ddot{\mathbf{q}}_{\boldsymbol{\rho}} + g_{\boldsymbol{\lambda}} \boldsymbol{\lambda}_{\boldsymbol{\rho}} + g_{\boldsymbol{\rho}}) dt. \quad (2)$$

In equation (2) the derivatives of functions  $w$  and  $g$  are known, since the objective function has a known expression. On the contrary, the magnitudes  $\mathbf{q}_{\boldsymbol{\rho}}$ ,  $\dot{\mathbf{q}}_{\boldsymbol{\rho}}$ ,  $\ddot{\mathbf{q}}_{\boldsymbol{\rho}}$  and  $\boldsymbol{\lambda}_{\boldsymbol{\rho}}$  are the sensitivity matrices solution of a set of  $p$  DAE systems, called the Tangent Linear Model (TLM) of the equations of motion.

The test case considered in this work is the five-bar mechanism shown in Figure 1. The sensitivities of this system are well known because they were previously obtained using several different formulations and approaches [11, 12]. The problem posed was the sensitivity analysis of following objective function dependent on the solution of the equations of motion:

$$\psi = \int_{t_0}^{t_F} (\mathbf{r}_2 - \mathbf{r}_{20})^T (\mathbf{r}_2 - \mathbf{r}_{20}) dt \quad (3)$$

where  $\mathbf{r}_2$  is the global position of the point 2 and  $\mathbf{r}_{20}$  is the initial position (at  $t = t_0$ ) of the same point. As parameters to obtain the sensitivities, the natural lengths of the springs were chosen  $\boldsymbol{\rho}^T = [L_{01}, L_{02}]$ .

## Acknowledgments

The support of the Spanish Ministry of Economy and Competitiveness (MINECO) under project DPI2016-81005-P and the post-doctoral research contract Juan de la Cierva No. JCI-2012-12376 is greatly acknowledged.

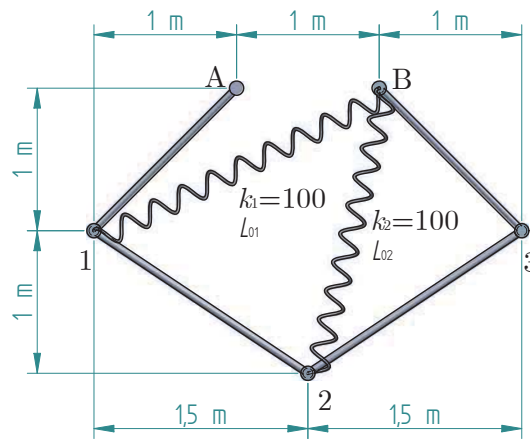


Figure 1: The five-bar mechanism

## References

- [1] C. O. Chang, P. E. Nikravesh. Optimal design of mechanical systems with constraint violation stabilization method. *Journal of Mechanisms, Transmissions and Automation in Design*, 107(4):493–498, 1985. doi: 10.1115/1.3260751.
- [2] E. Haug. Computer aided optimal design: structural and mechanical systems, chapter Design sensitivity analysis of dynamic systems. Number 27 in NATO ASI series. Series F, Computer and systems sciences. Springer-Verlag, 1987.
- [3] D. Bestle, J. Seybold. Sensitivity analysis of constrained multibody systems. *Archive of Applied Mechanics*, 62:181–190, 1992. doi:10.1007/BF00787958.
- [4] J. Pagalday, A. Avello. Optimization of multibody dynamics using object oriented programming and a mixed numerical-symbolic penalty formulation. *Mechanism and Machine Theory*, 32(2):161–174, 1997. doi:10.1016/S0094-114X(96)00037-7.
- [5] A. Schaffer. Stability of the adjoint differential-algebraic equation of the index-3 multibody system equation of motion. *SIAM Journal on Scientific Computing*, 26(4):1432–1448, 2005. doi:10.1137/030601983.
- [6] A. Schaffer. Stabilized index-1 differential-algebraic formulations for sensitivity analysis of multi-body dynamics. *Proceedings of the Institution of Mechanical Engineers Part K- Journal of Multi-Body Dynamics*, 220(3):141–156, 2006. doi:10.1243/1464419JMBD62.
- [7] J. Cuadrado, R. Gutierrez, M. Naya, P. Morer. A comparison in terms of accuracy and efficiency between a mbs dynamic formulation with stress analysis and a non-linear fea code. *International Journal for Numerical Methods in Engineering*, 51(9):1033–1052, 2001.
- [8] D. Dopico, A. Luaces, M. Gonzalez, J. Cuadrado. Dealing with multiple contacts in a human-in-the-loop application. *Multibody System Dynamics*, 25(2):167–183, 2011. doi:10.1007/s11044-010-9230-y.
- [9] R. Pastorino, E. Sanjurjo, A. Luaces, M. A. Naya, W. Desmet, J. Cuadrado. Validation of a Real-Time Multibody Model for an X-by-Wire Vehicle Prototype Through Field Testing. *Journal of Computational and Nonlinear Dynamics*, 10(3):031006, 2015. doi:10.1115/1.4028030.
- [10] D. Dopico, F. González, J. Cuadrado, J. Kövecses. Determination of holonomic and nonholonomic constraint reactions in an index-3 augmented lagrangian formulation with velocity and acceleration projections. *Journal of Computational and Nonlinear Dynamics*, 9(4):041006–041006, 2014. doi:10.1115/1.4027671.
- [11] D. Dopico, Y. Zhu, A. Sandu, C. Sandu. Direct and adjoint sensitivity analysis of ordinary differential equation multibody formulations. *Journal of Computational and Nonlinear Dynamics*, 10 (1)(1):1–8, 2014. doi:10.1115/1.4026492.
- [12] D. Dopico, A. Sandu, C. Sandu, Y. Zhu. *Multibody Dynamics*, chapter Sensitivity Analysis of Multibody Dynamic Systems Modeled by ODEs and DAEs, 1–32. Computational Methods in Applied Sciences. Springer International Publishing Switzerland, 2014. doi:10.1007/978-3-319-07260-9.

# Position Control of Flexible Chain Using Wave Based Control

Michael Valášek, Filip Šáfr, Zdeněk Neusser, Jan Pelikán,

Faculty of Mechanical Engineering  
Czech Technical University in Prague  
Technická 4, 166 07 Prague 6, Czech Republic  
[Michael.Valasek; Filip.Safr; Zdenek.Neusser; Jan.Pelikan]@fs.cvut.cz

## Abstract

Quality of motion control of a mechanical system is closely related to system's dynamic properties which usually limit the overall performance of mechatronic system. There are different approaches how to deal with the dynamic response of a mechanical system in order to achieve acceptable positioning times and accuracy. This paper describes an application of wave based control which is one of the newer approaches in motion control.

Theory of wave based control as well as an experiment will be demonstrated on 1D chain of lumped masses and springs (Fig. 1). Such chain can also stand as a representation of 1D continuum and eventually be expanded to model 3D continuum.

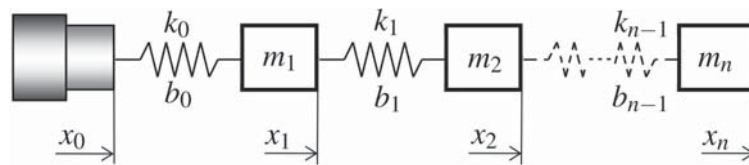


Figure 1: Chain of concentrated masses

$$m_i \ddot{x}_i = b_i(\dot{x}_{i+1} - \dot{x}_i) + k_i(x_{i+1} - x_i) - b_{i-1}(\dot{x}_i - \dot{x}_{i-1}) - k_{i-1}(x_i - x_{i-1}) \quad \text{for } i = 1, \dots, n-1$$

$$m_n \ddot{x}_n = -b_{n-1}(\dot{x}_n - \dot{x}_{n-1}) - k_{n-1}(x_n - x_{n-1}) \quad (1)$$

Motion of chain with  $n$  lumped masses depicted in Fig. 1 can be traditionally described by a system of  $n$  ordinary differential equations (1). The wave based control however originates from different description based on an idea of mechanical waves propagating through the chain [1]. In this description a virtual wave propagates through the mechanical system from the actuator to the free end of the chain where it is redirected back in the system and propagates in opposite direction toward the actuator. Position of each lumped mass  $x_i(t)$  in any given time is then determined by a sum of the forward traveling wave  $a_i(t)$  and the returning wave  $b_i(t)$ . Such mathematical model of physical system by means of transfer functions is depicted in Fig. 2, where  $X_i(s)$ ,  $A_i(s)$  and  $B_i(s)$  are Laplace transforms of masses positions  $x_i(t)$  and wave signals  $a_i(t)$ ,  $b_i(t)$ .

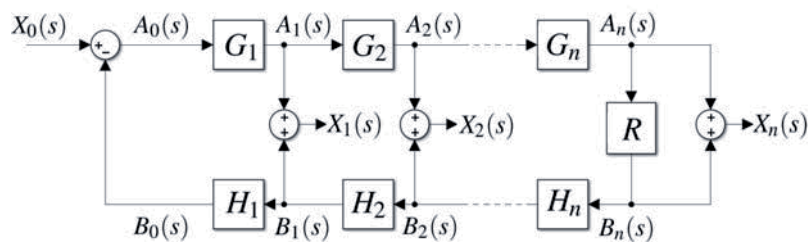


Figure 2: Scheme of wave based model

The idea of wave based control is then in sensing the returning wave and controlling the actuator in such a way that this returning wave is absorbed instead of being reflected back to the system. This control action terminates the motion at the desired position while effectively suppressing vibrations in the system. Various researches and experiments had shown, that control system based on this idea is applicable on many different control related problems with beneficial impact on stability and control performance [2].

However the key feature of wave based control is the fact, that very little has to be known about the controlled system's dynamic properties to successfully implement the control (as opposite to for example input shaping or model predictive control [3]). Neither the knowledge of complete actual state of the system during the control is needed. The control action is based on very localized information about the system (for example in the case of 1D lumped masses chain it is position of the first mass  $x_1$  and roughly the stiffness  $k_0$  and first mass itself  $m_1$ ).

The main goal of this paper is to introduce experimental results of wave based control applied on real mechanical system. This system was built as a physical (rotary/torsional) representation of an idealized chain of concentrated masses and springs.

The system itself can be seen in Fig. 3. It consists of three identical aluminum flywheels connected with two thin steel shafts, third (shorter) shaft connects the first flywheel to an actuator, which in this case is servomotor Omron R88M-W1K030F-BS2. Each of the flywheels is supported by two deep groove ball bearings and fitted with rotary encoders Renishaw SR030A to measure its position. Total moment of inertia of each flywheel assembly is  $0,016\text{kgm}^2$ . The connecting shafts are made of steel wire with diameter  $6\text{mm}$  and are connected to flywheels by bellows type couplings.

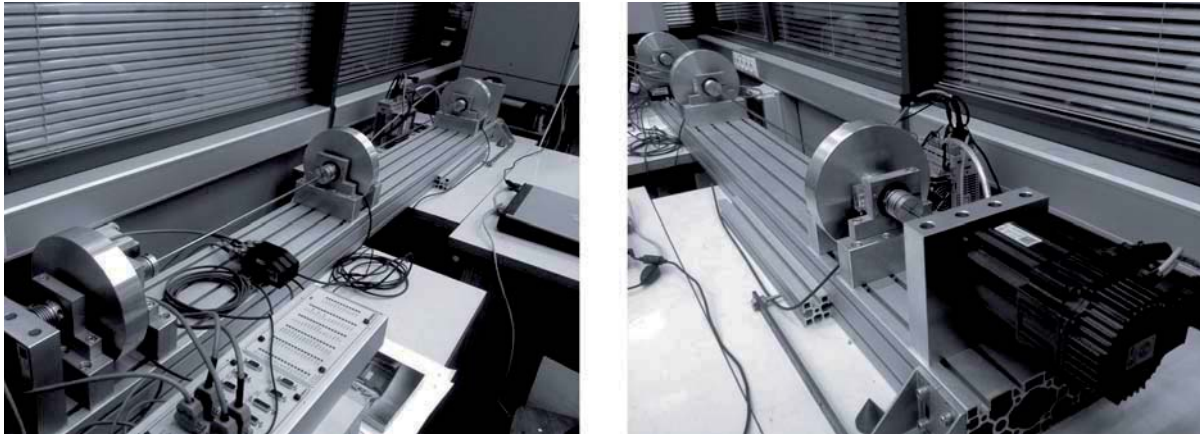


Figure 3: Mechanical system used for measurements

To control the actuator Yaskawa SGDM-10DE servo drive was used in traditional cascade control mode with position feedback loop closed from servomotor's encoder. This combination of servomotor and servo drive can introduce peak moment  $9,5\text{Nm}$  into the mechanical system.

The signal with servomotor desired position used as an input into the servo drive was generated by the wave based control loop. The input for this control loop (i.e. signal sensing the returning wave) was taken from the first flywheel's encoder.

### Acknowledgments

The research has been supported by the Czech Science Foundation, Project No. P101-11-2110 "Advanced input shaping control for precise positioning of mechanisms" and Project No. 17-20943S "Active multidimensional vibration absorbers for complex mechanical structures based on delayed resonator method".

### References

- [1] W. J. O'Connor. Wave-based Modelling and Control of Lumped, Multibody Flexible. *Proceedings of Multibody Dynamics*, ECCOMAS Thematic Conference, 2005.
- [2] M. Valášek. O. Marek. Stability analysis of wave-based control of flexible systems. The 1st Joint International Conference on Multibody System Dynamics IMSD: 1-8, Lappeenranta, 2010.
- [3] P. Beneš. M. Valášek. Optimized re-entry input shapers. *Journal of Theoretical and Applied Mechanics*, 54(2), pp. 353-368. 2016.

## Modelling of slender elements in offshore engineering using the rigid finite elements method

Iwona Adamiec-Wójcik, Łukasz Drąg, Stanisław Wojciech

Faculty of Management and Transport  
University of Bielsko-Biala  
Willowa 2, 43-309 Bielsko-Biala Poland  
ldrag@ath.bielsko.pl

### Abstract

In marine technology, commonly used elements are ropes and risers. These are slender elements with the dominance of one dimension (length), which during operation are subjected to large lifting movements caused by ship manoeuvres, sea waving and currents. When modelling elements of this type, many difficulties may be encountered caused by, among other causes, the need to include additional dynamic loads caused by the water environment impact, such as associated water and hydrodynamic drag force that can significantly affect the analysed systems' dynamics [1,2]. Dynamic models including slender elements are often formulated for the purpose of control. But this requires the adoption of several simplifying assumptions. The model has to balance the accuracy of modelling (mapping of the system's main features) with its numerical efficiency (the shortest possible simulation time of a single calculation case). In control applications, the considered systems' motion equations need to be repeatedly integrated, for instance when solving optimization tasks or when preparing learning sets for artificial neural networks (ANN). Neural networks can then be used for real time control [3].

Widely used in slender structures' modelling is the rigid finite elements method (RFEM) [4]. In the classical approach [5], rigid finite elements (rfe) have, in the case of spatial arrangements, six degrees of freedom. They are connected by spring-damping elements (sde), which take into account the susceptibilities: to shear and bending (in both directions), longitudinal and torsional. This approach produces high-frequency vibration in dynamic analysis of a system digitized by this method. The advantage of this method is, however, the block structure of mass matrix. The formulation of this method presented in [6,7] enables the elimination of large shear and longitudinal stiffness, and provides continuity of displacements. At the same time, it makes the mass matrix full, which significantly reduces the numerical efficiency. In turn, [8] shows a modification of RFEM that allows the elimination of longitudinal and shear deformations and does not require significant changes in the motion equation generation algorithm. It allows to take advantage of the both current formulations without taking over their disadvantages. It allows the elimination of high shear stiffness, and (if allowed) of longitudinal and torsional stiffness, without significant changes in the overall motion equation generation algorithm. It also retains the block structure of mass matrix. This is achieved by separating rigid finite elements, as in the classical method, and then combining them by geometric constraint equations.

Motion and constraint equations of elements  $0 \div n$  of a slender link can be written in the form:

$$\mathbf{M}\ddot{\mathbf{q}} - \mathbf{D}\mathbf{F} = \mathbf{f}, \quad (1.1)$$

$$\mathbf{D}^T \ddot{\mathbf{q}} = \mathbf{G}. \quad (1.2)$$

where:  $\mathbf{M} = \text{diag}\{\mathbf{M}_0, \mathbf{M}_1, \dots, \mathbf{M}_n\}$  – block-diagonal mass matrix

$\mathbf{M}_i = \mathbf{A}_i - \mathbf{M}_{i,a}$ ,  $\mathbf{A}_i, \mathbf{M}_{i,a}$  – mass, riser, and added water matrices

$\mathbf{q} = [\mathbf{q}_0^T, \mathbf{q}_1^T, \dots, \mathbf{q}_n^T]^T$  – vector of member's generalized coordinates

$\mathbf{f} = [\mathbf{f}_0^T, \mathbf{f}_1^T, \dots, \mathbf{f}_n^T]^T$  – vectors of generalized forces ( $\mathbf{f}_i = \mathbf{b}_i + \mathbf{f}_{i,w}$ ),

$\mathbf{f}_{i,w}$  – vector of generalized forces, incl. forces from water associated impact

$\mathbf{F}$  – vector of constraint reaction

$\mathbf{D} = \overline{\mathbf{D}} - \mathbf{D}_i$  – block-diagonal matrix of constraint reaction coefficients

$\mathbf{G}$  – vector of the right sides of constraint equations

Movement at each rigid finite element is described by vector components:

$$\mathbf{q}_i = [x_{i,1} \quad x_{i,2} \quad x_{i,3} \quad \varphi_{i,3} \quad \varphi_{i,2} \quad \varphi_{i,1} \quad \Delta_i]^T, \quad (2)$$

where:  $x_{i,1}, x_{i,2}, x_{i,3}$  – coordinates of the centre of mass of element  $i$ ,

$\varphi_{i,1}, \varphi_{i,2}, \varphi_{i,3}$  – Euler angles of rotation,

$\Delta_i$  – longitudinal elongation.

An important feature of the slender element description method presented in [8] is the ability to easily reduce the number of generalized coordinates describing the motion of rigid elements. Their number and the corresponding rigid element stiffness coefficients, significantly affect the computation time. Therefore, the issue of reduction of redundant degrees of the elements' freedom becomes critical.

Presented at this conference will be a model with five degrees of freedom in the task of riser bending moment optimisation (Fig .1), in which the vector of generalized coordinates is:

$$\mathbf{q}_i = [x_{i,1} \quad x_{i,2} \quad x_{i,3} \quad \varphi_{i,3} \quad \varphi_{i,2}]^T. \quad (3)$$

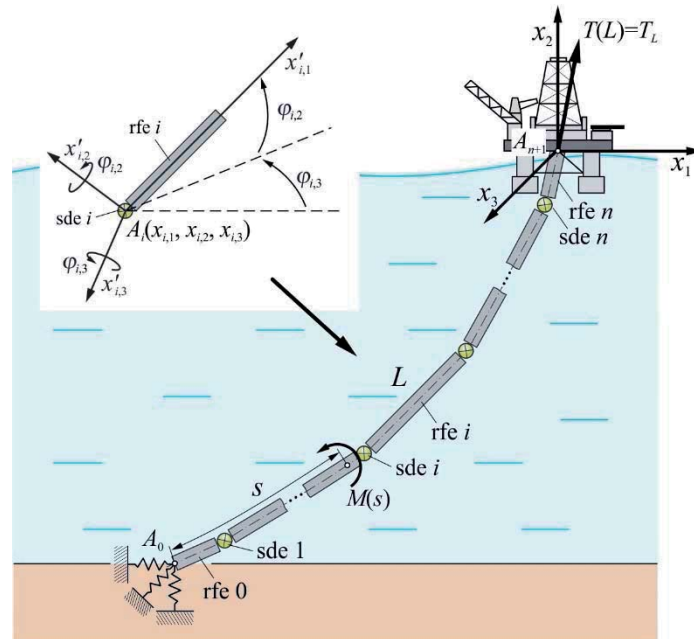


Figure 1. Analysed riser design

The longitudinal and torsion strains (stiffness coefficients of the spring and damping elements reproduce only the member's bending susceptibility) is neglected by deleting the last two rows and columns in matrices  $\mathbf{A}_i$ . Whereas in matrices  $\bar{\mathbf{D}}$  and  $\mathbf{D}_i$  and in vectors  $\mathbf{f}_i$  the two last rows should be deleted (removed). It is acceptable and justified in studies of ropes' and risers' dynamics. This results in the capacity to increase the step of system motion equations' integration.

The model was comprehensively validated by comparison with results of measurement of and calculations obtained with other models [9] in terms of the own vibration frequency, static deflection and maximum bending moments.

## References

- [1] I. Adamic-Wójcik, L. Brzozowska, Ł. Drag. An analysis of dynamics of risers during vessel motion by means of the rigid finite element method. *Ocean Engineering*. 106:102-114, 2015.
- [2] X. S. Xu, S. W. Wang. A flexible segment model based dynamics calculation method for free hanging marine risers in re-entry. *China Ocean Engineering*. 26(1):139-152, 2012.
- [3] Ł. Drag. Model of an artificial neural network for payload positioning in sea waves. *Ocean Engineering*. 115:123-134, 2016.
- [4] E. Wittbrodt, I. Adamic-Wójcik, S. Wojciech. *Dynamics of flexible multibody system, Rigid Finite Element Method*. Springer, Berlin, Heidelberg, New York, 2006.
- [5] J. Kruszewski, W. Gawroński, E. Wittbrodt, F. Nejbar, S. Grabowski: *Rigid Finite Element Method*. Arkady, Warszawa, 1975 (In Polish).
- [6] I. Adamic-Wójcik. *Modelling dynamics of multibody systems using homogenous transformations*. Bielsko-Biała University Press, Bielsko-Biała, 2003.
- [7] S. Wojciech. *The dynamics of plane link mechanisms with the flexibility of links and the friction as well as the clearance in the joints*. Scientific Papers of Lodz University of Technology, Mechanika 66, 1984 (in Polish).
- [8] Ł. Drag. Application of dynamic optimisation to the trajectory of cable-suspended load. *Nonlinear Dynamics*. 84(3):1637-1653, 2016.
- [9] I. K. Chatjigeorgiou. A finite difference formulation for the linear and nonlinear dynamics of 2D catenary risers. *Ocean Engineering*. 35:616-636, 2008.

# Active Vibrations Attenuation by Controlling Relative Motion of Selected Masses, FE Modeling

Walerian Szyszkowski, Ehsan Sharbati

Department of Mechanical Engineering  
University of Saskatchewan  
57 Campus Dr, Saskatoon, S7N5A9, Canada  
walerian.szyszkowski@usask.ca

## Abstract

If internal/external passive damping is almost absent in a vibrating system (main body) then the attenuation effects can be generated by imposing a precisely synchronized relative motion of its one or more components (parts). The dynamic interaction between the main body and the moving parts triggers the Coriolis type forces that are capable of producing both attenuation and amplification effects in every cycle of the system's vibrations. The attenuation effects are made prevailing by carefully controlling the relative motion's phase and frequency [1]. This provides a unique means for actively reducing vibrations in the system. A new finite element (FE) procedure is presented that handles interaction of a main body of any shape with several masses moving along arbitrary paths. The procedure is suitable for control purposes, it treats the moving part as a controller (with its imposed motion as input and the system's response as output) to generate its motion patterns resulting in attenuation.

The 'standard' FE analyses (such as used in vehicle-bridge or vehicle-rail tract simulations involving typically only constant, i.e. not controlled, relative velocities [2]) are essentially inapplicable to such a problem, mostly because it requires imposing too complex geometrical constraints on the relative motion of the components considered.

In our procedure the main body (Figure 1a) can be meshed by any elements appropriate to simulating its vibrations with sufficient accuracy. A controlled part of mass  $m$  is then forced to move along a prescribed path relative to the system. The path itself is modeled by a guiding beam attached to the vibrating body at nodes (Figure 1b). The properties of the beam represent either a real guiding rail or they may be fictitious. The moving mass interacts with the system via the beam, and at a particular instant only one beam element is affected by it. This element, referred to as the composite element, and the forces related to the relative motion (referred to as the Coriolis forces), are indicated in Figure 1c.

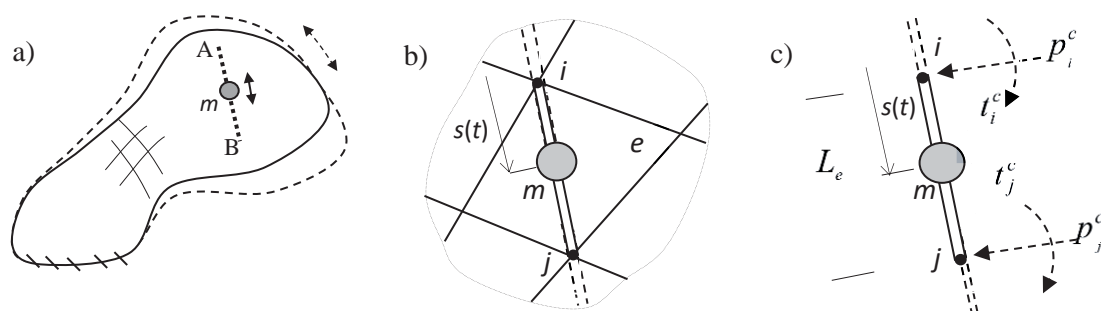


Figure 1: The vibrating system (a) the guiding beam (b), and the composite element (c)

Due to the relative motion the mass matrix of the composite beam is time-dependent. This makes, however, the mass matrix for the whole system also time-dependent that substantially complicates the analysis.

As shown in [3], in order to identify directly the Coriolis forces in the composite element, the inertia forces for the composite element are considered in the form:

$$\frac{d}{dt}[M_e(t)\dot{u}_e] = M_e(t)\ddot{u}_e + C_e\dot{u}_e = M_e(t)\ddot{u}_e + f_e^c \quad (1)$$

where  $C_s = \frac{dM_e}{dt} = m\dot{s} \frac{\partial}{\partial s} (N^T N)$  can be treated as an 'instantaneous' damping matrix (where  $\mathbf{N}=\mathbf{N}(\mathbf{s}(t))$  are the values of the beam's shape functions at the current mass location). The term  $f_e^c = C_e \dot{u}_e$  defines the nodal Coriolis forces indicated in Fig 1c. The matrix  $C_s$  and vector  $f_e^e$  depend explicitly on the current relative velocity  $\dot{s}$  of the mass and implicitly on its current position between the nodes of the element (the position is hidden in functions  $\mathbf{N}$ ).

Formula (1) permits writing the element equation in the following forms (in order to concentrate on the active attenuation any passive damping is omitted):

$$M_e(t)\ddot{u}_e + C_e \dot{u}_e + K_e u_e = F_e \quad \text{or} \quad M_e(t)\ddot{u}_e + K_e u_e = F_e - f_e^c \quad (2)$$

The first form indicates how the relative motion relates to periods of attenuation ( $C_s > 0$  if  $\dot{s} > 0$ ) and to periods of amplification ( $C_s < 0$  if  $\dot{s} < 0$ ), while the second form is more suitable for the practical simulation due to the fact that all the LHS terms can be routinely handled by typical FE software (in our case by ANSYS), in which  $f_e^e$  on the RHS can be easily calculated and added at each time step of the integration procedure. The system's attenuation is achieved by controlling forces  $f_e^e$  that are to be maximized in the periods of attenuation and minimized in the periods of amplification. The control scheme and the implementation and accuracy of the procedure will be discussed in details.

As illustration the test case of using relative motion of two small masses to attenuate vibrations of a frame is presented in Figure 2. For this particular case an effective active damping ratio of about 2.7% was generated.

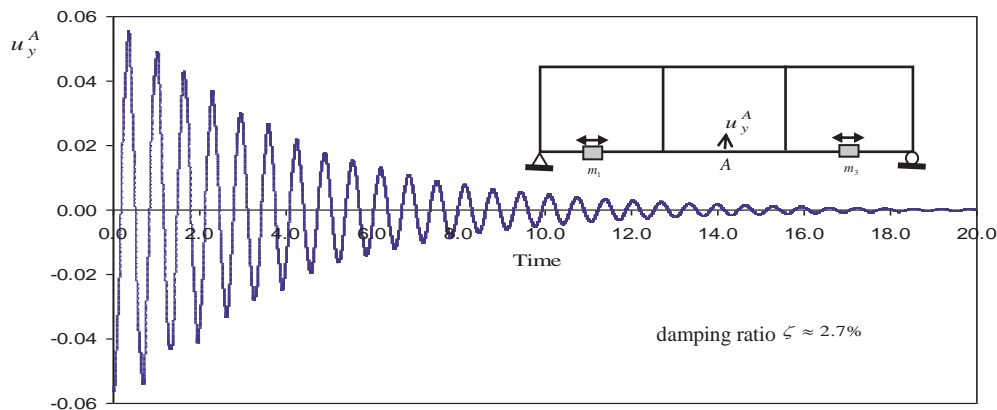


Figure 2: The response of vibrating frame controlled by motion of two masses.

## References

- [1] D.S.D. Stilling and W. Szyszkowski, Controlling angular oscillations through mass reconfiguration: a variable length pendulum case. *International Journal of Non-Linear Mechanics*, 37:89, 2002.
- [2] Y.B. Yang and C.W. Lin, Vehicle-bridge interaction dynamics and potential applications, **J. of Sound and Vibration**, 284:205, 2005
- [3] W. Szyszkowski and E. Sharbati, On the FEM modeling of mechanical system controlled by relative motion of a member: A pendulum-mass interaction test case, **Finite Elements in Analysis and Design**, 45:730, 2009

# On Control of Robot Manipulators with Flexible Joints

Aleksandr Andreev, Olga Peregudova

Faculty of Mathematics, Information and Aviation Technologies  
Ulyanovsk State University  
Leo Tolstoy street, 42, 432017 Ulyanovsk, Russia  
AndreevAS@ulsu.ru, peregudovaoa@gmail.com

## Abstract

A considerable number of researches have investigated the control problem for robot manipulators with flexible joints [1] - [14]. By use a singular perturbation theory an adaptive control approach was proposed in [1] for flexible-joint robot manipulators under the assumption of weak joint elasticity. By use a passivity-based approach an adaptive control scheme was proposed in [2] regardless of the joint flexibility value. By use an integral manifold approach an adaptive controller for flexible joint robot was obtained in [4]. The control results which are obtained in [1], [2] and [4] assume the full state measurement of the elastic joint robots, namely the control inputs are computed using link and motor shaft positions and velocities. Both the smooth output tracking control regulator with dynamical feedback linearization and the variable structure control scheme for the flexible joint manipulators are obtained in [3]. To define globally tracking controllers three stabilization techniques such as decoupling-based schemes, backstepping design procedure and passivity-based approach [6] have been applied.

The control results in [6]–[11] assume the availability of the link positions, velocities, accelerations, jerks as well as of the motor velocities.

The objective of the work is to design a controller that will provide a asymptotic stability of a program motion of a manipulator with flexible joints by use only motor position sensors and link accelerometers.

Consider the dynamic model of robot manipulators with elastic gearboxes, i.e. elastic joints, defined by the following equations [13]

$$A(q)\ddot{q} + C(q, \dot{q})\dot{q} + g(q) + D(\dot{q} - \dot{Q}) + K(q - Q) + d(q, \dot{q}) = 0 \quad (1)$$

$$J\ddot{Q} + D(\dot{Q} - \dot{q}) + K(Q - q) = u \quad (2)$$

where  $q \in \mathbb{R}^n$  and  $Q \in \mathbb{R}^n$  represent the link angles and motor angles respectively,  $A(q) \in \mathbb{R}^{n \times n}$  is the inertia matrix for the rigid links,  $J \in \mathbb{R}^{n \times n}$  is the diagonal matrix of actuators inertias reflected to the link side of the gears,  $J = \text{diag}\{j_1, j_2, \dots, j_n\} > 0$ , the Coriolis and centrifugal torques are described by  $C(q, \dot{q})\dot{q}$ ,  $g(q)$  represents the gravitational terms,  $D = \text{diag}\{d_1, d_2, \dots, d_n\} > 0$  is the viscosity matrix of the springs at the joints,  $d(q, \dot{q})$  is the vector of the link viscous damping,  $K = \text{diag}\{k_1, k_2, \dots, k_n\} > 0$  is the joint stiffness matrix and  $u \in \mathbb{R}^n$  is the input torque.

For the robot model (1), (2), define a set  $X$  of the program motions as

$$X = \{q^{(0)}(t) : [t_0, +\infty) \rightarrow \mathbb{R}^n : \|q^{(0)}(t)\| < g_0, \|\dot{q}^{(0)}(t)\| < g_1, \|\ddot{q}^{(0)}(t)\| < g_2\}$$

where functions  $q^{(0)}(t)$  are differentiable at least two times with respect to  $t$ ,  $g_i$  ( $i = 0, 1, 2$ ) are some positive constants,  $t_0 = \text{const} \geq 0$ ,  $\|\cdot\|$  is Euclid vector norm.

We assume that  $Q$  and  $\dot{q}$  are directly measured. Define as measured output  $z \in \mathbb{R}^{2n}$  the vector  $z = (z_1, z_2)' = (Q, \dot{q})'$ . The stabilization problem can be stated as that of constructing a control law  $u = u(t, Q, \dot{q})$  which provides an asymptotic stability for a given program motion  $q^{(0)}(t) \in X$  of the robot (1), (2).

For the dynamical model (1), (2), define the new state vector  $(q, \dot{q}, S)'$  and the new control input  $v$  as follows

$$S = D\dot{Q} + K(Q - q) \quad (3)$$

$$v = DJ^{-1}u + (DJ^{-1}D - K)\dot{q} + KD^{-1}Kq - KD^{-1}KQ \quad (4)$$

Then, we obtain the state equations as

$$A(q)\ddot{q} + C(q, \dot{q})\dot{q} + g(q) + D\dot{q} + d(q, \dot{q}) = S \quad (5)$$

$$\dot{S} = (-DJ^{-1} + KD^{-1})S + v \quad (6)$$

Let  $q^{(0)}(t) \in X$  be some program motion. Define the function  $S = S^{(0)}(t)$  as

$$S^{(0)}(t) = A(q^{(0)}(t))\ddot{q}^{(0)}(t) + C(q^{(0)}(t), \dot{q}^{(0)}(t))\dot{q}^{(0)}(t) + g(q^{(0)}(t)) + D\dot{q}^{(0)}(t) + d(q^{(0)}(t), \dot{q}^{(0)}(t)) \quad (7)$$

We use the following linear dynamical observer [13]

$$\begin{aligned} \dot{\xi}_1 &= \xi_3 + L_1(z_1 - \xi_1), & \dot{\xi}_2 &= \xi_4 + L_2(z_1 - \xi_1) \\ \dot{\xi}_3 &= -J^{-1}K\xi_1 + J^{-1}K\xi_2 - J^{-1}D\xi_3 + J^{-1}D\xi_4 + J^{-1}u + L_3(z_1 - \xi_1), & \dot{\xi}_4 &= L_4(z_1 - \xi_1) + z_2 \end{aligned} \quad (8)$$

where the gain matrixes  $L_j = \text{diag}\{l_{j1}, l_{j2}, \dots, l_{jn}\}$ ,  $j = 1, 2, 3, 4$  have the following form [13]

$$\begin{aligned} l_{1i} &= a_{3i} - d_i/j_i, & l_{2i} &= j_i a_{1i}/k_i - j_i d_i a_{0i}/k_i^2 \\ l_{3i} &= a_{2i} - d_i a_{3i}/j_i + (d_i^2 - k_i j_i)/j_i^2, & l_{4i} &= j_i a_{0i}/k_i \end{aligned} \quad (9)$$

the coefficients  $a_{ji}$  ( $j = 1, \dots, 4$ ,  $i = 1, \dots, n$ ) of the associated characteristic polynomial

$$p_i^*(\lambda) = \lambda^4 + a_{3i}\lambda^3 + a_{2i}\lambda^2 + a_{1i}\lambda + a_{0i}$$

with the desired set of roots  $\lambda_{ji}$ ,  $j = 1, 2, 3, 4$ .

By use the backstepping design procedure [15] and the result [16] we obtain that the control law

$$\begin{aligned} u &= (E - JKD^{-2})B(\xi_4 - \dot{q}^{(0)}(t) + p(\xi_2 - q^{(0)}(t))) + D^{-1}JB(\ddot{q} - \ddot{q}^{(0)}(t) + \\ &+ p'(\xi_2 - q^{(0)}(t))(\xi_4 - \dot{q}^{(0)}(t))) - D^{-1}J\dot{S}^{(0)}(t) + (KJD^{-2} - E)S^{(0)}(t) + \\ &+ (D^{-1}JK - D)\xi_4 - JK^2D^{-2}\xi_2 + JK^2D^{-2}Q \end{aligned}$$

with (7) stabilizes the program motion  $q^0(t) \in X$  of the robot (1), (2).

### Acknowledgments

The research was supported by the Russian Foundation for Basic Research (grant No. 15-01-08482) and the Ministry of Education and Science of Russia within the framework of state order for scientific research.

### References

- [1] F. Ghorbel, J.Y. Hung and M.W. Spong. Adaptive control of flexible-joint manipulators. IEEE Control Systems Magazine, 9-13, 1989.
- [2] R. Lozano and B. Brogliato. Adaptive control of robot manipulators with flexible joints. IEEE Transactions on Automatic Control, 37, 2:174-181, 1992.
- [3] H. Sira-Ramirez, S. Ahmad, M. Zribi. Dynamical feedback control of robotic manipulators with joint flexibility. IEEE Transactions on Systems, Man and Cybernetics, 22, 4:736-747, 1992.
- [4] Fathi Ghorbel, Mark W. Spong. Adaptive Integral Manifold Control of Flexible Joint Robot Manipulators. Proceedings of the 1992 IEEE International Conference on Robotics and Automation, 707-714, 1992.
- [5] M. Spong, H. Seth and M. Vidyasagar. Robot Dynamics and Control, New York-Wiley, 2004.
- [6] B. Brogliato, R. Ortega, R. Lozano. Global tracking controllers for flexible-joint manipulators: a comparative study. Automatica, 31, 7:941-956, 1995.
- [7] A. De Luca. Dynamic control of robots with joint elasticity. Proceedings of the IEEE International Conference on Robotics & Automation, 152-158, 1988.
- [8] A. De Luca. Feedforward/Feedback laws for the control of flexible robots. Proceedings of the 2000 IEEE International Conference on Robotics & Automation. San Francisco, CA, 2000, 233-240, 2000.
- [9] A. De Luca, B. Siciliano, L. Zollo. PD control with on-line gravity compensation for robots with elastic joints: Theory and experiments. Automatica, 41, 1809-1819, 2005.
- [10] S. Moberg. On modeling and control of flexible manipulators. Linkoping University, Linkoping, 2007.
- [11] G. Palli, C. Melchiorri, A. De Luca. On the feedback linearization of robots with variable joint stiffness. IEEE International Conference on Robotics and Automation, 1753-1759, 2008.
- [12] S. Ozgoli and H. D. Taghirad. A survey on the control of flexible joint robots. Asian Journal of Control, 8, 4:1-15, 2006.
- [13] A. De Luca, D. Schroder, M. Thummel. An acceleration-based state observer for robot manipulators with elastic joints. 2007 IEEE International Conference on Robotics and Automation, 3817-3823, 2007.
- [14] S. Avila-Becerril, A. Loria, E. Panteley. Global position-feedback tracking control of flexible-joint robots. IEEE American Control Conference, Jul 2016, Boston, MA, United States, 2016.
- [15] H. Khalil. Nonlinear systems, Pearson, 3 edition, 2001. ISBN-13: 978-0130673893
- [16] A. S. Andreev and O. A. Peregudova. On stabilization of program motions of holonomic mechanical systems. Automation and Remote Control, 77, 3:416-427, 2016.

## Cloth-like Structures with Distributed Active Damping

Petr Beneš<sup>1</sup>, Zbyněk Šika<sup>1</sup>, Martin Hromčík<sup>2</sup>, Radek Krejza<sup>1</sup>

<sup>1</sup>Faculty of Mechanical Engineering  
Czech Technical University in Prague  
Technická 4, 166 07 Prague 6,  
Czech republic  
[petr.benes; zbynek.sika;  
radek.krejza]@fs.cvut.cz

<sup>2</sup>Faculty of Electrical Engineering  
Czech Technical University in Prague  
Technická 2, 166 27 Prague 6,  
Czech republic  
xhromcik@fel.cvut.cz

### Abstract

The active damping or vibration control is a very common task in mechatronics especially if the passive damping properties of mechanical components are not sufficient. In case of thin and light materials, the possibilities of damping properties tuning by some geometric modifications are very limited. On the other hand, more and more cheap and miniature active components are available on the market. The aim of this paper is the investigation of active damping of the cloth-like thin material using distributed active elements and sensors.

The physical model of cloth is based on the regular grid of nodes. These nodes represent uniformly distributed mass of the cloth. The nodes are connected one to other by springs or by kinematic constrains for defined constant length. In that case, nodes represent spherical joints as well. The dissipative properties of the material are modelled using shear dampers and flexion dampers. Moreover there is a viscous damping applied on each node representing the interaction with air. The model was create using the Lagrange equations of mixed type and the numerical calculation was stabilized using Baumgarte's approach. The unknown parameters of the model were identified experimentally - the movement of the cloth sample was captured by camera and rangefinder sensor during precisely specified manipulation and image processed [1]. Then the model parameters were optimized until the simulation results met the measured ones (Fig 1).

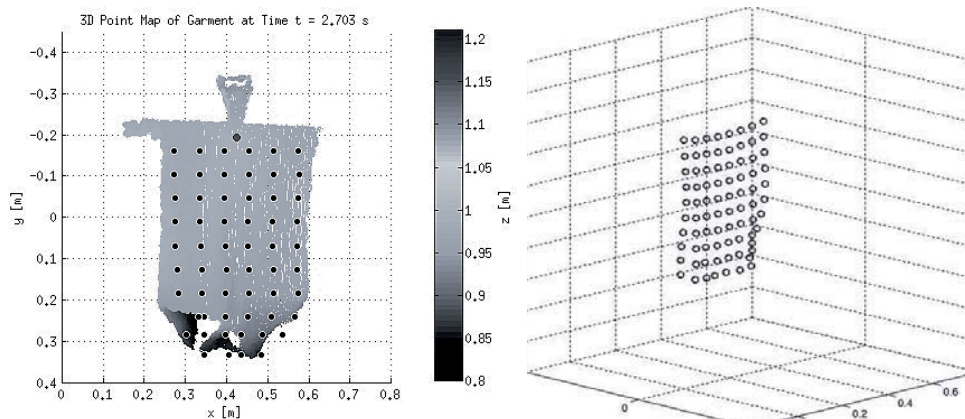


Figure 1. Identification of cloth parameters a) image processing, b) simulation model

The identified cloth model was used as a basis for simulation experiments with active control. The sensor/actuator pairs were added into the model structure. These consist of simple proportional velocity-feedback loops [2], [3]. The whole control systems is decentralized and the control of actuators is based on local information. Several variants with different numbers and placing of active elements in the structure were simulated. The aim of the whole control synthesis was to find the best set of proportional gains.

The considered mechanical system is non-linear. The control synthesis was performed for linearized variant however the results of synthesis were tested using the original non-linear model as well. The simplest variant – same gain for all loops – was far from optimal. In order to cover all modes including the higher ones, many of lower modes were unnecessarily overdamped and the power consumption was extremely high. Therefore the optimization was performed with two main objective functions – minimization of the maximal gain and maximization of angle  $\alpha$  in the pole placement region (Fig. 2). The overdamping was suppressed by optimization of the ratio between the number of real poles and the total number of poles. The width of the region  $\epsilon$  was optimized as well (Fig.2).

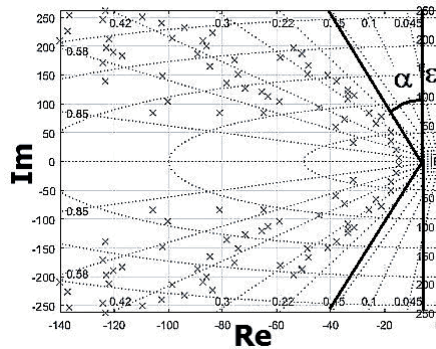


Figure 2. Optimization - pole placement

Fig. 3 shows the comparison of responses to disturbance in the form of chirp signal (0.1-50 Hz) when the resulting optimized active damping is used or not. In this simulation each second node was controlled by the active element and the vibration were reduced approx. ten times.

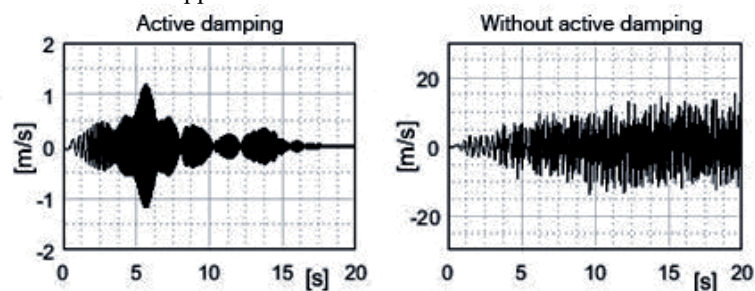


Figure 3. Chirp disturbance response – velocity of reference point

Generally experiments confirmed expected behavior – the higher number of active elements means better control of damping properties but increasing power consumption. More interesting results were obtained when active elements weren't distributed uniformly and some local areas were influenced more than the others. There is still large area for ongoing research focused on optimization of the placing of active elements [4]. Moreover in our simulations we expected that active elements are physically identical. The only differences between them are caused by different gains in control loops. The more advanced optimization can take more types of active elements into account.

The results show that the proposed strategy is capable to deal with the design of “smart” cloth-like materials with controlled mechanical properties. The experimental identification of parameters gives realistic cloth models, which could be used for further design and optimization of the distribution of active elements. The next steps in research will be focused on the distributed control with the nearest neighbor feedback and the combination of the simple controllers with the more complex design methods. The detailed modelling of different variants of actuators and sensors is under intensive development as well.

## Acknowledgments

This work is supported by the grant GA 16-21961S entitled „Mechatronic structures with heavily distributed actuators and sensors “ of Czech Science Foundation.

## References

- [1] M. Neoral. *Extraction of features from moving garment* (bachelor thesis). CTU in Prague, FEE – Dept. of Cybernetics, Prague 2014.
- [2] W.K. Gawronski. *Advanced Structural Dynamics and Active Control of Structures*, Springer-Verlag New York, Inc., 2004.
- [3] A. Preumont. *Vibration Control of Active Structures An Introduction*, 2nd Edition, *Solid Mechanics and its Application*, Volume 96, Kluwer Academic Publishers, 2002.
- [4] T. Haniš, M.Hromčík. Optimal sensors placement and spillover suppression, *Mech. Syst. Signal Process.*, Volume 28, pp. 367-378, 2012.

# Parameter Identification of a Torsional Vibration Damper in Frequency Domain Using Adjoint Fourier Coefficients

**Thomas Lauß\***, **Stefan Oberpeilsteiner\***, **Wolfgang Steiner\***, **Karin Nachbagauer\***,  
**Stefan Reichl†**,

\*Faculty of Eng. and Environmental Sciences  
University of Applied Science Upper Austria  
Stelzhamerstraße 23, 4600 Wels, Austria

E-Mail: [thomas.lauss, stefan.oberpeilsteiner, karin.nachbagauer, wolfgang.steiner]@fh-wels.at

†BMW Motoren GmbH  
Diesel Engine Development  
Hinterbergerstraße 2, A-4400 Steyr  
E-Mail: stefan.reichl@bmw.com

## Abstract

The adjoint method (see, e.g., [1, 2]) is a very powerful tool for parameter identification or optimal control in time domain. In most cases the results lead to some kind of best-fit solution, which means that high frequency components with low amplitudes are not considered. However, in this contribution we present an approach for the identification of parameters which influences the system at special frequencies or frequency ranges. The basic idea is to compute the Fourier coefficients for the relevant oscillations. Then, the cost function is the difference of the amplitudes from the simulation and a measured value e.g., from a test bench. The derivation and computation of the gradient of the cost function with the adjoint method is presented and applied to a four-cylinder engine in order to identify the parameters of a torsional vibration damper (TVD).

## Problem definition

We consider a multibody system of differential algebraic equations (DAE)

$$\mathbf{M}(\mathbf{q})\ddot{\mathbf{q}} + \mathbf{C}_q^T(\mathbf{q})\boldsymbol{\lambda} = \mathbf{f}(\mathbf{q}, \dot{\mathbf{q}}, \mathbf{p}, t), \quad \mathbf{C}(\mathbf{q}) = \mathbf{0} \quad \text{with} \quad \mathbf{q}(0) = \mathbf{q}_0 \quad \text{and} \quad \dot{\mathbf{q}}(0) = \mathbf{v}_0 \quad (1)$$

in which  $\mathbf{q}$  denotes the generalized coordinates with its time derivatives  $\dot{\mathbf{q}}$  and  $\ddot{\mathbf{q}}$ .  $\mathbf{M}$  is the symmetric mass matrix and  $\mathbf{f}$  represents the vector of generalized and gyroscopic forces. The algebraic constraint  $\mathbf{C}(\mathbf{q})$  influences the system equations by the constraint force  $\mathbf{C}_q^T(\mathbf{q})\boldsymbol{\lambda}$ . Moreover,  $\mathbf{p}$  is a vector of parameters to identify and  $y(t) = g(\mathbf{q}, \dot{\mathbf{q}})$  is the system output. Introducing time dependent Fourier coefficients  $a_k$  and  $b_k$  by setting

$$\dot{a}_k = \frac{2}{T}y(t) \sin(\omega_k t) \quad \dot{b}_k = \frac{2}{T}y(t) \cos(\omega_k t) \quad \text{with} \quad a_k(0) = 0 \quad \text{and} \quad b_k(0) = 0, \quad (2)$$

where  $T$  is the final end time and  $\omega_k$  is the  $k$ -th frequency of interest. The cost function in Mayer-form to be minimized is

$$J(\mathbf{p}) = S(T, \mathbf{q}, \dot{\mathbf{q}}) = \sum_{k=1}^N (a_k^2(T) + b_k^2(T) - \bar{A}_k^2)^2 \longrightarrow \min \quad (3)$$

in which  $\bar{A}_k$  is the measured amplitude of the  $k$ -th frequency.

## The adjoint gradient computation

Following the basic idea of the adjoint method in the work by Nachbagauer et al. [2], the gradient can be computed efficiently as follows. First of all the cost function of Eq. (4) is extended about the system equations (1) and the differential equation of the Fourier coefficients (2). Note, that this procedure does not influence the cost function, if the system equations are fulfilled. Hence, the extended cost function is given by

$$\begin{aligned} \bar{J}(\mathbf{p}) = & \frac{1}{4} \sum_{k=1}^N (a_k^2 + b_k^2 - \bar{A}_k^2)^2 + \int_0^T \left\{ \boldsymbol{\xi}^T (\dot{\mathbf{q}} - \mathbf{v}) + \boldsymbol{\zeta}^T (\mathbf{M}\dot{\mathbf{v}} - \mathbf{f}(\mathbf{q}, \mathbf{v}, \mathbf{p}, t) + \mathbf{C}_q^T \boldsymbol{\lambda}) + \boldsymbol{\mu}^T \mathbf{C}(\mathbf{q}) \right\} dt \\ & + \sum_{k=1}^N \int_0^T \alpha_k (g(\mathbf{q}, \mathbf{v}) \cos(\omega_k t) - \dot{a}_k(t)) dt + \sum_{k=1}^N \int_0^T \beta_k (g(\mathbf{q}, \mathbf{v}) \sin(\omega_k t) - \dot{b}_k(t)) dt \end{aligned} \quad (4)$$

in which  $\boldsymbol{\xi}$ ,  $\boldsymbol{\zeta}$  and  $\boldsymbol{\mu}$  are arbitrary Lagrange multipliers corresponding to the system states and  $\alpha_k$  and  $\beta_k$  are Lagrange multipliers corresponding to the Fourier coefficients. Next, the variation of the cost function is carried out, followed by an integration by parts. Finally, we define the Lagrange multiplier as the adjoint variables in order to avoid the computation of the relation between the variation in the states  $\delta\mathbf{q}$ ,  $\delta\mathbf{v}$ ,  $\delta\boldsymbol{\lambda}$ ,  $\delta a_k$ ,  $\delta b_k$  and the variation in the parameter  $\delta\mathbf{p}$ .

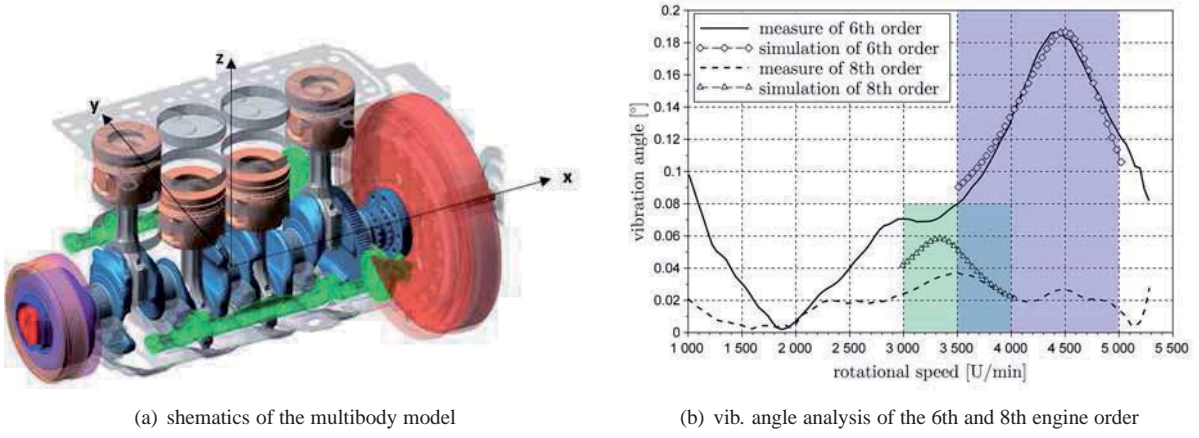


Figure 1: 4-cylinder combustion engine

The adjoint Fourier coefficients are constant and given by  $\alpha_k = [(a_k^2 + b_k^2 - \bar{A}_k^2) a_k] |_{t=T}$  and  $\beta_k = [(a_k^2 + b_k^2 - \bar{A}_k^2) b_k] |_{t=T}$  and the adjoint differential algebraic equations read

$$\dot{\boldsymbol{\zeta}} = \mathbf{A}\boldsymbol{\zeta} + \mathbf{C}_q^T \boldsymbol{\mu} + g_q G(t), \quad \frac{d}{dt}(\mathbf{M}\boldsymbol{\xi}) = -\boldsymbol{\xi} - \mathbf{f}_v^T \boldsymbol{\zeta} + g_v G(t) \quad \text{and} \quad \mathbf{C}_q \boldsymbol{\zeta} = 0 \quad (5)$$

where  $\boldsymbol{\zeta}(T) = 0$ ,  $\boldsymbol{\xi}(T) = 0$  and  $\mathbf{A} = (\mathbf{M}\mathbf{v})_q^T - \mathbf{f}_q^T + (\mathbf{C}_q^T \boldsymbol{\lambda})_q^T$  and  $G(t) = \sum_{i=1}^N (\alpha_k \cos(\omega_k t) + \beta_k \sin(\omega_k t))$ . Finally, the gradient is

$$\nabla J = - \int_0^T \mathbf{f}_p^T \boldsymbol{\xi} dt.$$

Note, that it is also possible to construct the discrete adjoint system, followed by Lauß [1]. The advantage of the presented method in [1] is, that the stability and accuracy of the backwards time integration of the adjoint differential algebraic equations (5) is guaranteed.

### Example: Parameter identification of a torsional vibration damper (TVD)

We consider a four-cylinder engine (see Fig. 1(a)) with a flexible crankshaft model, which can be described by differential algebraic equations in the form of Eq. (1). The goal is to identify the parameters of the TVD, which is modeled with two Maxwell elements, such that the vibration angle of the crankshaft of the 6th and 8th engine order coincide with a measured value. For the parameter identification we use  $N = 35$  points in the frequency domain. In Fig. 1(b) the vibration angle of the 6th and 8th engine order is compared with the simulation of the identified parameter and the measured vibration angle. The time integration and the gradient computation is implemented in C++ and the optimization is done in SCILAB with the nonlinear optimization routine `optim()`. After 50 iterations the solution converges and the computation time was about 1 hour and 50 minutes on a standard computer. However, using two Maxwell elements for the model of the TVD, the accordance of the 8th engine order (see in Fig. 1(b)) cannot be improved.

## References

- [1] T. Lauß, S. Oberpeilsteiner, W. Steiner, and K. Nachbagauer. The Discrete Adjoint Gradient Computation for Optimization Problems in Multibody Dynamics. *ASME J. Comput. Nonlinear Dyn.*, Nov 2016.
- [2] K. Nachbagauer, S. Oberpeilsteiner, K. Sherif, and W. Steiner. The Use of the Adjoint Method for Solving Typical Optimization Problems in Multibody Dynamics. *ASME J. Comput. Nonlinear Dyn.*, Apr 2015.

# Model Based Filtering on the Horizontal Axis Wind Turbine. Towards a Holistic Approach: Load Measurement, Predictive Maintenance, Mechanical Design Assessment and Certification.

Javier Ros<sup>1</sup>, Aitor Plaza<sup>1</sup>, Xabier Iriarte<sup>1</sup>, Gorka Gainza<sup>1,2</sup>

<sup>1</sup> IMAC Center & ISC -Institute of Smart Cities, Department of Mechanical Engineering,  
Public University of Navarre,  
Campus de Arrosadia s/n, Pamplona-Iruña, 31006, Spain  
[jros,aitor.plaza,xabier.irarte,gorka.gainza]@unavarra.es

<sup>2</sup> ARESSE Engineering  
P.I. Berriainz, Pamplona-Iruña, 31013, Spain  
ggainza@aresse.com

## Abstract

Today, to a great extent, it has become clear that a good deal of the expected upcoming advances in the context of machine design, testing, operation and maintenance (to cite some), will come from the hand of the addition of “Intelligent features” having an impact on the different stages of the machine life-cycle (design, prototype, validation, certification, control, operation, predictive maintenance,...).

In this work we center our attention on the Horizontal Axis Wind Turbines (HAWT), an interesting context because of the current and foreseen relevance of the wind energy generation at a global scale. It is well known that such demand is and is expected to be covered by the aforementioned wind turbine configuration.

This “Intelligent features” are expected to lower the Total Cost of Ownership (TCO) of wind energy infrastructures making them more competitive against other energy generation technologies. These features have been present in this industry from the very beginning. This means basically the Supervisory Control And Data Acquisition (SCADA) systems used for the autonomous control and operation, and remote operation and supervision of the wind turbines. But, generally speaking, the features of such systems used to be very conservative, they usually deal with a bare minimum of requirements for the monitoring and control required for the HAWT operation.

Nowadays predictive maintenance relies mainly on the analysis of very basic SCADA data, putting important limitations on the requirement for a fully-fledged predictive maintenance. Operation data can be also fundamental for the assessment of new HAWT designs, and their testing and validation, but usually the SCADA data is not enough to cope with all the belts and whistles that mechanical engineering practitioners would dream of. This is because it is already known that there are failure modes with an important impact on the TCO that are difficult to predict based on standard SCADA data. For example, some failure modes of: blade, tower, foundation and low speed axis, are infamous in this context.

Now that high MW HAWT are becoming the fact in the wind energy industry, the introduction of additional sensors has become a very attractive option. Obviously with HAWT have been deployed with a very important number of sensors, but these are mostly prototypes for experimental research. It frequently happens that special sensors are deployed in an HAWT, but usually in a limited number of specimens, for a short period of time, and/or for the assessment of a very specific issue, during the so called measurement campaigns.

Meanwhile, more exigent updated or even new specifications have been worked out, related to mechanical design, validation and certification more relevant ones are the IEC 61400-1 standard that applies for large onshore wind turbines [1], the IEC 61400-3 for offshore wind turbines [2], the 61400-13 TS that stipulates the measurement of generic mechanical loads for wind turbines [4] and the IEC 61400-22 concerned with conformity testing and certification of Wind Turbines [5]. These are referred here as they are more relevant in the mechanical engineering context. These new specifications require the estimation and or measurement of loads, displacements, accelerations,... in addition with other measurements usually performed already standardized in the SCADA, low speed shaft position, pitch angles, high speed shaft velocity,... Frequently the specification tells what it is desired to know without specifying how to perform the measure. This presents several difficulties, which sensors, where, calibration requirement, a dome sort of model based inference. Also requirements in terms of information or measurements required by different specifications, is regarded as unrelated.

Model based nonlinear filtering appears here as a tool that can be used suit most of the needs of the specifications in the most “Intelligent” way regarding the current technological scientific panorama. The possibilities of this kind of filters (i.e. Extended Kalman Filter) are well known. If a proper combination of model and sensors are correctly tuned: state, load, calibration and estimation of unknown inputs, to cite some, can be made available in a robust way. IEC 61400-13 TS [4] that stipulates required and suggested loads and accelerations measurements. Starting from these requirements for the case of high MW wind turbines, we propose to analyze High end Extended Kalman filter strategies with the purpose of allowing a detailed state estimation, detailed load estimation, sensor calibration, robustness of the measurement chain. We criticize the specification and propose measurement strategies, desirable additional measurements and even procedures to fulfill these objectives. The

presence of a detailed model compatible with the ones used to assess the design and specifications in IEC 61400-1, and IEC 61400-22 [1, 5], leads to an holistic approach that allows to satisfy simultaneously the requirements of Load Measurement, Predictive Maintenance, Mechanical Design Assessment and Certification, at least if such a system becomes a standard wind turbine monitoring equipment.

### **Acknowledgments**

This work has been partially supported by “Servicio de Innovación y Transferencia del Conocimiento de Gobierno de Navarra” contract number: 0011-1365-2016-000092.

### **References**

- [1] International Electrotechnical Commission. Wind Turbines - Part 1: Design Requirements (IEC 61400-1). Technical report, International Electrotechnical Commission, 2005.
- [2] International Electrotechnical Commission. Wind Turbines - Part 3: Design of Offshore Wind Turbines (IEC 61400-3). Technical report, International Electrotechnical Commission, 2008.
- [3] International Electrotechnical Commission. Wind Turbines - Part 4: Design requirements for wind turbine gearboxes. (IEC 61400-4). Technical report, International Electrotechnical Commission, 2012.
- [4] International Electrotechnical Commission. Wind Turbines - Part 13: Measurement of Mechanical Loads (IEC 61400-13 TS). Technical report, International Electrotechnical Commission, 2001.
- [5] International Electrotechnical Commission. Wind Turbines - Part 22: Conformity Testing and Certification of Wind Turbines (IEC 61400-22 TS). Technical report, International Electrotechnical Commission, 2008.
- [6] International Electrotechnical Commission. Wind Turbines - Part 23: Full-scale structural testing of rotor blades (IEC 61400-24). Technical report, International Electrotechnical Commission, 2014.

# Design optimization of planetary gear trains under dynamic constraints and parameter uncertainty

Erich Wehrle<sup>1</sup>, Franco Concli<sup>1</sup>, Luca Cortese<sup>2</sup>, Renato Vidoni<sup>1</sup>

<sup>1</sup>Faculty of Science and Technology  
Free University of Bozen-Bolzano  
Universitätsplatz 5  
39100 Bozen, South Tyrol · Italy

[Erich.Wehrle, Franco.Concli, Renato.Vidoni]@unibz.it

<sup>2</sup>Mechanical and Aerospace Engineering Department  
Università di Roma “La Sapienza”  
via Eudossiana 18  
00184 Rome, Italy

Luca.Cortese@uniroma1.it

## Abstract

Planetary gear trains or epicyclic gearing are mechanical systems for the transfer and translation of rotation and torque. Planetary gear trains can be found in such high technological systems as automotive transmissions, aircraft motors and wind turbines to mundane products as pencil sharpeners. In this work, the vibrational behavior of planetary gear trains is of concern as this can lead to detrimental effects including fatigue, comfort and acoustics.

Lumped-parameter models are useful in early development phases of planetary gear sets to assess the modal response and optimize performance. This design phase is, though, plagued by uncertainty, which if neglected can lead to drastically suboptimal designs. Methods are herein demonstrated to optimally design planetary gear sets, which ensures proper performance with respect to resonance frequencies under parameter uncertainty.

In this study, a parametric lumped-parameter model is developed for the analysis of a generic planetary gear train. This lumped-parameter modeling approach was originally introduced by [3] and has been further established and advanced by [1, 4, 5], amongst others. The dynamic model, having  $3(3 + n_p)$  degrees of freedom, is formulated via the equations of motion

$$\underline{m}\ddot{\underline{u}} + \underline{d}\dot{\underline{u}} + \underline{k}\underline{u} = \underline{F}, \quad (1)$$

where  $\underline{m}$ ,  $\underline{d}$ , and  $\underline{k}$  are the mass, damping and stiffness matrix, while  $\ddot{\underline{u}}$ ,  $\dot{\underline{u}}$ ,  $\underline{u}$  and  $\underline{F}$  are the acceleration, velocity, displacement and the external force vectors. This serves as the basis to find the system of free vibrations. The parametric model in this work is used to ascertain the resonance behavior of such free vibration. Lumped-parameter models are accurate in terms of eigenfrequencies and their eigenmodes, yet require extremely low computational effort, allowing for numerical optimization and uncertainty analysis [2]. Although the model framework is independent of the specific case, the benchmark planetary gear train in this work is driven by the sun and the output on the carrier (see fig. 1). There are three planetary gears and the ring gear is fixed.

Methodologies utilizing optimization are introduced to design generic planetary gear trains; three formulations are shown. Mass and inertia terms are used as design variables. The first formulation is a simple unconstrained maximization of the lowest eigenfrequency. The objective function in the second formulation is minimum mass while the constraints ensure that the design avoids critical frequencies. The frequency ranges have been avoided by formulating the constraint functions after a method introduced by [6]. Although this creates a disjoint design space, gradient-based optimization methods, which strictly seen are therefore no longer applicable, have been successfully utilized. Finally, a novel metric is introduced in which the avoidance of critical frequency ranges assessed. The Python toolbox for optimization DESOPTPY [7] including various optimization algorithms and methods is used. Efficient gradient-based methods are preferred here, yet gradient-free methods including genetic algorithms found in DESOPTPY are used for comparison purposes.

The stiffness values of planetary gear sets are afflicted with uncertainty and correspondingly the stiffness parameters used in this lumped-parameter model are treated as intervals. Bounded intervals are used as statistical distributions are assumed to be unavailable in such early development phases. Although resulting in more conservative designs, this method requires no precise statistical information and instead by bounding tolerances or ranges of possible values. The uncertainty analysis is carried out using an efficient optimization-based minimization–maximization method. The uncertain stiffness parameters are used to find the possible range of the resonance frequencies, which in turn are used in the optimization process.

Central to the efficiency of this work is analytical sensitivity analysis. This has been implemented to provide accurate sensitivities of system responses with respect to design variables, system parameters and uncertain parameters. Postprocessing assessments via sensitivities of the optimal results are included, which investigates the effect of the constraint limits (frequency ranges) and uncertainty levels (uncertain stiffnesses) on the objective function.

The results are then summarized providing insight on the design of planetary gear trains in various applications, with and without optimization methods.

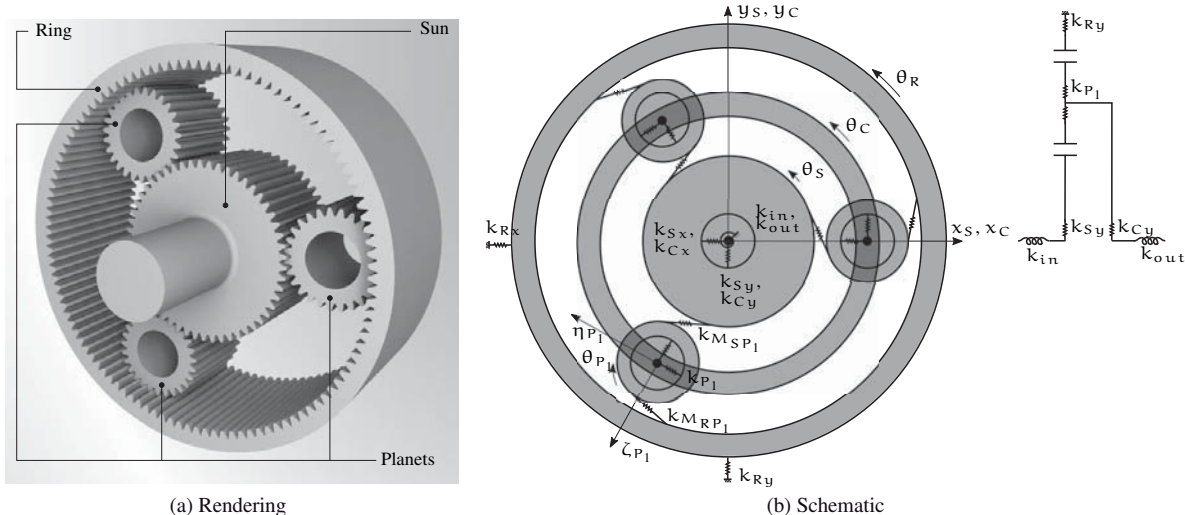


Figure 1: Planetary gear train

### Acknowledgments

This work is supported by the project CRC 2016 - TN2077 “Dynamic models for vibration and noise reduction in planetary gear trains” funded by the Free University of Bozen-Bolzano.

### References

- [1] M. Botman. Epicyclic gear vibrations. *Journal of Engineering for Industry*, 98(3):811–815, 1976.
- [2] C. G. Cooley and R. G. Parker. A review of planetary and epicyclic gear dynamics and vibrations research. *Applied Mechanics Reviews*, 66(4):040804–1–040804–15, 2014.
- [3] F. F. Cunliffe, J. D. Smith, and D. B. Welbourn. Dynamic tooth loads in epicyclic gears. *Journal of Engineering for Industry*, 96(2):578–584, 1974.
- [4] A. Kahraman. Natural modes of planetary gear trains. *Journal of Sound and Vibration*, 173(1):125–130, 1994.
- [5] A. Kahraman. Planetary gear train dynamics. *Journal of Mechanical Design*, 116(3):713–720, 1994.
- [6] C. Roß. *Strukturoptimierung mit Nebenbedingungen aus der Dynamik*. Dr.-ing. diss., Lehrstuhl B für Mechanik, Technische Universität München, 1991.
- [7] E. J. Wehrle. *Design optimization of lightweight space frame structures considering crashworthiness and parameter uncertainty*. Dr.-ing. diss., Lehrstuhl für Leichtbau, Technische Universität München, 2015.

# Intelligent Sliding Mode Control of an Overhead Container Crane

Wallace M. Bessa<sup>1,2</sup>, Svenja Otto<sup>2</sup>, Edwin Kreuzer<sup>2</sup>, Robert Seifried<sup>2</sup>

<sup>1</sup> Department of Mechanical Engineering  
Federal University of Rio Grande do Norte  
Campus Universitário Lagoa Nova, 59078-970 Natal, Brazil  
wmbessa@ct.ufrn.br

<sup>2</sup> Institute of Mechanics and Ocean Engineering  
Hamburg University of Technology  
Eißenendorfer Straße 42, 21073 Hamburg, Germany  
[svenja.otto,kreuzer,robert.seifried]@tuhh.de

## Abstract

Overhead container cranes are typical underactuated multibody systems since they have less independent control inputs than degrees of freedom. They play an essential role in cargo handling operations at ports and in the industrial sector. In order to ensure safe operating conditions, undesirable load swing should be avoided during the execution of a certain task. In this case, a feedback control scheme could be adopted to automatically prevent oscillation of the load. However, the design of accurate controllers for this kind of problem can become very challenging inasmuch as the load swing cannot be controlled directly. Moreover, overhead crane dynamics are frequently uncertain, e.g. due to unknown friction forces, and are also subject to external disturbances such as wind loads.

In this contribution, an intelligent controller is proposed for an underactuated overhead container crane subject to both parameter uncertainties and unmodeled dynamics. The adopted approach is based on the sliding mode method to confer robustness against modeling inaccuracies and external disturbances. Additionally, an adaptive fuzzy inference system is embedded within the control law to improve set-point regulation and trajectory tracking. In order to evaluate the performance of the proposed intelligent scheme, the control law was implemented and tested in a 1:6 scale experimental container crane, available at the Institute of Mechanics and Ocean Engineering at Hamburg University of Technology. The experimental setup, as shown in Figure 1a, consists of a trolley and a container with dimensions 0.35 m × 0.37 m × 0.86 m that is attached to the trolley by four cables.

Since the trolley moves along only a linear axis, planar motion is assumed, yielding the equation of motion:

$$\begin{bmatrix} M+m & m \sin \theta & ml \cos \theta \\ m \sin \theta & m & 0 \\ ml \cos \theta & 0 & ml^2 \end{bmatrix} \begin{bmatrix} \ddot{x} \\ \ddot{l} \\ \ddot{\theta} \end{bmatrix} = \begin{bmatrix} m\dot{\theta}(\dot{\theta}l \sin \theta - 2\dot{l} \cos \theta) \\ m(l\dot{\theta}^2 + g \cos \theta) \\ -ml(2\dot{l}\dot{\theta} + g \sin \theta) \end{bmatrix} + \begin{bmatrix} u_x \\ u_l \\ 0 \end{bmatrix}. \quad (1)$$

Here,  $u_x$  and  $u_l$  are, respectively, the control forces acting on the trolley and the cables,  $x$  is the trolley position,  $l$  stands for the length of the cables,  $\theta$  represents the swing angle,  $M$  is the mass of the trolley, and  $m$  is the container mass. It should be emphasized that only the variables  $x$  and  $l$  can be directly actuated. The swing angle  $\theta$ , on the other hand, is an unactuated variable.

Now, following the sliding mode method, a stable manifold should be established in the state space. Here, the switching variables are defined according to the general approach proposed by Ashrafiuon and Erwin [1]:

$$\mathbf{s} = \begin{bmatrix} \alpha_x & 0 \\ 0 & \alpha_l \end{bmatrix} \begin{bmatrix} \dot{\tilde{x}} \\ \dot{\tilde{l}} \end{bmatrix} + \begin{bmatrix} \lambda_x & 0 \\ 0 & \lambda_l \end{bmatrix} \begin{bmatrix} \tilde{x} \\ \tilde{l} \end{bmatrix} + \begin{bmatrix} \alpha_\theta \\ 0 \end{bmatrix} \dot{\tilde{\theta}} + \begin{bmatrix} \lambda_\theta \\ 0 \end{bmatrix} \tilde{\theta}. \quad (2)$$

Here,  $\mathbf{s} = [s_x \ s_l]^\top$  is the switching vector,  $\alpha_n$  and  $\lambda_n$  (with  $n = x, l, \theta$ ) are parameters that must be properly chosen in order to ensure the stability of the sliding surface [1], and  $\tilde{x} = x - x_d$ ,  $\tilde{l} = l - l_d$ , and  $\tilde{\theta} = \theta - \theta_d$  are the tracking errors, with subscript  $d$  representing the desired values for each variable.

Conventionally, sliding mode based schemes are implemented with a discontinuous term in the control law, but a known drawback of this approach is the resulting chattering phenomenon. In order to avoid the undesired effects of the control chattering, a thin boundary layer neighboring the switching surface could be adopted, by replacing the discontinuity with a continuous interpolation inside the boundary layer. This substitution can minimize or, when desired, even completely eliminate chattering. However, it turns a perfect tracking into a tracking with guaranteed precision problem, which actually means that a steady-state error will always remain.

Thus, in order to enhance the control performance, an adaptive fuzzy compensator  $\hat{\mathbf{d}} = [\hat{d}_x \ \hat{d}_l]^\top$  is combined with a smooth sliding mode controller:

$$\mathbf{u} = - \begin{bmatrix} -(\alpha_\theta \cos \theta - \alpha_x l)/Ml & (\alpha_\theta \cos \theta - \alpha_x l) \sin \theta / Ml \\ -\alpha_l \sin \theta / M & \alpha_l (m \sin^2 \theta + M) / Mm \end{bmatrix}^{-1} \begin{bmatrix} \alpha_\theta (2\dot{l}\dot{\theta} + g \sin \theta) / l + \\ \alpha_l (l\dot{\theta}^2 + g \cos \theta) + \\ + \hat{d}_x - \alpha_x \ddot{x}_d - \alpha_\theta \ddot{\theta}_d + \lambda_x \dot{\tilde{x}} + \lambda_\theta \dot{\tilde{\theta}} + K_x \text{sat}(s_x / \phi_x) \\ + \hat{d}_l - \alpha_l \ddot{l}_d - \lambda_l \dot{\tilde{l}} + K_l \text{sat}(s_l / \phi_l) \end{bmatrix}, \quad (3)$$

where  $\mathbf{u} = [u_x \ u_l]^\top$  is the proposed control signal,  $K_x$  and  $K_l$  are the related control gains,  $\text{sat}(\cdot)$  is the standard saturation function, and  $\phi_x$  and  $\phi_l$  define the width of the associated boundary layers.

Each compensation term is computed using the Takagi-Sugeno-Kang inference method [3]:  $\hat{d}_m = \hat{\mathbf{D}}_m^\top \Psi_m$  (with  $m = x, l$ ), where  $\hat{\mathbf{D}}_m = [\hat{D}_{m1}, \hat{D}_{m2}, \dots, \hat{D}_{mR}]^\top$  are vectors containing the attributed values  $\hat{D}_{mr}$  to each rule  $r$ ,  $\Psi_m = [\psi_{m1}, \psi_{m2}, \dots, \psi_{mR}]^\top$  are vectors with components  $\psi_{mr} = w_{mr} / \sum_{r=1}^R w_{mr}$  and  $w_{mr}$  is the firing strength of each rule. With the view to reduce the number of fuzzy sets and rules, the switching variables  $s_m$ , instead of all state variables, are considered in the premise of the related fuzzy rules. The vectors of adjustable parameters are automatically updated by the adaptation laws  $\dot{\hat{\mathbf{D}}}_m = \varphi_m s_m \Psi_m$ , where  $\varphi_m$  are strictly positive constants related to the adaptation rate [2].

Finally, the proposed intelligent controller is evaluated in the experimental overhead container crane for both stabilization and trajectory tracking problems. Figure 1b shows, for example, the overlaid video frames related to the tracking of a semicircle trajectory around an obstacle.

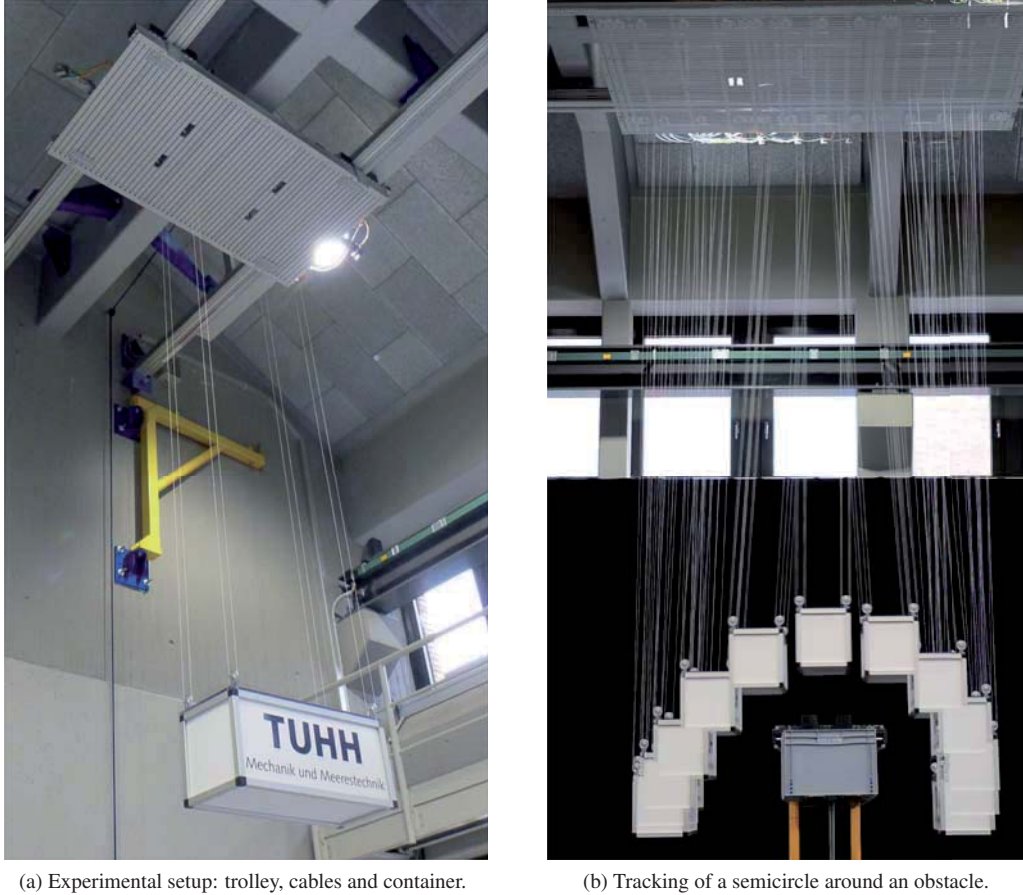


Figure 1: Overhead container crane at the Institute of Mechanics and Ocean Engineering.

Due to the ability of the adopted adaptive fuzzy algorithm to recognize and compensate for unmodeled dynamics, e.g. friction or damping forces, the improved performance of the proposed intelligent sliding mode controller over the conventional counterpart could be clearly verified in all conducted experiments.

### Acknowledgments

The authors would like to acknowledge the support of the Alexander von Humboldt Foundation, the Brazilian Coordination for the Improvement of Higher Education Personnel and the Brazilian National Research Council.

### References

- [1] H. Ashrafiuon, R. S. Erwin. Sliding mode control of underactuated multibody systems and its application to shape change control. *International Journal of Control*, 81:1849-1858, 2008.
- [2] W. M. Bessa, R. S. S. Barrêto. Adaptive fuzzy sliding mode control of uncertain nonlinear systems. *Controle & Automação*, 21:117-126, 2010.
- [3] J.-S. R. Jang, C.-T. Sun, E. Mizutani. *Neuro Fuzzy and Soft Computing: A Computational Approach to Learning and Machine Intelligence*. Prentice Hall, New Jersey, 1997.

## **Section**

# **SOFTWARE DEVELOPMENT AND COMPUTER TECHNOLOGY**



# Multibody System Dynamics at the University of Minho: Teaching and Research Activities

Paulo Flores

Department of Mechanical Engineering  
University of Minho  
Campus de Azurém, 4804-533 Guimarães, Portugal  
pflores@dem.uminho.pt

## Abstract

It is well known that Multibody System Dynamics field has a long and prolific history over the last decades. Multibody Dynamics has its roots in Classical Mechanics and becomes an important and independent multidisciplinary area thanks to the impressive computer developments. As a consequence, there are several methodologies available to model, study, analyze and control kinematics and dynamics of mechanical systems, nevertheless, the fact that most of them have been developed from few fundamental mechanical principles. In a simple way, there are three main methods to derive the equations of motion, namely the Newton-Euler approach, the Lagrange technique and Kane formulation [1-3].

The fundamentals that govern the motion laws for multibody systems were well established since century XVIII. In addition, the numerical methods necessary to solve the equations of motion were known more than 100 years ago. However, the scientific area of multibody system dynamics has emerged over the last five decades, when the development of several computational codes allows for the automatic generation, assemble and resolution of the equations of motion for complex constrained mechanical systems [4]. After 70's, the methodologies of multibody systems have reached a high degree of maturity, which were materialized by a good number of publications in the form of textbooks. Additionally, three scientific journals specially devoted to multibody dynamics were created, namely Multibody System Dynamics, Journal of Multi-Body Dynamics and Journal of Computational and Nonlinear Dynamics.

Over the last few decades, thanks to the developments at both software and hardware levels, it was possible to access to multibody computational tools able to model, simulate and analyzed mechanical system in academic and industrial environments that permit the inclusion of realistic characteristics such as flexibility of bodies, geometric properties, real time situations, etc. The high level of different characteristics associated with multibody dynamics formulations has been a reality over the last years with low computational costs and high level of reliability and an accuracy of results [5]. Shabana [6] advocated that the future of multibody dynamics implies the identification of the relations between different formulations, inclusion of contact-impact events, interaction with control methodologies, identification of experimental procedures as well as the incorporation of large deformations. This idea was corroborated by Schiehlen [1] who stated that "Challenging applications include biomechanics, chaos and nonlinearity, robotics and society and vehicle control ... multibody system dynamics turn out to be a very lively and promising research subject".

As it was previously mentioned, the research activities in the field of multibody dynamics has been intense and fertile over the last decades, however, the teaching activities related to the different methodologies of multibody systems is still an area of development. This ideas has been presented by Schiehlen [7] in a very interesting paper published in the occasion of 10th anniversary of Multibody System Dynamics journal. It can be said that the current panorama has similarities with the genesis of finite element method, when the first teaching courses were offered in the 60's and nowadays there must not exist any Mechanical or Civil engineering program that do not include a course special devoted to finite element method. In fact, there are only few universities offering special courses on multibody dynamics [8-12].

This work deals with the genesis and development of the teaching and research activities at the University of Minho. Special emphasis is given to the courses that are offered in the field of multibody dynamics at bachelor, master and PhD programs. The close relation with other courses, such as Dynamics, Numerical Methods, Computational Mechanics, etc., is object of study in this work, as well as the interaction with research activities in the area of multibody dynamics. The pre-requisites, objectives, teaching methodologies, evaluation, will be object of discussion in this work. In addition, several demonstrative examples of application will be presented and used to discuss the main assumptions and procedures in teaching multibody dynamics. The use of commercial and/or internally developed codes is also an important topics for teaching the fundamentals of multibody dynamics and also to perform the research activities. To address these issues, this work describes a recently developed course that relies on the Automatic Computation of Multibody Systems offered in the PhD Mechanical Engineering program of the University of Minho. Moreover, the ideas and constraints enforced by Bologna Declaration in the reorganization of Higher Education will be discussed [13-15].

## Acknowledgments

The author expresses his sincere thanks to Professor Manuel Seabra Pereira from Technical University of Lisbon (Portugal), Professor Christoph Glocker from ETH-Zurich (Switzerland), Professor Ahmed Shabana from University of Illinois (USA), Professor Hamid Lankarani from Wichita State University (USA), Professor Javier Cuadrado from University of La Coruna (Spain), Professor Parviz Nikravesh from The Arizona University (USA), Professor Paul Fiset from Université Catholique de Louvain (Belgium) and Professor García de Jalón from University Politécnica of Madrid (Spain) who have helped and commented on the development of the new course on multibody dynamics that has been offered at the University of Minho since 2010.

## References

- [1] W. Schiehlen. Multibody system dynamics: Roots and perspectives. *Multibody System Dynamics*, 1:149-188, 1997.
- [2] H. Rahnejat. Multi-body dynamics: historical evolution and application. *Proceedings of the Institution of Mechanical Engineers, Part C: Journal Mechanical Engineering Science*, 214:149-173, 2000.
- [3] P. Eberhard, W. Schiehlen, Computational dynamics of multibody systems: History, formalisms, and applications. *Journal of Computational and Nonlinear Dynamics*, 1:3-12,2006.
- [4] P.E., Nikravesh. *Computer-aided analysis of mechanical systems*. Prentice Hall, Englewood Cliffs, New Jersey, 1988.
- [5] J. Ambrósio, M.S. Pereira. *Desenvolvimentos Recentes no Cálculo Automático de Sistemas Mecânicos: Teoria e Aplicação*. Atas do VI Congresso Ibero-Americano de Engenharia Mecânica – CIBEM6, Departamento de Engenharia Mecânica, Universidade de Coimbra, Coimbra, (edited by A.M. Dias), Vol. I, 1-20, 2003.
- [6] A.A.Shabana. Flexible multibody dynamics: review of past and recent developments. *Multibody System Dynamics*, 1:189-222, 1997.
- [7] W. Schiehlen. Research trends in multibody system dynamics. *Multibody System Dynamics*, 18:3-13, 2007.
- [8] P. Flores, *Relatório da Unidade Curricular Cálculo Automático de Sistemas Multicorpo*. University of Minho, internal publication, 2010.
- [9] M., Cavacece, E.R. Pennestrí, R. Sinatra. Experiences in Teaching Multibody Dynamics. *Multibody System Dynamics*, 13:363-369, 2005.
- [10] F. Braghin, F. Cheli, P. Mantegazza, P. Masarati, G. Quaranta, G. *Multibody Dynamics Teaching Experience at Politécnico di Milano*. In Multibody Dynamics 2007, International Conference on Advances in Computational Multibody Dynamics, Milan, Italy, June, 25-28 2007, 8p.
- [11] P. Fiset, J.C. Samin. Teaching Multibody Dynamics from Modeling to Animation. *Multibody System Dynamics*, 13:339-351, 2005.
- [12] J. García de Jalón, A. Callejo. A straight methodology to include multibody dynamics in graduate and undergraduate subjects. *Mechanism and Machine Theory*, 46(2):168-182, 2011.
- [13] J.C.F. Teixeira, J.F. Silva, P. Flores. Development of Mechanical Engineering Curricula at the University of Minho. *European Journal of Engineering Education*, 32(5):539-549, 2007.
- [14] F. Marques, P. Flores, J.C.P. Claro, H.M. Lankarani. A survey and comparison of several friction force models for dynamic analysis of multibody mechanical systems. *Nonlinear Dynamics*, 86(3):1407-1443, 2016.
- [15] F. Marques, A.P. Souto, P. Flores. On the constraints violation in forward dynamics of multibody systems. *Multibody System Dynamics*, 39(4):385-419, 2017.

## Synchronous Machine Electromechanical and Mechanical Analogy Model Comparison

Michael Valášek<sup>1</sup>, Martin Nečas<sup>1</sup>, Zdeněk Neusser<sup>1</sup>, Jan Pelikán<sup>1</sup>, Petr Neuman<sup>2</sup>

<sup>1</sup>Faculty of Mechanical Engineering  
Czech Technical University in Prague  
Technická 4, 166 07 Prague, Czech Republic  
[Michael.Valasek, Martin.Necas, Zdenek.Neusser, Jan.Pelikán]@fs.cvut.cz

<sup>2</sup>Neureg, assoc.  
Studnická 2128/27, 193 00  
Prague, Czech Republic  
neumanp@volny.cz

### Abstract

The synchronous machine is one of the most important parts of the power grid. To ensure the grid stability it is necessary to control the power sources connected in the grid together with electric appliances, which can cause instability as electric consumption demands change the conditions in the grids and power sources must adapt to such demands. In the past, the properties of synchronous machines were investigated on a mechanical model, because the theory of electrical machines was unknown [1], [2]. At present the general models of electric machines are already known, e.g. Park's model - Park's transformation [3], [4], or another [5], [6]. All these models are complicated, complex and require deep knowledge of electrical engineering, as well as math and physics. The mechanical model of synchronous machine (MMSM) in the Figure 1 is open for broad engineering community to be used for dynamic stability simulations neglecting the internal electrical engine details.

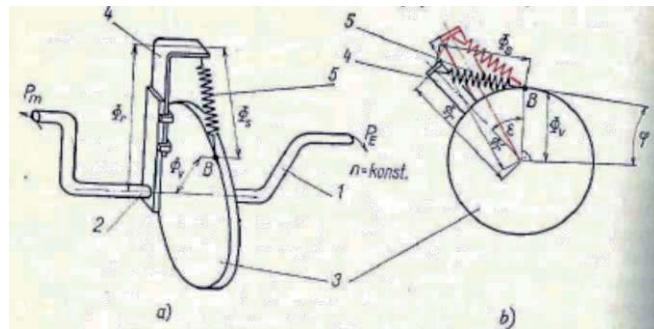


Figure 1. Mechanical model of a synchronous machine (MMSM).

Simple power system (alternator) and its equivalent mechanical model is used, see Figure 1. Load flow is equivalent of the mechanical torque and voltage controller is equivalent of the mass-rod system [7]. According to [8] and [9] electrical air-gap power  $P_e$  can be simplified using equation (1).

$$P_e = \frac{U_v U_r}{X} \sin \epsilon \quad (1)$$

Variable  $U_v$  in equation (1) represents the terminal stator voltage, variable  $U_r$  represents internal (rotor) magnetic field, variable  $X$  is the machine and wire reactance and angle  $\epsilon$  is the torque (loading) angle. This simplified electrical behavior creates connection between mechanical model and electromechanical model of synchronous machine.

Alternator function could be clearly explained on the mechanical model analogy in Figure 1. This device consists of two shafts having a common axis. The parts of the mechanical model of synchronous machine are explained in Table 1. Disk 3 is mounted on shaft 1, shaft 2 has mounted arm 5. Disk length  $\Phi_r$  can be changed. Arm 4 and disk 3 are interconnected by spring 5.

Disk diameter corresponds to  $\Phi_v$  magnetic flux and hence to the voltage at the terminals of the alternator. Direction of this flux can be imagined as the connecting line between point B, where the spring is attached and the center of the disk. Length of arm 4 represents magnetic flux  $\Phi_r$ , length of spring 5 represents magnetic flux  $\Phi_s$ . If we try to rotate shaft 2 faster than the shaft 1 rotates, it begins to stretch the spring 5, arm 4 starts to swing relatively to point B increasing their mutual angle, which represents load angle  $\epsilon$ . It is obvious that the larger  $\Phi_r$  is (i.e. direct current excitation of the rotor), the smaller load angle  $\epsilon$  is for transferring the same torque from one shaft to another.

**Table 1.** Mechanical model variable explanation

stator current, current stator windings	$I_S$
excitation current	$I_b$
limit excitation current	$I_{b0}$
resulting / required magnetic field, (the terminal voltage of the alternator size of the diameter of the disk 3)	$\Phi_V$
magnetic field (spring length 5)	$\Phi_S$
rotor magnetic field, (DC excitation current to the rotor, length of arm 4)	$\Phi_r$
the load / loading angle (the mutual angle between the arm 4 relative to the point B on the disk 3)	$\varepsilon$
Power	$P$
driving mechanical power (input)	$P_m$
actual active power supplied to the grid	$P_E$

The main aim of this paper is simulation verification of mechanical model of synchronous machine with electromagnetic representation covering mechanics of synchronous machine. The mechanical model of synchronous machine is open for broad engineering community to be used for dynamic stability simulations neglecting the internal electrical engine details. Using mechanical model would facilitate the application of modern non-standard methods (Wave-based, adaptive, predictive, etc.) on smart control and optimizing of electrical machines - synchronous and asynchronous, AC and DC.

### Acknowledgments

This research has been realized using the support of EU Regional Development Fund in OP R&D for Innovations (OP VaVpI) and The Ministry of Education, Youth and Sports, Czech Republic, project # CZ.1.05/2.1.00/03.0125 Acquisition of Technology for Vehicle Center of Sustainable Mobility, the support of The Ministry of Education, Youth and Sports program NPU I (LO), project # LO1311 Development of Vehicle Centre of Sustainable Mobility and the support of Technological Agency, Czech Republic, programme Centres of Competence, project # TE01020020 Josef Božek Competence Centre for Automotive Industry. This support is gratefully acknowledged.

### References

- [1] S. B. Griscom. A Mechanical Analog to the Problem of Transmission Stability. *The Electric Journal*, XXIII(5):230-235, 1926.
- [2] J. Pavelka. *Synchronous Machines* (in Czech). SNTL, Prague, 1965.
- [3] R. Park. Two Reaction Theory of Synchronous Machines. *Transactions of the AIEE*, 48:716-730, 1929.
- [4] C. Concordia. Two Reaction Theory of Synchronous Machines with Any Balanced Terminal Impedance. *Transactions of the AIEE*, 56:1124-1127, 1937.
- [5] T. Laible. *Die Theorie der Synchromachine im nichtstationären Betrieb*. Springer-Verlag, Berlin, Göttingen, Heidelberg, 1952.
- [6] J. Měříčka, Z. Zoubek. *The general theory of electrical machines* (in Czech). SNTL, Prague, 1973.
- [7] H. W. Weber. New Frequency and Power Oscillations in the Enlarged Westeuropean Interconnected Network Reasons and Counter Measures. *Preprints of the IFAC/CIGRE Symposium on Control of Power Systems and Power Plants*, 85-90, 1997.
- [8] L. P. Singh. *Advanced Power System Analysis and Dynamics*. New Age International (P) Ltd, New Delhi, 2006.
- [9] J. Machowski, J. W. Bialek, J. R. Bumby. *Power System Dynamics and Stability*. John Willey & Sons Ltd, Chichester, 1998.

# A new Software for Solving Inverse Problems in Multibody Dynamics

Karin Nachbagauer<sup>1</sup>, Thomas Lauß<sup>1,2</sup>, Stefan Oberpeilsteiner<sup>1,2</sup>, Wolfgang Steiner<sup>1</sup>

<sup>1</sup> Faculty of Engineering and Environmental Sciences  
University of Applied Science Upper Austria  
Stelzhamerstraße 23, 4600 Wels, Austria

[karin.nachbagauer, thomas.lauss, stefan.oberpeilsteiner, wolfgang.steiner]@fh-wels.at

<sup>2</sup> Institute of Mechanics and Mechatronics  
Vienna University of Technology  
Getreidemarkt 9/325, 1060 Wien, Austria

## Abstract

In the last few years inverse problems are becoming more and more important in the community of multibody system dynamics. The current paper presents an easy to use software for solving inverse problems in multibody dynamics which includes various strategies for the solution of parameter identification and/or optimal control problems in time- or frequency-domain. The software bases on the adjoint method which enables an efficient computation of the gradient for an objective function [1]. For complex multibody systems, an efficient strategy for the combined forward and backward simulation of the state and the co-state (adjoint) equations is implemented. Therefore, the software enables not only efficient applications in industry, but allows as well the analyses and investigation of new research ideas within this field.

## 1 The adjoint approach

A general approach to an inverse problem is the formulation as an optimization task. In this case, the main task is the identification of actuating forces/moments or parameters of a multibody system which minimize a time-continuous cost function  $J$ , e.g., the mean deviation of a system output from a measured signal. The bottleneck is, on the one hand, the large number of degrees of freedom of a multibody system which includes flexible bodies and, on the other hand, the expensive computation of the gradient of the cost function  $J$ . Especially, in the field of multibody systems, the effort of the computation of the gradient of a cost function is significantly reduced by using the adjoint method. The basic idea of the adjoint method is the introduction of additional adjoint variables determined by a set of adjoint differential equations from which the gradient can be computed straightforward. This main idea directly corresponds to the gradient technique for trajectory optimization pioneered by Bryson and Ho [2]. Various authors have utilized the adjoint method in the field of multibody system already more than twenty years ago, as e.g., [3–5], but nevertheless, the topic still provides open research potential as several contributions were published recently [1, 6–9]. The main goal of this contribution is the realization of the adjoint method for the gradient computation in order to solve both, parameter identification and/or optimal control problems as well as in time- or in frequency-domain within one software tool. The software is controlled by an easy-to-write input file in text-format, in which the domain and the parameters for the adjoint method can be selected and varied easily. It enables a wide range of applications, driven both by research questions and industrial problems. Various examples show the clear structure in the model file and the input file as well as the user interface for the software.

## 2 Available strategies for the adjoint method: (classical) continuous or discrete adjoint method

The use of the classical adjoint method for a multibody system described by a system of differential-algebraic equations of index 3 for optimal control problems or parameter identification applications has been presented in [1]. In this work, for the implicit time integration of the multibody system the classical HHT-algorithm [10, 11] is utilized, while a backward differentiation scheme is used for the adjoint system. An alternative and maybe more natural approach is the discrete adjoint method, presented in [8], which constructs a finite difference scheme for the adjoint system directly from the HHT-algorithm which is used for the solution of the equations of motion. The discrete adjoint method provides two main advantages as compared to the classical adjoint method, namely that no separate solver is necessary to solve the adjoint differential algebraic system backward in time, and, in case accelerations are included in the cost function, the Jacobian entries for the discrete adjoint computation simplify significantly. Both methods are implemented in the presented software.

### 3 Available domains: time- or frequency-domain

Depending on the inverse problem to solve, one can choose between classical time-domain or frequency-domain based procedures in the user interface. In most cases of the classical method in the time-domain, the results lead to some kind of best-fit solution, which means that high frequency components with low amplitudes are not considered. However, the identification of parameters which influence the system at particular frequencies or frequency ranges is an important issue. The basic idea is to compute the Fourier coefficients for the relevant oscillations and include the according amplitudes in the cost functional, see the work by Lauß et al. [9] for details. Therein, the parameter identification of a torsional vibration damper based on spectral data from a test bench is presented as an application of the adjoint method in frequency-domain.

### Acknowledgments

K. Nachbagauer acknowledges support from the Austrian Science Fund (FWF): T733-N30.

### References

- [1] K. Nachbagauer, S. Oberpeilsteiner, K. Sherif, W. Steiner. The Use of the Adjoint Method for Solving Typical Optimization Problems in Multibody Dynamics, *Journal for Computational and Nonlinear Dynamics*, Vol.10, Nr.6, 061011, doi: 10.1115/1.4028417, 2015.
- [2] A. E. Bryson, Y. C. Ho. *Applied Optimal Control*, Hemisphere, Washington, DC, 1975.
- [3] E.J. Haug, R.A. Wehage, N.K. Mani. Design sensitivity analysis of large-scaled constrained dynamic mechanical systems, *Trans ASME*, Vol.106, 156-162, 1984.
- [4] D. Bestle, P. Eberhard. Analyzing and Optimizing Multibody Systems, *Mech. Struc. Mach.*, Vol.20, 67-92, 1992.
- [5] P. Eberhard. Adjoint Variable Method for Sensitivity Analysis of Multibody Systems Interpreted as a Continuous, Hybrid Form of Automatic Differentiation, *Proc. of the 2nd Int. Workshop on Computational Differentiation*, Santa Fe. Philadelphia: SIAM, 319-328, 1996.
- [6] L. Petzold, S. Li, Y. Cao, R. Serban. Sensitivity analysis for differential-algebraic equations and partial differential equations, *Computers and Chemical Engineering*, Vol.30, 1553-1559, 2006.
- [7] J.-Y. Ding, Z.-K. Pan, L.-Q. Chen. Parameter identification of multibody systems based on second order sensitivity analysis, *International Journal of Non-Linear Mechanics*, Vol.47, 1105-1110, 2012.
- [8] T. Lauß, S. Oberpeilsteiner, W. Steiner, K. Nachbagauer. The Discrete Adjoint Gradient Computation for Optimization Problems in Multibody Dynamics. *Journal for Computational and Nonlinear Dynamics*, Vol.12, Nr.3, 031016, DOI 10.1115/1.4035197, 2016.
- [9] T. Lauß, S. Oberpeilsteiner, K. Nachbagauer, W. Steiner. Parameter Identification of a Torsional Vibration Damper in Frequency Domain Using Adjoint Fourier Coefficients, *Proceedings of the ECCOMAS Thematic Conference on Multibody Dynamics*, Prague, June 19-22, 2017.
- [10] H.M. Hilbert, T.J.R. Hughes, R.L. Taylor. Improved numerical dissipation for time integration algorithms in structural dynamics, *Earthquake Engineering and Structural Dynamics*, Vol.5, 283-292, 1977.
- [11] D. Negrut, R. Rampalli, G. Ottarsson, A. Sajdak. On the Use of the HHT Method in the Context of Index 3 Differential Algebraic Equations of Multibody Dynamics, *Int. J. Numer. Meth. Engng*, 1-24, 2000.

## **Section**

## **ROBOTICS**



# Cable Driven Spherical Mechanism Quadrosphere Enhanced by 3 DOF Piezo-actuated Platform

Zbyněk Šika<sup>1</sup>, Petr Beneš<sup>1</sup>, Michael Valášek<sup>1</sup>, Jiří Volech<sup>1</sup>, Karel Kraus<sup>1</sup>,

Radek Bulín<sup>2</sup>, Michal Hajžman<sup>2</sup>, Pavel Polach<sup>2</sup>

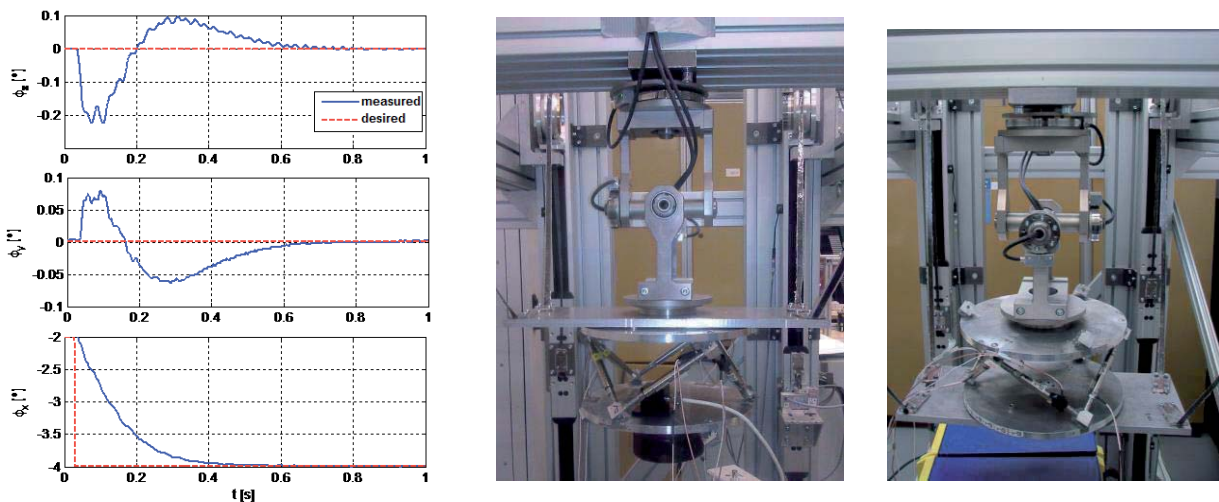
<sup>1</sup>Faculty of Mechanical Engineering  
Czech Technical University in Prague  
Technická 4, 166 07 Prague, Czech Republic  
[zbynek.sika, petr.benes, michael.valasek,  
jiri.volech, karel.kraus]@fs.cvut.cz

<sup>2</sup>Faculty of Applied Sciences  
University of West Bohemia  
Univerzitní 22, 306 14 Pilsen,  
Czech Republic  
[rbulin, mhajzman,  
ppolach]@ntis.zcu.cz

## Abstract

The cable/fibre driven variants of parallel kinematic mechanisms (PKM) combine the concept of parallel machines with the usage of cables instead of rigid links. This solution removes many weaknesses of PKM and brings further advantages. The number of kinematic joints can be lower, the weight is typically very low, the workspace is larger and easily reconfigurable and the construction is cheaper compare to the mechanisms with traditional links and joints. Natural and indeed necessary is the anti-backlash control [1]. The application area of cable driven PKM is very large ranges from the cargo handling [2] and astronomic applications [3], [4] to humanoid-arm manipulators [5] or snake-like manipulators.

The demonstrator of the cable driven mechanism QuadroSphere (Fig. 1) has a moving platform with 3 DOF driven by four fibres that performs a spherical motion around a central point. The triple of revolute joints is equipped with three rotational encoders for position feedback. The tension in cables/fibres is measured by force sensors. The stand is controlled by the dSpace DS1103 controller board through four AC servo drives. The motion control combines the position and force control in order to ensure that fibres are under tension [6]. The control approach was tested using many desired trajectories and motions of the demonstrator platform, e.g. the step response in Fig. 1 a). The implemented control scheme prevents mutual fighting of particular drives and ensures the tension in fibres.



a) Experiments with motion control

b) Demonstrator with 6 DOF secondary platform positioned by piezoactuators

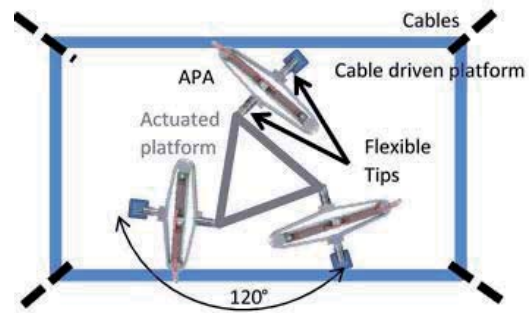
Figure 1. Demonstrator of cable driven spherical mechanism QuadroSphere

One drawback of the cable driven PKM is relatively low resultant stiffness and consequently the relatively narrow frequency bandwidth of end-effector motion control. To avoid these problems the concept of a multi-level mechanisms has been introduced. The term multi-level means a hierarchical structure composed from the cable driven primary platform for large and slower component of the motion and the secondary platform connected to the primary one for the small and higher frequency motion components [7]. The primary experiments with multi level structure use small Stewart platform driven by 6 piezoactuators in the cubic architecture (Fig. 1 b)). Two different structure configurations were analysed and tested. The external variant (left) has the active structure

outside the main kinematic loops created by fibres and the positioned tilting platform. The principle of acting in this configuration is similar to 6 DOF active vibration absorber. The internal variant (right) has the active piezo structure inside the main kinematic loops created by fibres and the positioned tilting platform. The piezoactuators used for the primary experiments were available in the laboratory at the time of experiment but they weren't optimized for the given platform and the experiments showed that their stroke  $60\ \mu\text{m}$  is rather small for correction of positioning error of primary cable driven platform (Fig. 2a)). Currently the experimental testing of multi-level spherical mechanism demonstrator using additional platform (Fig. 2b)) positioned by 3 mechanically amplified piezoactuators („APA” with stroke up to approximately 300 micrometers) is under preparation.



a) Demonstrator of spherical cable driven platform



b) Scheme of added secondary 3 DOF platform

**Figure 2.** Concept of cable driven spherical mechanism enhanced by 3 DOF platform

The multi-level robots/manipulators have the potential to improve properties of the pure cable driven variants. The combination of lightweight manipulator with large workspace with the ability to perform highly dynamic maneuvers is unique. The first presented control strategy based on combination of the position and force control of fibre driven platform is fully functional that was proved by test on experimental stand but it doesn't fully utilize potential of redundantly actuated platform. The second strategy - centralized control with force distribution among all actuators enables better control of tension distribution in cables. In the combination with the H-infinity approach that was applied on superimposed active platform it is suitable to effectively control multi-level mechanism. Simulation experiments performed on the simulation model proved that the control concept fulfill expectations – cable driven platform is suitable for low frequency components and high frequency part is performed by piezo-actuated platform. The simulation experiments give the promising results, the experiments will follow.

## Acknowledgments

The paper has originated in the framework of solving the project of the Czech Science Foundation No. 15-20134S entitled “Multi-level Light Mechanisms with Active Structures”.

## References

- [1] M. Valášek and M. Karásek, "Kinematical Analysis of HexaSphere," *Conference Proceedings of Engineering Mechanics*, pp. 1371–1378, 2009.
- [2] Y. Patel and P. George, “Parallel Manipulators Applications—A Survey,” *Modern Mechanical Engineering*, vol. 2, pp. 57-64, 2012.
- [3] B. Zi, Z. Zhu and J. Du, “Analysis and control of the cable-supporting system including actuator dynamics,” *Control Engineering Practice*, vol. 19, pp. 491-501, 2011.
- [4] G. Meunier, B. Boulet and M. Nahon, “Control of an Overactuated Cable-Driven Parallel Mechanism for a Radio Telescope Application,” *IEEE Transactions on Control Systems Technology*, vol. 17 No. 5, pp. 1043-1054, 2009.
- [5] Q. Chen, W. Chen, G. Yang and R. Liu, “An Integrated Two-Level Self-Calibration Method for a Cable-Driven Humanoid Arm,” *IEEE Transactions on Automation Science and Engineering*, vol. 10 No.2, pp. 380-391, 2013.
- [6] T. Skopec, Z. Šika and M. Valášek, “Calibration using adaptive model complexity for parallel and fiber-driven mechanisms,” *Robotica*, vol. 34, pp. 1416-1435, 2016.
- [7] P. Svatoš, Z. Šika, P. Beneš, M. Hajžman and J. Závřel, "Cable Driven Mechanisms with Added Piezo Active Platform," *Bulletin of Applied Mechanics*, vol. 11, no. 38, no. ISSN 1801-1217, 2015, pp. 19-24.

## On the Use of Principal Vectors in Multibody Dynamics

Volkert van der Wijk

Faculty of Mechanical, Maritime and Materials Engineering  
Department of Precision and Microsystems Engineering - Mechatronic System Design  
Delft University of Technology, Mekelweg 2, 2628 CD, Delft, The Netherlands  
v.vanderwijk@tudelft.nl

### Abstract

Otto Fischer's method of principal vectors from well over a century ago [1] has proven to be of enormous value for the design of dynamically balanced mechanisms, i.e. mechanisms that do not exert dynamic reaction forces and moments to their base for all motions [2]. This is because of its geometrical insight in the system's dynamics, which has led to an extensive development of the theory in the recent years. Some fundamentals of the method have also been used in the 70's to physically interpret a simpler form of dynamic equations in a.o. [3, 4] where principal vectors were referred to as 'barycentric vectors'. The question is what we can learn and how we can further benefit from this method. The aim here is not solely analysis, but rather to use the method as a starting point in the design of mechanisms with specific desired dynamic properties.

By example of a double pendulum it is shown how the Lagrange equations of motions can be written to depend solely on lengths (principal dimensions) and reduced inertia terms. The results are discussed and interpreted at the end.

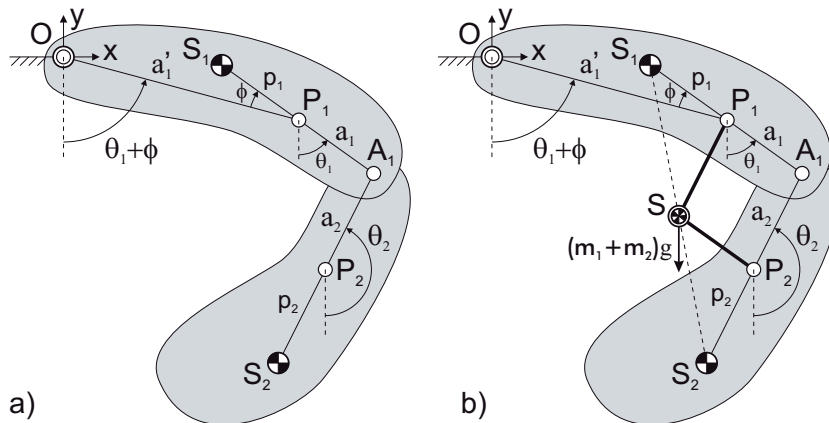


Figure 1: a) General double pendulum of two rigid bodies connected with revolute pairs in  $A_1$  and in base pivot  $O$ , the base joint; b) The parallelogram  $A_1P_1SP_2$  with principal dimensions  $a_1$  and  $a_2$  traces the common CoM  $S$  for all motions. The gravity force applies in  $S$ .

Figure 1a shows a planar double pendulum of two rigid bodies with revolute pairs in  $A_1$  and in base pivot  $O$ . Each body has a mass  $m_i$  and inertia  $I_i$  about a generally located center of mass (CoM)  $S_i$  and their motions are described with angles  $\theta_i$ . Figure 1b shows that the common CoM  $S$  of both bodies can be traced for all motions with a parallelogram  $A_1P_1SP_2$  with dimensions  $a_1$  and  $a_2$ , which are named the principal dimensions [2]. These are the lengths of the principal vectors describing the locations of the principal points  $P_1$  and  $P_2$  in each element and are determined by  $m_1p_1 = m_2a_1$  and  $m_2p_2 = m_1a_2$ . With  $a'_1$  and constant angle  $\phi$  the location of  $S$  can be described with the principal dimensions as:

$$x_S = a'_1 \sin(\theta_1 + \phi) + a_2 \sin(\theta_2 - \pi), \quad y_S = -a'_1 \cos(\theta_1 + \phi) - a_2 \cos(\theta_2 - \pi) \quad (1)$$

Generalized from Fisher [1, 2], the kinetic energy of the double pendulum can be written as:

$$T = m_{tot}\left\{\frac{\dot{x}_S^2}{2} + \frac{\dot{y}_S^2}{2}\right\} + m_{tot}\left\{\frac{\chi_1^2}{2}\dot{\theta}_1^2 + \frac{\chi_2^2}{2}\dot{\theta}_2^2 - a_1a_2\cos(\theta_1 - \theta_2)\dot{\theta}_1\dot{\theta}_2\right\} \quad (2)$$

with the reduced inertias  $\chi_i$  written as  $m_{tot}\chi_1^2 = I_1 + m_1p_1^2 + m_2a_1^2$  and  $m_{tot}\chi_2^2 = I_2 + m_1a_2^2 + m_2p_2^2$ . The first term is the kinetic energy of the absolute motion of the common CoM and the second term is the kinetic energy of the double pendulum motion relative to the common CoM. More details of this formulation can be found in [2]. With the derivatives of Eqs. (1) substituted, the kinetic energy can be rewritten as:

$$T = m_{tot}\left\{\frac{\chi_1^2 + a_1^2}{2}\dot{\theta}_1^2 + \frac{\chi_2^2 + a_2^2}{2}\dot{\theta}_2^2 - (a_1a_2\cos(\theta_1 - \theta_2) + a_1'a_2\cos(\theta_1 + \phi - \theta_2))\dot{\theta}_1\dot{\theta}_2\right\} \quad (3)$$

Then with the potential energy  $V = -m_{tot}g(a_1'\cos(\theta_1 + \phi) - a_2\cos\theta_2)$  the Langrange equations of motion can be obtained as:

$$(\chi_1^2 + a_1'^2)\ddot{\theta}_1 - (a_1a_2\cos(\theta_1 - \theta_2) + a_1'a_2\cos(\theta_1 + \phi - \theta_2))\ddot{\theta}_2 - (a_1a_2\sin(\theta_1 - \theta_2) + a_1'a_2\sin(\theta_1 + \phi - \theta_2))\dot{\theta}_2^2 = -ga_1'\sin(\theta_1 + \phi) \quad (4)$$

$$(\chi_2^2 + a_2^2)\ddot{\theta}_2 - (a_1a_2\cos(\theta_1 - \theta_2) + a_1'a_2\cos(\theta_1 + \phi - \theta_2))\ddot{\theta}_1 + (a_1a_2\sin(\theta_1 - \theta_2) + a_1'a_2\sin(\theta_1 + \phi - \theta_2))\dot{\theta}_1^2 = ga_2\sin\theta_2 \quad (5)$$

The right side of the equations shows the influence of the applied gravity force, depending solely on the gravity  $g$  and principal dimensions  $a_1'$  and  $a_2$ . Evaluation of the left side shows that it solely depends on the principal dimensions  $a_1$ ,  $a_2$ , and  $a_1'$  together with the reduced inertia terms. Both equations are similar with coefficients  $a_1a_2$  and  $a_1'a_2$ . With other methods these equations generally result with coefficients writing *mass times length times length*. The advantage of this formulation is that the coefficients are based on the graphical construction in Fig. 1b. This enhances intuitive investigation and optimization of the system dynamics. For instance for a given motion  $\ddot{\theta}_i(t)$ ,  $\dot{\theta}_i(t)$ , and  $\theta_i(t)$  the required action forces/moments or maximum reaction forces/moments could be optimized by deriving the optimal values for  $a_1$ ,  $a_2$ , and  $a_1'$ . Subsequently from these principal dimensions the exact mass parameters may be derived.

As example the situation that  $a_1' = 0$  and  $a_2 = 0$  where  $P_1$  and  $O$  coincide and  $P_2$  and  $A_1$  coincide. Then the gravity terms at the right side become zero. This means that the double pendulum has become gravity balanced. All sin and cos terms on the left then also disappear with which the equations of motion reduce to the linear decoupled set:

$$\chi_1^2\ddot{\theta}_1 = 0, \quad \chi_2^2\ddot{\theta}_2 = 0 \quad (6)$$

How such an optimization can be used for other situations and other mechanisms is topic of discussion and further research and is essential to reveal the full potential of this method.

## References

- [1] O. Fischer. Theoretische Grundlagen für eine Mechanik der Lebenden Körper. Teubner, Leipzig, 1906.
- [2] V. van der Wijk. Methodology for Analysis and Synthesis of Inherently Force and Moment-balanced Mechanisms - Theory and Applications (dissertation). University of Twente (free download: <http://dx.doi.org/10.3990/1.9789036536301>), 2014.
- [3] J. Wittenburg. Dynamics of Systems of Rigid Bodies. B.G. Teubner Stuttgart, 1977.
- [4] R. E. Roberson. Dynamics of Multibody Systems. Springer-Verlag, 1988.

## Robust rest-to-rest motion planning for cranes through a variational solution

Paolo Boscarì<sup>1</sup>, Dario Richiedei<sup>1</sup>

<sup>1</sup> Università degli Studi di Padova, DTG  
Stradella S. Nicola, 36100 Vicenza, Italy  
paolo.boscarì@unipd.it, dario.richiedei@unipd.it

### Abstract

The operation of overhead cranes requires to deal with the problem of damping or eliminating the load oscillation that naturally occur during and after the motion. Such a problem is usually tackled both in literature and in industrial practice through closed-loop control or through open loop control. The latter approach consists in designing optimal command profiles that move the load to the desired position without residual load oscillations. One of the most critical issues in the development of effective command references is the robustness with respect to the unavoidable model uncertainty. Despite its relevance, this problem has been explored less frequently.

An effective approach to include robustness specification in rest-to-rest motion planning of oscillatory systems is the one introduced and tested numerically in [1], which is for the first time validated experimentally in this work. The proposed solution is based on the formulation of the trajectory planning problem as a Two-Point Boundary Value Problem (TBPVP) to be solved through some well-established and reliable methods. In order to account for robustness, the proposed method is based on a new definition of the standard TBPVP by including the sensitivity functions of the dynamic model of the plant and by adding suitable additional boundary conditions. Additionally, some new features are included in the problem formulated in this work, to deal with the characteristics of real systems with finite control bandwidths.

In its nominal form, a rest-to-rest motion planning problem can be translated into a variational problem as follows. The dynamics of the flexible system should be described by a system of first-order ordinary differential equations (ODEs),  $\dot{\mathbf{x}}(t) = \mathbf{\Omega}(\mathbf{x}, \mathbf{u}, t, \eta)$  in which  $\mathbf{x}(t)$ ,  $\mathbf{u}$ ,  $t$  and  $\eta$  are the state, the input, the time and a generic scalar model parameter, respectively. The properties of the trajectory can be shaped by choosing the suitable cost function, defined as the time integral of the function  $\mathbf{f}(\mathbf{x}, t, \mathbf{u}, \eta)$  evaluated over the execution time, with desired initial and final states  $\mathbf{x}(t_0)$  and  $\mathbf{x}(t_f)$  as the boundary conditions. The solution of the TPBVP problem can be solved, in its nominal form, by defining the Hamiltonian  $\mathcal{H} = \mathbf{f} + \boldsymbol{\lambda}^T \mathbf{\Omega}$ , where  $\boldsymbol{\lambda}(t) = [\lambda_1, \dots, \lambda_N]^T$  are the Lagrangian multipliers. According to the Pontryagin Minimum Principle, the necessary conditions for the optimal solution are:

$$\frac{\partial \mathcal{H}}{\partial \mathbf{u}} = \mathbf{0}; \quad \dot{\mathbf{x}}(t) = \frac{\partial \mathcal{H}}{\partial \boldsymbol{\lambda}}; \quad \dot{\boldsymbol{\lambda}}(t) = -\frac{\partial \mathcal{H}}{\partial \mathbf{x}} \quad (1)$$

The conditions in Eq. (1) can be written as a single equation by defining the minimizing Hamiltonian  $\mathcal{H}^* = \mathcal{H}(\mathbf{u}^*(t))$ , with  $\mathbf{u}^*(t)$  as the input such that  $\frac{\partial \mathcal{H}}{\partial \mathbf{u}} = \mathbf{0}$ . The minimizing Hamiltonian can be used to define a system of ODEs with the augmented state vector  $\mathbf{y}(t) = [\mathbf{x}, \boldsymbol{\lambda}]^T$ :

$$\dot{\mathbf{y}} = \begin{bmatrix} \frac{\partial \mathcal{H}^*}{\partial \boldsymbol{\lambda}} \\ -\frac{\partial \mathcal{H}^*}{\partial \mathbf{x}} \end{bmatrix} \quad (2)$$

The solution in Eq. (2) is the nominal solution for the rest-to-rest motion planning problem, since the effects of the perturbation to the parameter  $\eta$  are neglected.

The robust motion planning problem can be defined by augmenting the dynamic model with the sensitivity functions of  $\mathbf{\Omega}$ , i.e. its partial derivative with respect to  $\eta$ , leading to the augmented system  $\mathbf{\Omega}_r$  and state  $\mathbf{x}_r$ :

$$\dot{\mathbf{x}}_r(t) = \begin{bmatrix} \dot{\mathbf{x}}(t) \\ \dot{\mathbf{s}}(t) \end{bmatrix} = \begin{bmatrix} \mathbf{\Omega}(\mathbf{x}, \mathbf{u}, t, \eta) \\ \frac{\partial \mathbf{\Omega}(\mathbf{x}, \mathbf{u}, t, \eta)}{\partial \eta} \end{bmatrix} = \mathbf{\Omega}_r(\mathbf{x}, \mathbf{u}, t, \eta) \quad (2)$$

The robust problem can be solved through the method described by Eqs. (1) and (2), with obvious modifications of the meaning of the terms. Some additional boundary conditions can be set. In particular, the values of the sensitivity functions  $\mathbf{s}(t)$  are set to zero at both initial and final time to impose minimal sensitivity of the solution to possible mismatches between the real and the modeled plant.

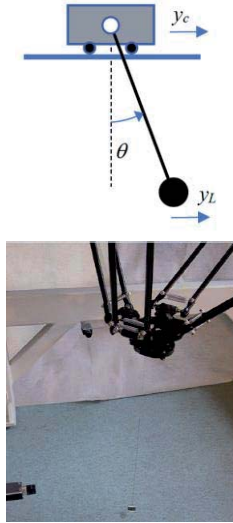


**Figure 1.** Scheme and picture of the studied system

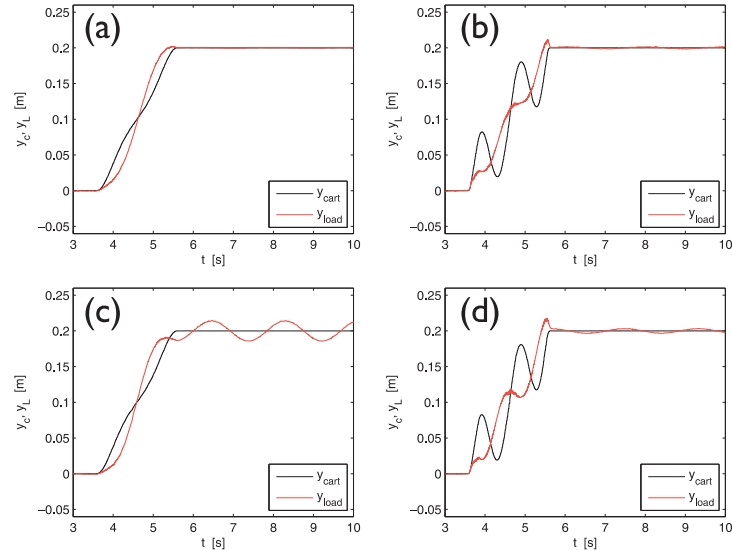


**Figure 2.** Experimental results: nominal (a,c) and robust trajectories (b,c), with nominal (a,b) and perturbed plants (c,d)

The model can be further augmented to include simplified models of the controlled actuator dynamic and hence to ensure feasibility of the generated motion profiles in real systems. Additionally, unlike other works in literature (see e.g. [2]), it can be applied to plants described by nonlinear dynamics, with both forces or accelerations as the model input.

Experimental results have been obtained using the testbed shown in Fig. 1, in which an Adept Quattro robot is used to mimic the motion of the cart of an overhead crane. A massless pendulum with length equal to 0.962 m is attached to the cart and the angular position of the pendulum  $\theta$  is measured using a camera. The experimental results shown in Fig. 2 compares the nominal and robust trajectories synthesized through the proposed method. All measurements refer to a sample motion consisting in a translation of the cart equal to 0.2 m in 2 s. The output of the problem solution is the time history of the desired position for the cart, which is used as the command references for the robot closed-loop position control.

The plot in Fig.2(a) shows the results of the application of the nominal trajectory to the nominal plant with no model mismatch, by showing the measured position of the cart  $y_c$  and the measured position of the suspended load  $y_L$ . The plot (b) shows the results obtained by synthesizing the command reference with the robust approach and, again, with the nominal plant. In particular, the robustness improvement has been obtained by including the sensitivity function with respect to the natural frequency of the load swing vibrational mode. In both cases the prescribed rest-to-rest conditions are obtained, since the residual oscillation of the load is negligible. The slightly lesser accuracy obtained in the case of robust planning is mainly due to the limited tracking precision of the robot observed during high dynamic motion. It should be noticed that the nominal trajectory, as shown in Fig.2(a), has only positive values of the cart speed. In contrast the robust command reference in Fig.2(b) imposes both positive and negative speeds. This feature results in higher peak values of cart speed and acceleration, and in harmonic components with higher frequency, thus making the tracking more difficult.

In order to test the actual robustness improvement brought by the proposed method, two further results are shown in Fig.2(c-d). Such tests consist in performing the same motion with a pendulum length reduced by 0.18 m. This modification induces an increase of the natural frequency of the load oscillation and therefore a sensible mismatch between the modeled and the actual plants. As can be seen in Fig.2(c), the application of the nominal trajectory results in a large residual oscillation of the load, while a noticeably lower amplitude is obtained by using the robust trajectory. This result confirms that the proposed method can be effectively used to improve the robustness to parametric mismatches between the model of the plant used for trajectory planning and the actual plant.

Other results, not reported here, has shown that the proposed techniques can effectively plan much faster motion profiles, lasting less than half of the oscillation period, and can be extended to overhead cranes with double and triple pendulum as well.

## References

- [1] P. Boscaroli, A. Gasparetto, Robust model-based trajectory planning for nonlinear systems, *Journal of Vibration and Control*, 22(18), 3904-3915, 2016
- [2] T.A. Hindle, T. Singh Desensitized minimum power/jerk control profiles for rest-to-rest maneuvers. *American Control Conference*, 2000, vol.5, pp. 3064-3068, IEEE

## Comparison of Distributed Model Predictive Control Approaches for Transporting a Load by a Formation of Mobile Robots

Henrik Ebel<sup>1</sup>, Ehsan Sharafian Ardakani<sup>1</sup>, Peter Eberhard<sup>1</sup>

<sup>1</sup>Institute of Engineering and Computational Mechanics  
University of Stuttgart  
Pfaffenwaldring 9, 70569 Stuttgart, Germany  
[henrik.ebel, ehsan.sharafian, peter.eberhard]@itm.uni-stuttgart.de

### Abstract

Over the last couple of years, technological advances have made it seem increasingly feasible to solve complicated tasks by employing a group of autonomous systems that need to cooperate to achieve a common goal. Driven by the possible advantages like increased flexibility and robustness, this has led to a growing scientific interest in the development of distributed control schemes that make this vision realizable from a control-theoretic point of view [1, 2].

In this context, this paper compares different distributed formation control approaches based on model predictive control (MPC) [3]. Specifically, the presented control schemes are used to govern the motion of omnidirectional mobile robots that shall maintain a given formation shape while following a path through a previously unknown environment. As illustrated in Figure 1, the setup of the control schemes is motivated by the task of letting the formation transport an elastic plate purely by normal and friction forces.

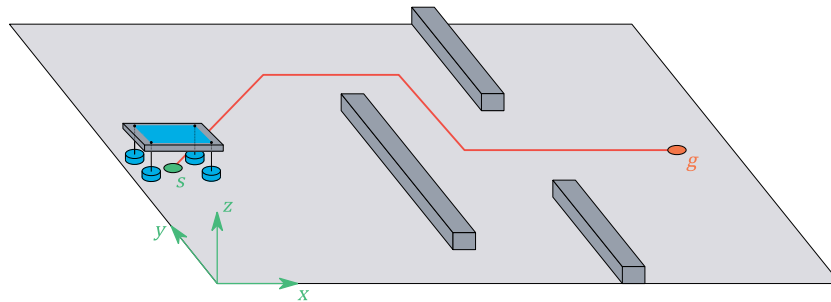


Figure 1. Illustration of the plate transportation task

The intricacy of this task motivates the choice of model predictive control since it allows to explicitly constrain the movements of the robots to the end of improving the transportation performance. However, typically, MPC is applied to systems where one central entity solves an overall optimization problem to determine the optimal control behavior. In contrast to that, the distributed control of mobile robots necessitates that each robot solves its own optimization problem and may only exchange information with the other robots before and after the optimization. Fortunately, in recent years, a multitude of algorithms and methods have been developed that make it possible to apply model predictive control to a group of distributed systems [1].

The specific schemes proposed and compared in this paper are rooted in the general theory presented in [4] and [5]. These two approaches are fundamentally different in their optimization and communication strategies. In [4], the systems optimize and transmit information sequentially one after another, while in [5], they can optimize concurrently but possibly need several optimization and communication iterations to achieve a satisfying performance. These and further theoretic differences lead to inherently different proposed formulations of the optimization problems for this paper's formation control task. In the sequential approach, hereafter denoted as sequential distributed MPC (SDMPC), only dynamically decoupled systems can be considered. Therefore, in each robot's MPC optimization problem, directly the individual robots' dynamical properties are used. Consequently, the considered overall system dynamics does not contain any couplings between the robots. All couplings necessary to achieve the cooperative formation control goal are present in the cost function. In contrast to that, in the proposed optimization problem of the iterative distributed MPC (IDMPC) scheme, an artificially designed system is used that contains all of the robots' dynamics, the dynamics of the formation's center of mass, and the dynamics of the robots relative to this center of mass. In principal, the formation control task then comes down to tracking a trajectory with this system in a distributed fashion by using IDMPC. Thus, while the system dynamics of the artificial system is more elaborate and contains more states, the cost function is decidedly

simpler. This motivates the usage of a simplified robot model in the construction of the artificial system to obtain a simpler overall model.

The performance of the two schemes is carefully examined in various simulations. These include situations in which the robots have to shrink the formation in order to squeeze through narrow passages in the environment. The simulations reveal that the two schemes have their individual merits and weaknesses not only on a theoretical level, but also in the perceivable control performance. Importantly, the proposed IDMPC-based scheme may allow for shorter sampling times in real-world applications since, for feasibility, even a single iteration is enough, and, at least in the conducted simulations, already modest numbers of iterations deliver a rather satisfying control performance. This applies especially to the pure formation control task. However, when transporting a plate purely by normal and friction forces, it becomes apparent that the IDMPC controllers lose some control compared to the SDMPMPC controllers because of the usage of the simplified robot model.

Nevertheless, the simulation results show that both of the proposed schemes are fully functional and capable of solving the formation control task in a satisfactory manner. This is exemplified in the simulation results of Figure 2 in which some results obtained with the SDMPMPC scheme are displayed. Furthermore, additionally conducted simulations indicate that the employed controllers are sufficiently robust so that robots can join and leave the formation during system runtime.

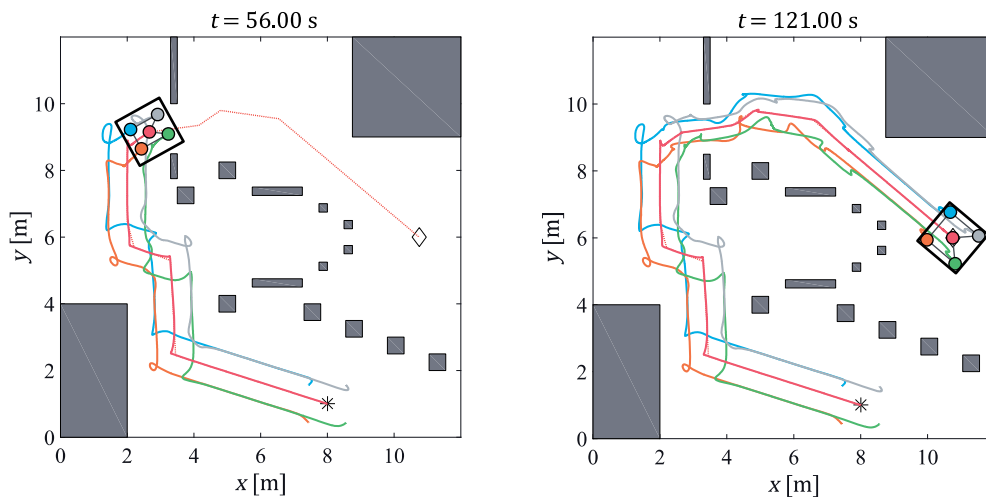


**Figure 2.** Five mobile robots transport a plate through an environment. The plate's traveling height is higher than the obstacles. The proposed SDMPMPC scheme is used to control the robots.

## Acknowledgments

This research was partially funded by the German Research Foundation via the Cluster of Excellence SimTech at the University of Stuttgart. This support is highly appreciated.

## References

- [1] R. Scattolini. Architectures for Distributed and Hierarchical Model Predictive Control - A Review. *Journal of Process Control*, Vol. 19, No. 5, pp. 723-731, 2009.
- [2] F. Bullo, J. Cortés, S. Martínez. *Distributed Control of Robotic Networks*. Princeton University Press, Princeton, 2009.
- [3] J. Maciejowski. *Predictive Control with Constraints*. Pearson Education, Harlow, 2001.
- [4] M.A. Müller, M. Reble, F. Allgöwer. Cooperative Control of Dynamically Decoupled Systems via Distributed Model Predictive Control. *International Journal of Robust and Nonlinear Control*, Vol. 22, No. 12, pp. 1376-1397, 2012.
- [5] A.N. Venkat, J.B. Rawlings, S.J. Wright. Stability and Optimality of Distributed Model Predictive Control. In *Proceedings of the 44<sup>th</sup> IEEE Conference on Decision and Control*, pp. 6680-6685, 2005.

# Performance of a Quasi-Holonomic Mobile Robotic Carrier in the Dynamics Mimicking System

Avi Weiss<sup>1</sup>, Uri Ben Hanan<sup>2</sup>

<sup>1</sup> Department of Mechanical Engineering  
Ort Braude Academic College of Engineering  
51 Snunit, Karmiel, Israel  
avi@braude.ac.il

<sup>2</sup> Department of Mechanical Engineering  
Ort Braude Academic College of Engineering  
51 Snunit, Karmiel, Israel  
ubenhana@braude.ac.il

## Abstract

The dynamics mimicking system was introduced in [1]. The idea is to provide wheelchair users with the ability to traverse rough terrain and even stairs without changing their wheelchair and, especially important, their user interface, which is the way they control the motion of their wheelchair. This is done using a system comprising a carrier robotic platform with capability to traverse rough terrain carrying a dynamics mimicking system, on which the wheelchair stands. The dynamics mimicking system reads the motion of the wheels of the wheelchair and interprets the readings to the desired motion of the wheelchair. This, in turn, is translated into commands to the robotic carrier that performs the desired motion instead of the wheelchair. A basic system was constructed as proof of concept that utilized miniature robotic systems with differentially actuated wheels, which is similar to the way a wheelchair is controlled. However, a wheelchair controls only two wheels, while the robotic system has four. This means that the robotic system always has slip, and as a result, the mimicking is not always accurate. Furthermore, since the robotic system is non-holonomic, it cannot accurately mimic the motion of the wheelchair unless the rotation center of the wheelchair exactly coincide with that of the carrier robot [2]. To improve the ability of the robot to mimic the motion of the wheelchair, a holonomic carrier is preferable. This may be accomplished either by using omnidirectional wheels (e.g., Mecanum wheels) or by allowing steering of all four wheels. The Mecanum wheels are not very practical since the terrain we are interested in traversing is rough and, in many cases, such as a sandy beach, extremely unfriendly for such wheels. The second solution, steerable wheels, allows all required degrees of motion, but not instantaneously, thus we refer to it as a quasi-holonomic solution. The left hand side of Figure 1 shows the suggested robotic system with integrated dynamics mimicking and a wheelchair on top. The right hand side shows the actual system built.

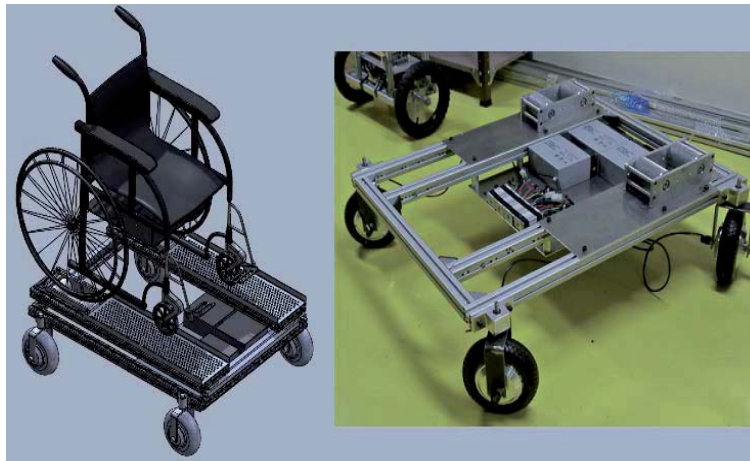


Figure 1: Dynamics mimicking system on a quasi-holonomic carrier robot.

The kinematic model is described in Figure 2. Each wheel of the robotic carrier has a its own steering angle as marked. The input speeds of the wheelchair's driving wheels are marked as  $u(1)$  for the right hand wheel and  $u(2)$  for the left hand wheel.  $d$  is the distance between the wheelchair's wheels,  $w$  is the width of the robotic carrier and  $h$  is the distance between the wheelchair's wheels and the rear wheels of the robotic carrier. Utilizing an instantaneous center of rotation approach for the kinematics, we mark  $x$  as the distance between the robotic carrier and the instantaneous center of rotation along the line connecting the wheelchair's wheels. Thus, we have:

$$x = \frac{d}{u(1) - u(2)} u(2) \quad (1)$$

and from here the steering angles for the wheels are obtained. The problems arise as the changes of the steering angles are not instantaneous due to steering motors limitations. Thus, while the steering angles may be known, one

may not simply command the motors to get to the proper angles at maximum rotational speed. The normals to the velocity vectors of all the wheels must meet at a single point throughout the entire steering process, or there would be slip. Furthermore, if the system already has a certain velocity, the delay in getting to the steering angles creates a deviation from the trajectory anticipated by the user.

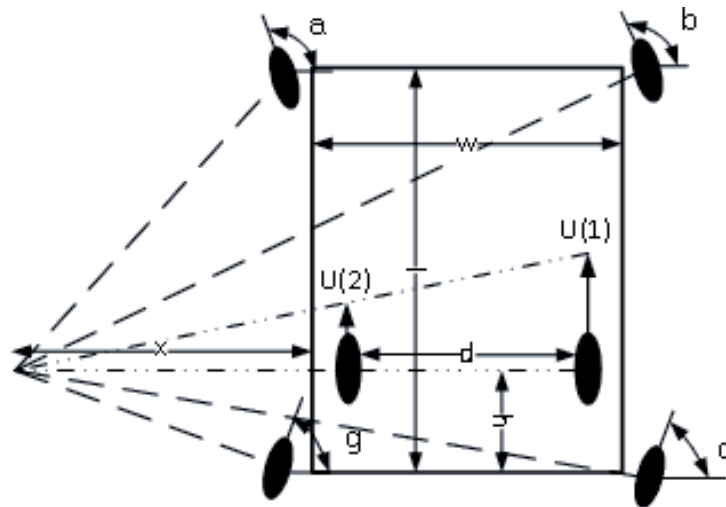


Figure 2: Kinematic model of the carrier robot with the wheelchair's driving wheel illustrated.

Initial results show that using the maximal angular speed of the steering motors, while getting to the correct steering angles the fastest, yields slip during the maneuver as well as trajectory deviations. An approach that prevents slip by maintaining an instantaneous center of rotation throughout the maneuver is using a velocity that is proportional to the change in the steering angle of each wheel. That is, we evaluate the largest steering change, and use the maximal velocity for that wheel. The time to get to the proper angle is then calculated, and the remaining steering commands are evaluated accordingly. Thus, if we mark the required steering angles as  $\theta_i, i = 1, 2, 3, 4$ , we obtain:

$$\begin{aligned}\theta_{max} &= \max \theta_i \\ t &= \frac{\theta_{max}}{\omega_{max}} \\ \omega_i &= \frac{\theta_i}{t}\end{aligned}\tag{2}$$

where  $\omega_{max}$  is the maximal angular velocity of the steering motors and  $\omega_i$  are the required steering motor speeds for the remaining wheels.

## References

- [1] A. Weiss, G. Avigad, U. Ben Hanan. Dynamics Mimicking of Wheelchair as a Mobility Enhancing Platform. ECCOMAS Multibody Dynamics, Barcelona, Spain, July 2015.
- [2] A. Weiss, G. Avigad, U. Ben Hanan. Enhancing Wheelchair Mobility Through Dynamics Mimicking. Proceedings of the 3rd International Conference on Mechanical engineering and Mechatronics. Prague, Czech Republic, August 14-15, 2014.

## Increase of Stiffness in Physically Cooperating Robots

Michael Valasek, Martin Necas, Ladislav Mráz

Faculty of Mechanical Engineering  
 Czech Technical University in Prague  
 Technicka 4, 16607 Praha 6, Czech Republic  
 Michael.Valasek@fs.cvut.cz

### Abstract

The industrial robots have full range of spatial motion and the industrial robots are cheaper than machine tools so the robots can be suitable for carrying out many manufacturing operations like machining. However, the industrial robots have low stiffness, lower than machine tools, it is leading into unacceptable inaccuracies of robot motions under the loading forces from the machining. The goal of robot development is to increase its stiffness.

The proposed solution is to use the physically interconnected robots that cooperate through the robotic interface attached to both grippers of the robots (Fig. 1). This procedure has increased the stiffness but not in sufficient manner.

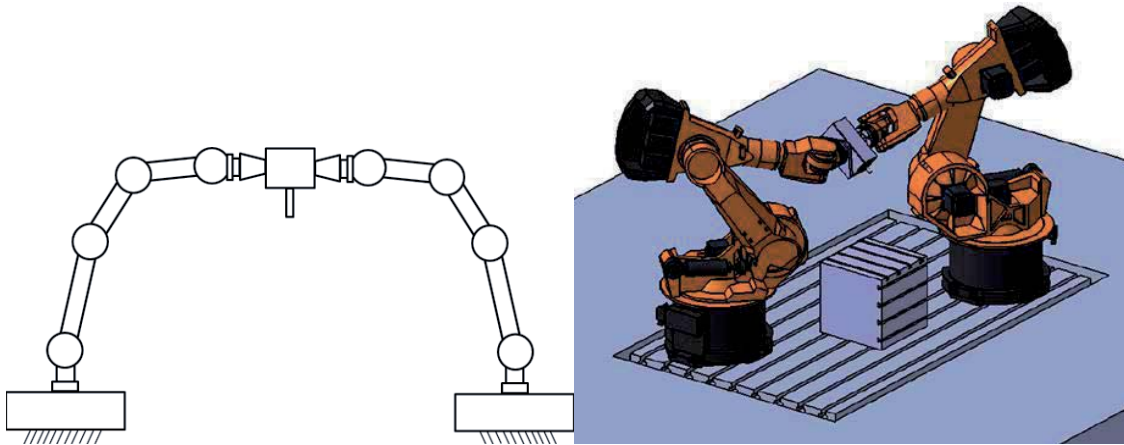


Figure 1 a): The scheme of physically cooperating robots      b) The working concept

However, this can increase the resulting stiffness only 3.5 times, i.e. from 0.5 N/um into  $3.5 \cdot 0.5 = 1.75$  N/um. In order to increase the stiffness more times the additional measurement inside the robot joints (Fig. 2) has been implemented [1, 2].

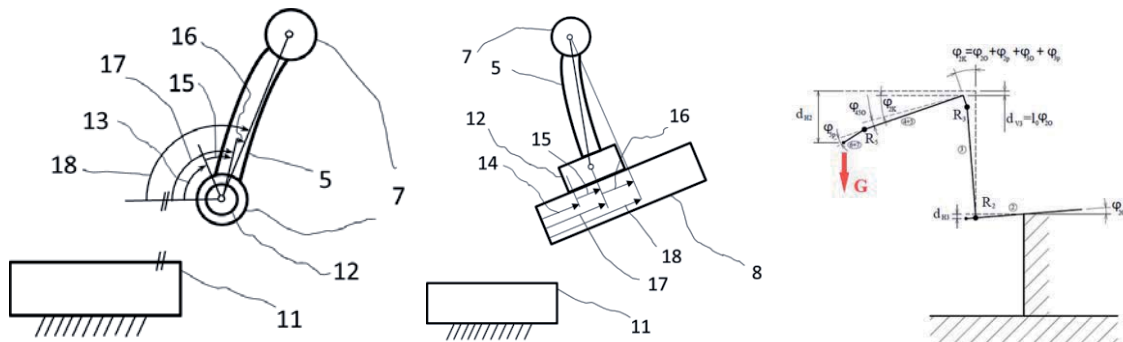


Figure 2 Measurements of deformation in robotic joints: revolute and prismatic. Correction variables.

These joint deformation measurements can serve as the measurement of internal forces within robotic arms. Based on the knowledge of internal forces the deformation of robotic arms due to the bending

and torsion can be estimated (Fig. 3). These measured and estimated deformations can be used for the correction of determination of kinematic position

$$r_E = T_{12}^d T_x(dx_2) T_z(dz_2) T_{\varphi x}(d\varphi_{x2}) T_{\varphi z}(d\varphi_{z2}) \quad (1)$$

$$T_{23}^d T_x(dx_3) T_y(dy_3) T_{\varphi x}(d\varphi_{x3}) T_{\varphi y}(d\varphi_{y3})$$

$$T_{34}^d T_{45}^d T_x(dx_5) T_z(dz_5) T_{\varphi x}(d\varphi_{x5}) T_{\varphi z}(d\varphi_{z5})$$

$$T_{56}^d T_{67}^d [0 \quad y_{6k} \quad 0 \quad 1]^T$$

where the matrix  $T_{i,i+1}^d$  expresses the transformation between the coordinate systems  $i$  and  $i + 1$ , which takes into account also the torsional deformation of shafts. The stiffness is given as

$$K_E = \frac{F}{d} \quad (2)$$

where  $F$  is the force acting on the end point and  $d$  is its overall deformation. If the part  $u$  of overall deformation  $d$  can be determined, then it is possible to compensate this part of deformation. Then the improved robot stiffness is

$$K_{E_{new}} = \frac{F}{(1-u)d} = \frac{1}{(1-u)} K_E \quad (3)$$

It has been achieved the determination of the deformation above 85% ( $u > 0.85$ ). This has increased the stiffness by further factor 7 times. Thus the resulting stiffness is  $3.5 \cdot 7 \cdot 0.5 \text{ N/um} > 12 \text{ N/um}$  and this stiffness is already within the stiffness of realistic machine tool. The carried out experiments with machining confirmed these assumptions.

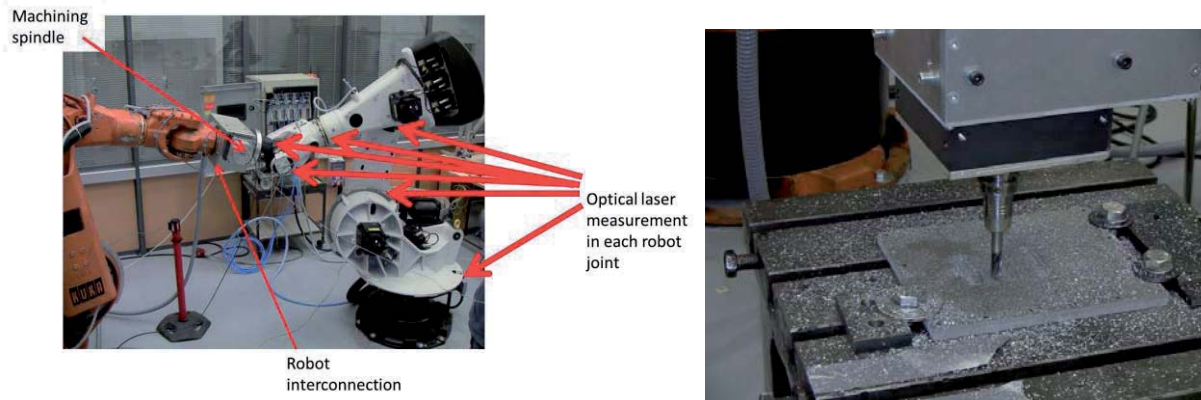


Figure 3. Additional sensors on the robot and its machining.

The resulting robot stiffness above 10 N/um is very promising. The industrial robot has achieved the stiffness comparable with the stiffness of machine tools. The carried out experiments with machining (Fig. 3) confirmed these assumptions.

## References

- [1] M. Valasek, M. Necas, L. Binar: Method of determining a position of a cutting tool center fastened in a cooperating clamping head and cooperating clamping head and the cooperating clamping head, Patent CZ2012474/EP2743040A2, UPV, Prague 2012
- [2] M. Valasek, V. Bauma, Z. Sika, O. Svatos: A method and a device for change of rigidity of a serial or parallel basic movable mechanism, especially of industrial robots and machine tools, CZ304673/EP2705934A2, UPV, Prague 2014

# Kinematic Design of a Multiple Motion-type Parallel Manipulator based on the 3-RRS Mechanism

Weidong YU<sup>1,2</sup>, Hao WANG<sup>1,2</sup>, Genliang CHEN<sup>1,2</sup> and Longhai ZHAO<sup>1,2</sup>

<sup>1</sup> State Key Laboratory of Mechanical System and Vibration  
Shanghai Jiao Tong University  
Shanghai 200240, P.R. China.

<sup>2</sup> Shanghai Key Laboratory of Digital Manufacture for Thin-walled Structures  
Shanghai Jiao Tong University  
Shanghai 200240, P.R. China.

[yuweidong, wanghao, leungchan, fhqdxix1988]@sjtu.edu.cn

## Abstract

This paper presents the kinematic design of a three degree-of-freedom (DOF) parallel manipulator (PM) with multiple motion types. As shown in Fig. 1, the proposed parallel manipulator is based on the 3-RRS architecture whose motion type can be switched by means of re-arranging the directions of the passive revolute joints. When all the passive revolute joints intersect at one point  $O$ , the PM becomes a 3-DOF spherical mechanism, referred to as Type 1, in which the platform is moved on the surface of a sphere. Otherwise, if all the revolute joints are parallel to each other, as shown in Fig. 3, the PM has one translational (along Z-axis) and two rotational (about X- and Y-axis, respectively) DOF [1-5]. The kinematics analysis of the PM is performed based on the closed loop equations. The inverse kinematic Jacobian is derived for the two motion types and the motion characteristics of the moving platform are obtained.

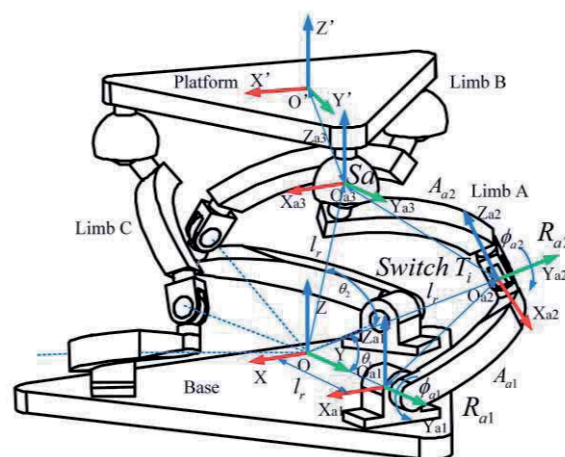


Figure 1. 3-RRS PM: all the passive revolute joints intersect at  $O$

The 3-RRS PM consists of three identical reconfigurable limbs connecting the base to the platform, Limb A, B and C. Each limb consists of two revolute joints  $R_{ij}$  ( $i = a, b, c; j = 1, 2$ ), a sphere joint  $S_i$  and two rods  $A_{ij}$  from the bottom up. Each rod  $A_{ij}$  consists of two parts  $A_{ijk}$  ( $k = 1, 2$ ) which are connected by *Electromagnetic Switch*  $T_{im}$  ( $m = 1, 2$ ). The motion type of the PM is switched by changing the working position of *Electromagnetic Switch*  $T_{im}$ . These *Electromagnetic Switches* have only two working positions. The detailed internal structure of the *Electromagnetic Switch* is shown in Fig. 2.

In motion type 1, when all the passive revolute joints intersect at one point  $O$ , switches are locked at one position. If we want to switch to motion type 2, control the platform to move to the initial pose at which the surfaces of the platform and base are parallel and the three sides of the two triangles are parallel accordingly. Then the axes of Switch  $T_{im}$  in each link are collinear, *Electromagnetic Switch*  $T_{im}$  can be switched to another working position at which the direction of revolute joints  $R_{i2}$  in each link is parallel to  $R_{i1}$ . After locking the switches, the PM will be able to move in motion type 2 [6,7].

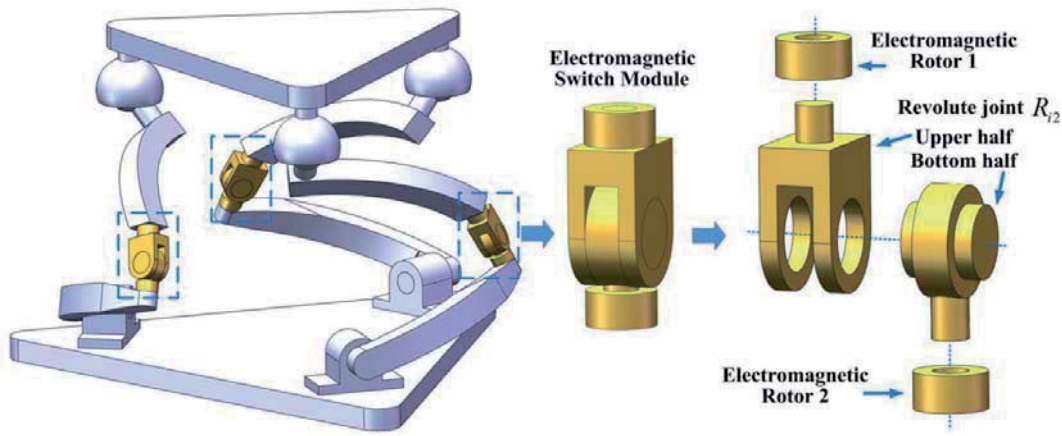


Figure 2. Detailed structure of Electromagnetic Switch

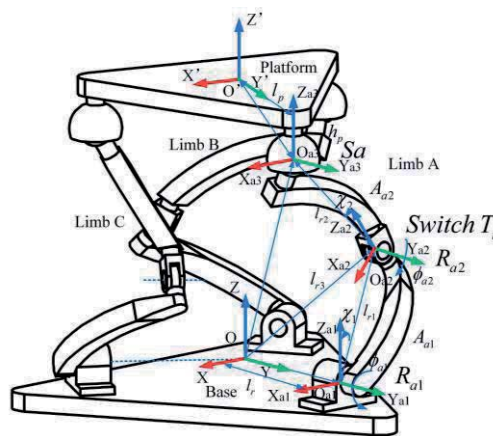


Figure 3. 3-RRS PM: all the revolte joints are parallel to each other

## Acknowledgments

This work is partially supported by National Natural Science Foundation of China (Grant No. 11472172), Research Fund for the Doctoral Program of Higher Education of China (Grant No. 2013007311003), and the National Basic Research Program of China (973 Program) (Grant No. 2014CB046600).

## References

- [1] Wang, Jiegao, and Clément M. Gosselin. Static balancing of spatial three-degree-of-freedom parallel mechanisms. *Mechanism and Machine Theory* 34.3, 437-452,1999.
- [2] Gosselin, C. M., Jaouad Sefrioui, and Marc J. Richard. On the direct kinematics of spherical three-degree-of-freedom parallel manipulators with a coplanar platform. *Journal of Mechanical Design* 116.2, 587-593,1994.
- [3] Gosselin, C. M., Jaouad Sefrioui, and Marc J. Richard. On the direct kinematics of spherical three-degree-of-freedom parallel manipulators of general architecture. *Journal of Mechanical Design* 116.2, 594-598, 1994.
- [4] Di Gregorio, Raffaele. The 3-RRS Wrist: A New, Very Simple and Not Over-Constrained Spherical Parallel Manipulator. ASME 2002 International Design Engineering Technical Conferences and Computers and Information in Engineering Conference. American Society of Mechanical Engineers, 2002.
- [5] Di Gregorio, Raffaele. The 3-RRS wrist: a new, simple and non-overconstrained spherical parallel manipulator. *Journal of Mechanical Design* 126.5,850-855,2004:
- [6] Dai, Jian S., and J. Rees Jones. Mobility in metamorphic mechanisms of foldable/erectable kinds. *Journal of mechanical design* 121.3, 375-382,1999.
- [7] Gan, Dongming, Jian S. Dai, and Qizheng Liao. Mobility change in two types of metamorphic parallel mechanisms. *Journal of Mechanisms and Robotics* 1.4, 041007,2009.

# On Optimal Laws of Groups of Walking Robots Motion while Solving Formation Task

Eugene Briskin, Alexander Maloletov

Department of Theoretical Mechanics  
Volgograd State Technical University  
28, Lenin Ave., Volgograd, 400005, Russia  
dtm@vstu.ru

## Abstract

Usually the formation task is formulated as the task of the seats distribution in the formation between robots an accordance with any criterion, for example in order to minimize the distance, which robots of group have to overcome [1-7]. There are also other possible criteria: the time required for formation of robots the structure [8]; the energy consumption for reformation robots structure [9]; forces developed by actuators [10] and others.

The task of ground robots or robots interactive with supporting surface is complicated by failure of profile ground practicability and maneuverability of robots with traditional types of movers (wheels and tracks). Walking robots, for example as “Ortonog” (fig. 1.a) or sprinkle machine with walking supports (fig. 1.b), have high practicability and perfect maneuverability – it can commit any pressigned plane movement [11]. So the group of walking robots like “Ortonog” as system of solid bodies are considered in this paper.

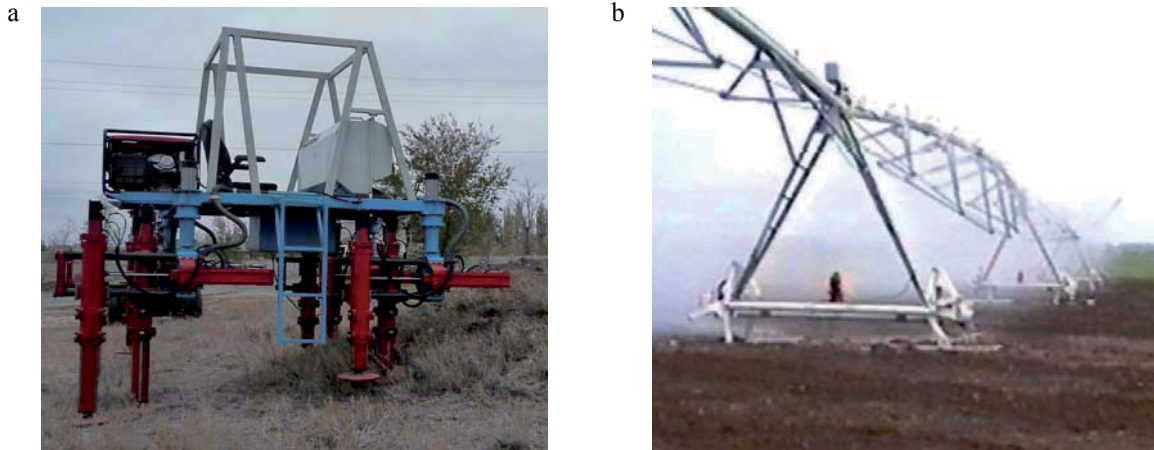


Figure 1. Walking machines

The aim is the formation of the laws of walking robots motion while solving formation task and ensuring minimum of asked criteria.

The determination of optimum laws of motion is based on the methods of the classical calculus of variations. These methods allows us to solve problems as a single-criterion and multi-criteria optimization. In general case the criteria of optimization has a form

$$I = \sum_{i=1}^n k_i H_i \quad (1)$$

Here  $k_i$  are weighting factors, set manually or automatically, for example using the method of “character” of robots group [12];  $H_i$  are indicators of the quality

$$H_i = \int_0^{\tau} F_i(t, \mathbf{q}, \dot{\mathbf{q}}, \ddot{\mathbf{q}}) dt \rightarrow \min \quad (2)$$

Here  $\tau$  is period of motion;  $t$  is time;  $\mathbf{q}, \dot{\mathbf{q}}, \ddot{\mathbf{q}}$  are vectors of generalized coordinates, velocities, accelerations;  $F_i$  are functions which are defined by the kinematic or dynamic model of mechanical system.

So using of Euler-Poisson equations guarantee the determination of optimum laws of motion. In the case of multi-criteria problem we obtain the point on the Pareto frontier.

$$\frac{d^2}{dt^2} \frac{\partial \Phi}{\partial \ddot{q}_j} - \frac{d}{dt} \frac{\partial \Phi}{\partial \dot{q}_j} + \frac{\partial \Phi}{\partial q_j} = 0, \quad \Phi = \sum_{i=1}^n k_i F_i \quad (3)$$

In general case a function of the quality  $\Phi$  can be depended on derivatives of order higher than second.

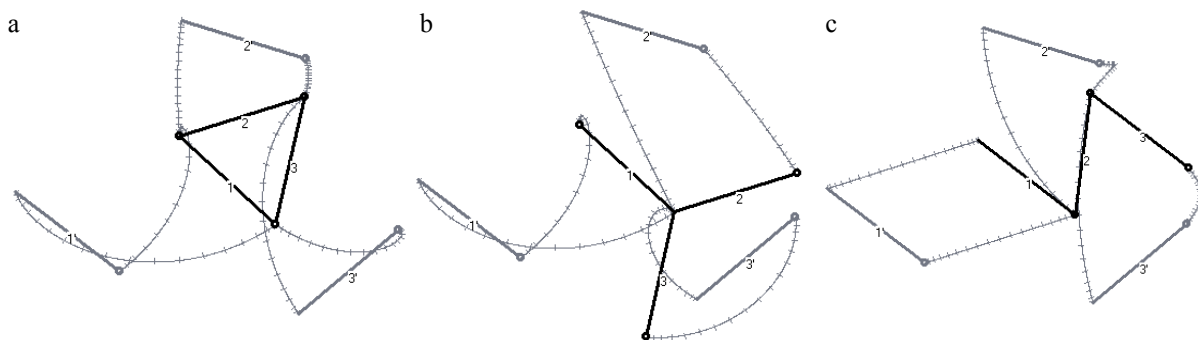


**Figure 2.** Examples of solution of the formation task

1', 2', 3', 1, 2, 3 are accordingly the vectors characterizing the situating of walking machines in the start and end time. The criteria of optimization is minimum of the sum of RMC accelerations. The curves with serifs show the trajectories of edges of machines.

The software for calculating optimal control laws of robots has been developed. Figure 2 shows examples of how the algorithm works for 3 robots which form different formations.

### Acknowledgments

This work is executed at financial support of the Russian Fund of Basic Researches (14-08-01002 a, 16-48-340957 r\_a).

### References

- [1] M. A. Lewis, K. H. Tan. High Precision Formation Control of Mobile Robots Using Virtual Structures. *Auton. Robots.* 4:387-403, 1997.
- [2] V. G. Gradetsky, I. L. Ermolov, M. M. Knyazkov, S. A. Sobolnikov. Design of Moving Communication Network on the Base of Ground Autonomous Mobile Robots. *Mechatronics, Automation, Control.* 11:27-32, 2011.
- [3] H. W. Kuhn. The Hungarian method for the assignment problem. *50 Years of Integer Programming 1958-2008.* Springer Berlin Heidelberg, pages 29-47, 2010.
- [4] D. Sutantyó, S. Kernbach, P. Levi. Multi-Robot searching algorithm using Lévy flight and artificial potential field. *2010 IEEE Safety Security and Rescue Robotics.* IEEE, pages 1-6, 2010.
- [5] J. P. Desai, J. Ostrowski, V. Kumar. Controlling formations of multiple mobile robots. *Proceedings. 1998 IEEE International Conference on Robotics and Automation.* 4:2864-2869, 1998.
- [6] M. Mesbahi, F. Y. Hadaegh. Formation flying control of multiple spacecraft via graphs, matrix inequalities, and switching. *Journal of Guidance, Control, and Dynamics.* V. 24, No2, pages 369-377, 2001.
- [7] P. K. C. Wang. Navigation strategies for multiple autonomous mobile robots moving in formation. *Journal of Robotic Systems.* No 2 (8), pages 177-195, 1991.
- [8] D. Ivanov, I. Kaliaev, S. Kapustjan. Formation task in a group of quadrotors. *Robot Intelligence Technology and Applications.* Springer International Publishing, pages 183-191, 2015.
- [9] E. S. Briskin, Y. V. Kalinin. On energetically efficient motion algorithms of walking machines with cyclic drives. *Journal of Computer and Systems Sciences International.* 50:348-354, 2011.
- [10] E. S. Briskin, V. V. Chernyshev, A. V. Maloletov, N. G. Sharonov. Comparative analysis of wheeled and walking machines. *7th IARP RISE-ER 2013: proceedings of 7th Int. symposium,* pages 99-107. St. Petersburg, 2013.
- [11] E. S. Briskin, I. P. Vershinina, A. V. Maloletov, N. G. Sharonov. On the control of motion of a walking machine with twin orthogonal rotatory movers. *Journal of Computer and Systems Sciences International.* 53:464-471, 2014
- [12] E. S. Briskin, A. V. Maloletov, N. G. Sharonov, Ya. V. Kalinin, A. V. Leonard, V. A. Serov, V. A. Shurygin. Walking robot "character" as element of intelligent system. *Advances in Cooperative Robotics: Proceedings of the 19th International Conference on Climbing and Walking Robots and the Support Technologies for Mobile Machines, CLAWAR 2016,* pages 386-394, 2016

# Modelling and Control Synthesis of Flexible Robot Arm Equipped with Additional Sensors

Volech Jiří<sup>1</sup>, Zbyněk Šika<sup>1</sup>, Beneš Petr<sup>1</sup>, Valášek Michael<sup>1</sup>

<sup>1</sup> Faculty of Mechanical Engineering  
CTU in Prague  
Technická 4, Praha 6, 166 07, Czech Republic  
[jiri.volech; zbynek.sika; petr.benes;  
michael.valasek]@fs.cvut.cz

## Abstract

The work deals with the problem of improving the accuracy of the robot with serial kinematic structure by feedback control and an auxiliary measuring its deformations. As a first step the dynamic model of the robot (Figure 1) has been created [1] using the composite method for the flexible mechanism [2]. When the recursive formalism for the flexible bodies is applied the final system of equations of motion is obtained

$$\begin{bmatrix} \mathbf{M}^R(\mathbf{q}, \mathbf{E}) & \mathbf{M}^{RF}(\mathbf{q}, \mathbf{E}) & \mathbf{0} \\ (\mathbf{M}^{RF}(\mathbf{q}, \mathbf{E}))^T & \mathbf{M}^F(\mathbf{q}, \mathbf{E}) & \mathbf{0} \\ \mathbf{0} & \mathbf{0} & \mathbf{M}^M \end{bmatrix} \begin{bmatrix} \ddot{\mathbf{q}} \\ \ddot{\mathbf{E}} \\ \dot{\mathbf{q}}_M \end{bmatrix} = \begin{bmatrix} \mathbf{Q}^R(\mathbf{q}, \dot{\mathbf{q}}, \mathbf{E}, \dot{\mathbf{E}}, \mathbf{q}_M, \dot{\mathbf{q}}_M) \\ \mathbf{Q}^F(\mathbf{q}, \dot{\mathbf{q}}, \mathbf{E}, \dot{\mathbf{E}}, \mathbf{q}_M, \dot{\mathbf{q}}_M) \\ \mathbf{Q}^M(\mathbf{q}, \dot{\mathbf{q}}, \mathbf{E}, \dot{\mathbf{E}}, \mathbf{q}_M, \dot{\mathbf{q}}_M) \end{bmatrix}. \quad (1)$$

The symbol  $\mathbf{M}^R$  represents the part of mass matrix related to the „rigid“ motion,  $\mathbf{M}^F$  is the part of the mass matrix representing the „flexible“ motion and  $\mathbf{M}^{RF}$  represents the interconnection of them. The symbol  $\mathbf{M}^M$  represents the mass matrix of the rotors. The symbols on the right-hand side are the corresponding generalized force vectors.

With the notation  $\mathbf{y} = [\mathbf{q}, \mathbf{E}, \mathbf{q}_M]^T$ , the system (1) can be easily described by

$$\mathbf{M}_y \ddot{\mathbf{y}} = \mathbf{Q}_y. \quad (2)$$

And denoting  $\mathbf{x}_1 = \mathbf{y}$  and  $\mathbf{x}_2 = \dot{\mathbf{y}}$  the system of differential equations of the first order can be obtained

$$\dot{\mathbf{x}} = \begin{bmatrix} \dot{\mathbf{x}}_1 \\ \dot{\mathbf{x}}_2 \end{bmatrix} = \begin{bmatrix} \mathbf{x}_2 \\ \mathbf{M}_y^{-1} \mathbf{Q}_y \end{bmatrix}.$$

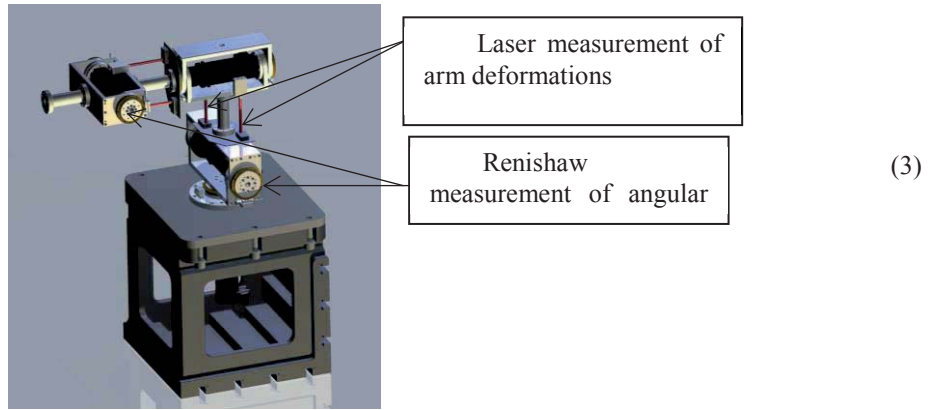


Figure 1. Model of construction of the experimental stand

First step in designing the suitable control, which takes into consideration the signals from additional sensors, is to optimization of a cascade control system and the second is optimization of H-infinity robust control system. In second step the results from first step was used.

*Computed Torques* realizes the linearization of the dynamic system through the inverse dynamics. This approach works in the whole workspace of the mechanism but on the other hand there are high hardware requirements if we want to execute computation in real time [3]. Inverse dynamics of the robot arm (4) is derived through Newton-Euler's equations.

$$\boldsymbol{\tau} = \mathbf{M}(\mathbf{q})^{-1} \cdot \mathbf{Q}(\mathbf{q}, \dot{\mathbf{q}}, \ddot{\mathbf{q}}). \quad (4)$$

All parts are considered as rigid bodies. We use there only the classic joint coordinates for description of arm position  $\mathbf{q} = [q_1, q_2, q_3, q_4]^T$ . Driving torques  $\boldsymbol{\tau} = [M_1, M_2, M_3, M_4]^T$  which realize motion  $\mathbf{q}, \dot{\mathbf{q}}, \ddot{\mathbf{q}}$  are computed from (4). Combined eqn. (3) and eqn. (4) is a new input  $\mathbf{r}$  in case that we use pid regulator.

$$\ddot{\mathbf{q}} = \mathbf{r} \quad (5)$$

Input acceleration  $\ddot{\mathbf{q}}$  in eqn. (5) is modified depending on the used regulator.

$$\mathbf{r} = \ddot{\mathbf{q}}_d + \mathbf{K}_P(\mathbf{q}_d - \mathbf{q}_m) + \mathbf{K}_I \int_0^t (\mathbf{q}_d - \mathbf{q}_m) dt + \mathbf{K}_D(\dot{\mathbf{q}}_d - \dot{\mathbf{q}}_m). \quad (6)$$

Where  $\mathbf{K}_p$ ,  $\mathbf{K}_I$ , and  $\mathbf{K}_D$  are linear feedback gain matrices. Desired position, velocity and acceleration of joint coordinates  $\mathbf{q}_d$ ,  $\dot{\mathbf{q}}_d$ ,  $\ddot{\mathbf{q}}_d$  are obtained from inverse kinematics of the mechanism. Motor positions and velocities  $\mathbf{q}_m$ ,  $\dot{\mathbf{q}}_m$  are measured by sensors or in case of simulation obtained from the flexible dynamic model.

Any control of the physical system has some source of uncertainties. For this case the uncertainty are mainly due to unknown payload on the robot end-effector, modelling errors on the actuator constant and the dimensions of the robots construction. To achieve more precise control this uncertainty has to be taken in to account. In equation (7) the  $\mathbf{q}$ ,  $\dot{\mathbf{q}}$ ,  $\ddot{\mathbf{q}}$  are dependent on the robots dimensions and can have some degrees of uncertainty.

$$\boldsymbol{\tau} = \mathbf{M}(\tilde{\mathbf{q}})^{-1} \cdot \mathbf{Q}(\tilde{\mathbf{q}}, \dot{\tilde{\mathbf{q}}}, \ddot{\tilde{\mathbf{q}}}) \quad (7)$$

Where  $\tilde{\mathbf{q}}$ ,  $\dot{\tilde{\mathbf{q}}}$ ,  $\ddot{\tilde{\mathbf{q}}}$  represent the real version of the  $\mathbf{q}$ ,  $\dot{\mathbf{q}}$ ,  $\ddot{\mathbf{q}}$  respectively. To diminished these errors the compensation method has to be made and since the  $H_\infty$  control method is based on linear system [4] and the robot dynamics is a highly nonlinear, can be using the  $H_\infty$  method directly a very complicated. The  $H_\infty$  method is better use just as the compensation tools of the remaining uncertainty. Therefore it is better to first use of the nonlinear feedback linearization such as computed torque to render the nominal system linear. The linearized system of the robot must be transformed to  $H_\infty$  synthesis Figure 2.

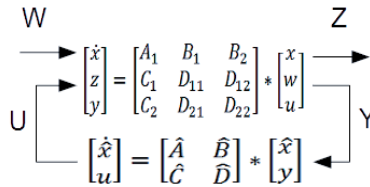


Figure 2. Augmented system for  $H_\infty$  synthesis

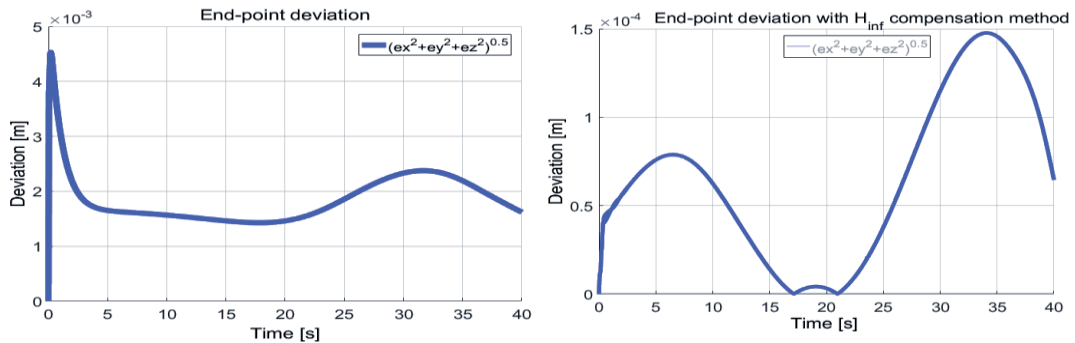


Figure 3. Results

This approach was tested on the fully compliant mathematical model and as results shown Figure 3 it has potential to enhance the controlling of large serial kinematic structure equipped with additional sensors. However the on-line control of the robot based on the additional auxiliary measurement can be difficult. The feasibility is going to be tested on ongoing construction of experimental stand.

## Acknowledgments

The authors appreciate the kind support by the grant SGS16/208/OHK2/3T/12 Mechatronics and adaptronics 2016 of CTU in Prague and the grant GA13-39057S “Position Feedback Based Stiffness Increase of Robots by Redundant Measurement” of the Czech Science Foundation.

## References

- [1] J. Volech, L. Mráz, Z. Šika, M. Valášek: Model of Flexible Robot with Deformation Detection, Procedia Engineering, Volume 96, 2014, Pages 510-516, ISSN 1877-7058
- [2] T. Vampola, M. Valášek: Composite Rigid Body Formalism for Flexible Multibody Systems. Multibody System Dynamics, 2007, Volume 18, Issue 3, pp 413-433
- [3] O. Sörnmo, B. Olofsson, A. Robertsson, Johansson R.: Increasing Time-Efficiency and Accuracy of Robotic Machining Processes Using Model-Based Adaptive Force Control. 10th IFAC Symposium on Robot Control – SYROCO 2012, pp. 543-548, Dubrovnik 2012.
- [4] J.V. Burke, D. Henrion, A.S. Lewis and M.L. Overton: HIFOO - a MATLAB package for fixed-order controller design and  $H_\infty$  optimization. In Fifth IFAC Symposium on Robust Control Design, Toulouse, 2006

# Development of Structure and Behavioral Model for Screw Driving In-pipe Inspection Robot based on Adaptive Mechanism on Legs

Krešimir Osman<sup>1</sup>, Zdenko Kovačić<sup>2</sup>

<sup>1</sup>Termo Servis Ltd.  
Sales and Technical Department  
Ul. grada Vukovara 72, 10000 Zagreb  
Croatia  
kresimir.osman@gmail.com

<sup>2</sup>University of Zagreb, Faculty of  
Electrical Engineering and Computing  
Unska 3, 10000 Zagreb  
Croatia  
zdenko.kovacic@fer.hr

## Abstract

The authors' idea was to present in this article the beginning of their research in the development of in-pipe inspection robot, where they aimed to present a robot's structure and the derived behavior model (mathematical model) We should notice that the presented robot is based on the main motion mechanism using the screw principle, including an adaptive mechanism applying its wheels' pressure to the pipeline wall.

Due to their importance, because pipelines made of various materials are used as a tool for transporting media such as oil, gas, water and other media and blends used in various industries, they should be managed in a particularly careful manner [1]. Please note that the issues concerning interior pipeline inspection are discussed below. This in particular pertains to the inspection of pipelines as part of their regular maintenance and cleaning. Substantial funds are allocated to such purposes to prevent different types of damage, cracks, wear and different types of corrosion on and within them. In practice, depending on the intended use of the pipeline, different approaches are used to their inspection for the purpose of assessing their condition and, in case repair is possible, different approaches are used to their economical repair and reconstruction. To avoid any permanent damage to pipelines, regular cyclical inspections should be performed that may provide us with information about the physical conditions of pipelines and damage to their material [2].

Pipeline inspection robots have recently been increasingly used for that purpose and their design and control currently represent one of the most attractive areas of service robotics [1]. Efforts have been used to develop a robot structure that will, controlled by its algorithm, very easily overcome all possible requirements on its way through the observed pipeline's configuration such as: brackets under different angles, T-pieces, narrowing and widening points, as well as pipeline ascents and descents under various angles (when the pipeline follows the terrain).

One of the usual classifications of pipeline inspection robots available in literature was proposed by Hirose et al. [3] and supplemented by Choi et al. [4], and is based on a robot motion mechanism. Most structures of pipeline inspection robots are based on one of these classifications established by said authors or a combination of two or more of them. Presented below are the relevant pipeline inspection robot motion mechanisms: a) Pig type, b) Wheel type, c) Caterpillar type, d) Wall-press type, e) Walking type, f) Inchworm type, g) Screw type, h) snake type, and i) variable velocity Pig type.

The robot structure presented in this paper is based on several of the above mentioned basic classifications. First, the aforementioned engine rotation in the propulsive section allows it to move using a screw, where it revolves not only around its own axis, but also around the axis of the pipeline it passes through. This reduces the complexity of the robot's mechanism. In addition, the robot may be classified according to a wheel-based motion mechanism, which is very common in commercial versions of this type of robot, driven by wheels on a propulsive and several pairs of wheels on a driven section. The pressure applied by a pair of wheels against the pipeline wall (which is also one of the basic motion mechanism classifications for this type of robot) allows it to adapt to different pipeline dimensions and smoothly pass curved pipeline sections such as brackets, T-pieces, etc., where its stability is maintained by using a leg with two jackets. The angle between the leg jackets in the propulsive and driven parts of the robot, which also maintains the necessary pressure applied by a pair of wheels against the pipeline wall, is controlled using a pneumatic cylinder. The pressure of a pair of wheels is enabled using a force sensor and an actuator (slider), which results in better traction of the leg against the pipeline wall and allows it to adjust to its interior diameter on that side as well. In that case, it is necessary to maintain the angle between the wheel pair on driven and wheels on propulsive section using the actuator. It is important to note that the propulsive and driven sections have three legs with two ankles and that the leg in the driven section is moved by 60° in relation to that same leg in the propulsive section. A CCD camera will be mounted on the front propulsive section of the robot for the purpose of inspecting the condition of the pipeline's interior surface. The robot is supplied with power through a power cable and a communication cable is also attached to it.

Some of the articles available in literature [5] have already presented the robot's motion based on the screw principle, with its propulsive and driven sections, and its motions enabled by maintaining the necessary pressure of the wheels against the pipeline wall [6].



# Adaptive Learning Control Algorithms for KUKA LWR 4+ Robots

Łukasz Woliński<sup>1</sup>

<sup>1</sup> Institute of Aeronautics and Applied Mechanics  
Warsaw University of Technology  
Nowowiejska 24, 00-665 Warsaw, Poland  
lwolinski@meil.pw.edu.pl

## Abstract

From the variety of robot control methods, the model-based ones offer good tracking performance often exceeding the other types of controllers. The more detailed the model, the better the results. However, that approach requires the knowledge of the dynamic parameters such as links' masses, moments of inertia, joint friction coefficients, etc. The identification of these parameters is often a demanding task requiring careful planning of the experiment and several iterations [1]. Moreover, some dynamic parameters might vary in robots of one kind, requiring separate identification of each robot. Preliminary experiments carried on two KUKA LWR 4+ robots showed subtle but apparent differences in the dynamic properties of the manipulators [2]. The parameters not included in the rigid-body model, such as friction coefficients, were believed to be responsible for that differences. To sufficiently account for that phenomena in the detailed dynamic model, the identification would have to be performed on both manipulators.

As mentioned, using the dynamic model of the manipulator in the control system might present difficulties. One of the possible solutions is to use the learning control algorithms such as adaptive control or artificial neural networks (ANN). With that approach, parameters of the controller are updating itself on-line during the robot motion and good position tracking is ensured.

In this paper, an adaptive and NN controller for the 7DOF LWR 4+ manipulator were studied and implemented in MATLAB/Simulink. The matrix-form equation of motion of the manipulator is given by:

$$\mathbf{M}(\mathbf{q})\ddot{\mathbf{q}} + \mathbf{C}(\mathbf{q}, \dot{\mathbf{q}})\dot{\mathbf{q}} + \mathbf{G}(\mathbf{q}) + \boldsymbol{\tau}_{dist} = \boldsymbol{\tau} \quad (1)$$

where  $\mathbf{q} \in \mathbb{R}^{7 \times 1}$  is the vector of joint coordinates,  $\mathbf{M}(\mathbf{q}) \in \mathbb{R}^{7 \times 7}$  is the manipulator inertia matrix,  $\mathbf{C}(\mathbf{q}, \dot{\mathbf{q}})\dot{\mathbf{q}} \in \mathbb{R}^{7 \times 1}$  is the Coriolis and centrifugal force vector,  $\mathbf{G}(\mathbf{q}) \in \mathbb{R}^{7 \times 1}$  is the gravitational force vector,  $\boldsymbol{\tau} \in \mathbb{R}^{7 \times 1}$  contains driving torques in joints and  $\boldsymbol{\tau}_{dist}$  represents disturbances and unmodeled dynamics.

The adaptive control law is formulated as [3]:

$$\boldsymbol{\tau} = \mathbf{Y}(\mathbf{q}, \dot{\mathbf{q}}, \ddot{\mathbf{q}}_d) \hat{\boldsymbol{\theta}} - \mathbf{K}\mathbf{s} \quad (2)$$

where  $\mathbf{s} = \dot{\mathbf{q}} - \dot{\mathbf{q}}_r$ ,  $\dot{\mathbf{q}}_r = \dot{\mathbf{q}}_d + \boldsymbol{\Lambda}\mathbf{e}$  and  $\mathbf{e} = \mathbf{q}_d - \mathbf{q}$  is the position error,  $\mathbf{q}_d$  is the desired joint trajectory and  $\boldsymbol{\Lambda} \in \mathbb{R}^{7 \times 7}$  is a symmetric positive definite matrix while  $\hat{\boldsymbol{\theta}} \in \mathbb{R}^{8 \times 1}$  is an estimate of the 8 dynamic parameters identified as the most important in the model. The manipulator regressor matrix  $\mathbf{Y}(\mathbf{q}, \dot{\mathbf{q}}, \ddot{\mathbf{q}}_d) \in \mathbb{R}^{7 \times 8}$  is based on the linearity-in-parameters property of the rigid body dynamic model.

The parameter adaptation law is given by:

$$\dot{\hat{\boldsymbol{\theta}}} = -\boldsymbol{\Gamma}\mathbf{Y}^T(\mathbf{q}, \dot{\mathbf{q}}, \ddot{\mathbf{q}}_d)\mathbf{s} \quad (3)$$

where  $\boldsymbol{\Gamma} \in \mathbb{R}^{8 \times 8}$  is a positive definite matrix.

In case of the ANN controller, the equation describing the control law is expressed as [4]:

$$\boldsymbol{\tau} = \mathbf{W}^T \boldsymbol{\sigma}_a + \mathbf{K}\mathbf{r} \quad (4)$$

where  $\mathbf{r} = \dot{\mathbf{e}} + \boldsymbol{\Lambda}\mathbf{e}$  is the filtered tracking error,  $\mathbf{K} \in \mathbb{R}^{7 \times 7}$  is the gain matrix,  $\mathbf{W} \in \mathbb{R}^{8 \times 7}$  is the matrix of weights and biases of the hidden (second) layer. The augmented vector  $\boldsymbol{\sigma}_a \in \mathbb{R}^{8 \times 1}$  is defined as:

$$\boldsymbol{\sigma}_a = \begin{bmatrix} 1 \\ \boldsymbol{\sigma}(\mathbf{V}^T \mathbf{X}) \end{bmatrix} \quad (5)$$

and it contains outputs of the hidden layer neurons  $\boldsymbol{\sigma} \in \mathbb{R}^{7 \times 1}$  which are sigmoid functions.  $\mathbf{V} \in \mathbb{R}^{36 \times 35}$  is the matrix of weights and biases of the input (first) layer while  $\mathbf{X} = [1 \quad \mathbf{e}^T \quad \dot{\mathbf{e}}^T \quad \mathbf{q}_d^T \quad \dot{\mathbf{q}}_d^T \quad \ddot{\mathbf{q}}_d^T]^T \in \mathbb{R}^{36 \times 1}$  is the augmented vector of the inputs to the neural network.

The weights are updated using the augmented backprop tuning:

$$\dot{\mathbf{W}} = \mathbf{F}\boldsymbol{\sigma}_a(\mathbf{L}\mathbf{r})^T - \mathbf{F}\boldsymbol{\sigma}'_a \mathbf{V}^T \mathbf{X}(\mathbf{L}\mathbf{r})^T - k_w \mathbf{F} \|\mathbf{L}\mathbf{r}\| \mathbf{W} \quad (6)$$

$$\dot{\mathbf{V}} = \mathbf{B}\mathbf{X}(\boldsymbol{\sigma}'_a \mathbf{W}\mathbf{L}\mathbf{r})^T - k_w \mathbf{B} \|\mathbf{L}\mathbf{r}\| \mathbf{V} \quad (7)$$

where the design parameters  $\mathbf{F} \in \mathbb{R}^{8 \times 8}$ ,  $\mathbf{B} \in \mathbb{R}^{36 \times 36}$  and  $\mathbf{L} \in \mathbb{R}^{7 \times 7}$  are positive definite matrices and  $k_w$  is a positive scalar.  $\boldsymbol{\sigma}'_a \in \mathbb{R}^{8 \times 7}$  is a derivative of  $\boldsymbol{\sigma}_a$ , defined as:

$$\boldsymbol{\sigma}'_a = \begin{bmatrix} 0 & 0 & 0 & \dots & 0 \\ \sigma_1(1-\sigma_1) & 0 & 0 & \dots & 0 \\ 0 & \sigma_2(1-\sigma_2) & 0 & \dots & 0 \\ \vdots & \vdots & \ddots & \dots & \vdots \\ 0 & 0 & 0 & \dots & \sigma_7(1-\sigma_7) \end{bmatrix}. \quad (8)$$

In the simulation, the end-effector trajectory was chosen to follow a circle with the radius of  $0.3(m)$  for 10 seconds:

$$\mathbf{r}_d(t) = \begin{bmatrix} 0.276 \\ -0.3 + 0.3 \cos\left(\frac{\pi}{5}t\right) \\ 0.124 + 0.3 \sin\left(\frac{\pi}{5}t\right) \end{bmatrix} (m) \quad (9)$$

and the manipulator was subjected to disturbances.

One of the results – the position error on the x-axis – is shown in Figure 1. It is visible that ANN performed better than the adaptive controller. As the latter relies on the linearity-in-parameters assumption, any unmodeled dynamics can worsen the position tracking even though the parameters are constantly updating. On the other hand, the ANN does not rely on the linear structure of the dynamic model and is able to compensate any nonlinearities.

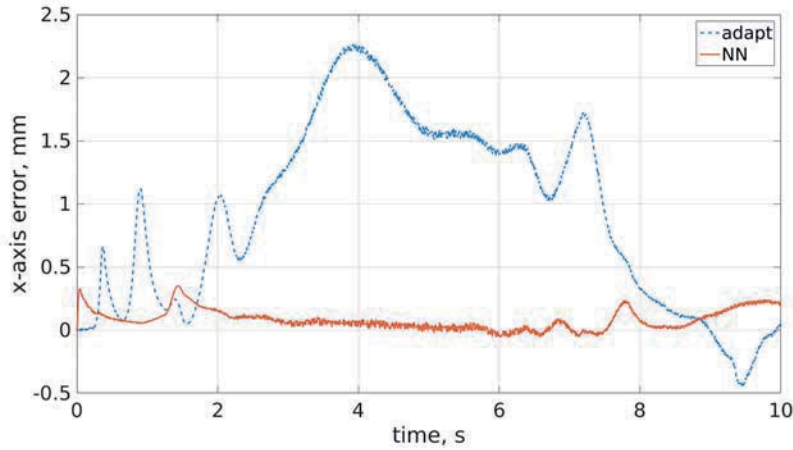


Figure 1: X-axis position error

Obtained simulation results are promising and will help with the implementation on the real LWR 4+ robot. The results of the implemented controllers will be shown on the conference.

### Acknowledgments

This research was supported by the National Science Centre (Poland) grant no. DEC-2012/07/B/ST8/03993.

### References

- [1] J. Swevers, W. Verdonck and J. De Schutter. Dynamic Model Identification for Industrial Robots. In: IEEE Control Systems, vol. 27, no. 5, pages 58–71, 2007.
- [2] Ł. Woliński and M. Wojtyra. Comparison of Dynamic Properties of Two LWR 4+ Robots. In: ROMANSY 21 - Robot Design, Dynamics and Control. Proceedings of the 21st CISM-IFTOMM Symposium, pages 413–420, June 2016, DOI: 10.1007/978-3-319-33714-2.
- [3] J.-J. E. Slotine, T. Bitto and W. Li. On the Adaptive Control of Robot Manipulators. In: The International Journal of Robotics Research, vol. 6, no. 3, pages 49–59, September 1987.
- [4] F. L. Lewis. Neural network control of robot manipulators. In: IEEE Expert, vol. 11, no. 3, pages 64–75, June 1996.

## Proportional-derivative and model-based controllers used for a serial type manipulator in case of a variable mass payload

Krzysztof Lipinski

Mechanical Department  
Gdansk University of Technology  
ul. Narutowicza 11/12, 80-233 Gdańsk Poland  
klipinsk @ pg. gda. pl

### Abstract

When the revolute joints composed manipulators are considered, they are characterized by nonlinear behaviours in most of the cases (especially, when driven over some larger operating space). Linear controllers may not be adequate for them. Accuracy of the motion control can be low. Nonlinear control technique could be a solution. There exist a number of nonlinear control architectures and design techniques. Some of the most frequent approaches are: classical PID control, PID control with model-based estimation, feedforward control with an inverse model, predictive control, and internal model control. In the present research, the feed-forward model-based controllers are considered. Detail knowledge of sophisticated models of the nonlinear processes is a critical point, as well as precise determination of values of the actual parameters of the model.

Operation with the model-based controller is a promising option, but its application is not a straightforward task, especially in case of complex systems. It can be hard to establish a reasonable complex numerical model of the controlled plant. It could be hard to estimate its parameters and it could be hard to certificate the reliability of the control. As in lot of the practical tasks, where the low cost controllers are required, the model-based controllers are eliminated because of their higher costs (according to the higher cost of the controller, as well as the cost of longer and more complex preparation and tests). Simplification to linearized formulations is an option in the reduction of the costs, but then the exponential stability can be preserved for the nominal configuration, only. Any unavoidable deviation can destabilise the system. Finally, none of the modelling methods and the parameter estimation procedures will guarantee the perfect matching between the plant and the model.

In generally, there is no unique way to obtain the nonlinear models of the processes. Physical or experimental considerations are the most popular methods. However, theoretically obtained models are low accurate in most of the cases and experimental modelling (identification) has to be employed independently or in parallel. In-between different types of approaches, the most popular are: basis function models; fuzzy models; neural network models; local models approach; storage-based (look-up tables) models.

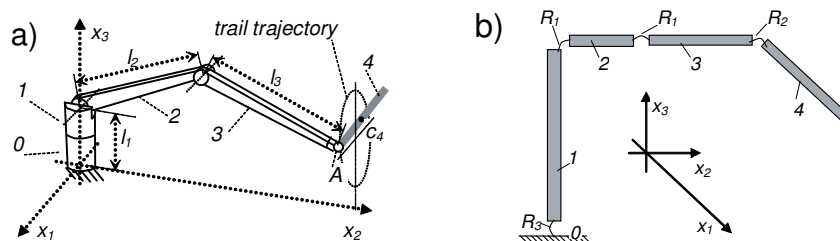


**Figure 1.** Description of the considered manipulator: a sketch of its structure (a); its multibody model (b);  
 $R_i$  – a rotational joint, its axis is collinear to  $i^{th}$  axis of the body fixed coordinate system

In the present considerations, model equations are prepared according the roles of the multibody modelling [1, 2]. Initially, all joints of the multibody structure are cut and replaced by the joint interactions. Free body diagrams are composed for all the bodies and their Newton/Euler dynamics equations are written. These equations are combined with the matching formulas expressing velocities and accelerations. Then, symbols of successors' forces and successors' torques are eliminated. Joint interactions are projected on directions of the joint mobility. Finally, components in front of the joint acceleration are collected as elements of the mass matrix. The dynamics equations are written as [1, 2]

$$M(\mathbf{q}) \cdot \ddot{\mathbf{q}} + \mathbf{F}(\dot{\mathbf{q}}, \mathbf{q}, \mathbf{f}_e, \mathbf{t}_e, t) = \mathbf{Q} \quad (1)$$

where:  $\mathbf{M}$  – mass matrix;  $\mathbf{F}$  – column composed of velocity depend inertial effects;  $\mathbf{Q}$  – column composed of joint actuations;  $\mathbf{f}_e$  – column composed of the external forces acting on the system bodies;  $\mathbf{t}_e$  – column composed of the external torques acting on the system bodies;  $t$  – time.

A sketch of the physical model is visualised in Fig. 1 for the considered system. Its gripper is considered as the variable mass element (in Fig. 1.a, denoted as #4). All links are considered as rigid bodies, they are joined by a set of single degree of freedom joints, in order to form a shape of an open kinematical chain (Fig. 1.b).

In addition to the equations, parameters have to be identified, too. Generally speaking, in case of the manipulator structure, there is a long list of the parameters that may be identified once and easily (e.g. distances, arms' inertias). Some external identification procedures can be used during the assembling process for it. These parameters are considered as known in the presently performed tests. The main hesitation is related to mass of the operated payload (located in the gripper). Intraoperative variability of its mass has to be taken account, together with the lack of pre-information about its actual value at the actually considered technological process.

The present tests are limited to numerical considerations, only. As a manipulator with a model-based controller is considered, two numerical sub-models (separate blocks) of the plant have to be introduced in the numerical program. The first block is understood as the model of the real plant. An original set of the inertia parameters is associated with this block. The second block is understood as the one implemented in the controller. Another set of the inertia parameters is associated with this block. When these two models and these two sets coincide, required path can be realised correctly (Fig. 2.a). Problems appear when the models or parameters differ. The model-based feedforward controller does not ensure satisfactory performance in this case (Fig. 2.b-d). To correct it, a closed loop PD feedback controller (Fig. 2.e) is added in the control structure (for each for each of the controlled joints). The PD feedback adjusts the endpoint motion to its required path. Possibility of mass identification is verified and introduced in the controller. A short run of a trial circular path is proposed at beginning of each of the operations. History of the PD signal obtained during the trial motions allows us to identify the mass of the payload. During the main operations, the identified value replaces the initial one in the controller, in order to minimise the path error and to reduce work of the feedback controller.

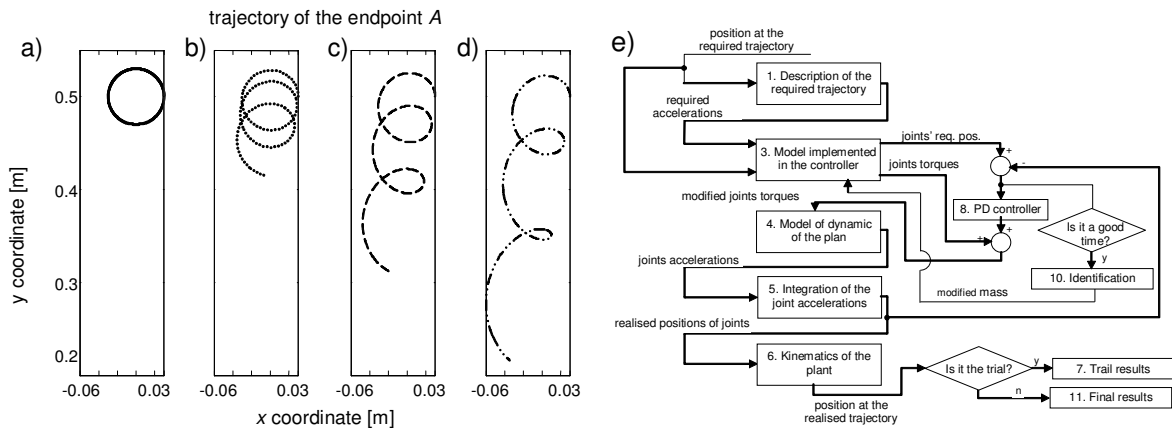


**Figure 2.** Imprecise value of the payload mass: the reference path  $m_c = m_p$  (a);  $m_c = 0.99 \cdot m_p$  (b);  $m_c = 0.97 \cdot m_p$  (c);  $m_c = 0.95 \cdot m_p$  (d) [3]; structure of the considered numerical program (e)

Some partial results, related to a limited case of a single unknown parameter, were presented by the Author in [3]. At the present case, more complex situation is considered. Simultaneous identification of two unknown parameters is considered. The presently considered parameters are: mass of the payload and position of its mass centre. The tests verify that the unrequited effects are significant in case of the non precise knowledge of the values of the inertia parameters and that the trajectory errors can cumulate significantly. As it was expected, direct application of a limited proportional closed-loop controller is non sufficient. For some values of the loop amplification coefficients the trajectory errors can raise significantly. Such errors can destabilise the trajectory considerably. Proportional/differential controllers are effective. With these controllers, obtained trajectories are closer to the required ones. Additional fitting is obtained, when identification of the inertia parameters is performed.

## References

- [1] P. Fiset, J.C. Samin. *Symbolic Modeling of Multibody System*, Kluwer Acad. Pub., 2003.
- [2] K. Lipiński. *Multibody Systems with Unilateral Constraints in Application to Modelling of Complex Mechanical Systems*, Wydaw. Politechniki Gdańskiej, Seria Monografie 123, Gdańsk, 2012 (in Polish).
- [3] K. Lipiński. Proportional-Derivative and Model-Based Controllers for Control of a Variable Mass Manipulator. *Applied Mechanics and Materials*, 831: 54-62 2016.

# Optimal Point to Point Trajectory Planning with Collision Avoidance for Dual Arm Setup

Dominik Kaserer, Hubert Gatringer, Andreas Müller

Institute of Robotics  
Johannes Kepler University Linz  
Altenbergerstraße 69, 4040 Linz, Austria  
{dominik.kaserer, hubert.gatringer, a.mueller}@jku.at

## Abstract

Nowadays it is a common scenario for industrial robotic manipulators utilized in a production environment to be placed in close spatial proximity of other manipulators and share at least a part of their workspace. The tasks of the different manipulators may often be independent so that collisions between the robots are likely. Moreover the robotic motions have to be performed optimally in the sense of e.g. minimum time or minimum consumed energy. Hereafter the case of a simultaneously time optimal point to point (PtP) motion for two manipulators sharing their workspace with the additional requirement of collision avoidance is treated. The problem of obtaining optimal motions while simultaneously avoiding collisions is a challenging task allowing for different solution approaches [1]. The easiest one may be to command the robot motions consecutively and neglect collision avoidance, but this is not satisfying at all because it does not allow for global time optimal motions of both manipulators. A well established approach for simplification of the optimization of PtP motions is to split the problem in the optimization of the geometric paths (higher level) and searching for an optimal solution along these geometric paths (lower level) as pursued in [2]. In contrast to [1], where the collision avoidance is considered at the lower level optimization, the geometric paths of the manipulators' end-effectors are not fixed and therefore adapted by the higher level optimization to obtain faster solutions as well as to avoid collisions. Both manipulators are considered to have the same priority, meaning that the geometric paths of both manipulators are adapted by the solver to avoid collisions. In the following sections the formulation and solution of the optimization problem will be briefly described and experimental results are provided.

The dual arm setup with two 6-DOF industrial manipulators  $i = \{1, 2\}$  visualized in Fig. 1 is considered here. The optimization problem

$$\begin{aligned} \min_{\mathbf{q}_i, \dot{\mathbf{q}}_i, \ddot{\mathbf{q}}_i, \tau_i} J & \quad J = \int_0^{t_{E,1}} 1 dt + \int_0^{t_{E,2}} 1 dt \quad (2) \\ \text{s.t. } \underline{\mathbf{q}}_i \leq \mathbf{q}_i \leq \bar{\mathbf{q}}_i & \\ |\dot{\mathbf{q}}_i| \leq \bar{\dot{\mathbf{q}}}_i & \quad \dot{s}_i = \frac{ds_i}{dt} \rightarrow dt = \frac{ds_i}{\dot{s}_i} \\ |\ddot{\mathbf{q}}_i| \leq \bar{\ddot{\mathbf{q}}}_i & \\ \underline{\tau}_i \leq \tau_i \leq \bar{\tau}_i & \\ \underline{d} \leq d_j & \quad J = \int_0^1 \frac{1}{\dot{s}_1} ds_1 + \int_0^1 \frac{1}{\dot{s}_2} ds_2 \quad (3) \end{aligned}$$

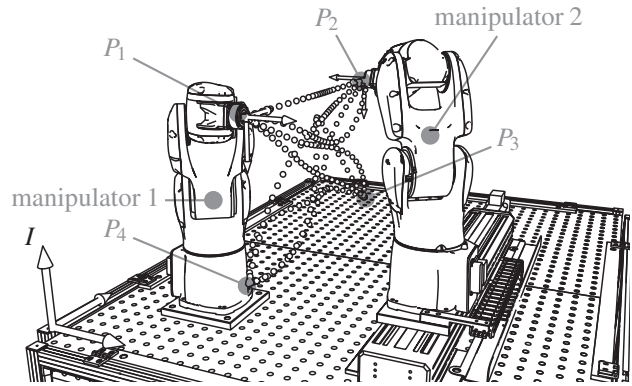


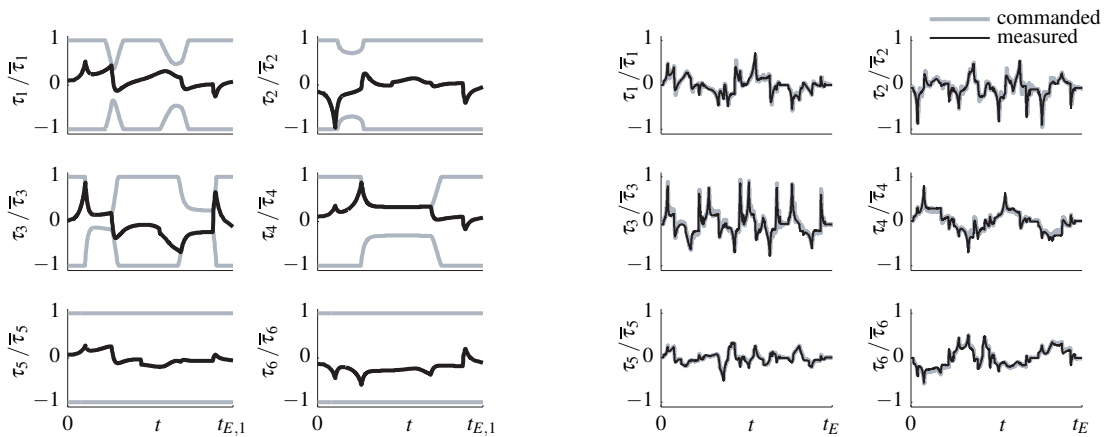
Figure 1: Dual arm setup and visualization of optimized trajectories

with the joint coordinates  $\mathbf{q}_i$ , the respective minimum and maximum values  $\underline{\mathbf{q}}_i$  and  $\bar{\mathbf{q}}_i$  and the velocity and acceleration limits  $\bar{\dot{\mathbf{q}}}_i$  and  $\bar{\ddot{\mathbf{q}}}_i$  is treated. The unknown trajectory durations  $t_{E,i}$  in the cost function  $J$  in (2) are substituted using the derivatives of the path parameters  $s_i$ . For the computation of the joint torques  $\tau_i$  dynamic models of the manipulators in terms of the equations of motion  $\mathbf{M}_i(\mathbf{q}_i) \ddot{\mathbf{q}}_i + \mathbf{c}_i(\dot{\mathbf{q}}_i, \mathbf{q}_i) = \tau_i$  with the mass matrices  $\mathbf{M}_i(\mathbf{q}_i)$  and the nonlinear terms  $\mathbf{c}_i(\dot{\mathbf{q}}_i, \mathbf{q}_i)$  are used. By the higher level optimization geometric paths for position and orientation of the end-effectors are planned and adapted in the upper optimization level considering joint limits and a minimal distance  $\underline{d}$  between the robot bodies. The geometric paths  $\mathbf{z}_{E,i} = [\mathbf{r}_{E,i}^T(s_i), \mathcal{Q}_{E,i}^T(s_i)]^T$  for both end-effectors are defined in the world frame  $I$  in terms of the position vector  $\mathbf{r}_{E,i}(s_i)$  and the unit quaternion  $\mathcal{Q}_{E,i}(s_i)$  describing the orientation. An iterative inverse kinematics algorithm on position level utilizing the geometric Jacobian

$\mathbf{J}_i = \left[ \left( \frac{d\mathbf{v}_{E,i}}{dq_i} \right)^T \left( \frac{d\omega_{E,i}}{dq_i} \right)^T \right]^T$  with linear and angular velocities  $\mathbf{v}_{E,i}$  and  $\omega_{E,i}$  is used to transform the geometric paths in the joint space. For limitation of the distances  $d_j$  to  $\underline{d}$  the robot bodies (and also environmental objects, which should be taken into account) are modeled by convex hulls according to [3]. Each body of the robots is represented by several sub bodies which can be easily described by the convex hull of at most 3 points and the spherical extension of this convex hull. It turned out that there are 58 body pairs for which collisions can occur in the present setup. For these possible collision pairs the minimal distance  $d_j$ ,  $j \in \{1 \dots 58\}$  has to be taken into

account. The higher level optimization is solved using a nonlinear solver. Every evaluation of the cost function  $J$  requires the computation of optimized path parameter trajectories  $s_i(t)$  with  $s_i(0) = 0$  and  $s_i(t_{E,i}) = 1$  along the given geometric paths which is solved by dynamic programming [4] here. Within the dynamic programming algorithm limitations of the motors are considered as velocity and torque constraints on joint level. Limitation of the joint acceleration at the beginning and at the end of the trajectory makes it possible to directly command the obtained trajectory to the robot without any special treatment (e.g. jerk limitation). To obtain feasible solutions for application on the real robots it is of major importance to consider friction effects and the torque characteristics  $\tau(\omega)$  of the motors with motor torque  $\tau$  and rotation speed  $\omega$  in the lower level optimization, because these effects gain significance with increasing velocities.

In order to demonstrate the effectiveness of the proposed approach, 4 points in the common workspace of the manipulators are chosen (see Fig. 1 for details). Initial geometric paths are computed for each manipulator which are then adapted by the higher level optimization to generate collision free trajectories with minimal trajectory duration. The optimization problem (1) was solved for four different trajectories connecting the edge points shown in Fig. 1. The resulting motor torques  $\tau$  of the first manipulator for the first trajectory are visualized in Fig. 2(a). Due to the consideration of the torque characteristics for each motor the admissible motor torque drops when the respective motor velocity is near the maximal value. Figure 2(b) compares the computed motor torques commanded as a feed forward torque to the manipulator and the measured motor torque for all four trajectories for manipulator 1. The results show that the used robot model reproduces the real behavior of the robot very well. Collision free,



(a) Normalized motor torques for the first optimized trajectory of manipulator 1

(b) Normalized feed forward motor torques (commanded) and measured motor torques for all four optimized trajectories for manipulator 1

Figure 2: Obtained results for manipulator 1

time optimal trajectories for simultaneous movement of two manipulators sharing the same workspace are derived.

### Acknowledgments

This work has been supported by the Austrian COMET K2 program of the Linz Center of Mechatronics (LCM).

### References

- [1] F. Debrouwere. Optimal Robot Path Following - fast solution methods for practical non-convex applications. KU Leuven, 2015.
- [2] H. Gatringer, M. Oberherber, K. Springer. Extending continuous path trajectories to point-to-point trajectories by varying intermediate points. International Journal of Mechanics and Control, vol. 15, no. 1, pages 35–43, 2014.
- [3] E. G. Gilbert, D. W. Johnson, S. S. Keerthi. A fast procedure for computing the distance between complex objects in three-dimensional space. IEEE Journal on Robotics and Automation, vol. 4, no. 2, pages 193–203, 1988.
- [4] R. Johanni. Optimale Bahnplanung bei Industrierobotern. Technische Universität München, 1988.

# Coordinate-Free Decomposition of the Rigid Body Displacement: A Davenport Dual Angles Approach

Daniel Condurache<sup>1</sup>

<sup>1</sup>Department of Theoretical Mechanical  
“Gheorghe Asachi” Technical University of Iasi  
D. Mangeron Street no.59, 700050, Iasi,  
Romania  
daniel.condurache@tuiasi.ro

## Abstract

In this paper, using the exponential parametrization of Lie group of orthogonal dual tensors  $\underline{S}\mathbb{O}_3$ , the problem of the decomposition of a rigid displacement by a sequence of three displacements with specified screw axis is solved. It will be determined either the closed form the dual angles of the screw displacements (translation and rotation) or the necessary and sufficient conditions when this decomposition is possible. The results are coordinate-free and they are obtained using only algebraic elements of tensor calculus. In the specific case of a screw axis is perpendicular to the other two, the decomposition is possible for any rigid displacement. So, a result that generalizes the Davenport decomposition in case of rotation is obtained.

For rigid motion, the kinematic equations that links the instantaneous dual angular velocity to the time variation of a dual Davenport angle are deduced. The cases of singularity of the decomposition are identified and a physical interpretation of these cases is given.

The problem of the decomposition of a rigid displacement seen by a sequence of three rigid displacements, with specified screw-axis is a fundamental one in the theoretical kinematics field.

Noting cu  $SE_3$  the Lie group of the rigid displacements, the problem is formalized as following:

$$g = g_1, g_2, g_3 \quad (1)$$

where  $g, g_k \in SE_3, k = \overline{1,3}$ .

In this paper, the necessary and sufficient conditions are given in order to take place the decomposition (1) and then  $g_k \in SE_3, k = \overline{1,3}$  are determined. The above result was obtained using the isomorphism between the Lie group of the rigid displacements  $SE_3$  and the Lie group of the orthogonal dual tensors  $\underline{S}\mathbb{O}_3$  introduced by author in [1], [2], [3]. In contrast to other approaches [4], [5], the transference principle is not used to solve the problem.

In the case of a rigid motion, the kinematics equations are determined and this permits the recovery of the rigid body motion knowing the instantaneous twist of the body. The solutions are free of coordinate and they are expressed in closed form.

For the particular case of spherical displacements,  $g, g_k \in S\mathbb{O}_3 \subset SE_3, k = \overline{1,3}$ , the known results are recovered [6], [7], [4], [8], [5], [9], [10].

We need some preliminary results given by the below lemmas.

**Lemma 1.** Being  $\underline{a}, \underline{b}, \underline{c} \in \mathbb{R}$  with  $Re(\underline{a}^2 + \underline{b}^2) \neq 0$ . Than, the equation

$$\underline{a} \cos \underline{\alpha} + \underline{b} \sin \underline{\alpha} = \underline{c} \quad (2)$$

has the solution  $\underline{\alpha} \in \mathbb{R}$  if and only if

$$Re(\underline{a}^2 + \underline{b}^2 - \underline{c}^2) > 0 \quad (3)$$

If the condition (3) is fulfilled, the solutions are:

$$\underline{\alpha} = \text{artan2}[\underline{bc} \pm \underline{ad}, \underline{ac} \mp \underline{bd}] \quad (4)$$

where we have denoted

$$\underline{d} = \sqrt{\underline{a}^2 + \underline{b}^2 - \underline{c}^2}. \quad (5)$$

**Lemma 2.** For any orthogonal dual tensor  $\underline{R} \in \underline{S}\mathbb{O}_3$ ,  $\underline{R} = \underline{R}(\underline{\alpha}, \underline{u})$  and any dual unit vector  $\underline{v}$  and  $\underline{w}$ , the following identity takes place:

$$(\underline{u} \times \underline{v}) \cdot (\underline{u} \times \underline{w}) \cos \underline{\alpha} + (\underline{u}, \underline{v}, \underline{w}) \sin \underline{\alpha} = \underline{w}[\underline{R} - \underline{u} \otimes \underline{u}]\underline{v} \quad (6)$$

**Lemma 3.** Let  $\underline{u}$  and  $\underline{v}$  two unit vectors so that  $Re(\underline{u} \times \underline{v}) \neq \mathbf{0}$ . The equation system

$$\begin{cases} \underline{R}\underline{u} = \underline{u} \\ \underline{R}\underline{v} = \underline{w} \end{cases} \quad (7)$$

admits unique solution  $\underline{R} \in \underline{S}\mathbb{O}_3$  if and only if the following condition is satisfied:

$$\underline{\mathbf{u}} \cdot \underline{\mathbf{v}} = \underline{\mathbf{u}} \cdot \underline{\mathbf{w}} \quad (8)$$

Now we can give the main theorem.

**Main Theorem:** If  $\underline{\mathbf{R}} \in \underline{S\mathbb{O}}_3$  and  $\underline{\mathbf{u}}_1, \underline{\mathbf{u}}_2, \underline{\mathbf{u}}_3$  three dual unit vectors, so that  $Re(\underline{\mathbf{u}}_2 \times \underline{\mathbf{u}}_1) \neq 0$ ,  $Re(\underline{\mathbf{u}}_2 \times \underline{\mathbf{u}}_3) \neq 0$ , the equation

$$e^{\alpha_1 \underline{\mathbf{u}}_1} e^{\alpha_2 \underline{\mathbf{u}}_2} e^{\alpha_3 \underline{\mathbf{u}}_3} = \underline{\mathbf{R}} \quad (9)$$

having unknown the dual angles  $\alpha_k \in \mathbb{R}$  with  $k = \overline{1,3}$ , admits solutions if and only if

$$|\underline{\mathbf{u}}_1(\underline{\mathbf{R}} - \underline{\mathbf{u}}_2 \otimes \underline{\mathbf{u}}_2)\underline{\mathbf{u}}_3| < \|\underline{\mathbf{u}}_2 \times \underline{\mathbf{u}}_1\| \|\underline{\mathbf{u}}_2 \times \underline{\mathbf{u}}_3\| \quad (10)$$

and

$$\underline{\mathbf{R}}\underline{\mathbf{u}}_3 \neq \pm \underline{\mathbf{u}}_1 \quad (11)$$

In relations (10) and (11), we have noted  $\underline{\mathbf{R}} = Re \underline{\mathbf{R}}$  and  $\underline{\mathbf{u}}_k = Re(\underline{\mathbf{u}}_k)$ , with  $k = \overline{1,3}$ .

If the screw-axes for  $\underline{\mathbf{R}}_1$  and  $\underline{\mathbf{R}}_3$  are perpendicular on the screw axes of  $\underline{\mathbf{R}}_2$ , the following conditions are met:

$$\begin{aligned} Re(\underline{\mathbf{u}}_1 \cdot \underline{\mathbf{u}}_2) &= 0 \\ Re(\underline{\mathbf{u}}_2 \cdot \underline{\mathbf{u}}_3) &= 0 \end{aligned} \quad (12)$$

In this case, the equation (10) of the **Main Theorem** becomes:

$$|\underline{\mathbf{u}}_1 \underline{\mathbf{R}} \underline{\mathbf{u}}_3| < 1. \quad (13)$$

valid for  $\forall \underline{\mathbf{R}} \in \underline{S\mathbb{O}}_3$ . Consequently, from **Main Theorem**, results that the dual angle  $\alpha_2$  can be determined for  $\forall \underline{\mathbf{R}} \in \underline{S\mathbb{O}}_3$ .

We will obtain the free of coordinates closed form solution for the **Davenport dual angles**. If  $\underline{\mathbf{u}}_3 = \underline{\mathbf{u}}_1$ , we will obtain the free of coordinates closed form solution for the **Euler dual angles**.

**Remark 1.** Parametrization of a rigid displacement through Davenport-Euler angles,  $\alpha_k, k = \overline{1,3}$  is minimal. This minimal parametrization presents singularities if

$$Re[\underline{\mathbf{R}}\underline{\mathbf{u}}_3 \times \underline{\mathbf{u}}_1] = 0 \quad (14)$$

The physical meaning of this singularity is that it appears if the tensor  $\underline{\mathbf{R}}$  transfers the screw-axis  $\underline{\mathbf{u}}_3$  in a screw-axis parallel with that one given by  $\underline{\mathbf{u}}_1$ .

In the specific case of a rigid motion, the kinematics equations are deduced and the motion is determined (via Davenport dual angles) knowing the instantaneous twist in space or in body frame:

$$\begin{cases} \underline{\dot{\alpha}} = \frac{1}{\langle \underline{\mathbf{u}}_1, \underline{\mathbf{u}}_2, \underline{\mathbf{u}}_3^* \rangle} [\underline{\mathbf{u}}_2 \times \underline{\mathbf{u}}_3^*, \underline{\mathbf{u}}_3^* \times \underline{\mathbf{u}}_1, \underline{\mathbf{u}}_1 \times \underline{\mathbf{u}}_2]^T \underline{\mathbf{R}}_1^T \underline{\boldsymbol{\omega}} \\ \underline{\alpha}(t_0) = \underline{\alpha}_0 \end{cases} \quad (15)$$

where  $\underline{\mathbf{u}}_3^* = \underline{\mathbf{R}}_2 \underline{\mathbf{u}}_3$

The results are of interest in inverse kinematics, control theory and multibody systems dynamics..

## References

- [1] D. Condurache and A. Burlacu, "Dual Tensors Based Solutions for Rigid Body Motion Parameterization," *Mechanism and Machine Theory*, vol. 74, no. April 2014, pp. 390-412, 2014.
- [2] D. Condurache and A. Burlacu, "Onboard Exact Solution to the Full-Body Relative Orbital Motion Problem," *AIAA Journal of Guidance, Control, and Dynamics*, vol. 39, no. 12, pp. 2638-2648, 2016.
- [3] D. Condurache and A. Burlacu, "Dual Lie Algebra Representations of the Rigid Body Motion," in *AIAA/AAS Astrodynamics Specialist Conference, AIAA Paper 2014-4347*, San Diego, 2014.
- [4] A. Rull and T. Frederico, "On Generalized Euler Angles," *New Trends in Mechanism and Machine Science*, vol. 24, pp. 61-68, 2015.
- [5] J. Wittenburg and L. Lilov, "Decomposition of a finite rotation into three rotations about given axes," *Multibody System Dynamics*, vol. 9, no. 4, pp. 353-375, 2003.
- [6] P. B. Davenport, "Rotations about nonorthogonal axes," *AIAA Journal*, vol. 11, no. 6, pp. 853-857, 1973.
- [7] A. H. J. de Ruiter and J. R. Forbes, "Generalized Euler Sequences Revisited," *Journal of Astronautical Science*, vol. 62, pp. 1-20, 2015.
- [8] G. Piovan and F. Bullo, "On coordinate-free rotation decomposition: Euler angles about arbitrary axes," *IEEE Transactions on Robotics*, vol. 28, pp. 728-733, 2012.
- [9] M. D. Schuster and L. F. Markley, "Generalization of the Euler angles," *Journal of the Astronautical Sciences*, vol. 51, no. 2, pp. 123-132, 2003.
- [10] C. D. Mladenova and I. M. Mladenov, "Vector decomposition of finite rotations," *Reports on Mathematical Physics*, vol. 68, no. 1, pp. 107-117, 2011..

# Selected Feedback Control Concepts in End-effector Trajectory Tracking of a Highly Flexible Manipulator

Merlin Morlock, Robert Seifried

Institute of Mechanics and Ocean Engineering  
Hamburg University of Technology  
21071 Hamburg, Germany  
[merlin.morlock; robert.seifried]@tuhh.de

## Abstract

In this talk various feedback control concepts for highly flexible manipulators are presented and their efficiency is evaluated by simulations and experiments. In this regard, the parallel manipulator depicted in Fig. 1 is considered. The manipulator consists of two movers which are actuated by linear servo-drives. Arms are mounted on top of each mover by revolute joints, being connected to each other by a third revolute joint in the middle of the long arm. At the end of this long and highly flexible arm an end-effector mass is attached. For details on the experimental setup see [1]. This experimental rig serves to investigate concepts for modern lightweight and consequently energy efficient manipulators. Typically a mass reduction of the system significantly decreases the stiffness. Thus, in contrast to traditional manipulators which are rigid, these lightweight manipulators have a considerable amount of compliance. This makes them interesting for modern robotics applications such as service robotics with human-machine interaction or medical robotics. Due to their energy efficiency they are also interesting for traditional robotics applications in manufacturing.



Figure 1: Experimental setup of a highly flexible parallel manipulator.

Due to body flexibility lightweight manipulators must be modeled as flexible multibody systems, whereby in such robotics applications the floating frame of reference approach is usually applied together with linear model reduction for the elastic bodies. This leads to compact models with a relatively low number of degrees of freedom which is very important for control design. Although, the considered system is highly flexible, the linear approximation is in most scenarios sufficient for describing the system dynamics.

In flexible manipulators the control inputs are often actuators which are collocated with the joints, yielding a similar system topology as for rigid manipulators. However, the elastic coordinates used for describing the body elasticity have no or only limited associated control inputs. Therefore, flexible manipulators are typically underactuated multibody systems, possessing less control inputs than degrees of freedom.

In this research, the control goal is trajectory tracking of the end-effector point located at the end of the long arm. The desired end-effector trajectories are predefined in time and space. Due to the underactuation this is a challenging task since the classical approach of inverse kinematics and dynamics known from rigid manipulators cannot be applied.

Since the manipulator performs a large working motion a so-called two design of freedom control structure is applied, combining feedforward control and feedback control. Due to the body flexibility the accurate determination of the end-effector state is difficult. Direct measurements, such as image tracking, are often not online capable and have rather limited frames per second. Thus, camera measurements are only used for offline validation purposes. For an online determination of the end-effector and the system state at a high sampling rate a nonlinear estimator is designed based on mover position and strain gauge measurements. Here, the common Unscented

Kalman Filter is adapted for flexible multibody systems with algebraic constraint equations providing the basis for end-effector feedback control.

In this talk all three components, feedforward control design, feedback control design and nonlinear state estimator design are briefly discussed. The main focus of this talk is on the design of the feedback part and its interplay with feedforward control.

The feedforward control is computed by a model inversion of the flexible multibody system. For given desired output trajectories the inverse model provides the required control inputs for exact output reproduction. Also, the trajectories of all coordinates of the system are obtained, which can be used in feedback control design. One efficient model inversion approach for underactuated multibody systems are the so-called servo-constraints [2, 3]. The inverse model of the considered flexible manipulator includes a dynamical part, which is called internal dynamics in nonlinear control theory [4]. The considered system has unstable internal dynamics if the end-effector point is used as system output [3]. In such a case a bounded solution can be computed from a boundary-value problem. Alternatively, by output relocation a new artificial system output can be designed close to the real system output but yielding stable internal dynamics. Thus, the inverse model can be computed by forward time integration. Such an alternative output can be designed by parameter optimization [3].

This feedforward control is then supplemented by additional feedback to account for small disturbances and uncertainties. One source of disturbance is friction in the linear drives. In the most simple case feedback action is just added using the mover position measurements to ensure that they follow the desired trajectories. Then, in the absence of any other disturbances it can be shown, that the end-effector follows the desired trajectory very closely, proofing the high accuracy of the feedforward control based on an inversion of the complete dynamics of the flexible multibody system [1].

Besides friction in the drives other disturbances and uncertainties e.g. in the initial condition or an uncertain end-effector mass are not as easy to overcome. More advanced feedback control strategies have to be applied. Thereby several approaches are presented and tested numerically and experimentally.

In a first approach the arm deformation is determined using strain gauges and feedback to the servo-drives [5]. This makes it possible to damp vibrations without the need for a state estimator. This approach is suited to damp large undesired vibrations before and after a trajectory tracking, but shows insufficient efficiency during trajectory tracking.

Alternatively, in a second approach a basic output feedback control of the end-effector state is designed. Hereby, an equivalent rigid model is linearized at selected working points and the first bending eigenmode is roughly compensated. As this controller uses the end-effector information much better results than in the first approach can be achieved.

Finally, in a third approach feedback linearization [4] based on servo-constraints is applied. Since the end-effector output yields unbounded internal dynamics the previously discussed output relocation approach is utilized. Thus, an exact input-output linearization can be performed. Within this approach the feedforward control is not needed, as the approach already includes the inverse model. Since feedback linearization requires full state feedback the nonlinear state estimator is crucial. The efficiency is compared to the other approaches, especially concerning external disturbances and parameter uncertainty.

## Acknowledgments

The authors would like to thank the German Research Foundation (DFG) for their financial support of the project SE1685/3-2 and Professor Peter Eberhard for providing the experimental setup at the Institute of Engineering and Computational Mechanics at the University of Stuttgart.

## References

- [1] M. Burkhardt, R. Seifried, P. Eberhard. Experimental studies of control concepts for a parallel manipulator with flexible links. *Journal of Mechanical Science and Technology*, Vol. 29, No. 7, pp. 2685-2691, 2015.
- [2] W. Blajer, K. Kołodziejczyk. A geometric approach to solving problems of control constrains: theory and a DAE framework. *Multibody System Dynamics*, Vol. 11, No. 4, pp. 343-364, 2004.
- [3] R. Seifried. *Dynamics of underactuated multibody systems*. Springer, Berlin, 2014.
- [4] A. Isidori. *Nonlinear control systems*. Springer, London, 1995.
- [5] M. Burkhardt, M. Morlock, R. Seifried, P. Eberhard: Active damping control for an underactuated multi-body system. *PAMM Proceedings in Applied Mathematics and Mechanics*, Vol. 15, pp. 59-60, 2015.

## Forward Kinematics Analysis of a Stewart Platform using Computer Vision Pose Estimation

Mohd.Zubair<sup>1</sup>, Vineet Mathew<sup>1</sup>, Sudipto Mukherjee<sup>1</sup>, Deepak K Gupta<sup>2</sup>

<sup>1</sup>Department of Mechanical Engineering  
 Indian Institute of Technology-Delhi  
 New Delhi, Delhi-110016, India  
 [mdzubair87, vineetdtu]@gmail.com,  
 sudipto@mech.iitd.ac.in

<sup>2</sup>Department of Neuroscience  
 AIIMS  
 Ansari Nagar, Delhi-110029, India  
 drdeepakgupta@gmail.com

### Abstract

In this paper computer vision is used to analyse the pose of the Stewart platform shown in Figure 1. To get a unique solution of the forward kinematics of the Stewart platform, a predefined library of ArUco markers has been used for pose estimation. The analytical solution for the forward kinematics problem of a Stewart platform is extremely non-linear and mathematically has multiple solutions [1]. By using computer vision, complexity decreases and speed increases [2]. The advantage of using ArUco markers is that a single marker has enough information for pose estimation [3].

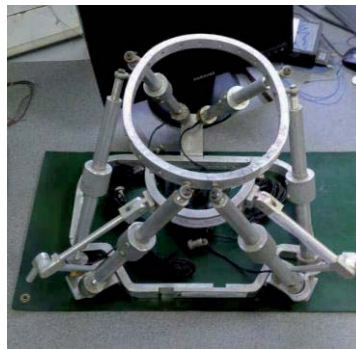


Figure 1. Stewart Platform setup on which markers are placed

In the case of serial manipulators the forward kinematics problem has an easy solution and the inverse kinematics problems are relatively quite tedious. A Stewart platform is an example of a closed loop parallel manipulator. It six legs having prismatic joint connecting a top mobile platform with a bottom fixed platform. The motion of the top platform is controlled by changing the lengths of the legs in various proportions [4]. For kinematic analysis the coordinate frame has been attached to fixed frame ( $XYZ$ ) and moving frame ( $X_0Y_0Z_0$ ). Vector  $\mathbf{b}_i$  and  $\mathbf{p}_i$  are the position vectors in respective frame as shown in Figure 2. A close loop equation can be written for each leg, thus vector loop equation for the base and moving platform is given by

$$\mathbf{q}_i = \mathbf{t}_0 + {}^pR_b \cdot \mathbf{p}_i \quad (1)$$

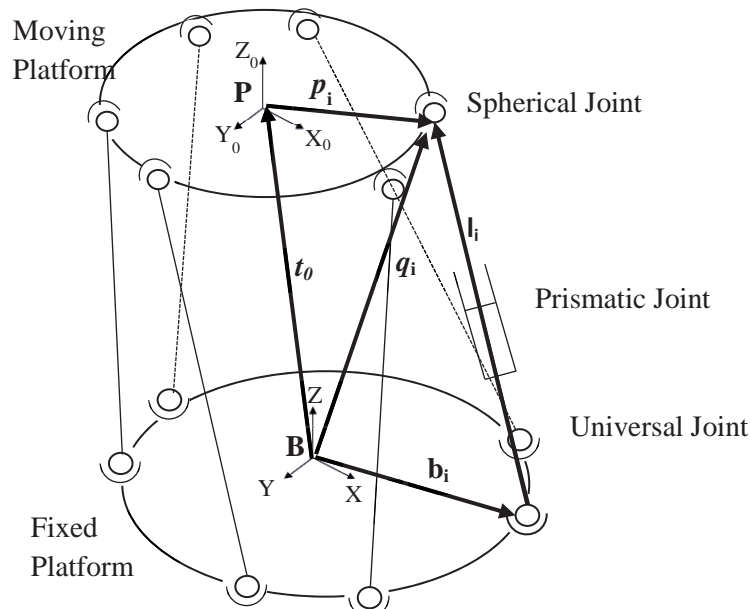


Figure 2. Labeled Stewart Platform schematic

With the use of predefined ArUco markers and computer vision techniques, the position and orientation of a marker can be determined with respect to the camera frame [5]. Figure 3 illustrates the experimental procedure adopted for analysing the forward kinematics of the Stewart platform.

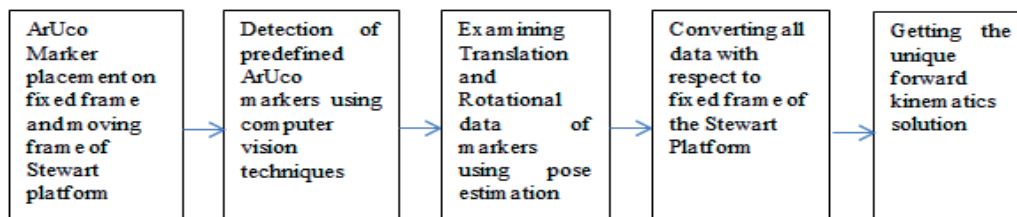


Figure 3. Flowchart of the experimental procedures

The position and orientation vectors of the marker in Figure 4 placed on the moving frame of the Stewart platform are tabulated in Table 1 and Table 2. The output for orientation is given using Rodrigues vectors. This output is then converted to a 3X3 rotation matrix and the extrinsic Euler angles for the X-Y-Z configuration are decomposed from the matrix.

Table 1. Translation vector components

$T_x$	-382.3489
$T_y$	-257.59445
$T_z$	1113.0265

Table 2. Rodrigues vector components

$R_x$	0.0675849
$R_y$	2.32048
$R_z$	-0.130508



Figure 4. ArUco marker detection

## Acknowledgments

We hereby acknowledge Mr. Sachin Kansal, PhD scholar, IIT Delhi for his assistance in doing the work. We also acknowledge Mechatronics Lab, Mechanical Engineering Department, IIT Delhi for providing the environment for carrying out the research activity.

## References

- [1] O. Ma and J. Angeles. Optimum Architecture Design of Platform Manipulator. *Advance Robotics*, IEEE, 1991, pp.1130-1135.
- [2] M. A. Sutton, W. J. Wolters, W. H. Peter, W. F. Ranson and S. R. McNeil. Determination of displacements using an improved digital correlation method. *Image vision computing*, 1986, pp 143-150.
- [3] S. Garrido-Jurado, R. Munoz-Salinas, F. J. Madrid-Cuevas, M. J. Marin-Jimenez. Automatic generation and detection of highly reliable fiducial markers under occlusion. *Pattern Recognition*, vol. 47, no. 6, pp. 2280-2292, 2014.
- [4] C. Gosselin. Determination of the Workspace of 6 DOF Parallel Manipulators. *Journal of Mechanical Design*, ASME, 1990, Vol. 112.
- [5] S. Garrido-Jurado, Rafael Munoz-Salinas, F. J. Madrid-Cuevas, R. Medina-Carnicer. Generation of fiducial marker dictionaries using Mixed Integer Linear Programming. *Journal of Pattern Recognition*, vol. 47, no. 6, pp. 2280-2292, 2014.

## Improved calibration of machine tools by redundant measurement

Michael Valasek, Filip Kovář

Faculty of Mechanical Engineering  
Czech Technical University in Prague  
Technická 4, 16607 Praha 6, Czech Republic  
Michael.Valasek@fs.cvut.cz

### Abstract

The paper deals with the new procedure of calibration of machine tools or robots by redundant measurements. The usage of laser tracker cannot provide sufficient accuracy of calibration within large workspaces. It is based on redundant measurements. The laser tracker measures the position of multiple reflectors firmly attached in the workspace. This enables to increase the accuracy of measurements several times.

The basic scheme of the described method consists of a laser tracker (tracker) placed in the machine and set of reflectors of the laser beam (reflectors). The reflectors could be arbitrarily placed in the workspace on the machine frame or on the workpiece. The reflectors could be also placed outside the workspace, for example on the construction of a hall etc. This scheme is shown in figure 1 of the patent [1].

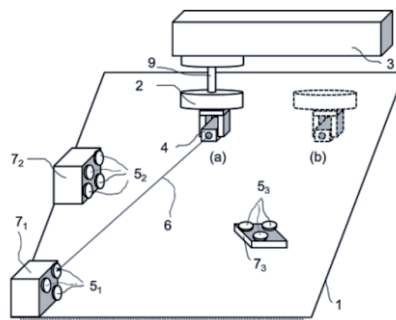


Figure 1: Measurement scheme

Figure 1 shows us workspace – 1, spindle – 2, headstock – 3, machine – 4, reflectors – 5, laser beam – 6, platforms holding reflectors – 7.

Measurement procedure starts by moving of the end-effector (corresponds to position of tracker) to the first position (Fig. 1 position (a)). In this position, the tracker measure the relative position of all reflectors (it means x, y, z of reflectors). After that the end-effector moves into the second position. (Fig. 1 position (b)). In this position the tracker measures all reflectors again. Similarly we measure the reflectors from all desired positions. From the measurement of reflectors in one position we obtain the relative position of all reflectors and one position of the tracker. With each new end point location and subsequent measurement we obtain redundancy. To determine the amount of redundancy we use formula:

$$E = \frac{v}{b} \quad (1)$$

where  $E$  means redundancy,  $v$  means binding equations and  $b$  is number of searched parameters.

Computation of measured data is based on modified Newton method, which is described by expressions:

$$\mathbf{F}_s = \mathbf{F}(\mathbf{R}_s, \mathbf{L}) \quad (1)$$

$$J_s = J(R_s, l)$$

$$\Delta R_s = -\lambda(J_s^T J_s)^{-1} J_s^T F_s$$

$$R_{s+1} = R_s + \Delta R_s$$

In equations (2)  $F$  is vector of coupling conditions,  $R$  means calibration parameters,  $l$  is measuring distances and  $J$  is jacobian. The algorithm begins with input of inaccurate calibration parameters  $R_0$ . Iterative calculation is carried out in a loop, until  $\|F\| \geq \varepsilon$  or  $\lambda \geq \varepsilon$ , where  $\varepsilon$  is sufficiently small number. In our method we chose the halving of step method (if it should occur in  $s + 1$  iteration divergence ( $\|F_{s+1}\| \geq \|F_s\|$ ), we will decrease step from  $\lambda$  to half of  $\lambda$ , so long as this condition is true).



Figure 2: Measurement scheme Machine Grata in TOS Varnsdorf and detail of laser tracker Leica AT901 (right)

For experimental tests, there was chosen the machine Grata in TOS Varnsdorf (see Fig. 3 – left) and measuring device the laser tracker Lieca AT901 (see Fig. 3 – right). Number of reflectors was 17 and number of position of trackers was 32.



Figure 3: Interferometer XM-60 of Renishaw

To results verification was chosen interferometer of Renishaw. The test results indicate more than 6-times improvement.

## References

- [1] Valášek, M., Nečas, M. Švéda, J., Zařízení pro redundantní optické měření a/nebo kalibraci polohy tělesa v prostoru. Užiténý vzor. Czech republic, 25815. 2013.
- [2] Štembera, J. Vliv vícenásobné redundance měření na přesnost kalibrace a měření,. Praha: Faculty of mechanical engineering, CTU in Prague

## **Section**

# **ROAD AND RAILROAD VEHICLE DYNAMICS**



## A soft soil contact model with adaptive level of detail for predicting off-road vehicle mobility

Alessandro Tasora<sup>1</sup>, Dario Mangoni<sup>1</sup>, Dan Negrut<sup>2</sup>, Radu Serban<sup>2</sup>, Paramsothy Jayakumar<sup>3</sup>

<sup>1</sup> Department of Industrial Engineering  
University of Parma  
V.le delle Scienze 181/A, 43100 Parma, Italy  
[alessandro.tasora,dario.mangoni]@unipr.it

<sup>2</sup> Department of Mechanical Engineering  
University of Wisconsin-Madison  
Madison, WI 53706-1572, USA  
[negrut,serban]@wisc.edu

<sup>3</sup>US Army Tank Automotive Research,  
Development, and Engineering Center  
Warren, MI 48397-5000, USA  
paramsothy.jayakumar.civ@mail.mil

### Abstract

This work presents a model for soft soil that can interact with wheeled or tracked vehicles in a multibody simulation framework. In sake of high performance, the soil is represented by arbitrary triangular meshes, where the level of detail of the mesh is automatically increased as tire lugs or track shoes come into contact.

Our model draws on the semi empirical wheel-soil model pioneered by Bekker and Wong [1–3]. As such, it requires few empirical parameters to be adjusted, and many of those values are already tabulated in literature for experimentally-tested soil samples. Following the ideas presented in the SCM Soil Contact Model [4, 5], our soil is represented by a three-dimensional mesh, hence it allows the case of arbitrary tire shapes.

Differently from the original SCM implementation, our algorithm uses a non-structured grid for the soil. In detail, instead of using a structured grid with equally-spaced rectangular elements, our model operates on a mesh of triangles with arbitrary size and topology. This allows scenarios where the soil mesh is shaped like a ring or a road with curves, without the need of adding nodes in areas that are not crossed by vehicles. Also, areas that are initially flat can be represented by a small number of triangles, thus saving memory and performance for areas that require small triangles; for instance when representing details such as bumps or trenches.

An additional improvement in performance comes from an algorithm that implements adaptive level of detail. This means that the triangle mesh is automatically refined in the surroundings of the tires (or tracks) of the running vehicle. When contact between a moving object and the soil is detected, a real-time refinement algorithm recursively splits contact triangles whose size exceeds a user-defined threshold; this process generates additional, smaller triangles that can compute contact forces with finer detail, as shown in Fig.1. As a side effect, also the visualization of the ruts is much more realistic and precise: the plastic deformation of the soil retains all the details of the wheel lugs without needing millions of nodes.

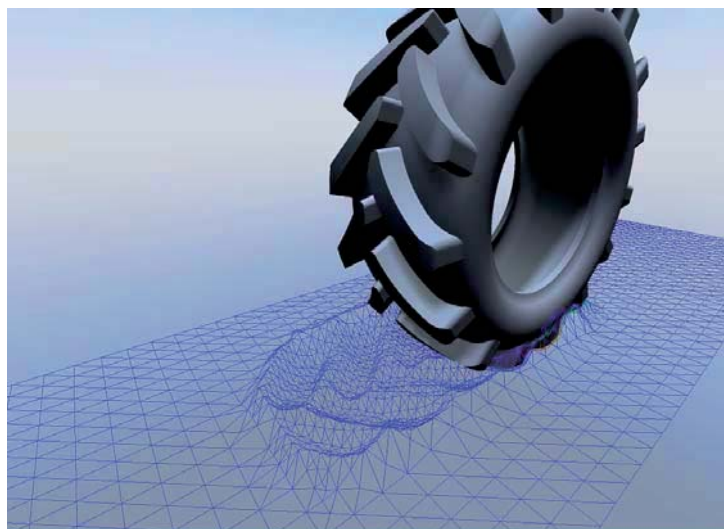


Figure 1: Example of adaptive soil refinement in the surroundings of the tire footprint.

When the vehicle goes away, after a time or distance threshold, the trailing ruts can be optionally simplified thanks to another algorithm that performs a mesh coarsening. Such algorithm merges fine triangles back into large triangles: this can keep the total number of triangles and nodes upper limited even after a long trip of the vehicle in the simulated environment.

Finally, an iterative algorithm performs an erosion of the deformed soil following the heuristic approach in [5]. The original idea, which runs a smoothing operator on a regular grid, here is extended to the case of unstructured grid of triangles by running a custom topological operator. This iteration is also in charge of creating the build-up of material in front and to the sides of the running tire.

We experienced that a purely plastic soil model does poses some difficulties to the numerical integration schemes used in multibody dynamics, especially when we tested stiff soils with vehicles that stay in place, a circumstance that often generates noisy or intermittent patterns of contact forces. This problem has been alleviated by introducing an additional and optional parameter, namely the soil elasticity, whose effect visible regularizes contact forces in those critical scenarios. Also, we introduced a basic soil damping coefficient whose effect is in favour of a more stable and robust integration, and that can be adjusted using experiments.

Thanks to the semi-empirical approach, the entire algorithm is local and it does not require the solution of linear systems. This means fast performance and, in many scenarios, low memory footprint. The biggest bottleneck comes from the collision detection step that detects the contact points. We adopt a general-purpose collision detection algorithm that finds the collision points by scattering ray-cast tests over an (virtually unlimited) set of shapes that describe tires, track shoes, legs or other vehicle/robot parts that come into contact with the soil. Such collision detection stage is accelerated by a broad-phase preprocessing step.

The entire algorithm has been implemented in the Project Chrono software library, and it has been used to study the performance of vehicles with variable numbers of wheels, as well as tracked vehicles [6]. The multi-body environment of Project Chrono allows also flexible tires, which can work together with the presented deformable soil. In this case, tires are modeled with multi-layered shells (each layer representing a ply of the tire) and solid brick elements that represent the lugs. All those finite elements can interact with the soft soil by exchanging contact forces over arbitrary patches, which are automatically detected by the collision engine.

Results have been compared with other, more detailed models (finite elements with plastic flow and granular soil with discrete elements) obtaining good agreement at a fraction of the computational cost.

## Acknowledgments

Disclaimer: Reference herein to any specific commercial company, product, process, or service by trade name, trademark, manufacturer, or otherwise, does not necessarily constitute or imply its endorsement, recommendation, or favoring by the United States Government or the Department of the Army (DoA). The opinions of the authors expressed herein do not necessarily state or reflect those of the United States Government or the DoA, and shall not be used for advertising or product endorsement purposes.

## References

- [1] M.G. Bekker. *Theory of land locomotion: the mechanics of vehicle mobility*. University of Michigan Press, 1956.
- [2] Jo-Yung Wong and AR Reece. Prediction of rigid wheel performance based on the analysis of soil-wheel stresses part i. performance of driven rigid wheels. *Journal of Terramechanics*, 4(1):81–98, 1967.
- [3] Jo Yung Wong et al. *Terramechanics and off-road vehicles*. Elsevier, 1989.
- [4] Andreas Gibbesch and B Schafer. Multibody system modelling and simulation of planetary rover mobility on soft terrain. In *8th International Symposium on Artificial Intelligence, Robotics and Automation in Space (i-SAIRAS 2005), Munich, Germany, September*, pages 5–8, 2005.
- [5] Rainer Krenn and Gerd Hirzinger. Simulation of rover locomotion on sandy terrain-modeling, verification and validation. In *Proceedings of the 10th Workshop on ASTRA, Noordwijk, The Netherlands*, 2008.
- [6] H. Mazhar, T. Heyn, A. Pazouki, D. Melanz, A. Seidl, A. Bartholomew, A. Tasora, and D. Negrut. Chrono: a parallel multi-physics library for rigid-body, flexible-body, and fluid dynamics. *Mechanical Sciences*, 4(1):49–64, 2013.

## Force estimation on a McPherson suspension by means of a state estimator and a multibody model

Enrico Risaliti<sup>1,2</sup>, Martijn Vermaut<sup>2,3</sup>, Jan Croes<sup>2,3</sup>, Bram Cornelis<sup>1</sup>, Wim Desmet<sup>2,3</sup>

<sup>1</sup>RTD Test Division  
Siemens Industry Software NV  
Interleuvenlaan 68, B-3001 Leuven, Belgium  
enrico.risaliti@siemens.com

<sup>2</sup> Department of Mechanical Engineering  
KU Leuven  
Celestijnenlaan 300 B, B-3001 Heverlee, Belgium

<sup>3</sup>Member of Flanders Make

### Abstract

External loads acting on mechanical systems represent important quantities which often need to be determined for design, control or monitoring purposes. For instance in the automotive sector so-called Wheel Center Forces (WCFs), i.e. the forces acting on the center of the vehicle wheels, are required in order to perform durability analyses [1]. WCFs can be directly measured by means of dedicated measurement wheels, but the latter turn out to be expensive, intrusive and time-consuming to install. An appealing alternative could be to virtually measure those forces by combining information coming from a system model and more economical, less intrusive and easier-to-install sensors. Virtual prototypes are indeed becoming available sooner and sooner in the development phase of a new vehicle. As soon as a virtual prototype becomes available, it can be used to enhance information coming from sensor data, and to infer quantities that are not directly measured or measurable. State estimation is the mathematical tool that can be used in order to combine simulation and sensors data and to estimate the quantity of interest.

In literature there already exist examples where finite element or multibody models are used in state estimators. In [2] simulation data of a finite element model of the steering knuckle are combined with sensor information coming from strain measurements. The unknown forces are modeled as a random walk process in order to be estimated by means of an augmented linear Kalman filter along with the states of the system. The performances of the approach are limited by the fact that the correct kinematic motion of the whole suspension is not well captured as only the finite element model of one component is considered. It therefore appears necessary to include a multibody model of the entire suspension in the state estimator. In [3] multibody models are used in non-linear Kalman filters in order to estimate the system states. Combined state-input estimation is instead performed in [4], where a reduced multibody model is used in an augmented Extended Kalman Filter (EKF). In this paper an approach similar to the one used in [3] is employed in order to perform state estimation with multibody models. By introducing a random walk model for the unknown force, also this latter quantity is estimated. The feasibility of the approach is illustrated by means of a virtual experiment on a McPherson suspension system.

A multibody system is generally described by a set of Differential Algebraic Equations (DAEs) as in addition to the equations of motion also constraint equations are present. In order to deal with a simpler non-constrained estimation problem, the system is transformed into a set of Ordinary Differential Equations (ODEs) by means of a penalty formulation in this work. The process equations for the estimation problem are reported below:

$$\dot{\mathbf{x}} = \begin{bmatrix} \dot{\mathbf{q}} \\ \dot{\mathbf{v}} \\ \dot{\mathbf{u}} \end{bmatrix} = \begin{bmatrix} \mathbf{v} \\ (\mathbf{M} + \Phi_q^T \alpha \Phi_q)^{-1} [\mathbf{B}\mathbf{u} - \mathbf{f} - \Phi_q^T \alpha (\dot{\Phi}_q \dot{\mathbf{q}} + 2\omega\zeta \Phi_q \dot{\mathbf{q}} + \omega^2 \Phi)] \\ \mathbf{0} \end{bmatrix} + \begin{bmatrix} \mathbf{w}_q \\ \mathbf{w}_v \\ \mathbf{w}_u \end{bmatrix}, \quad (1)$$

where the augmented state vector  $\mathbf{x}$  includes the generalized coordinates  $\mathbf{q}$ , the generalized velocities  $\mathbf{v}$  and the unknown inputs  $\mathbf{u}$ . The first two equations are the equations of motion in first order form, while the last one represents the random walk model for the unknown inputs.  $\mathbf{M}$ ,  $\Phi_q$ ,  $\Phi$  and  $\mathbf{B}$  are respectively the mass matrix, the constraint Jacobian matrix, the constraint vector and the input projection matrix.  $\mathbf{f}$  is the additional non-linear function of  $\mathbf{q}$  and  $\mathbf{v}$  which includes the gyroscopic effects and the effects of additional force elements.  $\alpha$ ,  $\omega$  and  $\zeta$  are the penalty factors introduced with the penalty formulation.  $\mathbf{w}_q$  and  $\mathbf{w}_v$  represent the process noise for the equations of motion while  $\mathbf{w}_u$  is the noise that characterizes the random walk model for the inputs.

Eq.1 forms the basis for a state space representation of the system, which is completely obtained once also a set of measurement variables is chosen and the relative measurements equations are written. This state space representation can be directly exploited in a non-linear Kalman filter in order to estimate the augmented state vector  $\mathbf{x}$ , which also contains the unknown inputs  $\mathbf{u}$ . In this work an EKF is used [5].

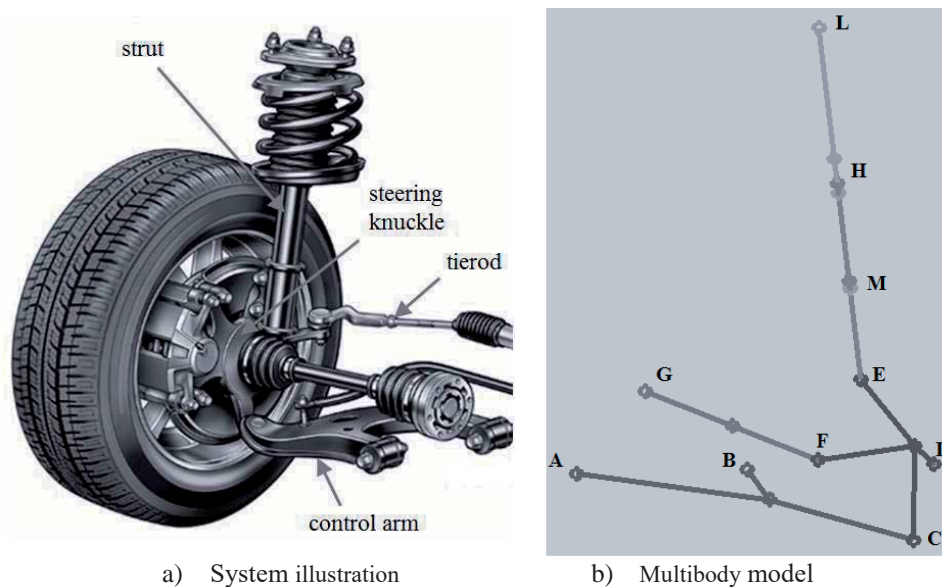


Figure 1. McPherson suspension system

In order to assess the feasibility of the approach, a numerical experiment is conducted on a McPherson suspension system for which an illustration is shown in Figure 1a. Figure 1b shows the multibody model used in the experiment. It is composed entirely of rigid bodies: the control arm (A,B,C), the steering knuckle (C,D,E,F), the tierod (G,F), the upper strut (L,M) and the lower strut (E,H). All the joints are ideal and the system is connected to the ground in points A, B, G and L. Linear elements are used to model the main spring and damping behavior. Point D represents the wheel center, where the external loads are applied.

Simulated measurements representing the suspension deflection and acceleration of the wheel center are generated for a loading case in which a vertical force at the wheel center is applied. The simulated measurements are then used to estimate the applied force by means of the state estimation approach described above. In order to increase the realism, modeling errors are introduced by considering a modified estimator model in which the stiffness constant value of the main spring is considerably reduced. The results show that the force estimation can be well accomplished.

## Acknowledgments

The authors gratefully acknowledge the European Commission for its support of the Marie Skłodowska Curie program through the ITN ANTARES project (GA 606817), and also the support of VLAIO (Flemish Innovation & Entrepreneurship) through the O&O project ENDURANCE (IWT. 150958).

## References

- [1] P. Johannesson and M. Speckert. *Guide to Load Analysis for Durability in Vehicle Engineering*. John Wiley and Sons, Ltd., Chichester, West Sussex, United Kingdom, 2014.
- [2] E. Risaliti, T. Tamarozzi, J. Van Caueren, B. Cornelis and W. Desmet. Virtual sensing of wheel center forces by means of a linear state estimator. *In International Conference on Noise and Vibration Engineering (ISMA2016)*, Leuven, Belgium, September 2016.
- [3] R. Pastorino, D. Richiedei, J. Cuadrado and A. Trevisani. State estimation using multibody models and non-linear Kalman filters. *International Journal of Non-Linear Mechanics*, 53:83-90, 2013.
- [4] F. Naets, R. Pastorino, J. Cuadrado and W. Desmet. Online state and input force estimation for multibody models employing extended Kalman filtering. *Multibody System Dynamics*. 32:317–336, 2014.
- [5] D. Simon. *Optimal state estimation: Kalman,  $H_\infty$  and nonlinear approaches*, John Wiley, New York, 2006.

# Optimal Control of the tilting modes transition for a Narrow Track Vehicle through MBS Modelling

Quentin Docquier, Timothée Habra, Nicolas Docquier, Paul Fiset

Institute of Mechanics, Materials and Civil Engineering  
Université Catholique de Louvain  
Place du Levant 2, 1348 Louvain-la-Neuve, Belgium  
quentin.docquier@uclouvain.be

## Abstract

**Introduction** Nowadays, traffic congestion is growing all over the world and has recently led to an increasing interest in the development of Narrow Track Vehicles (NTV). Narrow vehicles, characterized by a large height-to-track ratio, need to be tilted toward the inside of a turn to prevent them from overturning in case of high-speed cornering. Given NTVs mass and inertia, and for safety reasons, the vehicle tilt is controlled *actively* (i.e. by electric motors) instead of being controlled by the pilot as it is for traditional two-wheelers.

Two modes are possible for active tilt control. The Direct Tilt Control (DTC) consists in forcing the tilt with an actuator while the pilot steers the vehicle by turning the steering wheel (direct steering) (see Fig. 1.a). Conversely, for the Steering Tilt Control (STC), the steering wheel is decoupled from the wheels and an actuator steers the wheels to control the tilt (counter-steering) based on the measured steering wheel orientation (see Fig. 1.a). The DTC is stable for all speeds but leads to an important longitudinal torque in transient phase causing high energy consumption and reducing stability (wheel unloading). In turn, the STC is unstable at low speed but more efficient at high speed as it uses the lateral dynamic to tilt the vehicle. Previous investigations (see Fig. 1.b) showed the necessity to use the STC at higher speed and then to combine the two modes on the entire speed range [1]. The present work aims at optimizing the combination of both modes through optimal control [2]. The objective is to minimize the overall energy consumption related to tilting while ensuring a maximum safety and an accurate tracking of the tilt angle.

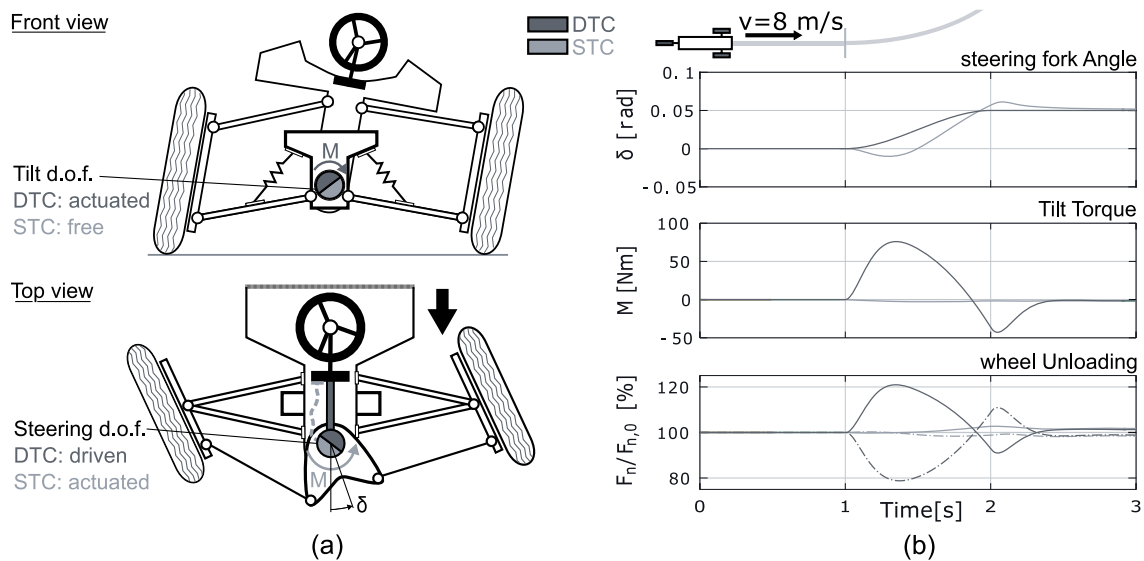


Figure 1: There exist two modes for active tilt control: the DTC and the STC. In the transient phase of cornering, the DTC can lead to an extensive torque causing a dangerous unloading and an important energy consumption [1].

**Vehicle modeling** The vehicle morphology and geometry used for the study correspond to a narrow three-wheelers, with a reverse-trike configuration, developed at the Université catholique de Louvain [3]. The rear axle unit is similar to the one of a motorbike. The front wheels unit is comparable to a traditional double wish-bone suspension except for the shocks' top connection which is not directly attached to the chassis but to an intermediate component: an articulated T-shaped pendulum (see Fig. 1). This mounting provides a rotational degree of freedom (d.o.f.) which can either be actuated (DTC) or let free (STC). The wheels can either be steered by the driver through the steering wheel (DTC) or controlled by an actuator based on the measured steering wheel orientation (STC).

The vehicle is modeled as a multibody system (MBS). Based on a formalism utilizing the relative coordinates [4], the equations of motions of the MBS are written as a system of Differential Algebraic Equation (DAE) :

$$\mathbf{M}(\mathbf{q})\ddot{\mathbf{q}} + \mathbf{c}(\mathbf{q}, \dot{\mathbf{q}}, \mathbf{g}) = \mathbf{Q}(\mathbf{q}, \dot{\mathbf{q}}) + \mathbf{J}^T \boldsymbol{\lambda} \quad (1)$$

$$\mathbf{h}(\mathbf{q}) = \mathbf{0} \quad \dot{\mathbf{h}}(\mathbf{q}, \dot{\mathbf{q}}) = \mathbf{0} \quad \ddot{\mathbf{h}}(\mathbf{q}, \dot{\mathbf{q}}, \ddot{\mathbf{q}}) = \mathbf{0} \quad (2)$$

with the symmetric generalized mass matrix  $\mathbf{M}$ , the generalized coordinates  $\mathbf{q}$ , the non linear dynamic vector  $\mathbf{c}$ , the generalized forces (torques)  $\mathbf{Q}$ , the constraint jacobian matrix  $\mathbf{J} = \frac{\partial \mathbf{h}}{\partial \mathbf{q}}$  and the algebraic constraints  $\mathbf{h}$  resulting, among others, from kinematic loops. The equations are derived using the ROBOTRAN software [5] developed at the UCL (Belgium). Based on a morphological description of the vehicle (masses, inertia, joints and lengths), the symbolic generator automatically writes expressions for the equations of the system. These are used for time integration (in real time) but also for modal analysis and quasi-static equilibrium in curves. Assuming a rigid connection for the steering assembly, such an equilibrium allows to relate the vehicle speed  $v$  and the steering of the vehicle (proportional to the steering wheel angle  $\delta_{SW}$ ) to a given tilt angle  $\theta$ .

**Optimal control** The problem of the transition between both modes can be treated as an Optimal Control Problem. The pilot desires to drive at a speed  $v(t)$  and turn the vehicle with a given steering wheel angle  $\delta_{SW}(t)$ . Through the quasi-static configuration [1], a reference trajectory for the tilt angle  $\theta_R(t)$  can be computed for a pair of  $v(t)$  and  $\delta_{SW}(t)$ . The objective is to minimize the tilt-related energy consumption by appropriately using the DTC or the STC and yet ensuring that the reference tilt angle  $\theta_R(t)$  is followed by the controller. To achieve this optimal control, a Model Predictive Control (MPC) aims at minimizing both the future deviation from the reference and the energy consumption related to the tilt control (DTC and STC) (see Fig. 2).

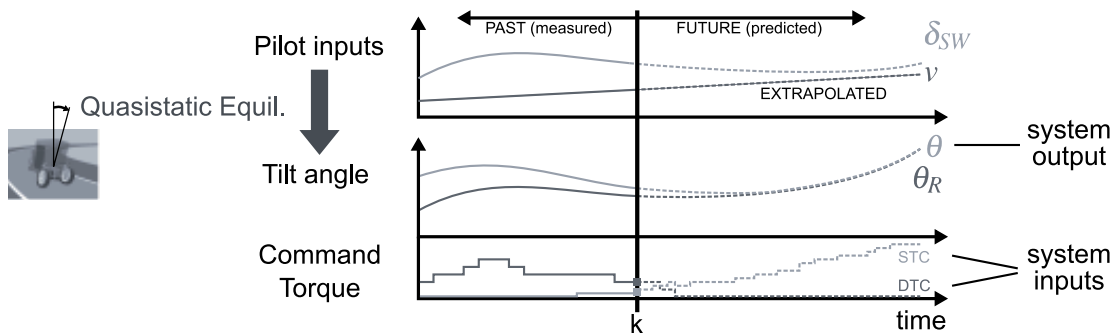


Figure 2: Predictive Control: at each time  $k$ , system inputs are optimally determined based on the predicted deviation from the reference and the energy consumption (qualitative graph).

The vehicle dynamics is strongly non-linear with respects to its speed. To design a controller that operates on the overall speed range, it is necessary to consider the field of non-linear predictive control with constraints. This involves solving a Non Linear Programming problem (NLP) [2] which is expressed for the decision variables  $\mathbf{x}$ .

$$\text{minimize } \mathbf{f}(\mathbf{x}) \quad (3)$$

$$\text{subject to } \mathbf{g}(\mathbf{x}) \text{ and } \mathbf{h}(\mathbf{x}) = \mathbf{0} \quad (4)$$

To formulate and solve the NLP problem, the software CasADi [6] developed at KUL (Belgium) provides interfaces to state-of-the-art NLP solvers through a symbolic approach. Such symbolic framework favors the use and the interfacing [7] of the symbolic equations of motion generated by ROBOTRAN.

**Expected results** First, a model predictive control will be implemented considering the two tilting modes separately (DTC or STC), for a given speed  $v$  and steering wheel angle  $\delta_{SW}(t)$ . In a second step, a driving scenario sweeping the overall speed range will be tested. By minimizing the energy consumption, the Optimal Control should lead to the transition from one mode to another depending on the speed. Through time simulation, tilt-related energy will be assessed and compared for the different controllers and for different optimization parameters.

## References

- [1] Q. Docquier, A. Verlé, P. Fiset, Narrow Tilting Vehicle (NTV) Control through Multibody Modelling: Comparison of Direct and Steering tilt Controls, Bicycle and Motorcycle Dynamics Symposium, 2016.
- [2] J. M. Maciejowski, Predictive Control with Constraints, Pearson Education, 2002.
- [3] A. Verlé, P. Fiset, A Dynamic-Based Approach for Road vehicle Design : Application to a Three-Wheeler, ECCOMAS Thematic Conference on Multibody Dynamics, 2015.
- [4] J.C. Samin and P. Fiset, Symbolic Modeling of Multibody Systems, Springer, 2003.
- [5] N. Docquier, A. Poncelet, P. Fiset, et al. Robotran: a powerful symbolic generator of multibody models in Mech. Sci, 4(1):199-219, 2013.
- [6] J. Andersson. A general-Purpose Software Framework for Dynamic Optimization. PhD thesis, Aremberg Doctoral School, KU Leuven, Department of Electrical Engineering (ESAT/SCD) and Optimization in Engineering Center, Kasteelpark Arenberg 10, 3001-Heverlee, Belgium, October 2013.
- [7] S. Manara, Trajectory optimization of multibody systems with contacts, IMTEK event, 2016.

## A Knife-Edge Wheel-Rail Contact Constraint Approach for the Multibody Simulation of Railway Vehicles

José L. Escalona<sup>1</sup>, Pedro Urda<sup>1</sup>, Sergio Muñoz<sup>1</sup>, Javier F. Aceituno<sup>2</sup>, Daniel García-Vallejo<sup>1</sup>, Rosario Chamorro<sup>1</sup>

<sup>1</sup>School of Engineering  
Universidad de Sevilla  
Camino de los Descubrimientos s/n, 41092,  
Sevilla, Spain  
[escalona, purda, sergiomunoz, dgvallejo  
rchamorro]@us.es

<sup>2</sup>Linares School of Engineering  
Universidad de Jaén  
Campus Científico-Tecnológico, 23700,  
Linares, Spain  
jaceitun@ujaen.es

### Abstract

Wheel-rail contact modeling is fundamental in the simulation of railway vehicles. Two approaches can be used to model it: the constraint approach and the elastic approach. The constraint approach results in smoother simulations as compared to the elastic approach that introduces high-frequency response. A hybrid method that combines constraint contact in the tread and elastic contact in the flange can also be used in multibody railroad simulations [1]. As the lateral excursion of the wheelset reaches the clearance due to the presence of the wheel flange the contact point moves from the wheel tread to the flange. This transition occurs for most wheel-rail profile combinations following a finite jump in the location of the contact point in the wheel and the rail. This transition is called the *two-point contact scenario*. An adequate simulation of this scenario is particularly important in small-radius curves because wheelsets can be struck in that position during steady curving. Derailment due to flange climbing can occur at any instant from this starting point.

Flange contact can be modeled using an elastic approach in a pure-elastic or in a hybrid method. In both cases flange contact appears as a result of an impact that requires a drastic and sudden reduction of the time step during simulation. This reduction affects seriously the efficiency of the simulations and it is very difficult to deal with in real-time simulations. In the method implemented in the railway simulation code Simpack the wheel-rail contact follows the so-called *quasi-elastic approach* [2] that transforms the wheel-rail contact constraint in such a way that contact transition from tread to flange becomes continuous. Using the quasi-elastic approach the wheel-rail dynamics is smoothen but the two-point contact scenario is not described.

The method presented in this paper reduces the wheel-rail profiles combination to an equivalent wheel profile that contacts an ideal rail that has no lateral dimension, like a wheel in contact with the edge of a knife. This is a classical approach that has been used in the railway dynamics literature [3]. In this paper this method is extended to account for two-point contact scenario and flange climb. To this end an analytically parametrized wheel profile is optimized such that the wheelset lateral kinematics is accurately described including wheel climb. In the resulting knife-edge contact constraint the contact point moves continuously in the equivalent wheel profile when the contact point jumps from the tread to the flange in the real wheel-rail profile combination. In order to simulate the two-point contact scenario avoiding flange impact the normal contact force is transferred smoothly from the tread and the flange at the real wheel profile when the contact point enters a predefined range in the equivalent wheel profile.

The advantage of the knife-edge contact constraint can be summarized as follows:

1. Contact constraints are simplified because they require a single profile and tangency constraints are not needed.
2. Contact constraints are smooth and continuous to the required order of derivative.
3. Two-point flange contact can be simulated with smooth transition of the load from the tread to the flange.
4. Flange climb can be accurately simulated.

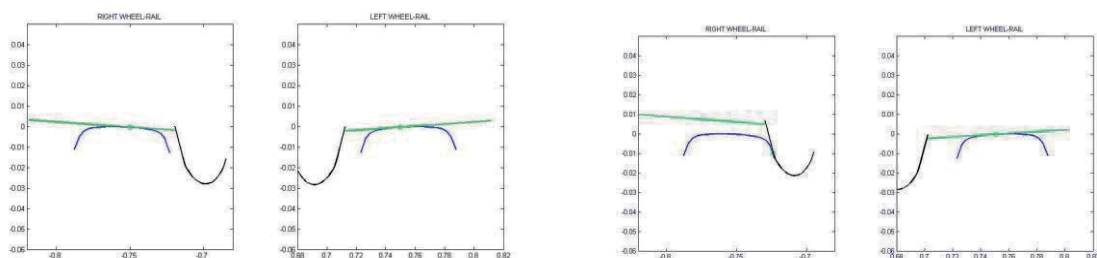
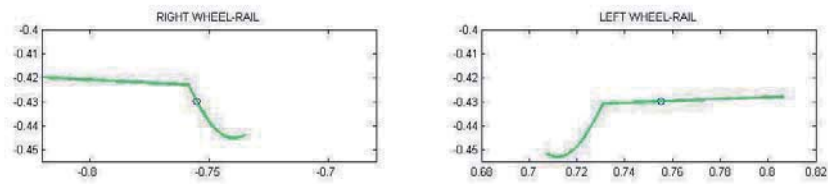
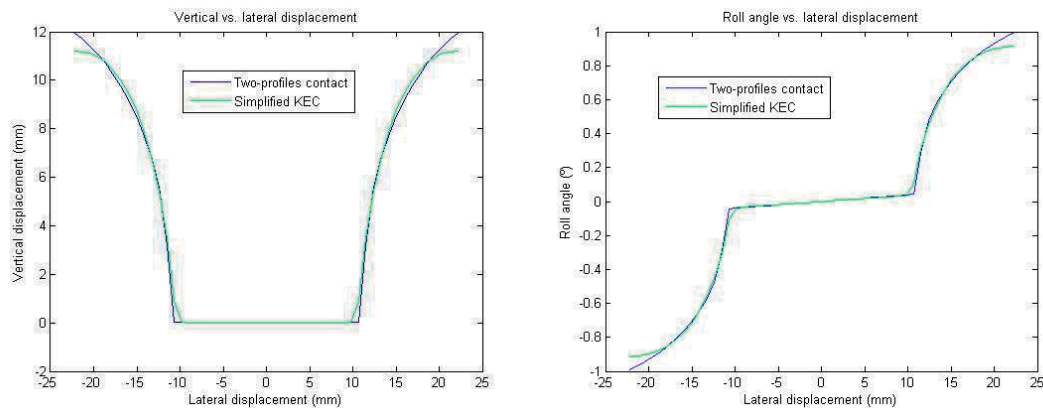


Figure 1. Wheel-rail constraint contact using two profiles. Tread contact (left) and flange climb (right)

Figure 1 shows the wheel-rail contact simulated with the real wheel and rail profiles. Figure 2 shows the situation with the equivalent and optimized wheel profile and knife-edge contact assumptions. Figure 3 shows the wheelset kinematics obtained with the two-profiles and the knife-edge contact assumptions. A very good agreement can be observed.



**Figure 2.** Wheel-rail knife-edge contact using equivalent wheel profile during wheel climb



**Figure 3.** Comparison of vertical wheelset displacement (left) and roll (right) as a function of lateral displacement with two-profiles and knife-edge contact

## Acknowledgments

This paper was funded by the Spain Ministry of Economy and Competitiveness under project reference TRA2014-57609-R. Their support is gratefully acknowledged.

## References

- [1] A. A. Shabana, K. E. Zaazaa, J. L. Escalona, J. R. Sany. Development of elastic force model for wheel/rail contact problems. *Journal of Sound and Vibration*, 269, 2004.
- [2] G. Shupp, C. Weidemann, L. Mauer. Modelling the contact between wheel and rail within multibody system simulation. *Vehicle System Dynamics*, 43(6-7):455-483, 2005.
- [3] A. H. Wickens. *Fundamentals of rail vehicle dynamics. Guidance and stability*. Swets & Zeitlinger Publishers, Lisse (Netherlands), 2003.

## Development of an Innovative Degraded Adhesion Model for Railway Multibody Applications

Enrico Boccini<sup>1</sup>, Elisa Butini<sup>1</sup>, Lorenzo Marini<sup>1</sup>, Martina Meacci<sup>1</sup>, Enrico Meli<sup>1</sup>, Andrea Rindi<sup>1</sup>

<sup>1</sup>Faculty of Mechanical Engineering  
University of Florence  
Via S. Marta n. 3, 50139 Florence, Italy  
[enrico.boccini, elisa.butini, lorenzo.marini, martina.meacci, enrico.meli, andrea.rindi]@unifi.it

### Abstract

A proper wheel-rail contact model is fundamental for studying wear, vehicle dynamics and vehicle safety in the railway field. For these reasons numerous studies on the modelling of the wheel-rail contact have been performed in the last years, most of them not considering the presence of a third body layer and an accurate degraded adhesion behavior. Indeed, the non-linear behavior of the adhesion coefficient and the presence of unknown contaminants are the primary causes of the difficulty in obtaining a realistic adhesion law. Moreover, large sliding on the contact surface occurs under degraded adhesion condition. For the abovementioned reasons an accurate model of the wheel-rail contact under degraded adhesion conditions challenges the researchers worldwide, and it is still an open problem in the academic field. Therefore, an innovative degraded adhesion model suitable for multibody applications is necessary to be developed.

In this work the authors present a contact model comprising a new adhesion model that takes into account some of the main phenomena characterising the degraded adhesion, such as large sliding at the contact interface, high energy dissipation, the consequent cleaning effect on the contact surfaces and the final adhesion recovery due to the removal of external unknown contaminants, a phenomenon caused by the high energy dissipation on the contact surfaces and by the consequent cleaning effect due to the friction forces. Besides, since most of the physical characteristics of the contaminants are totally unknown in practice, the followed approach will have to minimize the number of hardly measurable physical quantities required by the model.

As railway dynamic simulations are usually carried out with multibody software, the new approach has to be suitable to be employed within the wheel-rail contact models in multibody applications (e.g. Matlab-Simulink or Simpack environments) directly online and in real-time, and so it has to guarantee a good accuracy and a high numerical efficiency. For this reason, as the numerical performance is a primary concern, in practice it is impossible to model the contact by considering the wheel and the rail as generic elastic continuous bodies.

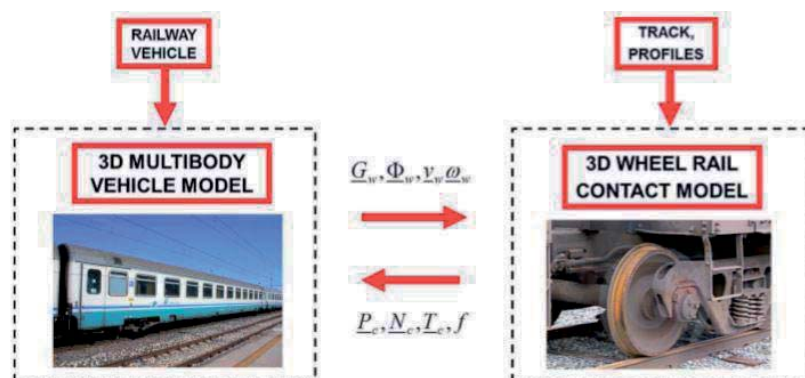
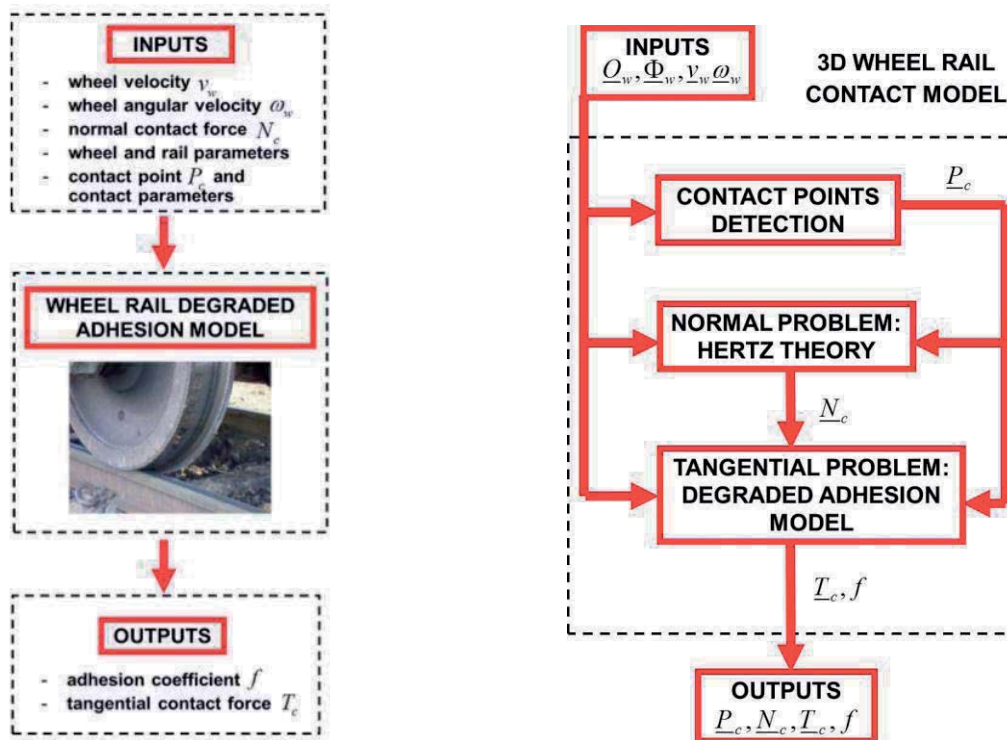


Figure 1. Architecture of the multibody model

From a logical point of view, the multibody model consists of two different parts that mutually interact during the dynamical simulation: the 3D model of the railway vehicle and the 3D wheel-rail contact model (Fig. 1). At each timestep the multibody vehicle model calculates position  $G_w$ , orientation  $\Phi_w$ , velocity  $v_w$  and angular velocity  $\omega_w$  of each wheel, while the contact model, starting from the knowledge of these quantities, evaluates the normal and tangential contact forces  $N_c$  and  $T_c$ , applied to the wheel in the contact point  $P_c$ , and the adhesion coefficient  $f$ .

Typically, simplified and efficient multibody contact models are characterized by three main logical parts: the contact point detection, here based on some innovative procedures recently developed by the authors in previous works [1] [2] [3], the normal problem solution, solved through the global Hertz theory to evaluate the normal contact forces  $N_c$ , and the tangential problem solution to compute the tangential contact forces  $T_c$  and the adhesion coefficient  $f$ ; the latter part includes also the adhesion model (Fig. 2).



**Figure 2.** Inputs and outputs of the degraded adhesion model and architecture of the wheel-rail contact model

In particular, a significant change into the solution of the tangential problem must be underlined. Initially, the tangential contact forces evaluation was performed by means of the global Kalker-Polach theory to compute the tangential contact forces  $T_c$  and the adhesion coefficient  $f$ . With an improvement of the adhesion law and the application of the algorithm FASTSIM the energy dissipation and the adherence recovery phenomenon are taken into account, and pressure and slip locally calculated with a discretisation of the contact surface can now be added as outputs. With the global and the implemented local model, some simulation and comparisons have been conducted, showing an improved accuracy in the results. The adhesion model presented will be validated soon thanks to experimental data provided by Trenitalia S. p. A and RFI.

## References

- [1] S. Margheri, M. Malvezzi, E. Meli, A. Rindi: *An innovative wheel rail contact model for multibody applications*. Wear 271 Issue 1, 462-471, 2011
- [2] E. Meli, S. Falomi, M. Malvezzi, A. Rindi: *Determination of wheel rail contact points with semianalythic methods*. Multibody System Dynamics 20 Issue 4, 327-358, 2008.
- [3] M. Malvezzi, E. Meli, S. Falomi: *Multibody modeling of railway vehicles: innovative algorithms for the detection of wheelrail contact points*. Wear 271 Issue 1, 453-461, 2011
- [4] O. Polach: *Creep forces in simulations of traction vehicles running on adhesion limit*. Wear 258, 992-1000, 2005
- [5] J. Kalker: *Three dimensional Elastic Bodies in Rolling Contact*. Kluwer Academic Publisher, NL, 1990
- [6] S. Iwnicki: *Handbook of Railway Vehicle Dynamics*. Taylor and Francis, Boca Raton, FL, USA, 2006
- [7] C. Esvelde: *Modern Railway Track*. Delft University of Technology, Delft, Netherlands, 2001

# Development of an Innovative Model to Study Wear Evolution Considering Wheel-Rail Conformal Contact

Elisa Butini<sup>1</sup>, Lorenzo Marini<sup>1</sup>, Martina Meacci<sup>1</sup>, Enrico Meli<sup>1</sup>, Andrea Rindi<sup>1</sup>

<sup>1</sup>Department of Industrial Engineering  
School of Engineering,  
University of Florence  
Florence, 50139, Italy

[elisa.butini, lorenzo.marini, martina.meacci, enrico.meli, andrea.rindi]@unifi.it

## Abstract

One of the main problem in railway systems, both dynamically (safety, comfort, etc..) and economically (planning of maintenance interventions maintenance, reduction of wheel and rail lifetime, etc..) is represented by the wear of wheel and rail profiles due to the wheel-rail interaction. The shape profile variation, caused by wear, influences in particular the dynamic behaviour of the vehicle and, in particular, the wheel-rail contact conditions. Hence, nowadays, one of the most important topics in the railway field, is the development of more accurate contact and wear models, useful both in vehicle design phase and for maintenance planning. More in detail, the conformal contact is very frequent in railway applications, especially in tracks where the curvature radius is limited and the wheel-rail profiles are affected by wear. This type of contact is characterized by more complex contact patch, where the hypotheses of single contact point, planar contact, elliptic contact are not verified. For this reason, the research for contact models, including conformal contact, are a crucial aspect to determine an accurate wear evolution and to optimize the maintenance of wheels and rails.

The complex problems arising from conformal contact are usually investigated through Finite Element (FE) approaches. The FE methods are critical in terms of computational load and time and are very difficult to be directly implemented in multibody software to perform dynamic real-time simulation. Therefore, the Authors have developed an innovative wear model where the conformal contact is carefully taken into account, according to the Piotrowski theory, without assuming hertzian hypothesis such elliptical shape, planar or symmetric contact patches. Furthermore, the Piotrowski approach has been extended to no-planar contact patch by means the introduction of natural abscissa in the wheel-rail surface discretization. Therefore, the main innovative aspect proposed in this work is the study of wear evolution when conformal contact conditions occurs.

The layout of the new wear model (see Figure 1) is made up of two separate blocks that mutually interact: the dynamics block where the dynamical analysis is carried out and the wear model block for the wear evaluation. The first one consists of two parts that interact online during the dynamic simulations creating a loop: a 3D multibody model, implemented in Simpack, of the railway vehicle taken into account and an innovative 3D conformal contact model based on an improvement of the Piotrowski theory implemented in a C/C++ user routine of Simpack. The contact model uses for the contact area detection a procedure based on an efficient version of the standard GRID method while the normal problem is solved in according to the innovative non-hertzian theory formulated by Piotrowski. Finally, the tangential problem is treated as an extension of the Kalker's Fastsim algorithm properly adapted for non-elliptical contact area through the use of an equivalent ellipse. The wear model (entirely implemented in MATLAB) starts from the outputs of the dynamic simulations (position and shape of the contact patches, contact pressures, etc..) and calculates the material removed by wear through an experimental law between the friction power produced by the tangential contact pressures and the material removed by wear. Finally, the worn profiles of wheel and rail are obtained subtracting the worn material from the wheel and rail old profiles. The new worn profiles are reintroduced into dynamics block as input of the vehicle model and the whole iterative process can proceed forward with the next discrete step. In fact, the whole model is based on a discrete process: in each discrete step one dynamic simulation and one profile update by means of the wear model are done while, within the discrete step, the profiles are supposed to be constant. Consequently the evolution of the wheel and rail geometry is described through several intermediate profiles.

A preliminary validation of this model is performed through experimental data related to a critical subway scenario.

The research activity has been performed in cooperation with Hitachi Rail Italy which provided the technical and experimental data needed to develop and validate the new wear model.

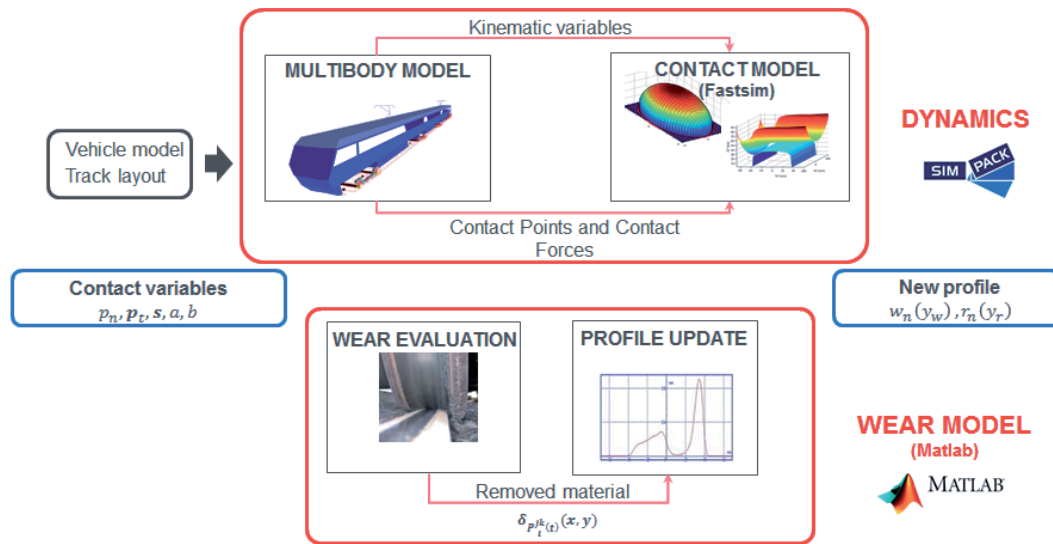


Figure 1. General architecture of the model

## Acknowledgments

Authors would like to thank Hitachi Rail Italy for providing the data relative both to the vehicle and to the experimental campaign.

## References

- [1] J. Piotrowski, W. Kik – *A simplified model of wheel/rail contact mechanics for non-Hertzian problems and its application in rail vehicle dynamic simulation*. Vehicle System Dynamics 46, 1-2, January – February 2008, 27 – 48
- [2] M. Ignesti, M. Malvezzi, L. Marini, E. Meli, A. Rindi – *Development of a wear model for the prediction of wheel and rail profile evolution in a railway system*. Wear 284-285 (2012), 1-17
- [3] F. Braghin, R. Lewis, R.S. Dwyer-Joyce, S. Bruni – *A mathematical model to predict railway wheel profile evolution due to wear*. Wear 261, 1253-1264, 2006.
- [4] A. Innocenti, L. Marini, E. Meli, G. Pallini, A. Rindi. – *Development of a wear model for the analysis of complex railway networks*” Wear 309 (2014), 174 – 191
- [5] J.J. Kalker – *Three-Dimensional Elastic Bodies in Rolling Contact*. Kluwer Academic Publishers, 1990.

# Motorway Sharing for Passenger Cars and Truck Platoons

Werner Schiehlen

Institute Engineering Computational Mechanics  
University of Stuttgart  
Pfaffenwaldring 9, 70569 Stuttgart, Germany  
werner.schiehlen@itm.uni-stuttgart.de

## Abstract

In road vehicle dynamics car automation and autonomous control are hot research topics. Among the anticipated benefits of automated cars is the reduction in traffic collisions caused by human-driver errors, such as delayed reaction time. Additional advantages could include higher speed limits, smoother rides and increased roadway capacity with minimized traffic congestion due to decreased need for safety distance, and higher speeds. Reduced traffic congestion and the improvements in traffic flow by widespread use of autonomous cars will also translate into better fuel efficiency and less fuel consumption, reduced air pollution and a lower carbon footprint from road travel.

In particular, trucks in a platoon are able to drive very close together reducing aerodynamic drag in a big way and bringing fuel-efficiency of as much as 20% depending on which test you're looking at. The smaller the distance between vehicles, the better the fuel economy. The following photo, Figure 1, shows a platoon of three Daimler trucks during the European Truck Platooning Challenge 2016 [1] driving from Stuttgart, Germany to Rotterdam, The Netherlands, on an empty motorway.



**Figure 1.** Daimler trucks during the European Truck Platooning Challenge 2016 [1]

Major research activities on autonomous started about thirty ago. The Eureka PROMETHEUS Project (PROgraMme for a European Traffic of Highest Efficiency and Unprecedented Safety, 1987-1995) was a large project in the field of driverless cars. From German universities Dickmanns [2] was the scientific leader and his research group dealt with dynamic vision resulting in the seeing passenger car 'VaMoRs-P' which drove 1995 without human interaction from Munich in Bavaria to Copenhagen in Denmark and return. In 1986 the California Partners for Advanced Transportation Technology Program were established, still known as PATH Berkeley, Shladover [3]. The partnership was a platooning pioneer. In 1994 it showed an Automated Highway System that used automated longitudinal control of a four-car platoon and they ramped that up to an eight-car platoon in 1997.

A smaller project dealt 1996 to 2001 with the platooning of two BMW passenger cars [4] using multibody system dynamics and nonlinear control for simulation and experiments at the University of Stuttgart.

The SARTRE Project (Safe Road Trains for the Environment, 2009-2012), funded by the European Commission under the Framework 7 Programme, aims to develop strategies and technologies to allow vehicle platoons to operate on normal public highways with significant environmental, safety and comfort benefits. SARTRE is led by Ricardo UK Ltd [5] and comprises a collaboration between companies in UK, Spain, Germany and Sweden. In 2012 a road train comprising a Volvo XC60, a Volvo V60 and a Volvo S60 plus one truck drove automatically in convoy behind a lead vehicle operating on a public motorway among other road users. The historic test in Spain was highly successful. Finally, the European Truck Platooning Challenge 2016 has to be mentioned again [1].

An open question remains how the very busy motorways in central Europe, as shown in Figure 2, could be shared between automated single passenger cars and larger truck platoons. Options discussed today are to use the most right lane or the most left lane for truck platoons, respectively. In any case, good motion control is most

essential and may be discussed at the session Road Vehicle Dynamics during ECCOMAS Conference Multibody 2017 in detail. For the dynamical modelling of the trucks the longitudinal motions including the energy saving aerodynamics and the vertical motions featuring the tire – road contact have to be considered.

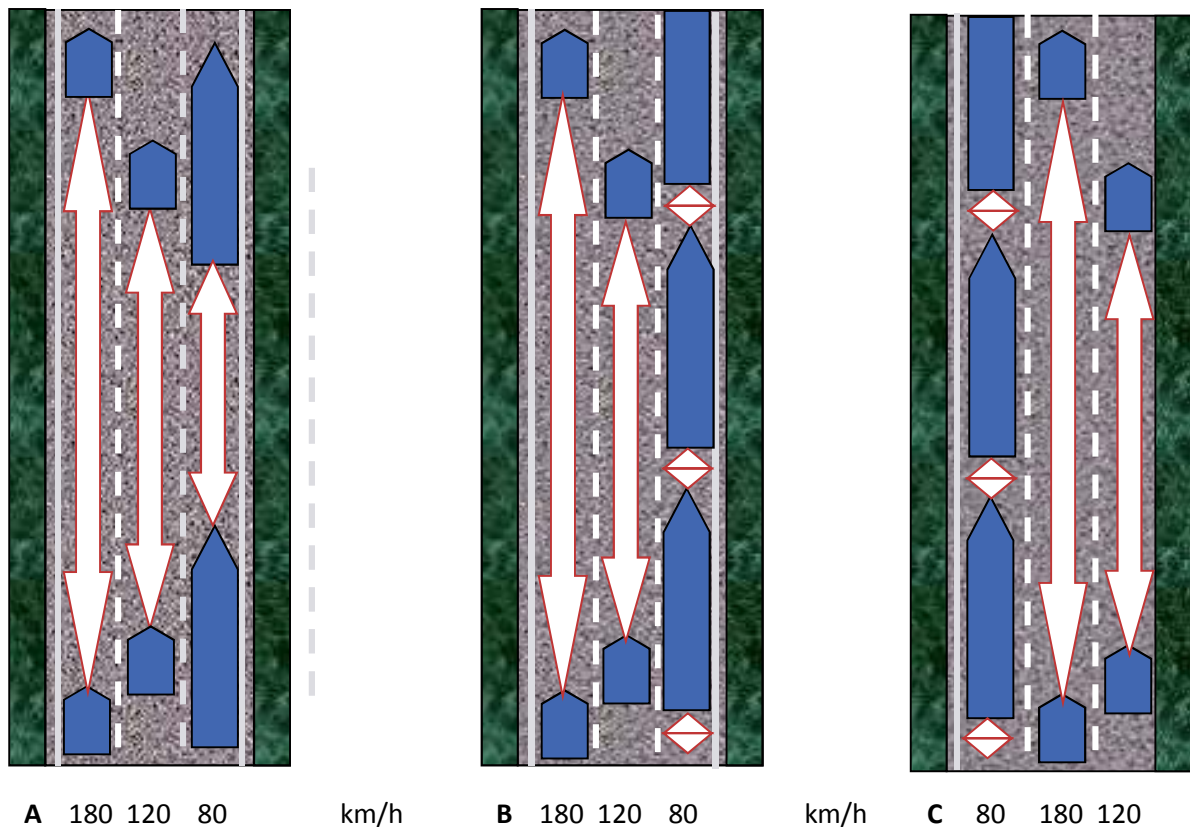


**Figure 2.** Lane utilisation by passenger cars and platoons

For the trucks gigaliners with 25 m length and 80 km/h speed are considered. The length of the cars is 5 m, the speed may vary between 120 and 180 km/h. The safety distance (red arrows) in m is speed dependent and is legally half of speed counted in km/h.

Today's standard lane utilization is depicted in Figure 2A. Even for fast cars there isn't any problem for exiting or entering a motorway. However, in a platoon the trucks don't need due to the common vehicle dynamics control any safety distance, they should drive as closely as possible for a maximum reduction of the air resistance and the related fuel consumption. That means a platoon is like a moving wall, and for a car it may be difficult or even dangerous to enter or exit the motorway for both, cars and platoons, see Figure 2B and 2C.

To overcome these problems there will be several options discussed: 1) New roads for platoons, 2) Same speed limits for cars and platoons, 3) Adaptive cruise control between all vehicles, cars and platoons, depending on their final destination. Most attractive is the third option. Then, the vehicles could be charged for the distance using the motorway. Finally, by a complete management of the space on the motorway traffic jams could be strongly reduced. Systems of demand dependent customer prices are very successfully used by airlines and railways. Late bookings get more and more expensive.

## References

- [1] V. Bulc. *European Truck Platooning Challenge 2016*. [www.eutruckplatooning.com](http://www.eutruckplatooning.com) , 2016.
- [2] E. Dickmanns. *Dynamic Vision for Perception and Control of Motion*. Springer, Berlin, 2007.
- [3] A. Shladover. PATH at 20 – History and Major Milestones. [www.path.berkeley.edu/about](http://www.path.berkeley.edu/about) , 2006.
- [4] A. Fritz, W. Schiehlen. Nonlinear ACC Simulation Measurement. *Vehicle System Dynamic*, 36:159-177, 2001.
- [5] T. Robinson. *SARTRE*. [www.sartre-project.eu/en/about/news/Sidor/Pressrelease120604.aspx](http://www.sartre-project.eu/en/about/news/Sidor/Pressrelease120604.aspx) , 2012.

# Assessment of the necessary width of a bicycle lane by means of multibody simulations on a bicycle-rider system.

A. L. Schwab<sup>1</sup>, J. P. Meijaard<sup>2</sup>

<sup>1</sup> BioMechanical Engineering  
Delft University of Technology  
Mekelweg 2, NL-2628 CD Delft  
The Netherlands  
a.l.schwab@tudelft.nl

<sup>2</sup> Olton Engineering Consultancy  
Deurningerstraat 7-101  
NL-7514 BC Enschede  
The Netherlands

## Abstract

### 1 Introduction

It can be observed that there is a wide variety in the width of bicycle lanes. It can range from wide to very narrow, see figure 1. Several guidelines disagree on the desired width of a bicycle lane [1, 2]. These guidelines are mainly based on observations and best practices. Instead of such an evolutionary approach we propose to determine the necessary width by means of a scientific approach. This accommodates out of the ordinary bicycles, like electrically assisted or recumbent bicycles. We hypothesize that the dynamic properties of the bicycle together with the rider control determine the needed width of the bicycle lane. The inherent lateral instability of the bicycle with fixed steer input results in unavoidable lateral contact point displacements to keep the bicycle upright. Additionally think of the act of countersteering to change heading direction.



Figure 1: Example of a very narrow bicycle lane, photo by Legreve.

### 2 Methods

To investigate the dynamics of the bicycle–rider system we use multibody dynamics models. For the bicycle model we use the so-called Carvallo/Whipple model, which has recently been benchmarked [3] and experimentally been validated by Kooijman *et al.* [4]. This model consists of a rear frame, front fork assembly and two wheels. The wheel–ground contact is non-holonomic, which results in a low-dimensional model with only three degrees of freedom: lean, steer and forward velocity. However, no such generally accepted model for a rider as a controller is available. Some initial work on an optimal preview controller has been done by Land [5], Savkoor [6], and for bicycles by Sharp [7], whereas Doyle [8] approaches the bicycle rider control from a psychological point of view. Experimental results on bicycle control together with an optimal control model are presented by Moore *et al.* [9]. An overview on rider control bicycles is presented by Schwab and Meijaard [10].

Instead of an often applied continuous controller we propose to use a bell-shaped controller as presented by Benderius [11]. To mimic a non-continuous observation of the state we introduce a zero-order hold filter [12]. Realistic perturbations are needed and we choose to perturb the bicycle roll rate, which can be caused by gusts of wind. Simulations at various forward speeds, sizes of perturbations and settings of the human controller give the lateral displacement of the contact point of the front wheel with respect to the centre line of the bicycle lane.

### 3 Conclusion

A useful method has been developed on the basis of multibody dynamics models to determine the lateral displacements of a perturbed bicycle–rider system. These displacements can be used as a guideline for the necessary width of a bicycle lane.

## References

- [1] CROW. Report Ontwerpwijzer fietsverkeer. pp.300, CROW, 13 June 2016.
- [2] D. J. Torbic, K. M. Bauer, C. A. Fees, D. W. Harwood, R. Van Houten, J. LaPlante, & N. Roseberry. Recommended Bicycle Lane Widths for Various Roadway Characteristics (No. Project 15-42), 2014.
- [3] J. P. Meijaard, Jim M. Papadopoulos, Andy Ruina, A. L. Schwab, Linearized dynamics equations for the balance and steer of a bicycle: a benchmark and review, *Proceedings of the Royal Society A* 463:1955-1982, 2007.
- [4] J. D. G. Kooijman, A. L. Schwab, and J. P. Meijaard. Experimental validation of a model of an uncontrolled bicycle, *Multibody System Dynamics* 19(1-2):115-132, 2008.
- [5] M. Land, and J. Horwood. Which parts of the road guide steering? *Nature* 377, no. 6547: 339, 1995.
- [6] A. R. Savkoor, and S. Ausejo. Analysis of driver's steering and speed control strategies in curve negotiation. In *The Dynamics of Vehicles on Roads and on Tracks-Supplement of Vehicle System Dynamics*, Volume 33. Proceedings of the 16th IAVSD Symposium held in Pretoria, South Africa, August 30–September 3, 1999, pp.94–109, 2000.
- [7] R. S. Sharp, Optimal stabilization and path-following controls for a bicycle. *Proceedings of the Institution of Mechanical Engineers, Part C: Journal of Mechanical Engineering Science*, 221(4), pp.415-427, 2007.
- [8] A. J. R. Doyle, The essential contribution to bicycle riding, in J. Patrick and K. Duncan eds., *Training, human decision making, and control*, Elsevier Science Publisher BV North Holland, pp.351-370, 1988.
- [9] J. K. Moore, J. D. G. Kooijman, A. L. Schwab, and M. Hubbard . Rider motion identification during normal bicycling by means of principal component analysis, *Multibody System Dynamics* 25(2):225-244, 2011.
- [10] A. L. Schwab, J. P. Meijaard. A review on bicycle dynamics and rider control, *Vehicle System Dynamics* 51(7):1059-1090, 2013.
- [11] O. Benderius, and G. Markkula. Evidence for a fundamental property of steering. In *Proceedings of the Human Factors and Ergonomics Society Annual Meeting*, vol. 58, no. 1, pp. 884-888. Sage CA: Los Angeles, CA: SAGE Publications, 2014.
- [12] J. Godthelp, *Studies on human vehicle control*. PhD diss., TU Delft, Delft University of Technology, 1984.

## Inerter Potential for Vehicle Vertical Dynamics

Pavel Steinbauer<sup>1</sup>, Jan Baněček<sup>1</sup>, Ondřej Kolda<sup>1</sup>, Pavel Houfek<sup>1</sup>, Tomáš Zemánek<sup>1</sup>

<sup>1</sup>Faculty of Mechanical Engineering  
Czech Technical University in Prague  
Technická 4, Praha 6, 16000, Czech Republic  
Pavel.Steinbauer@fs.cvut.cz, Jan.Banecek@fs.cvut.cz, Ondrej.Kolda@fs.cvut.cz,  
Pavel.Houfek@fs.cvut.cz, Tomas.Zemanek@fs.cvut.cz

### Abstract

Current vehicle suspension is designed to improve simple, but contradicting main criteria: Comfort level of passengers of load defined by their vibration exposition especially at higher frequencies ([1]) and maximized and even tyre contact force, which effects braking distance, manoeuvrability, but also pavement damage. In addition, it is also desirable to minimise roll, pitch under braking, acceleration and cornering (handling).

Design of automotive suspension was driven to its limits with passive traditional components like springs, dampers and tyres. Semi-active damping with controlled damper characteristics has been successfully used to decrease both road tyre dynamic force and braking distance ([2]). Active damping may improve vehicle behaviour using smart control algorithms, but it is so energy costly that it is not broadly used. Further improvement of vehicle suspension behaviour according to contradicting criteria can be achieved by introduction of additional components. In this paper, potential of novel element inerter is investigated, including design feasibility.

It has been shown long time ago ([3]) that arbitrary impedance can be achieved using sufficiently complex network of basic elements, i.e. resistors, capacitors and inductors in case of electric circuit. Using analogy between mechanical system and electrical circuit, considering equivalency between springs and inductors, dampers and resistors, masses and capacitors. Mass stands for grounded capacitor only. But capacitor is often connected to arbitrary nodes of electric circuit. So pure capacitance with both terminals free was missing. The mechanical design bypassing this empty spot was proposed by M. Smith ([4], [5]) and called it inerter. The basic idea is transformation of inertia D'Alembert couple of rotational motion of the flywheel into force acting between terminals of the inerter by moving screw. The flywheel has quite high moment of inertia while overall weight of the inerter device is kept low. So no substantial inertia force acts in the treated direction while force acting between inerter terminals is substantial. The inerter force  $F_I$  is proportional to the relative acceleration between inerter terminals and inertance constant  $b_I$  [kg]

$$F_I = b_I \frac{d}{dt} (\dot{z}_1 - \dot{z}_2) \quad (1)$$

Where  $\dot{z}_1$  is velocity of sprung mass,  $\dot{z}_2$  is velocity of unsprung mass. The inertance  $b_I$  is given by lead of a thread helix  $h$ [m] and flywheel moment of inertia  $J_f$ [kg.m<sup>2</sup>]

$$b_I = J_f \left( \frac{2\pi}{h} \right)^2 \quad (2)$$

Design of the investigated inerter is based on moving ball screw from the shelf and it is shown in the Figure 1a. The overall diameter is 85 mm, inertance  $b_I$  can be chosen in the range 9.7-50 kg.

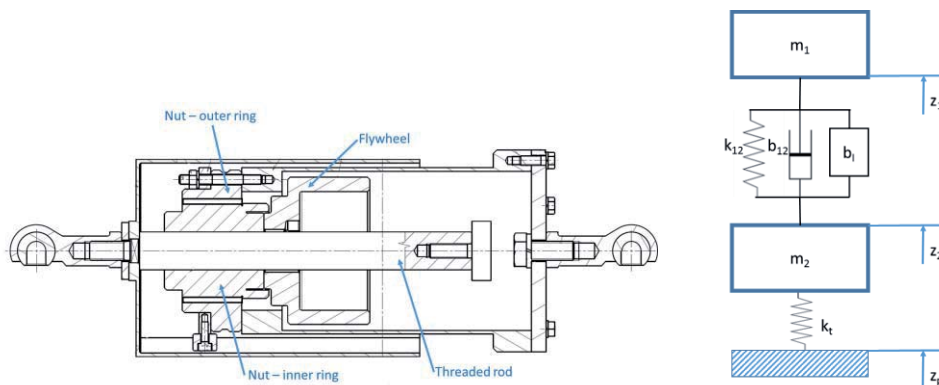
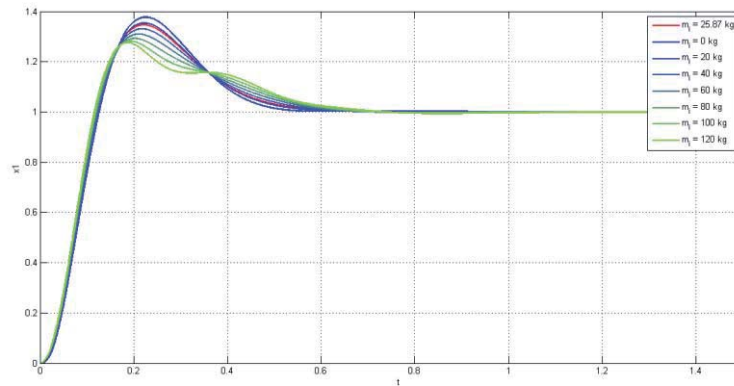


Figure 1. Inerter design (a), Quarter car vehicle vertical dynamics model (b)

The whole construction is dimensioned to withstand loading from acting forces and fits conceptually into current vehicle suspensions. So the inerter can be parametrized for optimal suspension performance. These parameters of the inerter were used for evaluation of its potential on the quarter car model based on the structure depicted in the Figure 1b.

Simulation experiments are demonstrated in the Figure 2 on response of sprung mass to step change of pavement height. The damping coefficient was selected to achieve damping near the critical in any investigated cases.



**Figure 2.** Step response of sprung mass position of quarter car model with inerter in parallel with the spring

The results show that peak amplitude of sprung mass motion is reduced when inerter device is used and properly tuned.

## Conclusions

The passive inerter was designed, including complete stress, design safety and durability calculation. The device does not add any substantial weight into the suspension, but allows to improve vertical dynamics behaviour. The designed inerter is feasible and it is being currently manufactured for laboratory tests on quarter car HIL model. Furthermore, the concept of passive inerter was investigated, using numerical simulation on quarter car model and multi-criteria optimization. The feasible range of available inertance values was selected based on designed inerter. Although connection of inerter's flywheel with electric motor has great potential ([6]), passive inerter without any electric components is much simpler and may improve suspension performance with contradicting requirements.

## Acknowledgments

This research has been realized using the support of EU Regional Development Fund in OP R&D for Innovations (OP VaVpI) and The Ministry of Education, Youth and Sports, Czech Republic, project # CZ.1.05/2.1.00/03.0125 Acquisition of Technology for Vehicle Center of Sustainable Mobility, the support of The Ministry of Education, Youth and Sports program NPU I (LO), project # LO1311 Development of Vehicle Centre of Sustainable Mobility, the support of SGS16/209/OHK2/3T/12 Modelling, control and design of mechanical systems 2016 of CTU in Prague and the support of Technological Agency, Czech Republic, program Centres of Competence, project # TE01020020 Josef Božek Competence Centre for Automotive Industry. This support is gratefully acknowledged.

## References

- [1] *Mechanical vibration and shock -- Evaluation of human exposure to whole-body vibration*, International Standard ISO 2631-1997
- [2] Kortuem, W., Valasek, M., Sika, Z., Schwartz, W., Steinbauer, P., & Vaculin, O., 2002. *Semi-active damping in automotive systems: design-by-simulation*. International journal of vehicle design, 28(1-3), 103-120.
- [3] BOTT, R.; DUFFIN, R. J. *Impedance synthesis without use of transformers*. Journal of Applied Physics, 1949, 20.8: 816-816.
- [4] Smith, M. C., 2005. *Force-controlling mechanical device*. Patent US 20050034943
- [5] Smith, M. C., 2002. *Synthesis of Mechanical Networks: The Inerter*. IEEE Transactions on Automatic Control, vol. 47, no. 10, s. 1648 – 1662.
- [6] WANG, Fu-Cheng; CHAN, Hsiang-An. *Vehicle suspensions with a mechatronic network strut*. Vehicle System Dynamics, 2011, 49.5: 811-830.

# Evaluation Criterion of Force Transfer through Mechanism

Michael Valasek, Jan Vich

Faculty of Mechanical Engineering  
Czech Technical University in Prague  
Technicka 4, 16607 Praha 6, Czech Republic  
Michael.Valasek@fs.cvut.cz, Jan.Vich@email.cz

## Abstract

The contemporary approach in the field of vehicle suspension brings a new mechanism with more than five bars ordered both in parallel and serial way [1]. These mechanisms have indisputable benefits in the wheel kinematic during bounce and rebound, but on the other hand it brings the increased complexity of the mechanisms. The complexity means beside other things unclear transfer of loading force in tire-road contact into the links of suspension and subsequently to the vehicle body. A global criteria evaluating the force transfer through suspension is described in this paper.

The load transfer from tire contact point to vehicle body can be split into two subsequent problems. The first one is a force transfer through the links (arms) and load applied to the links. The second one is a force interaction between the arms and the vehicle body. The first problem is mostly related to specific shape of the links while the second problem is more related to the global structure of the mechanism. The proposed evaluation criterion is focused on the second problem.

The kinematical scheme of such a contemporary suspension mechanisms is shown in Figure 1. It is based on Watt six-bar linkage. Thus the connection between the wheel hub and the vehicle body is performed by two serially ordered arms in both branches.

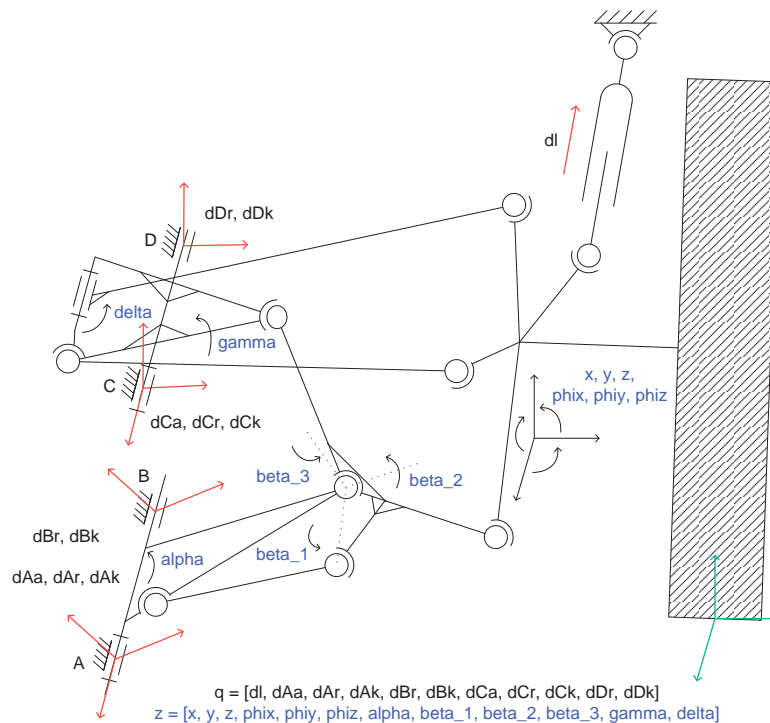


**Figure 1.** Suspension mechanism based on Watt six-bar linkage

The suspension arms are connected to the vehicle body in several discrete points. A set of relevant reaction forces  $F_r$  (depicted by red arrows in Figure 1) can be introduced at each of these connection points. There is a set of action forces at tire-road contact point, denoted  $F_a$  (depicted by green arrows in Figure 1). The force transfer from  $F_a$  to  $F_r$  is then expressed by matrix equation

$$A^* \cdot F_a = F_r \quad (1)$$

where  $A^*$  is the unknown matrix of a system. Different methods can be used in order to obtain matrix  $A^*$ . In the case of suspension system the principle of virtual work is suitable and can be written in form

$$F_q^T \cdot dq + F_z^T \cdot dz = 0 \quad (2)$$

where  $F_q$  are forces acting along independent virtual motions  $dq$  and analogically forces  $F_z$  act along dependent virtual motions  $dz$ . Time derivative of equations of motion yields

$$\begin{aligned} J_q \cdot dq + J_z \cdot dz &= 0 \\ dz &= -J_z^{-1} \cdot J_q \cdot dq \\ dz &= -J \cdot dq \end{aligned} \quad (3)$$

where  $dz$  are dependent coordinates,  $dq$  are independent coordinates and  $J$  is Jacobian of the system. Substitution form (3) into (2) we obtain

$$\begin{aligned} (F_q^T - F_z^T \cdot J) \cdot dq &= 0 \\ F_q^T - F_z^T \cdot J &= 0 \\ F_q &= J^T \cdot F_z \end{aligned} \quad (4)$$

Since forces  $F_z$  act along dependent coordinates, whereas forces  $F_a$  act on wheel at tire-road contact point, the addition force transformation matrix  $A_w$  between  $F_a$  and  $F_z$  has to be introduced.

$$F_z = A_w \cdot F_a \quad (5)$$

Substituting (5) into (4) we obtain

$$F_q = J^T \cdot A_w \cdot F_a \quad (6)$$

Providing  $F_q = F_r$  the equations (1) and (6) are equivalent and matrix  $A^*$  is defined by equation

$$A^* = J^T \cdot A_w \quad (7)$$

The mechanism in Figure 1 is described by 13 coordinates: position and angle of the wheel center point  $x, y, z, fix, fiy, fiz$ ; four angles of rotation  $alpha, beta_1, beta_2, beta_3, gamma, delta$  and a length of  $dl$ . The coordinate  $dl$  is the independent one as it directly describes bounce end rebound motion and the mechanism has only 1 DOF. Rest of these coordinates thus became dependent. Introducing virtual movements in direction of reaction forces  $F_r$  we obtain a set of 10 virtual independent coordinates, which stays equal to zero during whole wheel travel. The mechanism is than described by 12 equations of motion, 1+10 independent coordinates and 12 dependent coordinates. This principle of mechanism description enables to solve the kinematic of the mechanism and evaluates the values of the force transfer matrix  $A^*$  at the same time.

The mechanism arms have general mutual positions and furthermore, these positions are significantly varying during the wheel bounce and rebound. Therefore the force transfer matrix  $A^*$  has to be calculated in whole range of the wheel motion, respectively in discrete points in whole range of the wheel motion.

The most important aspect of evaluation of force transfer in suspension is a relation between the action forces and the reactions. Each column of matrix  $A^*$  describes the distribution of corresponding action force into the reactions. Therefore the evaluation criterion  $K_F$  can be introduced as maximum absolute column sum norm of matrix  $A^*$

$$K_F = \|A^*\|_1 = \max_j \sum_i |a_{ij}| \quad (8)$$

Smaller value of this criterion is better. The lowest teoretical value is 1 meaning that applied forces cause only reactions of the same magnitude in sum.

Effectivity of the action forces transfer and distribution to the vehicle body can be shown by applying of proposed criterion. Since the value of the criterion is strongly dependent on real dimensions of the mechanism, the criterion can be used for comparison of similarly sized mechanisms or has to be normalize to the most considerable dimensions.

## References

- [1] M. Plecnik and J. M. McCarthy, 2014. Vehicle suspension design based on a six-bar linkage, Proceedings of the ASME 2014 IDETC/CIE Conference, Paper No. DETC2014-35374, August 17-20, 2014, Buffalo, New York, USA.

## Estimation of railroad vehicle dynamics and track irregularities using data fusion techniques and computational methods

Javier F. Aceituno<sup>1</sup>, Pedro Urda<sup>2</sup>, Rosario Chamorro<sup>2</sup>, Sergio Muñoz<sup>2</sup>, Daniel García-Vallejo<sup>2</sup>, José L. Escalona<sup>2</sup>

<sup>1</sup>Linares School of Engineering  
Universidad de Jaén  
Campus Científico-Tecnológico, 23700,  
Linares, Spain  
jaceitun@ujaen.es

<sup>2</sup>School of Engineering  
Universidad de Sevilla  
Camino de los Descubrimientos s/n, 41092,  
Seville, Spain  
[purda, rchamorro, sergiomunoz, dgvallejo, escalona]@us.es

### Abstract

In this paper, a comparison between experimental and computational results of the dynamics of railroad vehicles is presented.

The experimental campaign consists on the use of a scaled railroad vehicle, designed and manufactured at the University of Seville [1], and tested in a 5-inch gauge scaled railroad track. This scaled track, where the prototype is tested, is measured every 20 mm for each rail to account for the track irregularities for validation purposes [2]. The dynamics of the vehicle is captured by three inertial measurement units (IMUs) installed at wheelset, bogie and carbody levels, and by two distance lasers that account for the effect of the primary and secondary suspension systems as shown in Fig. 1.



**Figure 1:** (Left): IMUs installation. (Right): primary suspension distance laser

Moreover, a computer-vision system shown in Fig. 2 is installed on the vehicle, which is formed by a high-speed recording video-camera and a guiding laser for each rail with the purpose of identifying the track geometry.



**Figure 2:** Computer-vision system

Regarding the computational approach, an efficient formulation of the equations of motion of railway vehicles that could simulate the motion of railway vehicles in real time is implemented. The numerical model includes the use of symbolic computations of the equations of motion of railway vehicles, moving reference frames, and wheel-rail tread and flange contact with pre-calculated lookup tables that can take into account the track irregularities [3].

In addition, a data fusion technique of the IMUs and computer vision systems to estimate the vertical and lateral track irregularities based on an analytical and computational study of the use of complementary filters is applied [4-6]. Sensor fusion algorithms based on complementary filters are designed such that low frequency irregularity measurements rely on the gyroscope signals and high frequency irregularity measurements are based on the accelerometer signal. The goal is to validate the track geometry estimation with the data fusion technique when the results are compared with the measured track irregularities [2].

The comparative study between the experimental and numerical results show that the proposed formulation together with the data fusion technique provide a precise description of the dynamics of railway vehicles and an accurate estimation of the track irregularities.

## Acknowledgments

This research was supported by the Spain's Consejería de Innovación, Ciencia y Empresa de la Junta de Andalucía under Project TEP-7280. This support is gratefully acknowledged.

## References

- [1] J.F. Aceituno, R. Chamorro, D. García-Vallejo, J.L. Escalona. On the design of a scaled railroad vehicle for the development of on-board systems. *Technical Report. Department of Mechanical and Manufacturing Engineering, University of Seville, Seville, 2016.*
- [2] J.F. Aceituno, R. Chamorro, S. Muñoz, J.L. Escalona. An innovative procedure of measured track irregularities. Application to scaled tracks. *Technical Report. Department of Mechanical and Manufacturing Engineering, University of Seville, Seville, 2016.*
- [3] J.L. Escalona, J.F. Aceituno. Modeling wheel-rail contact with pre-calculated lookup tables in arbitrary-geometry tracks with irregularities. *Proceedings of the ASME 2015 International Design Engineering Technical Conferences & Computers and Information in Engineering Conference IDETC/CIE 2015, Boston, MA, USA, 2015.*
- [4] W.T. Higgings. A comparison of complementary and Kalman filtering, *IEEE Trans. Aerospace and Electronic Systems*, Vol. AES-11 (3), 1975.
- [5] S.O.H. Madgwick, A.J.L. Harrison, R. Vaidyanathan. Estimation of IMU and MARG orientation using a gradient descent algorithm. *IEEE International Conference on Rehabilitation Robotics*, pp. 1-7, 2011.
- [6] S.P. Won, W.W. Melekand, F. Golnaraghi. A Kalman/particle filter based position and orientation estimation method using a position sensor/inertial measurement unit hybrid system. *IEEE Transactions on Industrial Electronics*, Vol. 57 (5), pp. 1787-1798, 2010.

# Numerical Investigation on the Dynamics of a High-Performance Motorcycle Equipped With an Innovative Hydro-Pneumatic Suspension System

Alberto Martini<sup>1,2</sup>, Gabriele Bellani<sup>1,3</sup>

<sup>1</sup>DIN – Dept. of Engineering for Industry  
University of Bologna  
V.le del Risorgimento 2, 40136 Bologna, Italy  
alberto.martini6@unibo.it

<sup>2</sup>CIRI – Advanced Applications in Mechanical  
Engineering and Materials Technology  
University of Bologna  
V.le del Risorgimento 2, 40136 Bologna, Italy

<sup>3</sup>CICLOPE Laboratory  
Center for International Cooperation in Long Pipe Experiments  
University of Bologna  
V. Fontanelle 40, 47121 Forlì, Italy  
gabriele.bellani2@unibo.it

## Abstract

Suspension systems heavily affect the dynamic response of vehicles and their investigation represents a central topic for the field of automotive applications. A new hydro-pneumatic shock absorber for wheeled vehicles, and in particular for motorcycles, has been recently developed [1]. Its most innovative feature is the presence of a hydro-pneumatic spring arranged in series with a coil spring (Fig. 1a). The device is expected to provide numerous benefits with respect to conventional shock absorbers, e.g. a better compromise between vehicle handling and riding comfort as well as easier and more flexible regulation capabilities. The hydro-pneumatic spring is composed of a gas spring and an oil circuit that transmits the elastic force to the coil spring (and vice versa). Because the gas spring preload is much higher than the preload of the coil spring, only the coil spring undergoes deflection for small displacements of the shock absorber (Fig. 1b). Conversely, for larger values of displacement, the equivalent stiffness of the suspension is determined by the contribution of both springs. Due to energy dissipation in the hydro-pneumatic circuit, the load/deflection characteristic curve exhibits a clear non-linear behavior, and in particular a hysteresis loop (Fig. 1b).

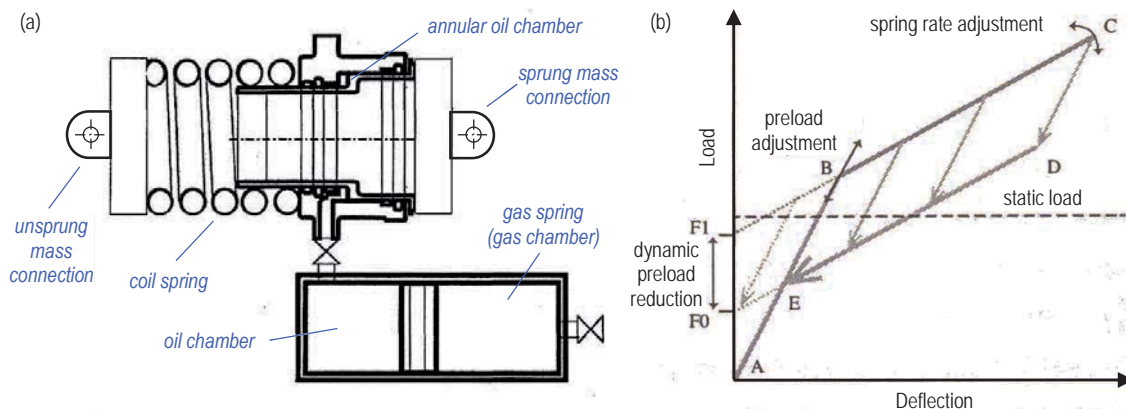


Figure 1. Hydro-pneumatic shock absorber: (a) drawing and (b) qualitative load/deflection curve

Aim of the present work is to provide a first assessment of the dynamic response of this hydro-pneumatic system when applied to the rear suspension of a high-performance motorcycle, with primary focus on the nonlinearities introduced by the hydro-pneumatic circuit. In particular, this work focuses on numerical simulations of the motorcycle in straight running at constant velocity, for different speeds and various road inputs. The goal is to compare the in-plane dynamics of the vehicle equipped with this strongly non-linear suspension with that of a standard suspension (linear spring), mainly in terms of both comfort and tire-road contact parameters.

Two different models are implemented within a multibody software environment, one for the conventional suspension system, the other for the hydro-pneumatic suspension system. The former is a 5 Degrees-of-Freedom (DOF) rigid-body planar model. Three DOFs describe the motion on a vertical plane (i.e. horizontal and vertical translations and pitch motion) of the sprung mass, which includes the mass of the rider (considered as a passive body rigidly connected to the frame). The fourth DOF describes the translation of the front fork. The fifth DOF is associated with the rotation of the swing arm. The corresponding generalized coordinates ( $q_i$ ,  $i=1,\dots,5$ ) are reported in Fig. 2. The assumption on planar behavior is acceptable for the test conditions of interest, since in-plane and out-of-plane motions can be considered as decoupled in straight running [2]. A simplified rider is

also considered acceptable for preliminary simulations, since its motion is expected to be relevant primarily for acceleration/breaking and cornering maneuvers [3]. Both the front and the rear shock-absorbers are modelled by using lumped stiffness and damping parameters characterized by constant values. Contact between each tire and road is modelled by means of a unilateral single-point viscoelastic force, hence taking into account possible wheel lift-off. The road profile exciting the vehicle dynamics is imposed independently on each wheel as a vertical displacement input function. This allows simulating the time delay between the two input displacements, which depends on the motorcycle actual speed.

In the second model, the rear shock absorber is replaced by the hydro-pneumatic device (Fig. 2). An additional DOF ( $q_6$ ) is associated with the device in order to study the detailed dynamics of its internal components. The coil spring is modelled with a lumped constant stiffness parameter, whereas the elastic force generated by the gas spring is described by a non-linear function. It is worth noting, however, that the gas spring is designed to exhibit linear behavior for the actual shock absorber stroke. The dissipative effects characterizing the oil circuit, as well as a damper arranged in parallel to the two springs (not represented in Fig. 1a), are modelled by using lumped constant damping parameters. Friction (including stiction) related to the cylinder seals of the annular oil chamber and between the gas and the oil chambers is also taken into account.

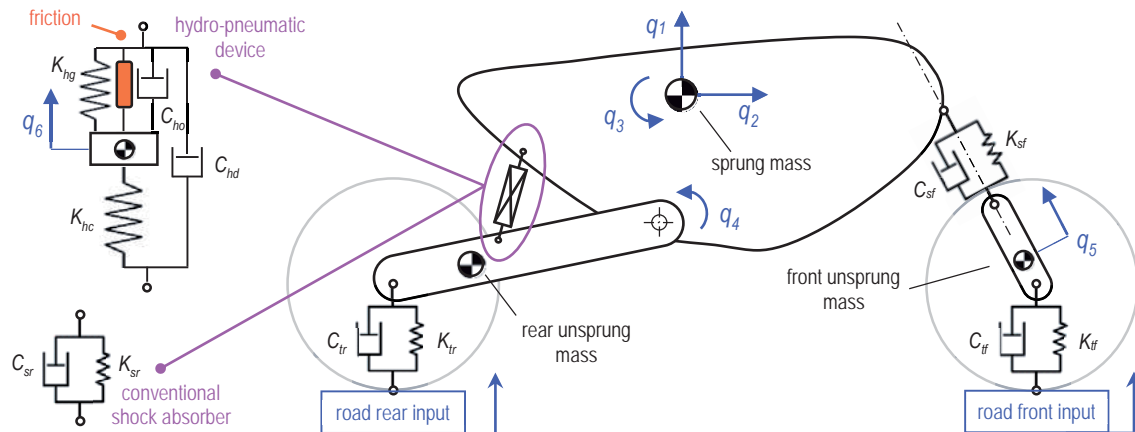


**Figure 2.** Schematics of the motorcycle multibody models

Firstly, natural frequencies and mode shapes are evaluated by linearization of the system around different operating configurations. Then, dynamic simulations of three road conditions are performed, namely random noise excitation, passage on a speed bump and wheels hitting a pothole, for different constant running speed values in the range between 10 and 60 m/s. The displacement input functions adopted for the first condition are synthesized according to the standard ISO 8608 [4], considering various road roughness classes. For the second and the third test conditions, idealized bump and pothole profiles are defined.

The dynamic response of the motorcycle is primarily analyzed in terms of two aspects, namely the vehicle handling performance and the riding comfort. The former aspect is assessed by considering the vertical forces acting between road and tires as a performance indicator of the traction (rear wheel) and braking (front wheel) capabilities. The latter property is evaluated by analyzing the accelerations exhibited by three locations of the sprung mass that are in contact with the rider (namely saddle, handlebar and footrests), in terms of root mean square value and frequency content. First simulation results confirm the effectiveness of the hydro-pneumatic shock absorber.

## Acknowledgments

Umbria Kinetics (Foligno, Italy) is kindly acknowledged for providing realistic parameters and data for the simulations.

## References

- [1] F. Giuliani, G. Bellani. Suspension for wheeled vehicle. Patent WO2015/155712A1, 2015.
- [2] R. S. Sharp, S. Evangelou, D. J. N. Limebeer. Advances in the Modelling of Motorcycle Dynamics. *Multibody System Dynamics*, 12(3):251–283, 2004.
- [3] G. Sequenzia, S. M. Oliveri, G. Fatuzzo, M. Cali. An advanced multibody model for evaluating rider's influence on motorcycle dynamics. *Proceedings of the IMechE, Part K: Journal of Multi-body Dynamics*, 229(2):193–207, 2015.
- [4] International Organization for Standardization. *Mechanical vibration - Road surface profiles - Reporting of measured data*. ISO 8608:2016.

# An overview of a Connected Autonomous Vehicle Emulator (CAVE)

Asher Elmquist, Dylan Hatch, Radu Serban, Dan Negrut

Department of Mechanical Engineering, University of Wisconsin-Madison, Madison, WI 53706-1572, USA  
 {amelmquist,dhatch2,serban,negrut}@wisc.edu

## Abstract

This project targets the creation of an open-source autonomous vehicle simulation framework whereby piloting control programs (PCPs) and vehicle response can be evaluated and improved in a safe environment. Through the interaction of hundreds of autonomous and avatar agents in a simulated environment, edge cases for self-driving vehicles can be analyzed thus accelerating research, development and technology deployment. The Connected Autonomous Vehicle Emulator (CAVE) developed builds upon four foundational components: (i) physics engine and dynamic vehicle support using Chrono and Chrono::Vehicle; (ii) virtual sensors support to provide self-driving algorithms with realistic data; (iii) multi-agent and vehicle-to-vehicle simulated communication support through a fast, low-latency server-client model; and, (iv) virtual environment for both physics and sensing to support edge cases for self-driving vehicles where physical testing is not feasible, including varying environmental conditions such as snow, rain, or fog.

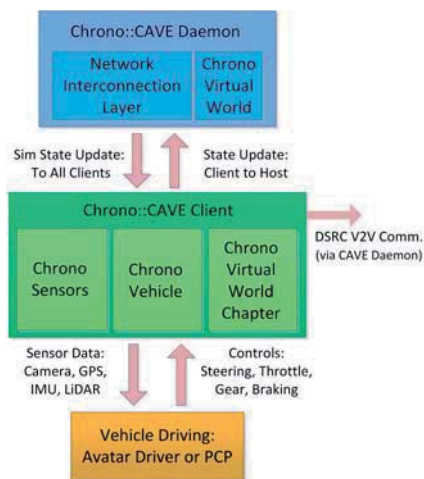


Figure 1: An overview of the CAVE.

As such, a template defines the basic modeling elements (bodies, joints, force elements), imposes the subsystem topology, prescribes the design parameters, and implements the common functionality for a given type of subsystem (e.g. suspension) particularized to a specific template (e.g. double wishbone).

Chrono::Vehicle provides an exhaustive collection of templates for various topologies of both wheeled and tracked vehicle subsystems, as well as support for modeling of rigid, flexible, and granular terrain, support for closed-loop and interactive driver models, and run-time and off-line visualization of simulation results.

A key aspect to testing autonomous vehicles on a simulated platform is producing realistic and reliable sensor data streams that mimic real world sensor data to the PCP, which depends on this information for path planning and obstacle avoidance. For instance, a vehicle approaching a stop sign should receive the same string of data from both a physical camera sensor mounted on front of a physical vehicle and from a virtual camera mounted on a virtual vehicle in the CAVE framework. This means that the process by which that virtual image is captured must introduce the same noise and uncertainty seen in the physical sensor. For a light dependent sensor such as a camera, LiDAR, or Infrared receiver, data is perceived dependent on scene-wide illumination as well as material reflectance and absorption properties. In the case of a camera, the sensor itself adds noise in reading of the light in addition to noise that is dependent on the photon levels present in the image capturing process [1]. The sensors implemented in Chrono are positioned to utilize physics base noise to generate realistic sensor data to send to the PCPs. For a LiDAR, which casts rays out and detects reflection, the dependence on scene, material, and environment is significant. For instance, a vehicle driving during a heavy snowfall may receive erroneous LiDAR data due to light scattering. A simple LiDAR is implemented in Chrono making use of collision detection for a given number of rays. This will be augmented with physics based noise dependent on sensor respective scene effects.

Core to the functionality of CAVE is its ability to simulate many autonomous and avatar vehicles in a distributed manner. The Chrono::CAVE daemon, see blue box in Fig. 1, allows for interaction of physics based vehicle models within this CAVE proving ground. The simulation of vehicle dynamics, sensor data, and path planning occurs locally; i.e., on the client side. Each client exchanges only world position and orientation data to the

server. The server disperses location information of all agents in the CAVE to each client, allowing for continued simulation without proprietary data exchange. The distributed nature of the simulation allows for rapid scaling of the CAVE without massive increase in computational burden on the server. All clients interact with each other through sensing and data passing, adding real world uncertainty and unpredictability for the autonomous vehicles. The agents can interact while being physically located and simulated hundreds of miles apart. The server will mandate and facilitate this vehicle interaction through a fast-network and simulation heartbeat. A second aspect of this server is to provide a means to simulate vehicle-to-vehicle connectivity. As vehicles begin to implement this standardization, simulating and providing a backbone for this protocol will enable the analysis of the impact of vehicle-to-vehicle communication or lack thereof.

The necessity for a realistic and physics based virtual environment is closely interwoven with each other aspect of the CAVE. With the purpose and goal of this framework being to test autonomous vehicle with stress on edge cases where physical testing is difficult or near impossible to facilitate, the replication of realistic physics and sensors is vital. To allow for this, the virtual environment in which the physics and sensing take place must match the real-world counterpart with a high degree of fidelity. The creation of such a virtual world should be based on replicating a given real-world location. For the initial CAVE design, this centers around the University of Wisconsin campus in Madison. World objects, such as traffic lights, road signs, buildings, and trees are important to include and understand from a sensor perspective. The virtual world should also provide edge cases seen from human interaction with autonomous vehicles. We inject the unpredictability of human behavior into the environment via avatar pedestrians, which partake in this proving ground through game console such as the Kinect. Avatar bicyclists and avatar drivers can also share the virtual streets with the CAVE autonomous vehicles by similar means of game controllers.

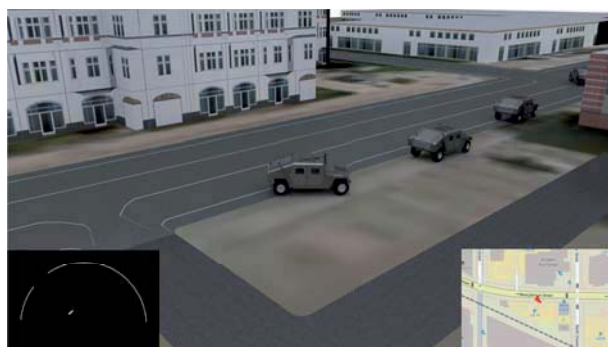


Figure 2: A convoy of vehicles four vehicles, of which the last three follow a leading avatar vehicle.

The demonstration shown in Fig. 2 represents the current progress of the CAVE project by implementing functionality from Chrono::Vehicle, multi-agent, sensors, and virtual world. This is setup with four vehicles simulated on separate clients, all connected to a single server. The lead vehicle is an avatar vehicle driven by a student and the three trailing vehicles are autonomous. The latter are equipped with virtual LiDAR, GPS, and IMU which are used in a simple driving algorithm. The output of these sensors is overlaid on the animation for the last vehicle in the convoy. The LiDAR on the left of the image is represented by dots located at the end of each LiDAR ray for readability. The GPS and IMU data are combined and displayed on a

map to show the location and orientation of the vehicle in the virtual world. The full animation can be found as video #130 [3].

## Acknowledgments

This project was partially sponsored by a University of Wisconsin RIC grant.

## References

- [1] Samuel W. Hasinoff, Frédo Durand, and William T. Freeman. Noise-optimal capture for high dynamic range photography. In *IEEE Conference on Computer Vision and Pattern Recognition*, 2010.
- [2] R. Serban and D. Negrut. Chrono::Vehicle – Template-Based Ground Vehicle Modeling and Simulation. Technical Report TR-2016-10: <http://sbel.wisc.edu/documents/TR-2016-10.pdf>, Simulation-Based Engineering Laboratory, University of Wisconsin-Madison, 2016.
- [3] Simulation-Based Engineering Lab (SBEL). Movies, Physics-Based Modeling and Simulation. <http://sbel.wisc.edu/Animations>. Accessed: 2015-06-09.
- [4] A. Tasora, R. Serban, H. Mazhar, A. Pazouki, D. Melanz, J. Fleischmann, M. Taylor, H. Sugiyama, and D. Negrut. Chrono: An open source multi-physics dynamics engine. In T. Kozubek, editor, *High Performance Computing in Science and Engineering – Lecture Notes in Computer Science*, pages 19–49. Springer, 2016.

# A variable time-step and variable penalty method for the index-3 augmented Lagrangian formulation with velocity and acceleration projections

Daniel Dopico, Emilio Sanjurjo, Javier Cuadrado, Alberto Luaces

Laboratorio de Ingeniería Mecánica  
University of A Coruña  
C/ Mendizábal s/n, 15403, Ferrol, Spain  
[ddopico,emilio.sanjurjo,aluaces]@udc.es,javicuad@cdf.udc.es

## Abstract

The index-3 augmented Lagrangian formulation with velocity and acceleration projections (the ALI3-P formulation) is an efficient and robust method to carry out the forward dynamics simulation of multibody systems modeled in dependent coordinates. The extension of the formulation to non-holonomic systems was accomplished in [1] and it was extensively used during many years for the real-time simulation of different systems with human and hardware in the loop, some of them including complex phenomena like flexibility [2], contact with friction [3, 4] or, more recently, non-holonomic constraints [1].

For almost all the applications tackled so far, a constant time step was employed, but for the case of non-real-time systems with intermittent contacts of high stiffnesses this is not the right approach, since the time step selected has to achieve the accuracy and robustness required in the hardest part of the whole simulation, thus affecting the overall simulation efficiency. On the contrary, a variable time step can speed-up the simulation when the integration is easier, allowing very small time steps when the integration is harder.

Even if there is a vast literature on variable time step algorithms and one previous work for the mentioned formulation, the relation between time step and penalty factors is not covered. This relation is crucial if a broad range of time steps is required. In this work, a variable time step and variable penalty ALI3-P formulation is proposed.

The algorithms developed are applied to the simulation of a real machine involved in a real situation: a diesel forklift rollover. The multibody model was built in the MBSLIM (Multibody Systems at Laboratorio de Ingeniería Mecánica) software package with mixed coordinates: 90 natural coordinates (12 points and 18 unit vectors) plus 9 angles and 2 distances, making a total of  $n = 101$  coordinates. A total number of  $d = 11$  mechanical degrees of freedom (DOF) have been considered: 6 DOF for the chassis rigid body motion, 4 DOF for the wheels rotations and 1 DOF for the rear rigid axle tilt. Besides, 5 additional kinematically guided motions, corresponding to degrees of freedom of the real machine have been considered: the mast swinging angle, the fork and upper mast lift and the rear wheels steering angles (related by the Ackerman steering condition). For these guided motions, rheonomic constraints have been employed and therefore they cannot be considered degrees of freedom from the mechanical point of view, nevertheless they are true additional DOF in the real machine that have been considered, making a total of 16 real degrees of freedom.

The model includes some problematic phenomena from the integration point of view, like tire forces and intermittent contacts with friction when the machine rolls over and slams into the pavement. The same model described in [5] was used for the tire forces with an improved collision detection algorithm that makes possible to come into contact on the tire shoulder, essential for rollover situations. The collisions between chassis or cabin and pavement have been modeled too, with the same approach proposed in [3].

The maneuver consists in the machine moving straight backward at full speed (10 km/h initially). One second after the simulation starts, the driver turns right completely.

Some snapshots of the interactive simulation are included in figure 1, proving that the careless maneuver results in the machine rollover. Some important magnitudes are represented in 3D: the green vectors are normal tire forces, the red ones are tangential tire forces, the yellow ones are center of mass accelerations for each body, a black vector represents the acceleration suffered by the driver and the purple one represents the velocity of the central point in the front axle.

## References

- [1] D. Dopico, F. González, J. Cuadrado, J. Kovacs. Determination of holonomic and nonholonomic constraint reactions in an index-3 augmented lagrangian formulation with velocity and acceleration projections. *Journal of Computational and Nonlinear Dynamics*, 9(4):041006–041006, 2014. doi:10.1115/1.4027671.
- [2] J. Cuadrado, R. Gutierrez, M. Naya, P. Morer. A comparison in terms of accuracy and efficiency between a mbs dynamic formulation with stress analysis and a non-linear fea code. *International Journal for Numerical Methods in Engineering*, 51(9):1033–1052, 2001.

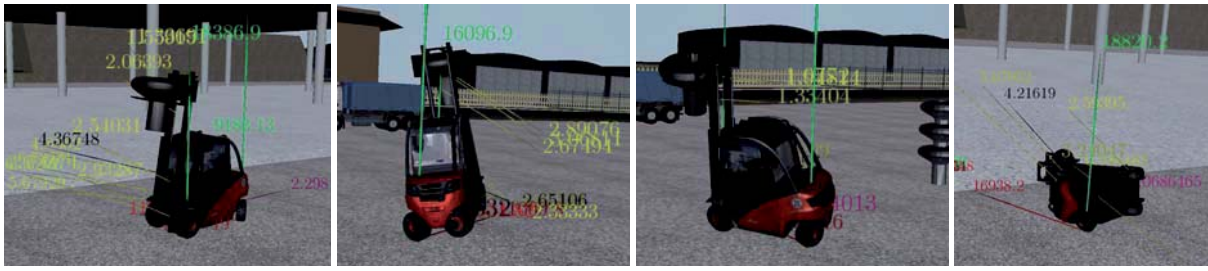


Figure 1: Rollover situation.

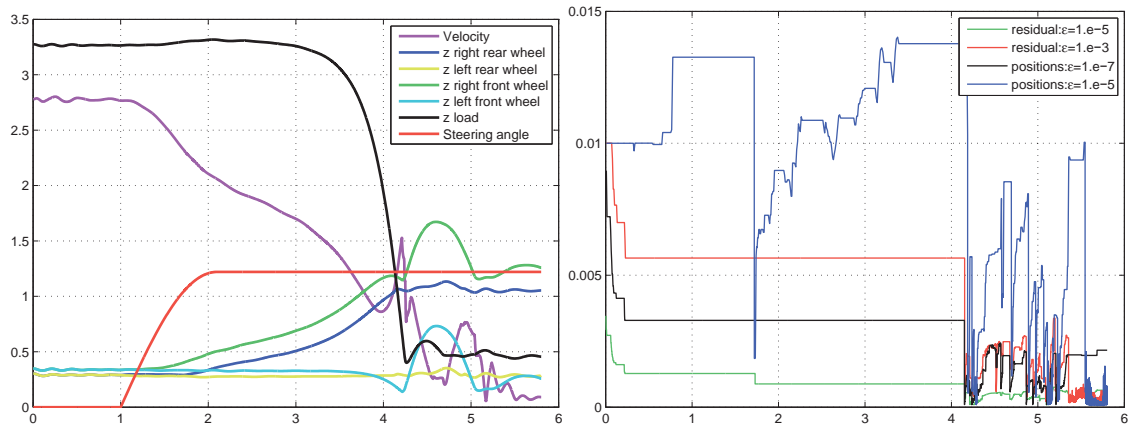


Figure 2: Maneuver results (left). Time step evolution (right): with residual of the equations of motion error  $e = \|\mathbf{f}(\mathbf{q}_{n+1})^{(i)}\|$  and positions error  $e = \|\mathbf{q}_{n+1}^{(i+1)} - \mathbf{q}_{n+1}^{(i)}\|$

- [3] D. Dopico, A. Luaces, M. Gonzalez, J. Cuadrado. Dealing with multiple contacts in a human-in-the-loop application. *Multibody System Dynamics*, 25(2):167–183, 2011. doi:10.1007/s11044-010-9230-y.
- [4] R. Pastorino, E. Sanjurjo, A. Luaces, M. A. Naya, W. Desmet, J. Cuadrado. Validation of a Real-Time Multibody Model for an X-by-Wire Vehicle Prototype Through Field Testing. *Journal of Computational and Nonlinear Dynamics*, 10(3):031006, 2015. doi:10.1115/1.4028030.
- [5] Y. Zhu, D. Dopico, C. Sandu, A. Sandu. Dynamic response optimization of complex multibody systems in a penalty formulation using adjoint sensitivity. *Journal of Computational and Nonlinear Dynamics*, 10(3):1–9, 2015. doi:10.1115/1.4029601.

# An Optimal Velocity Profile Design for 6 x 6 Unmanned Ground Vehicle Based on Real-time Traversability(RTT) Analysis

Hyosung Hong<sup>1</sup>, Jongboo Han<sup>1</sup>, Hajun Song<sup>1</sup>, Samuel Jung<sup>2</sup>,  
Sung-Soo Kim<sup>1</sup>, Mooncheol Won<sup>1†</sup>, Wan Suk Yoo<sup>2</sup>, Sanghyun Joo<sup>3</sup>

<sup>1</sup>Dept. of Mechatronics Engineering  
Chungnam National University  
99 Daehak-ro, Yuseong-gu,  
Daejeon, 34134, Korea  
[hyosung.hong, jbhan, hj\_song, sookim,  
mcwon]@cnu.ac.kr

<sup>2</sup>School of Mechanical Engineering  
Pusan National University  
2, Busandaehak-ro 63beon-gil,  
Geunjeong-gu, Busan, 46241, Korea  
Jung40L@gmail.com,  
wsyoo@pusan.ac.kr

<sup>3</sup>Agency for Defense Development  
Yuseong P.O. Box 35, Yuseong-gu, Daejeon, 34186, Korea  
jooshce@add.re.kr

## Abstract

Unmanned ground vehicles especially for the military applications have been developed for surveillance, mine removing, and even assaulting purpose. They are equipped with several different types of sensors, such as vision cameras, 3D laser scanners, and radars in order to gather the surrounding information for autonomous and remote operations. To reach the planned destinations, they are operating to follow the optimal path provided from a global and a local path planner. However, they have to be also required to operate with high speed in off-road situations. Thus, it is very important to determine the optimal velocity which guarantees vehicle stability through the real-time traversability(RTT) analysis [1]. To determine the optimal velocity of the unmanned ground vehicle before actually moving forward, the real-time on-board simulation must be carried out to predict vehicle stabilities with the scanned terrain data from the 3D laser scanners located on the front of the vehicle.

In this paper, an optimal velocity command profile for the 6 x 6 unmanned ground vehicle has been proposed based on RTT simulations. For the traversability simulations, a multibody dynamics and control model of the 6 x 6 unmanned ground vehicle has been proposed [2]. The 6 x 6 unmanned ground vehicle model consists of six arm type suspension systems with MR dampers and suspension springs, in-wheel motors, and tire elements [3]. The subsystem synthesis method has been applied for real-time multibody simulations [4]. Control systems consist of a preview optimal speed controller and a path following controller. The six longitudinal control tire force for each wheel can be determined by the distribution algorithm based on optimization scheme using the estimated vertical tire force [5]. In the RTT analysis module, real-time vehicle dynamics and control simulations are firstly carried out with the upcoming scanned terrain data. The simulation is carried out every 100 msec., and each simulation is a parallel processing of 7 constant speeds running of vehicle on 15-20m ahead terrain. Secondly, vehicle stability analysis is carried out according to the vehicle stability indices for heave, roll, pitch, and lateral motion. Finally, the optimal vehicle velocity profile is obtained as the maximum speeds (as a function of ahead distances) that result in all the vehicle stability indices being above the satisfactory limits from the RTT simulations. Since these optimal vehicle profile must be used as a command input of the actual unmanned ground vehicle, the RTT analysis module has to be implemented on-board. Thus the computation of the traversability analysis must be much faster than real-time. Real-time capabilities of the proposed model are investigated.

The suggested velocity profile design method is first tested on a test bed, where the actual vehicle is also modelled as the same MBD model used in RTT module. Figure 1. shows the obtained optimal velocity profile of the vehicle on an off-road terrain with a less strict stability criterion (non-conservative case) and a strict stability criterion (conservative case). Figure 2 shows the 3-D terrain and vehicle model used in the simulation.

In near future, the RTT analysis and optimal velocity profile routine will be implemented on a real unmanned vehicle and verified on off-road terrains

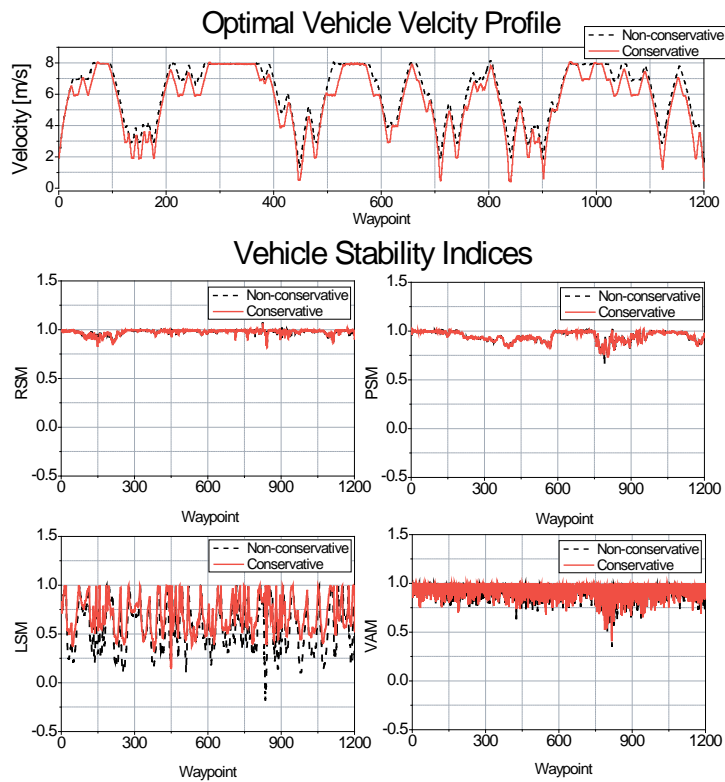


**Figure 1.** Optimal Velocity Profile Obtained from Simulation Test Beds

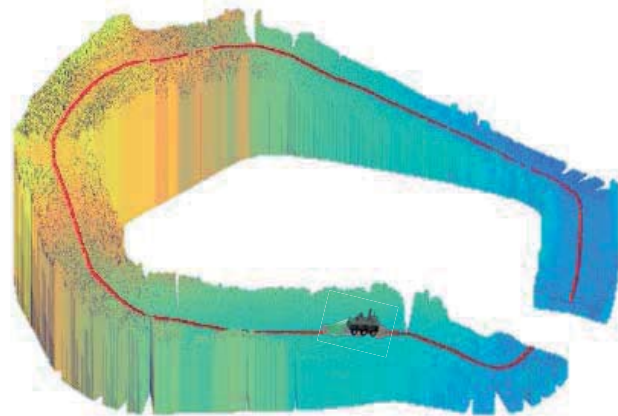


**Figure 2.** Off-road terrain model for UGV-RTT simulation

## References

- [1] Joo, S.H., Lee, J.H., Park, Y.W., Lee, J.H., and Yoo, W.S., Real Time Traversability Analysis to Enhance Rough Terrains Navigation for An 6 x 6 Autonomous Vehicle. *JMST*, 27/4:1125-1134, 2013.
- [2] Han, J.B., Hong, H.S., Song, H., Jung, S., Kim, S.S., Won, M.C., Yoo, W.S., Shin, J. and Park, Y.W., Multibody Dynamics and Control Model of 6 x 6 Unmanned Ground Vehicle for Real-time Traversability Analysis, *The 8<sup>th</sup> Asian Conference on Multibody Dynamics*, pages 124-125, 2016
- [3] Kang, H.C., Kim, S.S., and Lee, C.H., Parallel Processing with the Subsystem Synthesis Method for Efficient Vehicle Analysis. *JMST*, 29/7:2663-2669, 2015.
- [4] Kim, S-S., A Subsystem Synthesis Method for Efficient Vehicle Multibody Dynamics. *Multibody System Dynamics*, 7/2:189-207, 2002.
- [5] Mokhiamar, O., and Abe, M., Simultaneous Optimal Distribution of Lateral and Longitudinal Tire Forces for the Model Following Control. *ASME Journal of Dynamic Systems, Measurement, and Control*, 126:753-763, 2004.

## Physics-Based Tire-Soil Interaction Model and Validation for Off-Road Mobility Simulations

Hiroki Yamashita<sup>1</sup>, Paramsothy Jayakumar<sup>2</sup>, Mustafa Alsaleh<sup>3</sup>, Hiroyuki Sugiyama<sup>1</sup>

<sup>1</sup>Department of Mechanical & Industrial Eng.  
The University of Iowa  
Iowa City, IA 52242, USA  
[hiroki-yamashita,  
hiroyuki-sugiyama]@uiowa.edu

<sup>2</sup>Paramsothy Jayakumar  
US Army TARDEC  
Warren, MI 48397, USA  
paramsothy.jayakumar.civ@mail.mil

<sup>3</sup>Caterpillar Inc.  
Product Development & Global Technology  
Mossville, IL 61552, USA  
Alsaleh\_Mustafa\_I@cat.com

### Abstract

The vehicle-terrain interaction model is essential to demonstrate vehicle mobility capability on deformable terrains under various maneuvering scenarios, and the overall vehicle performance on sand and rough dirt roads needs to be carefully evaluated at various design stages, including drawbar pull, tire sinkage, and rolling resistance. Over the past decades, various simulation techniques have been proposed and utilized for modeling the vehicle and deformable terrain interaction. Empirical terramechanics models allow for a quick prediction of off-road mobility performance. Among others, a NATO Reference Mobility Model (NRMM) has been used for various military scenarios. Analytical and semi-empirical models, on the other hand, are utilized to better understand the tire-soil interaction mechanics using terramechanics theories. Since empirical and analytical terramechanics models cannot capture complex deformation as well as highly nonlinear material behavior of the soil, physics-based numerical models have been proposed to enable quantitative evaluation of the off-road mobility capability on deformable terrains using either continuum-based finite element (FE) or discrete element approaches.

Despite the fact many FE deformable tire-soil interaction simulation models have been proposed and validated, integration of these models into multibody vehicle simulation is not straightforward due to the essential difference in formulation and solution procedures adopted in general multibody dynamics computer algorithms and nonlinear finite element procedures. For this reason, co-simulation techniques are widely used to integrate the deformable tire and soil simulation models into the vehicle dynamics simulation framework. Use of co-simulation techniques, however, requires very small step size to assure the simulation accuracy, thus development of the tire-soil interaction model that can be fully integrated into multibody off-road mobility simulation framework is pursued in this study without co-simulation techniques. To this end, a high-fidelity deformable tire model based on the absolute nodal coordinate formulation proposed in the literature [1] is extended for use in off-road mobility simulations and validated against test data as shown in Fig 1. To model continuum soil behavior, a locking-free 9-node brick element is developed with the curvature coordinates at the center node using the capped Drucker-Prager failure criterion. Introduction of the curvature coordinates allows for considering the quadratic terms in the polynomial of the assumed displacement field, thus the linear distribution of the stresses and strains can be captured. This eliminates the reliance on the enhanced assumed strain method required to alleviate the element locking of the standard tri-linear 8-node brick element, thereby making the formulation and implementation of the continuum soil model straightforward. The multiplicative finite strain plasticity theory along with the capped Drucker-Prager failure criterion is utilized to account for the large soil deformation exhibited during the tire-soil interaction in addition to the soil compaction effect. The capped Drucker-Prager soil model is compared with the

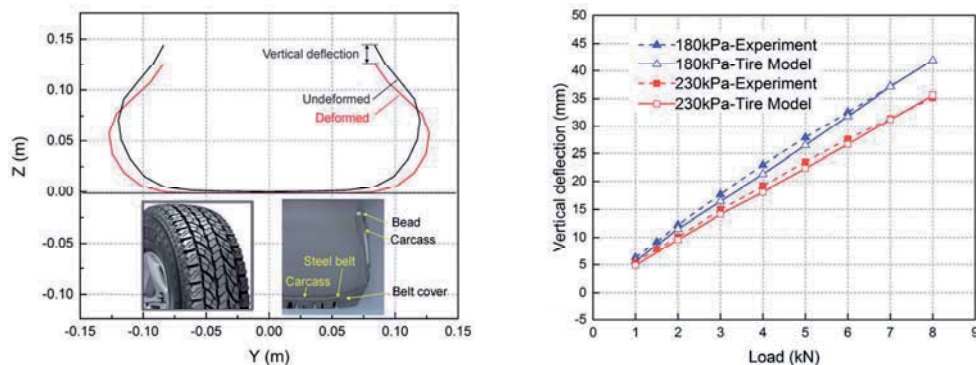


Figure 1. Deformable tire model and comparison with test results

soil elements in ABAQUS for the plate sinkage benchmark test of soil as shown in Fig. 2 for model validation. In order to identify soil parameters including cohesion and friction angle, the triaxial soil test is carried out. Using the soil parameters identified including the plastic hardening parameters, the continuum soil model developed is validated against the test data.

Using the deformable tire and soil models developed and validated against test data, the tire-soil interaction simulation model is developed and implemented in the general multibody dynamics computer algorithm. Use of the high-fidelity physics-based tire-soil simulation model in off-road mobility simulation, however, leads to a very large computational model for covering a wide range of terrains. Thus, the computational cost dramatically increases as the size of the soil model increases. To address this issue, a moving soil patch technique [2] is adopted as shown in Fig. 3 such that the soil behavior only in the vicinity of the rolling tire is solved in order to reduce the overall model dimensionality associated with the FE soil model. It is shown that use of this approach leads to a significant reduction in computational time while ensuring the accuracy, making the use of the physics-based deformable tire-soil simulation capability feasible in off-road mobility simulations. Finally, the tire-soil simulation model developed in this study is validated against test data obtained from a soil bin test facility under various tire-rolling test conditions.

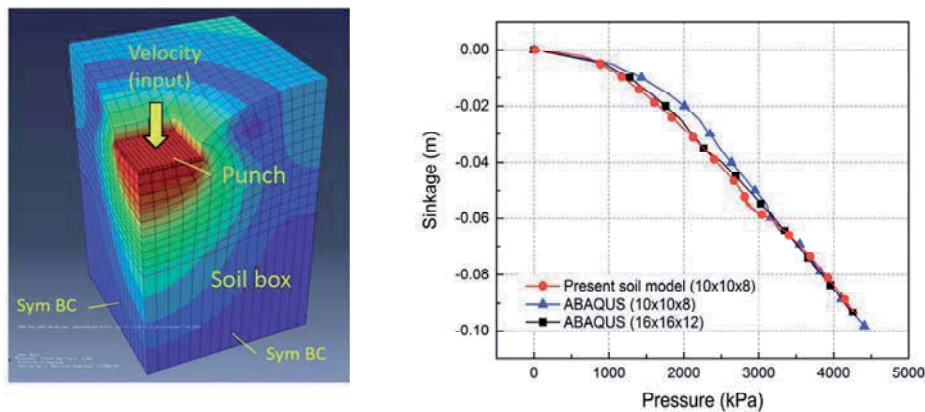


Figure 2. Pressure-sinkage benchmark test for the capped Drucker-Prager soil model

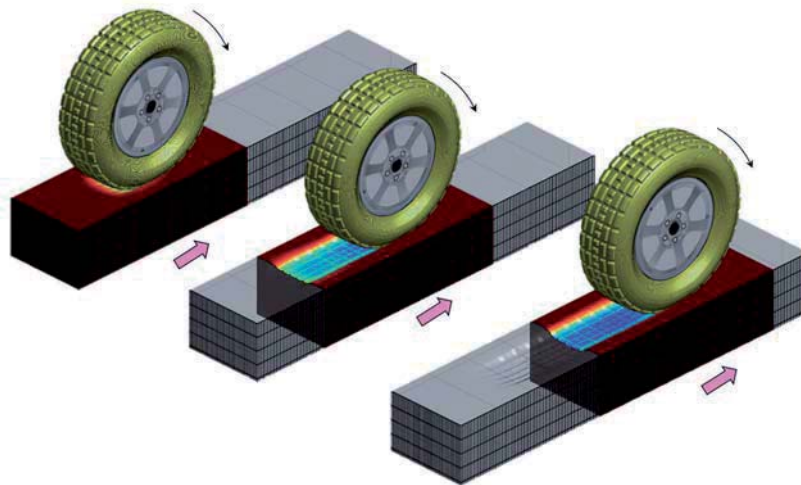


Figure 3. Tire-soil interaction simulation using moving soil patch technique

## References

- [1] Yamashita, H., Jayakumar, P., and Sugiyama, H., 2016, "Physics-Based Flexible Tire Model Integrated with LuGre Tire Friction for Transient Braking and Cornering Analysis", *ASME Journal of Computational and Nonlinear Dynamics*, vol. 11, 031017-1-17.
- [2] Wasfy, T. M., Jayakumar, P., Mechergui, D., and Sanikommu, S., 2016, "Prediction of Vehicle Mobility on Large-Scale Soft-Soil Terrain Maps Using Physics-Based Simulation", *Proceedings of the 2016 NDIA Ground Vehicle Systems Engineering and Technology Symposium (GVSETS)*, Novi, MI.

**Disclaimer:** Reference herein to any specific commercial company, product, process, or service by trade name, trademark, manufacturer, or otherwise, does not necessarily constitute or imply its endorsement, recommendation, or favoring by the United States Government or the Department of the Army (DoA). The opinions of the authors expressed herein do not necessarily state or reflect those of the United States Government or the DoA, and shall not be used for advertising or product endorsement purposes.

## Experimental Model of a Vehicle with an Assistant for Reversing with a Trailer

Jan Zavřel<sup>1</sup>, Petr Beneš<sup>1</sup>, Ladislav Vrbský<sup>1</sup>, Petr Denk<sup>1</sup>

<sup>1</sup>Department of Mechanics, Biomechanics and Mechatronics  
Czech Technical University in Prague  
Technická 4, CZ-16607, Czech Republic  
[Jan.Zavrel, Petr.Benes, Ladislav.Vrbsky, Petr.Denk]@fs.cvut.cz

### Abstract

This paper describes an assistant system used car backing, especially for backing with a trailer. The state of the art is reviewed and summarized in this document. The car backing system assisting a driver is considered to be very useful. It starts to offer as option by major vehicle manufactures. The software backing assistant helps the driver to back the vehicle trailer in a very easy way.

Recent parking and reversing assistants are currently actively researched and the commercial versions are offered as high gear options [1]. There are several ways how the reversing assistant can function. The majority of the backing assistants are based on video-based reversing assistants where reversing camera integrated into the vehicle's tailgate. The image is shown on the display of the radio unit or the navigation system. The video based assistant gives a better view of place behind the vehicle and enables the driver to identify obstacles, kids etc.

An assistant for reversing with a trailer is based on the car model and the trailer [2], [3]. The control method differs from car control. The driver can track the position of the trailer through the tailgate integrated camera. The driver gives commands to turn the trailer using a special driver. The car control unit controls the wheels.

It is necessary to establish equations (1-6) describing the behavior of a vehicle with a trailer. As the speed of the car is small, we do not consider the dynamics. The theory is based on the kinematic description only (Figure 1). The car model is simplified, too. We consider that car's back and front wheels have the same velocity and the front wheels have the same angles. A single-track model like a motorcycle is used for the computation. The model of the trailer unit considers one axle only.

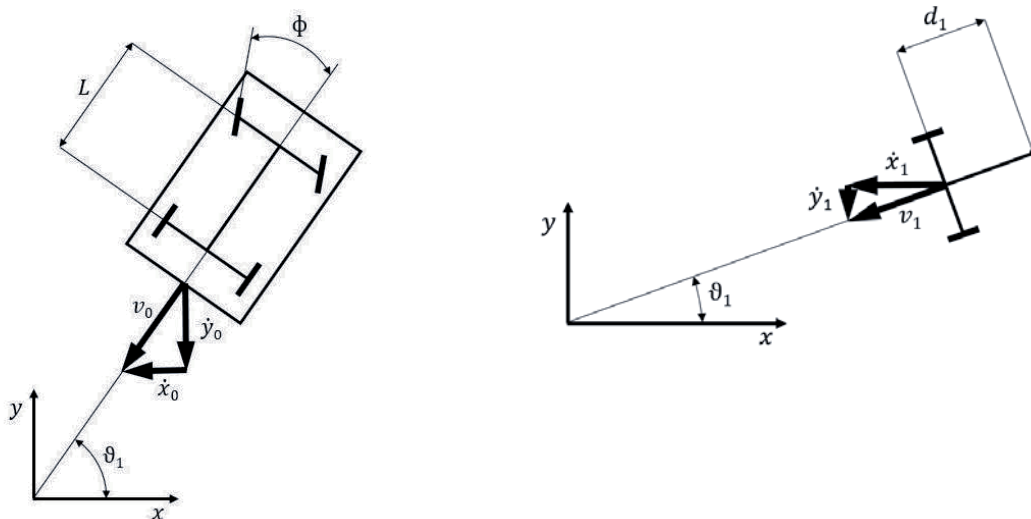


Figure 1. The simplified kinematical model of the car and trailer

The car and trailer are described by the following parameters:  $v_0$  – tangential car velocity,  $\dot{x}_0$  and  $\dot{y}_0$  – car velocity components,  $\vartheta_1$  - absolute angle of the car rotation,  $\Phi$  – angle of the front car axle,  $L$  – wheelbase,  $v_1$  – tangential trailer velocity,  $\dot{x}_1$  and  $\dot{y}_1$  – trailer velocity components,  $\vartheta_0$  – absolute angle of the trailer,  $d_1$  – distance between the car and the trailer and  $\vartheta_1$  – absolute angle of the car.

The car assistant needs to know tangential velocity  $v_0$  and angular velocity  $\omega_0$ . These velocities depend on velocity  $v_1$  and angular velocity  $\omega_1$ . The velocity  $\omega_0$  is the angular velocity of the car and  $\omega_1$  is the angular velocity of the trailer. These velocities are given also by the car driver through the special driver. Other

parameters are given by kinematic equations.

$$\dot{x}_1 = v_1 \cos \vartheta_1 \quad (1)$$

$$\dot{y}_1 = v_1 \sin \vartheta_1 \quad (2)$$

$$\dot{\vartheta}_1 = \omega_1 \quad (3)$$

$$\dot{x}_0 = (v_1 \cos \varphi_{10} + \omega_1 d_1 \sin \varphi_{10}) \cos \vartheta_0 \quad (4)$$

$$\dot{y}_0 = (v_1 \cos \varphi_{10} + \omega_1 d_1 \sin \varphi_{10}) \sin \vartheta_0 \quad (5)$$

$$\dot{\vartheta}_0 = \omega_0 = \frac{v_1}{d_0} \sin \varphi_{10} - \frac{\omega_1 d_1}{d_0} \cos \varphi_{10} \quad (6)$$

Angle  $\varphi_{10}$  is the relative angle between the car and the trailer. This approach and more complex models were simulated in the MATLAB-SIMULINK [4]. The results were tested on the physical model based on the LEGO platform (Figure 2). There were tested different approaches of sensors placement and the type of the driver's knob driver.

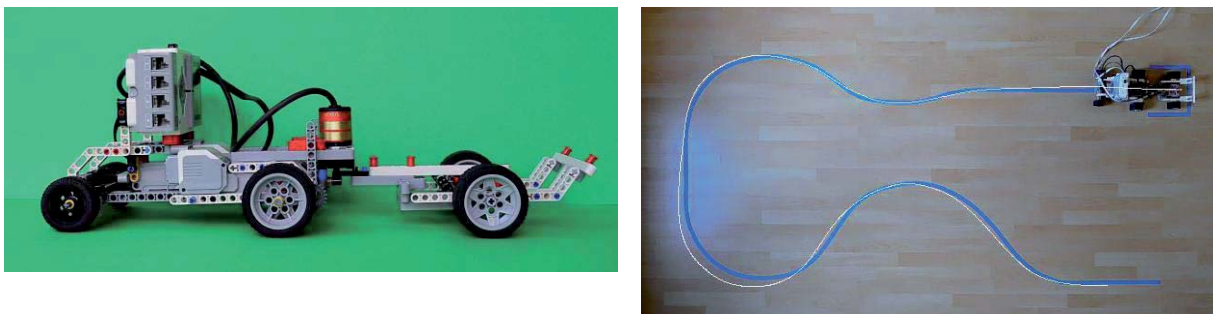


**Figure 2.** The physical model used for testing (on the left) and comparing the planned and real trajectory

## Conclusion

Procedures were derived for car backing and successfully tested. A car model was used for testing. Other possible positions of sensors and different types of user's drivers will be tested.

## Acknowledgments

The work has been supported by the grant SGS16/208/OHK2/3T/12 Mechatronics and adaptronics 2016 of CTU in Prague, The Technology Agency of the Czech Republic TAČR TH02011013 Advanced system for vehicle rear view monitoring with protection against damage and dirt and The Ministry of Education, Youth and Sports program NPU I (LO), project # LO1311 Development of Vehicle Centre of Sustainable Mobility.

## References

- [1] J. GOLSON. Ford Makes Backing Up a Trailer as Easy as Turning a Knob, 2015. [Online, 5/9/2016]. Available at: <http://www.wired.com/2015/05/ford-makes-backing-trailer-easy-turning-knob/>.
- [2] O. Sørtdalen. Conversion of the Kinematics of a Car with n Trailers into a Chained Form. IEEE Computer Society Press, ICRA 1, 1993, pp. 382-387.
- [3] A. a. J. W. Divilbiss: Trajectory Tracking Control of a Car-Trailer System. IEEE Transactions On Control Systems Technology, pp. 269-278, May 1997.
- [4] L. Vrbský. Experimentální model vozidla s asistentem pro couvání s přívěsem. ČVUT v Praze, Praha. 2014.

# Development of Steering Torque Simulator with Multibody Kinematic Model Considering Friction Characteristics of Steering Gear

Tadashi Iwasaki<sup>1</sup>, Hiroki Hoshino<sup>1</sup>, Taichi Shiiba<sup>1</sup>

<sup>1</sup> Department of Mechanical Engineering  
Meiji University  
1-1-1 Higashi-Mita, Tama-Ku, Kawasaki, Kanagawa, Japan  
[ce62011, ce62056, shiiba]@meiji.ac.jp

## Abstract

The function of the steering system is to give the driver directional control of the vehicle. The driver feels the force from the steering wheel which encompasses various information including the road and vehicle condition. The steering torque is considered as one of the most important information for the driver as the steering torque influences driver's judgment for next operation. In recent years, the adoption of the electronic controlled steering system with new technologies has been enlarged as well as the assist control of the steering torque. New technologies include the active steering system that changes the ratio of the steering rack stroke in response to the operation of the driver to optimize the vehicle behavior. These electronic controlled steering systems have interactions with other complex vehicle subsystems such as electronic stability controlled system, and it is difficult for developers to find the best solution from huge number of combinations of parameter settings with standard tools and test methods. In order to solve this problem, this study developed a steering torque simulator with the multibody kinematic model considering the friction characteristics of the steering gear. This developed steering torque simulator is shown in Figure 1.



Figure 1: Overview of steering torque simulator.

The steering torque simulator includes a steering torque generator and a PC which is used for the full vehicle dynamics analysis and the calculation of the steering torque. The configuration of the steering torque simulator is shown in Figure 2. The vehicle dynamics analysis is carried out by CarSim, which is a commercial software specialized for the real-time full vehicle simulation. The vehicle model of CarSim includes the characteristics of engine, transmission, brake and electronic stability control system. The 10-DOF model defined in CarSim is used for the vehicle dynamics calculation, and the detailed suspension characteristics such as the wheel alignment change are considered with a large number of look-up tables. In the multibody kinematic model, the knuckle vertical displacement and the tire force supplied by CarSim are used in order to calculate the steering torque. The program of the multibody kinematic analysis was written in C to realize the implementation to the real-time simulation environment. This approach can realize the high computational efficiency of the steering torque calculation and co-work with the real-time full vehicle simulation. The calculated steering torque is used as the command torque for the steering torque generator.

In this study, the deformation of the suspension metal parts as well as the play between the joints and the deflection of rubber bushes that connect the suspension parts in the actual vehicle are treated to be small enough to be ignored for the steering torque calculation. Therefore, all joints between the front suspension and the steering parts can be expressed as holonomic kinematic constraint. Furthermore, the inertia effect of the front wheels at the steering input is also ignored because the inertia effect is small enough in a usual condition with a steering input. The steering torque is calculated as one of the constraint forces.

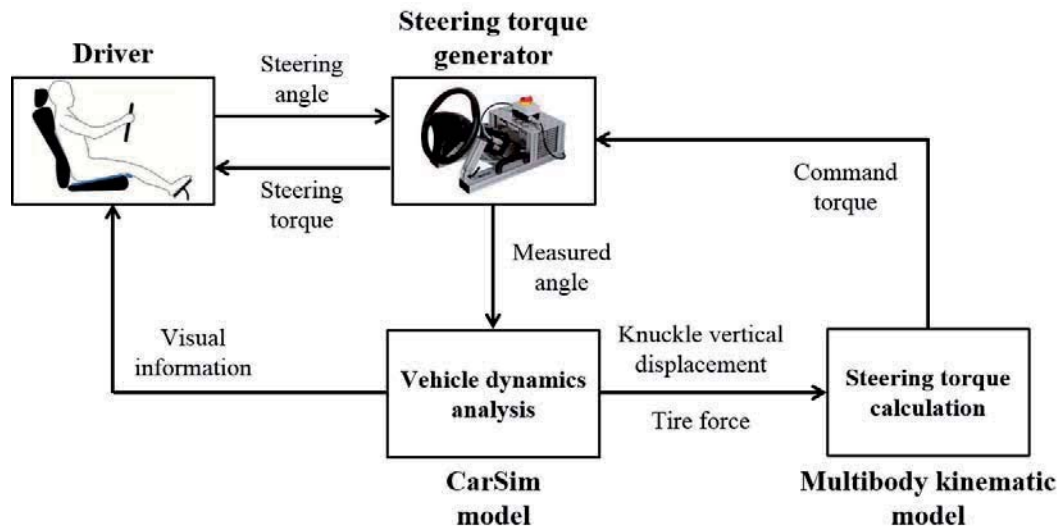


Figure 2: Configuration of steering torque simulator.

The characteristics of the steering torque are affected by the mechanical friction of the steering. Thus, it is desirable that the influences of the mechanical friction of the steering are considered in order to improve the precision of the steering torque, which is calculated in the multibody kinematic model. However, it is difficult to consider the influences of the mechanical friction because the mechanical friction of the steering gear changes complicatedly depending on a contact condition. In this study, the friction characteristics of the steering gear were evaluated by using the steering gear of a target vehicle to identify the friction model. The identified friction model of the steering gear is shown in Figure 3. This identified friction model was applied to the multibody kinematic model, and the steering torque was calculated.

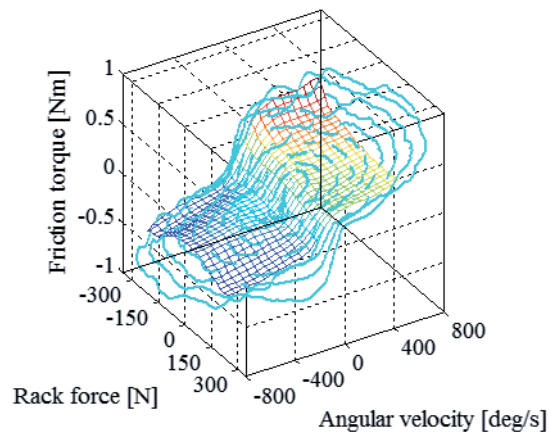


Figure 3: Identified friction model of steering gear.

## References

- [1] E. J. Haug. Computer Aided Kinematics and Dynamics of Mechanical Systems. Allyn ans Bacon, 1989.
- [2] M. Tsushima, T. Shiiba. Development of Hardware-In-the-Loop Simulation System for Steering Evaluation Using Multibody Kinematic Analysis. SAE paper. 2014-01-0086, 2014.
- [3] T. Shiiba, S. Sasaki, N. Takahashi. Dynamic Estimation of Applied Forces on Parallel Mechanism with Inverse Multibody Dynamics. The 1st Joint International Conference on Multibody System Dynamics, 2010.

## Estimation of commercial vehicle dynamics by means of real-time application in condition of high speed curvilinear maneuvers

Tumasov Anton, Butin Danila, Alexey Vasiliev, Viktor Kryaskov

Transport Systems Institute  
Nizhny Novgorod State Technical University n.a. R.E. Alekseev  
Minin str., 24, 603950 Nizhny Novgorod, The Russian Federation  
anton.tumasov@nntu.ru

### Abstract

The paper deals with the problem of estimation of vehicles dynamics by means of real-time application that allows analyzing the behavior of a vehicle in a real-time mode. This approach is necessary for development of HIL-testbench where the mechanical parts of a vehicle (wheels, suspensions, body, etc) simulated in a real-time application, but electronics systems presented by real devices (such as ECU) and work together with virtual vehicle in accordance with imitating maneuver.

The authors of the paper use VI-CarRealTime software that allows designing a vehicle model on the basis of MSC.Adams/Car models. The object of research was a light commercial vehicle (LCV) with cargo bed (the vehicles capacity is up to 3500 kg). The basis of research was LCV MSC.Adams/Car model (1 – 3, figures 1 – 3) validated by results of different laboratory and road tests (static rollover, high speed curvilinear maneuvers: line changing and running into the corner). This model was converted into VI-CarRealTime model that allows simulating LCV behavior in a real-time mode.

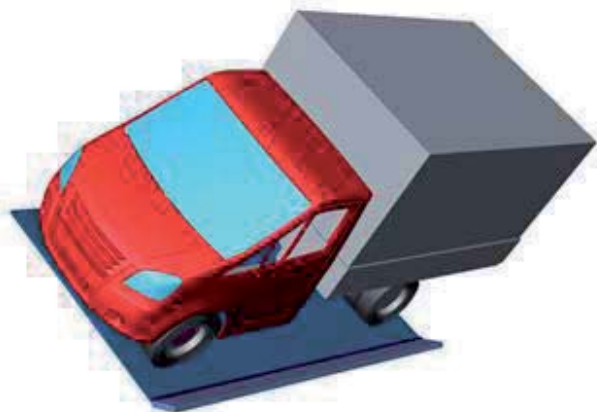


**Figure 1.** Static rollover test (rollover until the moment of kick off of both outer wheels):  
Simulation: 40,8°; Test: 40,0°; Discrepancy: 2,0%

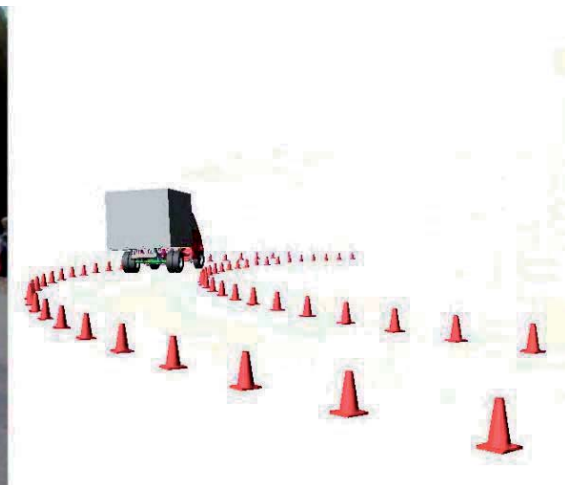


**Figure 2.** “Going into the corner” test (going with a higher speed until cornering breakaway will appear or vehicle will out of limits of a marking corridor): Simulation: 64,4 km/h; Test: 61,9 km/h; Discrepancy: 4,0%



**Figure 3.** “Line changing” test (going with a higher speed until cornering breakaway will appear or vehicle will out of limits of a marking corridor): Simulation: 75,6 km/h; Test: 73,0 km/h; Discrepancy: 3,5%

VI-CarRealTime LCV model used for imitation of two others high speed maneuvers: “sine with dwell” and “fish hook” that usually used for estimation of ECS systems efficiency.

This paper presented results of dynamics of LCV without any ECS influence. Such kinds of results are necessary for finding out of critical speeds when LCV lost its stability (beginning of essential skidding or rollover process).

The developed VI-CarRealTime LCV model will be used in of HIL-testbench with ECS system where the improvement of vehicle dynamics must be confirmed. The results presented in this paper and expected results from HIL-testbench should show that LCV model with ESC can perform “sine with dwell” and “fish hook” tests satisfactory on a speed over 80 km/h that is impossible for LCV model without ESC.

### Acknowledgments

This research done with the financial support from Ministry of Education and Science of the Russian Federation in the frame of the complex project “The establishment of the high-tech manufacturing of GAZ commercial vehicles family, equipped with intelligent driver assistance systems” under the contract №02.G25.31.0193 from 27.04.2016 (Governmental Regulation №218 from 09.04.2010).

### References

- [1] A. Tumasov, S. Kostin, D. Butin, A. Vasiliev, A. Vashurin, Y. Trusov / Estimation of influence of stiffness of chassis frame on LCV dynamics in conditions of curvilinear motion // Proceedings of the ECCOMAS Thematic Conference on Multibody Dynamics 2015, Barcelona, June 29 – July 2, 2015, pp. 1272-1278. <http://www.multibody2015.org/admin/files/fileabstract/a198.pdf>
- [2] A. Tumasov, K. Shashkina, G. Konikova, A. Groshev, A. Bezrukov, Y. Trusov Estimation Of Steerability And Cornering Stability Of Light Commercial Vehicle By Results Of Road Tests And Simulation. FISITA 2014 World Automotive Congress, the Netherlands, Maastricht, 2-6 June - F2014-IVC-048. <http://www.fisita2014.com/programme/sessions/F2014-IVC-048>
- [3] A. Tumasov, R. Musarsky, G. Konikova, A. Groshev, S. Kostin, Y. Trusov Estimation Of Light Commercial Vehicles Dynamics By Results Of Road Tests And Simulation . 16th International Conference on Advanced Vehicle Technologies (AVT), ASME 2014, USA, Buffalo NY, 17-20 August - DETC2014-34641. <http://www.asmeconferences.org/IDETC2014/ViewAcceptedAbstracts.cfm>

## Linearized Modal Analysis of Vehicle Powertrains

Josef Haslinger<sup>1</sup>, Günter Offner<sup>2</sup>, Martin Sopouch<sup>2</sup>, Bianka Barbara Zinkiewicz<sup>2</sup>

<sup>1</sup>Radon Institute for Computational and Applied Mathematics

Austrian Academy of Sciences and MathConsult GmbH

Altenberger Str. 69, 4040 Linz, Austria

josef.haslinger@mathconsult.co.at

<sup>2</sup>Advanced Simulation Technologies

AVL List GmbH

Hans-List-Platz 1, 8020 Graz, Austria

[guenter.offner, martin.sopouch, biankabarbara.zinkiewicz]@avl.com

### Abstract

In this study modal analysis of vehicle powertrains is considered. Modal analysis - the determination of natural frequencies and eigenmodes - provides essential insight into the dynamical behavior of mechanical systems. The mechanical systems under consideration is a multi-body system consisting of rigid and flexible bodies. These bodies are interconnected by nonlinear force elements. The time-dependent description of the system is based on the floating frame of reference approach. This approach leads to the standard system of second order differential-algebraic equations as used in the multi-body simulation software AVL-EXCITE [1]. The differential equation of this system is given as:

$$\mathbf{M}\mathbf{q}'' + \mathbf{D}\mathbf{q}' + \mathbf{K}\mathbf{q} = \mathbf{f}^{inertia}(\mathbf{y}, \mathbf{y}', \mathbf{y}'') + \mathbf{f}^{external}(\tilde{\mathbf{y}}, \tilde{\mathbf{y}}') \quad (1)$$

The vector of displacement variables of a single body consists of the global translation variables  $\mathbf{x}$ , the global rotational variables  $\boldsymbol{\theta}$ , and the local variables  $\mathbf{q}$ . They constitute the displacement vector  $\mathbf{y} = (\mathbf{x}^T, \boldsymbol{\theta}^T, \mathbf{q}^T)^T$  for a single body.  $\mathbf{M}$ ,  $\mathbf{D}$  and  $\mathbf{K}$  denote the mass, damping and stiffness matrix, resulting from spatial finite element discretization. Nonlinear inertia forces - like Coriolis and gyroscopic forces and torques - are collected in  $\mathbf{f}^{inertia}$ .

External forces and moments applied at a single body are covered by  $\mathbf{f}^{external}$ . This vector includes the forces and moments resulting from externally applied loads and torques, e.g. gravity or gas pressures. It also includes the forces and moments resulting from coupling between the bodies. Hence  $\mathbf{f}^{external}$  does not only depend on coordinates of the body itself, but also on possibly all states of other bodies, which are summarized in the vector  $\tilde{\mathbf{y}}$ .

Coupling between different bodies is modeled by force-elements (joints) and contained in  $\mathbf{f}^{joint}$  which is a part of  $\mathbf{f}^{external}$ . A typical joint constrains the motion of the connected bodies by exerting forces or moments on the connected nodes. Force-elements are preferred over algebraic constraints, as they often model radial or axial slider bearings, where clearance gaps, wear and lubrication are of importance. The joint forces/moments are a function of the relative positions and velocities of the connected nodes. For example, the following force law representing a nonlinear spring-damper combination is used for the coupling forces:

$$\mathbf{f}_{i,j}^{joint}(\mathbf{y}_i, \mathbf{y}_j, \mathbf{y}'_i, \mathbf{y}'_j) = \left( c_0 \left( \frac{c_{ref}}{c_0} \right)^{\frac{\Delta s_{ij}}{\Delta s_{ref}}} \Delta s_{ij} + d_0 \left( \frac{d_{ref}}{d_0} \right)^{\frac{\Delta v_{ij}}{\Delta v_{ref}}} \Delta v_{ij} \right) \mathbf{e}_{\Delta_{ij}} \quad (2)$$

where  $\Delta s_{ij}$  is the relative displacement (computed from  $\mathbf{y}_i$  and  $\mathbf{y}_j$ ) and  $\Delta v_{ij}$  the relative velocity (computed from  $\mathbf{y}'_i$  and  $\mathbf{y}'_j$ ) of the two connected nodes at bodies  $i$  and  $j$ ,  $s_{ref}$  is a reference displacement,  $c_0$  and  $c_{ref}$  are coefficients of spring stiffness, and  $d_0$  and  $d_{ref}$  are damping coefficients, respectively.  $\mathbf{e}_{\Delta_{ij}}$  represents the unit vector in direction of the two connected nodes.

The differential equation is completed by algebraic equations called reference conditions, which separate the global motion and elastic deformations in a unique manner [1]. The rotational motion  $\boldsymbol{\theta}$  of the global frame is parameterized by the four parameter family of quaternions [2]. The normalization condition of the quaternions gives another algebraic constraint on the single body level, in addition to the reference conditions.

In general, eigenmodes are viewed as periodic motions of the nonlinear system (1). The eigenvalue problem consists of finding solutions to the boundary value problem

$$\begin{bmatrix} \mathbf{y}(T) \\ \mathbf{y}'(T) \end{bmatrix} = \begin{bmatrix} \mathbf{y}_0 \\ \mathbf{y}'_0 \end{bmatrix}. \quad (3)$$

The initial values  $\mathbf{y}_0$  and  $\mathbf{y}'_0$  and the period  $T$  are unknown. Such a boundary value problem may be solved by the shooting method [3] where the states  $\mathbf{y}(T)$  and  $\mathbf{y}'(T)$  at the end of the period  $T$  are determined iteratively by numerical time integration of (1) from the initial states  $\mathbf{y}_0, \mathbf{y}'_0$ .

In this study, the application of modal analysis is restricted to systems where linearized analysis is applicable. In order to apply modal analysis, the highly nonlinear equations of motion are linearized at specified points in

time. Inertia and connections forces yield a contribution to the mass, damping, and stiffness matrix of the multi-body system, like the force equilibrium approach in [4]. As soon as a common reference frame can be chosen that renders the relative motion of the bodies independent of time, the resulting system of linearized differential equations has constant coefficients, A standard eigenvalue analysis such as the characteristic exponent method [6] is applied to extract natural frequencies and eigenmodes.

Some challenges associated with the linearized modal approach are addressed. For example, the linearization is dependent on the set of coordinates selected to describe the motion of the system, especially the coordinates used to describe global rotational motion of rigid bodies. In this contribution different sets of large orientation parameters (Euler angles and unit quaternions) lead to different forms of the linearized equations of motion and to different natural frequencies and eigenmodes, similar to [5].

The approach is evaluated by computing eigenvalues and eigenmodes of a vehicle powertrain. The vehicle powertrain consists of components like cranktrain/crankshaft, transmission including shafts, gearings, roller bearings as well as engine/transmission housing supported by mounts. Some of the bodies are flexible, some are rigid, some are rotating. The resulting eigenvalue problem is of medium size up to about 5000 degrees of freedom. The approach is validated against commercial software packages.

### **Acknowledgments**

Part of this work was supported by the Upper Austrian Government within the framework “Innovatives Oberösterreich 2020”.

### **References**

- [1] C. B. Drab, H. W. Engl, J. R. Haslinger, G. Offner, R. U. Pfau and W. Zulehner. Dynamic simulation of crankshaft multibody systems. *Multibody System Dynamics*, 22:133-144, 2009.
- [2] J. B. Kuipers. *Quaternions and Rotation Sequences*. Princeton University Press, Princeton, New Jersey, 1999.
- [3] G. Kerschen, M. Peeters, J. C. Golinval and A. F. Vakakis. Nonlinear normal modes, Part I: A useful framework for the structural dynamicist. *Mechanical Systems and Signal Processing*, 23:170-194, 2009.
- [4] J. S. Kang, S. Bae, J. M. Lee and T. O. Tak. Force equilibrium approach for linearization of constrained mechanical system dynamics. *Journal of Mechanical Design*, 125:143-149, 2003.
- [5] A. A. Shabana, M. H. Zaher, A. M. Recuero and R. Cheta. Study of nonlinear system stability using eigenvalue analysis: gyroscopic motion. *Journal of Sound and Vibration*, 330:6006-6022, 2011.
- [6] O. A. Bauchau and J. Wang. Stability analysis of complex multibody systems. *Journal of Computational and Nonlinear Dynamics*, 1:71-80, 2005.

## Behavior of Drivers with Road Departure Prevention Systems Using Driving Simulator

Seongchae Park<sup>1</sup>, Seungjun Choi<sup>2</sup>, Daegy Kim<sup>3</sup>, Donguk Kim<sup>4</sup>, Shengpeng Zhang<sup>5</sup>, Taeh Tak<sup>6</sup>,

<sup>1-5</sup>Graduate Student of Mechanical Engineering, Kangwon National University, 1 Kangwondaehak-gil, Chuncheon-si, Gangwon-do, 200-701, Republic of Korea  
Email:cpark91@kangwon.ac.kr

<sup>6</sup>Faculty of Mechanical Engineering Kangwon National University, 1 Kangwondaehak-gil, Chuncheon-si, Gangwon-do, 200-701, Republic of Korea  
Email: totak@kangwon.ac.kr

### Abstract

Road Departure Prevention System(RDPS) is one of ADAS's (Advanced Driver Assistance System), which prevents a vehicle from departing road boundaries by intervening to steering and/or braking control based on information obtained through vehicle mounted sensors, especially vision sensors. However, when RDPS is activated, there is a good possibility that the driver would not stay passive and instead interfere to steering and braking in some ways, thus the vehicle may not be controlled as originally designed. In order to design an effective and robust RDPS, it is necessary to account for the behavior of driver's interaction to RDPS. This study focuses on the measurement of driver's behavior when RDPS is active using a driving simulator.

Fig. 1 shows configuration of the driving simulator to investigate driver's behavior, where multibody vehicle dynamics simulation software CARMAKER calculates vehicle motion in response to steering wheel, brake and acceleration pedal inputs, and displays traffic situations on the Virtual Reality (VR) screen, and a motion capture system is attached to the driver to monitor the driver's behavior. A set of test scenarios that activate RDPS in various traffic situations are devised based on the accident data analysis related to road departure. Virtual driving tests are conducted using test drivers who are not informed on the activation of RDPS and related traffic situations. Behavior of drivers as well as the vehicle trajectory, vehicle speed, steering angle, steering torque, yaw rate, and lateral acceleration are measured.

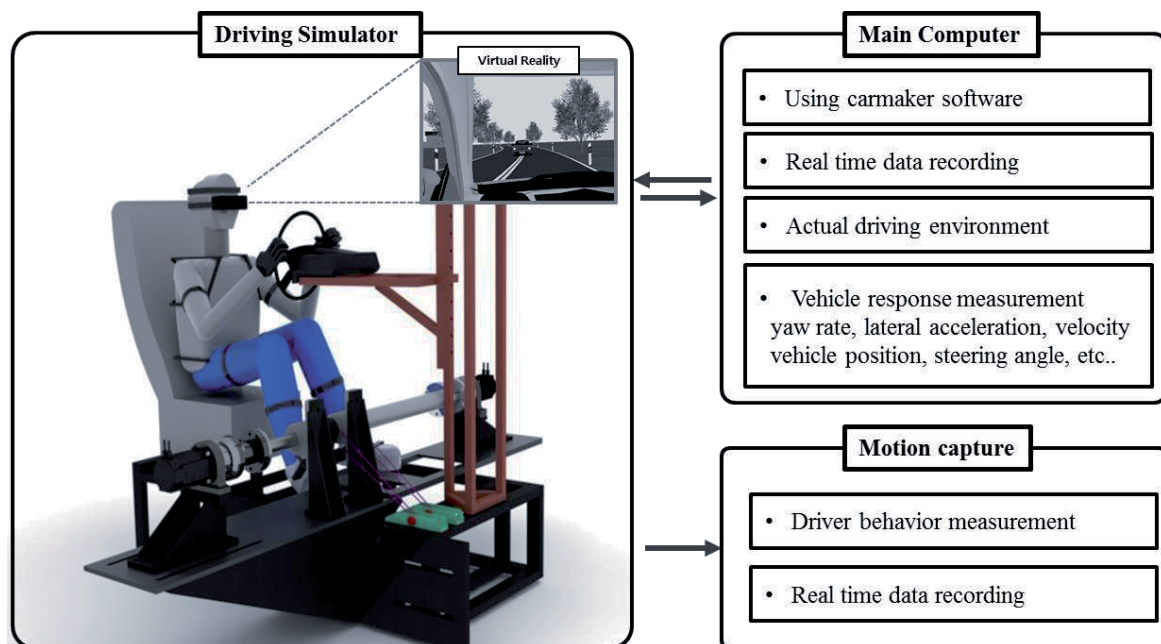
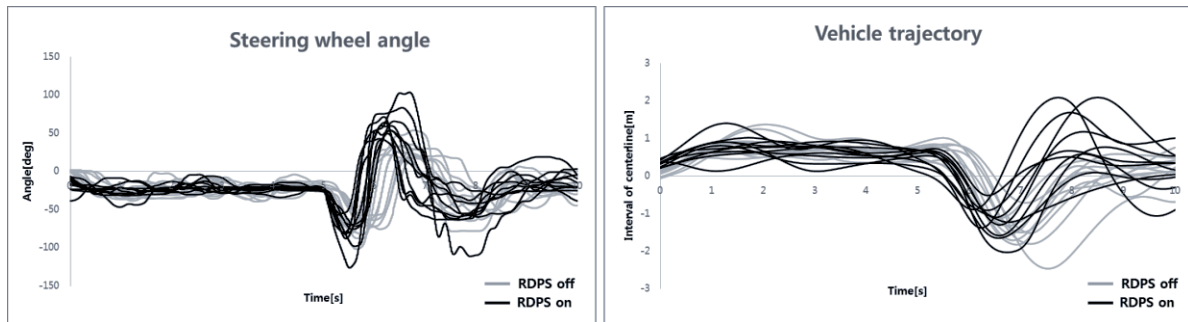


Figure 1. Configuration of the driving simulator



**Figure 2.** Steering wheel angle and vehicle trajectory.

Fig. 2 presents parts of test results, where steering wheel angle and vehicle trajectory are compared when RDPS is ON and OFF. In general, when RDPS is active, it is observed that drivers, prior to braking, tend to intervene to steering control more frequently, and resultantly contribute to preventing from departure from the road. However, in some cases, it is also observed that there is continued intervention by the drivers, and it can cause the vehicle instable and sometimes make the vehicle to depart from the road.

Through the research, it is concluded that the behavior of the driver affects the performance of RDPS significantly, thus driver behavior should be accounted for designing more effective and robust RDPS.

## References

- [1] National Highway Traffic Safety Administration. *A Compilation of Motor Vehicle Crash Data from the Fatality Analysis Reporting System and the General Estimates System*, NHTSA11 Traffic Safety Facts 2011, 2012
- [2] Diomidis I., Katzourakis, Student Member, IEEE, David A. Abbink, Riender Happee, Edward Holweg. *Steering Force Feedback for Human-Machine-Interface Automotive Experiments*, vol. 60, No. 1, pp. 32-43, IEEE Transactions on Instrumentation and Measurement, 2011
- [3] Diornidis I. Katzourakis, Joost C. F. de Winter, Moheesn Alirezaei, Matteo Cormo, Riender Happee. *Road-departure prevention in an emergency obsracle avoidance situation*, pp. 621-629, IEEE transaction on system, man and cybernetics : System 44, 2014,
- [4] Linus Liljeblad. *Driver response to a lane-departure prevention system*, Chalmers University of Technology, 2015

# Cable Dynamics and Fatigue Analysis for Digital Mock-Up in Vehicle Industry

Fabio Schneider<sup>1</sup>, Joachim Linn<sup>1</sup>, Tomas Hermansson<sup>2</sup>, Fredrik Andersson<sup>2</sup>

<sup>1</sup> Fraunhofer Institute for Industrial Mathematics  
Department Mathematical Methods in Dynamics and Durability  
Fraunhofer-Platz 1, 67663 Kaiserslautern, Germany  
[fabio.schneider,joachim.linn]@itwm.fraunhofer.de

<sup>2</sup> Fraunhofer Chalmers Research Centre for Industrial Mathematics  
Chalmers Science Park, SE-412 88, Gothenburg, Sweden  
[tomas.hermansson,fredrik.andersson]@fcc.chalmers.se

## Abstract

Numerical simulation has become an important aspect of modern industrial production processes. Very early in the process chain - even before the first prototypes are built - simulation is used for digital mock-up in order to discover possible problems and to improve certain components and their assembling.

In our work, we focus on the simulation of highly flexible components like cables and hoses, which is a challenging problem in vehicle industry. Already during the assembling steps but also later in regular usage, high loads and contacts with high friction should be avoided.

Considering slow or quasi-static motions, our software *IPS Cable Simulation* already offers the possibility to simulate flexible components interactively, i.e. in real-time, but also with high accuracy [1]. It is available as commercial software tool and has found a wide range of industrial applications in the last years (some examples can be found here [2]). Nevertheless, when it comes to fast excitations with high frequencies, inertia effects can not be neglected and dynamic simulation of cables is indispensable.

To achieve fast and accurate dynamic simulation, the cable is formulated as geometrically exact Cosserat rod, which allows rather rough discretization on a staggered grid (cf. Figure 1) and still leads to robust and realistic results. The Newton equations for the nodes  $x_n$  are given as

$$m_n \ddot{x}_n = f_n^x(x_{n-1}, p_{n-\frac{1}{2}}, x_n, p_{n+\frac{1}{2}}, x_{n+1}) \quad (1)$$

with mass  $m_n = \delta s_n \rho A$ . The Euler equations for quaternions  $p_{n-\frac{1}{2}}$  on the edge midpoints, which are used to describe rotations, are the index-3-DAEs

$$\mu_{n-\frac{1}{2}} \ddot{p}_{n-\frac{1}{2}} = f_{n-\frac{1}{2}}^p(p_{n-\frac{3}{2}}, x_{n-1}, p_{n-\frac{1}{2}}, x_n, p_{n+\frac{1}{2}}) - p_{n-\frac{1}{2}} \lambda_{n-\frac{1}{2}} \quad (2a)$$

$$0 = \frac{1}{2} (\|p_{n-\frac{1}{2}}\|^2 - 1) \quad (2b)$$

with quaternion mass  $\mu_{n-\frac{1}{2}} = \Delta s_{n-\frac{1}{2}} \rho 4Q(p_{n-\frac{1}{2}})IQ(p_{n-\frac{1}{2}})^T$ .

The right hand sides  $f_n^x$  and  $f_{n-\frac{1}{2}}^p$  include viscoelastic contributions from bending, torsion, tension and shearing. Its dependencies as given in (1) and (2a) guaranty a band structured Jacobian and, consequently, the resulting system can be solved efficiently. More details about the cable model can be found in [3].

Currently, we integrate the dynamic cable simulation in our software tool. Thus, users can generate flexible cables as before and only need to add some further information in order to enable dynamic simulations. These additional inputs are dynamic excitations and damping characteristics of the cable, which both are not necessary in quasi-static simulation.

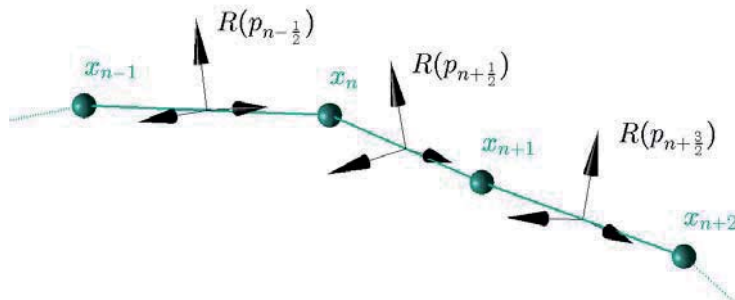


Figure 1: Staggered grid discretization of a geometrically exact Cosserat rod.

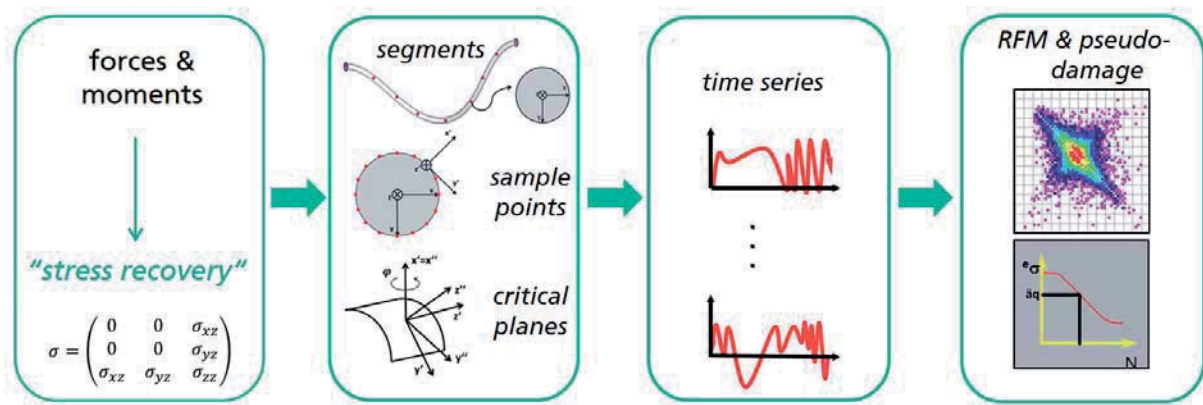


Figure 2: CLA overview - the computation of pseudo-damage values.

Concerning cable fatigue, i.e. damage due to dynamic (and also quasi-static) loads, we distinguish two approaches. On the one hand, we already provide a so called *comparative load analysis (CLA)* [4]. This method computes pseudo-damage values on the cable surface which do not predict the absolute lifetime of a component, but allow to compare several configurations to find the best one in the sense of damage. This computation includes the evaluation of one-dimensional comparison stresses which subsequently are treated by a rainflow counting and a standard Wöhler curve (detailed discussions on load data analysis can be found in [5]), as depicted in Figure 2. On the other hand, for absolute predictions of the component's lifetime, we can proceed as for the CLA but have to use component specific Wöhler curves. To generate these individual Wöhler curves in an efficient way is part of our ongoing research.

## References

- [1] J. Linn, T. Stephan: *Fast simulation of quasistatic cable deformations using discrete rod models*. Technical Report 144, Fraunhofer ITWM, 2008
- [2] *IPS Cable Simulation*: [www.flexstructures.de](http://www.flexstructures.de)
- [3] H. Lang, J. Linn, M. Arnold: *Multibody dynamics simulation of geometrically exact Cosserat rods*. *Multibody System Dynamics*, 25(3):285-312, 2011
- [4] F. Hoefft, T. Stephan, O. Hermanns: *Eine neue Methode zur vergleichenden örtlichen Beanspruchungsanalyse für Kabel und Schläuche*. SIMVEC Berechnung und Simulation im Fahrzeugbau 2010, VDI-Berichte Nr. 2107, ISBN 978-3-18-092107-5, pp. 297–309, 2010
- [5] P. Johannesson, M. Speckert: *Guide to load data analysis for durability in vehicle engineering*. Wiley, 2014

# Use of Joint Coordinates and Homogenous Transformations for Modelling of Articulated Vehicle Dynamics

Iwona Adamiec-Wójcik, Łukasz Drąg, Stanisław Wojciech

Faculty of Management and Transport  
University of Bielsko-Biala  
Willowa 2, 43-309 Bielsko-Biala Poland  
[i.adamiec@ath.bielsko.pl](mailto:i.adamiec@ath.bielsko.pl),  
[ldrag@ath.bielsko.pl](mailto:ldrag@ath.bielsko.pl),  
[swojciech@ath.bielsko.pl](mailto:swojciech@ath.bielsko.pl)

## Abstract

Articulated vehicles are widely used not only for transporting goods but also for performing heavy tasks in off-road terrains. Lateral and roll stability of such vehicles are widely studied due to the safety requirements. Most research papers are concerned with control of roll or steering angles or methods of preventing the jack-knifing [1-5]. Usually articulated vehicles are modelled as a system of single vehicle units. This contribution demonstrates how homogenous transformations can be used to model articulated vehicles. General equations of motion for a single unit vehicle are derived which take into account a complex range of phenomena in vehicle motion, and then an algorithm for generating equations for any articulated vehicle is presented.

The model of a single vehicle unit takes into account a vehicle body, suspensions, wheels and a steering system. It consists of an uneven number of rigid bodies, one of which represents a vehicle body. Motion of the vehicle body is described by one to six degrees of freedom describing the motion of the unit with respect to the preceding unit. Two models of the flexibility of suspensions are considered: in one the motion of the suspension with wheels is described as a function of the vertical displacement of the suspension and the rotation angle of the steering wheel while the second simplified approach limits the suspension and tire flexibility to the contact point between the tire and the road. The motion of a vehicle is performed on a planar, horizontal and undeformable road surface. The steering is reflected by additional functions describing the change in time of the steering angle of the wheels.

The equations of motion are derived using the Lagrange equations. All external forces and moments acting on the vehicle unit are included by means of the generalized forces. The following forces are taken into account: air resistance, drive, braking and aligning torques as well as forces describing the contact between the wheel and the road surface, which is described by the Dugoff-Uffelman model.

The motion of a single vehicle unit  $p$  in terms of its generalized coordinates [6]:

$$\mathbf{u}^{(p)} = \begin{bmatrix} \mathbf{q}^{(p)} & \tilde{\mathbf{q}}_z^{(p)T} \end{bmatrix}^T \quad (1)$$

where  $\mathbf{q}^{(p)} = \begin{bmatrix} \mathbf{q}^{(p-1)T} & \tilde{\mathbf{q}}^{(p)T} \end{bmatrix}^T$  is the vector of generalized coordinates of the unit body consisting of the generalized coordinates of the preceding unit and the coordinates describing the relative motion of unit  $p$  with respect to the preceding one;  $\tilde{\mathbf{q}}_z^{(p)} = \begin{bmatrix} \tilde{\mathbf{q}}_z^{(p,1)T} & \dots & \tilde{\mathbf{q}}_z^{(p,n_{zp})T} \end{bmatrix}^T$  is the vector with  $4n_{zp}$  elements describing the motion of  $n_{zp}$  suspensions and wheels with respect to the unit body.

The equations of motion of a single unit can be written as

$$\mathbf{A}^{(p)} \mathbf{u}^{(p)} = \mathbf{f}^{(p)} \quad (2)$$

which in view of the form of the vector of generalised coordinates can be presented in a block-matrix partitioned form:

$$\begin{bmatrix} \mathbf{A}_{11}^{(p)} & \dots & \mathbf{A}_{1,p-1}^{(p)} & \mathbf{A}_{1,p}^{(p)} & \mathbf{A}_{1,z}^{(p)} \\ \vdots & \ddots & \vdots & \vdots & \vdots \\ \mathbf{A}_{p-1,1}^{(p)} & \dots & \mathbf{A}_{p-1,p-1}^{(p)} & \mathbf{A}_{p-1,p}^{(p)} & \mathbf{A}_{p-1,z}^{(p)} \\ \mathbf{A}_{p,1}^{(p)} & & \mathbf{A}_{p,p-1}^{(p)} & \mathbf{A}_{p,p}^{(p)} & \mathbf{A}_{p,z}^{(p)} \\ \mathbf{A}_{z,1}^{(p)} & \dots & \mathbf{A}_{z,p-1}^{(p)} & \mathbf{A}_{z,p}^{(p)} & \mathbf{A}_{z,z}^{(p)} \end{bmatrix} \begin{bmatrix} \ddot{\mathbf{q}}^{(1)} \\ \vdots \\ \ddot{\mathbf{q}}^{(p-1)} \\ \ddot{\mathbf{q}}^{(p)} \\ \ddot{\mathbf{q}}^{(p)} \end{bmatrix} = \begin{bmatrix} \mathbf{f}_1^{(p)} \\ \vdots \\ \mathbf{f}_{p-1}^{(p)} \\ \mathbf{f}_p^{(p)} \\ \mathbf{f}_z^{(p)} \end{bmatrix} \quad (3)$$

where  $\mathbf{A}^{(p)} = \mathbf{A}^{(p)}(\mathbf{u}^{(p)})$  is the mass matrix and  $\mathbf{f}^{(p)} = \mathbf{f}^{(p)}(\mathbf{u}^{(p)}, \dot{\mathbf{u}}^{(p)})$  includes all components arising from potential energy and generalized forces resulting from external loads as well as from centrifugal and gyroscopic forces.

Using homogenous transformations articulated vehicles can be treated as open kinematic chains with low kinematic pairs which are in contact with the road by means of wheels. An articulated vehicle, for example a tractor with a trailer (Fig.1) is then treated as a system of four vehicle units and the equations of motion of the whole system are derived by combining the equations presented above.

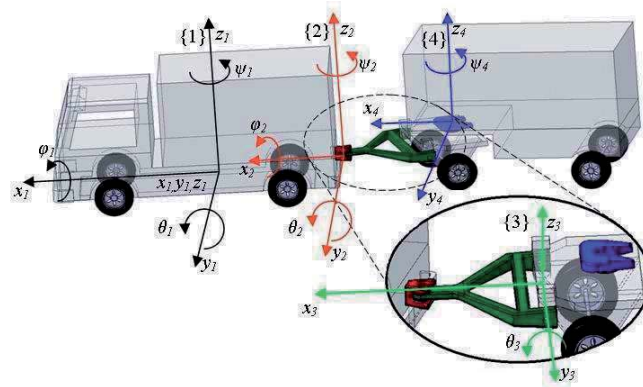


Figure 1. A truck with a trailer as a system of four units

The model enable us to consider friction in connections between the vehicle units. The influence of different models of friction on the articulated vehicle dynamics is presented in [7]. Dynamic optimisation methods are used for calibration of the model by the choice of motion and geometrical parameters describing forces between the tire and the road. The models of the vehicle have been verified by experimental measurements and those results together with the results of dynamic analysis of motion of articulated vehicles will be presented at the conference.

## References

- [1] P.Bolzern, R.M. DeSantis, A. Locatelli. An input-output linearization approach to the control of an n-body articulated vehicle. *Journal of Dynamic Systems, Measurement, and Control*, 123: 309-316, 2001.
- [2] D-H. Wu. A theoretical study of the yaw/roll motions of a multiple steering articulated vehicle. *Journal of Mechanical Engineering*, 215:1257-1265, 2001.
- [3] T. Kaneko, I.Kageyama. A study on the braking stability of articulated heavy vehicles. *JSAE Review*, 24:157-164, 2003.
- [4] M.Bouteldja, V. Cerezo. Jackknifing warning for articulated vehicles based on a detection and prediction system. *Proceedings of the 3rd International Conference on Road Safety and Simulation*, pages 14-16 Indianapolis, 2011.
- [5] X.Yang, J.Song, J. Gao. Fuzzy Logic Based Control of the Lateral Stability of Tractor Semitrailer Vehicle. *Mathematical Problems in Engineering*, doi.org/10.1155/2015/692912, 16 pages
- [6] I.Adamiec-Wójcik. *Modelling dynamics of multibody systems using homogenous transformations*. Lambert Academic Publishing, Köln, 2009.
- [7] I.Adamiec-Wójcik, J.Awrejcewicz, W.Grzegożek, S.Wojciech. Dynamics of articulated vehicles by means of multibody methods. In J. Awrejcewicz, M. Kaźmierczak, J. Mrozowski, P. Olejnik editors: *Dynamical systems: mathematical and numerical approaches*, pages 11-20, 2015.

# Tilting Child Safety Seat for Reducing the Lateral Acceleration Acting on Children when Vehicle Cornering

Nikolay Pavlov, Evgeni Sokolov

Faculty of Transport  
Technical University of Sofia  
8 Kl. Ohridski Blvd., 1000 Sofia, Bulgaria  
npavlov@tu-sofia.bg, evg\_sok@tu-sofi.bg

## Abstract

This research work studies the potential to reduce lateral acceleration acting on children when vehicle cornering. Tilting the car body in a turn is widely used in high-speed rail vehicles [6]. Vehicle body inclination when vehicle cornering is used also in small narrow vehicles [4]. Based on the theory of tilting vehicles, a multibody dynamic model of a passenger car-child safety seats system is created (Fig. 1).

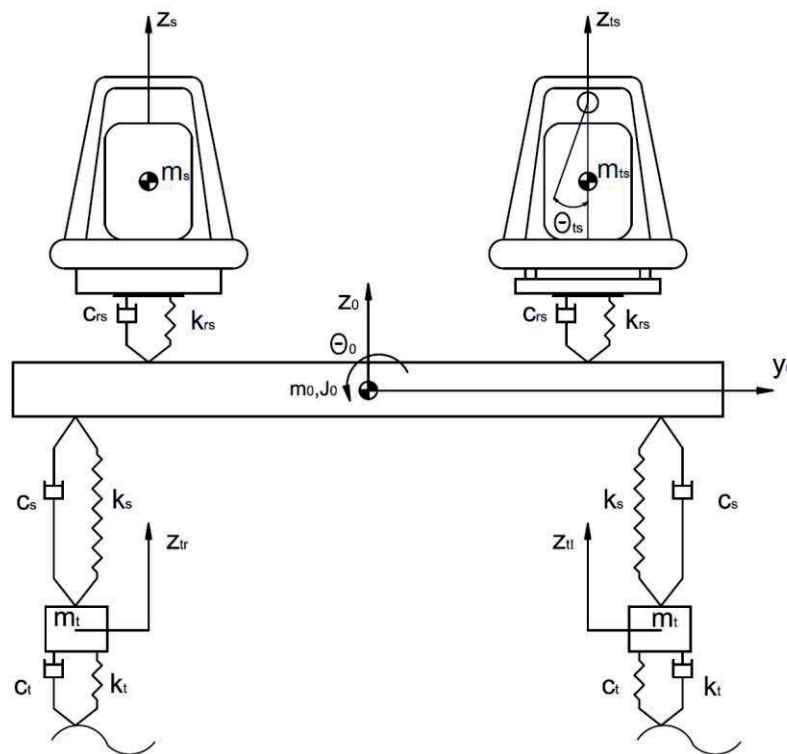


Figure 1. Multibody model of the system.

This model includes the sprung and the unsprung masses of the car, the car seat, and two child safety seats. One of them is conventionally installed on vehicle seat. The other one is mounted on special tilting frame. In this way the seat can rotate around cylindrical joint located above the mass center of the child-seat subsystem. The tilting seat can be examined as a physical pendulum [3].

The theoretical basis of the method is Lagrange equation of motion of second kind:

$$\frac{d}{dt} \left( \frac{\partial T}{\partial \dot{q}_i} \right) - \left( \frac{\partial T}{\partial q} \right) + \left( \frac{\partial \Pi}{\partial q} \right) + \left( \frac{\partial R}{\partial \dot{q}} \right) = F(t) \quad (1)$$

where  $T$  is the kinetic energy of the system,  $\Pi$  is the potential energy of the system,  $R$  is Rayleigh dissipation function,  $q_i$  are generalized coordinates and  $F(t)$  is function of disturbance.

When vehicle cornering the centrifugal force tilts the seat and the lateral acceleration acting on travelling child is reduced [2]. It will improve the ride comfort of children when travelling by car. The acceleration evaluation was performed by conducting various tests, such as double lane change maneuver [1, 5], slalom,

moving in a circle, road test on mountain roads etc. Some results obtained when system was tested on a proving ground are shown in Fig. 2.

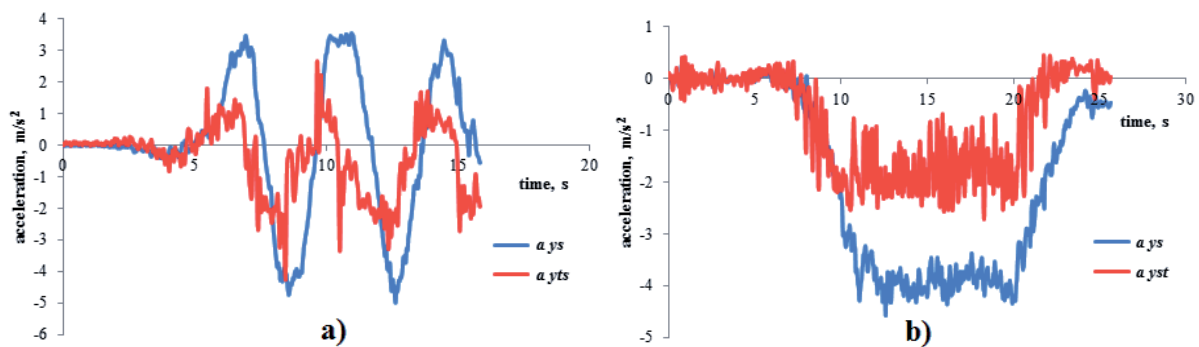


**Figure 2.** Lateral acceleration on conventional child seat ( $a_{ys}$ ) and tilting child seat ( $a_{yts}$ ) during a slalom test (a) and goes around a circle of radius 5,5 m (b). Vehicle speed is 20 km/h.

Fig. 3, a shows lateral acceleration on conventional and tilting seat when vehicle travels on mountain road, and Fig. 3, b shows their spectral densities.

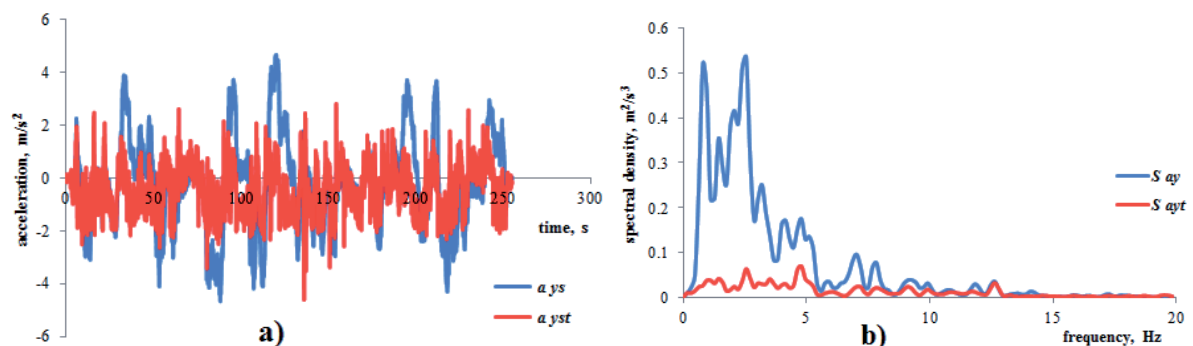


**Figure 3.** Lateral acceleration on conventional child seat ( $a_{ys}$ ) and tilting child seat ( $a_{yts}$ ) during a road experiment (a) and their spectral densities (b).

The results show that seat inclination has a significant effect on the reduction of lateral accelerations.

Finally, the multibody model is verified by comparing the calculated results with the proving ground test results.

## Acknowledgments

This research was supported by the National Science Fund of the Ministry of Education and Science of the Republic of Bulgaria [Grant No. ДМ 07/8 (December 17, 2016)].

## References

- [1] K. Reif. *Brakes, Brake Control and Driver Assistance Systems*. Springer, Wiesbaden, 2014.
- [2] M. Mauer, J. C. Gerdes, B. Lenz and H. Winner. *Autonomous Driving*. Springer, Berlin, 2016.
- [3] R. Andrzejewski and J. Awrejcewicz. *Nonlinear Dynamics of a Wheeled Vehicle*. Springer US, New York, 2005.
- [4] R. Hibbard and D. Karnopp. Twenty First Century Transportation System Solutions – a New Type of Small, Relatively Tall and Narrow Active Tilting Commuter Vehicle. *Vehicle System Dynamics*, Vol. 25, No. 5:321-347, 1996.
- [5] R. Rusev, R. Ivanov, G. Staneva and G. Kadikyanov. A Study of the Dynamic Parameters Influence over the Behavior of the Two-Section Articulated Vehicle during the Lane Change Maneuver. *Transport Problems*, Vol. 11, No. 1:29-40, 2016.
- [6] R. Persson, R. M. Goodall and K. Sasaki. Carbody Tilting – Technologies and Benefits. *Vehicle System Dynamics*, Vol. 47, No. 8:949-981, 2009.

## **Section**

# **BIOMECHANICS**



# Using Kinematic Rolling Surfaces for Fast Foot-Ground Modeling in the Forward Dynamics of Human Gait — A Sagittal Plane Analysis

Lennart Caspers<sup>1</sup>, Mario Siebler<sup>2</sup>, Harald Hefter<sup>2</sup>, Urbano LUGRÍS<sup>3</sup>, Andrés Kecskeméthy<sup>1</sup>

<sup>1</sup> Chair for Mechanics und Robotics  
University Duisburg-Essen  
Lotharstr. 1, 47057 Duisburg, Germany  
[lennart.caspers, andres.kecsekemethy]@uni-due.de

<sup>2</sup> Department of Neurology  
Heinrich-Heine University Düsseldorf  
Moorenstraße 5, 40225 Düsseldorf, Germany  
mario.siebler@mediclin.de, hoever@med.uni-duesseldorf.de

<sup>3</sup> Laboratory of Mechanical Engineering  
University of La Coruña  
15403 Ferrol, Province A Coruña, Spain  
ulugris@udc.es

## Abstract

Modeling of the foot-ground interaction is a topic of increasing interest for forward dynamics simulations of human gait, as it is essential for biofidelic and fast codes. Currently, most approaches use arrays of soft spheres or ellipsoids attached to a hind- and forefoot rigid body, interconnected by a revolute metatarsal joint, (e.g. [1], [2], [3]). This is accurate enough but (a) requires significant computational effort to find equilibrium configurations, and (b) induces superfluous high-frequency oscillations of the foot segments with respect to each other and the ground, both slowing down forward dynamics integration schemes. Recently, an alternative approach describing the rolling behavior of the foot by a surrogate disk with exponentially decaying radius as a function of foot tilt angle was presented [4], and a more or less recurrent kinematical rolling behavior of foot-ground interaction in the sagittal plane was verified in experiments for a large portion of the foot contact (see Fig. 1 (b), displaying average tilt angle over CoP progression (blue curve) and its standard deviation for 7 healthy walkers, as well as average curvature radius (red curve) and its standard deviation over CoP progression) [5]. Thus one may regard the foot-ground interaction as a higher joint from where individual motions will depart by small perturbations. This is analyzed in this paper for a simple forward dynamics period during the sagittal stance phase.

The disk-ground contact is parametrized by a virtual contact disk with exponentially decaying radius  $r(\alpha) = A(1 - e^{-C|\alpha|})$  whose rim touches the ground without slip at the immaterial contact point  $P$  (Fig. 1 (a)) [4], where  $A, C$  are shaping parameters. From this the physical rolling point (coinciding with the CoP) can be determined as follows: Let  $r^*$  be the distance of the immaterial contact point  $P$  from the footprint center  $C^*$  corresponding to  $P$  for  $\alpha = 0$ . For an infinitesimal increase  $d\alpha$ , point  $P$  progresses by  $dr^* = r' \cos \alpha d\alpha$  outwards, where  $(\cdot)' = \partial/\partial\alpha$  and  $dr^*$  is the projection of  $dr$  on the ground. The material rolling point  $\Omega$  currently having velocity zero must be at a distance  $\hat{r}^*$  from the point  $C^*$  such that the vertical velocity component  $\dot{z}_a = d\{r(\alpha) \sin \alpha\}/dt$  of the virtual disk center is equal to its vertical roll velocity component  $[\hat{r}^* - (r^* - r \cos \alpha)]\dot{\alpha}$ . Thus, one obtains

$$\hat{r}^* = r^* + r' \sin \alpha \quad , \quad \text{with} \quad r^*(\alpha) = \int_0^\alpha r'(\bar{\alpha}) \cos \bar{\alpha} d\bar{\alpha} = \frac{AC}{1+C^2} \left[ \sin \alpha e^{-C|\alpha|} + C(1 - \cos \alpha e^{-C|\alpha|}) \right] \quad . \quad (1)$$

Note that the exponential radius approach renders an explicit function for the roll distance in terms of the tilt angle  $\alpha$ , while ellipsoids require elliptic integrals for this purpose. In order to allow for more generic rolling surface shapes, a linear combination of several virtual exponential radius terms can be used such as

$$r(\alpha) = \sum_{i=1}^N A_i \left( 1 - e^{-C_i |\alpha|} \right) < \text{switch} \{ \alpha_i^* \} > \quad (2)$$

where “switch” turns on/off the individual terms depending on the angle  $\alpha_i^*$ . In the present case  $i = 1, 2$  are turned on *before*, and  $i = 3, 4$  are turned on *after* the switching angle  $\alpha^* = 0.0260$ . The other shaping parameters were chosen such that (1) curvature radius and its derivative ( $=0$ ) at  $\alpha = 0$  correspond to the average curve; (2) curvature radius and rolling distance at the interface  $\alpha^*$  match for the two pairs of exponential radius functions; and (3) the rest of the curvature progression matches as close as possible the average of measurement. The corresponding

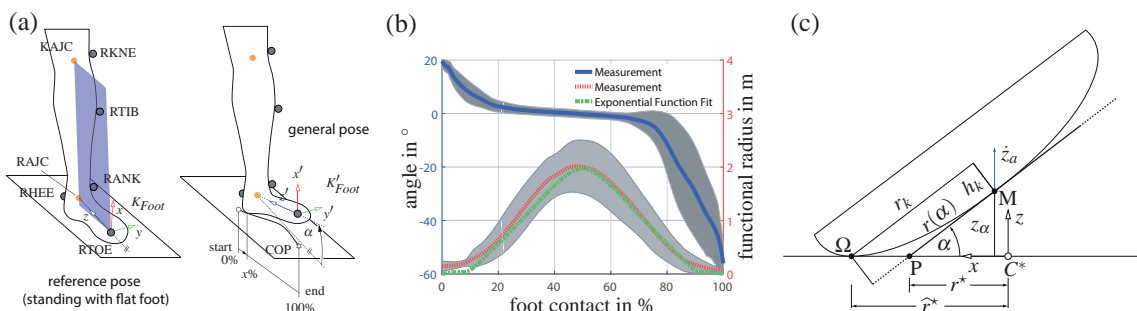


Figure 1: (a) definition of foot inclination angle  $\alpha$  and CoP progression  $x$  as percentage of total footprint length (b) experimental foot rolling results of 7 healthy walkers (c) exponential radius rolling surface in the sagittal plane.

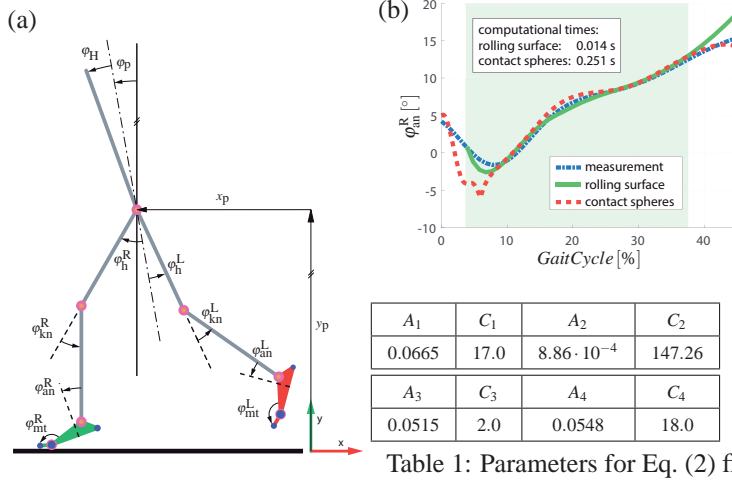


Table 1: Parameters for Eq. (2) fit

parameter	value		
$m_{total}$	65 kg	$k_{an,L}$	25.0 N/m
$\ell_{HAT}$	0.556 m	$k_{s1,heel}$	$6.5 \cdot 10^5$ N/m
$\ell_{Femur}$	0.417 m	$k_{s2,mt}$	$1.0 \cdot 10^9$ N/m
$\ell_{Tibia}$	0.435 m	$k_{s3,tip}$	$1.0 \cdot 10^9$ N/m
$\ell_{Footx}$	0.182 m	$e_{s1,heel}$	0.4
$\ell_{Footy}$	0.043 m	$e_{s2,mt}$	0.2
$\ell_{toe}$	0.05 m	$e_{s3,tip}$	0.2
$r_{s1,heel}$	0.025 m	$\mu_{st,heel}$	0.5
$r_{s2,mt}$	0.029 m	$\mu_{st,mt}$	0.9
$r_{s3,tip}$	0.023 m	$\mu_{st,tip}$	0.9

Table 2: Sphere-contact parameters

Figure 2: (a) Schematic two-dimensional multibody model from [6], (b) plot of the right ankle angle as a result of a forward dynamic simulation comparing viscoelastic spheres and virtual exponential disk with measurement data.

values are listed in Table 1, and the resulting curvature curve is shown in Fig. 1 (b) in green. Note that a fairly good fit is achieved by only nine parameters (in fact of which only 5 are independent).

Forward dynamics was analyzed for a simple two-dimensional biomechanical multibody walking model in the sagittal plane as presented in [6] (Fig. 2 (a)) using both viscoelastic spheres with Hunt-Crossley damping as in [2], and the here presented exponential rolling surface without metatarsal joints. Basic assumptions of the model were: (i) the pelvis is hinged to the inertial system via two prismatic joints ( $x_p$ ,  $y_p$ ) and one revolute joint ( $\varphi_p$ ); (ii) head and torso (HAT) are reduced to one rigid body connected by an ideal revolute joint ( $\varphi_H$ ) to the pelvis; and (iii) legs are chains of revolute joint/rigid link pairs starting at the hip-thigh joint ( $\varphi_h$ ) and followed by knee-shank, ankle-hindfoot, and metatarsal joint-forefoot ( $\varphi_{kn}$ ,  $\varphi_{an}$ ,  $\varphi_{mt}$ ). For the forward dynamics study, a real gait motion was first tracked and then a simulation with hybrid joint actuation comprising identical inputs for both models as (a) kinematically-driven (=rheonomic constraint) joints comprising  $\varphi_H$ ,  $\varphi_h$  and  $\varphi_{kn}$  for both legs as well as  $\varphi_{an}$  for the swing leg, and computed-torque controlled joints comprising  $x_p$ ,  $y_p$ ,  $\varphi_p$ ,  $\varphi_{an}$  of the stance leg, as well as both metatarsal joints for the viscoelastic sphere model. For the rolling surface case, simulation was started from the point of contact, as no impact is regarded at this point of the development. Due to the kinematical constraint, the rolling surface model has three degrees of freedom less than the viscoelastic sphere model, and the kinematics of the closed loop resulting from pelvis motion and kinematic foot rolling joint was solved numerically by Newton iterations. Fig. 2 (b) shows the resulting simulation results for the stance-foot ankle joint for the viscoelastic spheres (red dashed) and the virtual exponential disk (green solid). Compared to the measurement (blue dotted line), one can appreciate that the kinematic rolling surface model renders comparably good results — if not better — than the sphere contact between 3% and 35% of the gait phase, while performing approx. 18 times faster. The deviation after 35% is due to the missing foot contact of the opposite leg and the missing metatarsal joint torque control, which can be considered in future. This shows that modeling foot-ground contact by kinematic rolling surfaces might be an interesting alternative to soft sphere contacts for fast forward dynamics simulation of human gait.

Further work will be devoted to extend the virtual contact disk model to general spline fits, regularized impacts for foot strike, tangential compliance for soft foot pad deflection, as well as rotations also in the frontal plane.

## References

- [1] R. Pàmies-Vilà, J. M. Font-Llagunes, U. Lugrís, and J. Cuadrado, “Parameter identification method for a three-dimensional foot-ground contact model,” *Mechanism and Machine Theory*, vol. 75, pp. 107–116, 2014.
- [2] M. Millard, J. McPhee, and E. Kubica, “Multi-step forward dynamic gait simulation,” in *Multibody Dynamics*, pp. 25–43, Springer, 2009.
- [3] D. Lopes, R. Neptune, J. Ambrósio, and M. Silva, “A superellipsoid-plane model for simulating foot-ground contact during human gait,” *Computer Methods in Biomechanics and Biomedical Engineering*, vol. 19, no. 9, pp. 954–963, 2016.
- [4] A. Kecskeméthy, “Integrating efficient kinematics in biomechanics of human motions,” in *Procedia IUTAM*, (University of Waterloo, Canada), June 5–8 2011.
- [5] L. Caspers, U. Lugrís, and A. Kecskeméthy, “Foot-ground sagittal rolling behaviour during heel contact and its approximation by an exponential-curvature disk,” in *Proceedings of the IMSD*, (Montreal, Canada), May 29–June 2 2016.
- [6] P. Ferreira, F. Geu Flores, P. Flores, A. Kecskeméthy, and M. Siebler, “Modeling and analysis of an ankle-foot orthosis (AFO) using multibody methodologies,” in *Proceedings of the 5. Congresso Nacional de Biomechanica CNB2013*, (Espinho, Portugal), February 8–9 2013.

# Quantification of Intervertebral Efforts Using a Multibody Dynamics Approach: Application to Scoliosis

Gabriel Abedrabbo<sup>1</sup>, Olivier Cartiaux<sup>2</sup>, Philippe Mahaudens<sup>2</sup>, Christine Detrembleur<sup>2</sup>, Maryline Mousny<sup>2</sup>, Paul Fiset<sup>1</sup>

<sup>1</sup> Center for Research in Energy and Mechatronics (CEREM)  
Université catholique de Louvain  
Place du Levant 2, 1348  
Louvain-la-Neuve, Belgium  
gabriel.abedrabbo@uclouvain.be  
paul.fisette@uclouvain.be

<sup>2</sup> Neuro Musculo Skeletal Lab (NMSK)  
Université catholique de Louvain  
Brussels, Belgium  
maryline.mousny@uclouvain.be  
olivier.cartiaux@uclouvain.be  
philippe.mahaudens@uclouvain.be  
christine.detrembleur@uclouvain.be

## Abstract

**Context:** Spine surgery planning involves many decisions for which the surgeon has not enough information, and for which biomechanical models might be helpful. This has been illustrated by a study carried out at the École Polytechnique de Montréal [4], which shows a high variability in decision making in the planning of scoliosis surgery for an experienced group of surgeons. This variability is problematic because it could cause complications for the patient such as a revision surgery or an excessive limitation of spine mobility. Therefore, a biomechanical model for spine surgery planning might be useful in giving the surgeon sufficient information to propose the best treatment. In this context, the intervertebral efforts represent an essential input to help in the diagnosis and subsequently to guide surgical planning of scoliosis.

**Objectives:** This present research aims at developing a clinical protocol based on experimental data and on a multibody model of the upper body, to quantify the intervertebral efforts for idiopathic scoliotic adolescents in standing up position (statics) and during *moderate gait* (dynamics). The estimation of intervertebral efforts is based upon four interwoven topics: patient physiology, spine geometry, spine and pelvis kinematics and muscular forces. In line with this, to reach the final objective of this work, three targeted contributions must be achieved:

- The elaboration of a clinical protocol focusing on the assessment of the scoliotic patient parameters: necessary anthropomorphic data, spine shape and kinematics, and muscle force calibration;
- The development of a physiologically-based multibody model of the upper body, able to predict the kinematics and the dynamics of the spine during gait;
- The joint exploitation of the multibody model and of the experimental input, to allow exploring and discussing plausible solutions, in terms of internal efforts, thanks to the full potential offered by models and computer simulations.

**Methodology and illustrative Results:** As mentioned before, the accurate computation of the intervertebral efforts strongly depends on four pillars: patient physiology, geometrical identification, spine and pelvis kinematics and muscular forces inside the upper body. The proposed protocol addresses each of these problems, from both the clinical and the modeling points of view, as shown in Fig. 1.

The geometrical identification of the spine, using bi-planar X-rays, the computation of its kinematics from a limited amount of data and the impact of the patient physiology of the patient have been addressed in previous studies: [1],[3] and [2] respectively.

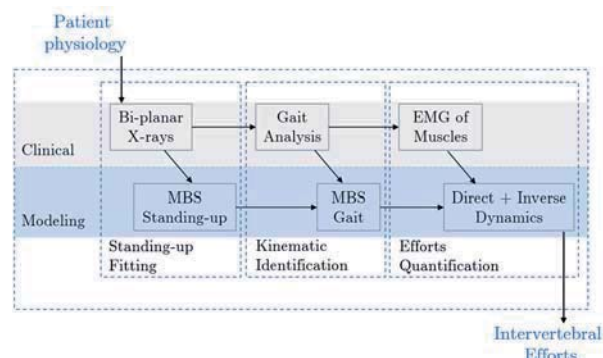


**Figure 1.** The general protocol is based on both clinical and modeling processes

The present contribution focuses on a global analysis of the protocol developed for this study for which a special attention will be paid to the computation of the muscular forces and the intervertebral efforts.

The model used includes 6 muscles representing the abdominal and back muscles groups (Fig.2-right). The muscular forces are estimated through its activation measured by EMGs. The correlation between the forces and activation was established via the David Back protocol (Fig. 2-left).

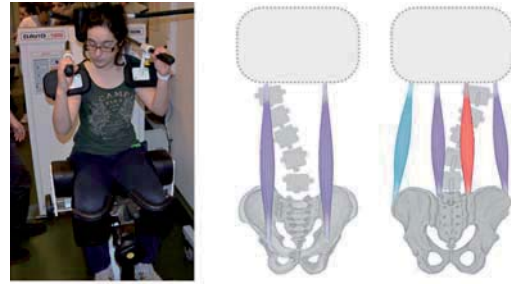


**Figure 2.** Muscular forces estimation: EMG calibration (left) and muscular activation (right). High activation in red, middle activation in purple and no activation in blue

An illustrative result obtained from our biomechanical model of the spine is shown in Fig. 3. It reveals the dynamic impact of the gait, by showing a significantly higher intervertebral —normal and shear— forces than in a standing up position (up to 125% higher).

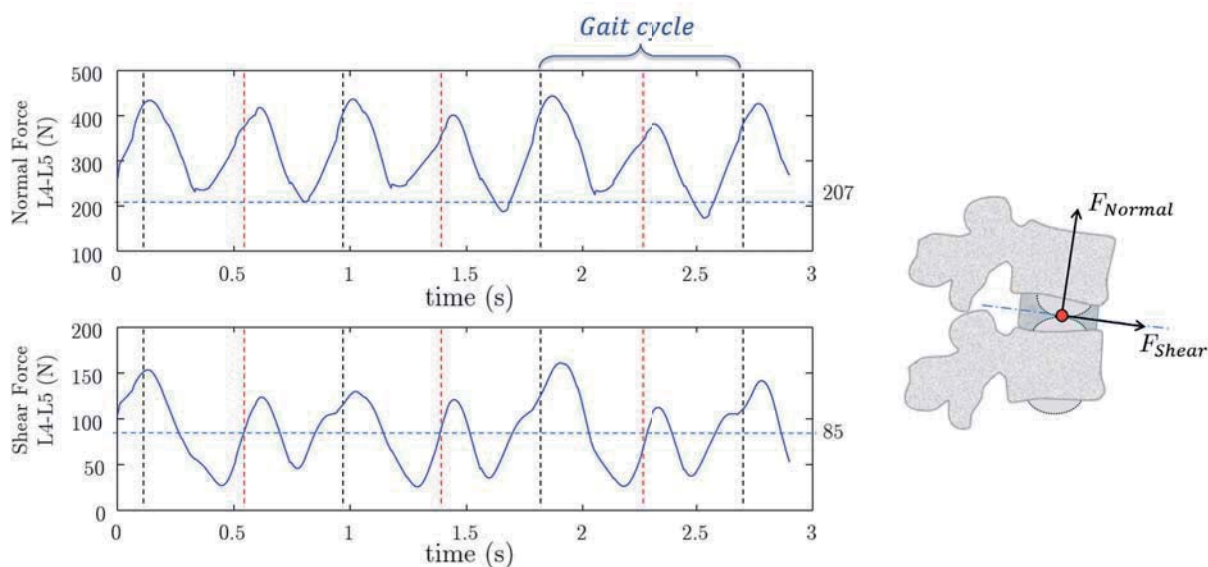


**Figure 3.** Dynamic intervertebral forces inside L5-S1: normal force (up) and shear force (down). The horizontal dotted line represents the intervertebral force for standing up position (Static). The vertical lines refers to the double stance phase of the gait cycle

## References

- [1] G. Abedrabbo, P. A. Absil, P. Mahaudens, C. Detrembleur, M. Raison, M. Mousny, and P. Fisette. A multibody-based approach to the computation of spine intervertebral motions in scoliotic patients. In *2nd Jt. Int. Conf. Multibody Syst. Dyn. May 29-June 1, Stuttgart, Ger., 2012*.
- [2] G. Abedrabbo, O. Cartiaux, P. Mahaudens, C. Detrembleur, and P. Fisette. Dynamic Analysis of the Spine : Impact of the Internal Organs Wobbling Motion During Gait. In *ECCOMAS Them. Conf. Multibody Dyn.*, pages 2–3, Barcelona, 2015.
- [3] G. Abedrabbo, M. Raison, P. Mahaudens, C. Detrembleur, M. Mousny, O. Cartiaux, and P. Fisette. Kinematic Identification of the Spine : a Multibody Approach. In *3rd Jt. Int. Conf. Multibody Syst. Dyn. 7th Asian Conf. Multibody Dyn. June 30-July 3, 2014, BEXCO, Busan, Korea*.
- [4] M. Robitaille, C. E. Aubin, and H. Labelle. Intra and interobserver variability of preoperative planning for surgical instrumentation in adolescent idiopathic scoliosis. *Eur. Spine J.*, 16(10):1604–1614, 2007.

# Influence of the Side Branches of the Human Vocal Tract on the Voice Quality

Tomáš Vampola<sup>1</sup>, Jaromír Horáček<sup>2</sup>

<sup>1</sup>CTU in Prague, Dept. of Mechanics,  
 Biomechanics and Mechatronics,  
 Technická 4, 166 07 Prague 6,  
 Czech Republic  
 Tomas.Vampola@fs.cvut.cz

<sup>2</sup>Institute of Thermomechanics,  
 Academy of Science of the Czech  
 Republic, Dolejškova 5, 182 00,  
 Prague 8, Czech Republic  
 JaromirH@it.cas.cz

## Abstract

The side branches of the human vocal tract exhibit antiresonance and resonance properties in the human voice frequency spectrum which influence the voice quality. This study investigates the possibility of these specific resonances to contribute to the speaker's formant cluster around 3-5 kHz. A reduced finite element (FE) models were created which allows numerical simulation of the effects of changing the parallel cavities on the acoustic resonance and antiresonance characteristics of the vocal tract. These models, created from an accurate three-dimensional (3D) FE models of the human vocal tract for vowel [a:,i:,u:], are computationally-effective and allows parametric changes of the parallel cavities continuously within the physiologic range. These changes are expected to play a role in voice therapy and operatic singing. While the influence of the geometric configuration of the main channel of the vocal tract on the vocal output has been studied rather extensively, the influence of side cavities of human vocal tract, has received less attention. Generally, these cavities have been reported to cause antiresonances in the resulting vocal spectrum, i.e., largely decreasing radiation of some of the spectral frequencies out of the mouth, particularly those around 4~--~5~kHz [1,4,5,6]. As such, their role for the resulting vocal intensity may be considered undesirable, since it contradicts the general goal of enhancing vocal output with the smallest vocal effort. However, newest studies with perceptual evaluations of sounds produced using 3D mathematical and physical models of the singers' vocal tracts revealed that the voice quality is perceived as being better when side branches are present. Furthermore, spectral analysis of singers indicates that the formant structure around 3-5 kHz is more complex than usually expected. A more detailed analysis shows that besides the antiresonances there are also new resonances which occur due to these side cavities. The sophisticated accurate 3D FE models of the vocal tract for vowels [a:,i:,u:] were created from the CT snaps. Their using for investigating the effect of vocal tract shape modifications on the changes in acoustic resonance properties is time consuming. Therefore the reduced FE models were created including all the dominant parallel cavities and their resonance and antiresonance frequencies were tuned to correspond to those of the full FE model. These reduced models were then used for analyzing the antiresonances, resonances and the pressure transfer function of the vocal tract. The accuracy of the results obtained using the reduced models were examined by comparing these to the results obtained with the full 3D FE model [2].

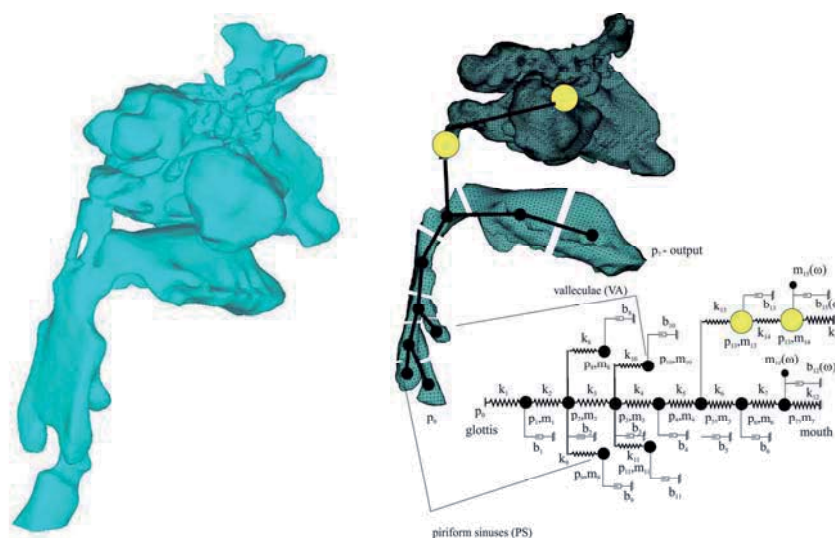


**Figure 1.** Volume model of the human vocal tract for vowel/a:/ (left). Simplified computational model of the human vocal tract for vowel/a:/ (right).

Based on the numerical analyzes can be concluded that the parallel cavities (without nasal cavity) influenced the voice quality for the vowels [a:,i:,u:] by different mechanism. For vowel [a:,u:] is most important the increasing of the parallel cavities near the human vocal fold. On the contrary for vowels [i:] are the phonation characteristics influenced most by the parallel cavities near the tonsils [2].

Velopharyngeal insufficiency (VPI) is an insufficient closing of nasal cavity (nasopharynx) and its airproof separation from the oral cavity (oropharynx). VPI leads to open nasality (rhinolalia aperta) affecting all oral speech sounds that should not be nasal. Small defects of the velopharyngeal closure become evident first by a different timber of the voice, bigger defects influence formant structure of vowels. The results for numerically simulated sound response of the human vocal tract for vowels /i:/ show considerable influence of VPI connecting the acoustic spaces of the vocal and nasal tracts of the FE models on phonation. In contrary, the influence of VPI on the acoustic pressure response for vowel /a:/ is smaller. This is in the qualitative agreement with the clinical acoustic data on velopharyngeal insufficiency. From presented results can be concluded, that for prediction of the voice quality is necessary correctly model the nasal cavities.

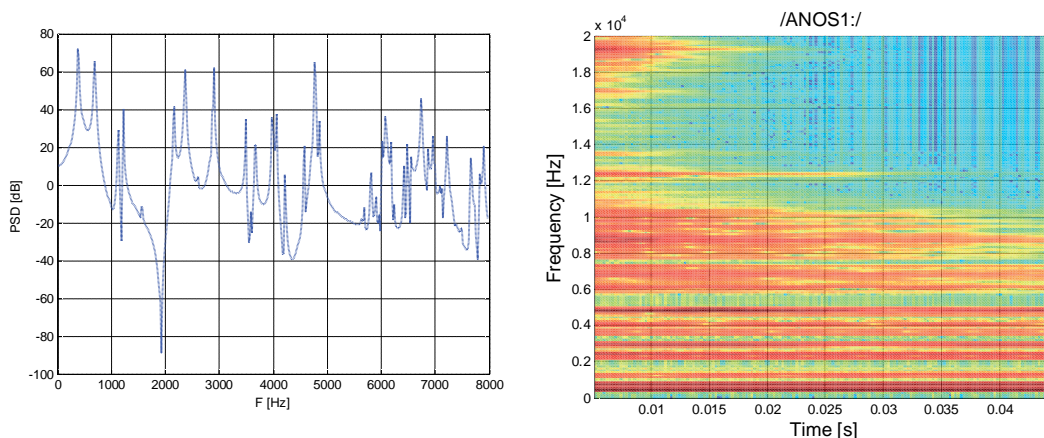


**Figure 2.** Acoustic pressure response computed at the lips (left), spectrogram of the computed acoustic pressure of the lips using the simplified model with VPI harmonically excited (right).

## Acknowledgments

The research is supported by the Grant Agency of the Czech Republic by project **No 16 01246S** Computational and experimental modelling of self-induced vibrations of vocal folds and influence of their impairments on human voice.

## References

- [1] J. Dang, K. Honda, "Acoustic characteristics of the piriform fossa in models and humans," *Journal of the Acoustical Society of America*, vol. 101, pp. 456-465, 1997.
- [2] T. Vampola, J. Horáček, J. G. Švec, "Modeling the influence of piriform sinuses and valleculae on the vocal tract resonances and antiresonances," *Acta Acustica United With Acustica*, vol. 101, pp. 594-602, 2015.
- [3] T. Vampola, J. Horáček, J. Vokřál, et al. "FE modeling of human vocal tract acoustics. Part II: Influence of velopharyngeal insufficiency on phonation of vowels," *Acta Acustica United With Acustica*, vol. 94, pp. 448 - 460, 2008.
- [4] K. Motoki, "Three-dimensional acoustic field in vocal tract," *Acoustical Science and Technology*, vol. 23, pp. 207-212, 2002.
- [5] S. Fujita, K. Honda, "An experimental study of acoustic characteristics of hypopharyngeal cavities using vocal tract solid models," *Acoustical Science and Technology*, vol. 26, pp. 353-357, 2005.
- [6] H. Takemoto, S. Adach, T. Kitamura, P. Mokhtari, K. Honda, "Acoustic roles of the laryngeal cavity in vocal tract resonance", *Journal of the Acoustical Society of America*, vol. 120, pp. 2228-2238, 2006.

# Validating Subject Multibody Dynamics Estimated Action with Measured sEMG at Lower Limb Muscles on different Gait modes

Carlos Rodrigues<sup>1</sup>, Miguel Correia<sup>2</sup>, João Abrantes<sup>3</sup>

<sup>1</sup>Centre for Biomedical Engineering Research  
Technology & Science Associate Laboratory  
R. Dr. Roberto Frias, 4200 - 465 Porto,  
Portugal  
carlos.b.rodrigues@inesctec.pt

<sup>2</sup>Faculty of Engineering  
University of Porto  
R. Dr. Roberto Frias, 4200-464 Porto,  
Portugal  
mcorreia@fe.up.pt

<sup>3</sup>MovLab – Interactions and Interfaces Lab  
Lusófona University of Humanities and Technologies  
Campo Grande 376, 1749-024 Lisboa, Portugal  
joao.mcs.abrantes@ulusofona.pt

## Introduction

Multibody dynamics (MBD) presents as a powerful tool for musculoskeletal model and neuromuscular control study towards decision support for prevention, diagnosis and treatment planning of specific subject skeletal and neuromuscular diseases, with large cost saving, subject comfort and intervention optimization [1]. Nevertheless kinematic and kinetic input data of human movement must be accurate and the employed model for simulation must be personalized to subject, task and moment of application. Also the results provided by the simulation with the musculoskeletal model must be compared with measured results for validation. Given the difficulty of direct measurement of internal actions, forces and force moments under natural conditions of movement, comparing estimated muscle actions by MBD with measured surface electromyography (sEMG) on different gait modes can provide assessment of model estimation.

The objective of this study is to compare estimated muscle actions by MBD with measured sEMG of selected muscles on different adopted gait modes, stiff knee gait (SKG) and slow running (SR) in relation to those registered at normal gait (NG). The scientific contribution of this work is to assess at the neural sEMG level registered differences at dynamic and kinematic operational level during NG, SKG and SR.

## Methods

Kinematic, kinetic and selected sEMG were collected at motion capture laboratory for one male subject (70 kg mass and 1.86 m height) during normal gait at comfortable auto-selected velocity, stiff knee gait with lower knee flexion and slow running at minimum velocity to ensure time period with both feet off the ground. Simultaneous recordings of ground reaction forces, skin markers attached to the lower extremity and sEMG were obtained with two AMTI force plates sampling at 2000 Hz, eight camera Qualisys system at 100 Hz and Noraxon wireless system at 2000 Hz. Marker protocol used for analysis at musculoskeletal model includes right and left anterior superior iliac spines, thigh superior, knee medial, knee lateral, shank superior, ankle medial, ankle lateral and toes. sEMG was recorded for soleus medialis (SM) and tibialis anterior (TA) of the subject's right leg and normalized to dynamic maximum voluntary contraction with counter movement jump for SM and right leg swing for TA. Musculoskeletal analysis was performed using AnyGait v. 0.92 set up for the experimental setup, starting with generation of stick-figure model based on a static trial, over-determinate kinematic analysis over the dynamic trial and joint angles, morphing Twente Lower Extremity Model (TLEM) to match the size and joint morphology of the stick-figure model for inverse dynamic analysis based on joint angles and kinetic boundary conditions. The outputs from the musculoskeletal model during one complete stride of NG, SKG and SR were assessed, namely ground reaction forces, computed joint angles, angular velocities and accelerations, joint moments, joint reaction forces, estimated muscle activities and processed sEMG for comparing different dynamic trials. AnyGait was set up to produce output using polynomial muscle recruitment criterion of power 3 and recorded sEMG was band-pass filtered at 10 Hz and 400 Hz, rectified and low-pass filtered at 6 Hz [2].

MBD estimated muscle activities and processed sEMG were obtained under the same conditions of joint angle, angular velocity and acceleration for all-time instants at each gait mode. Thus, despite different nature of estimated muscle activities and processed sEMG, these signals can be compared for the same time instant of the same movement performed by the same subject under the same conditions of joint angles, angular velocities and accelerations, to assess model validity. To overcome subjectivity of qualitative comparisons it was implemented alternative metrics to reproduce in a quantitative and objective way the interpretation of model results when compared to EMG activity patterns. For this purpose the shape of the wave form (magnitude) and time-of-arrival (phase) of both MBD predicted muscle activities and processed sEMG are quantified separately for magnitude (M) and phase (P) differences detection and combined (C) into a single metric for global agreement detection [3].

## Results

According to assessed results, ground reaction forces present typical characteristics of the ground contact type, with two maximum vertical values of lower magnitudes approximately 880 N and 770 N for gait trial, 680 N and 750 N for stiff knee gait and a single peak value with higher magnitude around 1600 N for slow running. Hip joint reaction forces follow the characteristic of the ground contact force, with two maximum vertical values of lower magnitudes 2700 N and 4400 N for gait trial and a 2400 N ripple and 3600 N for stiff knee gait with a single peak value of higher magnitude 6400 N for slow running. Knee joint reaction forces follow the characteristic of the ground contact force, with two maximum vertical values of lower magnitudes 3500 N and 4250 N for gait trial, a 1400 N ripple and a peak at 4500 N for stiff knee gait, with a single peak value of higher magnitude 12000 N for slow running. The 1400 N ripple at the stiff knee gait fading the first peak, approaching its profile to the slow running with the value of 12000 N peak force, far greater than all other maximum joint reaction forces. Ankle joint forces presents two local maximum around 3000 N and 6100 N for gait trial, with first local maximum fading around 2000 N and absolute maximum value 6000 N at stiff knee gait, with only one maximum value 14500 N for slow running.

Slow running presents higher joint knee angles, angular velocities and angular accelerations with maximum values 1.5 rad, 7.5 rad/s and 150 rad/s<sup>2</sup> than gait trial with maximum values 1.06 rad, 6 rad/s and 122 rad/s<sup>2</sup> as well as stiff knee gait with 0.7 rad, 4.8 rad/s, 55 rad/s<sup>2</sup>. Slow running presents higher ankle joint plantar flexion force moment with maximum value 240 Nm than gait trial with maximum value 124 Nm and stiff knee gait with 120 Nm. Gait trial presents higher maximum hip joint flexion force moment 77 Nm than at stiff knee gait trial with 70 Nm and slow running with 44 Nm.

The results from quantitative metric, Table 1, present better agreement between processed sEMG and MBD muscle estimated activity on P than on M, with better agreement on M for SM than TA at NG and SKG and the opposite at SR. Better combined agreement between SM processed sEMG and MBD muscle estimated activity for NG and SKG than at SR points to higher ability of the model to predict SM force patterns in agreement with EMG activity patterns at NG and SKG than at SR, with similar ability for prediction of TA on NG, SKG and SR.

**Table 1.** Metric values of magnitude, phase and combined differences between process sEMG and MBD muscle estimated activity for normal gait and stiff knee gait than at slow running

<i>Gait / Muscle</i>	<i>Magnitude (M)</i>	<i>Phase (P)</i>	<i>Combined (C)</i>
NG TA	-0.63	0.28	0.69
NG SM	-0.43	0.29	0.52
SKG TA	-0.65	0.30	0.72
SK SM	-0.45	0.26	0.53
SR TA	-0.47	0.36	0.59
SR SM	2.08	0.37	2.12

## Discussion and conclusion

MBD estimated muscle activities compares well with processed sEMG for each considered gait mode, namely on antagonist character of tibialis anterior and soleus muscle, featured by their activities and time instants of activation and inactivation at MBD predicted muscle activities and processed sEMG. Despite estimated muscle actions with MBD and measured sEMG express different physical quantities, these were obtained under the same conditions, thus minimizing the error on acquisition and comparing under dynamic conditions. MBD estimated muscle activities presents as a powerful alternative when sEMG is not viable and sEMG as a tool for MBD validation, with quantitative metrics of phase and magnitude contributing to overcome qualitative comparisons.

## References

- [1] A. Erdemir, S. McLean, W. Herzog and A.J. van den Bogert. Model-based estimation of muscle forces exerted during movements. *Clinical Biomechanics*, 22:131-154, 2007.
- [2] J. Rasmussen, M. de Zee and M.S. Andersen. *Assignment for the course in musculoskeletal modeling by multibody biomechanics*. Aalborg University: Dep. of Mechanical and Manufacturing Engineering, 2012.
- [3] L. E. Schwer. Validation metrics for response histories: perspectives and case studies. *Engineering with Computers*, 23(4): 295-309, 2007.

## What is sit-to-stand without a chair?

Valerie Norman-Gerum, John McPhee

Systems Design Engineering  
 University of Waterloo  
 200 University Ave W, N2L3G1 Waterloo, Canada  
 [vtgerum, mcphee]@uwaterloo.ca

### Abstract

To answer the title question, sit-to-stand without a chair is falling down – more on that later. And what is the result of predictive sit-to-stand simulation without an appropriate model of seat-chair contact? It cannot be expected to be natural sit-to-stand. Predictive simulation of activities of daily living, sit-to-stand included, are key to the discussion of why people move the way they do, understanding pathological motion and assessing interventions in silico. The predictions are sensitive to the model. In the case of sit-to-stand, between 18 and 77 percent of body weight is initially supported at the seat [1], and contact continues for the first thirty-four percent of the motion [2]. Thus, the model of seat-chair contact deserves attention. The goal of this work is to describe the vertical component of a seat-chair contact model appropriate for use in predictive simulation of sit-to-stand.

The buttocks to be modelled are transverse gluteus material, deep to adipose tissue, with a superficial layer of skin. The constitutive behaviour is commonly described as visco-hyperelastic. However, there is a void of information in the literature regarding the mechanical properties of soft biological tissues [3] from which this seat-chair model could benefit. In the least, a reasonable model for this application ought to be computationally inexpensive and produce physiological ranges and profiles of force for a typical sit-to-stand motion.

Previous predictive sit-to-stand research has modelled seat-chair contact using a Kelvin-Voigt model, rigid contact, or by omitting the chair entirely. The validity of these models has not been tested and the strategies have not been compared. When they are critiqued using the criterion above, that forces produced from normative sit-to-stand be physiological, none of these models meet the mark. Omission of a chair assumes an initial pose with the centre of mass well behind the base of support and a net joint moment demand to the ankles well in excess of their strength [4]. As you would if the chair were pulled out from under you, the appropriate response of a model seated without a chair is to fall down. Rigid contact models restrict the motion of the lower extremities in ways that are incongruous with experimentally observed sit-to-stand and the transitions at seat-off, the instant that contact is lost between buttock and chair, lead to discontinuities in force profiles and unachievable spikes in net joint moment profiles. The one constitutive model of seat-chair contact used in predictive simulation of sit-to-stand employs an exponential spring and linear damper Kelvin-Voigt element [5]. Still, as defined, all possible equilibrium positions for the spring render the element practically ineffective, implausibly sticky, or both. The evidence is clear that notions of omitting the chair from the model, or assuming rigid contact must be discarded. What is left is to take the cue from the material behaviour and small successes of the Kelvin-Voigt element and search for an appropriate lumped parameter, force-deformation model of seat-chair interaction.

Models of muscle and fat tissues used in other applications have represented the elastic behaviour as linear, exponential, and hyperelastic as characterized by neo-Hookean, Mooney-Rivlin, and Ogden strain energy functions. Incompressibility and uniaxial loading was assumed in order to describe point-to-point contact. The resulting constitutive equations are shown in Table 1.

**Table 1.** Constitutive relations assessed

<i>spring model</i>	<i>equation</i>	<i>number of parameters</i>
Linear	$F = -k_1 x$	1
Exponential	$F = -k_2 \lambda^{k_3}  x $	2
Neo-Hookean	$F = -1/2 (k_4 (\sqrt{(1/\lambda) - \lambda}))/\lambda$	1
Mooney-Rivlin	$F = -1/2 (k_6 \lambda^2 \sqrt{(1/\lambda) + k_5 \lambda \sqrt{(1/\lambda) - k_5 \lambda^2 - k_6}})/\lambda^2$	2
Ogden	$F = - (k_7 ((1/\lambda)^{(k_8/2)} - \lambda^{(k_8)}))/\lambda$	2

where  $k_s$  are material constants,  $x$  is the relative vertical displacement of the ischial tuberosity, and  $\lambda$  is the principal stretch.

These equations are used to describe the force developed in the spring of the Kelvin-Voigt element under deformation. Bounds are imposed on the force developed in the damper to allow the buttock to lift from the chair at seat-off. In the hyperelastic material models, where force is a function of stretch rather than position, an additional parameter was included to allow limited tuning to the vertical location of the ischial tuberosities, or sitting bones, from the mapped location on account of typical human variability. The best model will return the most plausible force profile when driven with typical sit-to-stand kinematics.

An experiment was used to determine these kinematics and kinetics. One participant performed sit-to-stand four times while in a motion capture suit with force plates below the feet and the chair as in Figure 1a. Data was collected at 120Hz and filtered using a dual-pass Butterworth filter with a cutoff frequency of 6Hz. Each trial was analysed for sit-to-stand event markers and was found characteristic of normative sit-to-stand. Sit-to-seat-off was then extracted from the series of data to be analyzed.

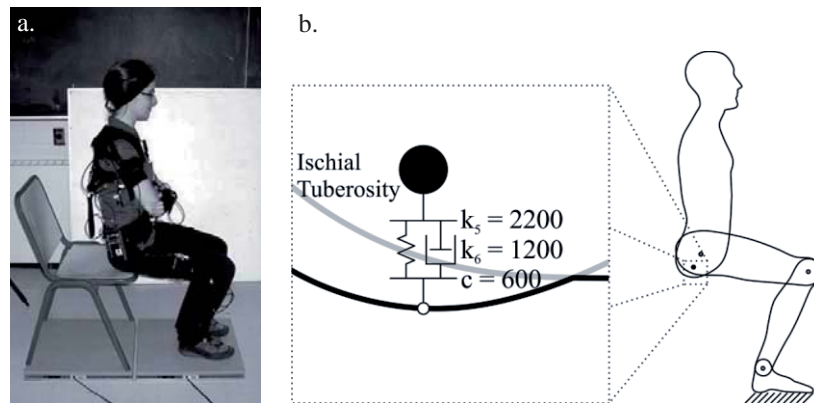


**Figure 1.** Sit-to-stand a. experiment and b. seat-chair model.

An optimization scheme was defined to identify best parameters for each model based on the experimental data collected in 3 of the 4 trials. Experimental ischial tuberosity movement was input and the forces calculated were compared to experimentally collected data in a least squares sense. The remaining error was compared across models. The Kelvin-Voigt model using the exponential spring was the poorest performer, although it met the most basic criterion of producing a reasonable force profile for sit-to-stand. The remaining models had improved performance and were comparable except for the one using a Mooney-Rivlin spring, which produced a force profile slightly closer to the experiment. To test for repeatability, the models with their best parameters were implemented using the data of the 4th trial and again the Kelvin-Voigt element with Mooney-Rivlin spring performed best. This model, including parameters, is shown in Figure 1b.

It is recommended, for this participant at least, that the Mooney Rivlin spring is used in the Kelvin-Voigt model of seat-chair interaction. It is a hyper-viscoelastic model, characteristic of the tissues of the buttocks, and when tested in kinematics typical of sit-to-stand, has provided continuous forces of physiological magnitude, most similar to those observed from experiment.

## Acknowledgments

This work was funded by the Natural Sciences and Engineering Research Council of Canada (NSERC) and Canada Research Chairs Program (CRCP).

## References

- [1] C.W.J. Oomens. Can Loaded Interface Characteristics Influence Strain Distributions in Muscle Adjacent to Bony Prominences? *Computer Methods in Biomechanics and Biomedical Engineering*, 6:171-180, 2003.
- [2] A. Kraij. Analysis of standing up and sitting down in humans: definitions and normative data presentation. *Journal of Biomechanics*, 23:1123-1138, 1990.
- [3] C.W.J Oomens. Mechanical Behavior and Properties of Adipose Tissue. In A. Gefen and D. Benayahu, editors, *The Mechanobiology of Obesity and Related Diseases*, pages 3-9. Springer-Verlag Berlin Heidelberg, 2015.
- [4] A.B. Schultz. Biomechanical analyses of rising from a chair. *Journal of Biomechanics*, 25:1383-1391, 1992.
- [5] B.A. Garner. *A dynamic musculoskeletal computer model for rising from a squatting or sitting position*. University of Texas at Austin, 1992.

# A Human Mannequin Head-and-Neck Multibody Model for the Simulation of High-Speed Impacts

Francisco González<sup>1</sup>, Urbano Lugrís<sup>1</sup>, Javier Cuadrado<sup>1</sup>,  
Marcos Rodríguez-Millán<sup>2</sup>, María Henar Miguélez<sup>2</sup>

<sup>1</sup>Laboratorio de Ingeniería Mecánica  
University of La Coruña  
Mendizábal s/n, 15403 Ferrol, Spain  
[f.gonzalez, ulugris]@udc.es, javicua@cdf.udc.es

<sup>2</sup>Department of Mechanical Engineering  
Universidad Carlos III de Madrid  
Av. Universidad 30, 28911 Leganés, Madrid, Spain  
[mrmillan, mhmiguel]@ing.uc3m.es

## Abstract

Helmets and body armours are often employed to decrease the occurrence of head- and torso-perforating injuries caused by ballistic projectiles, shrapnel, and other objects propelled by blast. However, even when these devices successfully defeat projectiles the user may still undergo Behind Armour Blunt Trauma (BABT) [1]. The effects of BABT on the human body are currently the subject of a number of research studies [2]; typical injuries range from skin laceration to bone fractures and contusions to internal organs. As a consequence, BABT need be considered during the development of personal protective armour components [3, 4].

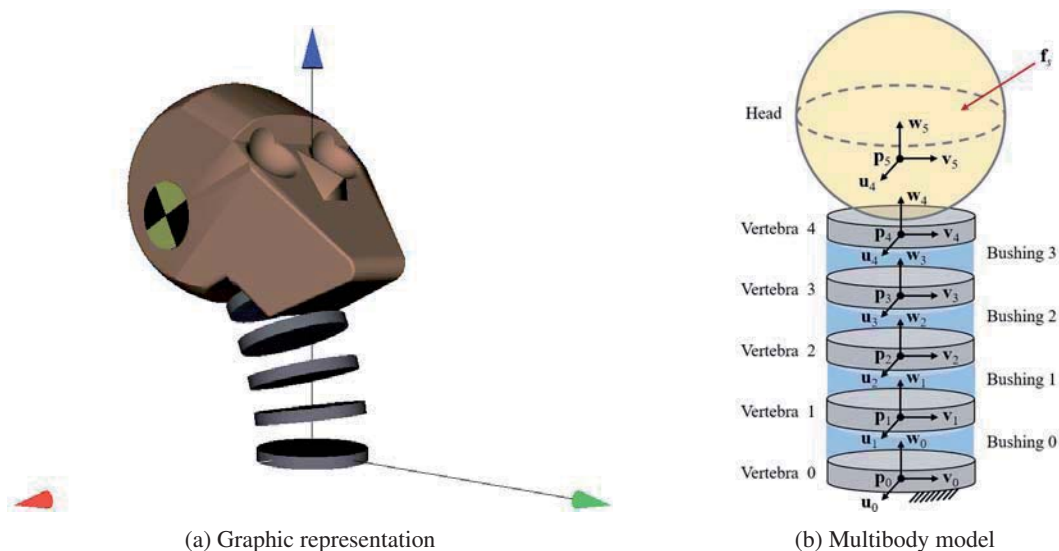
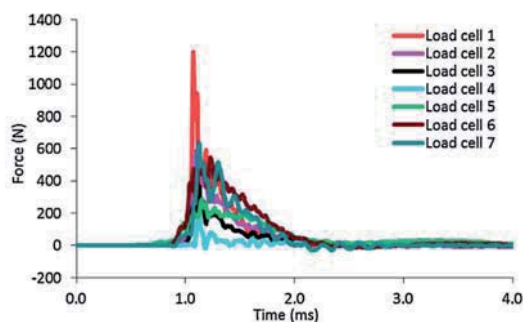


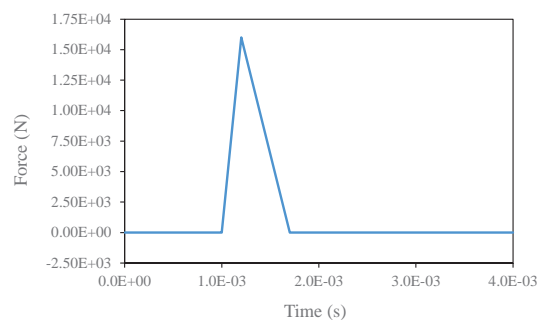
Figure 1: Computational model of the Hybrid III Dummy.

In this work we studied the effects of bullet impacts on subjects that wear protection helmets in order to predict their likelihood to suffer BABT. It was assumed that the helmet was able to defeat the bullet in all cases, so the head would not suffer any perforating injuries. However, the impact energy would still be transmitted to the subject, introducing significant accelerations in the system and giving rise to reaction efforts in the neck; these must be evaluated to determine up to what extent they may result in BABT. A computational multibody model of the head and neck of a Hybrid-III Dummy, shown in Fig. 1, was developed to this end. The model was formulated using natural coordinates; one point and three unit vectors were used to describe the motion of each body in the system. The vertebrae were connected by nonlinear bushings that allowed for relative three-dimensional motion between them. Each bushing was modelled as a six degree-of-freedom, linear elastic beam with bending-shear coupling and variable stiffness and damping properties. The head was pinned to the last vertebra via a revolute joint and a torsional spring. Bullet impacts were modelled with a set of time-varying forces  $\mathbf{f}_s$ . The number, location, and time history of these forces were adjusted to represent different impact scenarios that involved various types of ammunition and protective equipment. These forces can reach a peak value of up to 20 kN and typically have a rise period in the order of a tenth of a millisecond, while the total bullet energy is transmitted to the system in less than 3 ms [3]. Such force properties resulted in the need to use integration schemes with step-sizes in the order of  $10^{-6}$  s.

The forward-dynamics simulation of the bullet impacts and the subsequent dummy motion was carried out with several multibody formulations. Augmented Lagrangian and Hamiltonian algorithms were selected, as they have been proven to be efficient and robust and able to deal with impact forces and system discontinuities [5]. Their performance was tested in combination with explicit and implicit numerical integrators, namely the symplectic



(a) Experimental sample reported in [3]



(b) Force profile used in simulation

Figure 2: Time history of the forces transmitted from the helmet to the head during a bullet impact.

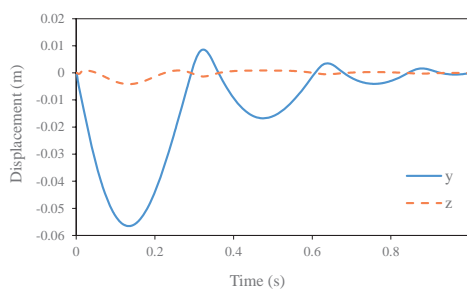


Figure 3: Displacement of the head COM during simulation.

Euler formula and the Newmark method. In the case of the implicit integrator, both fixed-point and Newton-Raphson iterative schemes were evaluated. These methods were implemented and compared in terms of efficiency, accuracy, and robustness using mbsLab, a C++ multibody system dynamics library developed at LIM [6].

In a preliminary set of numerical experiments, the impact force was modelled following the profile shown in Fig. 2b, which featured the same peak value, rising time, and impulse as experimental values reported in the literature. The asymmetric behaviour of the neck during flexion and extension was represented using a different bushing stiffness for each of these motions. The physical parameters of the bushings, including their stiffness and damping, will be adjusted in the near future with experimental data. All the tested methods delivered similar system motions, Fig. 3, successfully carrying out the integration with step-sizes larger than  $h = 4 \cdot 10^{-6}$  s.

### Acknowledgments

The authors acknowledge the financial support of the Ministry of Economy and Competitiveness of Spain and the ERDF (FEDER) program under Project RTC-2015-3887-8 and the post-doctoral research program Juan de la Cierva, contract No. JCI-2012-12376.

### References

- [1] L. Cannon. Behind Armour Blunt Trauma - An emerging problem, *Journal of the Royal Army Medical Corps*, 147 (1): 87–96, 2001.
- [2] D. J. Carr, I. Horsfall, C. Malbon. Is behind armour blunt trauma a real threat to users of body armour? A systematic review, *Journal of the Royal Army Medical Corps*, 162 (8): 8–11, 2016.
- [3] F. A. Pintar, M. M. G. M. Philippens, J. Zhang, N. Yoganandan. Methodology to determine skull bone and brain responses from ballistic helmet-to-head contact loading using experiments and finite element analysis, *Medical Engineering & Physics*, 35 (11): 1682–1687, 2013.
- [4] Y. Wen, C. Xu, S. Wang, R. C. Batra. Analysis of behind the armor ballistic trauma, *Journal of the Mechanical Behavior of Biomedical Materials*, 45: 11–21, 2015.
- [5] F. González, D. Dopico, R. Pastorino, J. Cuadrado. Behaviour of augmented Lagrangian and Hamiltonian methods for multibody dynamics in the proximity of singular configurations, *Nonlinear Dynamics*, 85(3): 1491–1508, 2016.
- [6] M. González, F. González, D. Dopico, A. Luaces. On the effect of linear Algebra implementations in real-time multibody system dynamics, *Computational Mechanics*, 41(4): 607–615, 2008.

# Multibody Biomechanical Analysis of Taekwondo Athletes

Giovanni Gerardo Muscolo, Darwin Caldwell, Ferdinando Cannella

Istituto Italiano di Tecnologia (IIT)  
Advanced Robotics Line  
Via Morego, 30, 16163, Genova, Italy  
[giovanni.muscolo, darwin.caldwell,  
ferdinando.cannella]@iit.it

## Abstract

This paper presents a multibody analysis of a standardized taekwondo athlete during execution of two kicks: 1) roundhouse kick performed with the rear foot (see Fig.1); 2) 360 roundhouse kick performed with the frontal foot (see Fig.1). 360 roundhouse kick (or also known as turning kick) is composed of a jumping rotation of 360 degrees around rotation axis (which colligates a point on the center of the head and the sacrum) before execution of the roundhouse kick. The objectives of this research are twofold: 1) to model a taekwondo athlete with a multibody analysis in order to understand the biomechanical behavior of the athlete and to optimize the jumping technics and the acceleration of the kick; 2) to analyze the multibody biomechanical behavior of taekwondo athletes in order to optimize ICT technology in fight tournaments.

The World Taekwondo Federation (WTF) [1] was founded in 1973. Taekwondo is one of the two Asian martial arts included in the Olympics. It made its debut as a demonstration Olympic sport at the 1988 Seoul Games, and became an official medal sport at the 2000 Sydney Games. The objective of Taekwondo is to land kicks and punches on the opponent's scoring zones [1, 2]. A kick or punch to the opponent's torso scores one point, an additional point is awarded if the attacker has his back to his opponent at the point of contact - so spinning kicks score two points. Punches to the head are illegal, but kicks score three points and a turning kick to the head scores four points. To be valid, shots must be of sufficient force. Competitors need powerful and explosive legs - to launch jumping attacks from the opponent and to support themselves during standing, single-leg kicks.

Technology is already widely used in the context of this sport [2]. The trunk of the athlete is protected by a sensorized corsage. The threshold of the impact force able to assign a point is calibrated for each weight level of competitors. The company developer of the corsage is also investigating the possibility to use sensorized helmets [3].

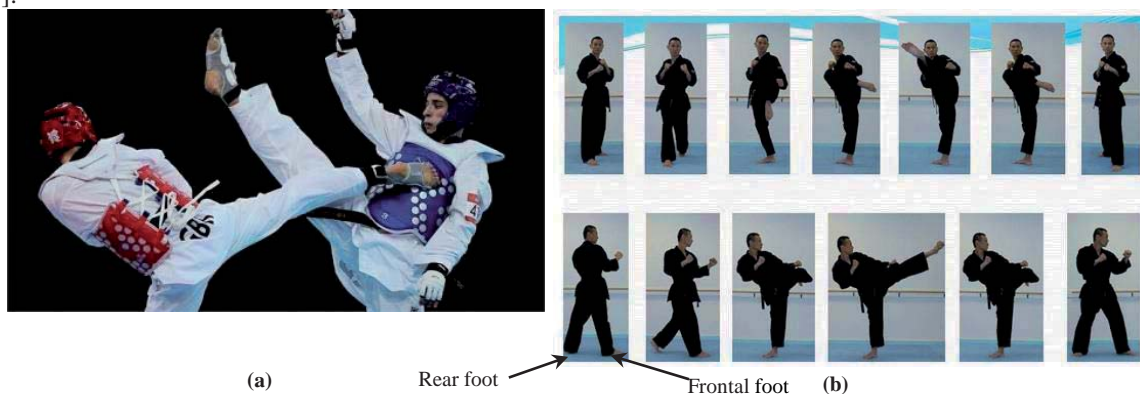


**Figure 1.** Roundhouse kick performed by the athlete with red corsage and red helmet during Olympic tournament London 2012 (a), and sequences to execute roundhouse kick (b).

To perform the Taekwondo roundhouse kicks, the kicking leg is basically lifted in an arc towards the front of the body and then the knee is rapidly extended until the instep of the foot hits the target (see Fig. 1b). In competition, the roundhouse kick is frequently used to get scores as it is a fast movement and provides a powerful attack. Previous studies showed that impact forces of roundhouse kicks were approximately 1000 N–3000 N in Taekwondo players [4]. Higher impact forces ( $1994.03 \pm 537.37$  N) were shown in the competitors as compared with the non-competitors ( $1477.90 \pm 679.23$  N). Even in the similar skill level athletes, the medalists performed stronger kicks than the non-medalists. Therefore, several researchers have investigated influential factors for powerful kicks regarding to kinematics and kinetics of the kicking leg. Concerning kinematics analysis, the kicking leg undergoes a wide range of motion of up to 100 knee flexion, and 45 ankle plantarflexion. During impact phase, knee flexion angle was significantly greater in highly skilled players (about 31) than in unskilled ones (about 20) whereas similar ankle plantarflexion was about 44 in both groups.

The paper proposed in [5] compared the impact characteristics of Taekwondo and Yongmudo (another martial art) player's 360 roundhouse kick (or turning kick) according to the target height. There was a significant difference

for impact force according to the target height approximately  $6400 \pm 898$  N, for the mid section and  $5419 \pm 659$  N, for the high section of taekwondo groups. In conclusion, as the 360 roundhouse kick was performed quicker by the Taekwondo players (respect to Youngmudo martial artists) with a similar impact force and more forward motion, it is evaluated to be a better technique of 360 roundhouse kicking.

The aims of this work is to find correlations between the dynamic of the kicking foot and the dynamic of the head in relation to the movement of the rotation axis. In particular, experimental tests performed in collaboration with some Taekwondo clubs underlined how  $\dot{\beta}$ ,  $\dot{\gamma}$ , and  $\dot{\theta}$  (see Fig.2) influence the force of the roundhouse kick and 360 roundhouse kick. This influence has been noted in other kicks, but only from experimental point of view. Analytical formulations on this theme for taekwondo kicks have not been found. The most important contribution of this research is to find a first analytical formulation between the acceleration of the kicking foot (point B of Fig.2) and acceleration of the head (point A of the Fig. 2) in relation to the angular position, speed, and acceleration of the rotation axis in the  $X_OZ_O$ ,  $Y_OZ_O$ , and  $X_RY_R$  planes.

The formulation and procedure is not shown in this extended abstract because a patent pending status is under development; it will be shown in the full paper (if accepted). The formulation, allowing to relates A and B to the rotation axis, permits to define novel technics for taekwondo jumping.

The paper is structured as follows: section I presents an introduction on taekwondo Olympic martial art sport and on roundhouse and 360 roundhouse kicks from a kinematic and dynamic point of view; section II shows the analytical formulation and the procedure proposed; section III describes the virtual model developed using MSC ADAMS multibody software and the performed simulations; section IV comments results. The paper end with conclusion. Future works are oriented to implement the formulation to 540 roundhouse kick (it has the same concept of the 360 roundhouse kick but the rotation before roundhouse kick is 540 degrees).

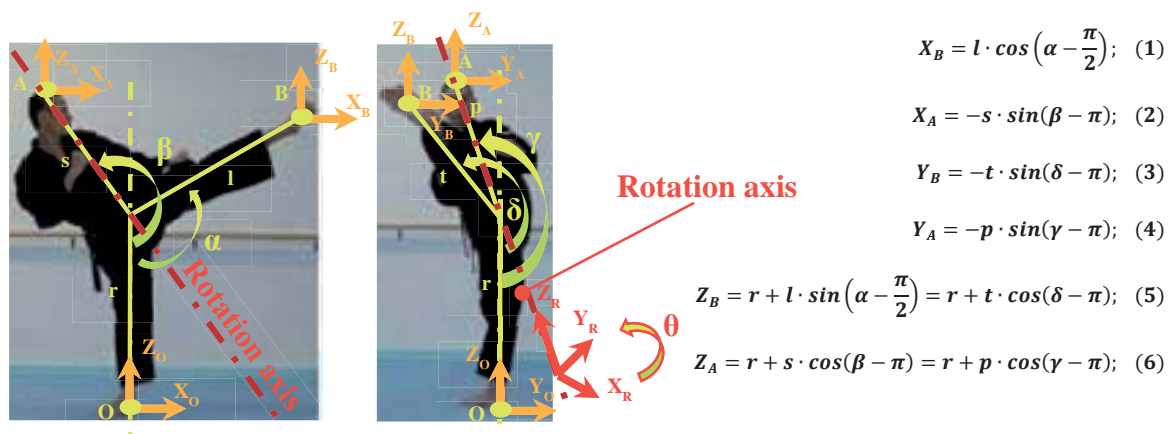


Figure 2. Roundhouse kick.

## Acknowledgments

The authors would like to thank to World Taekwondo Federation (WTF), Italian Federation of Taekwondo (FITA), and the Taekwondo Club Polisportiva Città dei Ragazzi of Genova, for technical discussions and improvements to define multibody system of a taekwondo athletes.

## References

- [1] Kazemi M., et al., A profile of Olympic taekwondo competitors (2006) *J Sports Sci Med*, 5, pp. 114-121.
- [2] Liebermann D. G., et al. , Advances in the application of information technology to sport performance (2002) *J Sports Sci*, 20, pp. 755-769.
- [3] DAEDO Company: <http://www.daedo.com/shop02/skin/shop.php>
- [4] Falco C., et al. Influence of the distance in a roundhouse kick's execution time and impact force in Taekwondo. *J Biomech* 2009;42:242–8.
- [5] O'Sullivan D., et al. Measurement and comparison of Taekwondo and Yongmudo turning kick impact force for two target heights. *J Sports Sci Med* 2009;8:13–16.

# Modelling of Real Car-to-Pedestrian Accident: Comparison of Various Approaches in the Car Bonnet Modelling

Jan Špička<sup>1</sup>, Jan Vychytil<sup>1</sup>, Jaroslav Mañas<sup>2</sup>, Petr Pavlata<sup>3</sup>, Jakub Motl<sup>4</sup>

<sup>1</sup> New Technologies – Research Centre  
University of West Bohemia  
Univerzitní 8, Pilsen, 306 14, Czech Republic  
[spicka, jvychyti]@ntc.zcu.cz

<sup>2</sup> MECAS ESI s.r.o.  
Brojova 16, 326 00 Pilsen, Czech Republic  
Jaroslav.Manas@esi-group.com

<sup>3</sup> Vision Consulting Automotive s.r.o.  
Rumunská 12, 120 00, Prague, Czech Republic  
petr.pavlata@vca.cz

<sup>4</sup> Transport Research Centre (CDV)  
Líšeňská 33a, 636 00, Brno Czech republic  
jakub.motl@cdv.cz

## Abstract

Purpose of this work is reconstruction of a real vehicle to pedestrian collision. The involved car model was Skoda Roomster and the participating pedestrian was 77 years old female. The geometry, mechanical parameters of the car, initial properties (position and velocity) as well as the anthropometric data of the female are known from the accident protocol, provided by CzIDAS project (Czech In-depth Accident Study). The car moved with the initial velocity equalling 30 km/h and hit the pedestrian from her left side by its right-frontal part.

The accident protocol contains also the description of the car damage and injury sustained by the pedestrian. The effort of the accident reconstruction was to not only to meet deformation of the vehicle (shape and maximal bonnet intrusion, see Figure 1), but also pedestrian injury.

**Human Model:** Virtual human body model VIRTHUMAN under Virtual Performance Solution (VPS) was used here for the performed simulations. The VIRTHUMAN model is a hybrid model that combines the advantages of two main modelling approaches: the deformable finite elements and rigid body segmentation within the MBS structure. The deformable elements representing external shape of the human body are connected via non-linear springs and dampers to the rigid segments. Such segments form an open tree structure based on the multibody principle. The particular rigid segments are connected via kinematic joints that represent real human joints (shoulder, elbow, knee, etc.) or breakable joints for description of a bone fracture. The VIRTHUMAN model is a fully scalable human model that takes into account the gender, age, height and weight of the particular subject [4]. The wide set of human anthropometric database [1] is a basement of automatic scaling algorithm, implemented in the model. The model was fully validated against large set of the validation tests. The full-body tests as well as detailed tests for the particular human body segments were performed to ensure the biofidelity of the VIRTHUMAN model [7]. This model was successfully used for the pedestrian modelling [6]. To assess the injury risk probability, an automatic algorithm for evaluation of the specified criterion based on various time-dependent quantities (e.g. forces, accelerations, displacements, torques and many others), was developed and implemented in the VIRTHUMAN model [2]. The investigated criteria limits are also scaled based on the human size. The list of the evaluated criteria is available in [6].



Figure 1: Deformed Skoda Roomster

**Car model:** The model of the car type Skoda Roomster was simplified on the external shape only, modelled via 2D shell elements, absent all the internal structures and reinforcements. The mass and inertia were additionally defined to represent the real car. However, such simplified model does not agree with the real collision scenario and the results will hardly correspond with the accident report. Since the car hits the pedestrian frontally and only frontal part sustained any damage, the rest of the car can be modelled via rigid bodies. The aim of this work was to test, compare and discuss pros and cons of various approaches for modelling of the car bonnet. Together, five different models were developed for the accident reconstruction:

- **Rigid model:** Car model consists only of rigid shell elements. Such model is suitable mainly for evaluation of the car kinematics. The collision with the pedestrian would be far from the reality, since the human is hit with the absolutely rigid structure.
- **Multibody model:** This model consists of deformable (MBS) frontal part and rigid "rest" of the car. In this model, three rigid segments (frontal bumper, bonnet and windshield) are connected via translational joints to a basic tree structure, see Figure 2a.
- **Segmented Multibody model:** The bonnet and the bumper were divided into large number of segments, see Figure 2b. These segments were connected to a basic rigid structure with the springs and dampers. The stiffness of the springs was set based on the EuroNCAP head-like-impactor testing for pedestrian protection

[3]. Based on the results of such experiment, the bonnet is segmented into the areas with the different rigidity. The spring stiffness was validated to correspond with the head-like-impactor testing.

- **Deformable Elastic Finite Element model:** This model consists of deformable shell elements with defined thickness and material properties. The rest of the car was again assumed as a rigid body for this purpose, see red coloured part at Figure 2c. The material of the bumper, bonnet and wind-shield was simplified to be a purely elastic.
- **Deformable Elastic Finite Element model with Reinforcement:** The FEM model here was improved with the bonnet reinforcement geometry definition. The reinforcement is shown in the Figure 2d. The reinforcement was modelled with the same elastic material as the bonnet.
- **Deformable Elastic-Plastic Finite Element model with Reinforcement:** The FEM model with the reinforcement was enhanced with the elastic-plastic definition of the material. With the advantage of performed experimental testing curve, the elastic-plastic material behaviour can be considered.

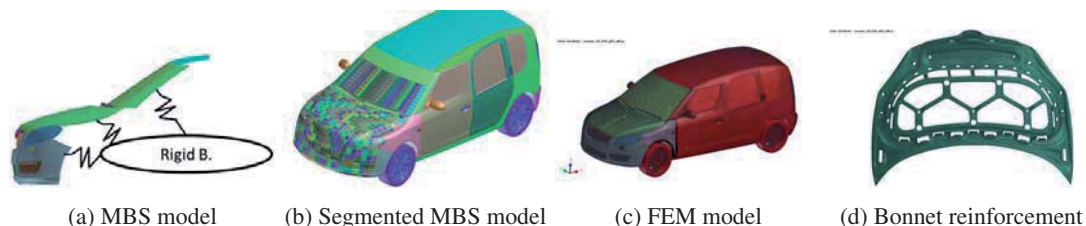


Figure 2: Skoda Roomster models

**Accident configuration:** The configuration of the accident was set up based on the available data from accident protocol, where initial position of the car and pedestrian were reported. Pedestrian was positioned in the desired walking position and placed tightly in front of the car. The car initial velocity was 30 km/h and it decelerates to zero velocity in 1650 ms. The walking speed of the pedestrian was assume as an average equalling 5 km/h [5]. The accident configuration is shown in the Figure 3. The investigated collision was modelled via five different models of the car bonnet and the results can be concluded as follows. The rigid model is not suitable for the car-to-pedestrian accident. MBS and segmented MBS models have advantages of fast calculation and they respect local stiffness of the bonnet. The deformable FEM model can respect real deformation of the car and meet the required pedestrian after impact motion. Enhancement of the FEM model with the reinforcement and definition of the real elastic-plastic material can improve the model for the reconstruction of the real car-to-pedestrian accident.

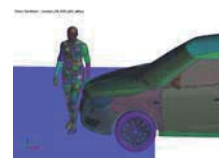


Figure 3: Configuration of the accident. Model VIRTHUMAN and Skoda Roomster

### Acknowledgments

The result was developed within the project co-financed by TAČR TA04030689 "Development of active car bonnet with respect to the diversity of the human population and implementation of the biomechanical model of human body" and financially supported internal by research project SGS-2016-059.

### References

- [1] P. Bláha. Antropometrie československé populace od 6 do 55 let: Československá spartakiáda 1985. Ústřední štáb Československé spartakiády, 1987.
- [2] ESI, Virthuman Postprocessing Manual, VPS Explicit MBS Model, Mecas ESI, Rev, 2. January 2015.
- [3] EuroNCAP, Assessment protocol – Adult occupant Protection, Version 7.0.3, November 2015.
- [4] L. Hynčík, J. Špička, J. Mañas, J. Vychytil. Stature Based Approach towards Vehicle Safety (No. 2015-26-0209). SAE Technical Paper, 2015.
- [5] J. Špička, J. Vychytil, L. Hynčík. Numerical Analysis of a Pedestrian to Car Collision : Effect of Variations in Walk. Applied and Computational Mechanics, 10(2): 139–160, Pilsen, 2016.
- [6] J. Vychytil, L. Hynčík, J. Mañas, P. Pavlata, R. Striegler, T. Moser, R. Valášek. Prediction of Injury Risk in Pedestrian Accidents Using Virtual Human Model VIRTHUMAN: Real Case and Parametric Study (No. 2016-01-1511). SAE Technical Paper, 2016.
- [7] J. Vychytil, J. Mañas, H. Čechová, S. Špirk, L. Hynčík, L. Kovář. Scalable multi-purpose virtual human model for future safety assessment. In SAE Technical Papers. SAE International, doi: 10.4271/2014-01-0534, 2014.

# Optimal Control of a Biomechanical Multibody Model for the Dynamic Simulation of Working Tasks

Michael Roller<sup>1</sup>, Staffan Björkenstam<sup>2</sup>, Joachim Linn<sup>1</sup>, Sigrid Leyendecker<sup>3</sup>

<sup>1</sup>Fraunhofer Institute for Industrial Mathematics  
Fraunhofer Platz 1, 67633 Kaiserslautern, Germany  
[michael.roller, joachim.linn]@itwm.fraunhofer.de

<sup>2</sup> Fraunhofer-Chalmers Centre  
Chalmers Science Park, SE-412 88 Gothenburg, Sweden  
staffan.bjorkenstam@fcc.chalmers.se

<sup>3</sup>Chair of Applied Dynamics  
University of Erlangen-Nuremberg  
Immerwahrstrasse 1, 91058 Erlangen, Germany  
sigrid.leyendecker@fau.de

## Abstract

In industry there is an increasing demand on simulating the dynamic motion of a worker and its interaction with the environment for an ergonomic assessment of tasks, for example the assembly of parts, or moving heavy objects. For given work instructions like "... move the part from A to B ...", a simulation should produce human like motion with realistic joint torques and muscle forces. Optimal control of a biomechanical multibody system [1, 2] is a good approach to create a simulation procedure for a digital human model that fulfills these requirements.

The human skeleton (or parts of it) are modeled as a multibody system (MBS), where, in contrast to [1, 2], a representation with minimal coordinates based on [3] is used due to performance issues [4, 5]. For a MBS with tree-like structure the equations of motion are a system of ordinary differential equation (ODE), turning into a system of differential algebraic equation (DAE) in the case of closed loop kinematics. Realistic inner forces can be obtained by including muscle models into the biomechanical MBS of the digital human. There are a variety of different muscle models [6] with different complexities. As in [2], we restrict ourselves to a string type Hill-model, where the active contractile element (CC) creates a pulling force depending on the actuation, the length and the contraction velocity of the muscle. This CC is connected in parallel to a (non-)linear spring (PEC), see Figure 1, that represents the passive stiffness of the tissue. A muscle is attached to the skeletal MBS in at least two body

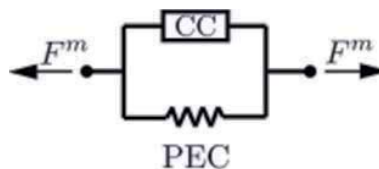


Figure 1: Simplified Hill muscle model

points, connected via a straight line. Hence, if the position and velocity of the bones are known, also the length and the contractile velocity of the muscle can be evaluated. With the help of these quantities and the activation the force  $F^m$  can be computed, which is acting on each point of the bones in the direction of the muscle.

Human like motions of such a biomechanical MBS are generated by optimal control, where the control signals are the activations of the muscles. This results in a time continuous optimization problem, including a mathematical model of the working task in the constraints, besides the equations of motion. Motion trajectories with given characteristics like e.g. minimal control effort, minimal kinetic energy or minimal execution time can be generated by choosing a specifically constructed objective. The continuous optimal control problem is solved by applying the so called DMOCC (*discrete mechanics and optimal control for constrained systems*) approach, including a variational integrator to solve the constrained equation of motions in time. The corresponding finite dimensional optimization is solved with the interior point method using the solver IPOPT [8].

This approach provides the possibility to simulate human-like motions of typical working procedures. For example, in Fig. 2 the simulation results of the task lifting a box from a lower to a higher position can be seen. Hereby, only the start and the end position are prescribed, the motion itself is completely generated by the optimal control approach with a descent objective function. The multibody model consists of two arms, where each has seven degrees of freedom and is fully actuated by 29 muscles. The contact of both hands and the box is realized with two phases [9], where in the second phase additional Lagrangian multiplier and constraints are added to the equation of motion such that the contact is closed. The corresponding constraint forces have to fulfill additional equation in every time step, such that Columbus friction law holds. Hence the model has to press the box to

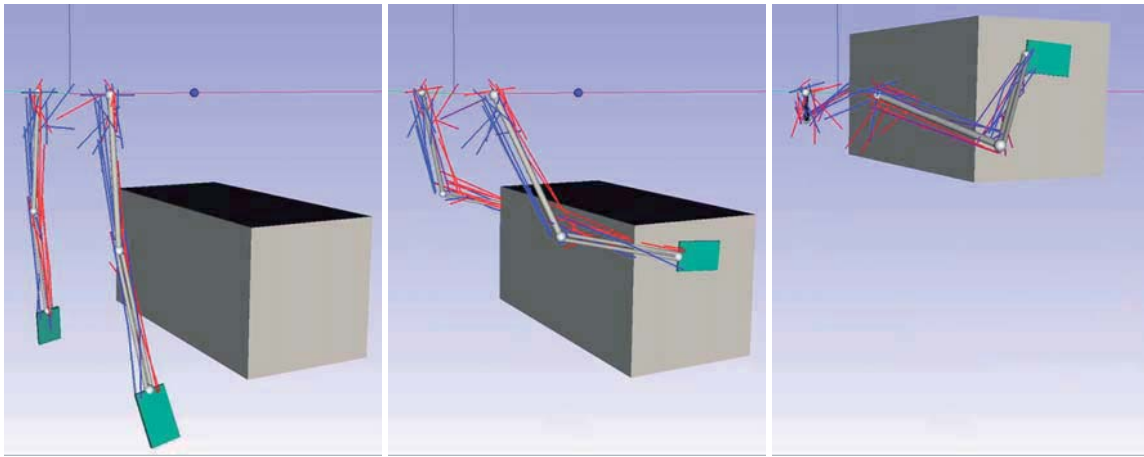


Figure 2: A box lifted by two arms actuated by muscles with friction included

produce a vertical force. Therefore, on each hand a few contact points are prescribed, which are moving with the coordinate system of the rigid body. Also the grasp position of the hands on the sides of the box are a result of the optimization process, because they are included as additional variables.

### Acknowledgments

This work was supported by the Fraunhofer Internal Programs under Grant No. MAVO 828 424.

### References

- [1] R. Maas and S. Leyendecker. Optimal control of biomechanical motion using physiologically motivated cost functions. *The 2nd joint international conference on multibody system dynamics*, 2012.
- [2] R. Maas and S. Leyendecker. Biomechanical optimal control of human arm motion. *Proceedings of the Institution of Mechanical Engineers, Part K: Journal of Multi-body Dynamics*, 2013.
- [3] R. Featherstone. *Rigid body dynamics algorithm*. Springer, 2014.
- [4] S. Björkenstam, N. Delfs, J. S. Carlson, R. Bohlin and B. Lennartson. Enhancing digital human motion planning of assembly tasks through dynamics and optimal control. *Procedia CIRP*, 44:20-25, 2016.
- [5] S. Björkenstam, S. Leyendecker, J. S. Carlson, and B. Lennartson. Inverse dynamics for discrete mechanics of multibody systems with application to direct optimal control. *Submitted for publication*, 2016.
- [6] F. E. Zajac. Muscle and tendon: properties, models, scaling, and application to biomechanics and motor control. *Critical reviews in biomedical engineering*, 17(4):359-411, 1989.
- [7] S. Leyendecker, S. Ober-Blöbaum, J. Marsden and M. Ortiz. Discrete mechanics and optimal control for constrained systems. *Optimal control applications & methods*, 31(6):505–528, 2010.
- [8] A. Wächter and L. T. Biegler. On the Implementation of a Primal-Dual Interior Point Filter Line Search Algorithm for Large-Scale Nonlinear Programming, *Mathematical Programming*, 106(1):25-57, 2006.
- [9] J. T. Betts. Survey of numerical methods for trajectory optimization. *Journal of guidance, control, and dynamics*, 21(2):193-207, 1998.

## Development of a tool for the sensitivity analysis of design parameters of femoral implants in the human body during gait

Benjamin Gervais<sup>1</sup>, Aurelian Vadean<sup>1</sup>, Myriam Brochu<sup>1</sup>, Maxime Raison<sup>1,2</sup>

<sup>1</sup>Department of Mechanical Engineering  
Polytechnique Montreal  
2500 Chemin de Polytechnique, H3T1J4  
Montreal, Canada  
benjamin.gervais, aurelian.vadean, myriam.brochu, maxime.raison@polymtl.ca

<sup>2</sup>Research Center  
CRME – Ste-Justine UHC  
5200 rue Bélanger Est, H1T 1C9  
Montreal, Canada

### Abstract

**Introduction:** In the domain of orthopaedic implant design and manufacturing, the stress analysis on implant is part of the standards. Today, these analyses are still carried out with simplified loading cases that do not represent the conditions closest to reality, but recommendations have been made for these analyzes to become more realistic in the future: e.g. for femoral implants, it was shown that loading during gait is a factor that can lead to failure of the implant and assembly screws [1], reinforcing the recommendation that dynamic conditions, such as gait, be taken into account in future analyzes of implant design parameters. Particularly, such a sensitivity analysis tool would allow manufacturers to improve their concepts of design and assembly of implants, and would guide surgeons in their personalized choice for each patient. However, such a tool does not exist yet: to date, one can find either effort analysis tools between implants based on dynamic rigid multibody models (e.g. [2]), or stress analysis tools in the bones based on flexible multibody dynamic models (e.g. [3]), and so to our knowledge no sensitivity analysis tool integrating flexible implants. Such a tool would require a flexible multibody inverse dynamic model of the human body, taking into account both the dynamics of the human multibody system during the motion and the flexibility of the bone-implant system in the human body. Thus, the objective is to develop a tool to analyze the sensitivity of the design parameters of femoral implants in the human body under dynamic conditions such as gait.

**Method:** To achieve this objective, a dynamic model of the human body integrating a flexible femoral implant was developed (Fig. 1) using *Motionview* software, from *Altair Engineering* (Troy, USA), which includes a flexible multibody dynamic modeling solution. For further details on the characteristics of the implant, which was a “locking compression plate”, and on the gait analysis data, including the data of joint movements ( $q$ ) and ground contact forces ( $F_p$ ), the reader is invited to consult Ref. [1]. To illustrate the interest of the sensitivity analysis tool, the abstract focuses on the impact of the implant length on the stress distribution through the implant and on the fracture deformation. This choice is justified by the fact that the length is one of the main implant design parameters, that the stress distribution in the implant allows to analyze the risk of failure [1], and that the fracture deformation enables to verify if the context is favourable to the bone healing. We compared four implants of different lengths (L1, L2, L3 et L4) on a linear scale from approximately the minimum length to the maximum length physically eligible for this case.

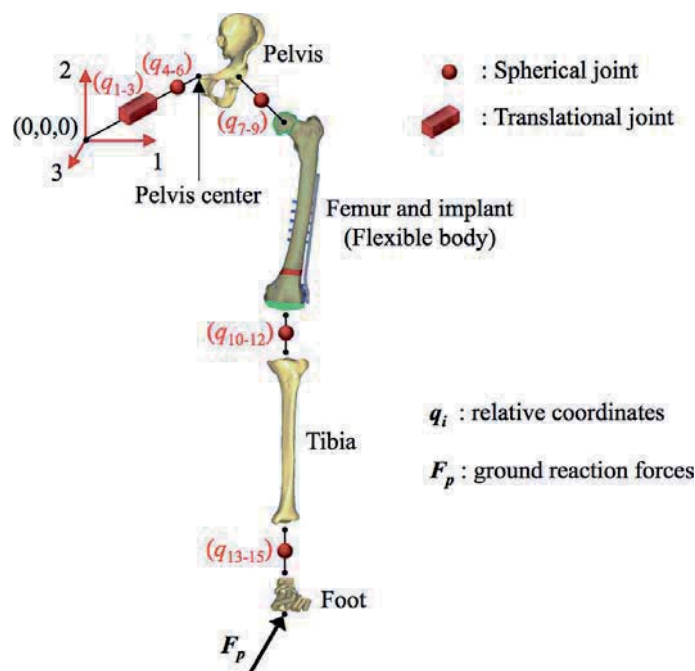
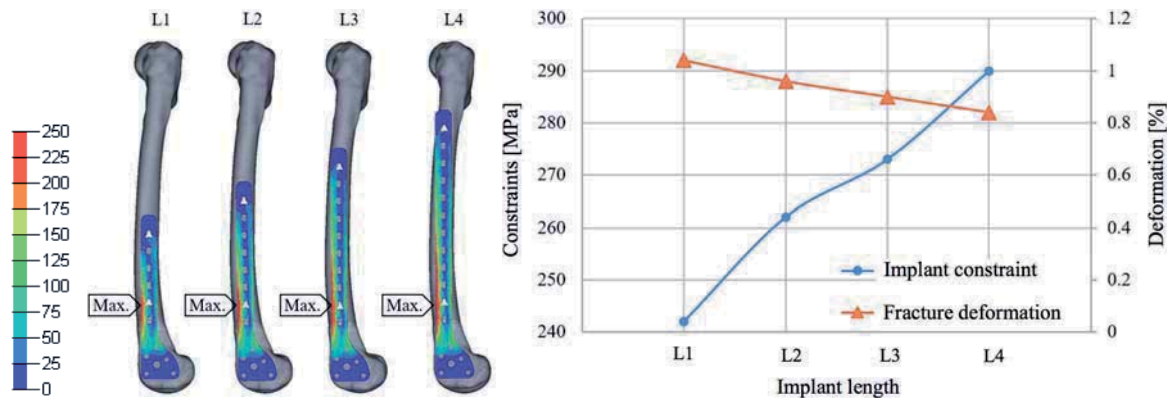


Fig. 1. Dynamic model of the human body integrating a flexible femoral implant.

**Results:** Fig. 2 compares the results of the flexible multibody model between four implant length variants. Fig. 2A compares the Von Mises stress distributions at the time of the largest loading on the implant. In this case study, this instant was identified at 48% of the gait cycle, i.e. just before the foot land on the ground on the side of the limb without implant. Fig. 2B compares maximal implant stresses and maximal fracture deformations.



**Fig. 2.** Comparison between the four implant lengths (L1 to L4): A. Von Mises stress distributions at the time of the largest sollicitation; B. maximal implant stresses and maximal fracture deformations.

Table 1 compares on the four implant lengths the values of: 1. maximal Von Mises stress; 2. volume where the stresses are considered high, exceeding the 200 MPa threshold corresponding to the red colour zone in Fig. 2A; 3. maximal deformation of the fracture, defined by Ref. [4].

**Table 1.** Quantitative comparison of constraints and deformations between the four implant lengths (L1 to L4).

Implant length	L1	L2	L3	L4
1. Maximal Von Mises stress [MPa]	242	262	273	290
2. Volume of high stress [mm <sup>3</sup> ]	48	131	240	360
3. Maximal deformation of fracture [%]	1.04	0.96	0.90	0.84

**Discussion and perspectives:** The objective was to analyze the impact of the main assembly parameters of a femoral implant on stress distribution through the bone-implant system during gait. This was achieved through the development of a dynamic model of the human body incorporating a flexible femoral implant. The most significant result seems to be the increase in the volume of high stress with the increase of implant length: 7.5 times higher (360 mm<sup>3</sup>) for the longer length, L4, relatively to the value (48 mm<sup>3</sup>) of the shorter length, L1. This shows a significant influence of the length of the implant on its resistance to fatigue, because the initiation of the cracks is in the region of high stresses and the risk of crack is correlated with the size of this region. Let us note that for the four models, the maximum stress is at the same location (Fig. 2A), i.e. on the edge of the implant and in the region of the first screw located near the fracture. Fig. 2B shows that the maximum stress in the implant increases with the increase of its length, with a 20% increase between the shortest length, L1 (242 MPa), and the longest, L4 (290 MPa), according to Table 1. Fig. 2B also shows that the maximal deformation of the fracture decreases while the length of the implant increase, such as the shortest implant, L1, records 24% greater (1.04%) maximal deformation than the longest implant, L4 (0.84%), according to Table 1. The prospects of this study are to extend the sensitivity analysis to all the design and assembly parameters. The incentive is to develop a tool for sensitivity analysis of orthopaedic implants on the stress distribution through the bone-implant system during dynamic conditions, such as gait, which would be transferable to the implant industry and orthopedic clinics.

## References

- [1] B. Gervais, A. Vadean, M. Raison, M. Brochu. Failure analysis of a 316L stainless steel femoral orthopedic implant. *Case Studies in Engineering Failure Analysis*, 5-6:30-38, 2016.
- [2] M. Yazji, M. Raison, et al. Are the mediolateral joint forces in the lower limbs different between scoliotic and healthy subjects during gait? *Scoliosis* 10(Suppl 2):S3; 4 pages, 2015.
- [3] A. Kłodowski, A. Valkeapää, A. Mikkola. Pilot study on proximal femur strains during locomotion and fall-down scenario. *Multibody System Dynamics*, 28:239-256, 2012.
- [4] S.M. Perren, A. Fernandez, P. Regazzoni. Understanding Fracture Healing Biomechanics Based on the “Strain” Concept and its Clinical Applications. *Acta Chir. Orth. Et Traum. Cechos.* 82:253-260, 2015.

# Dynamic Parameter Identification of an Upper Extremity Rehabilitation Robot Using GPOPS-II

Borna Ghannadi<sup>1</sup>, Reza Sharif Razavian<sup>1</sup>, John McPhee<sup>1</sup>

<sup>1</sup> Systems Design Engineering  
University of Waterloo  
200 University Ave. W., N2L3G1 Waterloo, Ontario, Canada  
[bghannad, rsharif, mcphee]@uwaterloo.ca

## Abstract

Rehabilitation robots are developed to provide rigorous, systematic and appealing health care for the therapy of post-stroke patients [1]. Three modes of assistive, corrective and resistive actions are the global strategies for rehabilitation robots [1]. In assistive mode, partially assistive controllers are widely used to control these robots using one of these methods: 1) Admittance/impedance control, 2) Attractive force field, 3) Model-based assistance, and 4) Offline adaptive control [1]. Recent progresses in development of nonlinear model predictive control (NMPC) motivate us to implement NMPC to generate an optimal hybrid assistive-corrective-resistive mode for an upper extremity rehabilitation robot. Similar to an impedance control, an NMPC requires a good estimation of the system dynamics, and a simpler model (fewer states) will decrease computation cost of the controller.

The dynamic parameter identification (DPI) of the system can be done by on-line or off-line methods [2]. System input-output matching, which is more accurate than other offline methods, is an optimization problem and can be done on an inverse/forward dynamics model of the system. In homotopy optimization [3], in which a forward dynamics model with an ordinary differential equation (ODE) system is used, inaccurate calculation of the finite differences will cause the divergence of the integrated system. Noisy input will exacerbate this problem. In inverse dynamics optimizations, inaccuracy in joint velocity calculations (caused by noise) may cause significant errors in identification. DPI methods are more applicable for open-chain robots. Workspace of closed chain robots is constrained, and it is not possible to run experiments on wider ranges. Besides, locking driving joints in these robots will not necessarily decouple their dynamic characteristics [2].

The upper extremity rehabilitation robot is a 2 degree-of-freedom parallelogram with sandwiched backlash ( $\approx 0.3$  degree) on two driving joints (Fig. 1.a). The robot has frictional joints and the manipulator moves on a frictional surface. These frictions can be modeled by the LuGre friction model, which is a general purpose dynamic friction model for robotic applications that combines the stiction and Stribeck effects with viscous friction [4]. However, implementing this model will increase the number of unknown parameters and states and this will lead to inefficient calculations. The objective of this project is to develop and identify an optimal dynamic model for the robot. It is required to find an optimal method for input-output matching of this closed-chain system with noisy inputs and outputs.

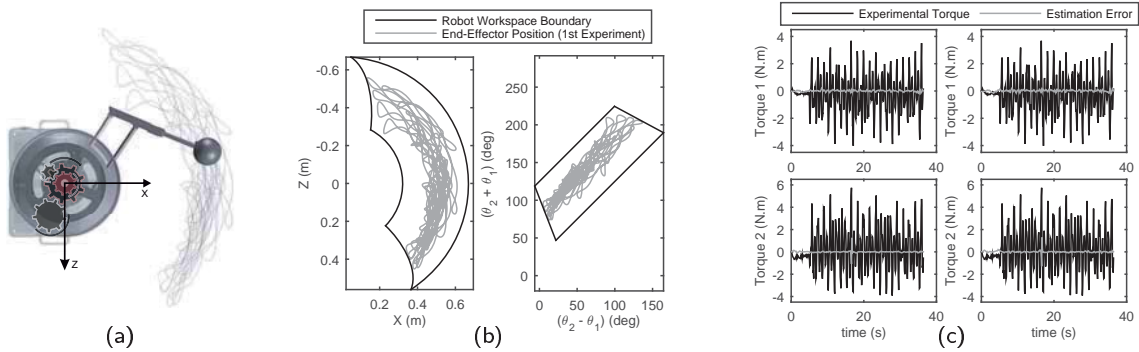


Figure 1: (a) Rehabilitation robot while performing first experiment , (b) Left plot: robot performance in curvilinear space, right plot: robot performance in rectilinear space. (c) DPI validation results for motor torques using approach 1 (left plots), and approach 2 (right plots).

Robot dynamic equations are:

$$\mathbf{M} \begin{Bmatrix} \ddot{\theta}_1 \\ \ddot{\theta}_2 \end{Bmatrix} + \mathbf{C} \begin{Bmatrix} \dot{\theta}_1^2 \\ \dot{\theta}_2^2 \end{Bmatrix} + \begin{Bmatrix} N_{j1} f_{j1} \\ N_{j2} f_{j2} \end{Bmatrix} + \mathbf{J}^T N_E \begin{Bmatrix} f_{Ez} \\ f_{Ex} \end{Bmatrix} + \mathbf{d} = \begin{Bmatrix} u_1 \\ u_2 \end{Bmatrix} \quad (1)$$

where  $\mathbf{M}$  and  $\mathbf{C}$  are the robot's inertia and Coriolis-centripital matrices,  $N_{j_i}$  is the frictional normal force on joint  $i$ ,  $f_{j_i}$  is the normalized frictional torque,  $\mathbf{J}$  is the geometric Jacobian matrix,  $N_E$  is the frictional normal force on the end-effector,  $f_{Ez}$  and  $f_{Ex}$  are the normalized frictional forces in the Cartesian space along Z and X directions respectively,  $\mathbf{d}$  is the vector of unknown dynamics and input noise, and  $u_i$  is the joint  $i$  driving torque. The frictional

normal forces are always positive and variable while the robot is operating in the whole workspace. Thus, we have modeled these forces with a positive definite second-order polynomial function of the joint angles. In the first approach, normalized frictional forces/torques are modeled with LuGre friction model; this model will introduce additional states (average bristle deflections) and parameters to the problem. Since additional states and parameters will increase the computation cost, as a second approach, a continuous velocity-based frictional model [5] is used to model the normalized frictional forces/torques. If we introduce  $\mathbf{p}$  as the vector of unknown dynamic parameters, the final format of the robot ODE system is:

$$\begin{cases} \text{Approach 1 : } \dot{\mathbf{x}}_{8 \times 1} = \mathbf{F}(\mathbf{x}_{8 \times 1}, \mathbf{u}_{2 \times 1}, \mathbf{p}_{43 \times 1}) \\ \text{Approach 2 : } \dot{\mathbf{x}}_{4 \times 1} = \mathbf{F}(\mathbf{x}_{4 \times 1}, \mathbf{u}_{2 \times 1}, \mathbf{p}_{37 \times 1}) \end{cases} \quad (2)$$

Since the robot has unknown dynamics and noisy inputs/outputs, it is not possible to use conventional DPI methods. GPOPS-II is used to solve multi-phase optimal control problems with unknown static parameters; this software combines variable-order adaptive orthogonal collocation methods with sparse nonlinear programming [6]. The main advantage of this software is the implementation of state-of-the-art nonlinear optimization methods. For solving a DPI problem, we set up the GPOPS-II environment with the following conditions:

$$\begin{cases} \text{Objective : } J = 0.5 \int_0^{t_f} ((u_1 - u_{1e})^2 + (u_2 - u_{2e})^2) dt \\ \text{Path constraint : } (\theta_1 - \theta_{1e})^2 + (\theta_2 - \theta_{2e})^2 \leq 5 \times 10^{-5} \end{cases} \quad (3)$$

where subscript  $e$  stands for experimental values. Based on the configuration of the GPOPS-II, it is desired to find optimal control inputs to a system with unknown dynamic parameters, where the control inputs track the experimental inputs, while the system output stays within the specified limits in the path constraint. In order to tune the GPOPS-II environment for solving the problem, the mesh size was set to a large value, then it was reduced to the sampling rate of the experiments (500 Hz). For experimental tests, since the robot's workspace has a curvilinear shape, controlling its end-effector in this space is not straightforward and will introduce some limitations in DPI. Thus, by changing variables, the curvilinear space is mapped into a rectilinear space (Fig. 1.b). Now the goal is: 1) move the end-effector in the mapped rectilinear space using sufficiently rich sinusoidal position inputs at 5 different frequencies rated from very low to high, 2) use recorded values of the experiments and run a 4-phase GPOPS-II problem for 4 experiments, and 3) validate the results by plugging the results of the fifth experiment into the identified system.

Results of the DPI show that identification errors are small, where the smallest signal to noise ratios for approaches 1 and 2 are 17.19 and 15.97, respectively. As the input frequency increases, the errors decrease. The reason is the dominance of the inertial terms in higher frequencies, while in lower frequencies frictional terms are more effective. Fig. 1.c shows the validation results for the fifth experiment using two approaches. The results of the second approach are pretty close to the first approach; thus, the robot dynamic model with the second approach is also valid. In this study, we have proposed a method for the DPI of the rehabilitation robot, which is a planar parallelogram with a sandwiched backlash and noisy inputs/outputs. This method can be extended to any closed-chain mechanism with noisy inputs/outputs. We have also demonstrated the efficiency of the continuous velocity-based friction over LuGre friction model. The continuous velocity-based model can estimate the system parameters with a good accuracy compared to the general purpose LuGre friction model.

### Acknowledgments

This work was funded by the Natural Sciences and Engineering Research Council (NSERC) and Canada Research Chairs (CRC) program. The authors wish to thank Quanser Inc. for providing the upper extremity rehabilitation robot, and the Toronto Rehabilitation Institute (TRI) for collaborating.

### References

- [1] T. Proietti, V. Crocher, A. Roby-Brami, and N. Jarrasse. Upper-Limb Robotic Exoskeletons for Neurorehabilitation: A Review on Control Strategies. *IEEE Reviews in Biomedical Engineering*, 9:4–14, 2016.
- [2] J. Wu, J. Wang, and Z. You. An overview of dynamic parameter identification of robots. *Robotics and Computer-Integrated Manufacturing*, 26(5):414–419, 2010.
- [3] C. P. Vyasarayani, T. Uchida, and J. McPhee. Single-shooting homotopy method for parameter identification in dynamical systems. *Physical Review E*, 85(3):036201, mar 2012.
- [4] H. Olsson, K. Åström, C. Canudas de Wit, M. Gäfvert, and P. Lischinsky. Friction Models and Friction Compensation. *European Journal of Control*, 4(3):176–195, jan 1998.
- [5] P. Brown and J. McPhee. A Continuous Velocity-Based Friction Model for Dynamics and Control With Physically Meaningful Parameters. *Journal of Computational and Nonlinear Dynamics*, 11(5):054502, jun 2016.
- [6] M. A. Patterson and A. V. Rao. GPOPS-II: A MATLAB Software for Solving Multiple-Phase Optimal Control Problems Using hp-Adaptive Gaussian Quadrature Collocation Methods and Sparse Nonlinear Programming. *ACM Transactions on Mathematical Software*, 41(1):1–37, oct 2014.

## Optimization Methods for Identifying Muscle Forces in a Spinal-Cord-Injured Subject during Crutch-Assisted Gait

Florian Michaud<sup>1</sup>, Urbano Lugrís<sup>1</sup>, Ye Ou<sup>2</sup>, Javier Cuadrado<sup>1</sup>, Andres Kecskeméthy<sup>1</sup>

<sup>1</sup>Lab. of Mechanical Engineering  
University of La Coruña  
Escuela Politecnica Superior,  
Mendizabal s/n, 15403 Ferrol, Spain  
florian.michaud@udc.es

<sup>2</sup>Institute of Mechanics and Robotics  
University of Duisburg-Essen  
Lotharstr. 1, 47057 Duisburg,  
Germany  
andres.kecskemethy@uni-due.de

### Abstract

Determination of muscle forces during gait (or any other exercise) by computer modeling and simulation is of great interest to extract the principles of the central nervous system (CNS) control, while avoiding the invasive character of in vivo experimental measurements.

In previous papers, the authors presented a comparison among four muscle recruitment criteria working on a static optimization scheme, and an additional criterion applied within a physiological optimization [1]. However, all methods were applied to healthy subjects and normal gait. People with spinal cord injury (SCI), or other neuromuscular diseases, have a different gait pattern which requires a specific analysis, especially when using assistive devices to walk (crutches, orthoses etc.).

Hence, in this work the subject was an adult female of mass 65 kg and height 1.52 m, with spinal cord injury at T11. In the experiment, she was wearing a pair of passive knee ankle-foot orthoses while walking over two embedded force plates, with the help of two instrumented crutches [2]. Her motion was captured by 10 optical infrared cameras that computed the position of 43 optical markers, as illustrated in Figure 1. Additionally, 15 electromyography (EMG) muscle signals were recorded at 1 KHz (4 at the right hip, 4 at the trunk, 4 at the right shoulder and 3 at the right arm). Signals were normalized and filtered using SSA with a window length of 250.

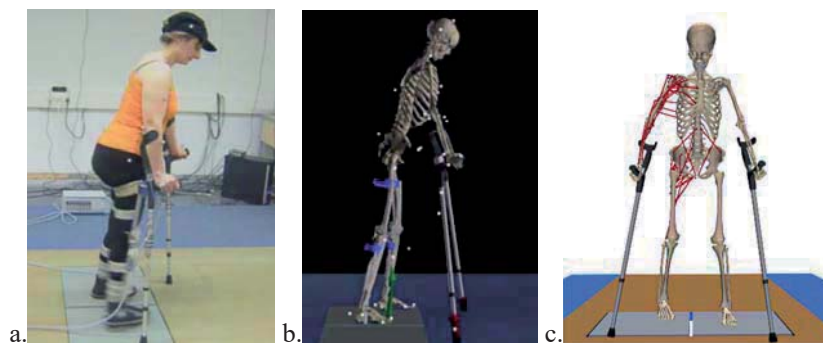


Figure 1. Gait of spinal cord injured subject assisted by passive orthoses and crutches: acquired motion (a), computational model (b) and musculoskeletal model (c).

The human 3D model consists of 18 anatomical segments: pelvis, torso, neck, head, and two hind feet, forefeet, shanks, thighs, arms, forearms and hands with the crutches rigidly connected to them. The segments are linked by ideal spherical joints, thus defining a model with 57 degrees of freedom (6 of the base body plus 51 of the joints). The musculoskeletal model (Figure 1, c.) is composed of 21 muscles at the right hip (after EMG measurement, some muscles were removed to adapt the model), 6 at trunk, 15 at the right shoulder and 11 at the right elbow whose properties were taken from [3].

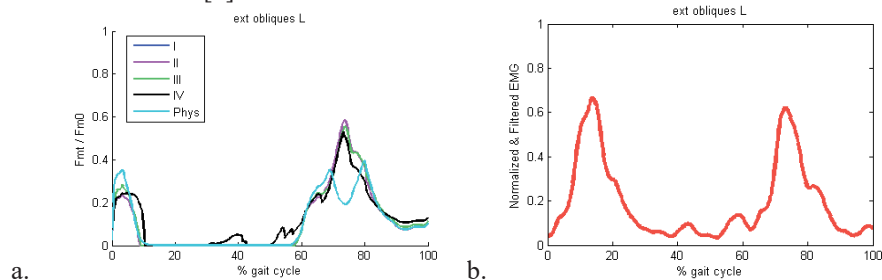


Figure 2. Normalized muscles forces obtained for left oblique extensor with 4 static and 1 physiological criteria using inverse dynamic analysis (a) and experimental data (b).

Four static optimization cost functions were considered and compared, whose mathematical formulations are shown in Table 1. Furthermore, physiological static optimization was implemented to take muscle dynamics into account by introducing dynamic muscle force constraints [4]. Results change depending on the muscle recruitment criteria used (Figure 2) and the experimental data obtained with the EMG was used to choose the criterion that best corresponded to the subject. Additionally, after selecting the best criterion, the cost function parameters were optimized to reduce differences between experimental data and simulation results [5].

**Table 1.** The four muscle recruitment criteria compared.

I	II	III	IV
$\sum_{i=1}^m F_i^2$	$\sum_{i=1}^m \left( \frac{F_i}{F_{i,0}} \right)^2$	$\sum_{i=1}^m \left( \frac{F_i}{A_i} \right)^2$	$\max \left\{ \frac{F_i}{F_{i,0}} \right\} \quad i = 1, 2, \dots, m$

Finally, this study confirmed that pathologic gait and normal gait present different patterns for the muscular activation due to assistive devices and incomplete muscle groups (Figure 3). Once again, it showed how important it is to personalize the model and optimization parameters to the subject in order to predict his neuromuscular behavior.

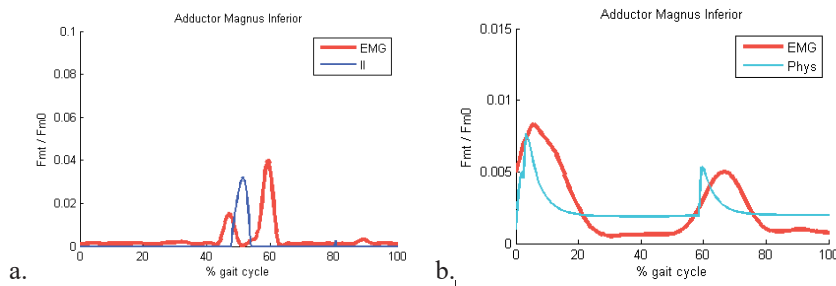


**Figure 3.** Results for SCI subject (a) and healthy subject (b).

## Acknowledgments

This work was funded by the Spanish MINECO under project DPI2015-65959-C3-1-R, cofinanced by the EU through the EFRD program.

## References

- [1] F. Michaud, U. Lugris, Y. Ou, J. Cuadrado, and A. Kecskemethy. Influence of muscle recruitment criteria on joint reaction forces during human gait. In J.M. Font, editor, *Proceedings of the ECCOMAS Thematic Conference on Multibody Dynamics*, pages 1024–1031. Barcelona, 2015.
- [2] U. Lugris, J. Carlin, A. Luaces, and J. Cuadrado. Gait analysis system for spinal cord-injured subjects assisted by active orthoses and crutches. *Journal of Multi-body Dynamics*, 227:363-374, 2013.
- [3] S.L. Delp, F.C. Anderson, A.S. Arnold, P. Loan, A. Habib, C.T. John, E. Guendelman, and D.G. Thelen. OpenSim: Open-source software to create and analyze dynamic simulations of movement. *IEEE Transactions on Biomedical Engineering*, 54:1940-1950, 2007.
- [4] W. Herzog, P. Binding. Cocontraction of pairs of antagonistic muscles: analytical solution for planar static nonlinear optimization approaches. *Mathematical Biosciences*, 118:83-95, 1993.
- [5] C. L. Bottasso, B. I. Prillustsky, A. Croce, E. Imberti, S. Sartirana. A numerical procedure for inferring from experimental data the optimization cost functions using a multibody model of the neuro-musculoskeletal system. *Multibody System Dynamics*, 16:123-154, 2006.

# Experimental Identification of Time-Delay of Human Balancing Using Cepstrum

Ambrus Zelei<sup>1</sup>, Dalma Nagy<sup>2</sup>, Csenge A. Molnár<sup>2</sup>, László Bencsik<sup>1</sup>, Tamás Insperger<sup>1,2</sup>

<sup>1</sup>MTA-BME Lendület  
Human Balancing Research Group  
Nádor u. 7., Budapest, 1051, Hungary  
zelei@mm.bme.hu, bencsik@mm.bme.hu

<sup>2</sup>Department of Applied Mechanics  
Budapest Univ. of Technology and Economics  
Műgyetem rkp. 3., Budapest, 1111, Hungary  
insperger@mm.bme.hu, nagy.dalma22@gmail.com,  
molnarcsege@gmail.com

## Abstract

In spite of the increasing efforts related to human balancing tasks, neural processes behind balancing mechanism are still not fully understood. The models that fit best to the different experimental results involve many uncertain factors. Consequently a wide range of various controller concepts and their modifications appear in the literature as possible candidates for human balancing, e.g. [1, 2, 3].

We suppose that a linear controller is appropriate for modeling the human balancing during balance board trials (see Fig. 1). As a fundamental example, balancing on a pinned balance board is also studied in [1], however the authors consider nonlinear terms in the feedback control. The human sensory system and vision provides information for the brain about the pose of the body, the angular velocity and acceleration of the head [2]. Thus, our model contains proportional, derivative and optionally acceleration feedback (PD and PDA respectively). These feedback terms are supposed to involve time delay in the closed-loop system [2, 3], for which the equation of motion assumes the form:

$$\mathbf{M}(\mathbf{q}(t))\ddot{\mathbf{q}}(t) + \mathbf{C}(\mathbf{q}(t), \dot{\mathbf{q}}(t)) = -\mathbf{P}\mathbf{q}(t - \tau_p) - \mathbf{D}\dot{\mathbf{q}}(t - \tau_D) - \mathbf{A}\mathbf{q}(t - \tau_A), \quad (1)$$

where gain matrices  $\mathbf{P}$ ,  $\mathbf{D}$  and  $\mathbf{A}$  contains 18 gain parameters in our model: proportional, derivative and acceleration feedback parameters for each of angles  $\vartheta$ ,  $\varphi_u$  and  $\varphi_l$  with respect to torques  $T_a$  and  $T_h$  exerted at the ankles and the hip, respectively. The controller model allows different values of time delays for each feedback term. The identification of these time delays is a challenging task, and many papers focus on it, e.g. [4].

If time delay and acceleration feedback is present at the same time, then the mathematical model of the controlled system is a neutral delay-differential equation (NDDE), because the term of highest derivative appears with a delayed argument. Neutral mechanical systems have the property that the discontinuities of the acceleration directly appear in the delayed terms, thus instead of smoothen slowly, the discontinuities accumulate [1, 3].

Our idea is to use the spectrum and cepstrum of the solution of NDDEs for the identification of time delay. In NDDEs the discontinuities and peaks do not smoothen therefore they are periodically repeated with a period equal to the time delay. A peak, which corresponds to the frequency of these periodic-like components of the signal, appears in the spectrum. Since the periodic signal is not sinusoidal, the peak in the spectrum involves higher harmonics too. These periodically repeated peaks in the spectrum (non-sinusoidal periodic function of frequency) generate peaks in the cepstrum (the spectrum of the spectrum) as well. All in all, we can say that the spectrum of a periodic signal usually contains finite number of peaks, but as a consequence of the time-delayed acceleration feedback, a peak appears in every equal interval of the domain of the spectrum and the cepstrum. Since the cepstrum is in time domain, this interval is equal to the delay of the system.

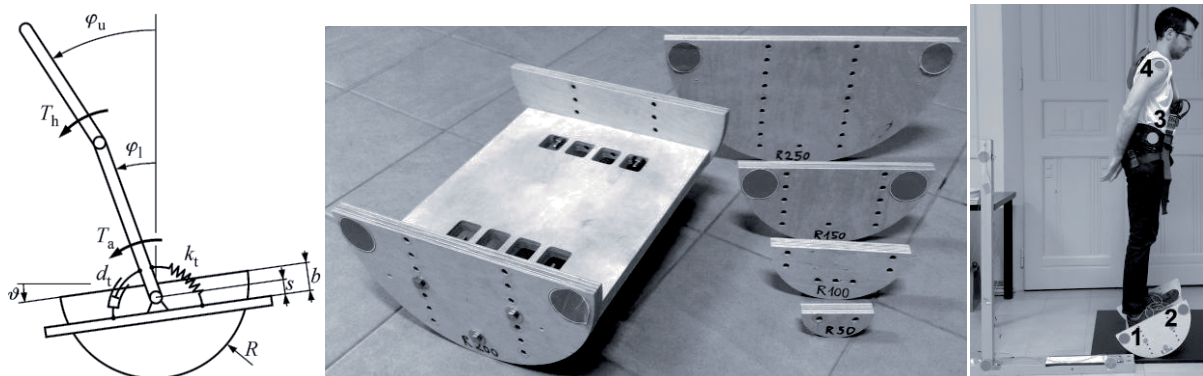


**Figure 1.** *left:* mechanical model of a balancing person on balance board; *middle:* balance board with interchangeable arcs; *right:* balancing person equipped with passive markers 1-4 for motion capturing

The idea was tested on a simulation result of a NDDE, for which the non-linear equation of motion of an inverted pendulum with PDA control was applied:

$$\ddot{\varphi}(t) - \frac{3}{2} \frac{g}{l} \sin(\varphi(t)) = -P\varphi(t - \tau) - D\dot{\varphi}(t - \tau) - A\ddot{\varphi}(t - \tau). \quad (2)$$

The spectrum and cepstrum of the numerical solution are shown in Fig 2 left. The peaks in the cepstrum indicate the pre-defined  $\tau = 0.2\text{s}$  time delay.

Laboratory experiments were carried out for 7 subjects balancing on a balance board with different radii (Fig 1 middle and right). The tilt angle  $\mathcal{G}$  of the balance board, the position of the hip and the shoulder was logged in the sagittal plane. A high resolution camera was used with 50Hz sampling frequency. The angles  $\varphi_u$  and  $\varphi_l$  of the lower and upper pendulum were calculated based on the measured marker positions.

If a subject was able to balance for 60 second without falling, then the trial was considered to be stable. For each subject 9 different  $R$  and  $h$  parameter sets were considered. In this work the spectrum and cepstrum analysis were carried out for the stable cases only.

The spectrum and cepstrum of the measured signals for  $\mathcal{G}$ ,  $\varphi_u$  and  $\varphi_l$  were analyzed. An example case is shown in Fig 2 middle and right panels respectively. The number of peaks of the cepstrum was determined for the queffrequency range between 0s and 1s. In this first trial of our concept, equal time-delays were assumed for the different terms:  $\tau = \tau_p = \tau_D = \tau_A$ . Assuming a uniform distance between the peaks, the average time delay was determined. The average value of the time-delay was about  $\tau = 85\text{ms}$ .

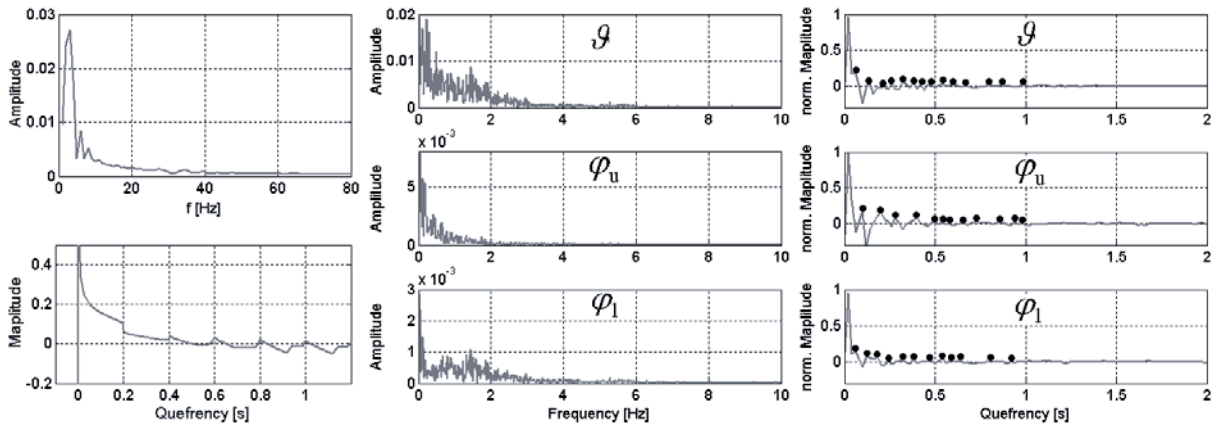


**Figure 2.** *left:* spectrum and cepstrum of a simulated signal; *middle and right:* spectrum and cepstrum of measured signals

Although, our results show the feasibility of the concept of determining the time-delay using cepstrum, a few issues have to be clarified in further research work. Human sense organs have dead zone, like artificial sensors [5]. The presence of dead zones causes nonlinearity, which affects the spectrum and the cepstrum. Multiple delays can cause intricate situation, and their separate identification may induce crucial problems.

The expected periodic-like pattern of the peaks appeared in the cepstrum, so the results do not exclude the validity of the linear compensator model and the possibility of the presence of the delayed acceleration feedback term.

## References

- [1] J. R. Chagdes, S. Rietdyk, M. H. Jeffrey, N. Z. Howard, A. Raman. Dynamic stability of a human standing on a balance board. *Journal of Biomechanics*, 46(15), 2593–2602, 2013.
- [2] G. Stépán. Delay effects in the human sensory system during balancing. *Transactions of the Royal Society A*, 367(1981), 1195-1212, 2009.
- [3] T. Insperger, J. Milton, G. Stépán. Acceleration feedback improves balancing against reflex delay. *Journal of the Royal Society Interface*, 10(79), Article No. 20120763, 2013.
- [4] X. X. Zhang, J. Xu. Identification of time delay in nonlinear systems with delayed feedback control. *Journal of the Franklin Institute*, 352(8), 2987–2998, 2015.
- [5] T. Insperger, J. Milton. Sensory uncertainty and stick balancing at the fingertip. *Biological Cybernetics*, 108(1), 85–101, 2016. (doi:10.1007/s00422-013-0582-2).

# Identification of Knee Ligament Properties by Multibody Optimisation

Evelyn Winter<sup>1</sup>, Robert Grawe<sup>1</sup>, Michael Stoltmann<sup>1</sup>, Philipp Bergschmidt<sup>3</sup>, Andreas Geier<sup>2</sup>,  
Rainer Bader<sup>2</sup>, Christoph Woernle<sup>1</sup>

<sup>1</sup> Chair of Technical Dynamics, University of Rostock, Justus-von-Liebig-Weg 6, 18055 Rostock, Germany  
{evelyn.winter, robert.grawe, michael.stoltmann, woernle}@uni-rostock.de

<sup>2</sup> Department of Orthopaedics, University Medicine of Rostock, Germany  
{andreas.geier, rainer.bader}@med.uni-rostock.de

<sup>3</sup> Department of Trauma Surgery, Orthopedics and Hand Surgery, Hospital in the southern part of Rostock,  
philipp.bergshmidt@kliniksued-rostock.de

## Abstract

Knee joint kinematics depends on complicated interactions of the geometry of the articulating joint surfaces, passive soft tissues and active muscles. The individual stiffness properties of the ligaments have an important contribution to the stabilisation; hence, impact kinematics as well as dynamics of the knee joint to a great extent and have to be addressed in musculoskeletal multibody simulation. Material characterisation of resected individual ligaments based on tensile tests does not take into account important test conditions like the attachment sites and wrapping around bones. To overcome these limitations, a procedure to characterise in-situ ligament forces has been developed, in which a six-axes robot under hybrid position and force control was used to move and load a human cadaveric knee [4]. The aim of the present contribution is the numerical identification of tibiofemoral ligament parameters while recording knee kinematics that results from ligament properties.

For the experimental analysis, a human cadaveric leg was completely dissected except from soft tissues belonging to ligaments and capsule. Osseous morphology and ligament insertions were reconstructed from CT and MRI scans. Based on these scans bone coordinate systems were defined as described in [3], and a digital model of the bone and soft tissue structures was built up in order to enable implementation into a multibody simulation model. For mechanical testing on the robot, tibia/fibula and femur were resected and casted into cups using bone cement and epoxy resin. To address the influence of the patella, the quadriceps tendon was statically loaded by a constant weight. Passive knee flexion of the human knee specimen was enforced by a six-axes industrial robot while tibiofemoral kinematics were being measured [4], in particular the vektor  $\mathbf{r}_{FT} = [\Delta r_x, \Delta r_y, \Delta r_z]^T$  and the knee-joint-angles  $\boldsymbol{\beta}_{FT} = [\gamma, \alpha, \beta]^T$  according to [3] that were defined between the tibia bone system  $K_T$  and the femur bone system  $K_F$ , Fig. 1a.

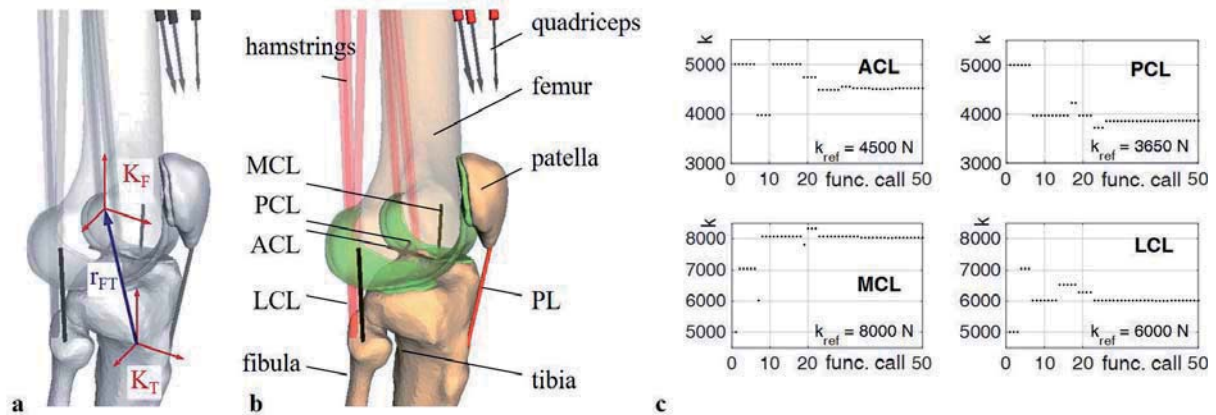


Abbildung 1: Multibody model of right knee. **a** lateral view: femur bone reference system  $K_F$  and tibia bone reference system  $K_T$ . **b** lateral view: multibody model with anterior and posterior cruciate ligament (ACL/PCL), lateral and medial collateral lig. (LCL/MCL), patellar lig. (PL). **c** Stiffness parameters  $k$  of the lig. ACL, PCL, LCL, MCL.

The native kinematics of the knee was analysed during a passive flexion up to  $120^\circ$  by moving the tibial component around the flexion angle  $\gamma$  under position control. The remaining five position coordinates, summarised in the vector  $\mathbf{g}^{\text{ref}}(\gamma) = [\Delta r_x, \Delta r_y, \Delta r_z, \alpha, \beta]^T$  were force/torque-controlled in such a way that the corresponding forces and torques are minimised and thereby making the joint finding its static equilibrium. Thus, for  $N$  prescribed discrete flexion angles  $\gamma_i$ , corresponding measurements

$$\mathbf{g}_i^{\text{ref}}(\gamma_i) = [ \Delta r_{xi} \quad \Delta r_{yi} \quad \Delta r_{zi} \quad \alpha_i \quad \beta_i ]_{\text{ref}}^T, \quad i = 1, \dots, N, \quad (1)$$

were obtained.

For ligament parameter identification this procedure was simulated by a musculoskeletal multibody model of the knee according to Fig. 1b. The most important ligaments (MCL, LCL, ACL and PCL acc. to [5]) were modelled with nonlinear dependencies of the ligament forces  $f$  from the corresponding ligament strains  $\varepsilon$  acc. to [1],

$$f(\varepsilon) = \begin{cases} 0 & \varepsilon < 0 \\ 0.25k \frac{\varepsilon^2}{\varepsilon_0} & 0 \leq \varepsilon \leq 2\varepsilon_0, \\ k(\varepsilon - \varepsilon_0) & \varepsilon > 2\varepsilon_0, \end{cases} \quad (2)$$

with the ligament stiffness parameter  $k$ , the strain  $\varepsilon_0 = 0.015$  which describes the change from quadratic to linear characteristic, the actual ligament length  $\ell$  and the ligament zero load length  $\ell_0$ , which influence the strain

$$\varepsilon = \frac{\ell - \ell_0}{\ell_0}. \quad (3)$$

The tibiofemoral joint is modelled by a polygonal contact model enabling the roll-glide movement [2]. The parametrisation of the multibody model was based on an alcohol-fixed human leg specimen that was CT-scanned and reconstructed acc. to [4], Fig. 1a. The pelvis, femur, tibia/fibula and patella were modelled as rigid bodies. The patellofemoral joint was modelled by a one-degree-of-freedom joint that describes the path of the patella along a femur-fixed path with the arc length  $s$ , identified from a previous polygonal contact simulation of the patellafemoral joint. Wrapping of the quadriceps tendon was then implemented by a skleronomic constraint depending on the patella arc length  $s$ .

The experimental procedure is simulated by calculating the equilibrium position of the tibia for given flexion angles  $\gamma_i$  without external loading on the tibia. This yields the relative position coordinates  $\mathbf{g}_i^{\text{mod}}$  in dependency of the ligament parameters summarised in the parameter vector  $\mathbf{p}$ ,

$$\mathbf{g}_i^{\text{mod}}(\gamma, \mathbf{p}) = [ \Delta r_{xi} \quad \Delta r_{yi} \quad \Delta r_{zi} \quad \alpha_i \quad \beta_i ]_{\text{mod}}^T, \quad i = 1, \dots, N. \quad (4)$$

Parameters  $\mathbf{p}$  were calculated subsequently by solving the nonlinear least squares problem

$$Z(\mathbf{p}) \equiv \sum_{i=1}^N \Delta \mathbf{g}_i^T \mathbf{W} \Delta \mathbf{g}_i = \min_{\mathbf{p}} \quad \text{with} \quad \Delta \mathbf{g}_i = \mathbf{g}_i^{\text{mod}}(\gamma_i, \mathbf{p}) - \mathbf{g}_i^{\text{ref}} \quad (5)$$

and the weighting matrix  $\mathbf{W} = \text{diag}(w_1, \dots, w_5)$  comprising weighting factors for the five coordinates  $\mathbf{g}$ . The optimisation problem is constrained by lower and upper bounds

$$p_j^{\min} \leq p_j \leq p_j^{\max}, \quad j = 1, \dots, 5. \quad (6)$$

The optimising problem is solved with the pattern search in MATLAB. The procedure was performed for the stiffness parameters of all ligaments (ACL, PCL, LCL and MCL). To obtain a well defined reference for testing the procedure, reference data for  $\mathbf{g}_i^{\text{ref}}(\gamma_i)$  according to (1) were generated by multibody simulation. Fig. 1c shows the trend of the stiffness parameters over the function calls during optimisation. It can be shown that the stiffnesses  $k$  of all ligaments converge to the known stiffness parameters  $k_{\text{ref}}$ . However, further investigations should determine the correct starting points of the ligaments.

Properties of ligaments have a major impact on knee joint kinematics. Herein, a method for in-situ ligament stiffness identification has been presented that enables consideration of individual ligament stiffness in musculoskeletal multibody simulation.

## References

- [1] L. Blankevoort, R. Huiskes. Ligament-bone interaction in a three-dimensional model of the knee. *J Biomech Eng.* 113(7): 263-269, 1991.
- [2] A. Geier, E. Winter, V. Polster, M. Schulze, A. Wree, D. Klüß, C. Woernle, R. Bader. Instantaneous screw axis for computed muscle torque control in the articulating human knee joint. *Proc. 4th Joint International Conference on Multibody System Dynamics (IMSD)*, Montreal, 2016.
- [3] E. S. Grood, W. J. Suntay. A Joint Coordinate System for the Clinical Description of Three-Dimensional Motions: Application on the Knee. *J Biomech Eng.* 105(2): 136-144, 1983.
- [4] R. Grawe, M. Krentzien, M. Schulze, P. Bergschmidt, A. Geier, D. Klüß, G. Wenzel, A. Wree, R. Bader, C. Woernle. Analysis of the elastic behavior of human knee ligaments by a robot under hybrid position-/force control. *Proc. 4th Joint International Conference on Multibody System Dynamics (IMSD)*, Montreal, 2016.
- [5] A. Ottoboni, V. Parenti-Castelli, N. Sancisi, C. Belvedere, A. Leardini. Articular surface approximation in equivalent spatial parallel mechanism models of the human knee joint: an experiment-based assessment. *Proc I. Mech E, Part H: Engineering in Medicine*, 224(9): 1121-1132, 2010.

## Use of analytical derivatives in an optimal control algorithm for the residual elimination problem of gait

Francisco Mouzo<sup>1</sup>, Urbano LUGRÍS<sup>1</sup>, Daniel Dopico<sup>1</sup>, Benjamin Fregly<sup>2</sup>, and Javier Cuadrado<sup>1</sup>

<sup>1</sup>Laboratorio de Ingeniería Mecánica  
University of La Coruña  
Mendizábal s/n, 15403 Ferrol, Spain  
[francisco.mouzo, ulugris, ddopico]@udc.es,  
javicuad@cdf.udc.es

<sup>2</sup>Computational Neuromechanics Lab  
University of Florida  
Gainesville, FL, 32611, USA  
fregly@ufl.edu

### Abstract

Optimal control is a well-known tool in the biomechanics field for gait analysis and prediction [1]. When solving an optimal control problem, first and second derivatives of the objective function and constraints (which may include the equations of motion in differential form) with respect to the design variables, states and controls are needed [2]. It is common to obtain first derivatives numerically by means of finite difference formulas, and to estimate the Hessian to avoid the calculation of second derivatives, which is very time consuming. Alternatively, it is possible to obtain symbolic expressions for the derivatives or use automatic differentiation [2]. In this work, the problem of analytically obtaining the first derivatives of the objective function and constraints is addressed for an optimal control problem that seeks to track an experimentally measured gait motion while making the simulated motion dynamically consistent. Results and efficiency are compared when using numerical and analytical first derivatives, respectively. For second derivatives, a Hessian approximation method is maintained in both cases.

Experimental walking data were collected from a healthy adult male, 34 years old, mass 85 kg, and height 1.82 m. All test procedures were approved by the local institutional review board, and the subject gave informed consent. The subject walked on a walkway possessing two embedded force plates (AMTI, AccuGait sampling at 100 Hz), and his motion was captured by 12 optical infrared cameras (Natural Point, OptiTrack FLEX:V100 also sampling at 100 Hz) that computed the position of 37 optical markers (red dots in Fig. 1).

A three-dimensional multi-body dynamic walking model of the subject was created by the authors [3], and is illustrated in Fig. 1. The model consisted of 18 anatomical segments: pelvis (base body), torso, neck, head, and two hindfeet, forefeet, shanks, thighs, arms, forearms and hands. The segments were linked by ideal spherical joints, thereby defining a model possessing 57 degrees of freedom (6 for the base body plus 51 for the joints). The computational model was defined using 228 mixed (174 natural + 54 angular) coordinates. Details about the treatment of captured data can be found in [3].

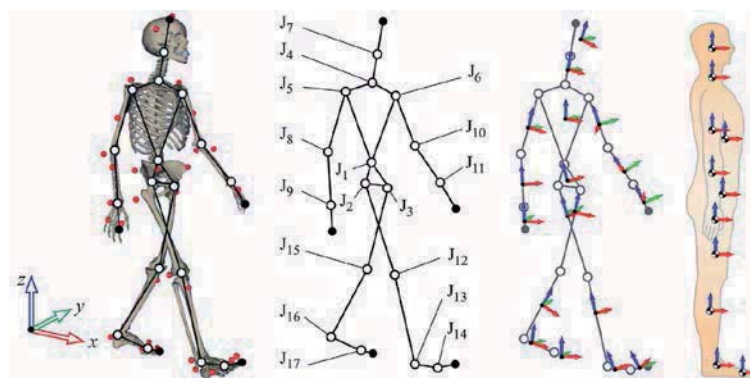


Figure 1. Human multibody model.

Given the experimental marker motion and force plate data, a direct collocation optimal control problem was formulated to find the dynamically consistent model motion that best fit the marker motion data. The optimal control problem possessed the following characteristics. The states were the generalized positions and velocities  $\mathbf{z}$  and  $\dot{\mathbf{z}}$  for the 57 independent degrees of freedom, and the controls were the associated generalized accelerations  $\ddot{\mathbf{z}}$  and the torques  $\boldsymbol{\tau}$  acting at the 51 controlled joint degrees of freedom. The objective function minimized the time integral over a complete gait cycle of the squared deviations between the generalized positions, velocities, and accelerations obtained from the model and those obtained from an inverse kinematic analysis, plus the squared deviations between the joint torques obtained from the model and those obtained from an inverse dynamic analysis. The dynamic constraints were trivial, as the generalized accelerations were used as controls. Dynamic consistency was imposed as a path constraint, forcing the residual forces and torques on the base body to be zero. This scheme using inverse dynamics increases the size of the problem, as the accelerations must be included as controls, but

proves to be more robust than the forward dynamics alternative.

The equations of motion were provided using the so-called matrix-R formulation [4], which leads to a system in the minimum number of 57 coordinates. Using this formulation, the inverse dynamic equations that provided the generalized forces were:

$$\mathbf{Q}_{ID} = \mathbf{R}^T \mathbf{M} \mathbf{R} \ddot{\mathbf{z}} - \mathbf{R}^T (\mathbf{Q} - \mathbf{M} \mathbf{R} \dot{\mathbf{z}}) = \mathbf{R}^T \mathbf{M} \mathbf{R} \ddot{\mathbf{z}} - \bar{\mathbf{Q}} \quad (1)$$

where  $\mathbf{R}$  is the matrix that projects the independent set of coordinates onto the dependent set,  $\mathbf{M}$  is the mass matrix in dependent coordinates, and  $\mathbf{Q}$  is the generalized force vector in dependent coordinates.

For the optimal control problem to be solved, the partial derivatives of the path constraints with respect to the states,  $\mathbf{z}$  and  $\dot{\mathbf{z}}$  and controls  $\ddot{\mathbf{z}}$  and  $\boldsymbol{\tau}$  were necessary. The derivatives with respect to the torques were trivial. The complexity arises in the derivatives of equation (1) with respect to  $\mathbf{z}$ ,  $\dot{\mathbf{z}}$  and  $\ddot{\mathbf{z}}$ , which are outlined using the following equations:

$$\frac{\partial \mathbf{Q}_{ID}}{\partial \mathbf{z}} = \left( \frac{\partial \mathbf{R}^T}{\partial \mathbf{z}} \mathbf{M} \mathbf{R} + \mathbf{R}^T \mathbf{M} \frac{\partial \mathbf{R}}{\partial \mathbf{z}} \right) \dot{\mathbf{z}} - \frac{\partial \bar{\mathbf{Q}}}{\partial \mathbf{z}} \quad (2)$$

$$\frac{\partial \mathbf{Q}_{ID}}{\partial \dot{\mathbf{z}}} = - \frac{\partial \bar{\mathbf{Q}}}{\partial \dot{\mathbf{z}}} \quad (3)$$

$$\frac{\partial \mathbf{Q}_{ID}}{\partial \ddot{\mathbf{z}}} = \mathbf{R}^T \mathbf{M} \mathbf{R} \quad (4)$$

The development of each of these partial derivative terms leads to extremely complex expressions involving tensor products that can be found in detail in [5]. Equations (1) through (4) were implemented in the software package MBSLIM [6], written in FORTRAN. For solving the optimal control problem, the commercial software GPOPS-II [7] was used.

**Table 1.** Results for the initial mesh.

<i>Derivatives method</i>	<i>Iterations until convergence</i>	<i>Time (s)</i>	<i>Time per iteration (s)</i>	<i>Objective</i>
GPOPS-II Sparse Central Diff.	16	399	24.94	1.084e-2
GPOPS-II Sparse Forward Diff.	18	225	12.5	1.14e-2
MBSLIM	17	123	7.24	1.033e-2

Results, summarized in Table 1, show that the three methods lead to almost the same solution in a similar number of iterations, but the use of analytical derivatives provides slightly better accuracy and much better efficiency.

## Acknowledgments

The support of the Spanish Ministry of Economy and Competitiveness (MINECO) under projects DPI2015-65959-C3-1-R (cofinanced by the European Union through the EFRD program) and DPI2016-81005-P is greatly acknowledged.

## References

- [1] A.J. van den Bogert, D. Blana, D. Heinrich. Implicit methods for efficient musculoskeletal simulation and optimal control. *Procedia IUTAM*, 2:297-316, 2011.
- [2] J.T. Betts. *Practical methods for optimal control using nonlinear programming*. SIAM, Philadelphia, 2001.
- [3] U. Lugris, J. Carlin, A. Luaces, J. Cuadrado. Gait analysis system for spinal cord injured subjects assisted by active orthoses and crutches. *Journal of Multi-body Dynamics*, 227(4):363-374, 2013.
- [4] J. Garcia de Jalon, E. Bayo. *Kinematic and dynamic simulation of multibody systems*. Springer-Verlag, New York, 1994.
- [5] D. Dopico, Y. Zhu, A. Sandu, C. Sandu. Direct and adjoint sensitivity analysis of ordinary differential equation multibody formulations. *Journal of Computational and Nonlinear Dynamics*, 10(1):011012, 2015.
- [6] MBSLIM multibody simulation library: <http://lim.ii.udc.es/MBSLIM/>.
- [7] M.A Patterson, A.V. Rao. GPOPS-II: A MATLAB software for solving multiple-phase optimal control problems using hp-adaptive Gaussian quadrature collocation methods and sparse nonlinear programming. *ACM Transactions on Mathematical Software*, 41(1):1-37, 2014.

## Human like Motion Generation for Ergonomic Assessment - a Muscle Driven Digital Human Model using Muscle Synergies

Marius Obentheuer<sup>1,2</sup>, Michael Roller<sup>1</sup>, Staffan Björkenstam<sup>3</sup>,  
Karsten Berns<sup>2</sup>, Joachim Linn<sup>1</sup>

<sup>1</sup>Fraunhofer Institute for Industrial Mathematics, Fraunhofer Platz 1, 67633 Kaiserslautern, Germany  
[Marius.Obentheuer, Michael.Roller, Joachim.Linn]@itwm.fraunhofer.de

<sup>2</sup>Robotics Research Lab  
Department of Computer Science  
University of Kaiserslautern  
Gottlieb-Daimler-Str., 67663, Kaiserslautern, Germany  
[obenth, berns]@rhrk.uni-kl.de

<sup>3</sup>Fraunhofer-Chalmers Centre  
Chalmers Science Park,  
SE-412 88, Gothenburg, Sweden  
staffan.bjorkenstam@fcc.chalmers.se

### Abstract

It is a well-known problem when controlling complex multibody systems (MBS) that there is an infinite number of possible ways to do a motion from a starting to an end configuration (kinematical redundancy). In biomechanical systems like musculoskeletal models the problem of anatomical redundancy has to be handled additionally. Here the number of actuators (muscles) in the model is higher than the number of kinematical degrees of freedom, which means that even one and the same motion can be generated by a multitude of different muscle actuations. Controlling a digital human model (DHM) in the scope of ergonomic assessment additionally adds some constraints to the generated motions. On the one hand the simulated task should be solved in a human like way, meaning the used forces, trajectories, velocities, accelerations etc. should be chosen in a way a real human might or at least can do it. Further on, it is important that the muscle activations used to generate these motions are similar to those which the human central nervous system (CNS) would choose as these data can be used to derive an assessment about how exhausting / ergonomic a motion (or repetitions of this motion, static postures...) will be for a human. Even there are many possible options, humans use quite stereotypical muscle activations across individuals to create motions. A long standing question in neuroscience and other disciplines is how the CNS chooses these patterns and solves the above described redundancy problems (the CNS additionally has to handle the problem of neurological redundancy, meaning that one and the same muscle is being innervated by several motor neurons).

One theory is that the CNS makes use of pre-defined building blocks (or modules) in the spinal cord which impose a specific pattern of muscle activation, although known as motion primitives or muscle synergies. By linearly combining these modules, instead of explicitly choosing which muscle to activate, the dimensionality is reduced what could simplify control whereas there is still a wide range of motor outputs that can be produced [1]. Another (but not contradistinctive) approach to explain interindividual muscle activation patterns is the optimality principle which assumes that the CNS minimizes some kind of cost function, whereas the "costs" to be minimized are not clear and there have been investigations on e.g. muscle activations, jerk, torque change, energy or time variance [2].

In our work we are not aiming on proving a control scheme of the CNS. Instead we concentrate on human like motion generation for ergonomic evaluation having a specific focus on inner loads and muscle activation signals. We use a DHM based on a full dynamic MBS model with *discrete mechanics optimal control* (DMOC) [3,4] which allows us to use, compare and combine the above described approaches in the application of human motion generation. The DHM can be actuated via joint torques, single muscles or muscle synergies (1D hill type muscle models [4]). To get human motion data for validation we have defined and setup a *basic reaching test* in the motion lab where the test subject stand in front of a plane and moves his hand (tip of middle finger) from a relaxed hanging start position to marked points (adjusted to its anthropometry) on the plane (see Fig. 1, *left* and *middle*). We measured about 150 different motions including different distances and orientations to the plane, weighted motions and distinct final hand orientations. The surface electromyography (sEMG) signals of 16 arm and shoulder muscles as well as the arm/hand/shoulder trajectories were recorded with a motion capture system.

With a *non-negative matrix factorization* (NMF) algorithm [5], we extracted *time invariant muscle synergies* (aka. *synchronous synergies*, *spatially fixed muscle synergies* or *muscle modes*) from the measured EMG data. The robustness of the extracted Synergies was evaluated by reconstructing the muscle activation signals of certain data sets using muscle synergies extracted from other data sets (different points and weights) and calculating the variance account for (VAF [6]). We have then built up the *basic reaching test* in our DHM simulation environment (see Fig. 1, *right*) and investigated the influence of (combined) different cost functions as well as the use of muscles

and muscle synergies as actuators to the resulting motions (trajectories, accelerations) and muscle activation signals. We showed that a weighted combination of certain cost functions results in human like motions and beside this provides more natural activation signals than the use of single cost functions. We further on showed that we can produce useful motions using muscles as actuators (actuated individual or via muscle synergies) which can deliver important data for ergonomic evaluation.

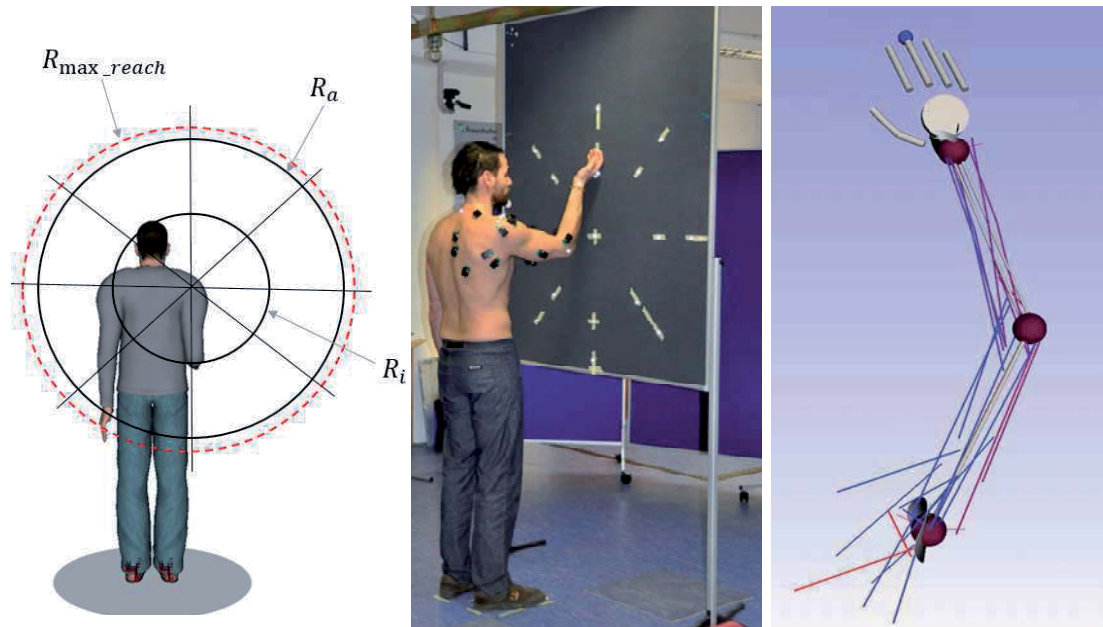


**Figure 1.** The basic reaching test: (left) The test setup with aiming point configuration adjusted to the subject's anthropometry. Inner radius ( $R_i$ ) corresponds to the upper arm length, outer radius ( $R_a$ ) equals 90% of the maximal reachability ( $R_{max\_reach}$ ). Aiming points were placed on the intersections of  $R_i$  and  $R_a$  with the horizontal and the vertical lines and their bisectrices. (middle) Test execution in the motion lab with motion capture system and sEMG measurement of 16 arm and shoulder muscles; (right) Test setup in our DHM simulation environment with a muscle driven model of the right arm. Upper arm, forearm and hand modeled as rigid bodies (grey) connected via joints (5 DOF, red balls with grey ellipsoids delimiting the range of motion) and actuated by hill type muscle models (blue and red lines, 29 muscles).

## Acknowledgments

This work was supported by the Fraunhofer Internal Programs under Grant No. MAVO 828 424.

## References

- [1] E. Bizzi, V.C.K. Cheung, A. d'Avella, P. Saltiel and M. Tresch. Combining modules for movement. *Brain Research Reviews*, 57:1:1-270, January 2008.
- [2] E. Todorov. Optimality principles in sensorimotor control. *Nature Neuroscience*, 7:907-915, 2004.
- [3] S. Björkenstam, J. S. Carlson, B. Lennartson. Exploiting sparsity in the discrete mechanics and optimal control method with application to human motion planning. *Eleventh IEEE International Conference on Automation Science and Engineering*, pp.769-774, Gothenburg, Sweden, 2015.
- [4] R. Maas, S. Leyendecker. Biomechanical optimal control of human arm motion. *Journal of Multi-Body Dynamics* 227:4:375-389, 2013.
- [5] M. C. Tresch, V. C. K. Cheung, A. d'Avella. Matrix Factorization Algorithms for the Identification of Muscle Synergies: Evaluation on Simulated and Experimental Data Sets. *Journal of Neurophysiology*, 95:4:2199-2212, 2006.
- [6] E. Chiovetto, B. Berret, I. Delis, S. Panzeri, T. Pozzo. Investigating reduction of dimensionality during single-joint elbow movements: a case study on muscle synergies. *Frontiers in Computational Neuroscience*, 7:11, 2016.

## Periodic servo-constraints in a stick balancing problem

László Bencsik<sup>1</sup>, Ambrus Zelei<sup>2</sup>

<sup>1</sup>MTA-BME Lendület  
Human Balancing Research Group  
Nádor u. 7., Budapest, 1051, Hungary  
zelei@mm.bme.hu,

<sup>2</sup>MTA-BME Research Group on Dynamics of  
Machines and Vehicles.  
Nádor u. 7., Budapest, 1051, Hungary  
bencsik@mm.bme.hu

### Abstract

To understand the human balancing is always a scientifically challenging task. As a model of human balancing many times the problem of stick balancing is studied [1], [2]. In that studies the main focus is on the stability of the delayed controller. In contrast here the focus is on the actuation of the model. The classical model of the stick balancing problem (see: Figure 1. left) is an inverted pendulum. The classical inverted pendulum model has 2DoF but only one control forces exists thus it can be modelled as an underactuated problem. In this work a periodic control technique will be applied, which is specially developed for underactuated systems [3].

In underactuated systems the task of inverse dynamics is not well defined. Some degrees-of-freedom cannot directly be controlled, and the corresponding generalized coordinates depend on the system dynamics only. Methods that are available in the literature introduces controlled and uncontrolled generalized coordinates, and solve for the inverse dynamics with a generalized computed torque control technique. Beside, the uncontrolled motion has to be calculated. This is often referred to as the internal- or passive dynamics of the system, which has to be stable to ensure the stability of the whole system. However, the stability of the internal dynamics depend on the controlled output/task. In case of the stick balancing the reducing of the inclination is the main control objective while the position of the bottom of the rod can be chosen as the internal dynamics. As a generalization the task in the control problem is formulated by additional constraints the so-called servo-constraints. In order to enhance the stability behaviour it is quite common to modify the original servo-constraints, because with this slight modification the otherwise unstable internal dynamics can be stabilized. A different approach when the servo constraints are not modified, but periodically changed in time [3]. In one period the servo constraints are for realizing the desired motion, while in the subsequent (typically shorter) period the servo-constraints are modified to stabilize the internal dynamics. The goal of this work is to show how the periodic controller can be used in stick balancing. The sliding pendulum which is the mechanical model of the stick balancing problem is shown in (see: Figure 1. right).

The equation of motion of the swinging pendulum can be derived using the Lagrange equation of the second kind using the inclination of the rod and the horizontal position of the slider as generalized coordinates  $\mathbf{q} = [x_1 \quad \mathcal{G}]^T$ , which is given in the following general form:

$$\mathbf{M}\mathbf{q} + \mathbf{c} = \mathbf{Q}_g + \mathbf{H}\mathbf{u}, \quad (1)$$

Using the generalized coordinates the main task of the robot is the control of the inclination and beside this as a secondary stabilizing control objective is the regulation of the position of the slider. These control goals can be defined with servo-constraints respectively

$$\hat{\gamma} = l \sin(\mathcal{G}) = 0 \quad \gamma_S = x_1 = 0. \quad (2)$$

Using the generalization of the computed torque control the required control force  $\mathbf{u}$  could be expressed from the following equation [3]:

$$\begin{bmatrix} \mathbf{M} & \mathbf{H} \\ \mathbf{I} & \mathbf{0} \end{bmatrix} \begin{bmatrix} \mathbf{q} \\ -\mathbf{u} \end{bmatrix} = \begin{bmatrix} -\mathbf{c} \\ -\dot{\gamma}_q \dot{\mathbf{q}} - k_D \dot{\gamma} - k_P \gamma \end{bmatrix}, \quad (3)$$

where  $\gamma = \kappa(t)\hat{\gamma} + (1 - \kappa(t))\gamma_S$  is the periodic servo-constraint where  $\kappa(t)$  realize the switching between the two control objective.

In order to show the usability of the proposed method a linear stability investigation was carried assuming a reflex delay. The results of the stability calculation are depicted in Figure 2 in the space of the free control gains  $k_D$  and  $k_P$ . The left hand side of Figure 2. shows the stable parameters when only the inclination of the rod is controlled. The right hand side of Figure 2. shows the stable parameters, when after each second step the original control is interrupted and the slider is controlled for one time interval.

It can be concluded that with the application of the periodic controller the control gain parameters can be selected from a wider range. Furthermore with the application of the periodic controller faster decay can be achieved.

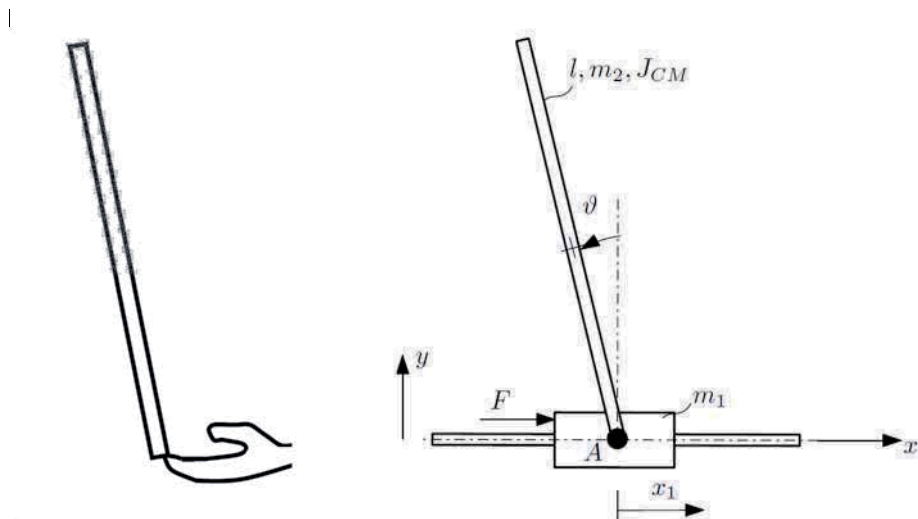


Figure 1. *left*: stick balancing problem; *right*: mechanical model of stick balancing

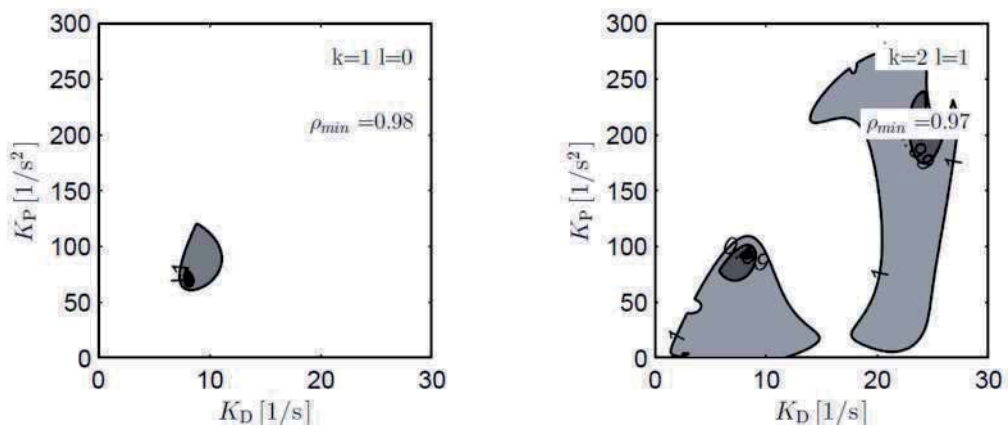


Figure 2. *left*: Stability chart of the conventional controller; *right*: Stability chart of the periodic controller

## References

- [1] Insperger T, Stick balancing with reflex delay in case of parametric forcing, *Communications in Nonlinear Science and Numerical Simulation*, 2160-2168, 16(4), 2011
- [2] G. Stépán, „Delay effects in brain dynamics”, *Phil. Trans. Roy. Soc A*, 367:1059-1062, 2009.
- [3] L. Bencsik, L. Kovács L., A. Zelei; Stabilization of Internal Dynamics of Underactuated Systems by Periodic Servo-Constraints; *International Journal of Structural Stability and Dynamics*, (available online)
- [4] Stability case study of the ACROBOTER underactuated service robot LL Kovács, L Bencsik *THEORETICAL AND APPLIED MECHANICS LETTERS* 7 pages. 2:(4), 2012

# Generating Optimal Gaits for the Biped Across Different Locomotion Modes

Lulu Gong, Zhenghai Zhang, Cichen Zhang, Weikang Zeng, Yunpeng Li

School of Life Sciences and Technology  
Tongji University  
No.1239, Road Siping, 200092 Shanghai, P.R. China  
lulugong@tongji.edu.cn

## Abstract

### *Objectives*

This paper proposes the optimal trajectory generation method for the biped walking across different locomotion modes with minimum energy consumption by using genetic algorithm trained neural network (GA-NN).

### *Methods*

The biped robot should be adaptive to the transition between different locomotion modes, such as transition from level walking to slopes ascending/descending. For a good system, the transitions should be automatic, seamless (no stopping) and natural. Young et al. [1] proposed the intent recognition strategy to allow the amputees to naturally transit between five different modes. Yang et al. [2] utilized Genetic Algorithm Optimized Fourier Series Formulation (GAOFSF) to generate stable gaits when the biped walking on slopes of different gradients. Considering energy efficiency and the stability of the robot locomotion, different optimization tools (such as genetic algorithm (GA) and GA-NN) were used to produce optimized gaits for the biped walking on uneven terrains, see e.g. Selene et al. [3] and Gong [4-6]. Vundavilli and Pratihar [7] found that GA-trained NN and GA-trained FL approaches were more adaptive compared to the analytical approach in creating optimal bipedal gaits. In addition, Gong and Schiehlen [8] and Gong [9] studied the motion/force control strategy for impactless biped walking stably on slopes and stairs. In this work, the optimal trajectories were generated by GA-NN for the biped walking across different locomotion modes. The 7-linked impactless bipedal model used in this paper was built with the multibody formalism Neweul-M2 [10].

In GA-NN algorithm, genetic algorithm is utilized to create the initial optimal trajectories of the lower limb joints for the biped walking uphill and downhill. GA design variables include the step length ( $s$ ) and the speed ( $v$ ). Then, one module of NN was used to generate optimal trajectories of the lower limb joints. The connecting weights of the NN were also generated by GA. The NN inputs were the initial optimal trajectories of the swing foot obtained by GA. The NN outputs were the final optimal coordinates of the swing foot. The biped locomotion transitions between different inclined surfaces with different angles ( $\gamma$ ) were investigated in this study. In order to minimize the energy consumption, the minimum specific resistance ( $\varepsilon$ ) is calculated [11], which is defined as:

$$\varepsilon(v) = \frac{P(v)}{mgv}, \quad (1)$$

where  $P$  is the mechanical power output and  $mg$  is the biped weight.

The optimal trajectories of the lower limbs were obtained for the biped walking uphill with different gradients changing from  $0^\circ$ ,  $+5^\circ$ ,  $+10^\circ$ ,  $+15^\circ$  to  $+20^\circ$ . The angles of slopes for downhill walking ranged from  $-20^\circ$ ,  $-15^\circ$ ,  $-10^\circ$ ,  $-5^\circ$  to  $0^\circ$ .

### *Results and Discussions*

The results show that the presented approach can generate stable human-like walking gaits for slopes with different specified gradients. The transitions between different locomotion modes are seamless. The GA-NN approach is able to generate more balanced gaits with lower energy consumption compared to GA approach.

This approach can be used effectively to produce stable gaits for walking on inclined surfaces with changing angles. Future work will focus on extending the approach to the 3D biped model walking across the complex environment.

## Acknowledgments

This work was supported by the NSFC Grant (No. 11402176), the Fundamental Research Funds for the Central Universities, and the National Key Research and Development Program of China, Stem Cell and Translational Research (No. 2016YFA0102200).

## References

- [1] A.J. Young, A. Simon, L.J. Hargrove. An intent recognition strategy for transfemoral amputee ambulation across different locomotion modes. *35<sup>th</sup> Annual International Conference of the IEEE EMBS*, pages 1587-1590. Osaka, Japan, 2013.
- [2] L. Yang, C.-M. Chew, T. Zielinska, and A.N. Poo. A uniform biped gait generator with offline optimization and online adjustable parameters. *Robotica*, 25:549-565, 2007.
- [3] L.C-M. Selene, C. Oscar, and T.A. Luis. Generation of walking periodic motions for a biped robot via genetic algorithms. *Applied Soft Computing*, 11:5306-5314, 2011.
- [4] L. Gong. Generation of optimal gaits for impactless bipedal walking on slopes via genetic algorithm. In *Proceedings of the 3rd Joint International Conference on Multibody System Dynamics and the 7th Asian Conference on Multibody Dynamics*, June 30-July 3, Busan, Korea, 2014.
- [5] L. Gong. Optimal trajectory generation for the biped walking on inclined surfaces. In *Proceedings of ECCOMAS Thematic Conference on Multibody Dynamics*, June 29-July 2, Barcelona, Spain, 2015.
- [6] L. Gong. Optimal gait generation for the biped crossing ditches. *The 4th Joint International Conference on Multibody System Dynamics*, May 29 – June 2, Montréal, Canada, 2016.
- [7] P.R. Vundavilli, D.K. Pratihar. Dynamically balanced optimal gaits of a ditch-crossing biped robot. *Robotics and Autonomous Systems*, 58(4):349-361, 2010.
- [8] L. Gong, W. Schiehlen. Impactless biped walking on a slope. *Theoretical & Applied Mechanics Letters*, 3(1): 013002, 2013.
- [9] L. Gong. Impactless biped walking on stairs. In *Proceedings of the ASME 2013 International Design Engineering Technical Conferences & Computers and Information in Engineering Conference (IDETC/CIE 2013)*, IDETC2013-12237, August 4-7, pages V07AT10A002, Portland, USA, 2013.
- [10] T. Kurz, P. Eberhard, C. Henninger, and W. Schiehlen. From Neweul to Neweul-M2: symbolical equations of motion for multibody system analysis and synthesis. *Multibody System Dynamics*, 24(1):25-41, 2010.
- [11] W. Schiehlen. Energy-optimal design of walking machines. *Multibody System Dynamics*, 13(1):129-141, 2005.

## Kinematic Validation Of A Human Thumb Model

Uday D. Phutane<sup>1</sup>, Michael Roller<sup>2</sup>, Staffan Björkenstam<sup>3</sup>, Joachim Linn<sup>2</sup>, Sigrid Leyendecker<sup>1</sup>

<sup>1</sup>Chair of Applied Dynamics  
University of Erlangen-Nuremberg  
Immerwahrstr. 1, 91058 Erlangen, Germany  
[uday.phutane, sigrid.leyendecker]@fau.de

<sup>2</sup>Fraunhofer ITWM  
Fraunhofer Platz 1,  
67663 Kaiserslautern, Germany  
[michael.roller, joachim.linn]@itwm.fraunhofer.de

<sup>3</sup>Fraunhofer-Chalmers Centre  
Chalmers Science Park  
SE-412 88 Göteborg, Sweden  
staffan@fcc.chalmers.se

### Abstract

The activity of grasping is possible due to the unique design of the human thumb and its complex movements viz. apposition, opposition etc. To simulate these complex movements, a physically correct model of the thumb is necessary. Anatomically, the thumb is made of three bones and three joints, namely the carpometacarpal (CMC) joint between the carpal (wrist) bone and the first metacarpal bone, the metacarpophalangeal (MCP) joint between the first metacarpal and the proximal phalanx bone and the interphalangeal (IP) joint between the proximal and distal phalanges.

The design of the CMC is of peculiar interest to researchers. It is a saddle joint [1] with rotations of flexion-extension (FE) and adduction-abduction (AA) and has been mathematically implemented in biomechanical models as a universal or cardan joint [2]. However, cadaver measurements [3] and more recently magnetic resonance (MR) imaging [4] have established that the CMC (and also the MCP) joints are composed with two axes of rotations which are non-orthogonal and non-intersecting, as opposed to a universal joint. Also, it has been studied that such a joint configuration is necessary to develop correct thumb tip forces in key posture and opposition posture [5].

Here, we develop a multibody model, similar to [6], of the thumb, as shown in Figure 1, with two degrees of freedom for the CMC and the MCP joints respectively and one degree of freedom for the IP joint. While the CMC and the MCP joints allow for motions of FE and AA, the IP joint allows only the motion of FE. The dimensions of the bones of the thumb are taken from [7] while the location and the orientation of the axes of the joints are obtained from [3].

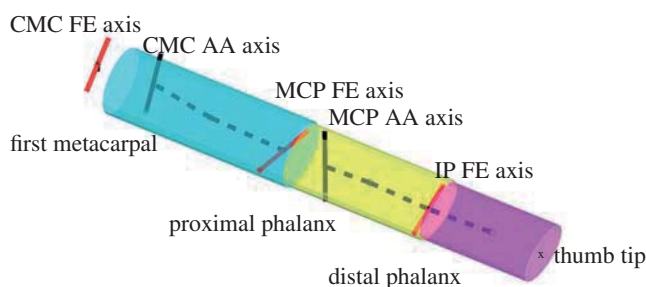


Figure 1: Thumb multibody model.

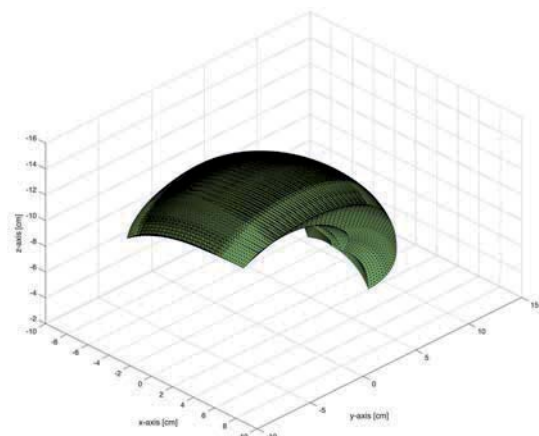


Figure 2: Point cloud of the thumb tip with maximum ROM.

To validate the realistic behavior of the model, we perform a two-fold validation test. Firstly, we plot the point cloud, as shown in Figure 2, of the work-space created by the tip of the thumb by moving the thumb kinematically in all its degrees of freedom and then calculating the volume using alpha shapes. There are two sets of limits on the range of motion (ROM), namely the maximum ROM and the grasp ROM. The grasp ROM limits are smaller than the maximum ROM as grasping while performing activities of daily living is not possible with the thumb at its anatomic extreme positions. Hence, grasp ROM yields lesser volume than maximum ROM. This reduction in the volume is a kinematic measure for a thumb model. We calculate the volume reduction for the thumb model

we created using parameters as stated above and also for four more thumb models obtained from Monte-Carlo simulations as described in [7]. These thumb models are representative of the anatomic variability of thumb FE and AA axes in general population and have differences such as the location of the MCP FE axis being distal to the MCP AA axis in two models and vice versa in the other two models. The reduction of volume for the thumb models from our simulations is found to be in the range of 71% to 75%. We compare these values with data from literature [8], wherein the volume reduction values vary between 68% and 76%.

Secondly, we compute the axial rotation of the thumb CMC joint in different postures. The axial rotation of the thumb is an outcome from the different positions of the thumb in FE and AA as the thumb CMC does not have an active third degree of freedom to rotate around its longitudinal axis. We compare the axial rotation of the first metacarpal for different FE and AA rotations with values from literature [1]. The axial rotation resulting in our simulation lies within the limits of the standard deviation of the literature values. The results for the two validation tests are in close agreement with the literature values and consequently the thumb model can be said to have been validated kinematically.

## References

- [1] W. P. Cooney, M. J. Lucca, E. Y. Chao and R. L. Linscheid, "The kinesiology of the thumb trapeziometacarpal joint", *The Journal of Bone and Joint Surgery*, vol. 63, no. 9, pp. 1371-1381, 1981.
- [2] J. L. Sancho-Bru, M. C. Mora, B. E. León, A. Pérez-González, J. L. Iserte and A. Morales, "Grasp modelling with a biomechanical model of the hand", *Computer Methods in Biomechanics and Biomedical Engineering*, vol. 17, no. 4, pp. 297-310, 2014.
- [3] A. Hollister, W. L. Buford, L. M. Myers, D. J. Giurintano and A. Novick, "The axes of rotation of the thumb carpometacarpal joint", *Journal of Orthopaedic Research*, vol. 10, no. 3, pp. 454-460, 1992.
- [4] P. Cerveri, E. De Momi, M. Marchente, G. Baud-Bovy, P. Scifo, R. M. L. Barros and G. Ferrigno, "Method for the estimation of a double hinge kinematic model for the trapeziometacarpal joint using MR imaging", *Computer Methods in Biomechanics and Biomedical Engineering*, vol. 13, no. 3, pp. 387-396, 2010.
- [5] F. J. Valero-Cuevas, M. E. Johanson and J. D. Towles, "Towards a realistic biomechanical model of the thumb: the choice of kinematic description may be more critical than the solution method or the variability/uncertainty of musculoskeletal parameters", *Journal of Biomechanics*, vol. 36, no. 7, pp. 1019-1030, 2003.
- [6] R. Maas and S. Leyendecker, "Biomechanical optimal control of human arm motion", *Journal of Multi-body Dynamics*, vol. 227, no. 4, pp. 375-389, 2013.
- [7] V. J. Santos and F. J. Valero-Cuevas, "Reported anatomical variability naturally leads to multimodal distributions of Denavit-Hartenberg parameters for the human thumb", *IEEE Transactions on Biomedical Engineering*, vol. 53, no. 2, pp. 155-163, 2006.
- [8] K. Dermizakis, A. Ioannides, and H.-T. Lin, "Robotic thumb grasp-based range of motion optimisation", in *35th Annual International Conference of the IEEE Engineering in Medicine and Biology Society (EMBC)*, Osaka, 2013.

# Optimal Control Prediction of a Dynamically Consistent Walking Motion for a Spinal Cord-Injured Subject Assisted by Orthoses

M. Febrer-Nafria<sup>1</sup>, F. Mouzo<sup>2</sup>, U. Lugris<sup>2</sup>, B.J. Fregly<sup>3</sup>, J.M. Font-Llagunes<sup>1</sup>

<sup>1</sup>Department of Mechanical Engineering  
Universitat Politècnica de Catalunya  
Diagonal 647, 08028 Barcelona, Spain  
[miriam.febrer, josep.m.font]@upc.edu

<sup>2</sup>Laboratory of Mechanical Engineering  
University of La Coruña  
Mendizábal s/n, 15403 Ferrol, Spain  
[francisco.mouzo, ulugris]@udc.es

<sup>3</sup>Department of Mechanical and Aerospace Engineering  
University of Florida  
231 MAE-A Building, Gainesville, FL 32611-6250, USA  
fregly@ufl.edu

## Abstract

Gait restoration is a high priority among spinal cord-injured (SCI) individuals. For those with incomplete SCI, the use of active orthoses (or exoskeletons) can improve the energy cost and aesthetics of their gait [1]. The authors are working on a project aimed at developing an active knee-ankle-foot orthosis (KAFO) to assist the gait of incomplete SCI subjects that can control hip rotation to some extent. The passive structure of this orthosis is tailored to the subject and built in an orthopedic workshop. Afterward, the actuation system and sensors are added to the passive structure to make the orthosis active and autonomous [2]. Simulations using subject-specific computational walking models that account for individual impairment can help in the selection of optimal gait-assistive devices for individual SCI subjects. This work deals with the development of a subject-specific simulation framework for the prediction of dynamically consistent walking motions of an SCI subject using orthoses and crutches.

Thus far, few published studies dealing with human motion prediction involve impaired or assisted motion. As examples, in [3], walking motions at different speeds for an individual post-stroke are predicted using a detailed subject-specific model, whereas in [1], the gait of an SCI subject assisted by active orthoses is studied. In the latter, the SCI impairment was modelled at the muscle level using muscle denervation parameters. However, a generic 2D computational model that does not correspond to a particular subject was used and the active orthoses were modelled as embedded in the lower limbs, omitting the physical interaction between the subject's body and the orthoses.

This work predicts a dynamically consistent walking motion, i.e., without a residual wrench acting on the pelvis, of an SCI subject assisted by passive orthoses (with no motors and sensors) and crutches. The simulation was generated by solving an optimal control problem that tracked experimental motion, where both joint angles and joint torques were unknowns. This approach allowed us to obtain a new motion that was close to the experimentally measured one, while also minimizing the pelvis residual wrench.

The experimental walking motion of an SCI female subject (41 years old, mass 65 kg and height 1.52 m) with injury at the T11 level wearing a pair of passive knee-ankle-foot orthoses and crutches was captured. Motion capture involved tracking 43 optical markers using 12 optical infrared cameras (Natural Point, OptiTrack FLEX:V100 sampling at 100 Hz). Ground reaction forces were collected using two force plates (AMTI, AccuGait also sampling at 100 Hz) and crutch-ground reaction forces were measured using instrumented crutches (Fig. 1). The skeletal model was based on the 3D full-body model from [4], developed in OpenSim [5] and scaled to the specific SCI subject.



**Fig. 1.** Gait of the SCI subject assisted by passive orthoses and crutches: experimental motion and computational model.

The optimal control problem was formulated as follows: Find joint angles  $\mathbf{q}(t)$ , joint angular velocities  $\mathbf{v}(t)$  and joint angular accelerations  $\mathbf{a}(t)$  (states,  $\mathbf{x}(t)$ ), and joint angular jerks  $\mathbf{j}(t)$  and joint torques  $\boldsymbol{\tau}(t)$  (controls,  $\mathbf{u}(t)$ ), which minimize differences between experimental data and predicted motion (cost function), subject to satisfying the dynamics equations (constraints). The cost function included terms that tracked experimental joint angles, joint angular velocities, joint angular accelerations and inverse dynamics torques, and a term that minimized joint angular jerks. The dynamics of the problem was formulated by simple dynamic constraints, where the states derivatives are part of states and part of controls (1). The equations of motion of the multibody system, obtained from OpenSim, were introduced as algebraic path constraints, where residuals were constrained to be zero (2) and torques obtained from inverse dynamics and torques guessed as controls were equated (3).

$$\dot{\mathbf{x}}(t) = [\dot{\mathbf{q}}(t), \dot{\mathbf{v}}(t), \dot{\mathbf{a}}(t)] = [\mathbf{v}(t), \mathbf{a}(t), \mathbf{j}(t)] \quad (1)$$

$$-\boldsymbol{\varepsilon}_0 \leq \mathbf{R}_{pelvis} \leq \boldsymbol{\varepsilon}_0 \quad (2)$$

$$-\boldsymbol{\varepsilon}_1 \leq \boldsymbol{\tau}_{IDA} - \boldsymbol{\tau} \leq \boldsymbol{\varepsilon}_1 \quad (3)$$

The optimal control problem was solved using GPOPS-II [6], an algorithm that uses a direct collocation method. Due to inaccuracies introduced during the experimental data collection and in the computational modeling, the total external reactions computed from the dynamic equations do not coincide with the ground reaction forces measured experimentally, i.e., the wrench applied to the six degrees of freedom (position and rotation) of the pelvis (base body) is not zero. Motion prediction allows slightly modifying the acquired motion and forces in order to minimize the pelvis residual wrench, resulting in a dynamically consistent subject-specific crutch walking motion.

As future work, the proposed methodology will be used to predict the walking motion of the same subject wearing a pair of active KAFOs, identical to the ones presented in [2]. In this case, the knee flexion-extension provided by the orthosis actuator will be allowed during swing phase; and it will be constrained during stance, as with the real prototype. This methodology could be useful as a support tool for the patient-tailored design of walking assistive devices, to simulate patient adaptation to the device, and to test virtually different control strategies.

## Acknowledgments

This work has been supported by the Spanish Ministry of Economy and Competitiveness under the project DPI2015-65959-C3-2-R, co-funded by the European Union through ERDF funds.

## References

- [1] D. García-Vallejo, J. M. Font-Llagunes, and W. Schiehlen. Dynamical analysis and design of active orthoses for spinal cord injured subjects by aesthetic and energetic optimization. *Nonlinear Dynamics*, 84(2): 559-581, 2016.
- [2] J. M. Font-Llagunes, D. Clos, U. Luginis, F. J. Alonso, and J. Cuadrado. Design and experimental evaluation of a low-cost robotic orthosis for gait assistance in subjects with spinal cord injury. In J. González-Vargas *et al.*, editors, *Wearable Robotics: Challenges and Trends. Proceedings of the 2<sup>nd</sup> Int. Symposium on Wearable Robotics*, pages 281-285. Segovia, Spain, 2016.
- [3] A. J. Meyer, I. Eskinazi, J. N. Jackson, A. V Rao, C. Patten, and B. J. Fregly. Muscle synergies facilitate computational prediction of subject-specific walking motions. *Frontiers in Bioengineering and Biotechnology*, 4:77, 2016.
- [4] S. R. Hamner, A. Seth, and S. L. Delp. Muscle contributions to propulsion and support during running. *Journal of Biomechanics*, 43(14): 2709-2716, 2010.
- [5] S. L. Delp, F. C. Anderson, A. S. Arnold, P. Loan, A. Habib, C. T. John, E. Guendelman, and D. G. Thelen. OpenSim: open-source software to create and analyze dynamic simulations of movement. *IEEE Transactions on Biomedical Engineering*, 54(11): 1940-1950, 2007.
- [6] M. A. Patterson, and A. V. Rao. GPOPS-II: a MATLAB software for solving multiple-phase optimal control problems using hp-adaptive gaussian quadrature collocation methods and sparse nonlinear programming. *ACM Transactions on Mathematical Software*, 41:1-37, 2014.

# Collective Bounce Helicopter Proneness: Moving Towards the Characterization of the *Worst Pilot*

Andrea Zanoni<sup>1</sup>, Vincenzo Muscarello<sup>2</sup>

Department of Aerospace Science and Technology  
 Politecnico di Milano  
 Via La Masa 34, 20156, Milan, Italy  
<sup>1</sup> [andrea.zanoni<sup>1</sup>, vincenzo.muscarello<sup>2</sup>]@polimi.it

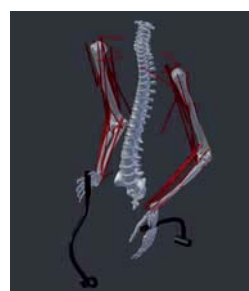
## Abstract

The interaction of the pilot with the helicopter dynamics is characterized not only by voluntary activity, which is intended to produce the control inputs required to perform a specific task, but also by involuntary actions. The latter is the result of the unintentional application of controls caused by vibrations of the cockpit. Such vibratory motion is filtered by the pilot's biomechanical characteristics and may produce involuntary control inputs through the so-called biodynamic feedthrough (BDFT [1]). Pilot's involuntary commands may further excite the dynamics of the vehicle, causing a degradation of the flight dynamics qualities, difficulties in achieving the desired performance and may ultimately produce an unstable closure of the control feedback loop [2, 3, 4].

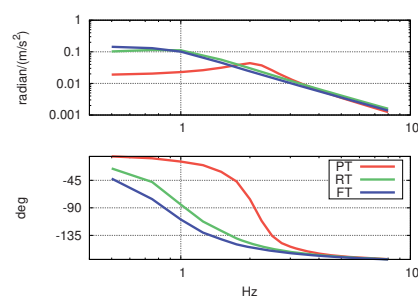
This problem, widely known as Pilot-Assisted Oscillation (PAO), may affect all kinds of aircraft whose pilot is accommodated within the vehicle and is thus subjected to its motion. Usually, PAO-related control inputs are characterized by frequencies between 2 – 8 Hz [5]; thus, in PAO events the interaction is with the aeroelastic modes of the vehicle. One of the most important PAO phenomena in helicopters is the so-called "Collective Bounce", caused by vertical vibrations of the cockpit. As a consequence of the most common cockpit and control inceptors layout, the vibrations induce a collective control input as a result of the biodynamics of the pilot's left arm. This, in turn, excites the vertical vibration by directly inducing a change in rotor thrust along the vertical axis. A closed-loop aeroelastic experiment involving the collective bounce was presented and discussed by Masarati et al. in [6]. In [7] Muscarello et al. pinpointed the phase margin reduction introduced by the main rotor coning mode in the collective pitch–heave loop transfer function as the key factor in the manifestation of collective bounce.

The investigation of PAO instabilities requires the capability to model aeroservoelastic phenomena as well as the dynamic behavior of the pilot. A simplified helicopter model, able to capture the collective bounce dynamics in hover, has been proposed in [7]. It consists of the vertical motion of the entire helicopter and the rotor coning motion. The pilot's BDFT can be modeled as a set of mechanical impedances between the motion of the seat and the resulting actuation of the control inceptors, since no voluntary action can be envisaged.

Experimental results obtained so far have shown how pilot's arms response to vibrations is characterized by an high level of variability [8]. As a consequence it should be considered as an highly uncertain element in the dynamic modeling of this kind of problems. Over the last several years, a detailed biomechanical multibody model of the pilot's body has been developed at Politecnico di Milano Aerospace Science and Technology Department: it features the full representation of the pilot upper limbs, each one possessing 7 degrees of freedom and actuated by a set of 25 Hill-type, one dimensional muscle actuators [9, 10]. The upper limbs model has been coupled with a Component Mode Synthesis model of the human torso to complete the description of the pilot's upper body dynamics.



(a) Biomechanical multibody model



(b) Identified pilot's BDFT

Figure 1: The biomechanical multibody model of the upper limbs and torso.

To assess the variability of the bioservoelastic interaction between the pilot and the vehicle with respect to the pilot's body characteristics, it is of crucial importance to be able to represent, as realistically as possible, a wide variety of pilots with possibly very different anthropometric parameters. To this end, the upper limbs model has been extended with a specific set of procedures to generate its geometrical, inertial and muscular properties [11] based on a set of very standard anthropometric data: stature, weight, age and sex. The present work extends the geometry scaling also to the CMS model of the torso to yield the scaling of the complete pilot's body model.

In order to assess the effects of the variability of the anthropometric data on the performance parameters with respect to PAO phenomena, a fully numerical procedure has been developed. It consists in several steps:

- a set of *random* anthropometric parameters is generated;
- the corresponding multibody model is built;
- the multibody model is simulated in order to identify the biomechanical transfer function between the seat vertical acceleration and the control inceptor displacement
- the resulting state space pilot model is simulated coupled with the simplified helicopter model, in order to evaluate the figures of (de-)merit with respect to PAO resilience;

The whole procedure is governed by a genetic (de-)optimization algorithm: that ultimately yields the *worst* possible combinations of anthropometric parameters for that particular rotorcraft.

## References

- [1] H. R. Jex and R. E. Magdaleno, "Biomechanical models for vibration feedthrough to hands and head for a semisupine pilot," *Aviation, Space, and Environmental Medicine*, vol. 49, no. 1–2, pp. 304–316, 1978.
- [2] M. D. Pavel, M. Jump, B. Dang-Vu, P. Masarati, M. Gennaretti, A. Ionita, L. Zaichik, H. Smaili, G. Quaranta, D. Yilmaz, M. Jones, J. Serafini, and J. Malecki, "Adverse rotorcraft pilot couplings — past, present and future challenges," *Progress in Aerospace Sciences*, vol. 62, pp. 1–51, October 2013. doi:10.1016/j.paerosci.2013.04.003.
- [3] M. D. Pavel, P. Masarati, M. Gennaretti, M. Jump, L. Zaichik, B. Dang-Vu, L. Lu, D. Yilmaz, G. Quaranta, A. Ionita, and J. Serafini, "Practices to identify and preclude adverse aircraft-and-rotorcraft-pilot couplings — a design perspective," *Progress in Aerospace Sciences*, vol. 76, pp. 55–89, 2015. doi:10.1016/j.paerosci.2015.05.002.
- [4] D. T. McRuer, *Aviation Safety and Pilot Control: Understanding and Preventing Unfavourable Pilot-Vehicle Interactions*. Washington DC: National Research Council, National Academy Press, 1997.
- [5] O. Dieterich, J. Götz, B. DangVu, H. Haverdings, P. Masarati, M. D. Pavel, M. Jump, and M. Gennaretti, "Adverse rotorcraft-pilot coupling: Recent research activities in Europe," in *34th European Rotorcraft Forum*, (Liverpool, UK), September 16–19 2008.
- [6] P. Masarati, G. Quaranta, L. Lu, and M. Jump, "A closed loop experiment of collective bounce aeroelastic rotorcraft-pilot coupling," *Journal of Sound and Vibration*, vol. 333, pp. 307–325, January 2014. doi:10.1016/j.jsv.2013.09.020.
- [7] V. Muscarello, G. Quaranta, and P. Masarati, "The role of rotor coning in helicopter proneness to collective bounce," *Aerospace Science and Technology*, vol. 36, pp. 103–113, July 2014. doi:10.1016/j.ast.2014.04.006.
- [8] M. Mattaboni, G. Quaranta, P. Masarati, and M. Jump, "Experimental identification of rotorcraft pilots' biodynamic response for investigation of PAO events," in *35th European Rotorcraft Forum*, (Hamburg, Germany), pp. 1–12, September 22–25 2009.
- [9] P. Masarati, G. Quaranta, and A. Zanoni, "Dependence of helicopter pilots' biodynamic feedthrough on upper limbs' muscular activation patterns," *Proc. IMechE Part K: J. Multi-body Dynamics*, vol. 227, pp. 344–362, December 2013. doi:10.1177/1464419313490680.
- [10] P. Masarati and G. Quaranta, "Bioaeroservoelastic analysis of involuntary rotorcraft-pilot interaction," *J. of Computational and Nonlinear Dynamics*, vol. 9, p. 031009, July 2014. doi:10.1115/1.4025354.
- [11] A. Zanoni and P. Masarati, "Geometry generation and benchmarking of a complete multibody model of the upper limb," in *4th Joint International Conference on Multibody System Dynamics*, (Montreal, Canada), May 29–June 2 2016.

## **Section**

# **AEROSPACE AND MARITIME APPLICATIONS**



## Equivalent Mass-Spring Models of Multibody Spacecraft for the Application of Wave-based Control

Joseph Thompson

School of Mechanical and Materials Engineering  
University College Dublin  
Belfield, Dublin 4, Ireland  
joseph.thompson@ucdconnect.ie

### Abstract

Wave-Based Control (WBC) is particularly effective for achieving rest to rest motion of under-actuated, cascaded, lumped flexible systems such as in Fig. 1. The motion of each mass  $x_1$  to  $x_n$  of this system can be considered as a superposition of rightwards and leftwards travelling components or waves, starting at the actuator  $x_0$ , travelling to the tip,  $x_n$ , and returning to the actuator. The control strategy is based on considering the motion of the actuator  $x_0$  as simultaneously launching rightwards travelling motion (waves) into the system while absorbing leftwards travelling motion coming back from the system. For rest-to-rest manoeuvres to a target displacement, the controller launches a wave into the system of half the target displacement and absorbs the returning wave after it has travelled to the end of the system and has been reflected back to the actuator. This absorption by the actuator moves the system the second half of the target displacement while absorbing vibrations. Thus position control and active vibration damping are combined in a single actuator motion. The resulting control strategies have many advantages, including robustness to modelling errors and system changes, minimal sensing and ease of implementation. The cascaded system of Fig. 1 is similar to a range of systems of practical engineering interest, including

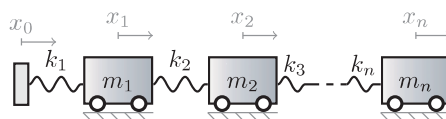


Figure 1: Non-uniform lumped system with one free and one moving boundary

robot arms, cranes, space structures and disk drive heads. Much work has been done on wave-based modelling and control of such systems [4, 3]. This paper asks the question: to what extent can this work be extended to a wider class of systems? This question is motivated by the control of spacecraft with features such as structural flexibility, flexible appendages and fuel slosh. Mathematical models of these systems, as presented to the control engineer, do not appear to have the same structure as a mass-spring string actuated at one end. Many systems for instance are modelled as multi-rigid-body systems [2] with multiple sensors and actuators or simply presented as a linear system in the form of a set of state space matrices. This leads to the following problem. Given a generic, SISO (single-input single-output), lightly damped mechanical system described by

$$\ddot{\mathbf{q}}(t) + \Lambda \mathbf{q}(t) = \mathbf{b}u(t) \quad (1)$$

$$y(t) = \mathbf{C}\mathbf{q}(t) \quad (2)$$

$$\Lambda = \begin{bmatrix} \lambda_1 & 0 & \cdots & 0 \\ 0 & \lambda_2 & \ddots & 0 \\ \vdots & \ddots & \ddots & \vdots \\ 0 & 0 & \cdots & \lambda_n \end{bmatrix} \quad (3)$$

under what conditions can this system be transformed into the equivalent of a mass-spring string such as in Fig.1 (for which WBC is known to work well)? Here  $u(t)$  is the input and  $y(t)$  is the output. We restrict ourselves to the case where the eigenvalues are real and distinct, i.e.

$$0 \leq \lambda_1 < \lambda_2 < \cdots < \lambda_n \quad (4)$$

The problem becomes if (and if so, how) this system can be transformed to a structure similar to that of the system in Fig.1. The required structure is

$$M\ddot{\mathbf{z}}(t) + K\mathbf{z}(t) = \hat{\mathbf{b}}u(t) \quad (5)$$

$$y(t) = \hat{\mathbf{C}}\mathbf{z}(t) \quad (6)$$

$$M = \begin{bmatrix} m_1 & 0 & \cdots & 0 \\ 0 & m_2 & \ddots & 0 \\ \vdots & \ddots & \ddots & \vdots \\ 0 & 0 & \cdots & m_n \end{bmatrix}, \quad K = \begin{bmatrix} k_1 + k_2 & -k_2 & 0 & \cdots & 0 \\ -k_2 & k_2 + k_3 & -k_3 & \ddots & 0 \\ 0 & -k_3 & \ddots & \ddots & \vdots \\ \vdots & \ddots & \ddots & k_{n-1} + k_n & -k_n \\ 0 & 0 & \cdots & -k_n & k_n \end{bmatrix} \quad (7)$$

An algorithm is developed to find a suitable coordinate transformation  $\mathbf{z} = P\mathbf{q}$  to achieve this objective. The problem may be first reduced to an inverse eigenvalue problem for a Jacobi matrix. This may be solved using the Lanczos algorithm as presented in [1]. It is found that there are many equivalent mass-spring systems depending on the desired forms of the input vector  $\hat{\mathbf{b}}$  and output matrix  $\hat{C}$ , that is, on the input-output structure of the system or the location(s) of actuators and sensors in the string.

The particular example we use to test the algorithm is a planar model of a rocket with a flexible structure as in Fig. 2. The model consists of three rigid bodies connected by two torsional springs. The base body has an attitude angle  $\theta$  relative to an inertial reference frame and the other bodies have relative angles  $\phi_1$  and  $\phi_2$  respectively between themselves and the segment below as shown. The rocket has a gimbaled engine producing a thrust  $T$  at an angle  $\delta$  to the main body and also a lateral thruster located on the bottom segment which produces a variable thrust  $f$ . Different test cases are examined where different actuators are used and attitude sensors are located at different positions along the rocket body i.e. on different segments. In each case an equivalent mass-spring model for the system is calculated.

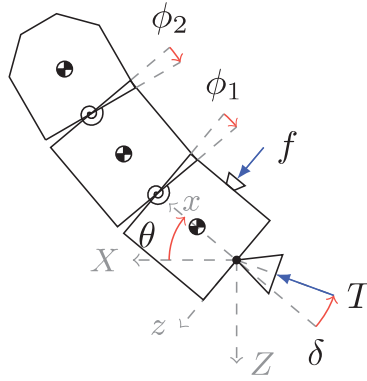


Figure 2: Segmented planar rocket model

### Acknowledgments

This research is funded by an Irish Research Council postgraduate scholarship

### References

- [1] GLADWELL, G. *Inverse problems in vibration*. Mechanics, dynamical systems. M. Nijhoff, 1986.
- [2] KANE, T. R., AND LEVINSON, D. A. Formulation of equations of motion for complex spacecraft. *Journal of Guidance, Control, and Dynamics* 3, 2 (Mar. 1980), 99–112.
- [3] O’CONNOR, W. J. Excellent control of flexible systems. *Control* (2005), 6181–6186.
- [4] O’CONNOR, W. J. Wave-like modelling of cascaded, lumped, flexible systems with an arbitrarily moving boundary. *Journal of Sound and Vibration* 330, 13 (2011), 3070–3083.

# Forward Dynamics of Fixed-Wing Aircraft with Attitude Reconstruction via Novel Quaternion-Integration Procedure

Zdravko Terze, Dario Zlatar, Viktor Pandža, Milan Vrdoljak

Faculty of Mechanical Eng. and Naval Arch.  
Chair of Flight Vehicle Dynamics  
University of Zagreb  
Ivana Lučića 5, 10002 Zagreb, Croatia  
[zdravko.terze, dario.zlatar, viktor.pandza, milan.vrdoljak]@fsb.hr

## Abstract

Unit quaternion representation (4-parameter description of spatial rotations) is widely used in flight simulation to overcome the limitations of the standard numerical ordinary-differential-equations (ODEs) based on three-parameters rotation variables (such as Euler angles), as they may impose kinematic singularities during aircraft's attitude reconstruction. However, these benefits do not come without a price, since the classical way of integrating rotational quaternions includes solving of differential-algebraic equations (DAEs) that requires numerical stabilization of the additional (explicitly-imposed) algebraic constraint enforcing the unitary norm of the quaternion. This can pose a problem in the case of longer flight simulations since improper numerical treatment of the quaternion-normalisation constraint may induce numerical drift into the simulation results. As a remedy, the proposed novel algorithm [1] circumvented DAE problem of quaternion integration by shifting update-integration-process from configuration manifold to the local tangential level of the incremental rotations (reducing thus integration to standard three ODEs problem at Lie algebra level). This can be done due to the isomorphism of the Lie algebras of the  $SO(3)$  rotation group and the unit quaternion  $Sp(1)$  group.

In order to study rotational kinematics of a local frame rigidly attached to an airplane airframe, we start with the kinematic reconstruction equation  $\dot{\mathbf{R}}(t) = \mathbf{R}(t)\tilde{\boldsymbol{\omega}}(t)$  that relates the angular velocity  $\boldsymbol{\omega}(t) \in \mathcal{R}^3$ , expressed in the local frame, and the time derivative of the frame rotation matrix  $\mathbf{R}(t)$  (aircraft attitude matrix). The assignment of the skew symmetric matrix  $\tilde{\boldsymbol{\omega}} \in so(3)$  to the vector  $\boldsymbol{\omega} \in \mathcal{R}^3$  is an isomorphism of  $so(3)$  and  $\mathcal{R}^3$  [2]. Similarly to Muthe-Kaas approach [3], we seek a solution of kinematic reconstruction equation in the form

$$\mathbf{R}(t) = \mathbf{R}_0 \exp(\tilde{\mathbf{u}}(t)), \quad (1)$$

where closed form of the exponential mapping on  $SO(3)$  is given by the Rodrigues formula [3] and  $\mathbf{u}(t) \in \mathcal{R}^3$  is the scaled instantaneous rotation vector, and  $\mathbf{R}_0$  is initial attitude. Then,  $\tilde{\mathbf{u}}(t) \in so(3)$  solves the ODE system in the Lie algebra

$$\dot{\tilde{\mathbf{u}}} = \text{dexp}_{-\tilde{\mathbf{u}}}^{-1}(\tilde{\boldsymbol{\omega}}(\mathbf{R}(t))), \quad \tilde{\mathbf{u}}_0 = \mathbf{0}, \quad (2)$$

where the operator  $\text{dexp}_{-\tilde{\mathbf{u}}}^{-1}$  admits the series expansion (see [3]).

Unit quaternions, which satisfy the unit length condition  $\|\mathbf{q}\| = q_0q_0 + \mathbf{q} \cdot \mathbf{q} = 1$ , form a group which is isomorphic to the symplectic group  $Sp(1)$  as well as to special unitary group  $SU(2)$ . The unit quaternion group is also isomorphic to the unit sphere in  $\mathcal{R}^4$ , defined as  $\mathcal{S}^3 = \{\mathbf{q} \in \mathcal{R}^4 \mid \|\mathbf{q}\| = 1\}$ . The rotational motion of a frame is thus described by  $\mathbf{q}(t) \in \mathcal{S}^3$ , where  $t$  denotes the time. Also, velocities  $\dot{\mathbf{q}} \in T_{\mathbf{q}}\mathcal{S}^3$  can be represented by introducing the vector space of skew-symplectic quaternions  $sp(1) = \{\boldsymbol{w} \in \mathcal{R}^4 \mid \boldsymbol{w} + \overline{\boldsymbol{w}} = (0, \mathbf{0})\}$  as tangent space to  $Sp(1) \cong \mathcal{S}^3$  at the group identity, where  $\overline{\boldsymbol{w}}$  is the conjugate of the pure quaternion  $\boldsymbol{w}$ . Hence,  $sp(1)$  is the Lie algebra of  $Sp(1)$ , which is isomorphic to  $so(3)$  and  $\mathcal{R}^3$ . The Lie algebra  $sp(1)$  is the set of pure quaternions isomorphic to  $\mathcal{R}^3$ , so that an element  $\boldsymbol{w} \in sp(1)$  can be assigned to a vector  $\mathbf{u} \in \mathcal{R}^3$ . For  $so(3)$  this assignment was  $\tilde{\mathbf{u}}(t) \in so(3)$ . In order to ensure that  $sp(1)$ ,  $so(3)$ , and  $\mathcal{R}^3$  are isomorphic as Lie algebras, the element  $\boldsymbol{w} = (0, 1/2\mathbf{u}) \in sp(1)$  is associated to the vector  $\mathbf{u} \in \mathcal{R}^3$ . Therefore, by following equation (1), we express update for the step in the form  $\mathbf{q}_{n+1} = \mathbf{q}_n \circ \exp_{\mathcal{S}^3}(\boldsymbol{w}_n) = \mathbf{q}_n \circ \exp_{\mathcal{S}^3}((0, 1/2\mathbf{u}_n))$ , where the closed form of the exponential mapping on  $\mathcal{S}^3$  is given by [4]

$$\exp_{\mathcal{S}^3}(\boldsymbol{w}) = \cos(1/2\|\mathbf{u}\|)(1, \mathbf{0}) + \frac{\sin(1/2\|\mathbf{u}\|)}{\|\mathbf{u}\|}(0, \mathbf{u}), \quad (3)$$

and  $\boldsymbol{w}_n$  is element of Lie algebra  $sp(1)$  associated to the incremental rotation vector, and  $\mathbf{u}_n \in \mathcal{R}^3$  is the  $n$ -th step incremental rotation vector that updates rotation, determined from

$$\dot{\tilde{\mathbf{u}}}_n = \text{dexp}_{-\tilde{\mathbf{u}}_n}^{-1}(\tilde{\boldsymbol{\omega}}(\mathbf{q}(t))), \quad \tilde{\mathbf{u}}_{n_0} = \mathbf{0}, \quad (4)$$

where the operator  $\text{dexp}_{\tilde{u}_n}^{-1}$  is introduced in [3] and  $\tilde{u}_n$  is initial condition. These equations should be integrated within each integration step together with the equations of aircraft dynamics, which determine velocity field  $\omega(t)$  from the acceleration field  $\dot{\omega}(t)$ . Since (4) is a system of ODEs defined in Lie algebra, that is a vector space, any standard vector-space ODE integrator can be used. Actually, an order of accuracy of the overall algorithm depends only on the accuracy of the ODE integrator that is utilized for solving (4).

As a numerical example of the proposed novel formulation, a 3D motion of the general aviation aircraft, modeled as a flat-earth 6DOF single rigid body problem, is discussed. North-East-Down (NED) coordinate system, is selected for the global inertial frame and is applied for the description of the trajectory. The aircraft dynamical model includes a full aerodynamic model as a function of the flight conditions, non-dimensional components of the aircraft angular velocity and controls, and includes model of the piston engine, which is based on the available power as a function of pressure, temperature, velocity and the engine RPM. Also, the aircraft has an implemented flight control system with longitudinal command and stability augmentation system. For the purpose of numerical integration, we use fixed time-step Runge-Kutta methods of the fourth order (RK4) for integration of the dynamical equations and rotation-vector Lie algebra ODEs (4) within the kinematical part of each integration step.

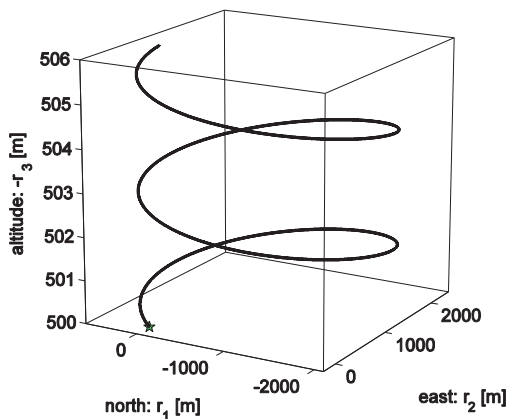


Figure 1. Trajectory  $r$  of aircraft's mass center

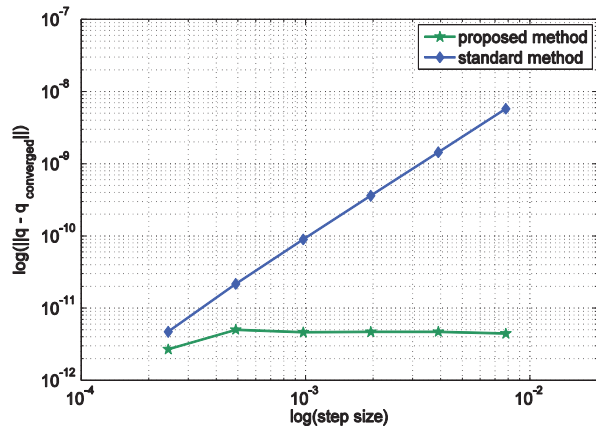


Figure 2. Convergence in the norm of error in aircraft's attitude quaternions

Trajectory of aircraft's mass center is shown in three-dimensional plot on Figure 1. In Figure 2, accuracy of the flight simulation with aircraft-attitude reconstruction via novel method is compared with the simulation that included standard quaternion integration [1]. The figure illustrates change of the norm of the rotation error for decreasing values of the integration step size, when two quaternion integration methods have been applied (note that aircraft dynamical models are identical in both cases, i.e. the only difference between the compared simulation procedures is the attitude reconstruction algorithm that is based on the novel and standard quaternion-integration algorithm). It is visible from the results that numerical integration of three non-linear ODEs in terms of incremental rotation vector (4) within the proposed novel algorithm follows a non-linear kinematical rotation update more accurately than integration of a four (linear!) ODEs (as it appears within the framework of the standard algorithm [1]), resulting in more accurate simulation results. Depending on the numerical case at hand - as it is in the presented flight example with 'slower' dynamics and steady rotation component within its 3D motion - this can allow for utilization of longer integration steps and overall better numerical accuracy. Also, it is important to note that method does not introduce any drift in the unitary norm constraint, i.e. quaternion maintains unit-length constraint (orthogonal kinematic relationship) during the whole time domain of the simulation.

To summarize, the proposed method avoids kinematic singularities that are pertinent for the Euler angles, but without imposing additional algebraic constraint to the mathematical model, as it is pertinent for the standard quaternion formulation. Besides that, the presented integration procedure may also exhibit numerical advantages in terms of better accuracy compared to the standard approach, especially in the cases of aircraft motion patterns with steady rotational component and 'slower' dynamics, when longer integration time-steps can be applied.

## References

- [1] Z. Terze, A. Mueller, D. Zlatar. Singularity-Free Time Integration of Rotational Quaternions Using Non-Redundant Ordinary Differential Equations. *Multibody Syst Dyn*, 38(3):201-225, 2016.
- [2] E. Hairer, C. Lubich, and G. Wanner. *Geometric Numerical Integration*. Springer, 2006.
- [3] Z. Terze, A. Müller, D. Zlatar. Lie-group Integration Method for Constrained Multibody Systems in State Space. *Multibody Syst Dyn*, 34(3):275-305, 2014.
- [4] P. Betsch, R. Siebert. Rigid body dynamics in terms of quaternions: Hamiltonian formulation and conserving numerical integration. *International Journal for Numerical Methods in Engineering*, 79(4):444-473, 2009.

# Attitude control of the Tether Space Mobility Device in extending and winding tether

Yu Uematsu<sup>1</sup>, Shoichiro Takehara<sup>2</sup>, Wataru Miyaji<sup>1</sup>, Yoshiaki Terumichi<sup>3</sup>

<sup>1</sup>Department of Science and Technology,  
Graduate School of Sophia University  
7-1 Kioi-cho Chiyoda-ku, Tokyo, 102-8554, Japan  
e-mail:yu.u123@eagle.sophia.ac.jp

<sup>2</sup> Department of Science and Technology,  
Sophia University  
7-1 Kioi-cho Chiyoda-ku, Tokyo, 102-8554, Japan  
e-mail:stakeha@sophia.ac.jp

<sup>3</sup> Department of Science and Technology,  
Sophia University  
7-1 Kioi-cho Chiyoda-ku, Tokyo, 102-8554, Japan  
e-mail:y-terumi@sophia.ac.jp

## Abstract

Recently the opportunity that a human is active in space increase by space development. It is expected that upsizing of manned space facilities such as the International Space Station. Therefore, an original means of transportation is necessary so that a human being is active effectively under microgravity environment. In this study, we propose a mobility device using tether named Tether Space Mobility Device (TSMD)[1]. TSMD is the mobility device that moves user by winding tether which is attached to the structure in the destination. An attitude control method of TSMD in extending and winding tether is examined by numerical analysis.

Figure1 shows the analytical model of TSMD. This model can simulate a series of movement extending and winding tether. The analytical model of TSMD is made of flexible body and three rigid bodies. In microgravity environment, it is expected that motion of tether involves large deformation. Therefore, tether is formulated using Absolute Nodal Coordinate Formulation (ANCF) which is suggested by Shabana[2]. Coupled motions between tether and rigid bodies are considered by multibody dynamics. Furthermore, the contact force between tether and arm is formulated by spring and damper elements to express the interaction between tether and arm.

Figure2 shows the experimental device of TSMD. The device is comprised of TSMD part and human imitate part. The experiment was performed under two-dimensional microgravity environment which is simulated by floating an experiment device using gas pressure to decrease contact resistance.

Figure3 shows the time history of angular velocity of COG of rigid body3 when it wind tether at constant speed. In figure3, a solid line is analytical result and dashed lines are experimental result, and both of them show qualitatively equal result. As a result of comparison between analytical and experimental result, proposed model is useful for verification of attitude control method of TSMD.

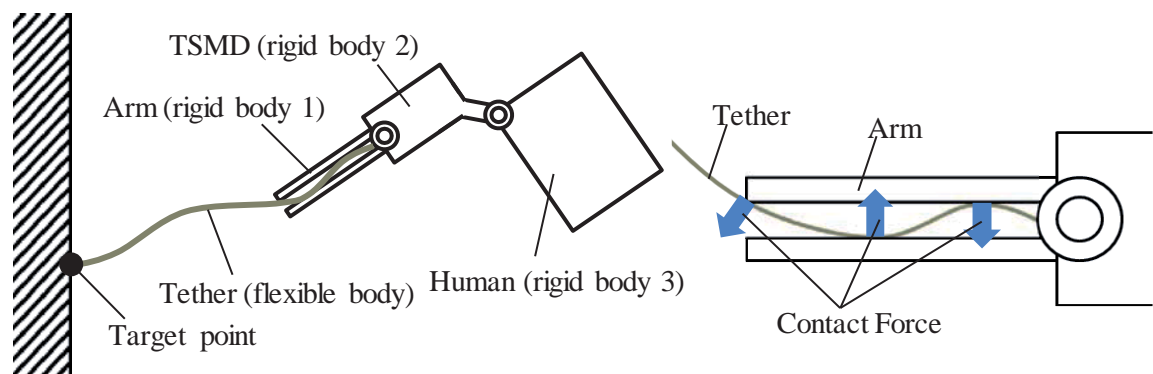
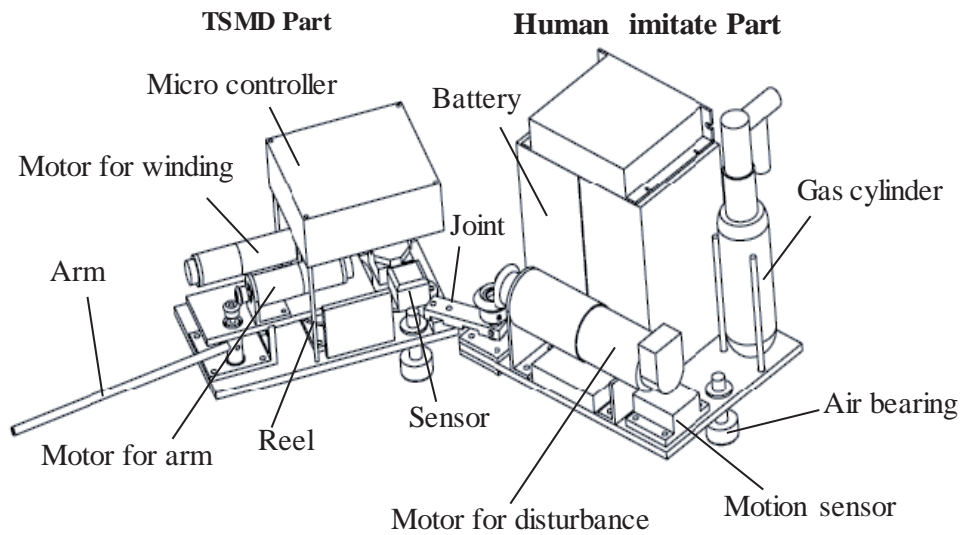
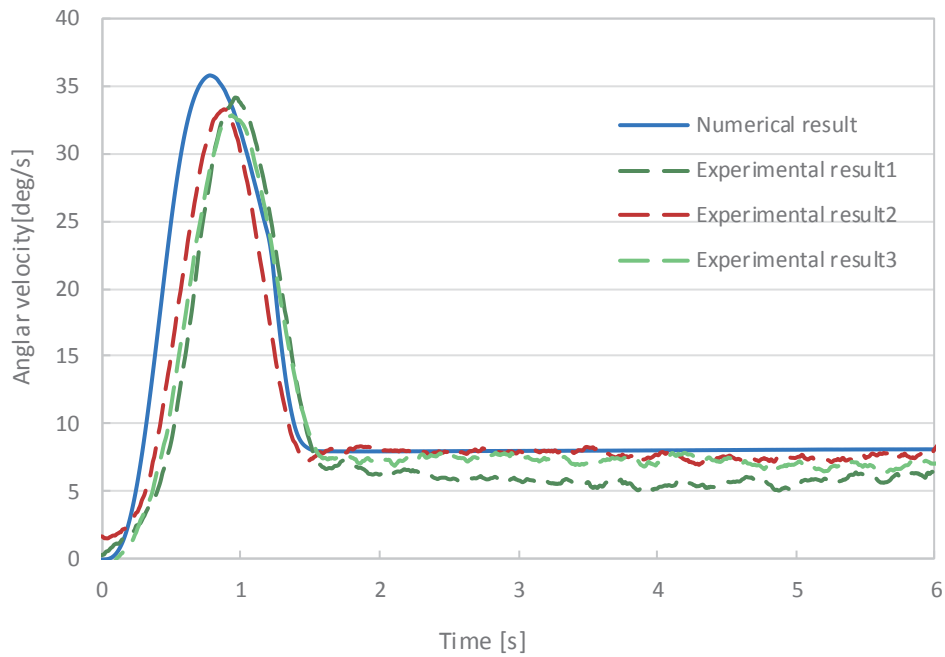


Figure 1. Analytical model of TSMD



**Figure 2.** Experimental device of TSMD



**Figure 3.** Time history of Angular velocity of TSMD

### Acknowledgments

This work was supported by JSPS KAKENHI Grant Number JP26820075.

### References

- [1] S. Takehara, T. Nishizawa, M. Kawarada, H. Hase, Y. Terumichi. Development of Tether Space Mobility Device, Computational Methods in Applied Sciences, Vol. 35, pages255-274, 2014.
- [2] H.A. Hussien, A.A. Shabana. Application of the Absolute nodal coordinate formulation to multibody system dynamics. Journal of sound and vibration, Vol. 214, No. 5, pages833-851, 1998.

# Deployment of a coilable boom based on corotational frame for flexible 3-D beams with large displacement and rotation

Zhuyong Liu, Tanhui Wu, Jiazhen Hong

School of Naval Architecture, Ocean and Civil Engineering  
Shanghai Jiao Tong University  
800 Dongchuan Road, 200240 Shanghai, China  
zhuyongliu@sjtu.edu.cn, wutanhui@163.com, jzhong@sjtu.edu.cn

## Abstract

Since the limit of the launchers' capabilities, the deployable structures were developed for the Aerospace Engineering. A coilable boom can be designed for a long deployed length with small boom storage. A coilable boom was usually comprised with large displacement and rotation beams, and the nonlinear dynamics of the system is rather complicated.

In this paper, a forward recursive formulation based on corotational frame is proposed for flexible beams with large displacement and rotation. The traditional recursive formulation has been successfully used for flexible multibody dynamics to improve the computational efficiency based on floating frame, in which the assumption of small strain and deflection is adopted. The proposed recursive formulation could be used for large displacement and rotation beams based on the corotational frame. It means that the recursive scheme is used not only for adjacent bodies but also for adjacent beam elements. The nodal relative rotation coordinates of the beam are used to obtain equations with minimal generalized coordinates in present formulation. The proposed formulation is different from Absolute Nodal Coordinate Formulation and the Geometrically Exact Beam Formulation in which the absolute coordinates are used.

The recursive scheme and minimal set of dynamic equations lead to a high computational efficiency in numerical integration. With using the relative coordinate a new element without singular was proposed in this formulation. Several numerical examples are carried out to demonstrate the validity of this formulation. And a coilable boom's deploying progresses are simulated by proposed formulation as shown in Figure 1.

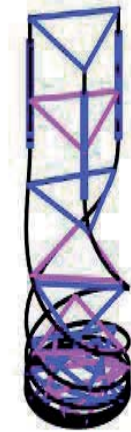


Figure 1. Deployment of a coilable boom

## Acknowledgments

The project was supported by the National Science Foundation of China (11132007,11202126), for which the authors are grateful.

## References

- [1] Puig, L., A. Barton, and N. Rando, A review on large deployable structures for astrophysics missions. *Acta Astronautica*, 2010. 67(1-2): p. 12-26.
- [2] Bae, D.-S. E.J. Haug, A Recursive Formulation for Constrained Mechanical System Dynamics: Part I. Open Loop Systems. *Mechanics of Structures and Machines*, 1987. 15(3): p. 359-382.



# A study on the effective deployment of tethered system via fast analysis method and experimental validation

Yoshiki Sugawara<sup>1</sup>, Shuntarou Oshima<sup>2</sup>, Yuri Touyama<sup>1</sup>, Sayako Sakama<sup>1</sup>

<sup>1</sup>Faculty of Mechanical Engineering  
 Aoyama Gakuin University  
 5-10-1 Fuchinobe, Chuo-ku, Sagami-hara-shi,  
 Kanagawa-ken, Japan  
 sugawara@me.aoyama.ac.jp,  
 a5613064@aoyama.jp,  
 sakama@me.aoyama.ac.jp,

<sup>2</sup>Faculty of Mechanical Engineering  
 Akita University  
 1-1, Tegatagakuen-machi Akita-shi,  
 Akita-ken, Japan  
 m9015104@wm.akita-u.ac.jp

## Abstract

In recent years, structure with extremely flexible elements are often employed in spacecraft in order to achieve large structure. One of those systems is tethered system which is attracting a lot of attention because such a system has potential to achieve various missions, for example orbit control, removal of orbital debris and so on. For reliable operation of such a system, behavior of them should be understood well before operation of them, therefore effective method of numerical analysis for such a system is strongly required. Finite element method (FEM) is often used for numerical analysis of systems with flexible component, but in general the calculation cost of FEM is not small and FEM requires long time to complete the analysis. Long time analysis make it impossible to handle the emergency case, to change mission phase dramatically in short time and so on. Therefore, numerical analysis with low calculation and moderate accuracy is beneficial and required.

Our previous study<sup>[1]</sup> proposed a numerical analysis method which utilizes the complementarity of the system which has extremely flexible element and the method provides a numerical analysis with fast calculation and moderate accuracy. For example, Figure 1 shows the behavior of simple case of the system with extremely flexible element. Introducing relative slack displacement  $s$  as the right figure shows, the acceleration of  $s$  and tensile force  $\sigma$  have complementarity relation in state transition from the state without “slack” to the state with “slack” as Figure 1 shows. That is, when  $\sigma$  has non-zero value,  $\ddot{s} = 0$ . On the other hand, when the value of  $\dot{s}$  becomes non-zero,  $\sigma$  becomes 0. Utilizing such a characteristic, our proposed method enables fast and moderately accurate analysis for the behavior of the system with extremely flexible element.

Our preliminary analysis revealed that attachment of intermediate masses to the tether have influence on behavior of deployment of tethered system and that there is a possibility of optimization of deployment sequence by additional masses to the tether. However, mathematical model of such a system is complex and it is difficult to execute aforementioned optimization in analytical method or conventional numerical analysis, i.e. FEM. On the other hand, our proposed method can provide fast calculation for deployment sequence of tethered system and it is easy to carry out a number of numerical analyses, and it leads to numerical optimization.

In this study, one dimensional deployment behavior of the tethered system shown in Figure 2 is analyzed by use of the proposed method. The tethered system consists of one main satellite and two tip satellites which are connected to the main satellite by tether. Tip satellites have propulsion systems which generate forces for deployment of tether. Furthermore, tether has some intermediate masses in order to change the deployment behavior. In the analyses, the mass of main satellite is 50[kg], mass of each tip satellite is 2[kg], total length of tether is 4[m], deployment force  $F$  given by propulsion systems is 5[N], number of additional mass on one tether is 7, length of tether between neighboring intermediate masses is 0.5[m] and all intermediate masses have same mass. Figure 3 shows the result of optimization obtained by the analyses. In Figure 3, the horizontal and vertical axis show mass of intermediate mass and settling time to complete deployment, respectively. As Figure 3 shows

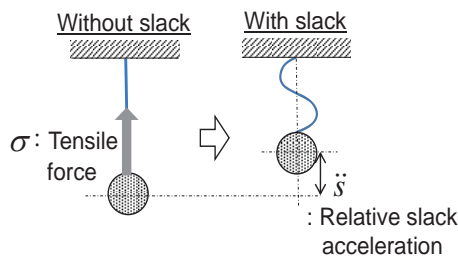


Figure 1. An example of complementarity relation of the system with extremely flexible elem.

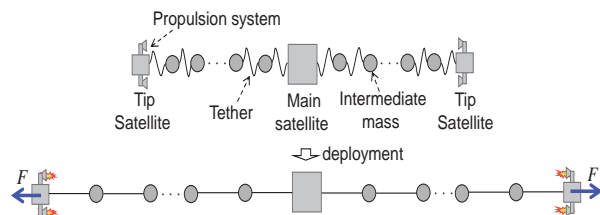


Figure 2. Analysis object (Tethered system)

settling time depends on the additional mass and it can be confirmed from the result that there exist optimum mass value which achieves minimum settling time, that is, optimum intermediate mass is about 0.17[kg] and the settling time at that mass is about 2[s]. Consequently, minimum settling time leads to minimum fuel consumption for propulsion systems and effective deployment can be achieved by attaching intermediate masses to the tethers. In other word, attaching masses to the tether leads to effective deployment without any active control.

In addition to numerical analysis, experimental validation is also carried out. Figure 4 shows experimental setup and Figure 5 shows schematic diagram of experimental setup and definition of coordinate. Considering the symmetric property of the tethered system shown in Figure 2, the setup is developed for half part of the system of Figure 2. Introducing pulley, deployment force is given by gravitational force applied to Mass 4 assumed as tip satellite and additional masses are attached to the slider in order to achieve low friction environment as space. In the experiment, 3 intermediate masses are attached to the tether and every mass have same value in one experiment. Figure 6 is the results of 4 experiments for 4 kinds of different additional masses (0.2, 0.3, 0.4, 0.5[kg]). It is clear from the time history of Mass 4 in Figure 6, the case of additional mass of 0.4[kg] shows shortest settling time and experimental results also show the existence of the optimum value of additional mass.

Comparison between numerical analysis and experiment does not show good correspondence and the reason comes from the friction of the slider and non-uniform characteristic of the tether. In order to execute more accurate experimental validation, model for numerical analysis should be improved and 2 dimensional case of deployment should be studied for practical use.

### Acknowledgments

This work was supported by KAKENHI 26420165.

### References

- [1] Y. Sugawara, S. Oshima, T. Chida “An analysis method for a system with mass and extremely flexible component and its application to analysis of deployable satellite” Proceedings of 7th ECCOMAS Thematic Conference Multibody Dynamics, Barcelona Spain, 2015.

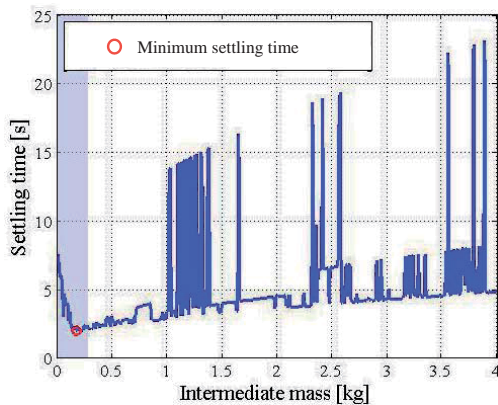


Figure 3. Result of numerical analysis

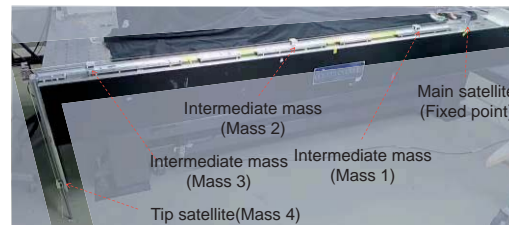


Figure 4. Experimental setup

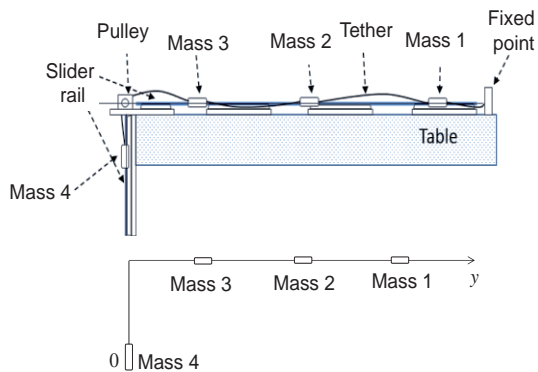


Figure 5. Schematic diagram of experimental setup (upper figure) and definition of coordinate (lower figure)

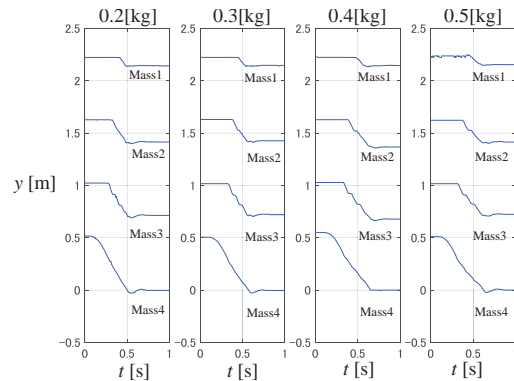


Figure 6. Results of experiment

## Modelling and Validation of a 3 MW Wind Turbine as a Basis for Structural Optimisation

Andreas Schulze<sup>1</sup>, János Zierath<sup>2</sup>, Roman Rachholz<sup>1</sup>, Sven-Erik Rosenow<sup>2</sup>, Reik Bockhahn<sup>2</sup>,  
Christoph Woernle<sup>1</sup>

<sup>1</sup> Chair of Technical Dynamics  
University of Rostock

Justus-von-Liebig-Weg 6, 18059 Rostock, Germany  
[andreas.schulze4, roman.rachholz, woernle]@uni-rostock.de

<sup>2</sup> W2E Wind to Energy GmbH

Strandstrasse 96, 18055 Rostock, Germany  
[jzierath, serosenow, rbockhahn]@wind-to-energy.de

### Abstract

With the increasing demand on renewable energy, the requirements on wind turbines with respect to higher performance while decreasing costs become more demanding on the design process. To meet these requirements a deep understanding of the overall wind turbine, comprising the mechanical structure, the aerodynamics and the plant controller, is needed at an early stage of the design process. Typically simplified multibody models of the overall turbine are used for early load calculations as basis for further component design. However, to ensure a thorough understanding of the dynamical behaviour during operation the development of detailed multibody models by means of general purpose multibody software is preferable, see [1].

The subject covered by this contribution is the development and experimental validation of a detailed multibody model of the W2E 120/3.0fc wind turbine designed by W2E Wind to Energy, Rostock, Germany. A prototype of this turbine is erected in Kankel, Mecklenburg-Western Pomerania, Germany. The prototype belongs to the class of wind turbines with horizontal axis, variable speed and variable pitch and has a rotor diameter of 120 m, a hub height of 100 m and a nominal rated power of 3 MW. Multibody modelling of this wind turbine is based on the concepts developed for a 2 MW wind turbine in [1]. The 3 MW turbine model and its validation are the basis for further optimisation studies.



Figure 1: Prototype of the W2E-120/3.0fc wind turbine.

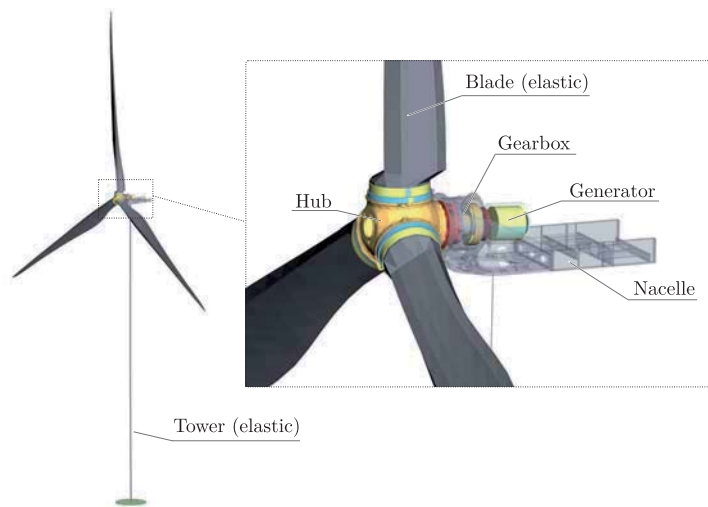


Figure 2: SIMPACK multibody model of the W2E-120/3.0fc wind turbine.

The multibody model of the 3 MW prototype in Figure 2 is built up in the general purpose multibody program SIMPACK [2]. The model comprises 110 degrees of freedom including flexible blades and a flexible tower as well as a detailed drive train model. The flexible tower is first modelled by means of finite beam elements in MSC.Nastran and then imported into SIMPACK via modal Craig-Bampton reduction [3]. For the flexible blades the SIMPACK blade generation tool is used. Equal to the tower buildup process, the blades are first modelled as finite beam elements followed by the coordinate reduction, whereby additional marker are applied for the application of aerodynamic loads. The drive train model includes a two stage planetary gear comprising rigid body parts connected via user-defined force elements to account for contact stiffness of pairing gears and torsional stiffness of the shaft.

The aim of developing a detailed multibody model of the wind turbine is to ensure a realistic representation of the overall turbine dynamics and structural loads during nominal power production and exceptional cases like controller faults or overload events. For this purpose it is necessary to model the aerodynamic forces and torques acting on the turbine blades as well as the interaction between turbine and controller. An interaction scheme

between multi body model, controller and aerodynamic code was developed in [1] that is appropriately adapted to the problem at hand.

Since the turbine prototype is part of type certification process extensive measurements have been conducted that are used for the validation of the multibody model. Therefore design load cases (DLC) classified by Germanischer Lloyd are simulated with the multibody model [4]. Simulation results and measurements are then compared based on statistical valuation. An exemplary comparison is given in Figure 3 where minimum, maximum and mean value of measurement and simulation are compared for the electrical power output and for the tilt bending moment at the tower base. Both curves in Figure 3 show sound correlation between simulation and measurements.

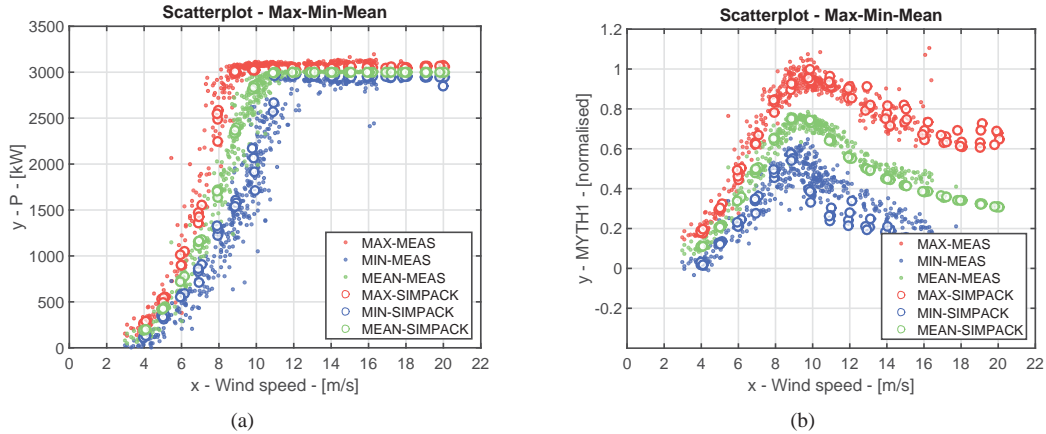


Figure 3: Comparing measurements with SIMPACK simulations: (a) electrical power (b) tilt bending moment at the tower base.

The validated wind turbine model lays the foundation for extensive dynamic optimisation studies. A first optimisation aims at an optimal relation  $\eta = f_1/f_2$  between the first eigenfrequencies of tower  $f_1$  and blades  $f_2$  to minimise structural loads during operation. Here it is assumed that changing the design variable  $\eta$  does influence neither the turbine mass nor the airfoil geometry of the blades. Therefore a simple scalar objective function can be introduced

$$Z(\eta) = \sum_{i=1}^m (w_i S_i(\eta) + \bar{w}_i \bar{S}_i(\eta)) + \sum_{j=1}^n (w_j M_j(\eta) + \bar{w}_j \bar{M}_j(\eta)). \quad (1)$$

Herein  $m$  DLC for different wind speed and turbulence intensities and  $n$  extreme load cases (ELC), defined by Germanischer Lloyd [4], are simulated by means of time integration of the multibody model. For each DLC  $i$ , the standard derivations of the tower base bending moment  $S_i$  and blade root bending moment  $\bar{S}_i$  are calculated and multiplied by the weighting factors  $w_i$  and  $\bar{w}_i$  respectively. For each ELC  $j$  the maxima  $M_j$  and  $\bar{M}_j$  of the respective bending moments are weighted with  $w_j$  and  $\bar{w}_j$ . With the objective function in (1) the constrained optimisation problem

$$\min \{Z(\eta) \mid \eta_{\min} \leq \eta \leq \eta_{\max}\} \quad (2)$$

is formulated. The problem stated in (2) is solved using methods available for constrained optimisation in Matlab [5]. Therefore a user-defined script is developed that couples the multibody code with the Matlab script.

### Acknowledgement

The research presented here is part of the DynAWind project funded by the German Federal Ministry for Economic Affairs and Energy under the grant number FKZ 0325228C/D.

### References

- [1] J. Zierath, R. Rachholz and C. Woernle. Field test validation of Flex5, MSC.Adams, alaska/Wind and SIMPACK for load calculations on wind turbines. *Wind Energy*, 19:1201-1222, 2016
- [2] SIMPACK. SIMPACK 9.7 Documentation. Simpack AG, Gilching, Germany, 2014.
- [3] R. R. Craig and M.C.C. Bampton. Coupling of Substructure for Dynamic Analyses. *AIAA Journal*, 6:1313-1319, 1968.
- [4] Germanischer Lloyd. IV Rules and Guidelines Industrial Service, Guidelines for the Certification of Wind Turbines, 2010.
- [5] MATLAB 2014b. The MathWorks, Inc., Natick, Massachusetts, United States, 2014.

## Table of Content

<b>Formulations and Numerical Methods .....</b>	<b>5</b>
A Simple Energy-Conserving Torsion-Free Beam Element for Multibody Applications .....	7
Adjoint Sensitivity Analysis of Three-Dimensional Beam Formulation .....	9
Convergence Rate Improvement in The HHT Integration Method for Index-3 DAEs of Multibody Dynamics .....	11
Multibody Kinematics by Means of Dual Constraints .....	13
Locally Nonlinear Strategies and Effective Preconditioners for Domain Decomposition Methods Applied to Large Flexible Multibody Systems .....	15
Interpolation Schemes for Geometrically Exact Beams: A Motion Approach .....	17
Computer Simulation of the Inverse Dynamics of Underactuated Mechanical Systems .....	19
On the Proper Orthogonal Decomposition for the Reduced-Order Modelling of Geometrically Nonlinear Elastic Bodies .....	21
Velocity-Based Three-Dimensional Beam Using the Energy Preserving Approach .....	23
Nullspace Method for the Analysis of Uniqueness of Reactions and Driving Forces in Redundantly Constrained Multibody Systems .....	25
Experimental Investigation and Numerical Modeling of Resultant-based Bending Plasticity in Cables .....	27
Application of a DAE Approach to Nonlinear Sloshing Problems.....	29
Dynamic Analysis of Thin Cables with Time-Varying Unwinding Velocity Condition and Transient-Tension Equations.....	31
Condensed Stiffness Matrices for the Model Reduction of Flexible Multibody Systems .....	33
Recursive Solution Procedures for Flexible Multibody Systems: Comparing Condensation and Transfer Matrix Methods.....	35
Indirect State and Force Estimator Based on Multibody Models.....	37
A Method for Calculating and Continuing Static Solutions for Flexible Multibody Systems .....	39
Stability Bounds For Step Size Ratios In Variable Time Step Implementations Of Newmark Integrators.....	41
Towards Higher Order Multi-Symplectic Lie-Group Variational Integrators for Geometrically Exact Beam Dynamics – Avoidance of Shear Locking.....	43

<b>Efficient Methods and Real-Time Applications.....</b>	<b>45</b>
Real-Time Estimation based on Multibody Dynamics for Automotive Embedded Heterogeneous Computing .....	47
Index-3 Divide And Conquer Algorithm For Efficient Multibody Dynamics Simulations .....	49
In-Extensible ANCF Cable Element for Real-Time Simulations .....	51
Study on Model Order Reduction of Flexible Multibody Systems.....	53
Constraint Reordering for Iterative Multi-Body Simulation with Contact.....	55
Dynamic Relaxation Method to Determine Equilibrium Configuration of Dynamic Models .....	57
Simplification of Multibody Direct Dynamics Models by Parameter Elimination .....	59
Comparative Analysis about High DOF Model and Low DOF Model of Rescue Robot .....	61
Performance Aspects of Real-Time Capable Flexible Multibody Simulations .....	63
<b>Parallelization methods .....</b>	<b>65</b>
Elimination Method for Parallelization of Flexible Multibody System Dynamics.....	67
A Co-Simulation Framework for High-Fidelity Simulation of Vehicle-Terrain Interaction .....	69
On-line Estimation of Wheel-Rail Contact Forces through Efficient Real-Time Models .....	71
<b>Flexible Multibody Dynamics .....</b>	<b>73</b>
Implementation of Shear Deformable Thin-Walled Beam Element for Flexible Multibody Dynamics .....	75
Kinetic Aspects of Discrete Cosserat Rods.....	77
Some Considerations on the Setup of Pseudo-Rigid Body Models for Single-Leaf Flexure Hinges in Compliant Mechanisms.....	79
The Use of Modal Derivatives in Determining Stroke-Dependent Frequencies of Large Stroke Flexure Hinges.....	81
FLEGX: Multibody Approach in Flexible Structure Design and Control .....	83
Approach for Modeling Flexible Bodies based on Experimental Data with Utilization in Elastic Multibody Simulation.....	85
Parallel Implementation of Flexible Multibody Dynamics Simulation Based on the Motion Formalism .....	87
A Discrete Hamilton-Pontryagin Approach to the Statics of Kirchhoff Rods.....	89
Dynamics of Spatial Flexible Multibody Systems with Interval Probabilities .....	91
Kinematic Calibration of a Six DOF Flexure-Based Parallel Manipulator.....	93

Avoiding Unphysical Vibrations Caused by Statically Correct Reduction of Elastic Multibody Systems.....	95
Comparison of Local and Global Approaches for Parametric Model Order Reduction for Systems with Distributed Moving Loads .....	97
Estimating Relative Eigenvalue Errors of Dynamic Model Reduction for Reliable Flexible Multibody Simulation .....	99
Calibration of Mechatronic Flexible Joint.....	101
Modal Testing on Wind Turbines for Validation of a Flexible Multibody Model.....	103
A Generalised Fourier Method to Solve the Initial Boundary Value Problem for Free Vibrating Viscoelastic Beam Models .....	105
Research on Form-finding and Deployment Dynamics for Modular Cable-Truss Antenna .....	107
Multibody Dynamics of Gear Pairs: Comparison Among Different Models.....	109
Comparison of Model Order Reduction Techniques for Flexible Multibody Dynamics using an Equivalent Rigid-Link System Approach.....	111
Modelling and Simulation of Mechatronic Flexible Joint .....	113
Two Approaches of the Rigid Finite Element Method to Modelling the Flexibility of Spatial Linkage Links.....	115
Kinematic and Dynamic Behavior of Hyperelastic Plate with External Force via Absolute Nodal Coordinate Formulation .....	117
On the Use of the Absolute Nodal Coordinate Formulation for the Dynamic Analysis of Rotating Shafts.....	119
<b>Contact Dynamics and Constraints .....</b>	<b>121</b>
Mathematical Tools for the Analysis of Smooth and Non-Smooth Systems with Redundant Constraints.....	123
Selection and Experimental Validation of Contact / Impact Models Suitable for Multibody Dynamics Simulations .....	125
Efficient Evaluation of Local and Global Deformations in Impact Simulations in Reduced Flexible Multibody Systems based on a Quasi-Static Contact Submodel .....	127
On the Generalized Friction Cone for Multibody Systems.....	129
A Discussion of Two Approaches for Studying the Dynamics of Dry Granular Material .....	131
A Spatial Revolute Joint Model with Clearance in Mechanisms Dynamics .....	133
Geometrical Interpretation of LCP Pivoting in Contact Dynamics.....	135
Geometric Non-Linear Dynamics of Shell System with Large Amount of Contact Based on the Co-Rotational Formulation .....	137

Comparison of Two Versions of the LuGre Model Under Conditions of Varying Normal Force .....	139
Modeling Rigid Body Multi-point Contact-Impact Transition for Event-Based Simulation Schemes .....	141
Modelling of the Nuclear Fuel Assembly Components as a Flexible 1D Continua with Inner and Outer Impact Interactions.....	143
Numerical Prediction and Experimental Validation of a Three-Dimensional Rod-Plate Impact.....	145
Experimental Investigation of Contact-impact In Multi-body System Using DIC Technique .....	147
Contact and Constraints in Analytical Dynamics .....	149
A 3D Volumetric Foot-Ground Model for Forward Dynamics.....	151
Gear Contact Model: Simulations and Measurement .....	153
Multibody Modelling of Friction Based Interaction between Turbine Blades .....	155
Dynamics of Falling Dominoes .....	157
Multibody Dynamics of a Flexible Legged Robot with Wheeled Feet.....	159
<b>Multiphysics and Coupled Problems .....</b>	<b>161</b>
Dynamic Simulation of the Inflation Gas of a Tire Under Operational Conditions....	163
Coupling a DEM Material Model to Multibody Construction Equipment .....	165
A Unitary Framework for Handling Fluid-Solid Interaction (FSI) Problems .....	167
An Efficient and Robust Standard Particle Interface for Multi-Flexible-Body Dynamics .....	169
Coupled Model for Simulating Turbocharger Rotors with Ball Bearings .....	171
Multibody Formulation of a Load-out Problem of a Mega Block Using Modular Transporters in Shipbuilding Industry.....	173
Damping Effect on Tall Building Low Frequency Vibration Using Two-Degree-of-Freedom Enhanced Coriolis Effect Damper .....	175
A Study on the Steering Jerk of a Wheel Loader Using MBD Simulation Including Hydraulic System .....	177
Investigation of Numerical Stability and Local Error for Continuous Co-Simulation Methods .....	179
Dynamic Analysis of a 3D Printer Based on the Delta Mechanism .....	181
Advance Modeling of Machine Tool Machining Process .....	183
<b>Benchmark Problems .....</b>	<b>185</b>
Comparison of Classical Multibody Simulation Methods with regard to the DAE Mathematica Solver .....	187

Benchmark Problems for the Linearization of Multibody Dynamics.....	189
Computational Modelling of the Parallel Cable Mechanism with the Added Active Structure .....	191
<b>Control and Optimization .....</b>	<b>193</b>
Fully Coupled Topology Optimization of Flexible Multibody Systems with Constraints .....	195
Variational Multirate Integration in Discrete Mechanics and Optimal Control.....	197
Forward Sensitivity Analysis of the Index-3 Augmented Lagrangian Formulation with Projections .....	199
Position Control of Flexible Chain Using Wave Based Control.....	201
Modelling of Slender Elements in Offshore Engineering Using the Rigid Finite Elements Method .....	203
Active Vibrations Attenuation by Controlling Relative Motion of Selected Masses, FE Modeling .....	205
On Control of Robot Manipulators with Flexible Joints.....	207
Cloth-like Structures with Distributed Active Damping.....	209
Parameter Identification of a Torsional Vibration Damper in Frequency Domain Using Adjoint Fourier Coefficients.....	211
Model Based Filtering on the Horizontal Axis Wind Turbine. Towards a Holistic Approach: Load Measurement, Predictive Maintenance, Mechanical Design Assessment and Certification. ....	213
Design Optimization of Planetary Gear Trains Under Dynamic Constraints and Parameter Uncertainty.....	215
Intelligent Sliding Mode Control of an Overhead Container Crane .....	217
<b>Software Development and Computer Technology.....</b>	<b>219</b>
Multibody System Dynamics at the University of Minho: Teaching and Research Activities .....	221
Synchronous Machine Electromechanical and Mechanical Analogy Model Comparison .....	223
A New Software for Solving Inverse Problems in Multibody Dynamics.....	225
<b>Robotics .....</b>	<b>227</b>
Cable Driven Spherical Mechanism Quadrosphere Enhanced by 3 DOF Piezo-actuated Platform.....	229
On the Use of Principal Vectors in Multibody Dynamics .....	231
Robust Rest-to-Rest Motion Planning for Cranes Through a Variational Solution .....	233

Comparison of Distributed Model Predictive Control Approaches for Transporting a Load by a Formation of Mobile Robots .....	235
Performance of a Quasi-Holonomic Mobile Robotic Carrier in the Dynamics Mimicking System.....	237
Increase of Stiffness in Physically Cooperating Robots .....	239
Kinematic Design of a Multiple Motion-type Parallel Manipulator based on the 3-RRS Mechanism .....	241
On Optimal Laws of Groups of Walking Robots Motion while Solving Formation Task .....	243
Modelling and Control Synthesis of Flexible Robot Arm Equipped with Additional Sensors.....	245
Development of Structure and Behavioral Model for Screw Driving In-pipe Inspection Robot based on Adaptive Mechanism on Legs.....	247
Adaptive Learning Control Algorithms for KUKA LWR 4+ Robots.....	249
Proportional-Derivative and Model-Based Controllers Used for a Serial Type Manipulator in Case of a Variable Mass Payload.....	251
Optimal Point to Point Trajectory Planning with Collision Avoidance for Dual Arm Setup .....	253
Coordinate-Free Decomposition of the Rigid Body Displacement: A Davenport Dual Angles Approach .....	255
Selected Feedback Control Concepts in End-effector Trajectory Tracking of a Highly Flexible Manipulator.....	257
Forward Kinematics Analysis of a Stewart Platform using Computer Vision Pose Estimation .....	259
Improved Calibration of Machine Tools by Redundant Measurement.....	261
<b>Road and Railroad Vehicle Dynamics .....</b>	<b>263</b>
A Soft Soil Contact Model with Adaptive Level of Detail for Predicting Off-Road Vehicle Mobility .....	265
Force Estimation on a McPherson Suspension by Means of a State Estimator and a Multibody Model.....	267
Optimal Control of the Tilting Modes Transition for a Narrow Track Vehicle through MBS Modelling .....	269
A Knife-Edge Wheel-Rail Contact Constraint Approach for the Multibody Simulation of Railway Vehicles.....	271
Development of an Innovative Degraded Adhesion Model for Railway Multibody Applications.....	273

Development of an Innovative Model to Study Wear Evolution Considering Wheel-Rail Conformal Contact.....	275
Motorway Sharing for Passenger Cars and Truck Platoons .....	277
Assessment of the Necessary Width of a Bicycle Lane by Means of Multibody Simulations on a Bicycle-Rider System.....	279
Inerter Potential for Vehicle Vertical Dynamics.....	281
Evaluation Criterion of Force Transfer through Mechanism.....	283
Estimation of Railroad Vehicle Dynamics and Track Irregularities Using Data Fusion Techniques and Computational Methods.....	285
Numerical Investigation on the Dynamics of a High-Performance Motorcycle Equipped With an Innovative Hydro-Pneumatic Suspension System.....	287
An Overview of a Connected Autonomous Vehicle Emulator .....	289
A Variable Time-Step and Variable Penalty Method for the Index-3 Augmented Lagrangian Formulation with Velocity and Acceleration Projections.....	291
An Optimal Velocity Profile Design for 6 x 6 Unmanned Ground Vehicle Based on Real-time Traversability(RTT) Analysis.....	293
Physics-Based Tire-Soil Interaction Model and Validation for Off-Road Mobility Simulations .....	295
Experimental Model of a Vehicle with an Assistant for Reversing with a Trailer.....	297
Development of Steering Torque Simulator with Multibody Kinematic Model Considering Friction Characteristics of Steering Gear.....	299
Estimation of Commercial Vehicle Dynamics by Means of Real-Time Application in Condition of High Speed Curvilinear Maneuvers.....	301
Linearized Modal Analysis of Vehicle Powertrains.....	303
Behavior of Drivers with Road Departure Prevention Systems Using Driving Simulator .....	305
Cable Dynamics and Fatigue Analysis for Digital Mock-Up in Vehicle Industry .....	307
Use of Joint Coordinates and Homogenous Transformations for Modelling of Articulated Vehicle Dynamics.....	309
Tilting Child Safety Seat for Reducing the Lateral Acceleration Acting on Children when Vehicle Cornering.....	311
<b>Biomechanics .....</b>	<b>313</b>
Using Kinematic Rolling Surfaces for Fast Foot-Ground Modeling in the Forward Dynamics of Human Gait - A Sagittal Plane Analysis.....	315
Quantification of Intervertebral Efforts Using a Multibody Dynamics Approach: Application to Scoliosis.....	317
Influence of the Side Branches of the Human Vocal Tract on the Voice Quality.....	319

Validating Subject Multibody Dynamics Estimated Action with Measured sEMG at Lower Limb Muscles on Different Gait Modes.....	321
What is Sit-to-Stand without a Chair? .....	323
A Human Mannequin Head-and-Neck Multibody Model for the Simulation of High-Speed Impacts.....	325
Multibody Biomechanical Analysis of Taekwondo Athletes.....	327
Modelling of Real Car-to-Pedestrian Accident: Comparison of Various Approaches in the Car Bonnet Modelling .....	329
Optimal Control of a Biomechanical Multibody Model for the Dynamic Simulation of Working Tasks .....	331
Development of a Tool for the Sensitivity Analysis of Design Parameters of Femoral Implants in the Human Body During Gait.....	333
Dynamic Parameter Identification of an Upper Extremity Rehabilitation Robot Using GPOPS-II.....	335
Optimization Methods for Identifying Muscle Forces in a Spinal-Cord- Injured Subject during Crutch-Assisted Gait.....	337
Experimental Identification of Time-Delay of Human Balancing Using Cepstrum .....	339
Identification of Knee Ligament Properties by Multibody Optimisation.....	341
Use of Analytical Derivatives in an Optimal Control Algorithm for the Residual Elimination Problem of Gait.....	343
Human like Motion Generation for Ergonomic Assessment - a Muscle Driven Digital Human Model using Muscle Synergies.....	345
Periodic Servo-Constraints in a Stick Balancing Problem.....	347
Generating Optimal Gaits for the Biped Across Different Locomotion Modes.....	349
Kinematic Validation Of A Human Thumb Model .....	351
Optimal Control Prediction of a Dynamically Consistent Walking Motion for a Spinal Cord-Injured Subject Assisted by Orthoses .....	353
Collective Bounce Helicopter Proneness: Moving Towards the Characterization of the Worst Pilot.....	355
<b>Aerospace and Maritime Applications .....</b>	<b>357</b>
Equivalent Mass-Spring Models of Multibody Spacecraft for the Application of Wave-based Control.....	359
Forward Dynamics of Fixed-Wing Aircraft with Attitude Reconstruction via Novel Quaternion-Integration Procedure.....	361
Attitude Control of the Tether Space Mobility Device in Extending and Winding Tether .....	363

Deployment of a Coilable Boom Based on Corotational Frame for Flexible 3-D Beams with Large Displacement and Rotation.....	365
A Study on the Effective Deployment of Tethered System via Fast Analysis Method and Experimental Validation.....	367
Modelling and Validation of a 3 MW Wind Turbine as a Basis for Structural Optimisation .....	369

**Index of Authors**

Aarts, Ronald G.K.M.....	93
Abedrabbo, Gabriel.....	317
Abrantes, João M. C. S. ....	321
Aceituno, Javier F. ....	271, 285
Adamiec-Wójcik, Iwona.....	203, 309
Alsaleh, Mustafa.....	295
Andersson, Fredrik.....	77, 307
Andreev, Aleksandr.....	207
Andrews, Sheldon.....	55
Arnold, Martin.....	41, 123
Augustynek, Krzysztof.....	115
Bader, Rainer.....	341
Baecker, Manfred.....	163
Banecek, Jan.....	281
Barbosa Rodrigues, Carlos Manuel.....	321
Barrere, Remi.....	187
Bauchau, Olivier A. ....	9, 17, 87
Bauma, Vaclav.....	101, 113
Beitelschmidt, Michael.....	85
Bellani, Gabriele.....	287
Ben Hanan, Uri.....	237
Bencsik, László.....	339, 347
Beneš, Petr.....	209, 229, 245, 297
Berglind, Luke.....	183
Bergschmidt, Philipp.....	341
Berns, Karsten.....	345
Bertails-Descoubes, Florence.....	89
Bessa, Wallace Moreira.....	217
Betsch, Peter.....	19
Björkenstam, Staffan.....	331, 345, 351
Blumentals, Alejandro.....	89
Bocchini, Enrico.....	273
Bockhahn, Reik.....	103, 369
Boscariol, Paolo.....	233
Boudon, Benjamin.....	187
Bowling, Alan Paul.....	141
Briskin, Eugene Samuilovich.....	243
Brochu, Myriam.....	333
Brown, Peter.....	151

Bruls, Olivier .....	17, 21, 133
Bulín, Radek.....	191, 229
Burger, Michael.....	165
Busch, Martin .....	179
Butin, Danila.....	301
Butini, Elisa.....	273, 275
Byrtus, Miroslav .....	155
Calabrese, Francesco .....	163
Caldwell, Darwin G.....	83, 159, 327
Callejo, Alfonso.....	9
Cammarata, Alessandro.....	33
Cannella, Ferdinando.....	83, 159, 327
Cardona, Alberto .....	133
Cartiaux, Olivier .....	317
Caspers, Lennart.....	315
Cavalieri, Federico .....	133
Cirelli, Marco .....	109
Collingridge, Mike.....	11
Concli, Franco .....	215
Condurache, Daniel .....	255
Cornelis, Bram .....	267
Cortese, Luca.....	215
Croes, Jan.....	267
Cuadrado, Javier .....	49, 189, 291, 325, 337, 343
Cugnon, Frederic .....	183
Czekanski, Alex.....	125
Češarek, Peter.....	27
de Boer, André.....	35
Deng, Xiaowei.....	147
Denk, Petr .....	297
Desmet, Wim .....	47, 267
Detrembleur, Christine.....	317
Dewes, Eva-Maria .....	15
Diebels, Stefan.....	27
D’Imperio, Mariapaola.....	83
Docquier, Nicolas .....	269
Docquier, Quentin.....	269
Dopico, Daniel .....	37, 199, 291, 343
Dörlich, Vanessa .....	27
Drąg, Łukasz.....	203, 309
Dreßler, Klaus .....	165
Dyk, Štěpán .....	143

Ebel, Henrik .....	235
Eberhard, Peter .....	95, 97, 235
Ekevid, Torbjörn .....	165
Ellenbroek, Marcel .....	35
Elmqvist, Asher .....	289
Enzenhöfer, Andreas .....	135
Erleben, Kenny .....	55
Escalona, José .....	71, 271, 285
Febrer-Nafría, Míriam .....	353
Fisette, Paul .....	269, 317
Flores, Paulo .....	221
Font-Llagunes, Josep M. ....	129, 353
Frączek, Janusz .....	25, 49
Fregly, Benjamin J. ....	343, 353
Fröhlich, Benjamin .....	97
Gail, Tobias .....	197
Gainza, Gorka .....	213
Galardi, Emanuele .....	71
Gallrein, Axel .....	163
Galvez, Javier .....	133
García Orden, Juan Carlos .....	7
García-Vallejo, Daniel .....	199, 271, 285
Gasparetto, Alessandro .....	111
Gattringer, Hubert .....	253
Geier, Andreas .....	341
Gervais, Benjamin .....	333
Ghannadi, Borna .....	335
Giovagnoni, Marco .....	111
Gong, Lulu .....	349
González, Francisco .....	49, 189, 199, 325
Grawe, Robert .....	341
Gupta, Deepak K. ....	259
Habra, Timothée .....	269
Hajžman, Michal .....	155, 191, 229
Hakvoort, Wouter B.J. ....	93
Ham, Seung-Ho .....	173
Hamed, Ashraf .....	11
Han, Jongboo .....	293
Hara, Kensuke .....	29
Haslinger, Josef .....	303
Hatch, Dylan .....	289
Hefter, Harald .....	315

Held, Alexander.....	195
Hermansson, Tomas.....	77, 307
Hira, Yuuki.....	175
Hong, Hyosung.....	293
Hong, Jiazhen.....	137, 145, 365
Hopf, Helge.....	85
Horáček, Jaromír.....	319
Hoshino, Hiroki.....	299
Houfek, Pavel.....	281
Hromcik, Martin.....	209
Hu, Haiyan.....	53, 91, 107
Hurskainen, Vesa-Ville Taneli.....	119
Huynh, Hoai Nam.....	155
Chamorro, Rosario.....	271, 285
Chang, Hanjiang.....	107
Chatterjee, Abhishek.....	141
Chatzisavvas, Ioannis.....	171
Chaudhry, M. S.....	125
Chen, Genliang.....	241
Chen, Peng.....	147
Choi, Jin Hwan.....	99, 169
Choi, Juhwan.....	99, 169
Choi, Seungjun.....	305
Insperger, Tamás.....	339
Iriarte, Xabier.....	59, 213
Iwasaki, Tadashi.....	299
Jang, Jin-Seok.....	31
Jankowski, Krystof Peter.....	125
Jayakumar, Paramsothy.....	265, 295
Jeong, Seung-Hyun.....	31
Jonker, Ben.....	75
Joo, Sanghyun.....	293
Jung, Samuel.....	57, 61, 293
Kang, Ji-Heon.....	31
Kaserer, Dominik.....	253
Kecskemethy, Andres.....	315, 337
Khude, Naresh.....	11
Kim, Daegyu.....	305
Kim, Donguk.....	305
Kim, Hyung-Ryul.....	31
Kim, Jin-Gyun.....	99
Kim, Kum-Woo.....	31

Kim, Minseok.....	177
Kim, Sung-Soo.....	293
Kim, Tae-Yun.....	57, 61
Kohlsche, Thomas.....	195
Kolda, Ondrej.....	281
Kovačić, Zdenko.....	247
Kovář, Filip.....	261
Kovecses, Jozsef.....	129, 135
Kraus, Karel.....	229
Krejza, Radek.....	209
Kreuzer, Edwin.....	217
Kry, Paul G. ....	55
Kryaskov, Viktor.....	301
Kwarta, Michal.....	131
Lang, Holger.....	105
Lauß, Thomas.....	211, 225
Lee, Hanmin.....	99
Lee, Heejong.....	177
Lee, Jae-Wook.....	31
Lee, Jimin.....	177
Lein, Claudius.....	85
Leitz, Thomas.....	43
Leyendecker, Sigrid.....	43, 105, 197, 331, 351
Li, Yunpeng.....	349
Linn, Joachim.....	27, 77, 307, 331, 345, 351
Lipinski, Krzysztof.....	251
Liu, Caishan.....	157
Liu, Cheng.....	53
Liu, Jinyang.....	147
Liu, Zhuyong.....	137, 145, 365
Lu, Daixing.....	171
Luaces, Alberto.....	189, 291
Ludovico, Daniele.....	83
Lugris, Urbano.....	315, 325, 337, 343, 353
Luo, Jingjing.....	117
Luo, Kai.....	53, 107
Mahaudens, Philippe.....	317
Malczyk, Pawel.....	49
Maloletov, Alexander Vasilievich.....	243
Manas, Jaroslav.....	329
Mangoni, Dario.....	265
Marini, Lorenzo.....	71, 273, 275

Martini, Alberto .....	287
Martinusi, Vladimir .....	21
Masarati, Pierangelo .....	181, 189
Mathew, Vineet.....	259
Matikainen, Marko Kalervo.....	119
Mazhar, Hammad .....	167
McPhee, John .....	151, 323, 335
Meacci, Martina.....	273, 275
Meijaard, Jacob P.....	39, 279
Meli, Enrico.....	71, 273, 275
Mentrasti, Lando .....	83
Miguélez, María Henar.....	325
Michaud, Florian .....	337
Mikkola, Aki Matti .....	51, 119
Minaker, Bruce .....	189
Miyaji, Wataru .....	363
Molnár, Csenge A. ....	339
Morlock, Merlin .....	257
Mousny, Maryline .....	317
Mouzo, Francisco.....	343, 353
Mráz, Ladislav .....	67, 239
Mukherjee, Sudipto.....	259
Müller, Andreas.....	253
Muñoz, Sergio .....	271, 285
Muscarello, Vincenzo.....	355
Muscolo, Giovanni Gerardo .....	159, 327
Nagy, Dalma.....	339
Nachbagauer, Karin.....	211, 225
Naya, Miguel Ángel.....	37, 47
Nečas, Martin.....	223, 239
Negrut, Dan .....	69, 131, 167, 265, 289
Neuman, Petr.....	223
Neusser, Zdeněk.....	153, 201, 223
Norman-Gerum, Valerie.....	323
Obentheuer, Marius .....	345
Ober-Blöbaum, Sina.....	197
Oberpeilsteiner, Stefan .....	211, 225
Offner, Guenter.....	303
Oh, Joo-Young .....	31
Okabe, Eduardo Paiva .....	181
Okuma, Masaaki .....	175
Olsen, Nicholas.....	69

Ortiz, Jose.....	11
Orzechowski, Grzegorz.....	51
Oshima, Shuntarou.....	367
Osman, Krešimir.....	247
Otto, Svenja.....	217
Ou, Ye.....	337
Ozturk, Erdem.....	183
Pandža, Viktor.....	361
Park, Seongchae.....	305
Paschkowski, Manuela.....	123
Pastorino, Roland.....	47
Pavlata, Petr.....	329
Pavlov, Nikolay Lyubenov.....	311
Pazouki, Arman.....	131, 167
Peiret, Albert.....	129
Pękal, Marcin.....	25
Pelikán, Jan.....	201, 223
Pennestri', Ettore.....	13, 79, 109
Peregudova, Olga.....	207
Phutane, Uday Dattaram.....	351
Pizzamiglio, Cristiano.....	83
Plakhotnik, Denys.....	183
Plaza, Aitor.....	59, 213
Polach, Pavel.....	191, 229
Rachholz, Roman.....	103, 369
Raison, Maxime.....	333
Rakhsha, Milad.....	167
Recuero, Antonio.....	69
Reichl, Stefan.....	211
Richiede, Dario.....	233
Rindi, Andrea.....	71, 273, 275
Risaliti, Enrico.....	267
Rixen, Daniel.....	15
Rodriguez Gonzalez, Antonio Joaquin.....	37, 47
Rodríguez-Millán, Marcos.....	325
Roh, Myung-Il.....	173
Roller, Michael.....	331, 345, 351
Romani, Benedetta.....	71
Ros, Javier.....	59, 213
Rosenow, Sven-Erik.....	103, 369
Sakama, Sayako.....	367
Sanjurjo Maroño, Emilio.....	37, 47, 291

Saura, Mariano .....	199
Scalera, Lorenzo.....	111
Seifried, Robert.....	63, 127, 195, 217, 257
Serban, Radu.....	69, 131, 265, 289
Sharafian Ardakani, Ehsan .....	235
Sharbati, Ehsan.....	205
Sharif Razavian, Reza.....	335
Shi, Jiabei .....	137
Shi, Tengfei.....	157
Shiiba, Taichi.....	299
Schiehlen, Werner.....	277
Schilder, Jurnan.....	35, 81
Schmitt, Alexander.....	63
Schmoll, Robert.....	171
Schneider, Fabio .....	77, 307
Schulze, Andreas.....	103, 369
Schwab, Arend L. ....	279
Schweizer, Bernhard.....	171
Siebler, Mario .....	315
Sinatra, Rosario.....	33
Sokolov, Evgeni Evgeniev.....	311
Song, Hajun.....	293
Sonneville, Valentin.....	17, 21, 87
Sopouch, Martin .....	303
Souchet, René Paul.....	149
Spicka, Jan .....	329
Steidel, Stefan .....	165
Steinbauer, Pavel .....	101, 281
Steiner, Wolfgang.....	211, 225
Stoltmann, Michael.....	341
Sugawara, Yoshiki.....	367
Sugiyama, Hiroyuki.....	295
Sulitka, Matěj.....	153
Szyszkowski, Walerian.....	205
Šáfr, Filip .....	201
Šika, Zbyněk.....	191, 209, 229, 245
Tak, Taeoh.....	305
Takehara, Shoichiro.....	363
Tasora, Alessandro.....	265
Teichmann, Marek.....	55, 135
Terumichi, Yoshiaki.....	363
Terze, Zdravko .....	361

Thompson, Joseph William .....	359
Tian, Qiang.....	53, 91, 107
Timmer Arends, Axel J.H. ....	93
Touyama, Yuri.....	367
Tschigg, Stephan.....	127
Tumasov, Anton.....	301
Uematsu, Yu .....	363
Urbaś, Andrzej.....	115
Urda, Pedro .....	271, 285
Vadean, Aurelian .....	333
Valášek, Michael .....	67, 101, 113, 153, 201, 223, 229, 239, 245, 261, 283
Valentini, Pier Paolo.....	13, 79, 109
Vampola, Tomáš .....	153, 319
van den Belt, Mieke.....	81
van der Wijk, Volkert.....	231
Vasiliev, Alexey .....	301
Velhote Correia, Miguel Paiva.....	321
Verlinden, Olivier.....	155
Vermaut, Martijn .....	267
Vidoni, Renato .....	111, 215
Vích, Jan .....	283
Vilela, David.....	189
Volech, Jiří.....	229, 245
Voss, Kevin H.J.....	93
Vrbský, Ladislav.....	297
Vrdoljak, Milan .....	361
Vychytil, Jan.....	329
Walker, Mario Patrick.....	175
Wang, Hao.....	117, 241
Wang, Jia.....	119
Wang, Jianyao.....	145
Wang, Zhe .....	91
Weber, Dietmar .....	165
Wehrle, Erich.....	215
Weiss, Avi.....	237
Wieloch, Victoria .....	41
Winter, Evelyn .....	341
Woernle, Christoph .....	103, 341, 369
Wojciech, Stanisław.....	203, 309
Wojtyra, Marek .....	25, 139
Woliński, Łukasz .....	249
Woller, Johannes .....	85

Won, Mooncheol .....	293
Wu, Tanhui.....	365
Yamashita, Hiroki .....	295
Yang, Yinping .....	19
Yi, Canming.....	117
Yoo, Wan Suk.....	31, 57, 61, 177, 293
Yoon, Seul-Gi .....	57
Yu, Haidong.....	117
Yu, Weidong.....	241
Zanoni, Andrea.....	355
Zavřel, Jan.....	191, 297
Zelei, Ambrus.....	339, 347
Zeman, Vladimír.....	143
Zemanek, Tomas .....	281
Zeng, Weikang .....	349
Zhang, Shengpeng.....	305
Zhang, Zhenghai .....	349
Zhao, Longhai.....	241
Ziegler, Pascal.....	95
Zierath, János.....	103, 369
Zinkiewicz, Bianka.....	303
Zlatar, Dario.....	361
Zubair, Mohd.....	259
Zupan, Dejan .....	23
Zupan, Eva.....	23

## Organizers



## Auspices



## Conference sponsors



## Institutional support



## Media partner

